FROM OPEN CONTAINERS TO CONFINED SUPRAMOLECULAR ARCHITECTURES

This dissertation is submitted for the degree of

"Doctor rerum naturalium"

TU Dortmund

Department of Chemistry and Chemical Biology

David Ocklenburg

technische universität dortmund

The work presented in this thesis has been conducted between January 2022 and December 2025 at the Department of Chemistry and Chemical Biology, TU Dortmund.

Principal Advisor:	Dr. David Van Craen
	Department of Chemistry and Chemical Biology,
	TU Dortmund
Coexaminer:	Prof. Dr. Sebastian Henke
	Department of Chemistry and Chemical Biology,
	TU Dortmund
Submission Date:	13.03.2026

Ich kann, was ich muß! o seltenes Geschick!
Ich will, was ich muß - - o doppeltes Glück.

Mein Herz ist an Stärke dem Felsen gleich,
Mein Herz ist, wie Blumen, sanft und weich.

Mein Wesen gleicht Glocken von strengem Metall:
Schlag kräftig d'ran, gibt es auch kräftigen Schall.

Mein Geist stürmt auf eiligem Wolkenruß hin;
Mein Geist spielt mit Kindern mit kindlichem Sinn.

Ich weiß, was ich will! Und weil ich es weiß,
Drum bann' ich's zu mir in den magischen Kreis.

Ich weiß, was ich will! Das ist ja die Kraft,
Die sich aus dem Chaos ein Weltall entrafft.

Ich weiß, was ich will! Und wenn ich's erreich',
Dann gelten der Tod und das Leben mir gleich.

Betty Paoli (1814-1894)

Awards and Scholarships

2022 Liebig PhD Fellowship, offered by the Fonds der Chemischen Industrie (FCI)

2025 Poster Prize at Tag der Chemie, Dortmund, Germany

Conferences and contributions

Poster presentations

July 2022	SupraChem, Mainz, Germany
September 2022	International Symposium on Confinement-controlled chemistry 2022
June 2023	International Symposium on Macrocyclic and Supramolecular Chemistry, Reykjavik, Iceland
September 2023	796th Heraeus-Seminar, Bad Honnef, Germany
February 2024	SupraChem, Ulm, Germany
May 2024	SupraParis, Paris, France
June 2024	Girona Seminar, Catalunya
März 2025	Tag der Chemie, Dortmund, Germany

Oral presentations

February 2024	Tag der Chemie, Dortmund, Germany
December 2024	PhD seminar at TU Dortmund, Dortmund, Germany
April 2025	Symposium with Clever and Friends, Dortmund, Germany

Publications

D. Ocklenburg, D. Van Craen, *Beilstein J. Org. Chem.* **2024**, *20*, 3007-3015.

D. Ocklenburg, Yannic Müller, Julian Holstein, D. Van Craen, *Guest induced formation of confined tri- and hexanuclear host-guest complexes* (manuscript in preparation).

Table of Content

Abstract

The work will investigate the preparation and characterization of charge-neutral Zn(II) metal organic cages based on bis(bidentate) hydroxyquinolate ligands, with focus on how ligand topology and functionality modulate anion recognition and guest-directed assembly. Building on a charge-neutral $[Zn_2L_2]$ host-complex presented by our group in 2022, various rational designed ligands were synthesized and self-assembled with $Zn(OAc)_2$ to yield discrete $[Zn_2L_2]$ architectures and others.

The first chapter will introduce three new bis(bidentate) ligands L^{mN3}-H_2, L^{N3}-H_2 and L^{crown3}-H_2 which are designed and synthesized to increase the functionality of the parent $[Zn_2L_2]$ cage. Spectroscopic and computational analysis indicate that expanded π-surfaces preserve the metal organic cages integrity while enabling additional host-guest π-interactions, and a crown-ether functionalized derivative demonstrates heteroditopic ion-pair binding.

Second, to address the challenge that strongly chelating oxalate can disrupt metal-ligand assemblies, a more flexible ligand L^{DB3}-H_2 was designed and synthesized to afford a robust charge-neutral $[Zn_2L^{DB3}{}_2]$ host-complex. This container forms a well-defined 1:1 oxalate host-guest complex in solution. UV/Vis titrations quantify binding and competition experiments demonstrate selective oxalate recognition over longer dicarboxylates and monocarboxylates. Dicarboxylates form host-guest complexes in a slow-guest exchange behavior, whereas mono-carboxylates demonstrate fast-exchange.

Finally, a tripodal bis(bidentate) ligand, L^{TP3}-H_3, enables guest-induced control over nuclearity and topology. Tricarboxylates template direct formation of trinuclear and hexanuclear onion-type host-guest complexes with architecturally appealing supramolecular features. ^{1}H NMR competition experiments reveal observable interconversion of a trinuclear species into a hexanuclear species and give insight in to the respective binding affinities. Kinetic studies suggest an associative-dissociative exchange-transformation mechanism with a substantial activation barrier.

Zusammenfassung

Die vorliegende Arbeit untersucht die Herstellung und Charakterisierung ladungsneutraler Zn(II)-metallorganischer Käfige auf Basis von bis(bidentaten) Hydroxychinolinat-Liganden, mit dem Schwerpunkt darauf, wie Ligandtopologie und -funktionalität die Anionenerkennung und gastgesteuerte Assemblierung modulieren. Aufbauend auf einem von unserer Arbeitsgruppe im Jahr 2022 vorgestellten ladungsneutralen $[Zn_2L_2]$-Wirtskomplex wurden verschiedene rational entworfene Liganden synthetisiert und mit $Zn(OAc)_2$ zur Bildung diskreter $[Zn_2L_2]$-Architekturen und weiterer Strukturen selbstassemblierend verknüpft.

Im ersten Kapitel werden drei neue bis(bidentate) Liganden, L^{mN3}-H_2, L^{N3}-H_2 und L^{crown3}-H_2, vorgestellt, die entwickelt und synthetisiert wurden, um die Funktionalität des ursprünglichen $[Zn_2L_2]$ Käfigs zu erweitern. Spektroskopische und computergestützte Analysen zeigen, dass erweiterte π-Flächen die Integrität der metallorganischen Käfige erhalten, während sie zusätzliche Wirt-Gast-π-Wechselwirkungen ermöglichen. Zudem zeigt ein Kronenether-funktionalisiertes Derivat eine heteroditopische Ionen-Paar-Bindung.

Zweitens wurde ein flexiblerer Ligand L^{DB3}-H_2 entworfen und synthetisiert, der die Bildung eines robusten, ladungsneutralen $[Zn_2L^{DB3}{}_2]$-Wirtskomplexes ermöglicht. Dieser Container bildet in Lösung einen wohldefinierten 1:1-Oxalat-Wirt-Gast-Komplex. UV/Vis-Titrationen quantifizieren die Bindung, und Konkurrenzexperimente zeigen eine selektive Oxalat-Erkennung gegenüber längeren Dicarboxylaten und Monocarboxylaten. Dicarboxylate bilden Wirt-Gast-Komplexe mit langsamem Gastaustausch, wohingegen Monocarboxylate ein schnelles Austauschverhalten zeigen.

Abschließend ermöglicht ein tripodal bis(bidentater) Ligand, L^{TP3}-H_3, eine gastinduzierte Kontrolle über Nuklearität und Topologie. Tricarboxylate ermöglichen die direkte Bildung von trinuklearen und hexanuklearen, zwiebelartigen Wirt-Gast-Komplexen mit architektonisch reizvollen supramolekularen Merkmalen. ^{1}H-NMR-Konkurrenzexperimente zeigen eine beobachtbare Umwandlung einer trinuklearen Spezies in eine hexanukleare Spezies und geben Einblicke in die jeweiligen Bindungsaffinitäten. Kinetische Untersuchungen deuten auf einen assoziativ-dissoziativen Austauschmechanismus mit einer erheblichen Aktivierungsbarriere hin.

1 General Introduction

In the last century, chemistry has learned to treat non-covalent interactions not as nuisance to be averaged out, but as design parameters with perspective to create materials with characteristic functionalities for making matter recognize, assemble and adapt. JEAN MARIE LEHN defined supramolecular chemistry at the Nobel lecture 1987 as "chemistry beyond the molecule". LEHN, together with PEDERSEN and CRAM, won the 1987 Nobel Prize in chemistry for founding host-guest chemistry and demonstrating that selective molecular recognition could be engineered with small synthetically accessible, purely organic receptors. These receptors are exemplified, among others, by crown-ethers[1], cryptands[2], cyclodextrins and calixarenes[3] whose preorganized cavities and non-covalent recognition units set the rules for selectivity and complementarity, which became a fundamental strategy for functional chemical systems.

The consequence is a shift in emphasis, from making molecules to programming interactions. Hydrogen bonding, electrostatics, π-π stacking, hydrophobic effects, halogen and chalcogen bonding and metal coordination, each non-covalent force reassembles a line of code in an intermolecular script. When these scripts are well written, they can produce astonishing nature-inspired properties, such as self-assembly[4,5a,5b,6,7,5c], molecular recognition[8,9], energy conversion[10,11], signal transduction[12,13] and adaptive reconfiguration.[14,15]

The world of metal-organic coordination cages (MOCs) provides a striking example as interdisciplinary script of science, written and extended by numerous developers.[16a,17,16b,16c,15,18,16d–k,19,16l–u,20–22] This work will introduce the world of cages from my personal experience, keeping it aligned with my own research while also adding further aspects to provide a broad overview of the sheer number of publications and reviews, including strategies for self-assembly, host-guest chemistry, and applications of MOCs.

In general, MOCs are formed by organic ligands coordinating to cationic metal centers or, sometimes, small metal clusters, to generate supramolecular architectures that reassemble cages.[19] These assemblies are often highly charged and create confined microenvironments within the bulk phase, defined by the specific functionalities within their cavities. The host-guest chemistry of MOCs presents a vast and versatile variety with profound implications for both fundamental and applied sciences.

The first reported metal-organic coordination cage in literature was discovered by SAALFRANK and co-workers in 1988, who presented the self-assembly of a $[Mg_4L_6]^{4-}$ tetrahedron upon mixing diethyl malonate, oxalyl chloride and methylmagnesium iodide (Figure 1.1, a).[4] With this discovery, the seed was not only planted; it already sprouted, ready to grow its branches into the vast expanse of science.[20–22] In 1995 FUJITA and co-workers presented a MOC based on *cis*-protected square-planar Pd(II) metal centers, coordinated by tripodal ligands based on a 1,3,5-triazine backbone equipped with pyridine coordination units (Figure 1.1, b).[7] The vertices of the self-assembled octahedral $[Pd_6L_4]^{12+}$ cage are capped by ethane-1,2-diamine ligands. The cavity of the $[Pd_6L_4]^{12+}$ octahedron is hydrophobic and electrophilic, thus it encapsulates a variety of neutral electron-rich aromatic and aliphatic molecules. Offering properties quite different from those of the bulk phase.[8]

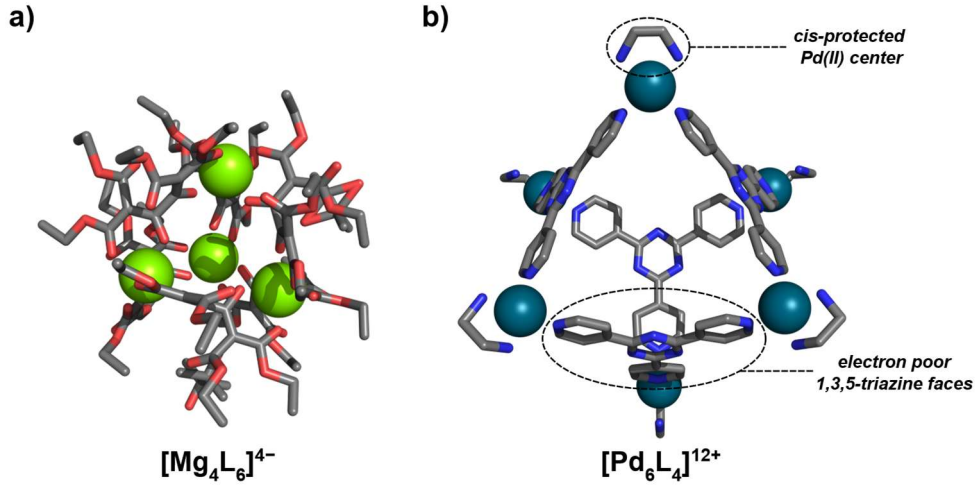

Figure 1.1: a) The first metal-organic coordination cage reported in literature was described by SAALFRANK et al.: a tetrahedral $[Mg_4L_6]^{4-}$ cage, in which the Mg(II) cations are bridged by malonate-derived ligands. b) The $[Pd_6L_4]^{12+}$ octahedral cage described by FUJITA, featuring its electron poor 1,3,5-triazine backbone, covering half of the surfaces of the octahedron. Hydrogen-atoms are omitted (C: grey, N: blue, O: red, Mg(II): green, Pd(II): dark turquoise).

Only a few years after FUJITA's discovery, RAYMOND and co-workers employed a strategy for the rational design and self-assembly of MOCs in 1998.[6] They demonstrated that geometric analysis can be employed in the rational design of templated self-assemblies of homochiral $[M_4L_6]^{12-}$ tetrahedral MOCs. They developed the self-assembly using C_2-symmetric bis(bidentate) catecholamide ligands.[23,6,24] The reaction of three equivalents of the ligand with two equivalents of $[M(acac)_3]$ (M = Ga(III), Al(III), Fe(III)) self-assembled into a triple-stranded helicate (Figure 1.2).[23,24] To avoid the formation of a $[M_2L_3]^{6-}$ helicate and to favor the formation of a tetrahedral $[M_4L_6]^{12-}$ assembly, the 1,4-substituted phenyl backbone was changed to a 1,5-substituted naphthalene backbone, causing the two catechol coordination units to be offset from one another. The tetrahedral $[M_4L_6]^{12-}$ is obtained from $[M(acac)_3]$ (M = Ga(III), Fe(III)) salts in combination with the new ligand, KOH and Et_4NCl. The crystal-structure of the tetrahedron proved that one of the NEt_4^+ counter-ions was located inside the cavity, highlighting the importance of the counter-ion for the self-assembly process. They also demonstrated that the templated guest could be exchanged for other alkylammonium derivates, depending on the binding affinities.[6]

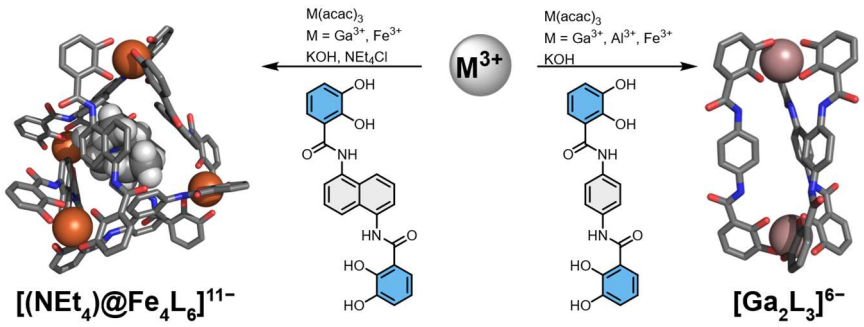

Figure 1.2: Left: Crystal structure of RAYMOND's rationally designed $[Fe_4L_6]^{12-}$ tetrahedron with encapsulated NEt_4^+. Right: Crystal structure of RAYMOND's triple stranded helicate $[Ga_2L_3]^{6-}$.

Another pioneering strategy for the self-assembly of MOCs was published by the same group in 1999. RAYMOND and co-workers demonstrated that identical ligands and metals can assembly into either a supramolecular triple helicate or a tetrahedron (Figure 1.3).[25] Adding NMe^{4+} converts the helicate quantitatively into the tetrahedron. Thus, beyond tuning ligand geometry[6], host-guest interactions offer systematic lines of code for the rational design and synthesis of supramolecular architectures. Remarkably, this type of guest-induced synthesis not only leads to a more favorable energetic state but to cage topologies otherwise inaccessible that express greater complexity and functions not available before transformation.[26,25]

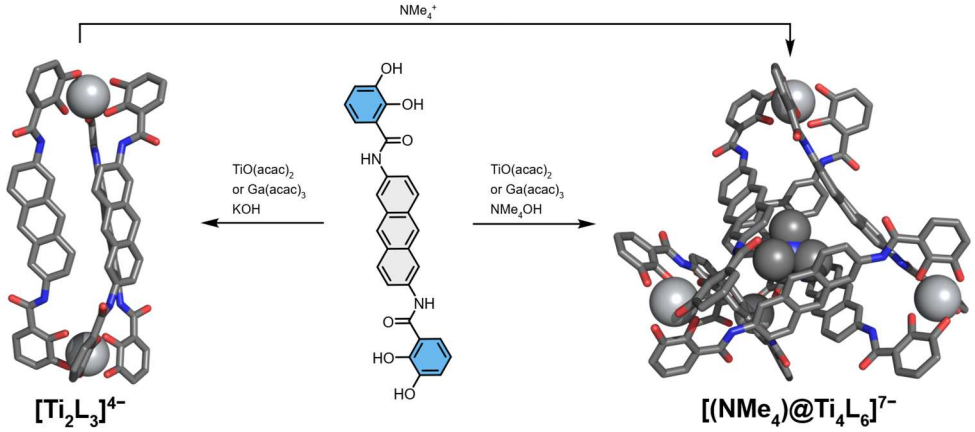

Figure 1.3: Crystal structure of the $[Ti_2L_3]^{4-}$ triple stranded helicate and the NMe_4^+ templated $[Ti_4L_6]^{8-}$ tetrahedron. It is possible to induce a helicate to cage transform by adding the template NMe_4^+ into the helicate.

RAYMOND and co-workers extended their symmetry-based design to the self-assembly of charged $[M_4L_4]$ tetrahedral cages (M = Ga(III), Al(III), In(III), Ti(IV)) by tris-bidentate symmetric ligands which coordinate four pseudo-octahedral metal-centers.[27] Tripodal-ligand designs offer many opportunities to alter functionalities of the self-assembled structures and enables charge-, size- and shape-selective guest encapsulation.[27,28,29] A follow up study was done by the group of RAYMOND and TOSTE, on how tuning the conformational landscape of the $[M_4L_4]^{12-}$ tetrahedral cages (M = Ga(III), Al(III), In(III)) controls guest binding and supramolecular catalysis. Using a $[Ga_4L_4]^{12-}$ cage that interconverts between S_4, C_3 and T conformers via Bailar twists as a model.[30] They showed systematic stabilization of specific high-energy conformers by installing distal chiral amides to lock the high-energy T state, by swapping Ga(III) for Al(III) of the larger In(III) to alter S_4/T thermodynamics and using a symmetry-matched tube-shaped guest ($CoCp^*_2{}^+$) to trap the transient C_3-symmetric conformer. Investigated with a van't Hoff-plot and ion-mobility measurements that map the ethalpic/entropic contributions of each state. They showed that in the dynamic Ga(III)-tetrahedra the $S_4 \rightarrow T$ conformational change is rate-limiting and suppresses catalysis of an aza-PRINS reactions. Whereas "locking" the active T conformer resorts strong

catalytic activity. The group proves, that effective supramolecular cage catalysis must have conformational exchange faster than the chemical step.[30]

Another recent design-approach to increase stability and functional tuneability of MOCs is the double-bridged Zn(II) MOC series, introduced by NITSCHKE and co-workers (Figure 1.4).[31] The dynamic covalent chemistry approach uses various subcomponents, which enforce a vertex geometry that orients aniline residues toward the cage faces, enabling dianiline-based cross-linking of edges to form rectangular tetratopic ligands within pseudo-cubic $[Zn_8L_6]^{16+}$ architectures. This double-bridging increases ligand denticity from bis-bidentate to tetra-bidentate without altering the overall cage size, but it changes the symmetry from chiral *O* (all-*Δ* or all-*Λ* in the single bridged $[Zn_8L_{12}]^{16+}$ cube) to achiral T_h in the double bridged cages, enforcing an alternating *Δ*/*Λ* arrangement of metal centers and yielding more rigid frameworks. Quantum-chemical calculations showed that the double-bridged cage is thermodynamically favored over the mono-bridged cube, with an entropic term that overcomes an enthalpic preference for the mono-bridged cage. Molecular dynamics simulations confirm that the double-bridged cage is significantly more ridged. Experimentally, double-bridged cages display markedly enhanced robustness towards high equivalents of competing ligands (aniline, DMSO and triflate) and show higher thermal stability, under conditions where the single-bridges cage undergoes rapid decomposition. Demonstrating that double-bridging as a general strategy to increase stability and functional tunability in MOCs.[31]

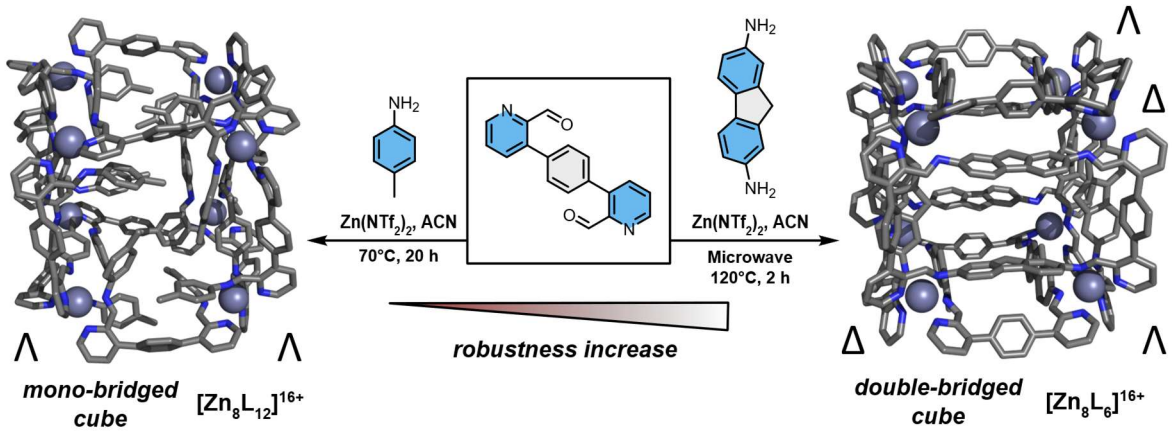

Figure 1.4: Crystal-structures of the self-assembly of mono- and double-bridged Zn(II) cages based on a dipicolinaldehyde-derivate. Left path: Subcomponent self-assembly with the dipicolinaldehyde-derivate, p-toluidine, and $Zn(NTf_2)_2$ gives the O-symmetric $[Zn_8L_{12}]^{16+}$ mono-bridged cube. Both cage enantiomers were present in the crystal. Right path: Self-assembly of the dipicolinaldehyde-derivate, 2,7-diaminoluorene, and $Zn(NTf_2)_2$ gives achiral double-bridged $[Zn_8L_6]^{16+}$ cube. The double-bridged cube was also formed through reaction of the mono-bridged cube with 2,7-diaminofluorene.

Another more ambitious approach to alter the properties of MOCs is the post-assembly modification.[32,17] In a recent report, MUKHERJEE and co-workers presented an elegant strategy to induce a post-assembly sulfoxidation of a phenothiazine-functionalized $[Pd_6L_3]^{12+}$ tube-like MOC, which enhances the MOC's ability to generate reactive oxygen species (ROS) under visible light without disrupting its overall architecture. Encapsulation of C_{70} within the tube and the oxidized-tube further boosts ROS formation by harnessing the fullerene's photosensitizing properties in acetonitrile, in which free C_{70} is otherwise poorly soluble. The combination of both post-assembly modification and C_{70} encapsulation in the oxidized-tube leads to a cooperative, substrate-independent acceleration of terpene oxidations, enabling near-quantitative conversions at catalytic loading and short irradiation times.[33]

Implementing multiple functionalities in the form of distinguishable building blocks within one discrete MOC architecture is difficult without risking a statistical mess.[18] CLEVER and co-workers could elegantly demonstrate a systematic series of interactively self-assembled heteroleptic $[Pd_2L_4]^{4+}$ lantern-shaped cages in which two square-planar Pd(II) metal-centers are coordinated by four distinct bis-pyridyl

ligands (L_A, L_B, L_C and L_D), due to cooperative effects. Exclusively forming a single low-symmetry $[Pd_2L_4]^{4+}$ cage-isomer with four different ligands under thermodynamic control, accessible through multiple different pathways.[18,34]

1.1 Host guest chemistry of charged MOCs

The self-assembly of a discrete MOC is the first step of exploring the non-covalent interactions offered by the implemented molecular functionalities of the cage's cavities and ligands. The host-guest chemistry of MOCs offers opportunities to selectively encapsulate molecules, enabling highly specific molecular recognition and separation.[35] Inside their confined cavities, MOCs can act as nanovessel, altering reaction pathways and rates by stabilizing transitions states or reactive species.[36a,36b,37,36c] MOCs are also explored as delivery systems, in which encapsulation controls solubility, protection, and release of drugs or catalysts.[38] Additionally, guest binding can change optical, redox or magnetic properties of the MOC, making them useful for sensing or signal amplification.[39]

The group of RAYMOND pioneered in the encapsulation and stabilization of different cationic molecules within the cavity of their highly negative charged tetrahedral MOC. Among others, they demonstrated the encapsulation of iminium-salts in aqueous solution[40], diazonium cations[41] and ruthenium organometallic species[37]. In this respect, further great examples for the encapsulation of reactive molecules by MOCs are presented by the groups of NITSCHKE[42], YOSHIZAWA[43] and CLEVER[44] (Figure 1.5). Each MOC enables the encapsulation of reactive species inside of the respective cavity, shielding the molecules from the bulk phase and altering their reactivity.

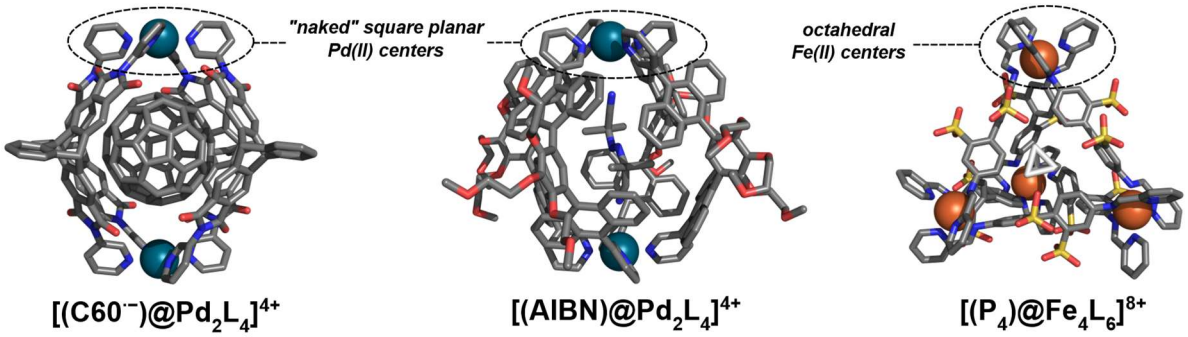

Figure 1.5: Crystal structures of host-guest systems, which stabilize the reactive guest-molecules in the bulk phase. Left: CLEVER's $[Pd_2L_4]^{4+}$ lantern-shaped cage, encapsulating and stabilizing a photochemically generated C60 radical. Middle: YOSHIZAWA's $[Pd_2L_4]^{4+}$ lantern-shaped cage, encapsulating and stabilizing AIBN and derivatives toward light irradiation. Right: NITSCHKE's $[Fe_4L_6]^{8+}$ tetrahedral cage, encapsulating and stabilizing white phosphorous toward air.

A recent report by BAILEY and co-workers demonstrated that MOCs can encapsulate and stabilize synthetic iron-sulfur clusters. Iron-sulfur clusters are particularly important for bioinspired synthesis, due to their ability to promote catalytic reactions. However, due to their instability they are challenging to handle outside of protein scaffolds. The group presented encapsulation of the reactive bioinorganic iron-sulfur cluster in tetrahedral $[M_4L_6]^{8+}$ (M = Fe(II), Ni(II), Zn(II)) MOCs, based on naphthalenediimide-containing ligand and 2-formylpyridine. The encapsulation is driven by electrostatics and dispersion interactions between the faces of the ligand and the guest cluster, which is stabilized against thermal decomposition by the MOC. They showed that 44% of iron-sulfur clusters remained stable after 17 days of encapsulation, but only 28% cluster remained stable in the non-encapsulated control.[45]

Another extraordinary example for how confinement modulates the properties of guest molecules is described by KLAJN and co-workers, using MUKHERJEE'S barrel-shaped cage.[10,46–50] They examined spiropyran[48], dihydropyrene and especially azobenzenes[46,50,49], showing that two trans-azobenzenes can co-encapsulate and, upon irradiation, one is expelled, leaving a single *cis*-isomer within the cavity.[50] They also formed a kinetically controlled ternary complex where anthracene and BODIPY co-occupy the cage, restoring BODIPY emission.[51] Building on these findings, they introduced

"disequilibration by sensitization under confinement" (DESC).[10] In DESC, azobenzene derivatives are co-encapsulated with sensitizer dyes (BODIPY or resorufin). The sensitizer absorbs a photon, undergoes intersystem crossing, and transfers triplet energy to the azobenzene (TET), promoting isomerization; the resulting steric crowding expels the isomerized guest from the cavity. This confined sensitization strategy increases azobenzene switching yields up to 98% at long wavelengths that are typically ineffective. Hence, dear Sir or Madam, this is an appropriate moment to give a shoutout to the 2016 Nobel Prize in chemistry laureates JEAN-PIERRE SAUVAGE, FRASER STODDART and BERNARD FERINGA for their pioneering work on the design and development of molecular machines, as the lines of code in the intermolecular script in the system described by KLAIJN enables it to operate as a light-driven molecular machine that converts light into chemical energy.[52]

1.1.1 Guest -induced self-assembly, exchange and transformations of metal-organic cages

The combination of organic ligands with metal cations does not always yield a discrete MOC, or it produces an undesired mixture of products, due to the dynamic nature of their metal-ligand bonds. Consequently, MOCs can transform between geometrically distinct structures assembled from the same set of components, giving MOCs an additional degree of freedom.[53] Guest-induced structural transformations and guest-templated self-assemblies therefore offer opportunities to alter both their structure and their functions.[54,53] In other words, an incoming guest can act as a stimulus that transforms an assembly into a new discrete MOC, effectively allowing the guest to "shape its own complementary host" in an "induced-fit" mechanism reminiscent of certain biological receptors.[55] Molecular inputs can lower the energetic barriers for interconversion and often template cages with new metal-ligand compositions (Figure 1.6).[56]

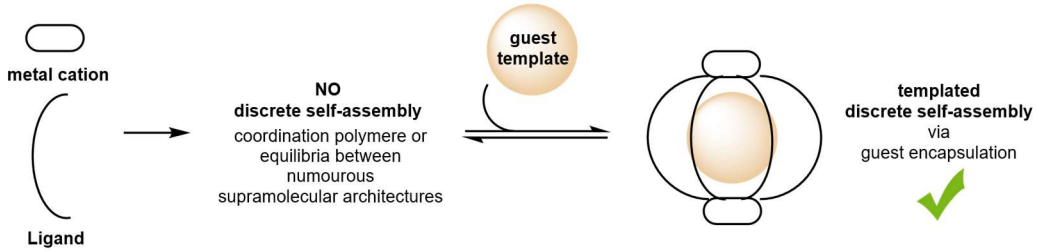

Figure 1.6: Abstract hypothetic case of a successful guest-templated self-assembly of a $[Pd_2L_4]^{4+}$ lantern-shaped cage.

The template effect highlights that preorganization and thermodynamic stabilization for the self-assembly of MOCs can be provided by well-defined noncovalent interactions between the ligands and the guest. In solution, nevertheless, formation of a single supramolecular entity from a host and a guest faces an entropic challenge. The process of guest binding must therefore establish specific and cooperative interactions that result in a favorable binding enthalpy, so that the entropic loss is compensated and the host-guest complex is stabilized.[57] However, encapsulation of a guest can be entropically favorable, as the release of solvent molecules from the MOCs cavity necessitates a reorganization of the solvent molecules in the bulk phase.[58] Nevertheless, guest uptake of an empty cage or guest-exchange processes must overcome energetic barriers, which can occur either via partial or full disassembly-reassembly, or via a slippage mechanism in which bonds rearrange without breaking and reforming.[59,58,60,61] CRAM, who reported binding processes for various large molecular guests in hemicarceplexes in 1991, introduced the term *constrictive binding*.[59] For a *constrictive guest release process*, the constrictive binding energy $\Delta G^{\ddagger}_{constrictive}$ describes the free energy which must be provided to the system to reach the transition-state for guest dissociation from the encapsulated state minus the free energy associated with binding.[59]

Equation 1

$$\Delta G^{\ddagger}_{constrictive} = \Delta G^{\ddagger}_{diss} - (-\Delta G^{0}_{a})$$

The standard free energy of binding ΔG^{0}_{a} for a simple 1:1 host-guest complex is:

Equation 2

$$H + G \rightleftharpoons HG$$

Equation 3

$$\Delta G^{0}_{a} = -RTlnK_a$$

Favorable binding processes give negative values for ΔG^{0}_{a}. The activation free energy for dissociation $\Delta G^{\ddagger}_{diss}$ of the host-guest complex is the free energy difference between the host-guest complex and the transition state of dissociation (Figure 1.7). For most guest exchange processes, rates of

dissociation are dictated by the reorganization of the host molecule required to create an open side of sufficient size to the bulk phase.[62] However, the steric demand of large guests is a determining factor.[63] The group around CRAM demonstrated that it is possible to manipulate host-guest dynamics by altering the structure of the host open sides.[64] Nevertheless, hemicarceplexes are purely organic receptors, but the scripted concept of *constrictive binding* is common in other host-guest systems, also for MOCs.

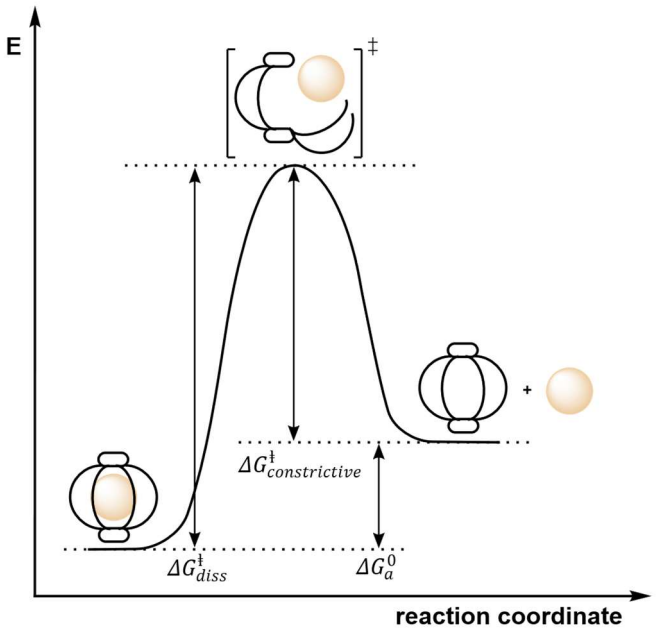

Figure 1.7: Energy diagram for a constrictive guest release process of a MOC.

RAUCHFUSS and co-workers, working with a charge-neutral $[\{CpCo(CN)_3\}_4(Cp^*Ru)_4]$ MOC and K^+ and Cs^+ as guests, found that the rate of guest-exchange depends on the size of the alkali-cations. The smaller K^+ cation was encapsulated fast (k = 300 M^{-1} s^{-1}), whereas exchange of the larger Cs^+ cation was markedly slower (k = 36 M^{-1} s^{-1}), consistent with a constrictive binding mechanism.[65]

In 2015 RAYMOND and co-workers reported that constrictive guest binding within their $[Ga_4L_6]^{12-}$ tetrahedron redirects an aza-PRINS cyclization of tethered amines toward an unusual pathway involving transannular 1,5-hydride transfer, in stark contrast to the hydration product formed in the bulk phase (Figure 1.8). Guest binding enforces a compact transition-state geometry that orients the nascent carbocation in close proximity to the more extended transition states that would lead to simple solvent capture. The nature of this transformation was probed by isotopic labeling studies and kinetic analysis, and the effect of nitrogen substitution was assessed. This pathway is uniquely available within the constrictive environment of a supramolecular nanovessel and is too high in energy to be observed in the bulk phase for this class of substrates.[66] RAYMOND's group, together with TOSTE, explored many reactions catalyzed by the $[M_4L_6]^{12-}$ and $[M_4L_4]^{12-}$ tetrahedra.[67,30]

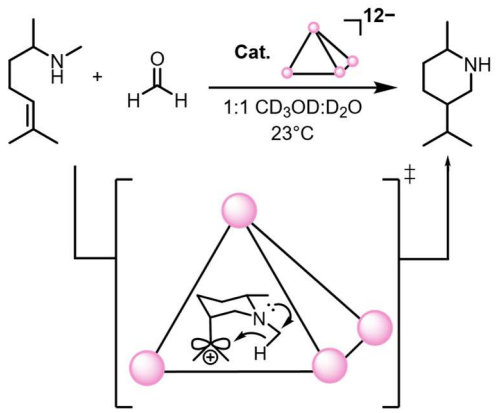

Figure 1.8: The tetrahedral $[Ga_4L_6]^{12-}$ cage catalyzes an aza-PRINS cyclization that feature a transannular 1,5-hydride transfer enabled by constrictive encapsulation.[66]

A classic example for a guest-exchange slippage mechanism that pushes the limits of nondissociative guest-exchange processes was presented by RAYMOND and co-workers.[58] The experiments are based on the host-guest behavior of the inclusion complexes of the $[Ga_4L_6]^{12-}$ tetrahedron.[6] The guest NEt_4^+ drives the self-assembly thermodynamically and becomes a constituent component of the assembly. Nevertheless, it is possible to exchange the guests within the void and keep the integrity of the cage. The process of guest-exchange is depending on the size of the individual guests. Cationic guests, such as NEt_4^+ PEt_4^+, NMe_4^+, $PMe_2Pr_2^+$ or NPr_4^+, are bound reversibly via a slippage mechanism, in which the faces of the $[Ga_4L_6]^{12-}$ tetrahedron are deforming and keep the coordinative bonds of ligands and metal intact. The negative $\Delta S^{\ddagger}$ values for guest self-exchange (NEt_4^+ PEt_4^+, $PMe_2Pr_2^+$ and NPr_4^+) suggest that bond rupture is not the active mechanism of guest exchange (Figure 1.9, A).[61] Bigger, sterically more demanding guests ($CoCp^*_2^+$) gave a drastic decrease of rate constants, presumably as a result of an energetically more demanding partial ligand-metal dissociation (Figure 1.9, B).[58] The guest exchange kinetics for the analogous $[Ti_4L_6]^{8-}$ and $[Ge_4L_6]^{8-}$ tetrahedrons produced almost identical rates of exchange, suggesting that guest exchange is not dependent on the nature of the metal-ligand interactions of the host.[60]

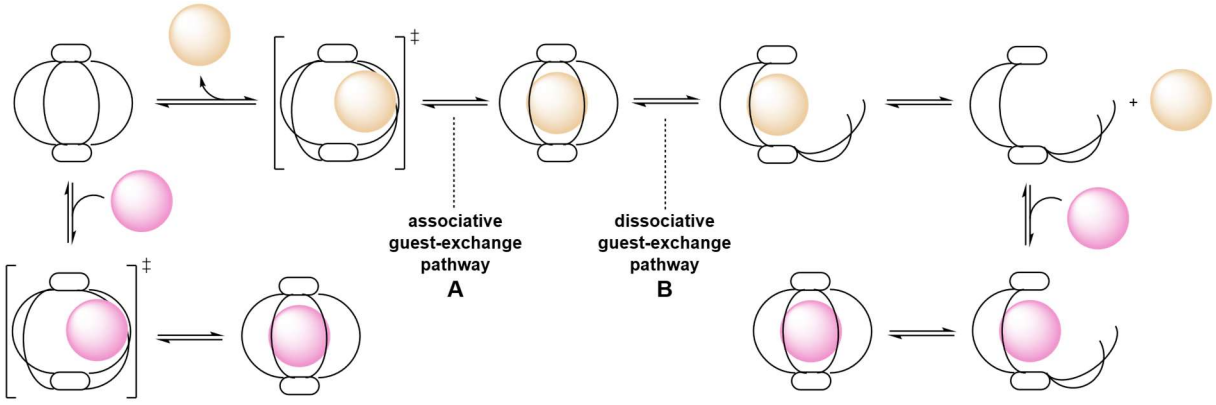

Figure 1.9: Two possible guest-exchange mechanisms for MOCs. Pathway A illustrates the associative mechanism, where expansion of the open sides would allow guest-exchange. Pathway B describes partial disassembly and reassembly in the constrictive guest-exchange process.[60]

To demonstrate a MOC with conformationally switchable faces for dynamically adaptive guest encapsulation, the recently reported pseudo-cubic $[Zn_8L_6]^{16+}$ MOC by NITSCHKE and co-workers has 2,6-naphthalene-based faces that can switch between endo and exo conformations, allowing dynamic modulation of the cage's cavity.[68] Host-guest studies showed that the pseudo-cubic cage forms 1:1 inclusion complexes with a number of molecules. These guests had sphericity-corrected volumes from 178 Å^3 (adamantane) to 599 Å^3 (tetrakis(4-chlorophenyl)borate), corresponding to 46-154% of the empty-cage cavity volume. Larger guests induced discrete, quantized expansion of the host's faces via

flipping of ligand panels from endo to exo, as evidenced by NMR spectroscopy (NOESY and DOSY) and ion-mobility mass spectrometry. Computational modelling showed that endo and exo faces are nearly isoenergetic and connected by a low-barrier pathway, supporting the existence of ten conformational states that map onto seven accessible cavity volumes, illustrating a general strategy for intrinsically adaptive metal-organic cages.[15]

In designing highly charged metal-organic cages for host-guest chemistry, electrostatic interactions inevitably play a central and often dominant role, exemplified by the dimerization process of $[Pd_2L_4]^{4+}$ lantern-shaped MOCs (Figure 1.10).[69] The formation of Pd(II)-based MOC interlocked structures, enabled by the lability of the metal-ligand bonds, allows initially monomeric cages to transform into more complex interlocked species once thermodynamic key criteria are fulfilled.[70,71] The group around CLEVER showed that the dimerization and guest selectivity of interpenetrated Pd(II) MOCs can be switched by the presence of anionic templates and ligand sterics. Dibenzosuberone-based ligands together with Pd(II) centers form a tetrafluoroborate templated interpenetrated cage $[BF_4@Pd_4L_8]^{7+}$, in which the central tetrafluoroborate anion enforces a compact inner cavity and small outer pockets that bind halides with high affinity (Figure 1.10, a). In the sterically bulkier ligands, tetrafluoroborate can no longer template the interpenetration, which causes the formation of a monomeric cage. However, smaller template anions, such as chloride, induce dimerization with chloride occupying the inner cavity (Figure 1.10, b). The occupation by the relatively small chloride shrinks the central cavity and enlarges the outer cavities, thereby inverting the binding preference of the outer cavities to larger anions such as ReO_4^-.[71]

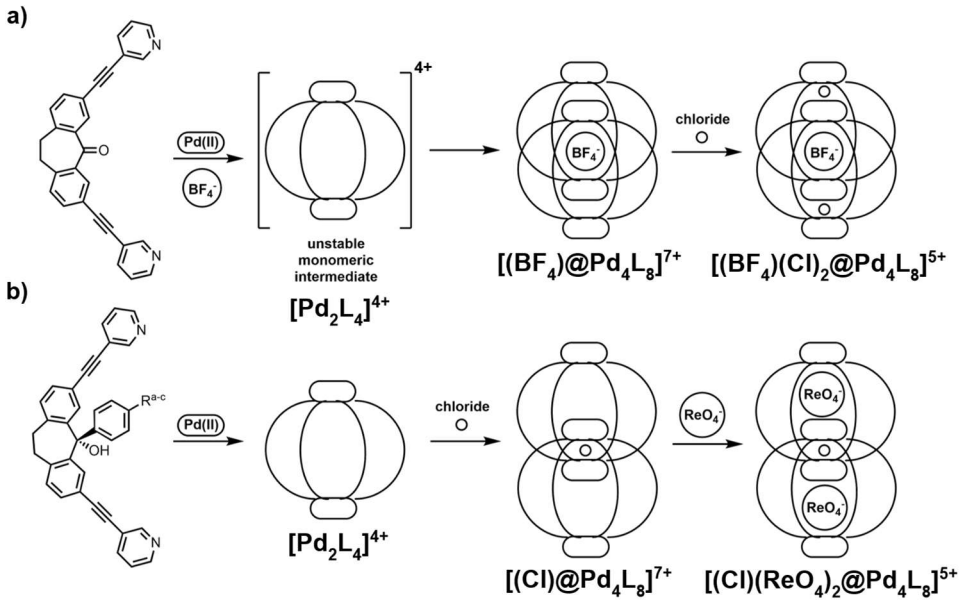

Figure 1.10: a) Upon addition of $[Pd(CH_3CN]_4](BF_4)_2$, the ligand self-assembles into an unstable monomeric lantern-shaped cage. Over time tetrafluoroborate templates the formation of the interpenetrated double cage, which is capable of binding chloride in the outer cavities. b) The bulky backbone ($R^a = CF_3$, $R^b = OCH_3$, $R^c = CH_3$) of the ligands prevent a double-cage formation with tetrafluoroborate, thus a stable monomeric $[Pd_2L_4]^{4+}$ lantern-shaped cage is formed. The addition of 0.5 equiv. of chloride induces the formation of the interpenetrated double cage. The two large outer cavities are capable of binding each one perrhenate anion.

In a similar double-cage host-guest system, the group around CLEVER demonstrated that the inner cavities can encapsulate neutral guest molecules after activation by a chemical signal. The addition of halide anions triggers a mechanical process, a compression of the double-cage along the Pd_4-axis, which preorganizes the central cavity for the subsequent inclusion of the neutral guest molecule. On the other hand, the neutral guest kinetically stabilizes the halide anions in the outer cavities.[13]

The design strategy of using tripodal ligands can, as well as bis-bidentate ligands, lead to the formation of complicated knotted cage frameworks, depending on their constitutional features. NITSCHKE and co-workers combined rigid tritopic formyl pyridines and tris(anilines) with Zn(II) coordination to access covalently linked trefoil perplaxane and trefoil tetrahedral knotted MOCs. By tuning subcomponent rigidity and steric bulk, the group achieved a rare bidirectional interconversion between an interwoven trefoil perplaxane and a non-interwoven $[Zn_4L_4]^{8+}$ tetrahedron, coupled to switchable encapsulation and release of anionic and neutral guest molecules. They further showed that introduction of flexible crosslinkers gives a template-free assembly of a trefoil tetrahedron, while crosslinking can kinetically lock ligand conformations, suppress adaptive face inversion and thus shut down guest binding. This study shows how ligand rigidity and flexibility together with subcomponent addition can control thermodynamics and kinetics in MOCs, allowing modulation of structural transformations and host-guest behavior.[29]

Another great example involving neutral hydrocarbons as guest molecules is a macrocycle reported by SUN and co-workers, which reassembles a combination of STODDART's blue box[72] and the 1,3,5-triazine backbone used by FUJITA[7], that can self-assemble with tetramethylethan-1,2-diamine (tmen) *cis*-capped Pd(II) centers into two interconverting MOCs (Figure 1.11). The ratio between the $[Pd_2L_2]^{12+}$ cage and $[Pd_1L_1]^{6+}$ structure can be tuned by solvent, temperature and concentration. The addition of flat polycyclic aromatic hydrocarbons induces the formation of the $[(guest)@Pd_1L_1]^{6+}$ host-guest complex, due to π-π stacking interactions of the electron deficient backbone and the guests. Whereas a large anionic guest induces the formation of a $[(guest)@Pd_2L_2]^{8+}$ host-guest complex. In the crystal structure of $W_{10}O_{32}^{4-}$ inside $[Pd_2L_2]^{12+}$, the decatungstate anion is in the middle of the cavity, due to electrostatic interaction and strong anion-π interactions, as well as multiple [C-H···O=W] interactions.[53]

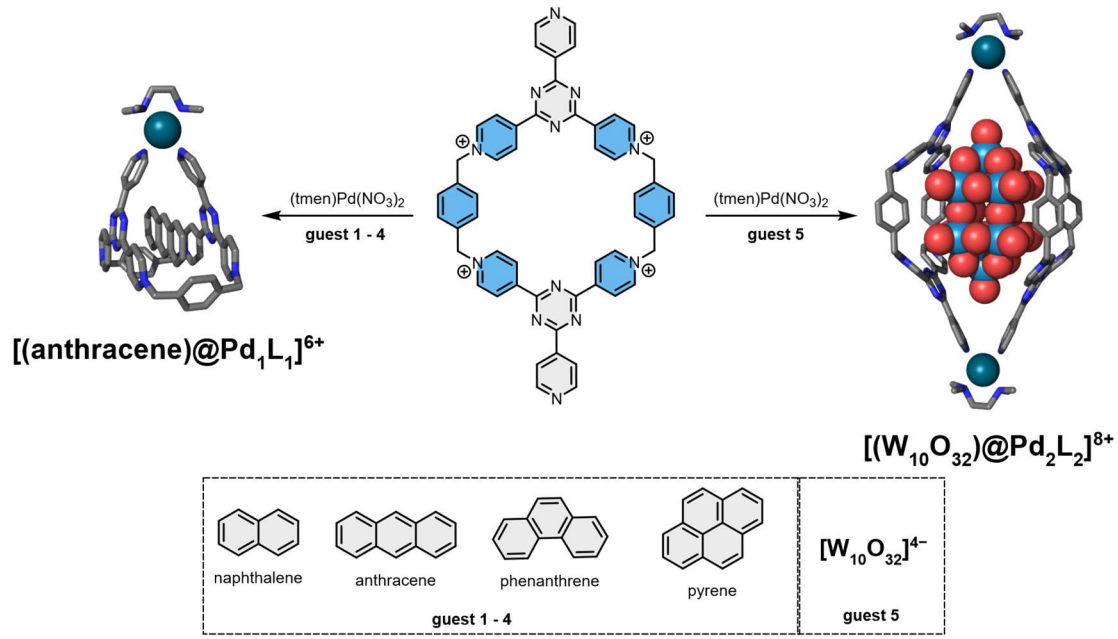

Figure 1.11: Controlled self-assembly of a $[Pd_1L_1]^{6+}$ or $[Pd_2L_2]^{12+}$ structural assembly via induced-fit binding of a guest.

A more recent example by the group of CLEVER for a guest induced transformation of a MOC was published in 2023 (Figure 1.12). The group demonstrated a self-assembled azulene-derived lantern-shaped $[Pd_2L_4]^{4+}$ cage undergoing a templated transformation with benzene-1,4-disulfonate into a tetrahedral shaped [(benzene-1,4-disulfonate)$_2$@$Pd_4L_8]^{4+}$ host-guest complex.[54] Remarkably, the guests can be released by the uptake of another MOC with higher affinity for the guest molecules[73], transforming the tetrahedral 2:2 host-guest complex back to the lantern-shaped $[Pd_2L_4]^{4+}$ cage.[54]

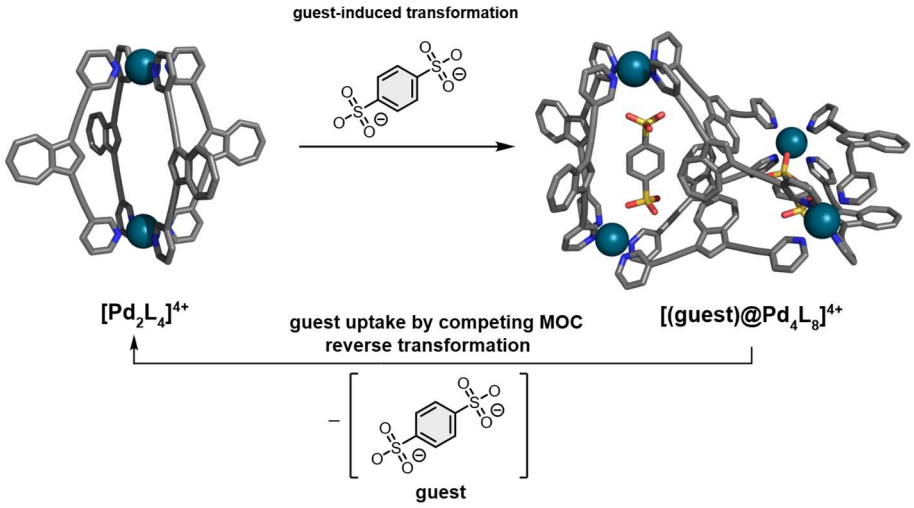

Figure 1.12: $[Pd_2L_4]^{4+}$ lantern-shaped MOC, which transforms into a tetrahedral shaped [(benzene-1,4-disulfonate)$_2$@$Pd_4L_8]^{4+}$ host-guest complex induced by benzene-1,4-disulfonate. Guest uptake by a competing MOC based on methylene blue[73] reverses the transformation to the lantern-shaped $[Pd_2L_4]^{4+}$ cage.[54]

A more dramatic scenario, in which the combination of organic ligands and metal cations does not lead to a self-assembly of a cage-like entity, was presented by the group of HIRAOKA in 2019. The group demonstrated that the self-assembly pathways can be controlled by template effects. In the absence of a suitable template, the system reaches a kinetically trapped state, which forms micrometer-sized sheets. However, in the presence of a tetrafluoroborate anion, the self-assembly of the ditopic ligands and Pd(II) afford a metastable MOC with encapsulated tetrafluoroborate, whose self-assembly was significantly accelerated by the kinetic template effect. Notably, the template anion not only converts the micrometer-sheets into host-guest-species, but also alter the self-assembly pathway itself from the beginning by the kinetic template effect on the early stages of the self-assembly.[74]

The biggest strength of MOCs, whether they are charged or charge-neutral, is their metal-driven self-assembly. Unfortunately, the dynamic metal-ligand bonds can also be their Achilles' heel. MOCs can easily disassemble by the addition of competitive coordinating or chelating anions, resulting in the decomposition or the formation of undesired products or mixtures.[75,76] Especially oxalate, the shortest dicarboxylate, as it forms strong chelate-complexes with all sorts of metal-cations.[77,78] On the other hand, this disadvantage of MOCs can be exploited as an opportunity to induce a function by using a chemical stimulus. Exemplified by the design and self-assembly of an anthracene-functionalized $[Pd_2L_4]^{4+}$ MOC based on a triphenylamine-derived ligand reported by XU and co-workers in 2023 (Figure 1.13). Due to the heavy-atom effect of Pd(II), the fluorescence of the anthracene bearing MOC is quenched. However, solubilized in DMSO and in the presence of competitive guest molecules like hydroxy, phosphate or acetate anions, the MOC is disassembled into free ligands and the respective Pd(II)-salts. Consequently, the fluorescence of the anthracene-derived ligand is enhanced, as evidenced by fluorescence titration studies. This anion-induced disassembly process enables the MOC to function as a stimuli-responsive fluorescent system.[75]

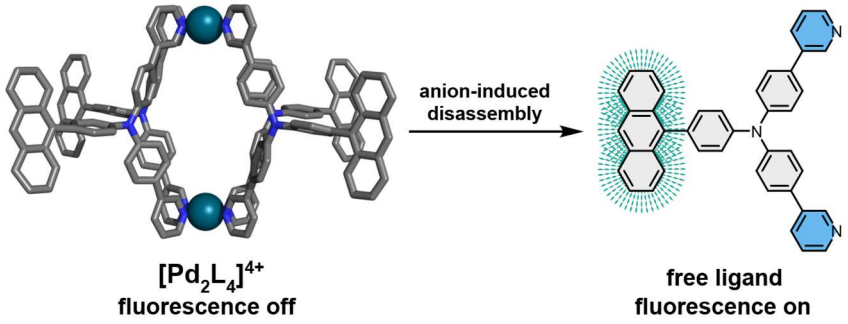

Figure 1.13: $[Pd_2L_4]^{4+}$ lantern-shaped MOC, which disassembles in solution upon addition of a hydroxy, phosphate or acetate anions. Consequently, the heavy-atom effect no longer interferes with the ligand fluorescence properties.

1.1.2 Charge-neutral MOCs and anion recognition

Binding guest molecules to a self-assembled MOC, which induces a transformation or a guest-exchange process is a lovely observation for a supramolecular chemist. However, to quantitively analyze a guest binding event, the overall integrity of the host MOC should ideally be consistent. The MOCs discussed so far are highly charged supramolecular entities. Given the focus on anion recognition, it is not surprising that both these entities are interacting with each other. In addition to that, there is the risk, that the counter-ions of the self-assembled MOC may interfere with the desired guest binding event, thus resulting in lower binding constants.[79] In this respect, MOCs with interfering counter-ions do not represent classical 1:1 host-guest systems, rather than equilibria between thermodynamically preferred host-guest systems and the counter-ions (Equation 1).

Equation 1

$$HG^1 + G^2 \rightleftarrows HG^2 + G^1$$

Two approaches can be used to mitigate this issue. One option is substitute competitive counter-ions with more frustrated anions like tetrakis[3,5-bis/trifluoromethyl)phenyl]borate[79], or to avoid any interfering ion-ion interactions between host and guest, fully charge-neutral, yet metal-driven self-assembled discrete ion receptors may help to overcome this issue.[76] Conceptually, the metal-driven design approach combines features of both, charge-neutral organic receptors and metal-driven self-assemblies. Furthermore, a charge-neutral MOC would benefit from the preorganization provided by its self-assembled topology, while avoiding competing counter-anions in its periphery.[76] Preferably, the synthesis of a MOC and its ligands should not suffer from a time-demanding synthesis with a challenging assembly of the final receptor, contrary to a lot of organic cages. The assembly of purely organic cages often depends on macrocyclization reactions or organic cage formations, which can

represent a significant bottleneck, for example due to low yields and sophisticated isolation processes.[80a,81,80b,80c] The cryptand-like, organic cage reported by FLOOD and co-workers in 2019 is a prominent example. A copper(I)-catalyzed alkyne-azide cycloaddition between a 2:3 stoichiometric mixture of tripropargylamine and a bisazide building block afforded the tripodal organic cage in 15% isolated yield. Nevertheless, the resulting rigid assembly incorporates six triazole units that act as classic C-H···anion recognition units, all oriented toward the internal cavity. Consequently, the purely organic cage binds chloride with exceptionally high binding constants.[81]

One design approach for charge-neutral MOCs, which is a *central part* of this thesis, is presented by VAN CRAEN and co-workers. The MOC is a charge-neutral $[Zn_2L_2]$ container with open sides. The bis-bidentate ligands consist of hydroxyquinoline coordination units that are linked with the phenyl backbone by a click reaction. The metal-precursor for the self-assembly of the $[Zn_2L_2]$ container is $Zn(OAc)_2$. Prior to self-assembly, the hydroxy groups of the ligands are deprotonated. This deprotonation is facilitated by the corresponding base acetate of the metal precursor, resulting in the formation of acetic acid as byproduct. The bis-bidentate ligands then self-assemble with Zn(II) into the $[Zn_2L_2]$ container, with the hydroxyquinolate units coordinating both Zn(II) centers probably in a tetragonal fashion and compensating the positive charges. Isolation of the bench-stable $[Zn_2L_2]$ container as a yellow powder is achieved by lyophilization, which removes both the solvent DMSO and the acetic acid byproduct, yielding a counter-anion free, charge-neutral $[Zn_2L_2]$ MOC that acts as a receptor for anions. The charge-neutral $[Zn_2L_2]$ container binds aliphatic and aromatic dicarboxylate of varying length in DMSO. The dicarboxylates coordinate to the LEWIS-acidic Zn(II) centers, creating a trigonal-bipyramidal coordination sphere around each Zn(II) center. The resulting 1:1 host-guest complexes, exemplified by the crystal structure of $[(NP)@L_2Zn_2]^{2-}$ with naphthalene-2,6-dicarobylate (NP^{2-}), exhibit exceptionally high binding constants with log $K_{1:1}$ = 8.16 (Figure 1.14) and for terephthalate (TP^{2-}) log $K_{1:1}$ = 7.59. Systemic studies with aliphatic dicarboxylates reveal a pronounced size selectivity. Pimelate shows the highest binding constant with log K = 7.42, because the carboxylate-carboxylate distance closely matches the Zn(II)-Zn(II) distance of ≈ 8 Å defined by the container. Shorter or longer aliphatic dicarboxylates bind weaker, due to the containers limited degree of freedom to adapt its Zn(II)-Zn(II) distance. Nevertheless, all dicarboxylates show slow guest-exchange behavior. In contrast, monoanions such as chloride, acetate and benzoate bind significantly weaker and show fast exchange behavior. Each monoanion forms 1:2 host-guest complexes with log β_2 between 5.04 and 6.93. The binding behavior of monoanion highlights that the high-affinity recognition is primarily driven by size-matching dicarboxylate coordination between the two Zn(II) centers. Limitations of this system include the low solubility of the free host $[Zn_2L_2]$, and the inability of the metal-driven self-assembly to bind the shortest dicarboxylates malonate and oxalate. In particular, oxalate acts as competitive chelator that can disrupt the integrity of the MOCs by coordinating to the metal centers.[76]

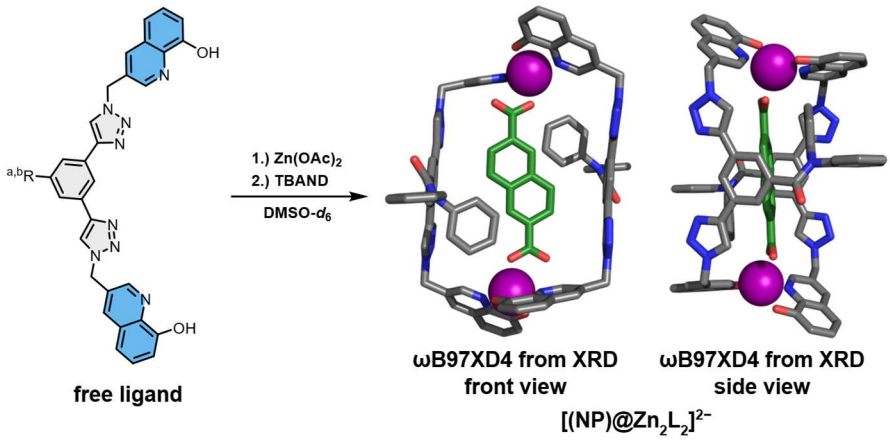

Figure 1.14: Self-assembly of the charge-neutral $[Zn_2L_2]$ container with the ligand (R^a = CON(Ph)$_2$, R^b = H) and $Zn(OAc)_2$ in a 1:1 ratio with subsequent guest binding of NP^{2-}. The structure of the host-guest complex $[(NP)@Zn_2L_2]^{2-}$ is represented by a calculated model from the X-ray diffraction data.

The group also demonstrated that the same charge-neutral [Zn_2L_2] container effectively acts as chiroptical receptor for mono- and dicarboxylate anions. The triazole-linker units of the ligand can adopt a *syn-syn* conformation, converting a meso-form into a racemic pair of *ΔΔ*- and *ΛΛ*-MOCs, with chiral guests inducing preferential enrichment of one enantiomer and giving rise to characteristic Cotton effects in the CD spectra. In particular, the host-guest complexes of *D*- and *L*-tartrate showed well-resolved CD signals.[82]

Comparable examples for dicarboxylate binding metal-organic cages are tris(2-pyridylmethyl)-based (TPMA) imine cages by ZONTA and co-workers, which form cationic bimetallic zinc complexes that bind dicarboxylates between both Zn(II) centers.[83,84,85] These supramolecular architectures are assembled by dynamic covalent chemistry, taking advantage of the preorganized aldehydic subcomponent and using diamines that can be varied to adjust the recognition properties of the final structures.[85,84] As a noteworthy curiosity: ZONTA and co-workers demonstrated that the lines of code of their Zn(II)-TPMA-based imine cage design approach can be executed directly in complex natural matrices, where naturally occurring components template the self-assembly. In other words, they were able to perform the self-assembly of their MOCs in DMSO-d_6 with a few drops of commercially available wines and fruit juices, using the naturally occurring dicarboxylic acids as templates.[86] This design approach exploits high selectivity combined with high stability, even in complex, competitive matrices.

Another, more historic, but comparable system, in which the guest molecules are clipped via LEWIS acid-base pairing interactions between two metal-centers within a preassembled MOC, was presented by the group of MAVERICK in 1984.[21,22] The group established a structurally defined, charge-neutral binuclear Cu(II) host-complex in which cavity dimensions and axial LEWIS-acidic coordination sites govern guest association and enable internal bridging by appropriately sized bidentate Lewis bases, such as pyrazine. In the following years, MAVERICK and co-workers further developed the design principles and extended their ligand library and substituted Cu(II) by different metal cations, e.g. Ni(II).[20]

2 Scope of the thesis

The projects presented in the following chapters are exploring a tiny part of the vast scientific space of metal organic cages. The work is aimed to investigate rational, ligand-based control of charge-neutral Zn(II) metal organic cages derived from hydroxyquinolate coordination units, with emphasis on anion/ion-pair recognition and guest-induced self-assembly pathways in competitive polar media. Among others, this work combines ligand synthesis, $Zn(OAc)_2$-driven self-assembly, solution-, solid- and gas-state characterization and computational modeling to relate structural modifications to host-guest formation.

The first chapter deals with the design and synthesis of ligands L^{mN3}-H_2, L^{N3}-H_2 and L^{crown3}-H_2 to expand the family of charge-neutral $[Zn_2L_2]$ complexes by either increasing π-surface to modulate solubility and aromatic dicarboxylate interactions, or by introducing crown-ether motifs to enable heteroditopic ion-pair recognition. The ligands are expected to self-assemble into charge-neutral $[Zn_2L_2]$ complexes, as they followed the design principles of the parent $[Zn_2L_2]$ complex. The resulting complexes $[Zn_2L^{mN3}{}_2]$, $[Zn_2L^{N3}{}_2]$ and $[Zn_2L^{crown3}{}_2]$ are characterized and screened in guest-recognition experiments, supported by 1D and 2D NMR, HRMS, and computational DFT calculations.

The second chapter presents the development of a flexible ligand L^{DB3}-H_2 to overcome the parent $[Zn_2L_2]$ complex limitations toward the discrete binding of short dicarboxylates and to resist oxalate-driven disassembly. Host-guest complex formation of $[Zn_2L^{DB3}{}_2]$ with several mono- and dicarboxylates is characterized by (VT)-NMR experiments, complemented by competition studies and 1D and 2D NMR-guided DFT/MD calculations to rationalize binding and integrity.

The third chapter introduces the synthesis and self-assembly pathways of a tripodal bis-bidentate ligand L^{TP3}-H_3. The ligand makes it possible to access higher nuclearity and more confined Zn(II)-based architectures with unexpected features. Because direct self-assembly with $Zn(OAc)_2$ yields ill-defined species, tricarboxylate templates are used to induce and control self-assembly of charged trinuclear $[Zn_3L_2]^{3-}$ and hexanuclear $[Zn_6L_4]^{3-}$ topologies. The obtained host-guest complexes are characterized and studied by competition experiments, as well as 1D and 2D NMR spectroscopy, X-ray diffraction analysis and HRMS.

3 Modifications of a charge-neutral Zn(II)-based metal organic cage

3.1 Introduction

The ligands L^{mN3}-H_2, L^{N3}-H_2 and L^{crown3}-H_2 were designed to expand the family of charge-neutral metal organic cages. Among other aspects, L^{mN3}-H_2, L^{N3}-H_2 and L^{crown3}-H_2 were intended to influence the solubility of the anticipated charge-neutral cages, thereby overcoming the solvent limitations of the previously reported $[Zn_2L_2]$ complexes by VAN CRAEN. The cages described by VAN CRAEN bind aromatic and aliphatic dicarboxylates with high binding constants. Suitable dicarboxylates must match the distance between the two Zn(II) centers in length to enable simultaneous coordination of both carboxylate groups. Upon guest binding, the Zn(II) centers increase their coordination number, forming a trigonal-bipyramidal coordination sphere.[76]

Expanding the π-surface of the solubility group may lead not only to improved solubility but also to higher binding-constants for the respective dicarboxylates. Ligand L^{mN3}-H_2 bears one naphthalene-substituent, and ligand L^{N3}-H_2 bears two naphthalene substituents, in place of the phenyl groups present in the parent cage. With a larger π-surface, the cavity may be stronger shielded from solvent molecules interacting with the guest anion. In the unpublished crystal structure of VAN CRAEN'S MOC as host-guest complex with naphthalene-2,6-dicarboxylate $[(NP)@Zn_2L_2]^{2-}$, the phenyl-substituents of the solubility group of the ligand's backbone interact via π-π interactions with the π-surface of the naphthalene guest.

Ligand L^{crown3}-H_2 was designed to self-assemble into a heteroditopic $[Zn_2L^{crown3}{}_2]$ species capable of binding ion pairs. The ligand backbone bears a 15-crown-5-ether, which readily forms host-guest complexes with sodium cations and thus functions as the cation recognition unit in the respective $[Zn_2L^{crown3}{}_2]$ species. As the self-assembled $[Zn_2L^{crown3}{}_2]$ bearded two crown-ether moieties, it was expected to form 2:2 host-guest complexes with ion pairs like NaCl.

3.2 Synthesis of ligands L^{mN3}-H_2, L^{N3}-H_2 and L^{crown3}-H_2

The synthesis of ligands L^{mN3}-H_2, L^{N3}-H_2 and L^{crown3}-H_2 all started from 3,5-dibromobenzoic acid (Figure 3.1). Full characterization and synthetic protocols are given in the experimental part associated with this chapter (chapter 3.7). The synthetic pathways for ligands L^{mN3}-H_2 and L^{N3}-H_2 were similar, starting with the synthesis of an acyl chloride a) and its subsequent amidation b) with naphthalene-2-amine and di(naphthalen-2-yl)amine, respectively. Followed by a SONOGASHIRA reaction c) with ethynyltrimethylsilane and basic deprotection of the TMS-groups d) gave the corresponding backbones of ligands L^{mN3}-H_2 and L^{N3}-H_2.

The synthetic pathway for the backbone of L^{crown3}-H_2 (Figure 3.1) started with the esterification e) of the carboxylic acid. Followed by a SONOGASHIRA reaction f) with ethynyltrimethylsilane and basic deprotection g) which gave 3,5-diethynylbenzoic acid. The final step in the synthesis of the L^{crown3}-H_2 backbone was the esterification h) of the carboxylic acid moiety with (1,4,7,10,13-pentaoxacyclopentadecan-2-yl)methanol, a 15-crown-5-ether derivative.

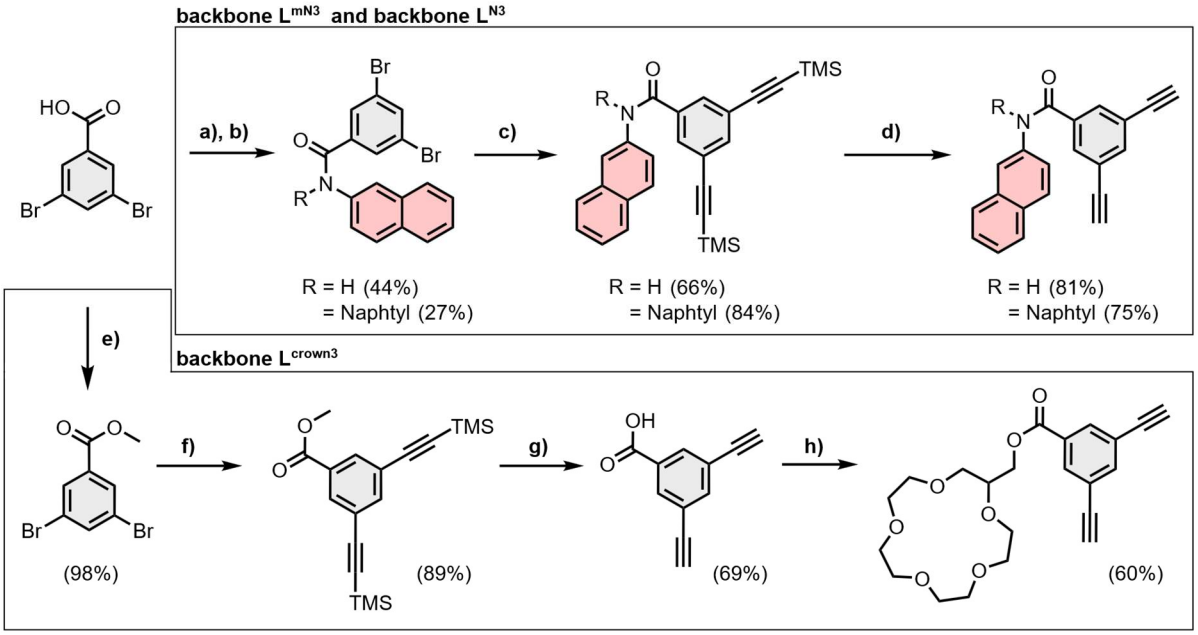

Figure 3.1: Backbone synthesis of L^{mN3}-H_2, L^{N3}-H_2 and L^{crown3}-H_2. a) $SOCl_2$, $CDCl_3$, reflux; b) L^{mN3}-H_2 R = H, $NH_2C_{10}H_7$, NEt_3, rt; L^{N3}-H_2 R = naphthyl, $NHC_{20}H_{14}$, NEt_3, rt; c) CuI, $[Pd(PPh_3)_2Cl_2]$, ethynyltrimethylsilane, NEt_3, 100°C; d) K_2CO_3, DCM/MeOH, rt; L^{crown3}-H_2 e) $SOCl_2$, MeOH, $CDCl_3$, reflux; f) CuI, $[Pd(PPh_3)_2Cl_2]$, ethynyltrimethylsilane, NEt_3, 100°C; g) KOH, THF/H_2O, 40°C; h) 15-crown-5-ether derivative, DCC, DMAP, DCM, rt.

The synthesis path (Figure 3.2) of the hydroxyquinoline coordination unit is literature known and began with a SKRAUP-type reaction i) of methacrolein and *o*-anisidine, which afforded 8-methoxy-3-methylquinoline, followed by the demethylation of the methoxy group j) with BBr_3. Afterwards, the free hydroxyl group was reacted with Boc anhydride k). To introduce an azide-functionality to the methyl group in position three of the Boc-protected hydroxyquinoline, the reactant was first reacted in a radical bromination with *N*-bromosuccinimide l), followed by a S_N2 reaction with sodium azide m), which afforded 3-(azidomethyl)quinoline-8-yl tert-butyl carbonate.[87,88,76]

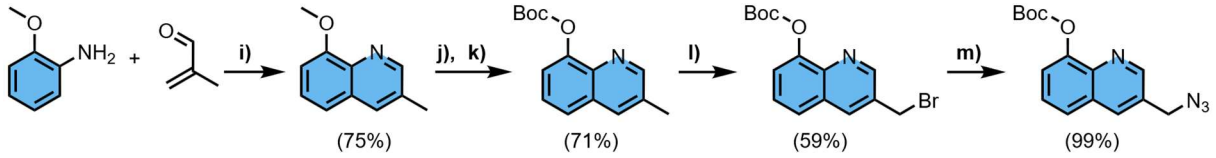

Figure 3.2: Synthesis of the Boc-protected hydroxyquinoline coordination unit. i) NaI, H_2SO_4 (70 wt%), reflux to rt; j) BBr_3, DCM, 0°C to rt; k) Boc_2O, NEt_3, DMAP (cat.), DCM, rt; l) NBS, AIBN, CCl_4, 80°C; m) NaN_3, acetone/H_2O, rt.

The final two steps of the synthetic pathway for the respective ligands (Figure 3.3) began with n) the 1,3-dipolar azide-alkyne HUISGEN cycloaddition. In this step, the terminal alkynes of the respective backbones reacted with the Boc-protected coordination unit bearing an azide functionality. The final step o) was the acidic deprotection of the Boc-groups, which afforded the respective bis-bidentate ligands in moderate yields with 53% for L^{crown3}-H_2 to 69% for L^{mN3}-H_2.

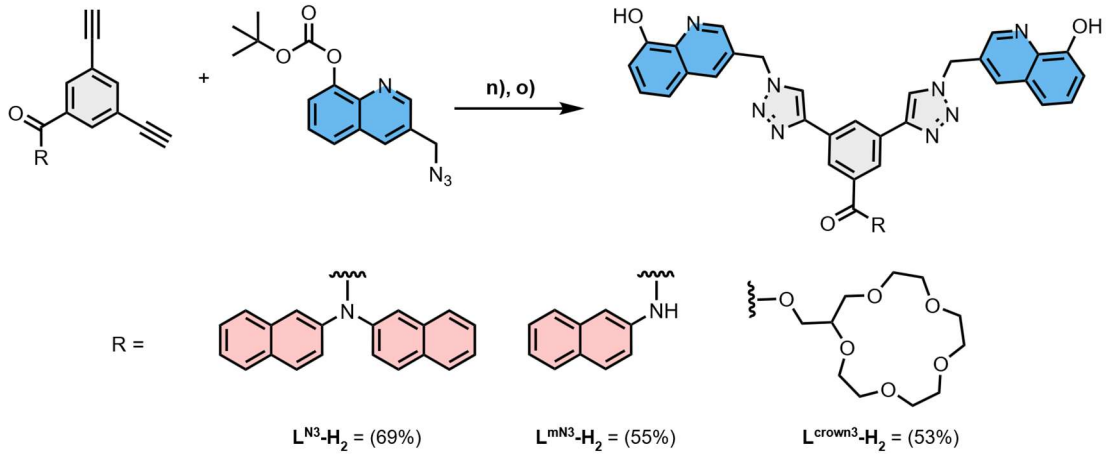

Figure 3.3: Final reaction steps of the synthesis of the ligands L^{mN3}-H_2, L^{N3}-H_2 and L^{crown3}-H_2. n) $CuSO_4$, Na-ascorbate, THF/H_2O, 60°C; o) TFA, DCM, rt.

3.3 Self-assembly of ligands L^{mN3}-H_2, L^{N3}-H_2 and L^{crown3}-H_2

The next step was the self-assembly of the respective bis-bidentate ligands L^{mN3}-H_2, L^{N3}-H_2 and L^{crown3}-H_2 with Zn(II) cations in DMSO-d_6. To self-assemble the respective charge-neutral containers, a solution of $Zn(OAc)_2$ was mixed with a stirring ligand solution in a 1:1 ratio, during which the reaction mixture turned yellow in each case. To ensure that the thermodynamic minimum is reached, the solutions were heated at 70°C for 12 h, which afforded the same ^{1}H NMR spectrum as after 1 h of stirring at room temperature. Using other Zn(II) salts ($ZnCl_2$ or $Zn(OTf)_2$) did not lead to a discrete self-assembly, highlighting the importance of the corresponding acetate counterion, which deprotonates the hydroxyquinolines, thereby enabling complexation and forming acetic acid as by product. Both the acetic acid and the solvent DMSO were removed during lyophilization, which afforded $[Zn_2L^{mN3}{}_2]$, $[Zn_2L^{N3}{}_2]$ and $[Zn_2L^{crown3}{}_2]$ as yellow, bench-stable powders.

3.3.1 Self-assembly of ligand L^{mN3}-H_2

The ^{1}H NMR spectrum of $[Zn_2L^{mN3}{}_2]$ showed a single set of proton signals after complexation, with most signals shifted downfield compared to those of L^{mN3}-H_2 (Figure 3.4). Signals corresponding to protons a and g, which are located next to the coordinating nitrogen atom of the hydroxyquinoline unit and the triazole-proton, respectively, showed downfield shifts. In contrast, signals corresponding to the peripheral protons of the hydroxyquinolate (c, d and e) showed a highfield shift, as well as the inner proton h of the ligand's backbone. These observations indicated successful coordination of the hydroxyquinolate units to Zn(II), confirming the self-assembly of $[Zn_2L^{mN3}{}_2]$. The assignment of each proton signal was carried out using 2D NMR spectroscopy (COSY Figure 3.50 and NOESY Figure 3.51 in the experimental part).

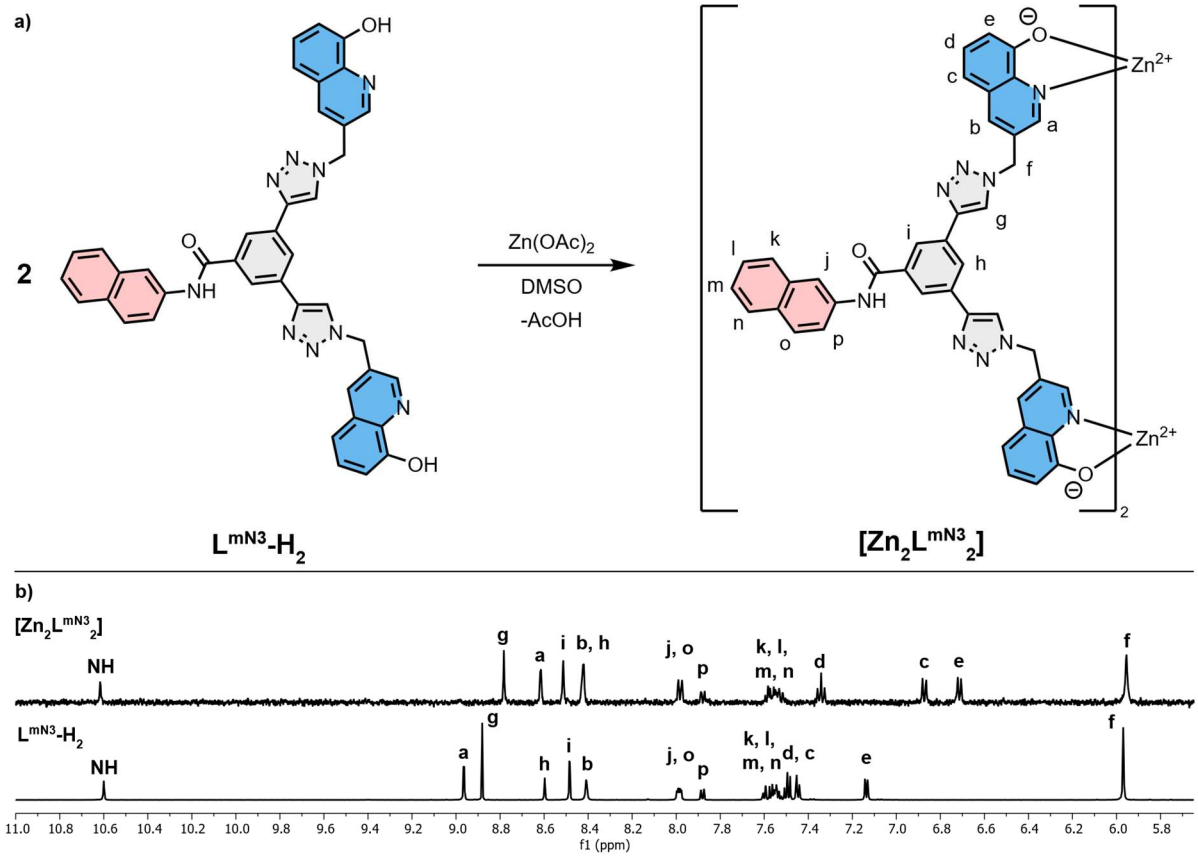

Figure 3.4: a) self-assembly of L^{mN3}-H_2 with $Zn(OAc)_2$ in a 1:1 ratio. b) staked ^{1}H NMR spectra of complex $[Zn_2L^{mN3}{}_2]$ and L^{mN3}-H_2 (DMSO-d_6, 500 MHz, 500 µM, 25°C).

The formation of $[Zn_2L^{mN3}{}_2]$ was further confirmed by negative ESI-MS, which showed a measured m/z value of 1631.3523 corresponding to an adduct of $[Zn_2L^{mN3}{}_2]$ (Figure 3.5) together with DMSO and a chloride anion, consistent with the calculated m/z value of 1631.2866. The spectra showed a plenty of signals with presumably Zn being an integral part of the measured signals, either way, many signals could not be assigned.

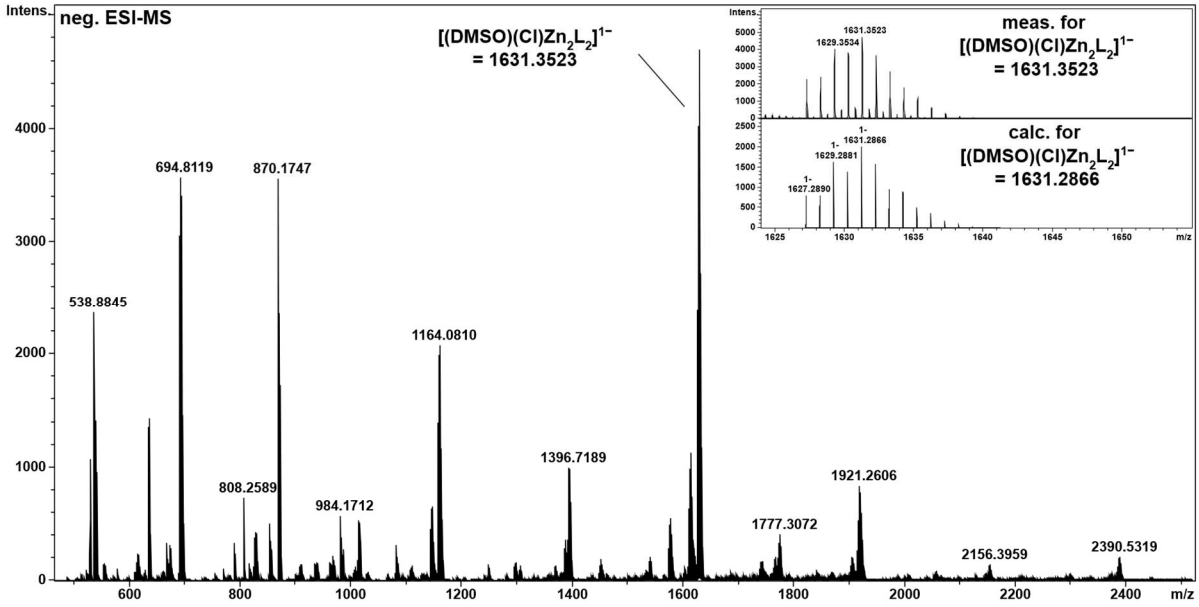

Figure 3.5: Negative ESI-MS spectrum of $[Zn_2L^{mN3}{}_2]$ as adduct with DMSO and chloride (DMSO/ACN).

3.3.2 Self-assembly of ligand L^{N3}-H_2

The ^{1}H NMR spectrum of $[Zn_2L^{N3}_2]$ showed a single set of signals, with downfield shifts for most of the proton signals compared to the ^{1}H NMR signals corresponding to ligand L^{N3}-H_2. The signals corresponding to proton a, located next to the coordinating nitrogen, shifted downfield, consistent with previously described charge-neutral $[Zn_2L_2]$ hosts.[76] Signals corresponding to the peripheral protons of the hydroxyquinolate (c, d and e) presented a highfield shift. This information indicated a successful coordination of the hydroxyquinolate units to Zn(II). Signal assignments were carried out using NMR spectroscopy (COSY Figure 3.84 and NOESY Figure 3.85, see chapter 3.7.8). The self-assembly of $[Zn_2L^{N3}_2]$ was further confirmed by DOSY experiments (D = 1.143 x 10^{-10} m^2 s^{-1}, see chapter 3.7.8).

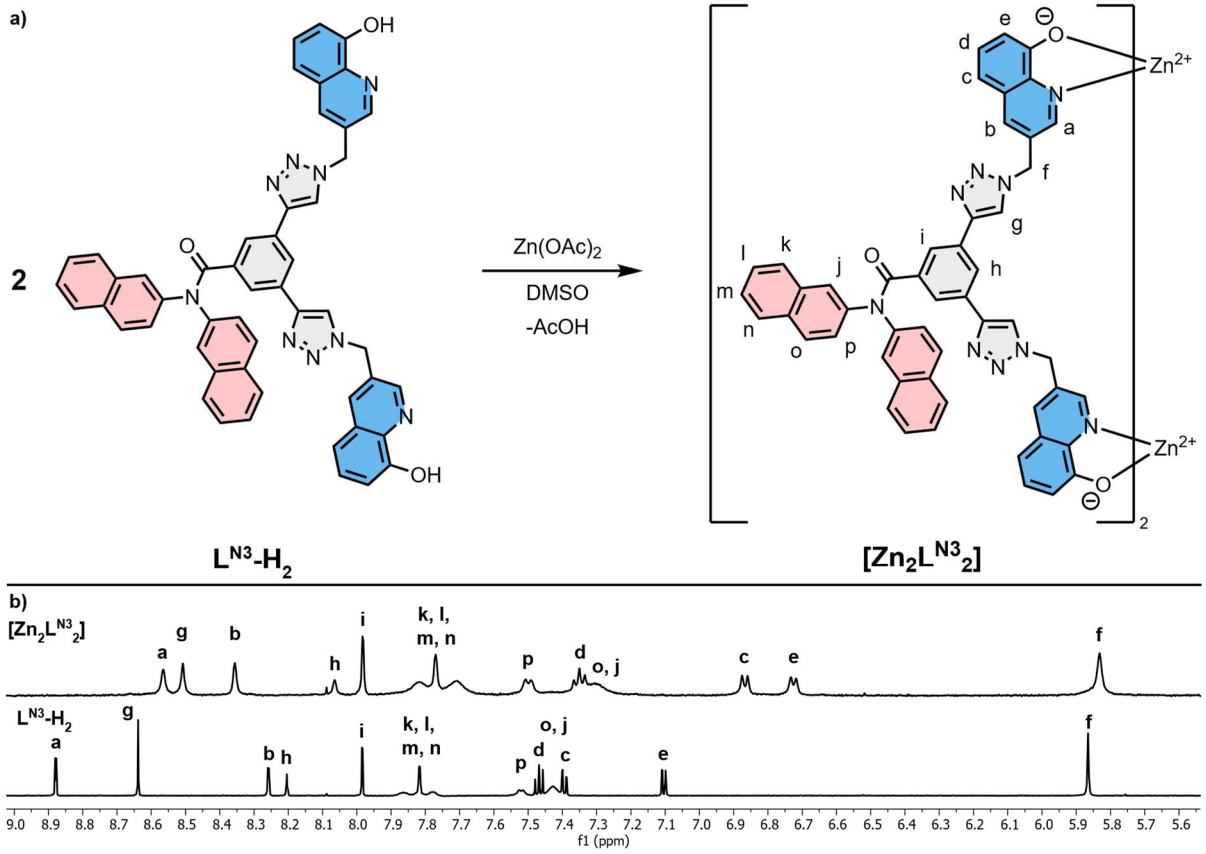

Figure 3.6: a) Self-assembly of L^{N3}-H_2 with $Zn(OAc)_2$ in a 1:1 ratio. b) Staked ^{1}H NMR spectra of complex $[Zn_2L^{N3}_2]$ and ligand L^{N3}-H_2 (DMSO-d_6, 500 MHz, 500 µM, 25°C).

Further, the self-assembly of $[Zn_2L^{N3}_2]$ was confirmed by negative ESI-MS as adduct with DMSO and chloride (Figure 3.7).

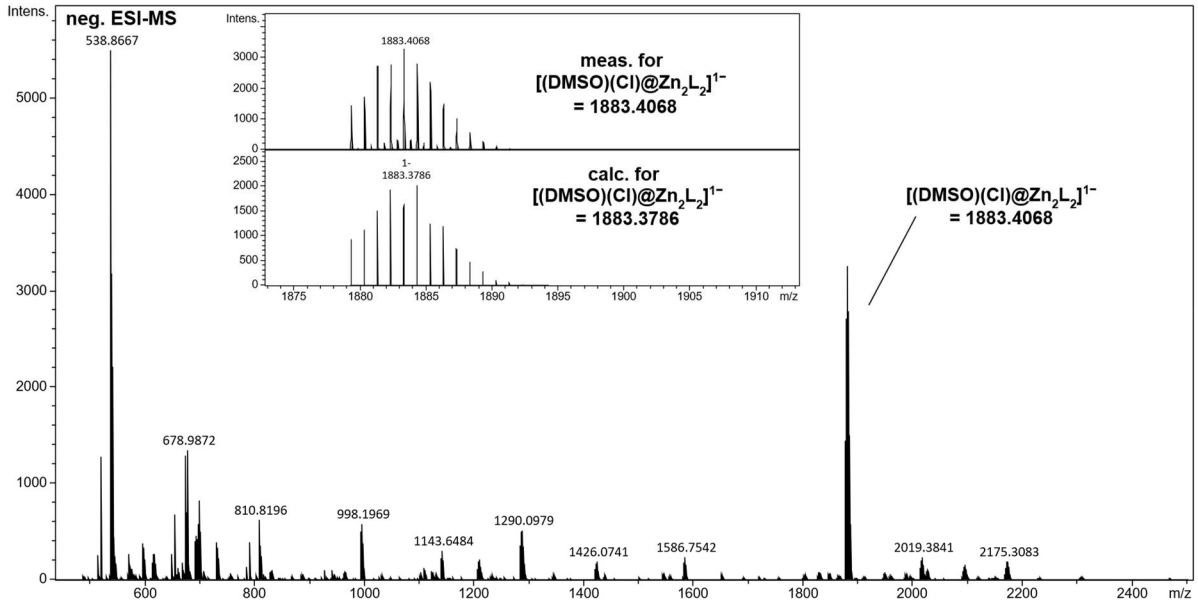

Figure 3.7: Negative ESI-MS spectrum of $[Zn_2L^{N3}_2]$ as adduct with DMSO and chloride (DMSO/ACN).

In the UV/Vis spectroscopy study of $[Zn_2L^{N3}_2]$ in DMSO-d_6 (Figure 3.8, a) two main absorbance-bands were present, one $\pi \rightarrow \pi^*$ transition at 345 nm and one $n \rightarrow \pi^*$ transition at 410 nm. A fit of the absorbance at 410 nm in different concentrations (0.5 µM – 100 µM) of $[Zn_2L^{N3}_2]$ (Figure 3.8, b) showed a linear Lambert-Beer correlation between absorbance and concentration of $[Zn_2L^{N3}_2]$.

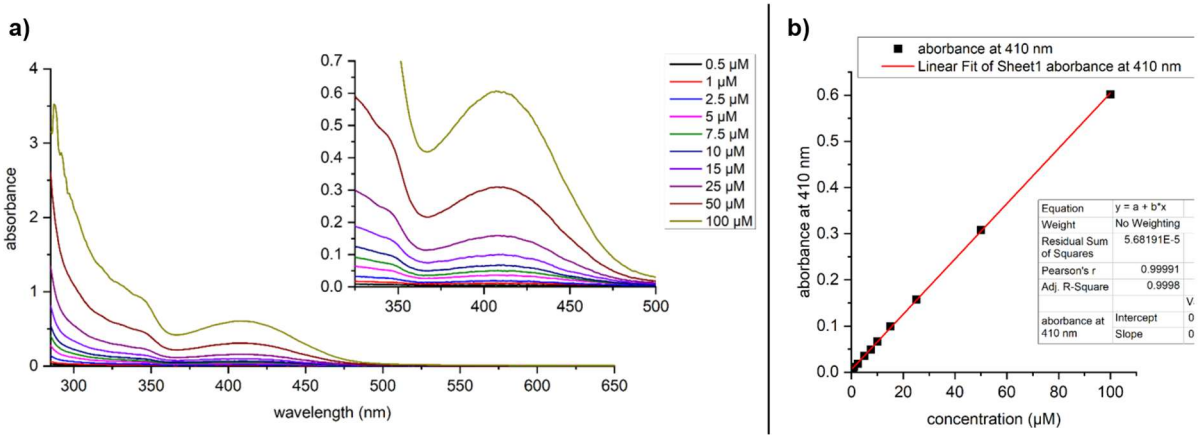

Figure 3.8: a) UV/VIS spectra of $[Zn_2L^{N3}_2]$ at concentrations between 0.5 µM and 100 µM; b) Linear fit of a Lambert-Beer plot of the absorbance at 410 nm.

3.3.3 Self-assembly of ligand L^{crown3}-H_2

The ^{1}H NMR spectrum of the self-assembled host $[Zn_2L^{crown3}{}_2]$ showed a single set of signals (Figure 3.9). In this spectrum, the signals of the protons from the inner backbone core (h and i) overlapped with the signal of proton b. Interestingly the signals of proton a and g, corresponding to the proton adjacent to the coordinating nitrogen atom and the triazole-proton, respectively, exhibited a highfield shift. The shifting behavior of the signals corresponding to the peripheral hydroxyquinolate moiety (c, d and e) was similar to that observed in the previously described hosts. The assignments of the signals in the ^{1}H NMR of $[Zn_2L^{crown3}{}_2]$ was carried out using 2D NMR spectroscopy (see chapter 3.7.9).

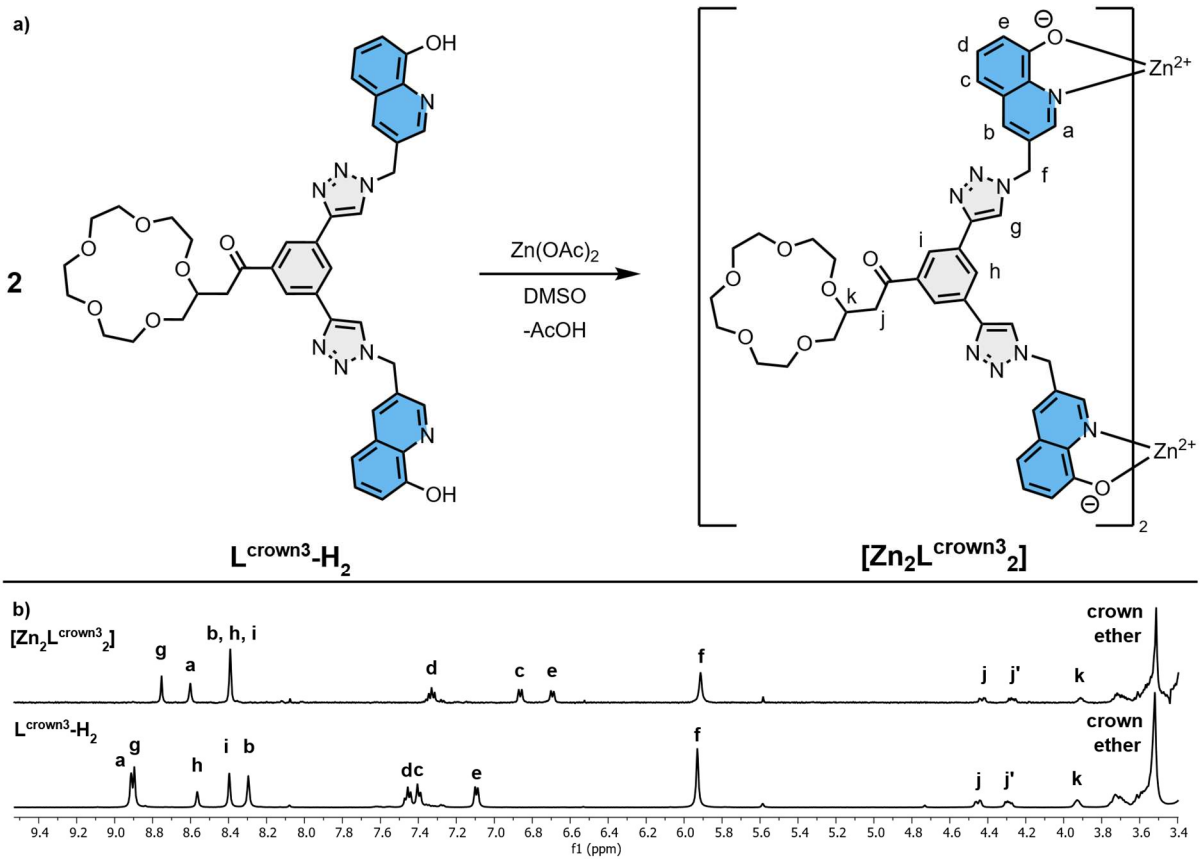

Figure 3.9: a) Self-assembly of ligand L^{crown3}-H_2 with $Zn(OAc)_2$ in a 1:1 ratio. b) Staked ^{1}H NMR spectra of complex $[Zn_2L^{crown3}{}_2]$ and ligand L^{crown3}-H_2 (DMSO-d_6, 500 MHz, 500 µM, 25°C).

The self-assembly of $[Zn_2L^{crown3}{}_2]$ was further confirmed by negative ESI-MS experiments (Figure 3.10). The spectrum showed a measured m/z value of 1767.3936 corresponding to a negatively charged adduct of a chloride anion and $[Zn_2L^{crown3}{}_2]$, matched the calculated m/z value of 1767.4091. The signal with the highest intensity appeared at m/z 901.1803 and corresponded to the two times negatively charged adduct of host $[Zn_2L^{crown3}{}_2]$ and two chloride anions.

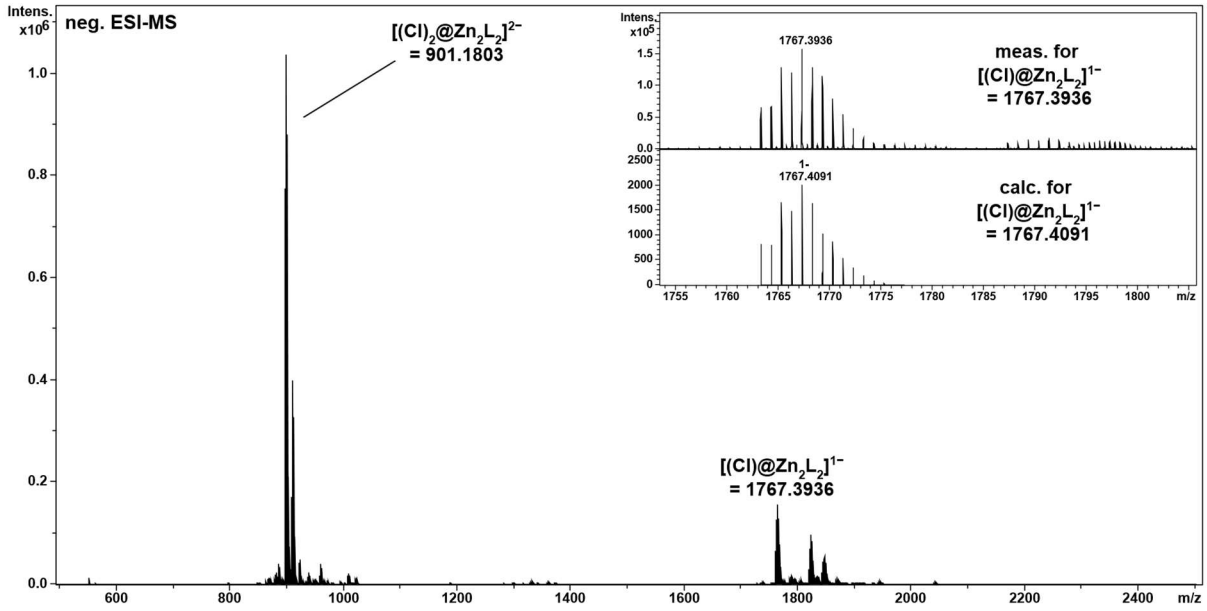

Figure 3.10: Negative ESI-MS spectrum of $[Zn_2L^{crown3}{}_2]$ as adduct with chloride (DMSO/ACN).

3.4 Guest Recognition experiments of $[Zn_2L^{mN3}{}_2]$, $[Zn_2L^{N3}{}_2]$ and $[Zn_2L^{crown3}{}_2]$

After characterization of the self-assembled charge-neutral containers $[Zn_2L^{mN3}{}_2]$, $[Zn_2L^{N3}{}_2]$ and $[Zn_2L^{crown3}{}_2]$, the next step was to test these hosts for their ability to bind the respective guest molecules (Figure 3.11 and Figure 3.14). The initial two dicarboxylates to be tested for $[Zn_2L^{mN3}{}_2]$ and $[Zn_2L^{N3}{}_2]$ were naphthalene-2,6-dicarboxylate NP^{2-} and terephthalate TP^{2-}. Both were intended to coordinate and bridge the two Zn(II) centers. The enlarged π-surfaces of the backbones in $[Zn_2L^{mN3}{}_2]$ and $[Zn_2L^{N3}{}_2]$ were intended to increase the binding of NP^{2-} and TP^{2-} (Figure 3.11, b) compared to the previous described $[Zn_2L_2]$ MOC by VAN CRAEN, by hovering over the bound guest inside of the cavity and interact via π-π-interactions and shielding the bound guest to interact with solvent molecules. Among these two aromatic dicarboxylates, the host $[Zn_2L^{N3}{}_2]$ was also intended to bind simple, aromatic molecules like benzene, naphthalene and pyrene via π-π-interactions. Since $[Zn_2L^{crown3}{}_2]$ was designed as a heteroditopic receptor for ion-pairs, it was tested with a variety of ion pairs (Figure 3.14).

3.4.1 Recognition experiments of $[Zn_2L^{mN3}{}_2]$ and $[Zn_2L^{N3}{}_2]$

The ^{1}H NMR titrations of $[Zn_2L^{mN3}{}_2]$ and $[Zn_2L^{N3}{}_2]$ with NP^{2-} and TP^{2-} (Figure 3.11) revealed a slow guest exchange behavior, comparable with the exchange behavior of these guests and VAN CRAEN'S previous described $[Zn_2L_2]$ container. Unfortunately, in all ^{1}H NMR test-titrations a major and a minor species was formed. Due to the formation of a minor species, calculating binding-constants from the ^{1}H NMR data of these titrations is prone to errors. Adding 10 equivalents of guest to $[Zn_2L^{mN3}{}_2]$ or $[Zn_2L^{N3}{}_2]$ and heating the sample for several hours at 70°C did not lead to a discrete host-guest complex formation in the respective ^{1}H NMR spectra (Figure 3.13).

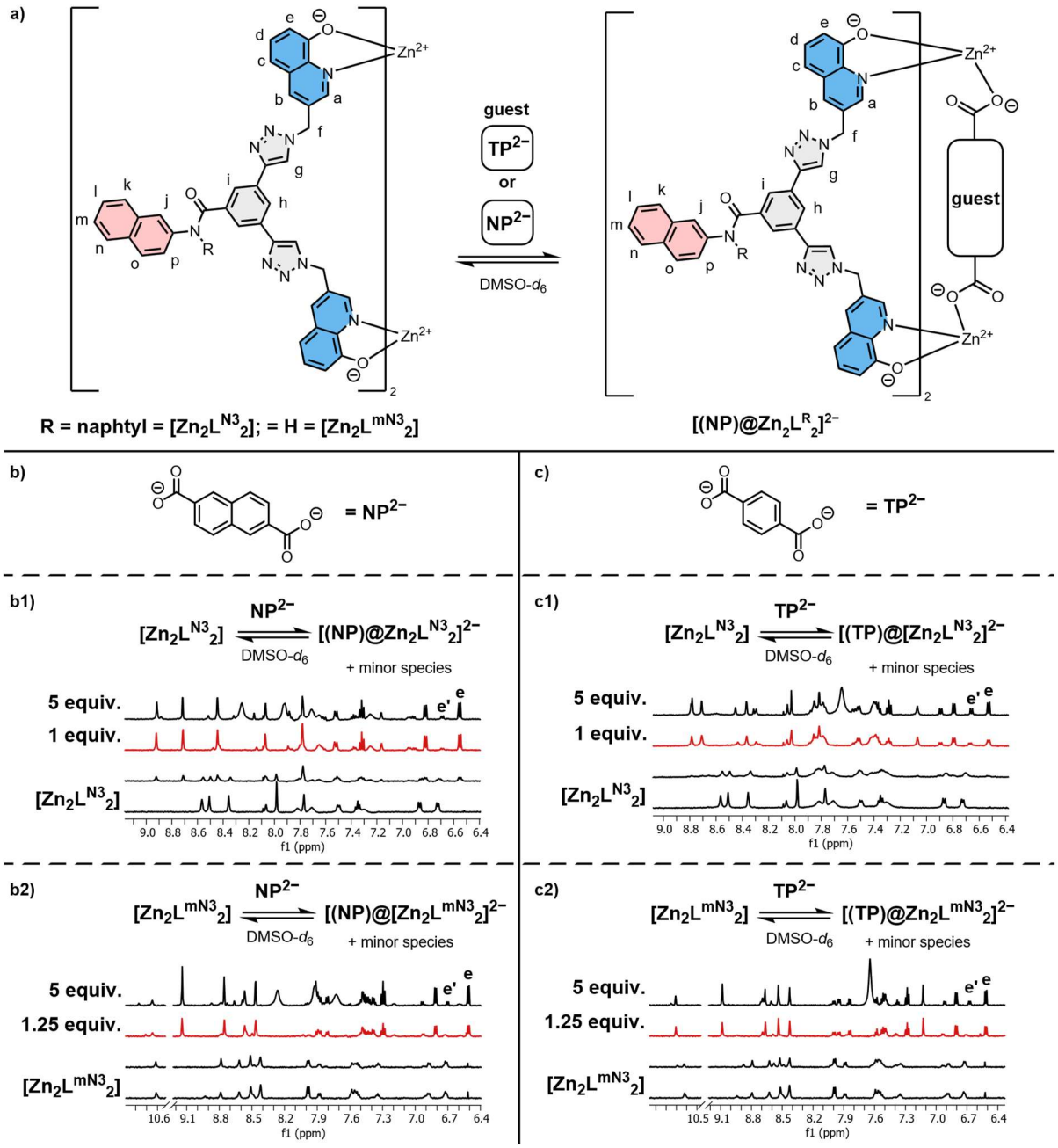

Figure 3.11: a) Host-guest formation of $[Zn_2L^{mN3}{}_2]$ and $[Zn_2L^{N3}{}_2]$ with NP^{2-} and TP^{2-}.
b) Structure of naphthalene-2,6-dicarboxylate NP^{2-}. c) Structure of terephthalate TP^{2-}.
b1) and b2) ^{1}H-NMR test titrations of $[Zn_2L^{mN3}{}_2]$ and $[Zn_2L^{N3}{}_2]$ with NP^{2-}.
c1) and c2) ^{1}H-NMR test titrations of $[Zn_2L^{mN3}{}_2]$ and $[Zn_2L^{N3}{}_2]$ with TP^{2-}
(all titrations, DMSO-d_6, 500 MHz, 500 µM 25°C).

The differences in diffusion coefficients between the respective major and minor species were very small, exemplified by the most pronounced difference, given by $[(NP)@Zn_2L^{mN3}{}_2]^{2-}$ (D_{minor} = 9.75 x 10^{-11} m^2 s^{-1} and D_{major} = 1.04 x 10^{-10} m^2 s^{-1}, see SI and Figure 3.13) probably due to the formation of complexes with different compositions of ligand, central Zn(II) cation and guest. Negative ESI-MS spectra of the host-guest complexes formed between $[Zn_2L^{mN3}{}_2]$ or $[Zn_2L^{N3}{}_2]$ and NP^{2-} or TP^{2-} showed m/z values corresponding to the respective two times negatively charged host-guest complexes (Figure 3.12).

Nevertheless, the minor species formed in the initial ^{1}H NMR titrations (Figure 3.11) could not be assigned and remained unidentified in all four cases. It was presumed that the integrity of the host was partially disrupted, which led to the formation of complexes with different compositions. The negative ESI-MS spectrum of $[(TP)@Zn_2L^{N3}{}_2]^{2-}$ showed a m/z value and isotopic pattern consistent with a $H[(TP)_2@Zn_2L^{N3}{}_1]^{1-}$ species (see chapter 3.7.8), which represents unexpected behavior of these host-guest systems and likely corresponds to the minor species observed in the initial ^{1}H NMR recognition experiments of $[Zn_2L^{mN3}{}_2]$ and $[Zn_2L^{N3}{}_2]$.

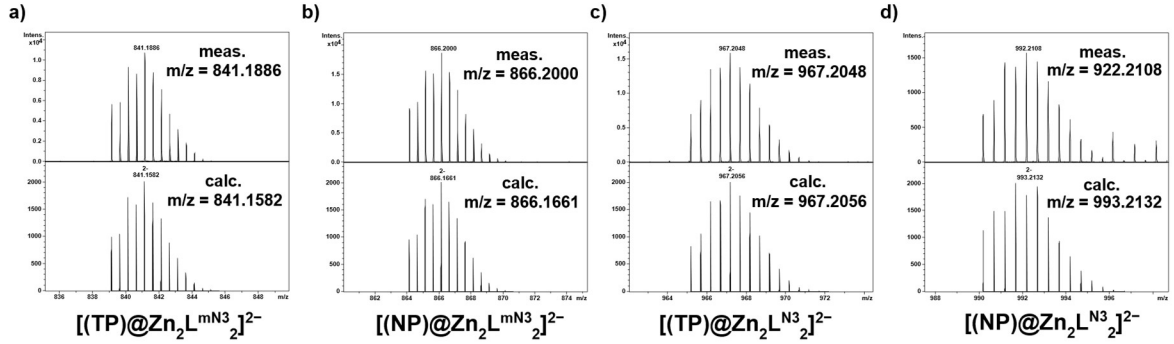

Figure 3.12: Excerpt from the negative ESI-MS spectrum of the host-guest complexes of $[Zn_2L^{mN3}{}_2]$ and $[Zn_2L^{N3}{}_2]$ with TP^{2-} and NP^{2-}.

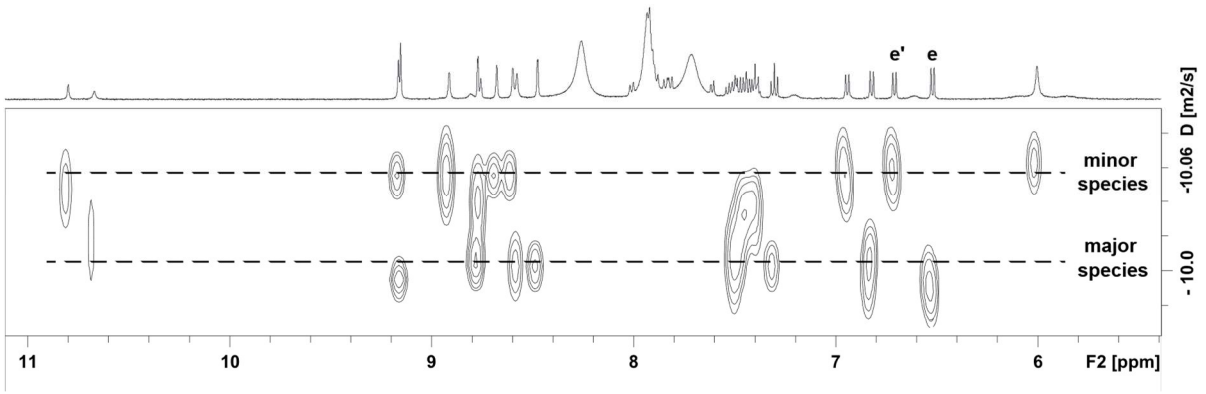

Figure 3.13: ^{1}H NMR DOSY spectrum (DMSO-d_6, 500 MHz, 1 µM, 25°C) of host-guest complex formation (10 equiv. NP^{2-} and heating to 70°C) of $[(NP)@Zn_2L^{mN3}{}_2]^{2-}$ (signal e) and minor species (signal e').

To investigate if the new charge-neutral hosts $[Zn_2L^{mN3}{}_2]$ and $[Zn_2L^{N3}{}_2]$ are able to bind flat aromatic compounds in DMSO-d_6, ^{1}H NMR recognition experiments are conducted. Initial ^{1}H NMR titrations of $[Zn_2L^{N3}{}_2]$ with simple, flat aromatic compounds show no shifts of signals upon addition and heating to 70°C and suggests no recognition under these conditions.

3.4.2 Guest Recognition experiments of [$Zn_2L^{crown3}{}_2$]

^{1}H NMR titrations of [$Zn_2L^{crown3}{}_2$] with ions pairs sodium chloride and sodium azide showed a fast-exchange behavior (Figure 3.14). The most pronounced shifts, although still small, corresponded to the signals of the hydroxyquinolate-units, which suggested the anions coordinate to the zinc-centers. Hence, presumably changing the coordination sphere from tetrahedral to trigonal-bipyramidal. As a noteworthy observation, the most pronounced shift in each of the ^{1}H NMR titrations of [$Zn_2L^{crown3}{}_2$] was performed by the signal corresponding to proton e. Leaving the question if the coordination happened axial outside of the cavity, or inside of the cavity. Triazole-protons are a well-known recognition unit for anions[89], nevertheless, the shifts of signals corresponding to the triazole-protons g were small (Figure 3.14). This suggested that the anions interacted with the Zn(II) centers rather than with the triazole-protons.

The signals corresponding to the crown ether also shifted, but only slightly (Figure 3.14, b and c). This suggested either interaction with sodium cations or conformational changes induced by chloride binding. To verify that chloride binding and the associated conformational changes of the receptor influenced the shifts of the crown ether signals, tetrabutylammonium chloride was tested as guest for [$Zn_2L^{crown3}{}_2$] in a ^{1}H HMR titration experiment. The shifts of the hydroxyquinolate signals were similar to the previous titration, and the crown ether signals likewise shifted (Figure 3.14, b1 and c1). With this information, it was not likely that sodium cations and the 15-crown-5-ether units strongly interacted with each other. The ^{1}H NMR titration experiments of [$Zn_2L^{crown3}{}_2$] with KPF_6 and $TBAPF_6$ showed no shifting signals, indicating that K^+ and PF_6^- were either too large to be recognized by the host or too strongly solvated.

The limitation of DMSO-d_6 as a solvent was problematic, particularly with regard to its influence on the interactions between crown ethers and cations. With its relatively high dielectric constant, DMSO itself coordinates alkali cations and thereby disrupted the desired host-guest interactions.

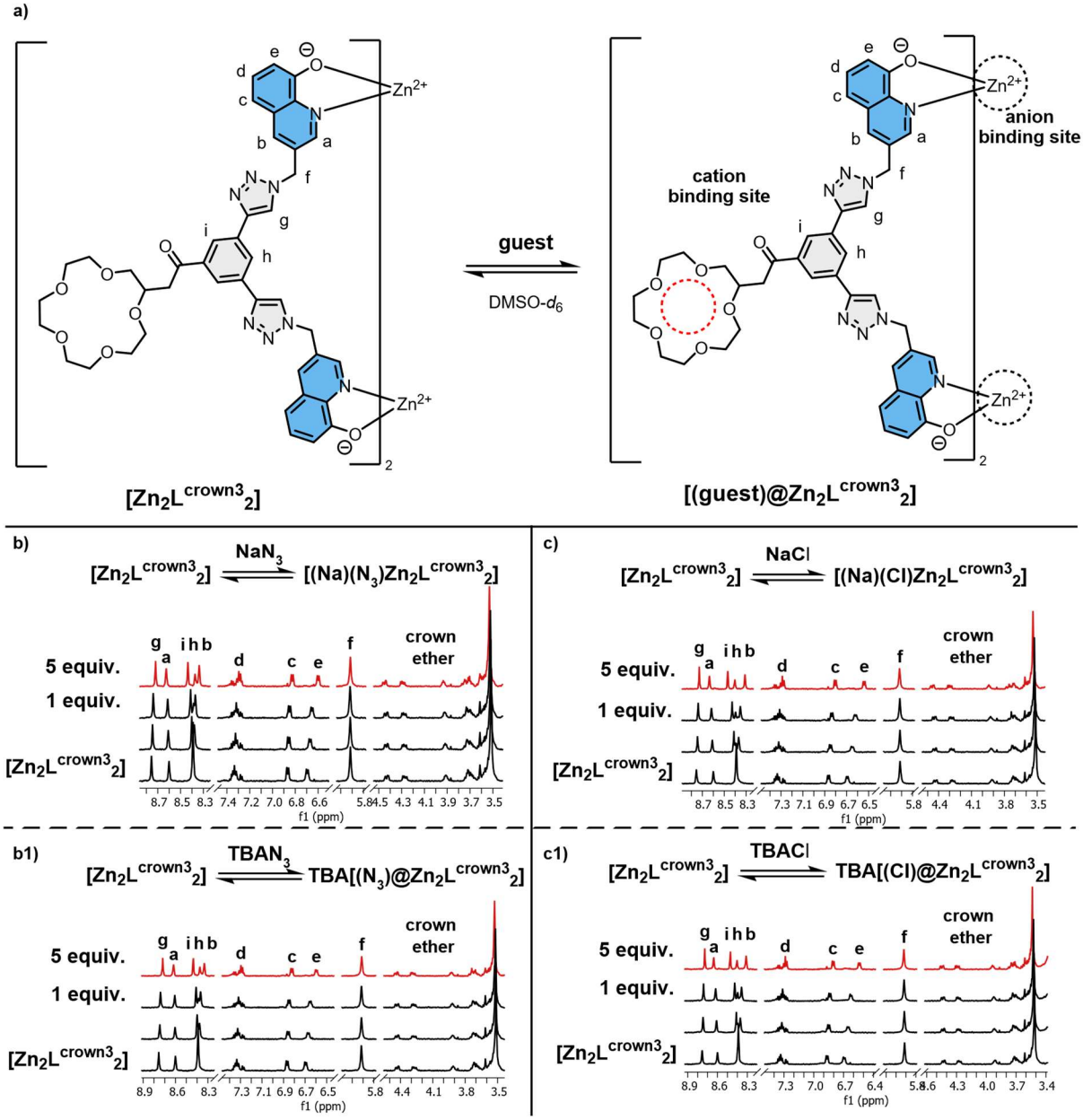

Figure 3.14: a) Host-guest formation of the heteroditopic ion pair receptor $[Zn_2L^{crown3}{}_2]$, showing both recognition sites. b) and b1) ^{1}H-NMR test titrations of $[Zn_2L^{crown3}{}_2]$ with NaN_3 and $TBAN_3$ c) and c1) ^{1}H-NMR test titrations of $[Zn_2L^{crown3}{}_2]$ with NaCl and TBACl (all titrations, DMSO-d_6, 500 MHz, 500 µM 25°C).

Nevertheless, the fast exchange behavior of $[Zn_2L^{crown3}{}_2]$ and NaCl in the ^{1}H NMR allowed calculation of a binding constant (Figure 3.15, a and b). It should be noted that the binding constant was influenced by the competitive behavior of DMSO as solvent. Due to this competition, and supported by the small signal shifts in the ^{1}H NMR test-titrations, the binding constant was expected to be relatively low. The complete fine ^{1}H NMR titration experiment is described in the experimental part. Fitting of the ^{1}H NMR data indicated primarily a 1:1 binding, as no inflection point was observed (Figure 3.15, c). For this 1:1 binding, BindFit[90,91] gave a binding constant K = 371 M^{-1} with an fitting error of ±2.6%. Considering that the host $[Zn_2L^{crown3}{}_2]$ possesses more than one recognition site for anions or cations, and the added

equivalents correspond to an excess, it was expected to observe an inflection point. Consequently, the 1:2-binding constant, due to the aforementioned limitations, was expected to be very small and therefore difficult to detect, both in terms of signal shifts in the ^{1}H NMR and appearance of inflection points in the fit.

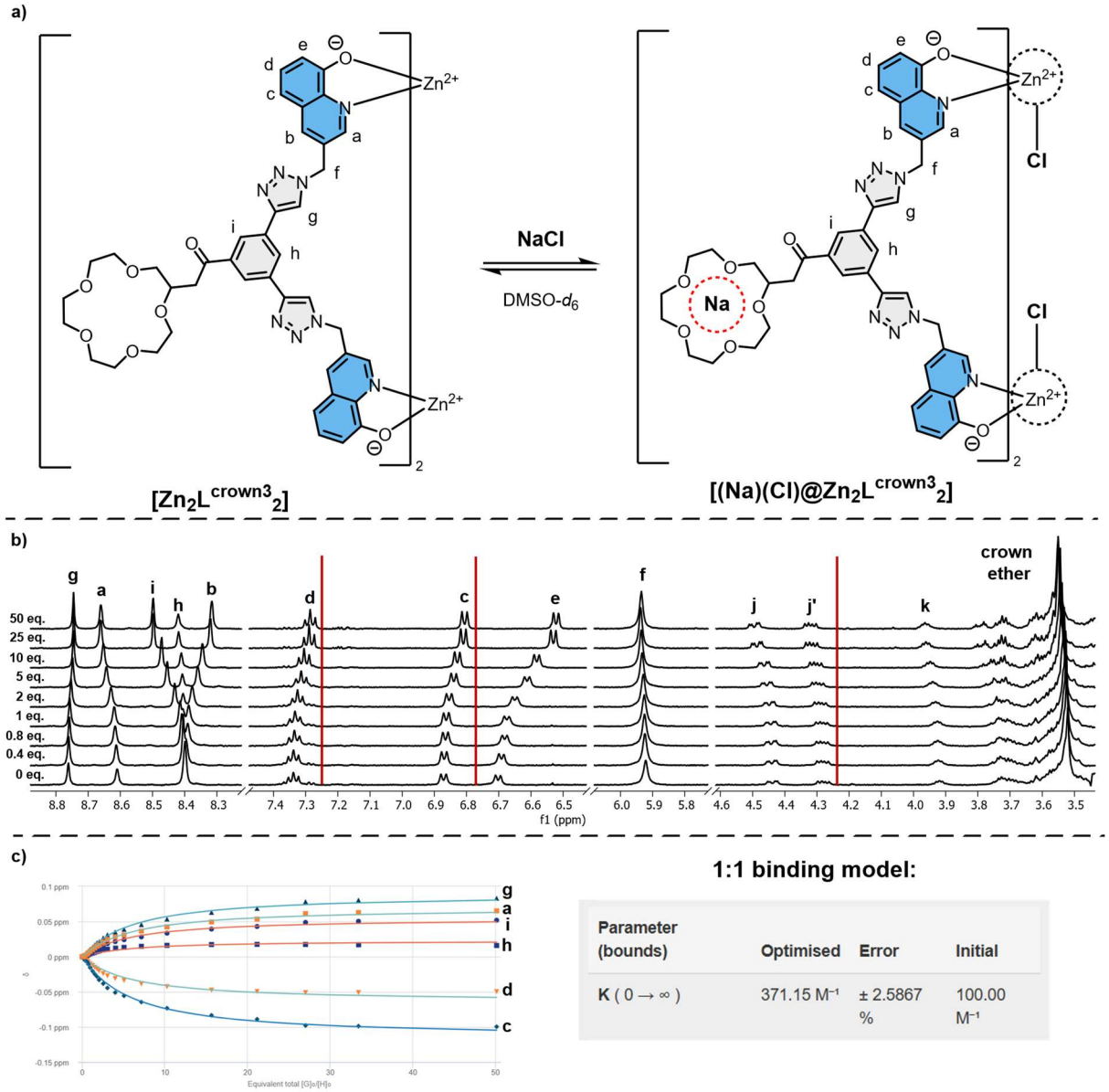

Figure 3.15: a) Host-guest formation of the heteroditopic ion pair receptor [Zn$_2$L$^{crown3}_2$] with NaCl in DMSO-d$_6$. b) An excerpt from the fine ^{1}H NMR titration of [Zn$_2$L$^{crown3}_2$] with NaCl (DMSO-d$_6$, 500 MHz, 500 µM 25°C). c) BindFit[91,85] plot of selected signals from the fine ^{1}H titration and the resulting binding constant K in a 1:1 binding model.

3.5 Crystallization, Computation and remarks

All crystallization attempts of $[Zn_2L^{mN3}{}_2]$, $[Zn_2L^{N3}{}_2]$ and $[Zn_2L^{crown3}{}_2]$ were unsuccessful. The most commonly used method for crystallization was slow-vapor diffusion. Crystallization experiments were carried out both with the host alone and in the presence of guests. However, combining DMSO with various anti-solvents consistently resulted either in amorphous precipitation or the formation of amorphous, yellow glass-like rod-materials (Figure 3.16). Despite extensive crystallization attempts under varying conditions, no single crystal suitable for X-ray diffraction could be obtained. This remains a limitation of unambiguous structural confirmation in the solid state.

Figure 3.16: Amorphous, yellow, glass-like rod-material formed from $[Zn_2L^{crown3}{}_2]$ with NaCl in DMSO and benzene as anti-solvent.

The failure of crystallization prevents absolute structural characterization. Nevertheless, computational studies of the hosts $[Zn_2L^{mN3}{}_2]$, $[Zn_2L^{N3}{}_2]$ and $[Zn_2L^{crown3}{}_2]$, together with the respective guests, were conducted. From NMR spectroscopy and the previously reported $[Zn_2L_2]$ container by VAN CRAEN, it was known that the major species in solution orients its triazole units in the backbone in a *syn-syn* conformation and that the crystal structure of $[(NP)@Zn_2L_2]^{2-}$ showed an achiral diastereomer. Additionally, in the case of $[Zn_2L^{mN3}{}_2]$ and $[Zn_2L^{N3}{}_2]$, it could be assumed that the dicarboxylates coordinate through both of their carboxylate units to the two Zn(II)-centers, as also observed in the previously reported $[(NP)@Zn_2L_2]^{2-}$ host-guest complex.[76] In the case of $[Zn_2L^{crown3}{}_2]$, it was assumed that the anionic guests are interacting with the Zn(II) centers from within the cavity, as the ^{1}H NMR titrations (Figure 3.15) also show shifting signals corresponding to the triazole-protons. Although the ^{1}H NMR titrations indicated weak interactions of the cationic guests with the 15-crown-5 ether of the backbone, the cations are presumed to bind the ether via dipole-dipole interactions, hovering above the cavity that accommodates the negatively charged guests. With this information it was possible to model the host-guest complexes of $[(NP)@Zn_2L^{mN3}{}_2]^{2-}$, $[(NP)@Zn_2L^{N3}{}_2]^{2-}$ and $[(Na)_2(Cl)_2@Zn_2L^{crown3}{}_2]$.

The starting geometry (Figure 3.17, a)) for the DFT optimizations of the host-guest complexes $[(NP)@Zn_2L^{mN3}{}_2]^{2-}$, $[(NP)@Zn_2L^{N3}{}_2]^{2-}$ and $[(Na)_2(Cl)_2@Zn_2L^{crown3}{}_2]$ was taken from an XRD-informed model and refined at the ωB97X-D4 level. In the model of $[(NP)@Zn_2L_2]^{2-}$, naphthalene-2,6-dicarboxylate bridged the two Zn(II) centers through both carboxylates, generating a trigonal-bipyramidal coordination sphere at each Zn(II). The structure also displayed auxiliary noncovalent interactions between host and guest. First, the phenyl backbone shows CH-π interactions with the protons of NP^{2-} at position four and eight. And second, weak hydrogen bonds between the hydroxyquinolate protons at position two and the carbonyl oxygen atoms of the guest. The approximately rectangular-shaped cavity has an area of ~140 Å^2, with a Zn(II)-Zn(II) distance of 13.0 Å and a phenyl-phenyl distance of 11.1 Å. This close geometric match between NP^{2-} and the $[Zn_2L_2]$ cage underscored the importance of the Zn(II)-Zn(II) distance for efficient dicarboxylate binding.

The calculated structures of the host-guest complexes $[(NP)@Zn_2L^{mN3}{}_2]^{2-}$ and $[(NP)@Zn_2L^{N3}{}_2]^{2-}$ exhibited the intended structural behavior (Figure 3.17 b)-c)). The enlarged π-surfaces of the naphthalene substituents extend over the guest and cavity, thereby reducing the solvent-accessible surface area. In these models, the distances between the π-surface of the backbone and that of the

guest are 3.4 Å and 3.5 Å for $[(NP)@Zn_2L^{mN3}{}_2]^{2-}$ and $[(NP)@Zn_2L^{N3}{}_2]^{2-}$, respectively, consistent with additional parallel-displaced π-π interactions between host and guest. Compared to the starting geometry, the trigonal-bipyramidal coordination spheres around the Zn(II) centers were slightly distorted, resulting in a modestly elongated Zn(II)-Zn(II) distance of 13.1 Å and a slightly compressed phenyl-phenyl distance of 10.9 Å in both complexes.

The calculated model of the host-guest assembly of the heteroditopic host $[Zn_2L^{crown3}{}_2]$ with sodium chloride (Figure 3.17, d)) reflected the NMR observations, showing coordination of the chloride anions to the Zn(II) centers and intramolecular complexation of the sodium cations by the crown ether moieties. The sodium cations were theoretically positioned above the coordinating chloride anions, stabilized by electrostatic interactions. This model, however, neglected the fact that in solution, DMSO presumably shields the interactions between the sodium cations and the crown ether moieties due to its high dielectric constant, as well as the missing inflection points in the ^{1}H NMR titrations. The model showed a sodium-chloride distance of 5.7 Å.

Furthermore, the calculated model of $[(Na)_2(Cl)_2@Zn_2L^{crown3}{}_2]$ exhibited an increased Zn(II)-Zn(II) distance of 13.7 Å compared to the previous models, presumably due to the presents of two chloride anions within the cavity, while the phenyl-phenyl distance slightly contracted to 10.5 Å. Overall, the calculated geometries of the host-guest structures $[(Na)_2(Cl)_2@Zn_2L^{crown3}{}_2]$, $[(NP)@Zn_2L^{mN3}{}_2]^{2-}$ and $[(NP)@Zn_2L^{N3}{}_2]^{2-}$ displayed cavity areas of approximately 140 Å^2.

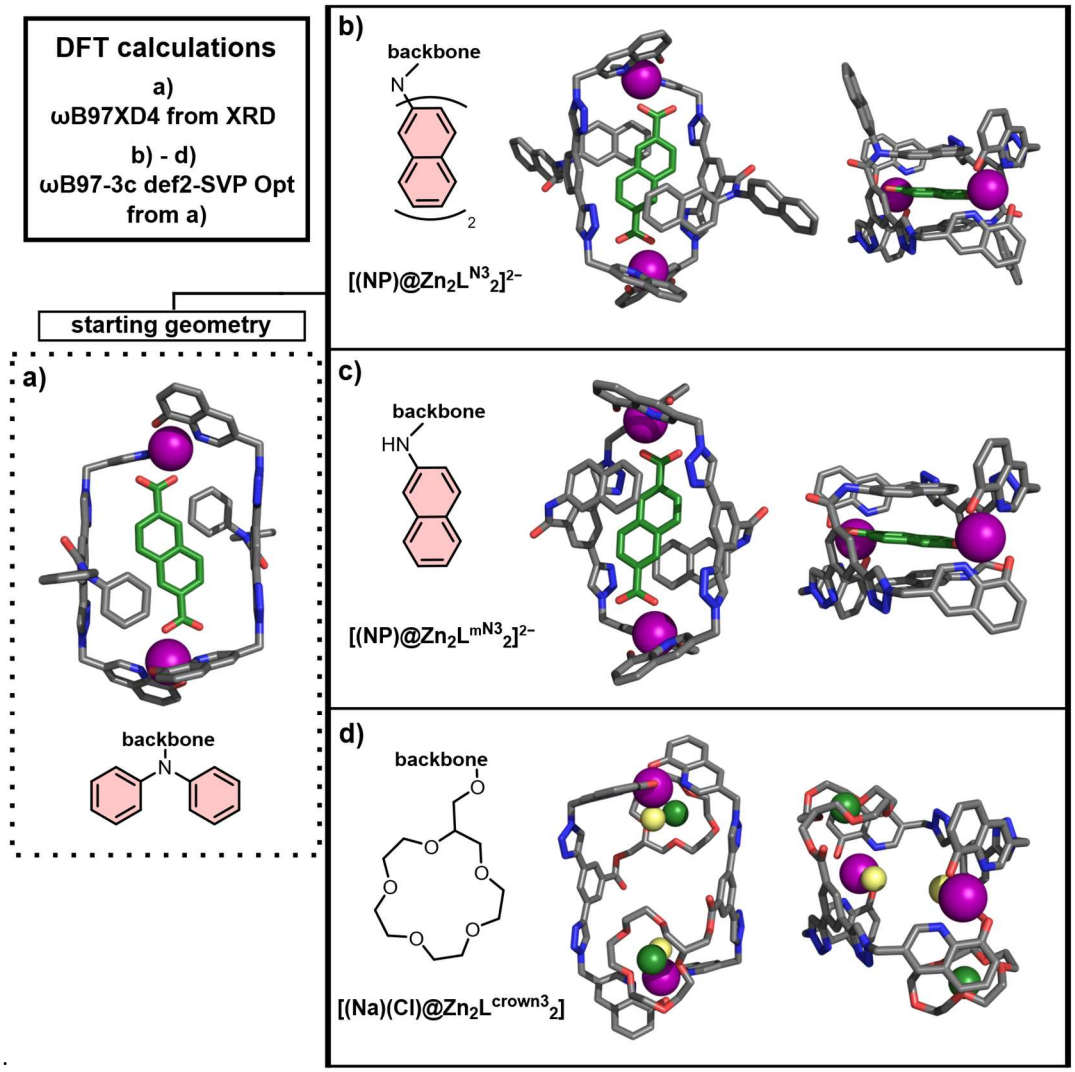

Figure 3.17: DFT calculations of the host-guest complexes of $[(NP)@Zn_2L^{mN3}{}_2]^{2-}$ and $[(NP)@Zn_2L^{N3}{}_2]^{2-}$ and $[(Na)_2(Cl)_2@Zn_2L^{crown3}{}_2]$, carbon atoms are shown in grey, nitrogen in blue, oxygen in red, chloride in green, sodium in yellow and Zn(II) is purple colored.

As a noteworthy observation, ^{1}H NMR titration experiments of $[Zn_2L^{crown3}{}_2]$ with Na_2NP showed a slow exchange binding behavior similar to that observed for complex $[Zn_2L^{mN3}{}_2]$ and $[Zn_2L^{mN3}{}_2]$ with $(TBA)_2NP$. Under the given conditions, both a major and a minor species were formed, making a reliable quantitative determination of the binding constants problematic. However, the ^{1}H NMR spectra showed an exchange behavior and chemical shift trends comparable to those of the analogous host-guest system, for which a discrete 1:1 host-guest complex and a binding constant are known. Therefore, it could be assumed that the binding constants of the present systems lie in a similar range, although it could not be conclusively determined due to the coexistence of multiple species.

3.6 Conclusion and Outlook

The ligands L^{mN3}-H_2, L^{N3}-H_2 and L^{crown3}-H_2 were designed and successfully synthesized to expand the family of charge-neutral Zn(II)-based metal-organic cages previously introduced by VAN CRAEN. By varying the backbone architectures, through the incorporation of extended π-surfaces (L^{mN3}-H_2 and L^{N3}-H_2) and a crown ether functionality (L^{crown3}-H_2), this study systematically explored how electronic extension and functional diversity influence self-assembly, solubility and host-guest recognition.

All three ligands self-assembled quantitatively with $Zn(OAc)_2$ in DMSO to form the anticipated charge-neutral complexes [$Zn_2L^{mN3}{}_2$], [$Zn_2L^{N3}{}_2$] and [$Zn_2L^{crown3}{}_2$]. NMR spectroscopy and ESI-MS confirmed successful coordination of the hydroxyquinolate units to Zn(II) and formation of discrete [Zn_2L_2] architectures. The acetate counterion again prove to be crucial, as it facilitated the deprotonation of the hydroxyquinoline units, which is an essential step in the self-assembly process.

The recognition studies revealed that [$Zn_2L^{mN3}{}_2$] and [$Zn_2L^{N3}{}_2$] maintained the fundamental binding behavior of VAN CRAEN'S system toward aromatic dicarboxylates such as NP^{2-} and TP^{2-}. The enlarged π-surfaces of these ligands increased the hydrophobic shielding of the cavity and enabled π-π interactions between the host backbone and the encapsulated aromatic guests, as supported by DFT modeling. Despite this, ^{1}H NMR titrations consistently showed the coexistence of a major and a minor species, which prevented precise quantitative evaluation of binding constants. Nonetheless, the similarity in binding behavior relative to the parent system suggested that the binding affinities remain in the same range, which confirmed that the expanded π-surface preserve structural integrity while modulating guest interactions.

The heteroditopic system [$Zn_2L^{crown3}{}_2$] demonstrated the feasibility of the integrating cation and anion recognition within a single charge-neutral container. NMR titrations and DFT models indicated chloride coordination to the Zn(II) centers and sodium binding to the crown ether moieties, forming ion-pair inclusion complexes. While DMSO's high dielectric constant likely weakened these electrostatic interactions in solution, the observed fast-exchange binding and calculated structures confirmed the underlying concept of cooperative dual-site recognition.

Crystallization efforts for all three hosts and their complexes were unsuccessful, highlighting the inherent challenge of isolating crystalline materials from charge-neutral architectures in polar solvents. Nevertheless, computational studies provided valuable insight into cavity geometries, host-guest distances, and interaction patterns, which showed consistent Zn(II)-Zn(II) distances and cavity areas across all systems.

From an academic perspective, this work contributed to the rational design of modular, charge-neutral coordination containers with tunable electronic and geometric properties. The presented ligands offer a versatile platform to study structure-function relationships, cooperative binding effects, and solvent influences in supramolecular assemblies. Future investigations should focus on fine-tuning ligand rigidity, introducing alternative metal centers, and employing less competitive solvents to enhance selectivity and enable crystallographic characterization.

In the broader scientific and applied context, these systems hold potential in several directions, for example:

- Selective molecular recognition and sensing, particularly of small anions and ion pairs in polar media
- Host-assisted catalysis, where confined cavities and adjustable coordination environments can stabilize reactive intermediates

In summary, the development of L^{mN3}-H_2, L^{N3}-H_2 and L^{crown3}-H_2 broadened the scope of neutral Zn(II)-based MOCs toward multifunctional host systems. These findings reinforce the principle that subtle ligand design modifications, whether electronic, structural or functional, can profoundly influence host-guest chemistry. Bridging the gap between fundamental supramolecular design and future real-world applications in recognition, separation and catalysis.

3.7 Experimental Part

3.7.1 General Information

All experiments were performed under argon atmosphere, when necessary. Chemicals and solvents were purchased from Sigma Aldrich, Acros Organics, Carl Roth, TCI Europe, VWR and ABCR. Dry solvents were purchased or purified with absorbent-filled columns in a solvent purification system (SPS). Monitoring of reactions were performed with thin layer chromatography using silica coated aluminium plates (Merck, silica 60, fluorescence indicator F_{254}, thickness 0.25 mm). For column chromatography, silica (Merck, silica 60, 0.02-0.063 mesh ASTM) was used as the stationary phase. UV-Vis spectra were obtained using a DAD HP-8453 UV-Vis spectrometer. High resolution Electrospray ionization (ESI) mass spectra were obtained using a Bruker ESI timsTOF (trapped ion mobility-time of flight) and Compact mass spectrometers (positive and negative mode). Samples were diluted with HPLC-grade acetonitrile. NMR spectra were recorded on Bruker AVANCE III 500, 600 and 700 MHz spectrometers. Chemical shifts were reported in ppm with residual solvent as reference: DMSO-d_6 (2.50 ppm for ^{1}H, 39.52 ppm for ^{13}C), $CDCl_3$ (7.26 ppm for ^{1}H, 77.16 ppm for ^{13}C). Abbreviations for signal multiplicity in the ^{1}H NMR spectra were indicated as: s, singlet; d, doublet; t, triplet; dd, doublets of doublets; m, multiplet; b, broad.

3.7.2 Deprotonation of carboxylic acids

The (di)carboxylic acids were dissolved in a small amount of MeOH (up to 5 mL), and one or two equivalents of TBA-hydroxide (1 M in MeOH) were added, depending on whether it was a mono- or dicarboxylic acid. Afterward, the mixture was vortexed for 30 min and the solvent was evaporated. A small amount of water (1-2 mL) was added to the remaining slurry residue to assist the final lyophilization process. The TBA-dicarboxylates were used without further purification. The TBA-salts of chloride and azide were commercially available.

3.7.3 Titration procedure

All preliminary qualitative NMR binding studies were performed at 500 µM in DMSO-d_6 with a Bruker NEO 500. All quantitative binding studies were performed dilution corrected. Binding constants were determined by ^{1}H NMR titration experiments, if not mentioned differently. The obtained data was fitted by BindFit[91,85].

3.7.4 Synthetic procedure of 3-(azidomethyl)-quinolin-8-yl-t-butyl-carbonate

Synthesis of 8-methy-3-methylquinoline

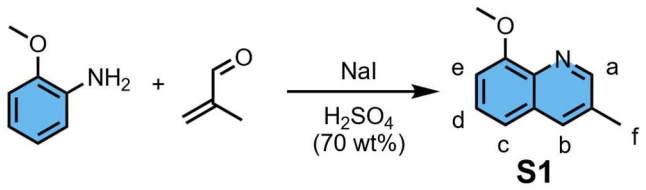

Figure 3.18: o-Anisidine and methacrolein in a SKRAUP-type reaction, which gives 8-methoxy-3-methylquinoline.

The synthesis of 8-methoxy-3-methylquinoline (**S1**) has been described in the literature and was followed accordingly.[88,76] First, sodium iodide (78.7 mg, 525 µmol, 1.5 mol%) and sulfuric acid (70%wt, 17.5 mL, 0.5 M) were mixed in a two neck round bottom flask, then *o*-anisidine (3.95 mL, 35 mmol, 1 equiv.) was added to the mixture and heated to 110°C. Once the reaction mixture reached 110°C and began refluxing, methacrolein (4.73 mL, 56 mmol, 1.6 equiv.) was added dropwise over a period of three hours. After the addition of methacrolein, the mixture was refluxed for three hours and then stirred at room temperature for an additional 16 h. The mixture was neutralized with a sat. $NaHCO_3$ solution and extracted with dichloromethane (2x). The combined organic layers were dried ($MgSO_4$) and the solvent was evaporated. Column chromatography (silica, pentane/EtOAc 1:1 to 1:2) gives 8-methoxy-3-methylquinoline (**S1**) as brown solid (75%, 4.53 g, 26.2 mmol).

^{1}H NMR (500 MHz, $CDCl_3$, 25°C): δ = 8.77 (d, *J* = 2.1 Hz, 1H, a), 7.88-7.85 (m, 1H, b), 7.41 (t, *J* = 8.0 Hz, 1H, d), 7.29 (dd, *J* = 8.2, 0.9 Hz, 1H, c), 6.97 (dd, *J* = 7.7, 1.2 Hz, 1H, e), 4.07 (s, 3H, OMe), 2.49 (s, 3H, f) ppm.

Synthesis of t-butyl-(3-methylquinolin-8-yl)-carbonate

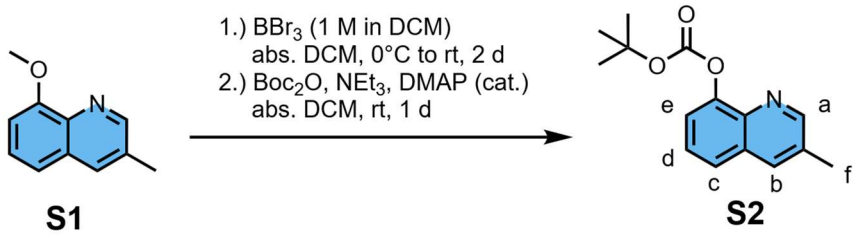

Figure 3.19: The methoxy moiety was deprotected with BBr_3, followed by the addition of the Boc protecting group using Boc anhydride.

The synthesis of *t*-butyl-(3-methylquinolin-8-yl)-carbonate (**S2**) is described in the literature and was followed accordingly.[76,88] 8-Methoxy-3-methylquinoline (**S1**, 2.08 g, 12.00 mmol, 1 equiv.) was transferred to a Schlenk tube and placed under argon atmosphere. **S1** was dissolved in dry dichloromethane (34.2 mL, 0.35 M) and the solution was cooled in an ice bath. Boron tribromide (1 M in DCM, 24.0 mL, 24.0 mmol, 2 equiv.) was added dropwise over 30 minutes to the cooled solution. Afterward, the reaction mixture was stirred at room temperature for two days. Then, the reaction mixture was quenched with water and neutralized with a sat. $NaHCO_3$ solution. Extraction with dichloromethane (5x), drying of the combined organic layers over magnesium sulfate and evaporation of the solvent under reduced pressure gives 3-methylquinolin-8-ol as brownish/red solid which was used without further purification. 3-Methylquinolin-8-ol was transferred into a Schlenk tube with dry dichloromethane (90 mL) under an argon atmosphere. Then, DMAP (220 mg, 1.8 mmol, 15 mol%), Boc-anhydride (3.14 g, 14.40 mmol, 1.2 equiv.) were added sequentially to the reaction mixture, followed by triethylamine (8.32 mL, 60.0 mmol, 5 equiv.). The mixture was stirred for one day at room temperature, washed with brine and the organic layer was dried over magnesium sulfate. Evaporation of the solvent under reduced pressure and purification via column chromatography (silica, pentane/EtOAc 6:1) gives *t*-butyl-(3-methylquinolin-8-yl)-carbonate (**S2**) as a brownish oil which becomes solid in the fridge (74%, 2.30 g, 8.87 mmol).

^{1}H NMR (500 MHz, $CDCl_3$, 25°C): δ = 8.79 (d, *J* = 2.1 Hz, 1H, a), 7.93 (s, 1H, b), 7.63 (dd, *J* = 8.0, 1.6 Hz, 1H, c), 7.48 (t, *J* = 7.7 Hz, 1H, d), 7.45 (dd, *J* = 7.5, 1.6 Hz, 1H, e), 2.51 (s, 3H, f), 1.60 (s, 9H, *t*Bu) ppm.

Synthesis of 3-(bromomethyl)-quinolin-8-yl-t-butyl-carbonate

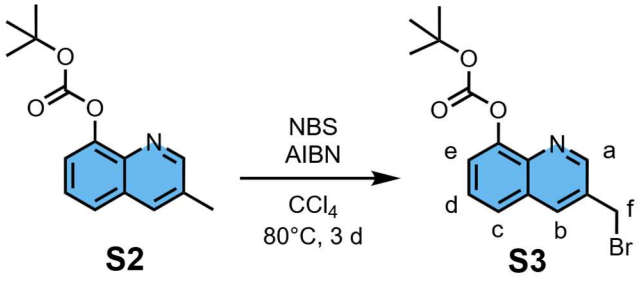

Figure 3.20: Radical bromination of the methyl substituent at position three of the precursor was performed using NBS as the bromine source and AIBN as the radical initiator.

The synthesis of 3-(bromomethyl)quinolin-8-yl-*t*-butyl-carbonate (**S3**) is described in the literature and was followed accordingly.[76,88] **S2** (519 mg, 2.00 mmol, 1 equiv.), NBS (356 mg, 2.00 mmol, 1 equiv.) and AIBN (16.4 mg, 0.10 mmol, 5 mol%) were put into a pressure tube, dissolved in CCl_4 (40 mL, 0.05 M) and the reaction mixture was stirred at 80°C for 48 h. Afterward, the reaction mixture was filtrated while still being hot. The filtrate was collected and the solvent was removed under reduced pressure. Column chromatography (silica, pentane/Et_2O 6:1) gives 3-(bromomethyl)quinolin-8-yl-*t*-butyl-carbonate (**S3**) as yellowish solid (59%, 396 mg, 1.17 mmol).
^{1}H NMR (600 MHz, $CDCl_3$, 25°C): δ = 8.95 (d, *J* = 2.2 Hz, 1H, a), 8.17 (d, *J* = 2.1 Hz, 1H, b), 7.70 (dd, *J* = 7.4, 2.2 Hz, 1H, c), 7.57-7.52 (m, 2H, d, e), 4.64 (s, 2H, f), 1.61 (s, 9H, *t*Bu) ppm.

Synthesis of 3-(azidomethyl)-quinolin-8-yl-t-butyl-carbonate

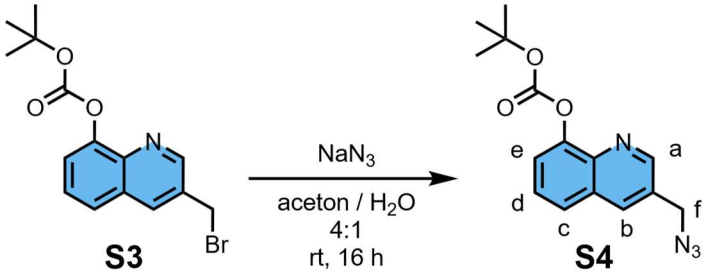

Figure 3.21: Nucleophilic substitution of the bromomethyl moiety with azide was carried out using sodium azide.

The synthesis of 3-(azidomethyl)quinolin-8-yl-*t*-butyl-carbonate (**S4**) is described in the literature and was followed accordingly.[76] **S3** (385.6 mg, 1.14 mmol, 1 equiv.) was transferred to a round bottom flask and dissolved in acetone (15 mL). Next, NaN_3 (111 mg, 1.71 mmol, 1.5 equiv.) was dissolved in 2 mL water and added to the reaction mixture, which was then stirred at room temperature overnight. The reaction mixture was washed with brine (2x), the organic layer was dried ($MgSO_4$) and the solvent was evaporated under reduced pressure. Column chromatography (silica, pentane / diethyl ether 4:1) gives 3-(azidomethyl)quinolin-8-yl-*t*-butyl-carbonate (**S4**) as colorless oil which becomes a colorless solid the fridge (99%, 338.8 mg, 1.13 mmol).
^{1}H NMR (500 MHz, $CDCl_3$, 25°C): δ = 8.88 (d, *J* = 2.2 Hz, 1H, a), 8.12 (d, *J* = 2.1 Hz, 1H, b), 7.73 (dd, *J* = 7.1, 2.5 Hz, 1H, c), 7.59-7.52 (m, 2H, d, e), 4.58 (s, 2H, f), 1.60 (s, 9H, *t*Bu) ppm.

3.7.5 Synthetic procedure of ligand L^{mN3}-H_2

Synthesis of 3,5-dibromo-*N*-(naphthalen-2-yl)benzamide

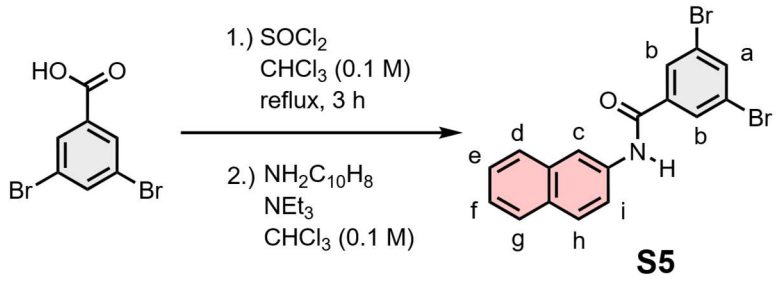

*Figure 3.22: Synthesis of the mono-substituted amide **S5** via a SCHOTTEN-BAUMANN reaction.*

3,5-dibromobenzoic acid (2.6 g, 9.3 mmol, 1 equiv.) and $SOCl_2$ (19.8 mL, 279.3 mmol, 30 equiv.) were dissolved in 100 mL of $CHCl_3$ (0.1 M) and refluxed for 3 h. The solvent was evaporated under vacuum on a Schlenk line, with a cold trap placed between the vacuum pump and the sample, so that excess $SOCl_2$ could subsequently be quenched. The remaining solid was dissolved in $CHCl_3$ and then, naphthalen-2-amine (4 g, 27.9 mmol, 3 equiv.) and NEt_3 (7.8 mL, 55.8 mmol, 6 equiv.) were dissolved in $CHCl_3$ (0.1 M) and added to the reaction mixture and refluxed for 4 days. The reaction mixture was diluted with DCM and a white solid was obtained by precipitation. The solid was filtered, washed with DCM and dried under vacuum. The mono-substituted amine **S5** was obtained as white solid (44%, 1.67 g, 4.1 mmol).

^{1}H NMR (500 MHz, DMSO-d_6, 25°C) δ = 10.62 (s, bs, 1H, NH), 8.27 (d, *J* = 1.8 Hz, 2H, b), 8.12 (t, *J* = 1.8 Hz, 1H, a), 8.05 - 7.96 (m, 2H, d, g), 7.87 (d, *J* = 8.1 Hz, 1H, i), 7.61 (dd, *J* = 7.3, 1.3 Hz, 1H, c), 7.58-7.53 (m, 3H, e, f, h) ppm. **^{13}C NMR** (126 MHz, DMSO-d_6, 25°C) δ = 163.37, 138.28, 136.20, 133.75, 133.61, 129.83, 129.03, 128.04, 126.42, 126.12, 126.02, 125.54, 123.76, 123.38, 122.64 ppm. **HRMS** (positive ESI-MS, ACN): m/z = 427.9062 ([M+Na$^+$], $C_{17}H_{11}Br_2NONa^+$, calc. 427.9080), 832.8251 ([2M+Na$^+$], $(C_{17}H_{11}Br_2NO)_2Na^+$, calc. 832.8270).

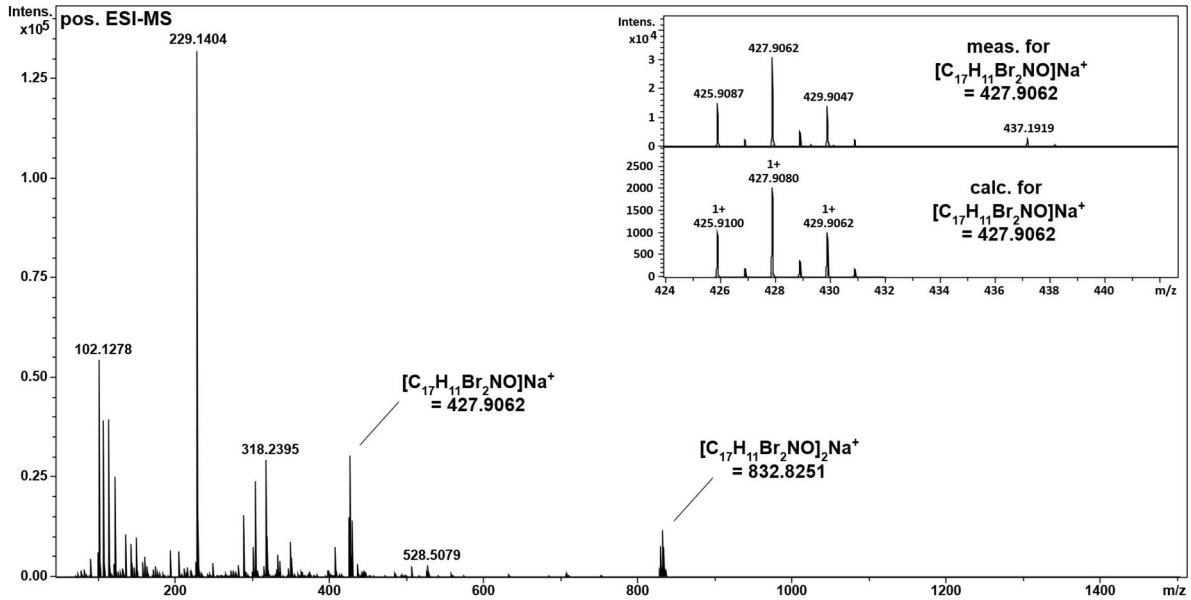

*Figure 3.23: Positive ESI-MS spectrum of the mono-substituted amine **S5** in ACN, representing the corresponding isotopic patterns and m/z values as adducts with sodium cations.*

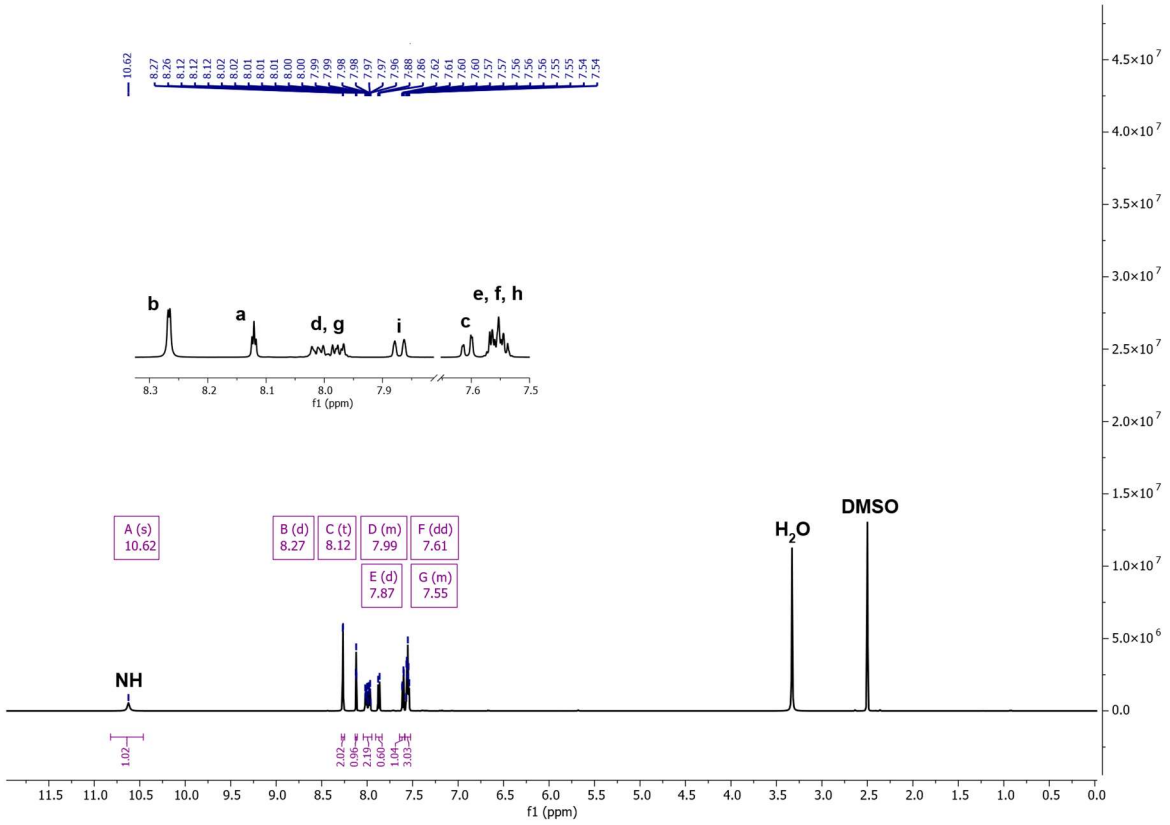

*Figure 3.24: ^{1}H NMR of the mono-substituted amide **S5** (DMSO-d_6, 500 MHz, 25°C).*

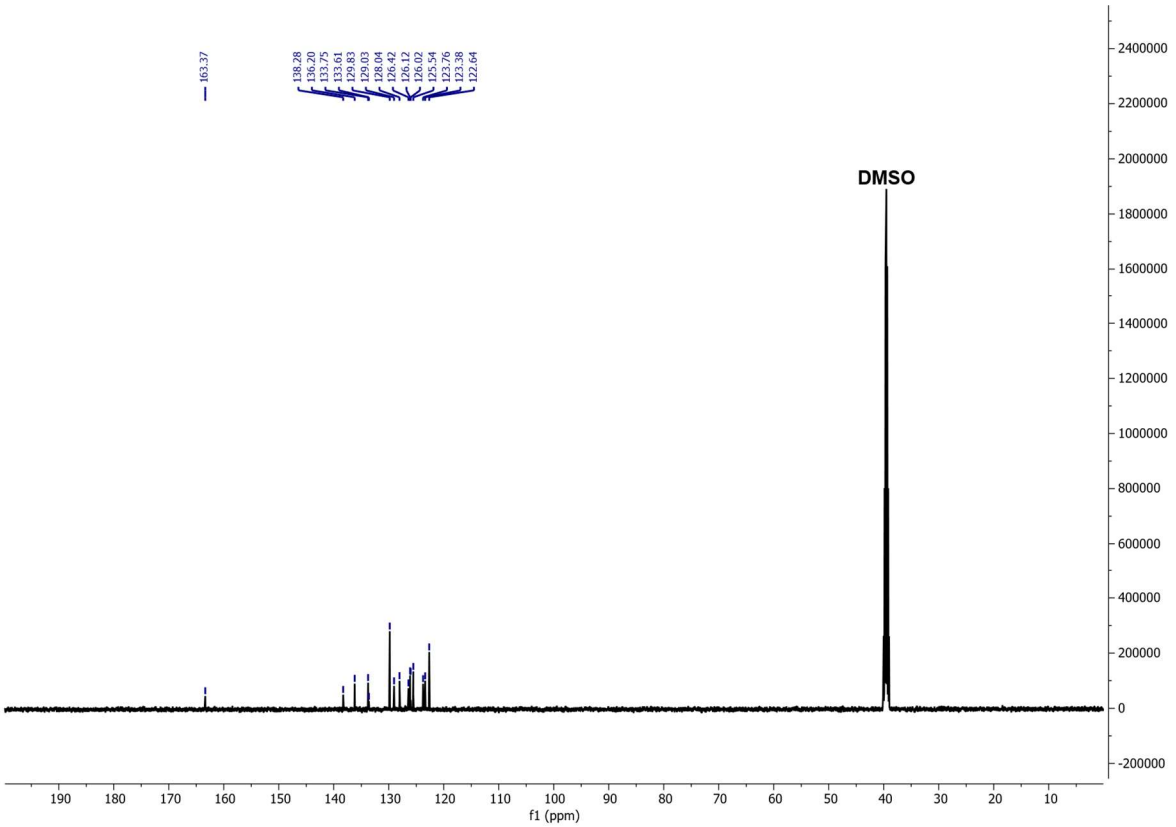

*Figure 3.25: ^{13}C NMR of the mono-substituted amide **S5** (DMSO-d_6, 126 MHz, 25°C).*

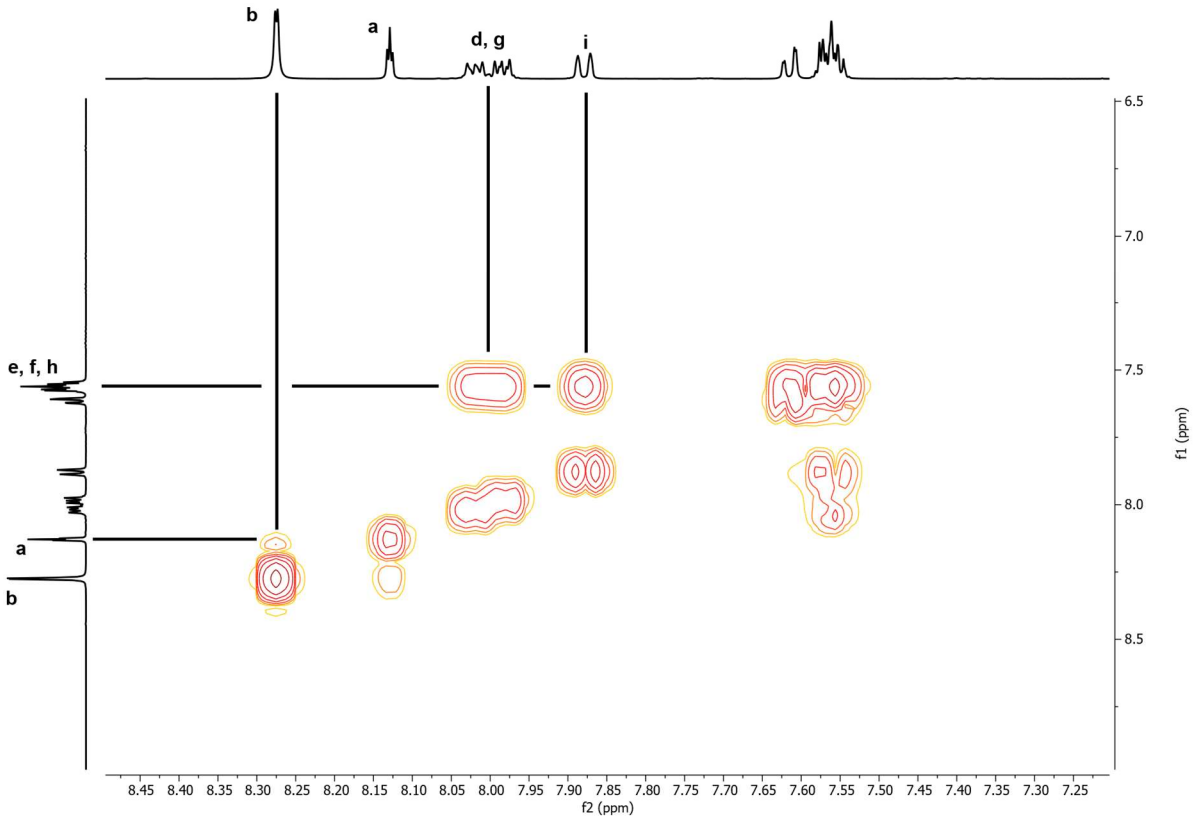

*Figure 3.26: ^{1}H COSY NMR of the mono-substituted amide **S5** (DMSO-d_6, 500 MHz, 25°C).*

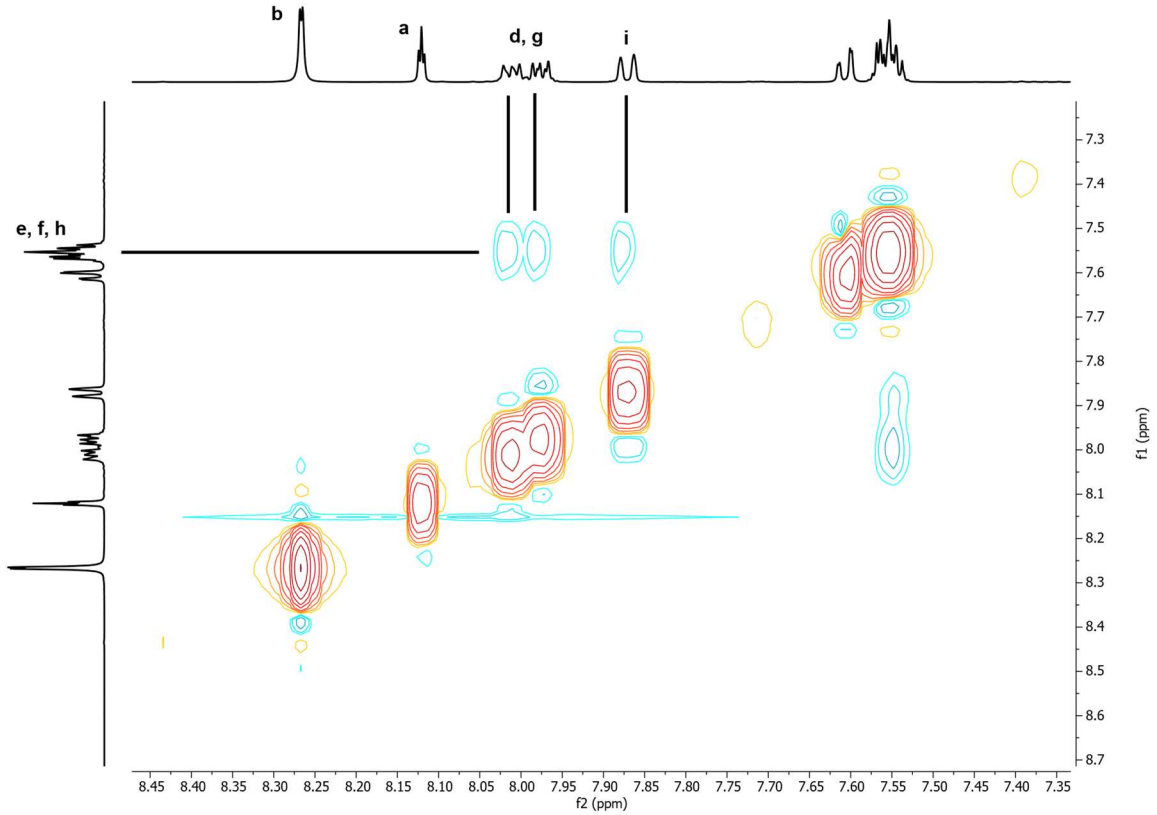

*Figure 3.27: ^{1}H NOESY NMR of the mono-substituted amide **S5** (DMSO-d_6, 500 MHz, 25°C).*

Synthesis of *N*-(naphthalen-2-yl)-3,5-bis((trimethylsilyl)ethynyl)benzamide

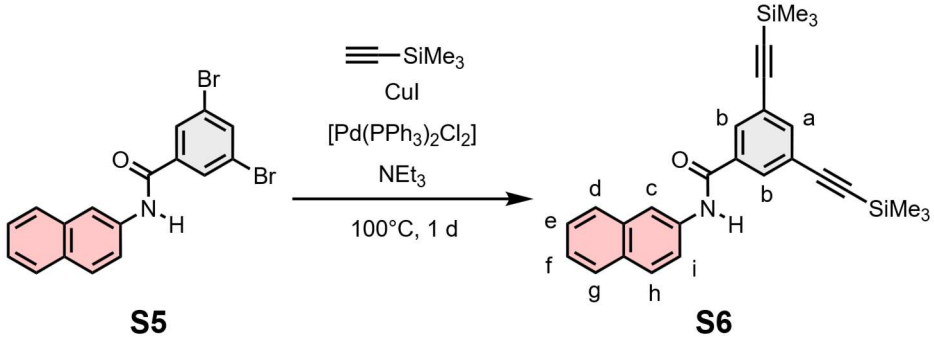

*Figure 3.28: Synthesis of the TMS protected acetylene intermediate **S6** via SONOGASHIRA coupling.*

S5 (50 mg, 0.123 mmol, 1 equiv.) and $[Pd(PPh_3)_2Cl_2]$ (8.66 mg, 0.012 mmol, 0.1 equiv.) were dissolved in 1.7 mL NEt_3. After three freeze pump thaws were performed, CuI (2.35 mg, 0.012 mmol, 0.1 equiv.) and TMS-acetylene (70 µL, 0.5 mmol, 4 equiv.) were added sequentially. The reaction mixture was stirred at 100°C for 1 day under an argon atmosphere. Afterward, the reaction mixture was diluted with DCM, transferred in a separation funnel and washed with NH_4Cl and brine. The organic layer was dried with $MgSO_4$ and the solvent was evaporated. Column chromatography (silica, pentane/Et_2O 25:1) gives the product **S6** as a yellowish solid (66%, 25.5 mg, 81.1 µmol).

^{1}H NMR (600 MHz, DMSO-d_6, 25°C) δ = 10.58 (s, 1H, NH), 8.15 (d, *J* = 1.5 Hz, 2H, b), 8.02-7.95 (m, 2H, c, i), 7.88 (dd, *J* = 7.1, 2.4 Hz, 1H, h), 7.74 (d, *J* = 1.6 Hz, 1H, a), 7.60-7.51 (m, 4H, d, g, e, f), 0.26 (s, 18H, TMS) ppm. **^{13}C NMR** (151 MHz, DMSO-d_6, 25°C) δ = 164.2995, 136.8676, 135.3910, 133.7712, 133.4913, 131.0706, 129.1152, 128.0580, 126.5660, 126.1365, 126.0446, 125.5455, 124.0055, 123.4342, 123.0944, 103.1874, 96.2936, -0.2462 ppm. **HRMS** (positive ESI-MS, ACN): m/z = 404.1821 ($[M+H^+]$, $C_{27}H_{29}NOSi_2H^+$, calc. 404.1860), 462.1633 ($[M+Na^+]$, $C_{27}H_{29}NOSi_2Na^+$, calc. 462.1680).

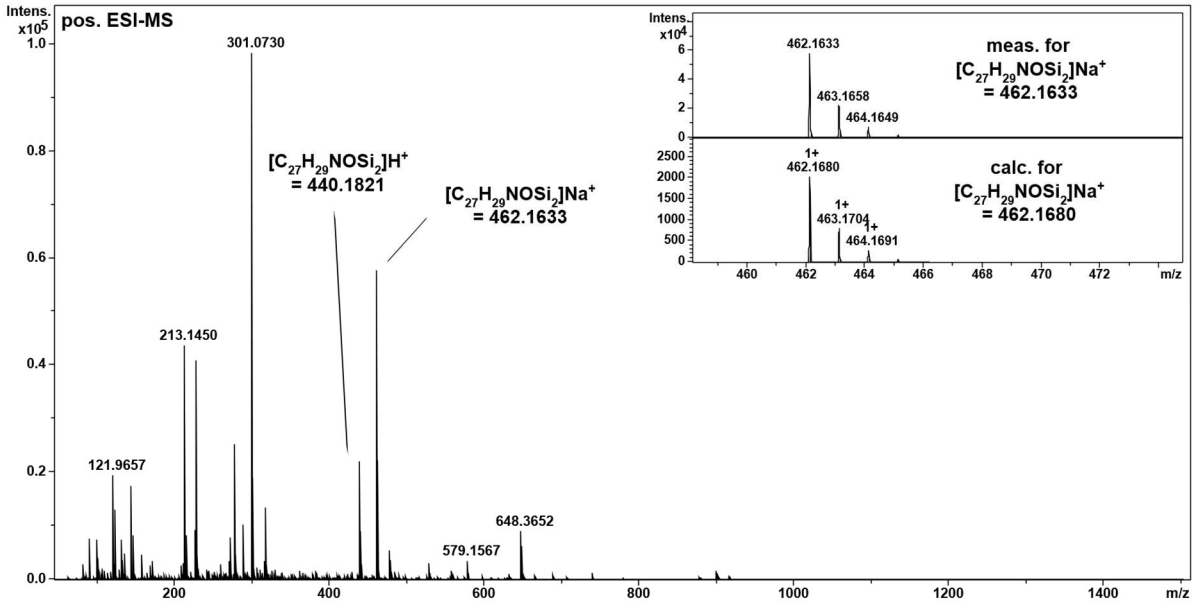

*Figure 3.29: Positive ESI-MS spectrum of the TMS protected acetylene intermediate **S6** in ACN, representing the corresponding isotopic patterns and m/z values as adducts with sodium and hydrogen cations.*

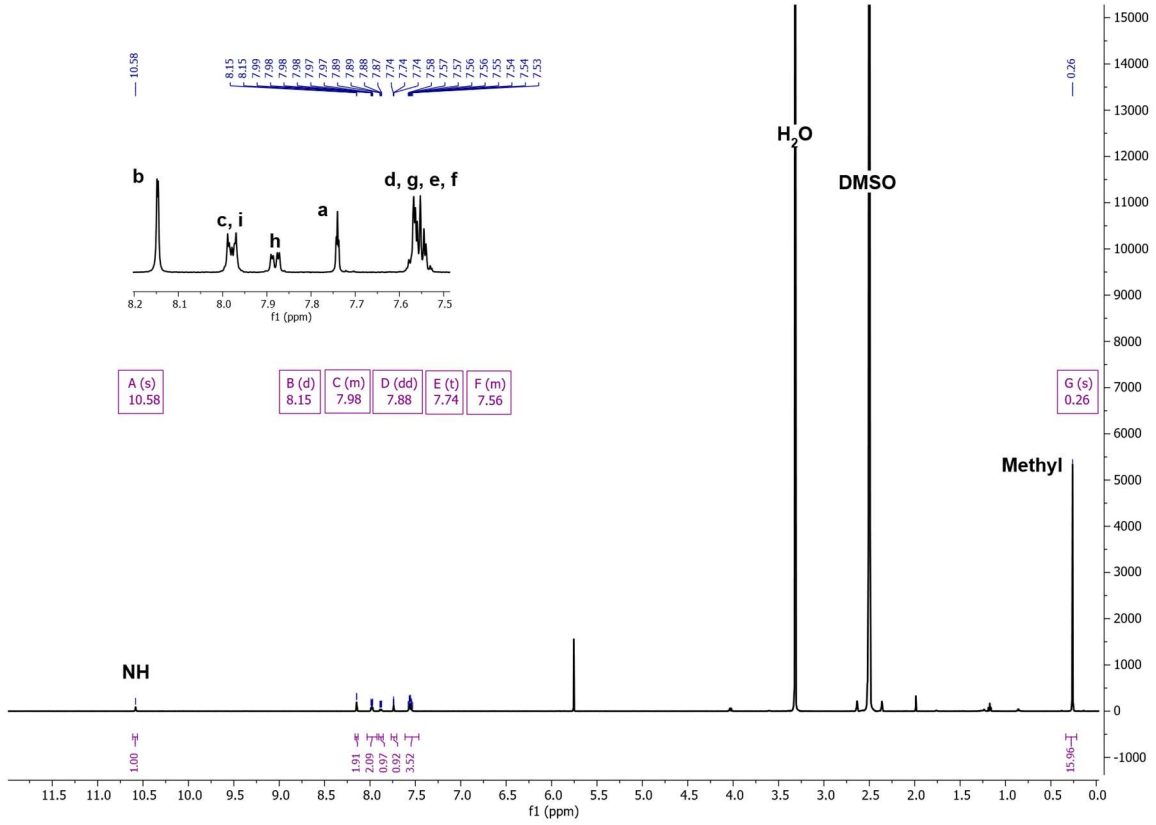

*Figure 3.30: ^{1}H NMR of the TMS protected acetylene intermediate **S6** (DMSO-d_6, 500 MHz, 25°C).*

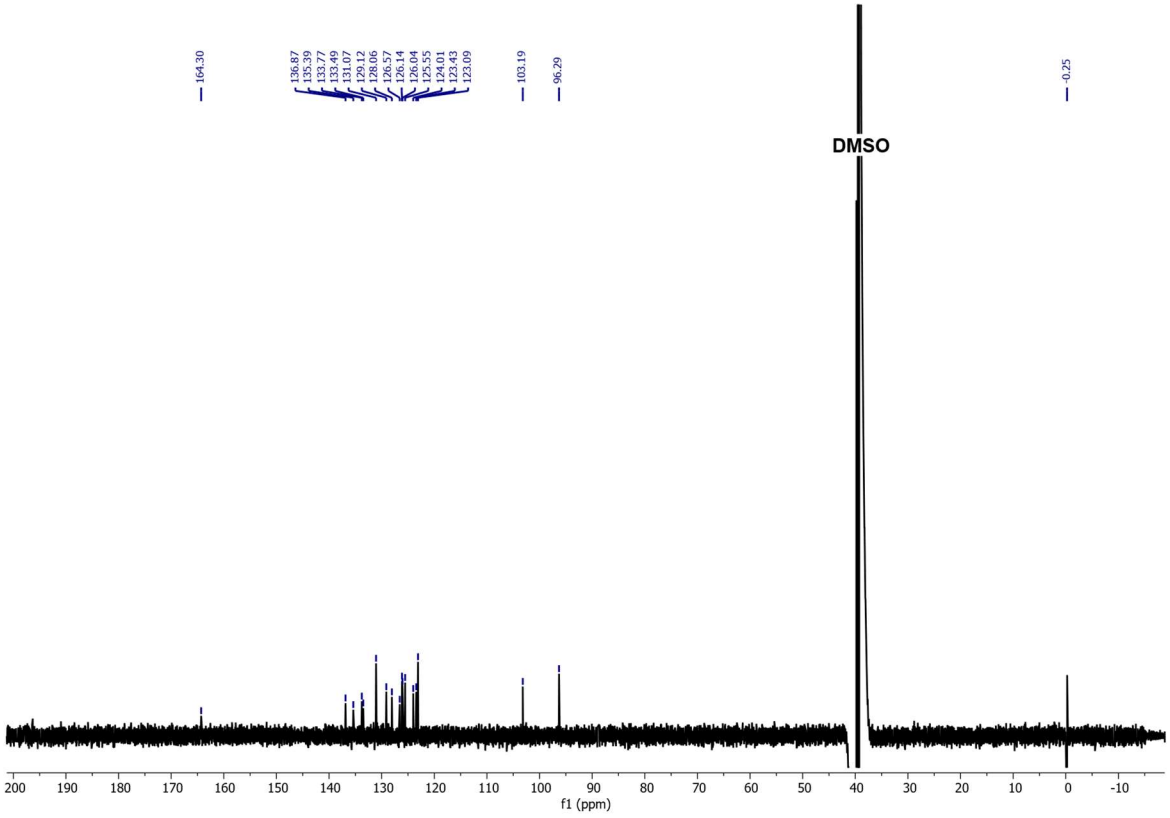

*Figure 3.31: ^{13}C NMR of the TMS protected acetylene intermediate **S6** (DMSO-d_6, 151 MHz, 25°C).*

Synthesis of 3,5-diethynyl-*N*-(naphthalen-2-yl)benzamide

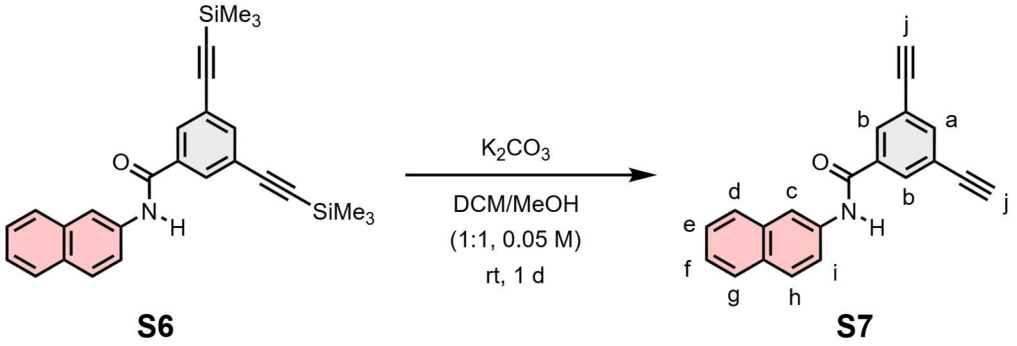

S6 **S7**

*Figure 3.32: Synthesis of the acetylene intermediate **S7** via removal of the silyl substituent.*

Compound **S6** (31.4 mg, 71.4 µmol, 1 equiv.) was dissolved in a mixture of DCM and MeOH (1:1), then K_2CO_3 (59.2 mg, 428 µmol, 6 equiv.) was added to the stirring solution. The dispersion was stirred at room temperature overnight. Afterward, the reaction solution was diluted with DCM and washed with water (2x). The organic layer was dried with MgSO4 and the solvent was evaporated under reduced pressure. Column chromatography (silica, pentane/Et_2O 20:1) gives the product **S7** as beige solid (81%, 17.1 mg, 57.9 µmol).

^{1}H NMR (600 MHz, DMSO-d_6, 25°C) δ = 10.60 (s, 1H, NH), 8.19 (s, 2H, b), 8.03 - 7.96 (m, 2H, d, g), 7.88 (d, *J* = 8.1 Hz, 1H, i), 7.82 (t, *J* = 1.4 Hz, 1H, a), 7.61 (d, *J* = 7.2 Hz, 1H, c), 7.59 - 7.53 (m, 3H, e, f, h), 4.42 (s, 2H, j) ppm. **^{13}C NMR** (151 MHz, DMSO-d_6, 25°C) δ = 164.36, 137.06, 135.45, 133.75, 133.41, 131,31, 129.04, 128.05, 126.52, 126.13, 126.06, 125.52, 123.91, 123.35, 122.68, 82.58, 81.79 ppm. **HRMS** (positive ESI-MS, ACN): m/z = 318.0853 ([M+Na$^+$], $C_{21}H_{13}NONa^+$, calc. 318.0889), 613.1807 ([2M+Na$^+$], $(C_{21}H_{13}NO)_2Na^+$, calc. 613.1886).

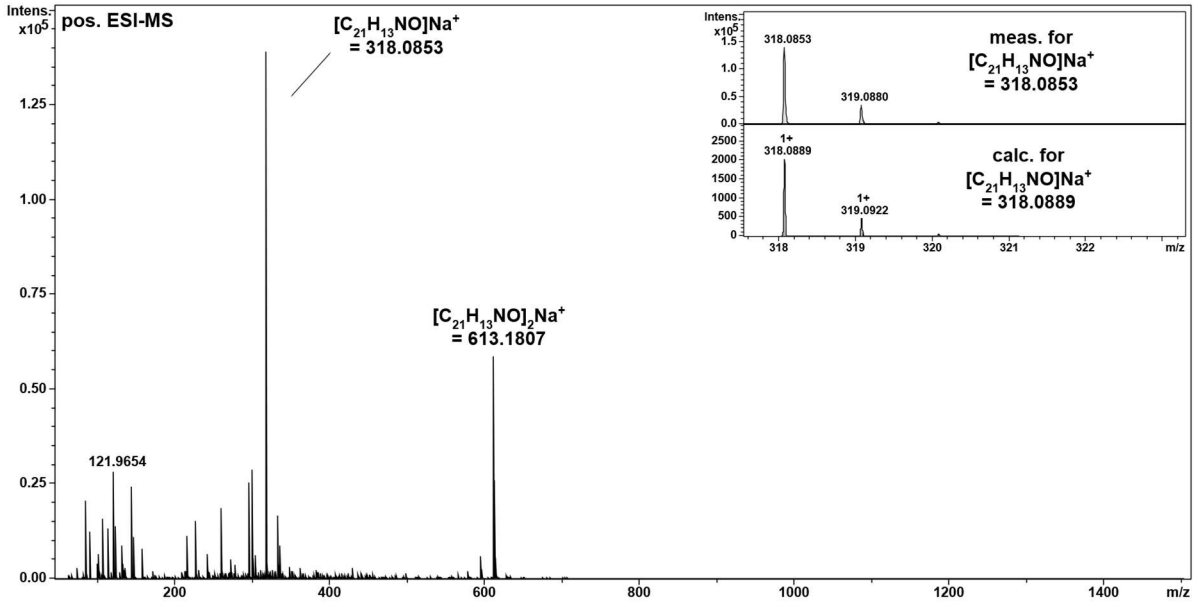

*Figure 3.33: Positive ESI-MS spectrum of the acetylene intermediate **S7** in ACN, representing the corresponding isotopic patterns and m/z values as adducts with sodium cations.*

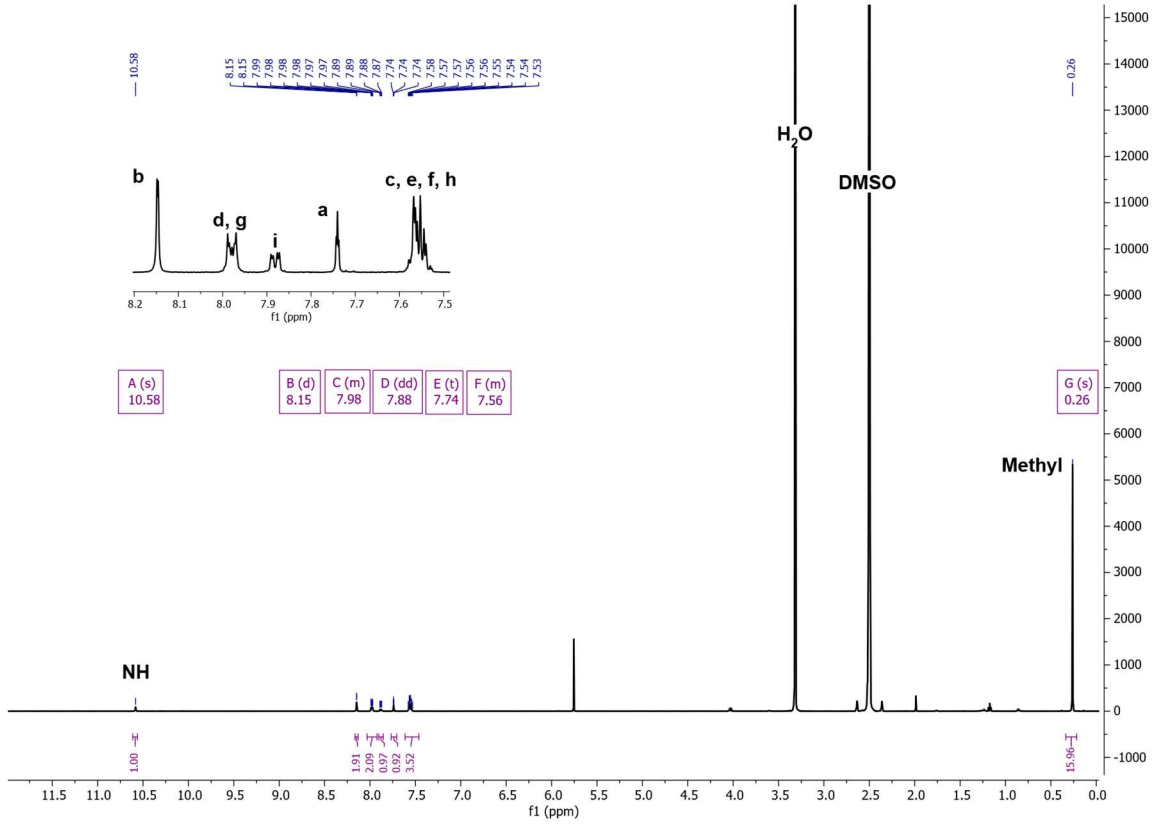

*Figure 3.34: ^{1}H NMR of the acetylene intermediate **S7** (DMSO-d_6, 600 MHz, 25°C).*

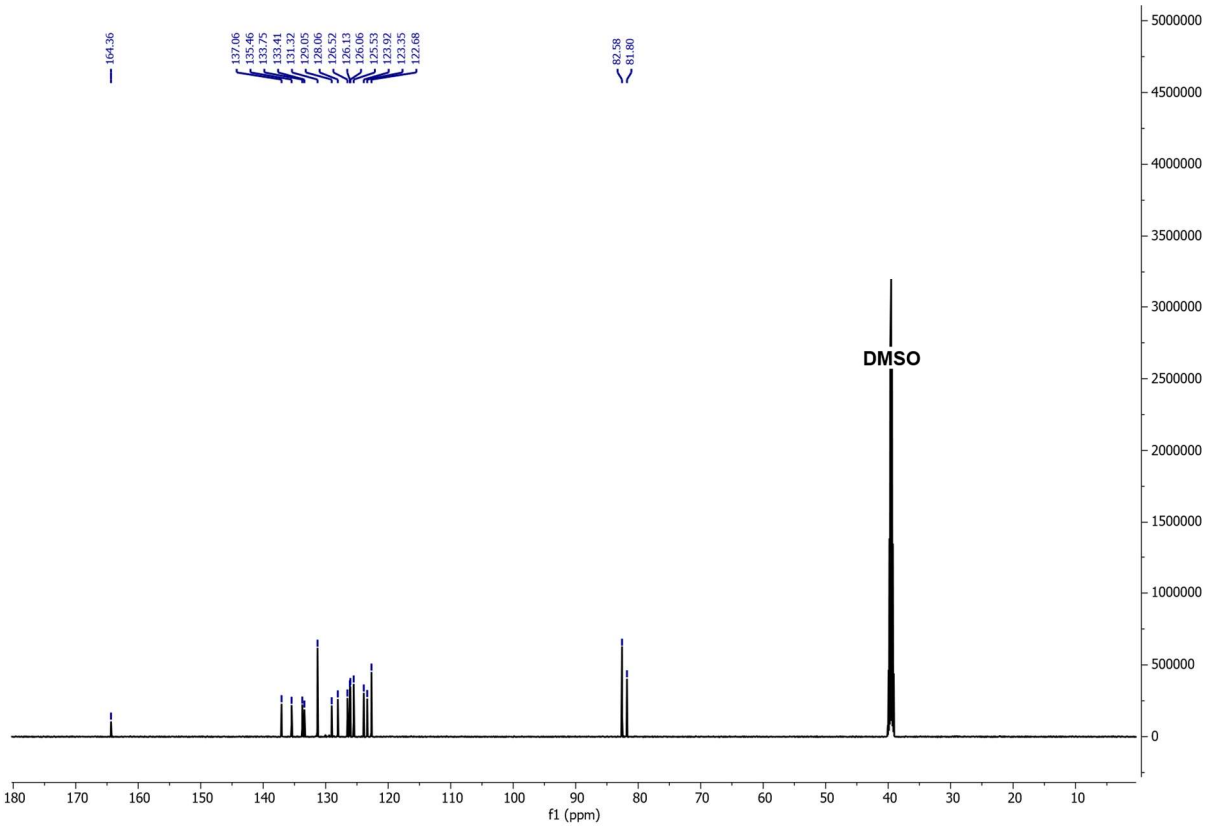

*Figure 3.35: ^{13}C NMR of the acetylene intermediate **S7** (DMSO-d_6, 151 MHz, 25°C).*

Synthesis of the BOC protected ligand L^{mN3}

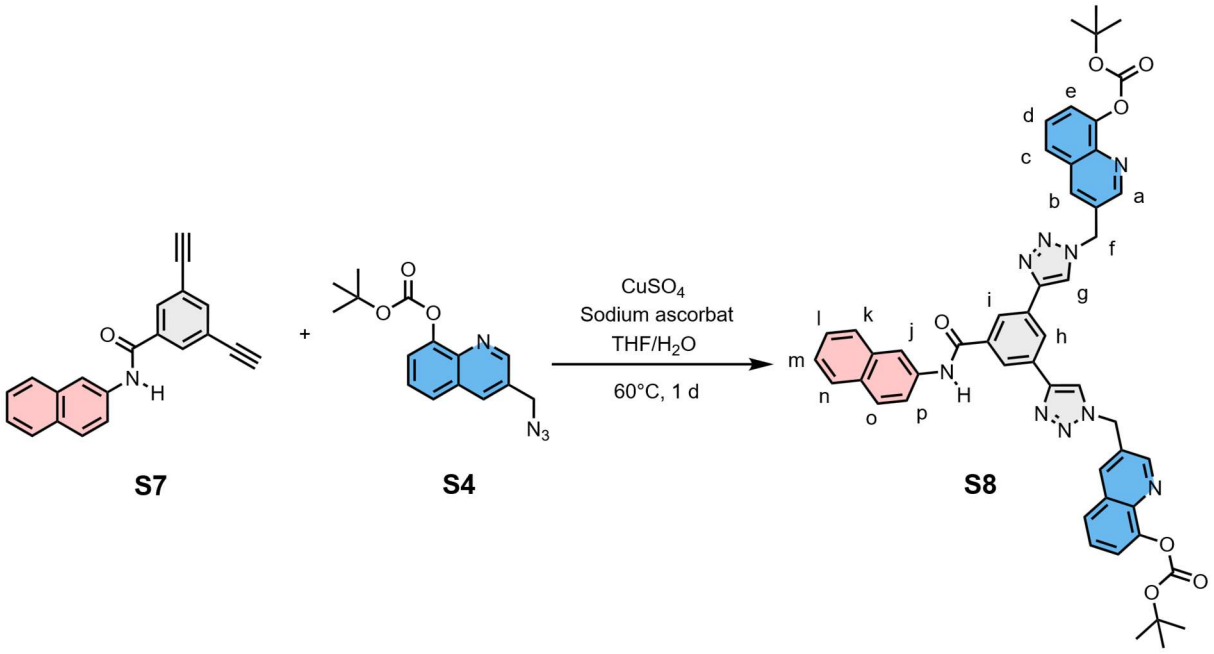

*Figure 3.36: 1,3-dipolar HUISGEN cycloaddition of di-alkyne **S7** and azide **S4** gave the Boc-protected ligand **S8**.*

The azide **S4** (50.1 mg, 166.9 µmol, 2.2 equiv.) was transferred into a Schlenk tube and dissolved in THF. The solution was degassed for 20 min with argon. $CuSO_4$ (0.6 mg, 3.8 µmol, 0.05 equiv.) and sodium-ascorbate (60.1 mg, 303.4 µmol, 4 equiv.) were dissolved in small amounts of water and added sequentially. Backbone **S7** (22.4 mg, 75.8 µmol, 1 equiv.) was added under argon, the solution was heated to 60 °C and stirred for 16 h. The reaction solution was diluted with DCM and the organic layer was washed with EDTA (0.25 M), brine and saturated NH_4Cl solution. The aqueous layer was extracted with DCM (3x). The combined organic layers were dried with Na_2SO_4 and the solvent was evaporated under reduced pressure. Column chromatography (silica, DCM/MeOH gradient 0 % - 3 %) yielded the Boc-protected derivative **S8** as white solid (37.3 mg, 41.6 µmol, 55%).

^{1}H NMR (600 MHz, DMSO-d_6, 25°C) δ = 10.60 (s, 1H, NH), 9.00 (d, *J* = 2.1 Hz, 2H, i), 8.91 (s, 2H, g), 8.60 (t, *J* = 1.6 Hz, 1H, h), 8.50 (d, *J* = 1.6 Hz, 2H, a), 8.43 (d, *J* = 2.1 Hz, 2H, b), 8.02 - 7.96 (m, 2H, j, p), 7.94 (dd, *J* = 8.0, 1.7 Hz, 2H, c), 7.88 (d, *J* = 8.1 Hz, 1H, o), 7.66-7.58 (m, 5H, d, e, k), 7.59-7.52 (m, 3H, l, m, n), 5.98 (s, 4H, f), 1.48 (s, 18H, *t*Bu) ppm. **^{13}C NMR** (151 MHz, DMSO-d_6, 25°C) δ = 165.83, 151.14, 150.59, 146.81, 146.10, 140.05, 136.00, 135.41, 133.78, 131.52, 129.74, 129.16, 128.49, 128.08, 127.09, 126.42, 126.19, 126.09, 126.00, 125.58, 124.60, 124.06, 123.91, 123.38, 122.56, 121.49, 83.05, 54.91, 50.76, 27.25. **HRMS** (positive ESI-MS, DCM): m/z = 448.6696 ([M+2H$^+$], $C_{51}H_{47}N_9O_7^{2+}$, calc. 448.6794), 896.3310 ([M+H$^+$], $C_{51}H_{46}N_9O_7^+$, calc. 896.3515).

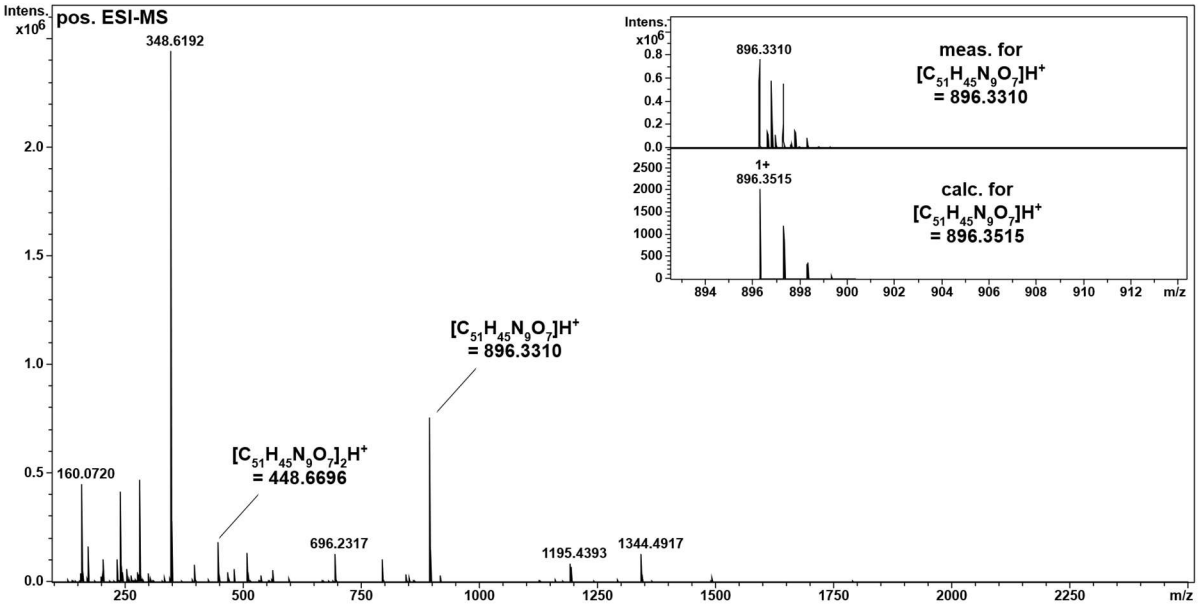

*Figure 3.37: Positive ESI-MS spectrum of the BOC protected ligand **S8** in DCM.*

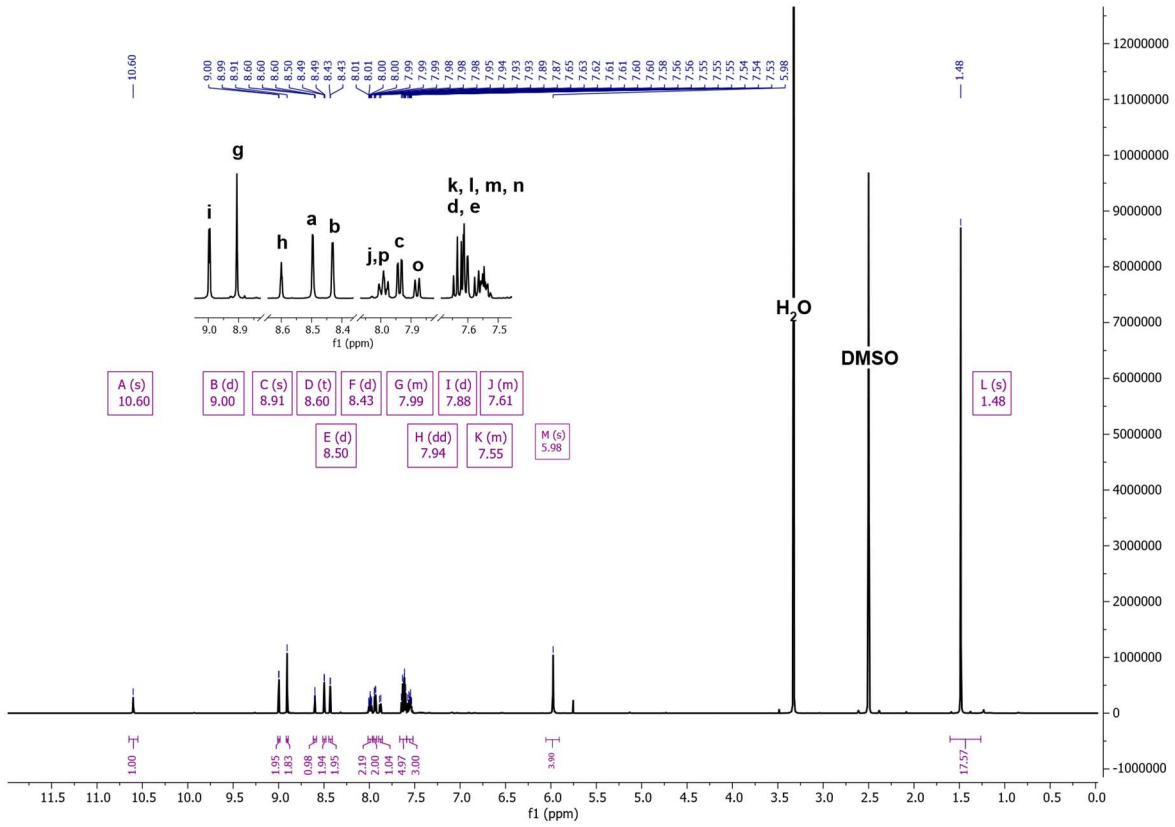

*Figure 3.38: ^{1}H NMR spectrum of the BOC protected ligand **S8** (DMSO-d_6, 600 MHz, 25°C).*

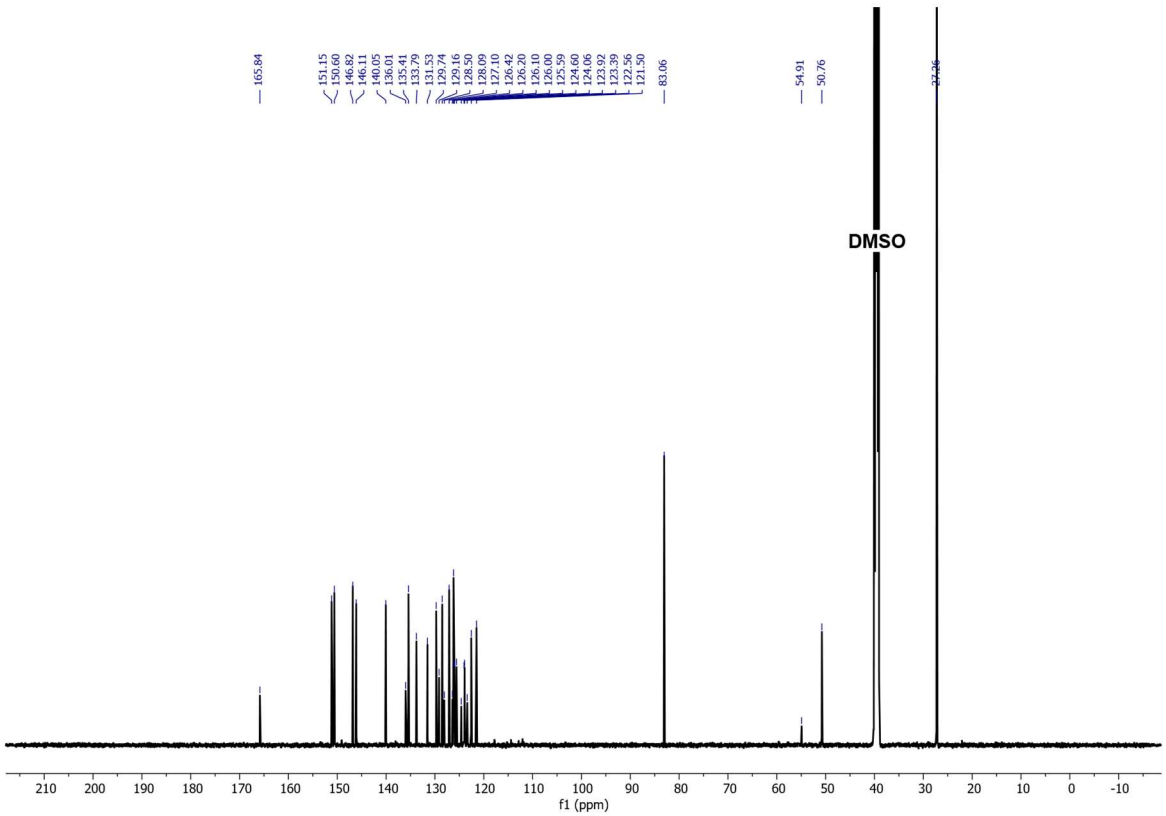

*Figure 3.39: ^{13}C NMR of the BOC protected ligand **S8** (DMSO-d_6, 151 MHz, 25°C).*

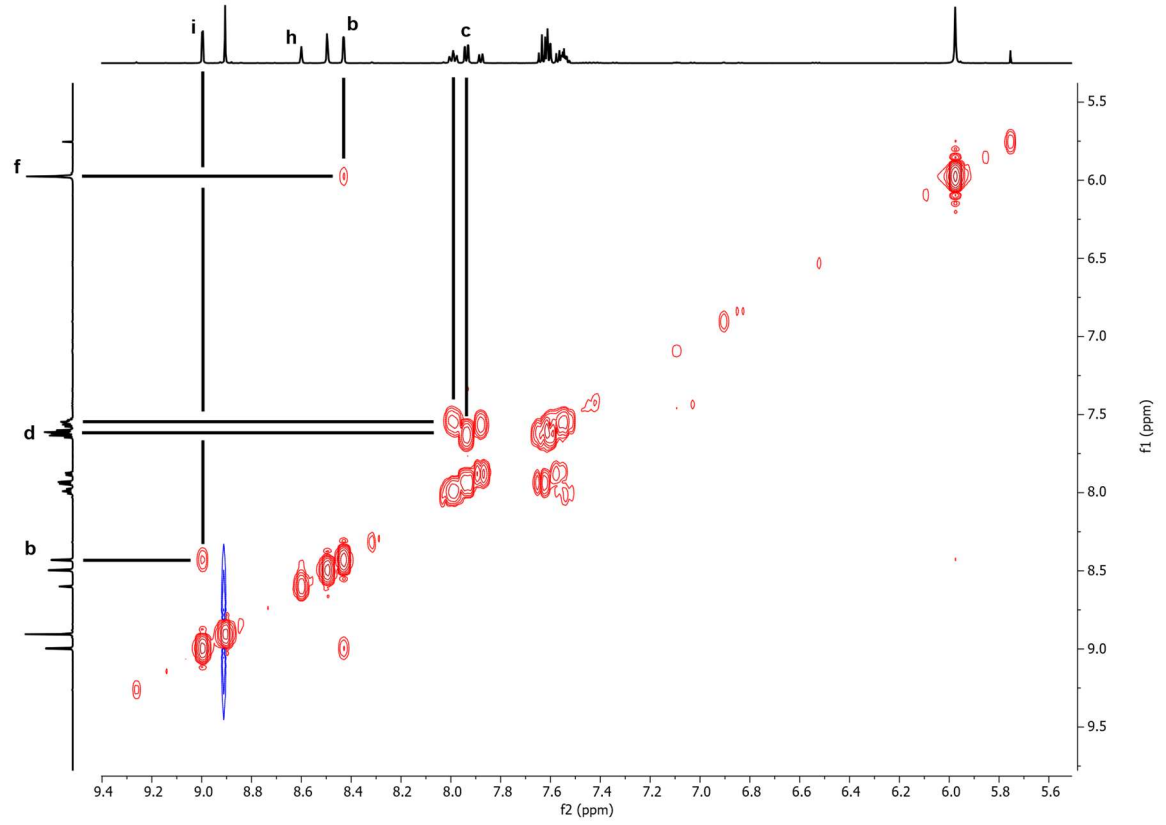

*Figure 3.40: ^{1}H COSY NMR of the BOC protected ligand **S8** (DMSO-d_6, 600 MHz, 25°C).*

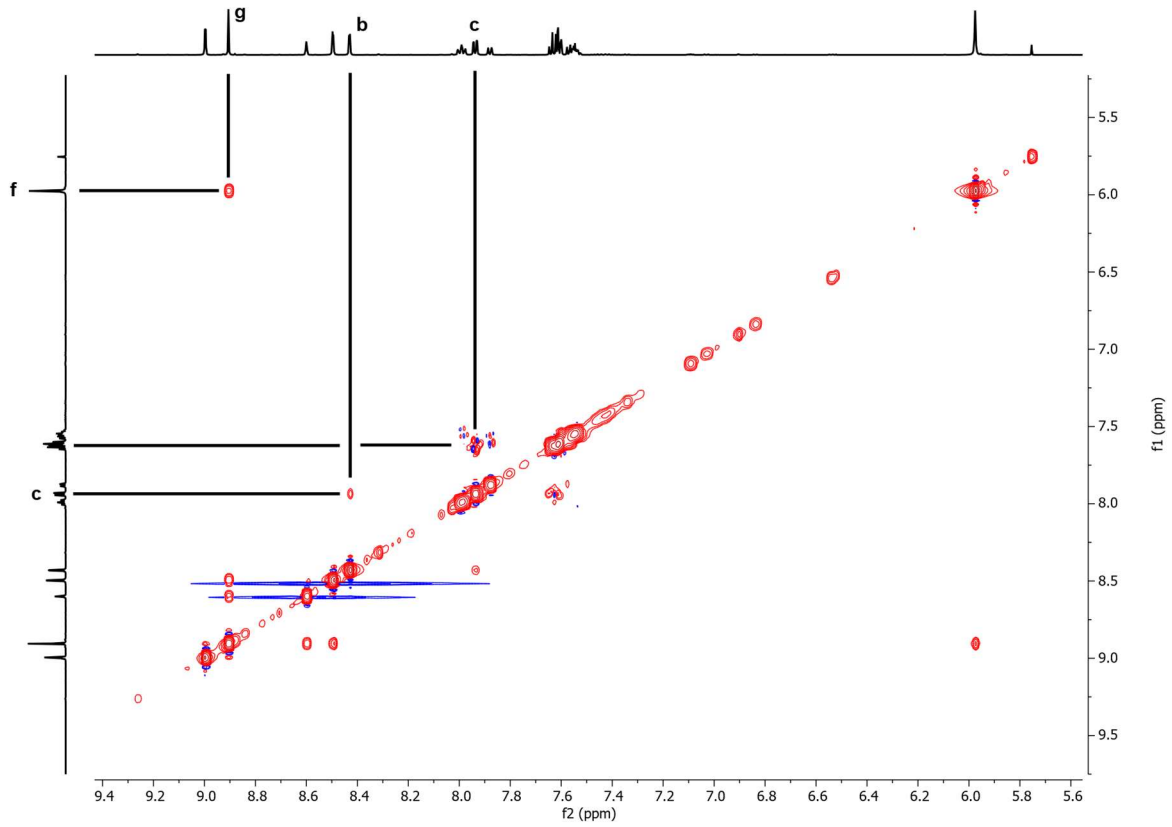

*Figure 3.41: ^{1}H NOESY NMR of the BOC protected ligand **S8** (DMSO-d_6, 600 MHz, 25°C).*

Synthetic procedure of the ligand L^{mN3}-H_2

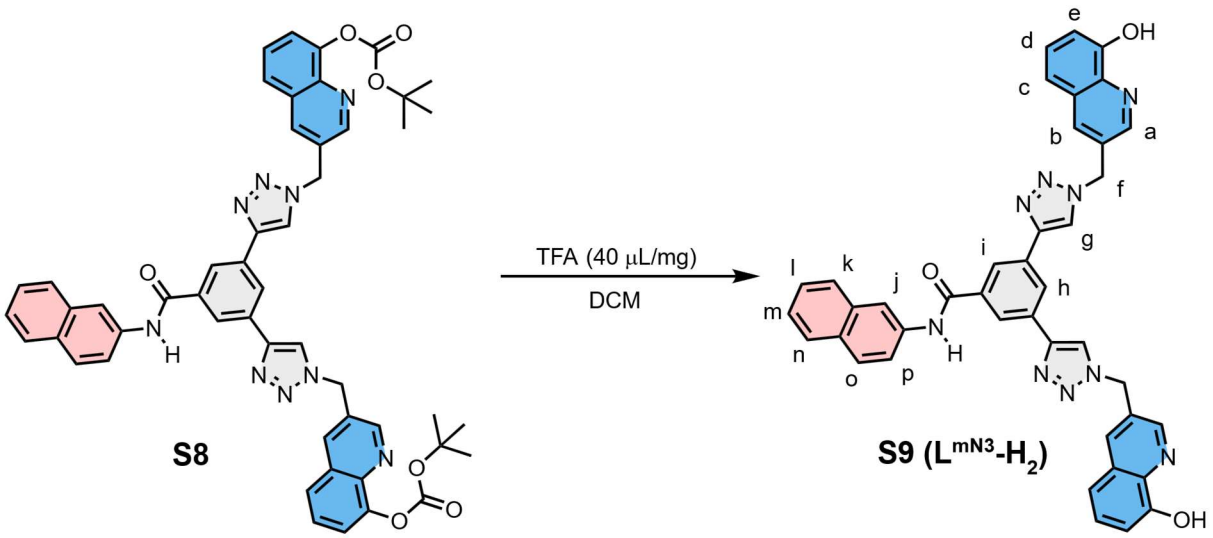

*Figure 3.42: Boc-deprotection of **S8** with TFA gave ligand **S9** (L^{mN3}-H_2).*

The BOC-protected derivative **S8** (10 mg, 11.2 µmol, 1 equiv.) was dissolved in DCM and treated with TFA (40 µL/mg). After 1 h the reaction mixture was neutralized with sat. $NaHCO_3$. As soon as the reaction mixture reached a pH of around 7, the product **S9** precipitated as yellow solid. The reaction mixture was decantated and the yellow solid was washed with water. The yellow solid was redissolved in plenty of DCM, washed with brine and the organic layer was dried via Na_2SO_4. The solvent was evaporated until there was a residue organic layer present. Pouring Et_2O into the residue gives the ligand **S9** as a beige powder (99%, 7.7 mg, 11.1 µmol).

^{1}H NMR (600 MHz, DMSO-d_6, 25°C) δ = 10.60 (s, 1H, NH), 8.96 (d, *J* = 2.2 Hz, 2H, b), 8.88 (s, 2H, g), 8.60 (t, *J* = 1.6 Hz, 1H, h), 8.48 (d, *J* = 1.6 Hz, 2H, i), 8.41 (s, 2H, a), 8.01-7.97 (m, 2H, p, j), 7.88 (d, *J* = 8.0 Hz, 1H, o), 7.61-7.52 (m, 4H, k, l, m, n), 7.50 (t, *J* = 7.9 Hz, 2H, d), 7.45 (dd, *J* = 8.3, 1.4 Hz, 2H, c), 7.14 (dd, *J* = 7.5, 1.3 Hz, 2H, e), 5.97 (s, 4H, f) ppm. **^{13}C NMR** (151 MHz, DMSO-d_6, 25°C) δ = 165.82, 152.88, 147.83, 146.06, 136.01, 133.79, 133.77, 131.53, 129.32, 129.16, 128.52, 128.42, 128.10, 126.44, 126.11, 126.01, 125.59, 124.50, 124.05, 123.93, 123.37, 122.49, 117.92, 116.79, 114.85, 112.45, 50.77 ppm. **HRMS** (positive ESI-MS, ACN): m/z = 696.2320 ([M+H$^+$], $C_{41}H_{29}N_9O_3^+$, calc. 696.2466), 348.6196 ([M+2H$^+$], $C_{41}H_{29}N_9O_3^{2+}$, calc. 348.6269).

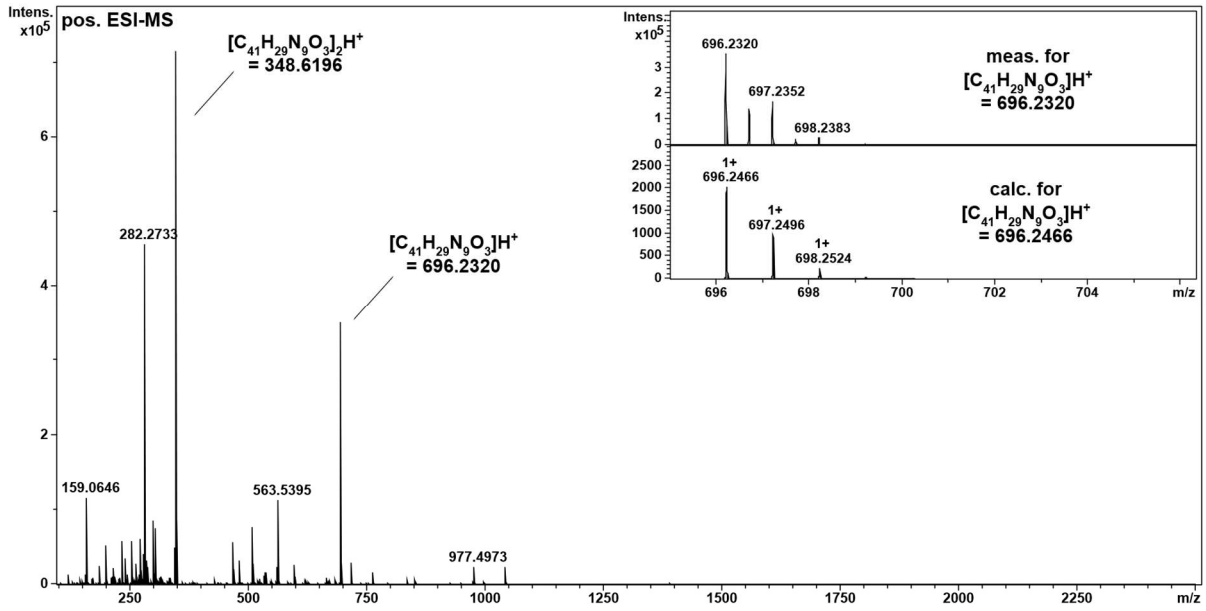

*Figure 3.43: Positive ESI-MS spectrum of the ligand **S9** (L^{mN3}-H_2) in DCM.*

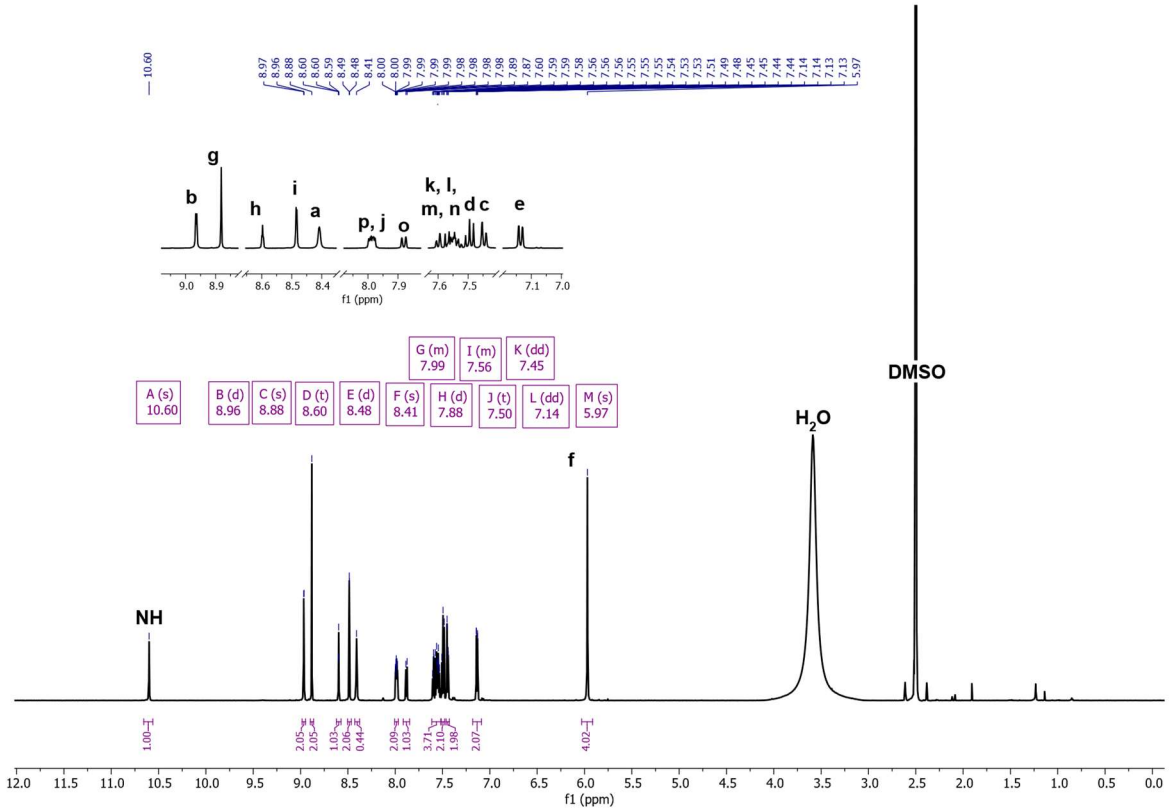

*Figure 3.44: ^{1}H NMR of the ligand **S9** (L^{mN3}-H_2) (DMSO-d_6, 600 MHz, 25°C).*

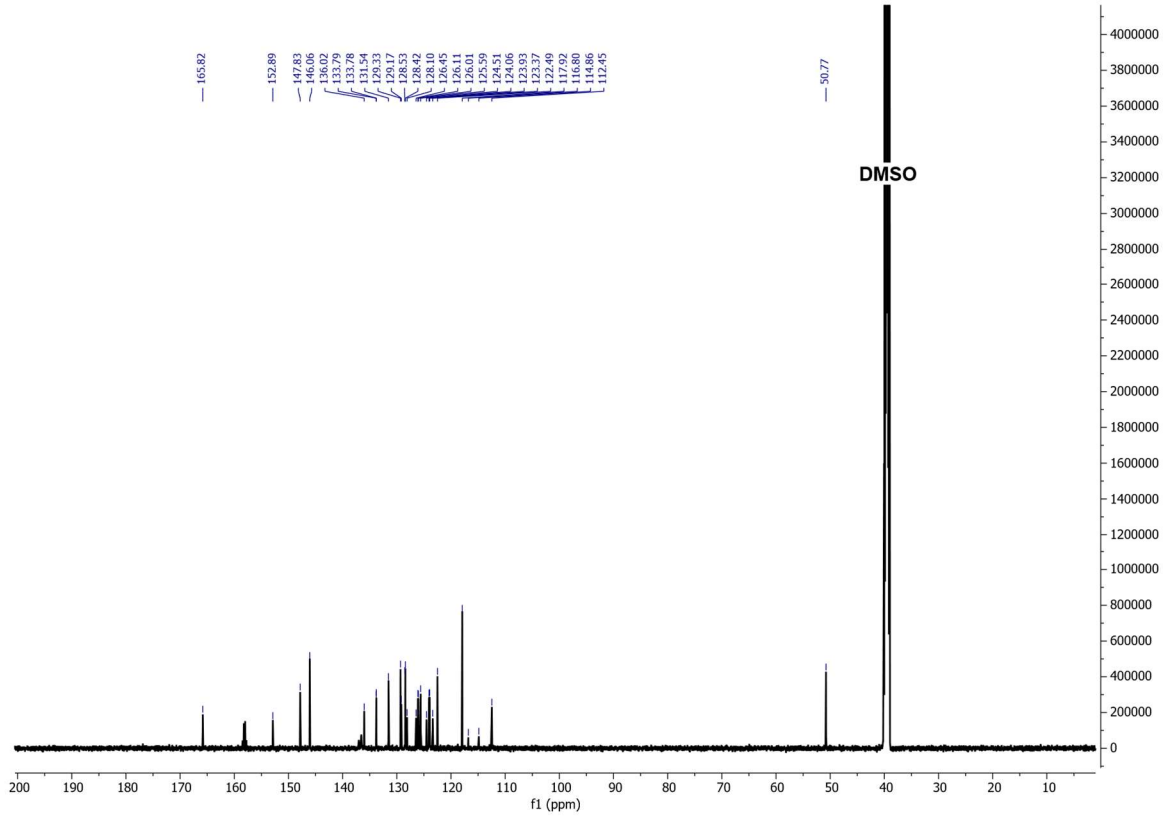

*Figure 3.45: ^{13}C NMR of the ligand **S9** (L^{mN3}-H_2) (DMSO-d_6, 600 MHz, 25°C).*

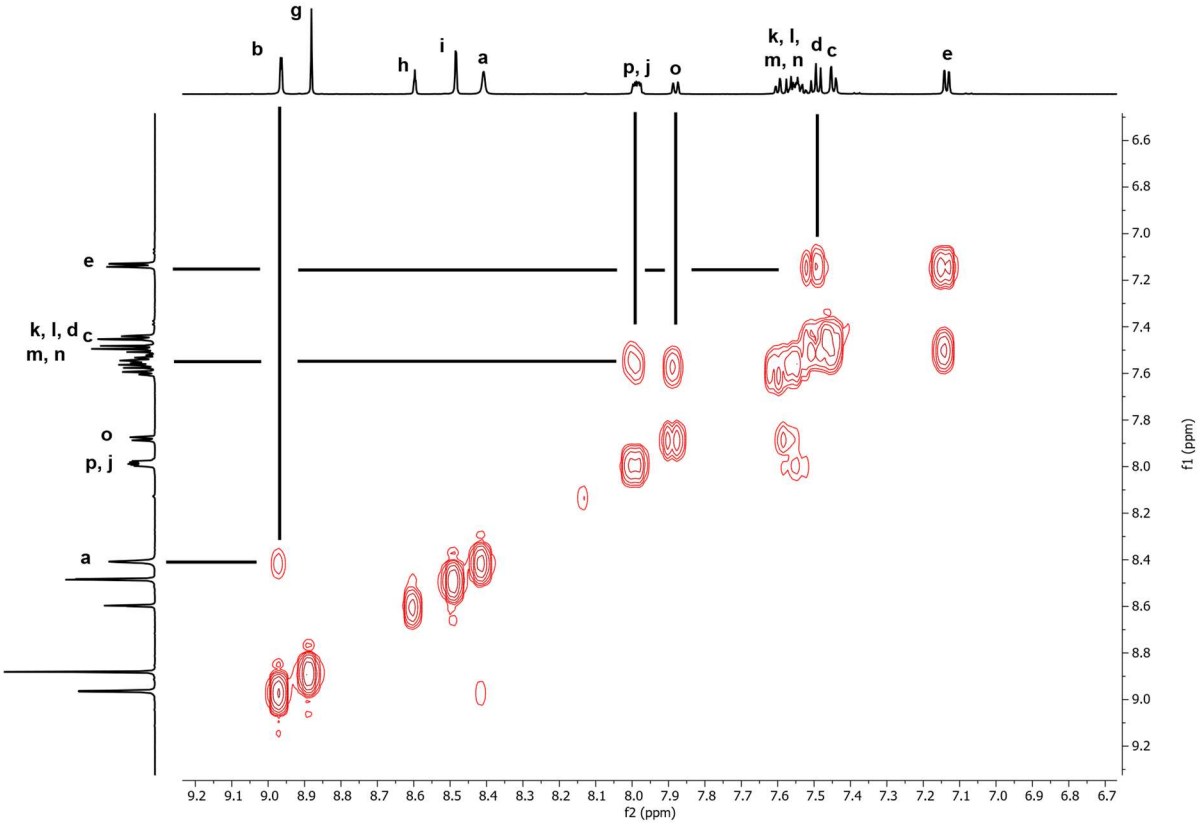

*Figure 3.46: ^{1}H COSY NMR of the ligand **S9** (L^{mN3}-H_2) (DMSO-d_6, 600 MHz, 25°C).*

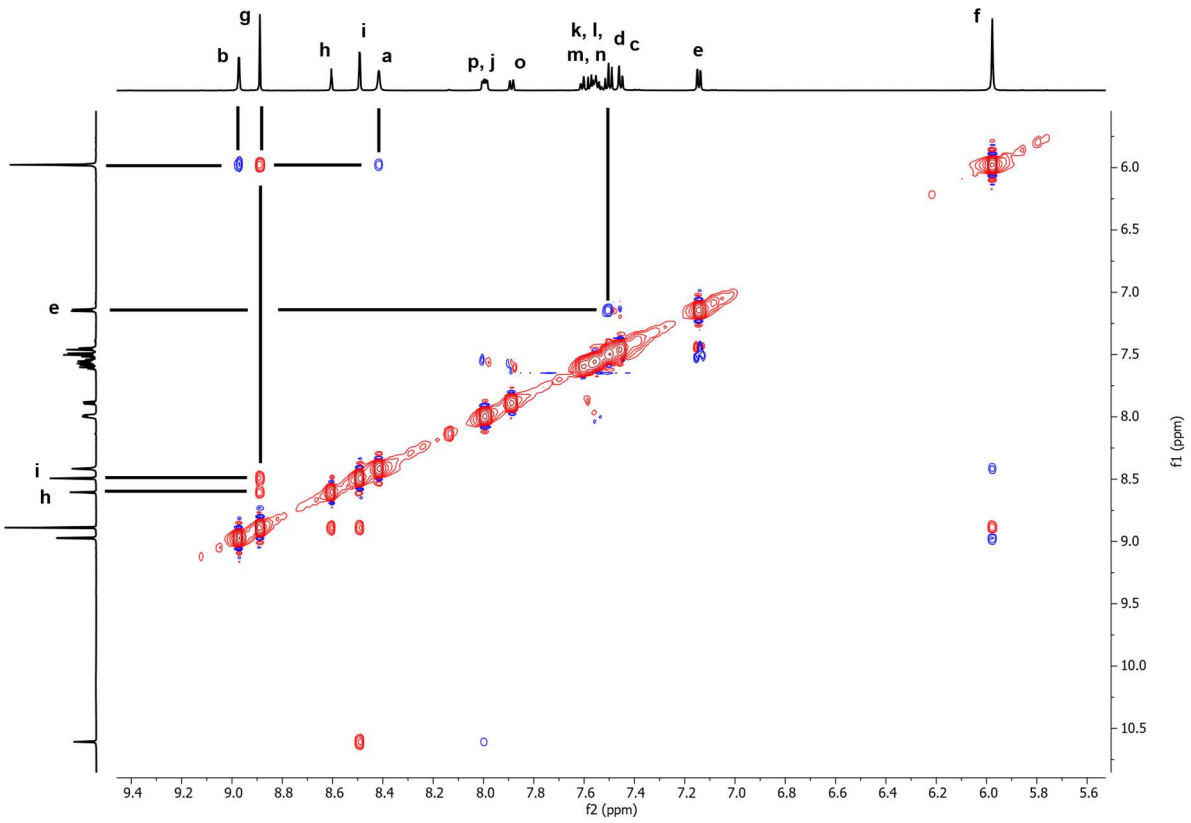

*Figure 3.47: ^{1}H NOESY NMR of the ligand **S9** (L^{mN3}-H_2) (DMSO-d_6, 600 MHz, 25°C).*

3.7.6 Self-assembly of ligand L^{mN3}-H_2 with $Zn_2(OAc)_2$

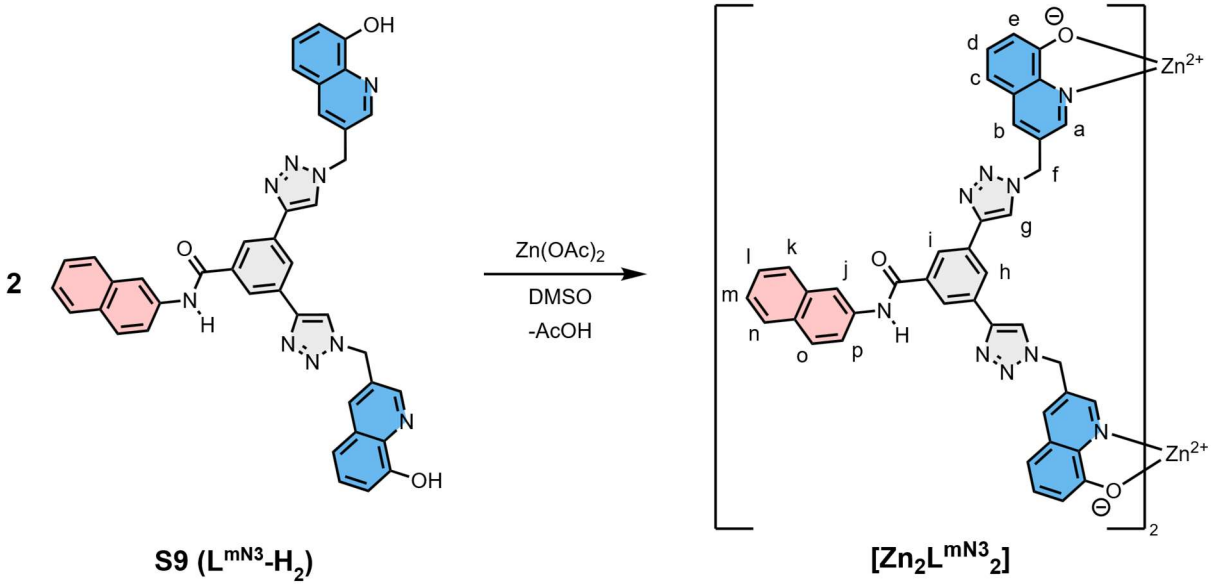

*Figure 3.48: Self-assembly of the ligand **S9** (L^{mN3}-H_2) and $Zn(OAc)_2$ in a 1:1 ratio.*

Ligand **S9** (L^{mN3}-H_2) (1 equiv.) and $Zn(OAc)_2$ (1 equiv.) were dissolved separately in DMSO-d_6.The zinc acetate solution was added to the stirring ligand solution which resulted in a colour change to yellow. After 1 h the solvent as well as the by-product acetic acid were removed via lyophilization, which yields the complex $[Zn_2L^{mN3}{}_2]$ as a yellow solid with quantitative yield.

^{1}H NMR (600 MHz, DMSO-d_6, 25°C) δ = 10.62 (s, 1H, NH), 8.78 (s, 2H, g), 8.62 (s, 2H, a), 8.51 (d, *J* = 1.4 Hz, 2H, i), 8.42 (m, 3H, b, h), 7.98 (d, *J* = 8.3 Hz, 2H, j, o), 7.88 (d, *J* = 8.0 Hz, 1H, p), 7.61-7.46 (m, 4H, k, l, m, n), 7.34 (t, *J* = 7.9 Hz, 2H, d), 6.87 (d, *J* = 8.0 Hz, 2H, c), 6.71 (d, *J* = 7.6 Hz, 2H, e), 5.96 (s, 4H, f) ppm. **HRMS** (positive ESI-MS, ACN): m/z = 1631.3523 ($[M+DMSO+Cl]^-$, $C_{82}H_{54}N_{18}O_6Zn_2SO(CH_3)_2Cl^-$, calc. 1631.2866).

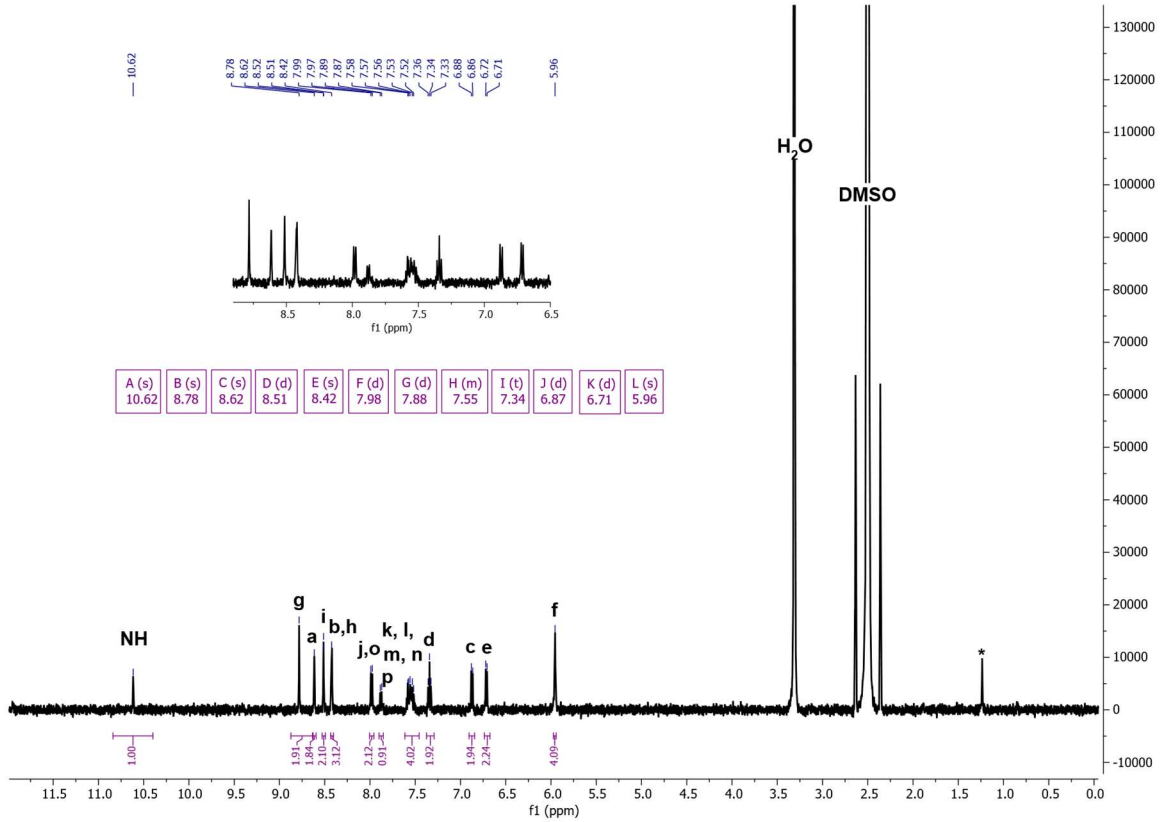

Figure 3.49: ^{1}H NMR spectrum of complex [$Zn_2L^{mN3}_2$] (DMSO-d_6, 600 MHz, 25°C).

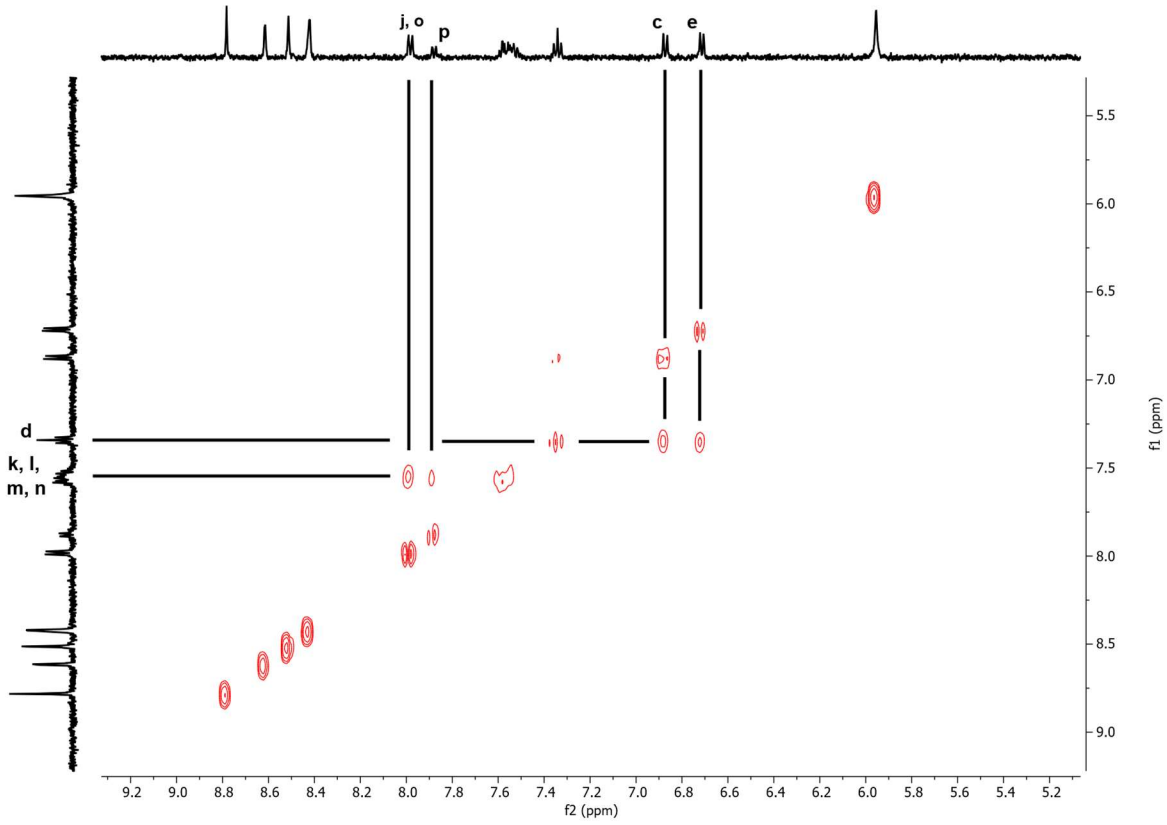

Figure 3.50: ^{1}H COSY NMR spectrum of complex [$Zn_2L^{mN3}_2$] (DMSO-d_6, 600 MHz, 25°C).

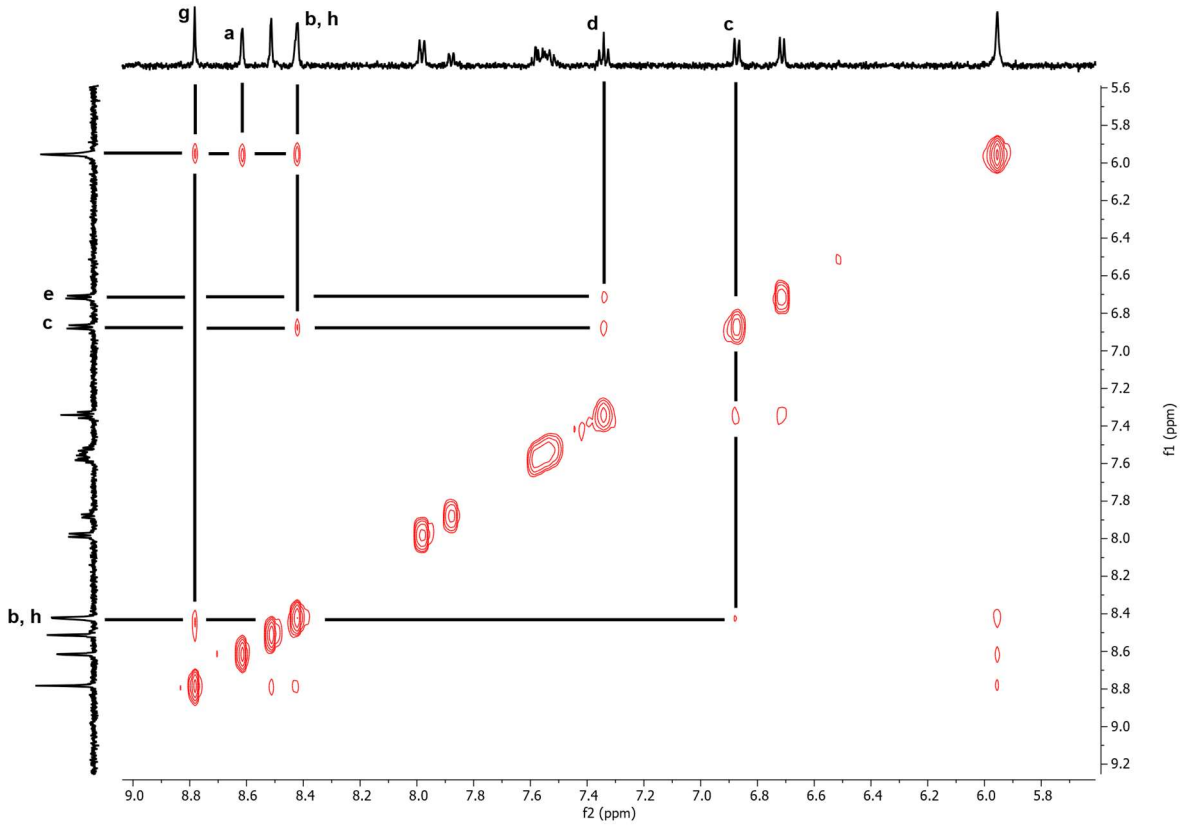

Figure 3.51: ^{1}H NOESY NMR spectrum of complex [$Zn_2L^{mN3}_2$] (DMSO-d_6, 600 MHz, 25°C).

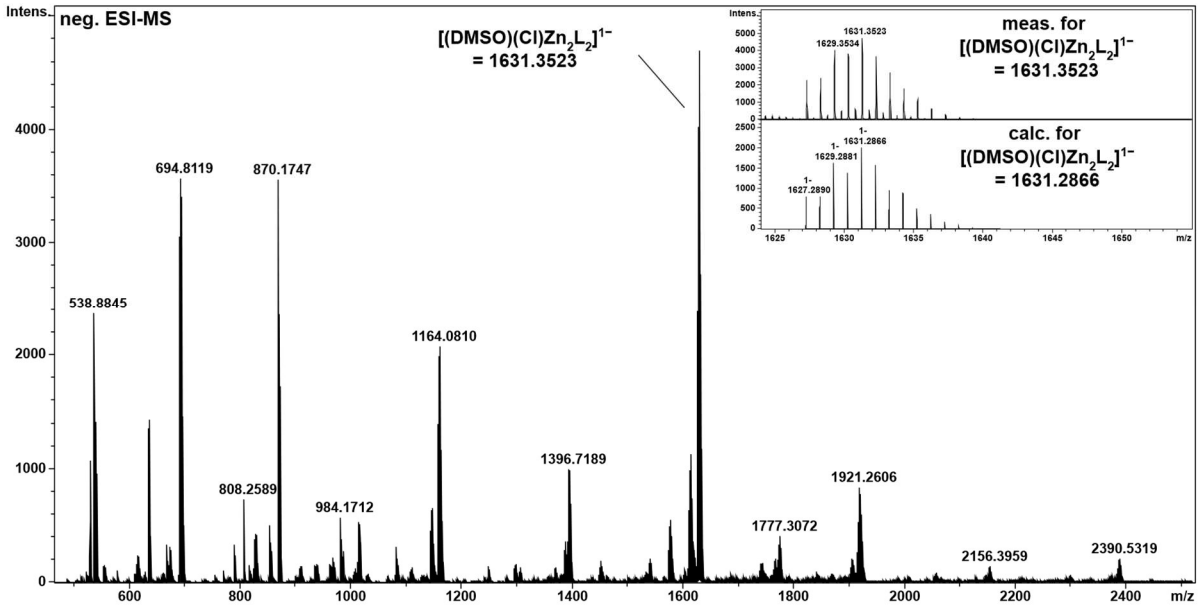

Figure 3.52: Negative ESI-MS spectrum of [$Zn_2L^{mN3}_2$] as adduct with DMSO and chloride in DMSO/ACN (1:9).

Anion-Binding studies of $[Zn_2L^{mN3}{}_2]$ with TBA_2TP and TBA_2NP

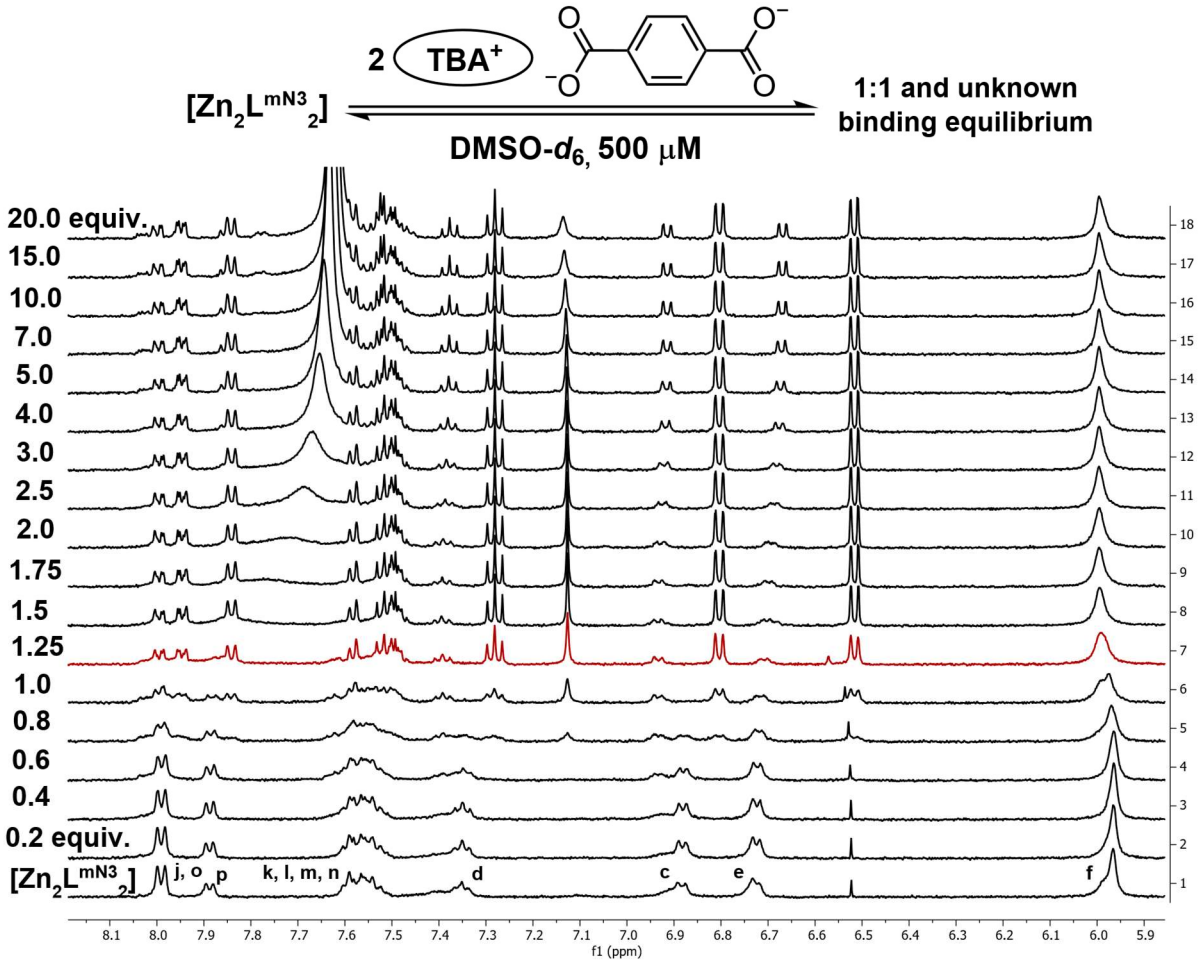

Figure 3.53: ^{1}H NMR titration of host $[Zn_2L^{mN3}{}_2]$ and TBA terephthalate (TP^{2-}) showing intermediate to slow binding fashion (DMSO-d_6, 500 MHz, 500 μM, 25°C).

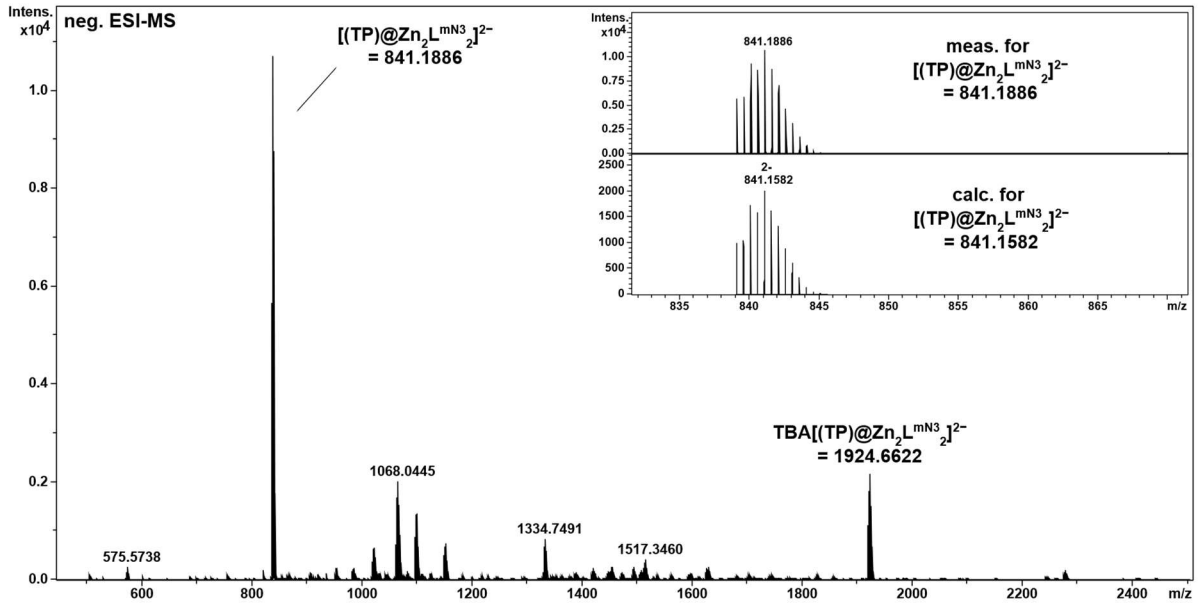

Figure 3.54: Negative ESI-MS spectrum of $[(TP)@Zn_2L^{mN3}{}_2]^{2-}$ in DMSO/ACN (1:9).

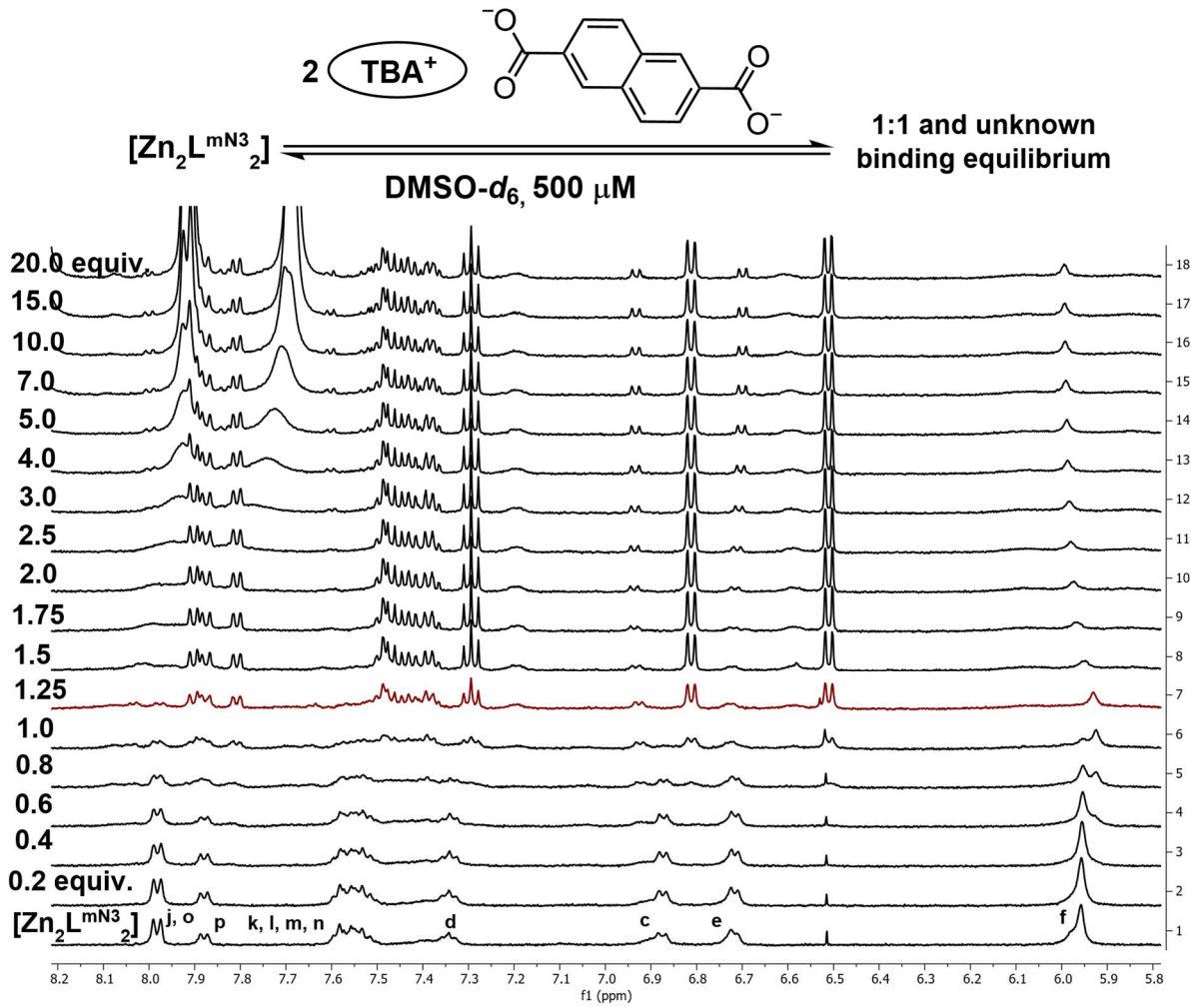

Figure 3.55: ^{1}H NMR titration of host $[Zn_2L^{mN3}{}_2]$ and TBA naphthalene-2,6-dicarboxylate (NP^{2-}) showing intermediate to slow binding fashion (DMSO-d_6, 500 MHz, 500 µM, 25°C).

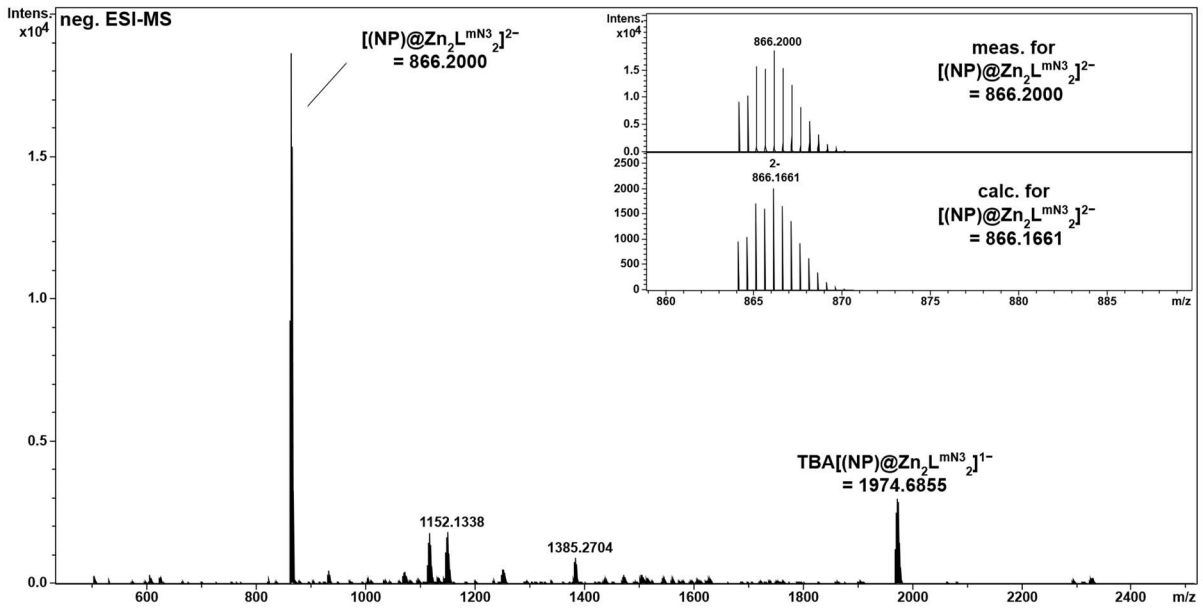

Figure 3.56: Negative ESI-MS spectrum of $[(NP)@Zn_2L^{mN3}{}_2]^{2-}$ in DMSO/ACN (1:9).

3.7.7 Synthetic procedure of ligand L^{N3}-H_2

Synthesis of 3,5-dibromo-*N*,*N*-di(naphthalen-2-yl)benzamide

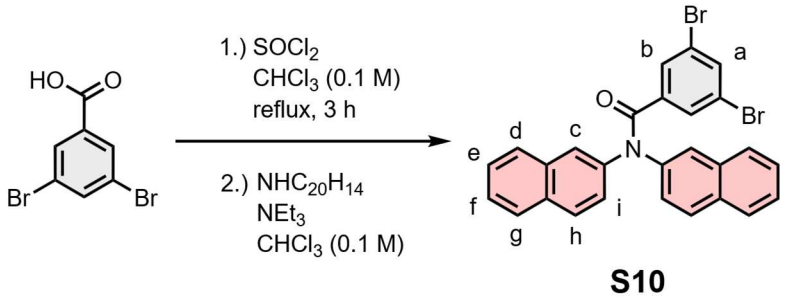

*Figure 3.57: Formation of the acid chloride and subsequently SCHOTTEN-BAUMANN reaction, which gave precursor **S10**.*

3,5-dibromobenzoic acid (485 mg, 1.73 mmol, 1 equiv.) and $SOCl_2$ (3.68 mL, 51.98 mmol, 30 equiv.) were dissolved in 11 mL of $CHCl_3$ (0.1 M) and refluxed for 3 h. The solvent was evaporated under vacuum on a Schlenk line, with a cold trap placed between the vacuum pump and the sample, so that excess $SOCl_2$ could subsequently be quenched. The remaining solid was dissolved in $CHCl_3$ and then, di(naphthalen-2-yl)amine (700 mg, 2.60 mmol, 1.5 equiv.) and NEt_3 (483.3 µL, 3.47 mmol, 2 equiv.) were dissolved in $CHCl_3$ (0.1 M) and added to the reaction mixture and refluxed for 4 days. The reaction mixture was diluted with DCM, washed with $NaHCO_3$ and brine. Afterwards the organic layer was dried with $MgSO_4$, the solvent was evaporated under vacuum and column chromatography (silica, pentane/Et_2O 75:1 to 50:1 to 20:1) gives the product **S10** as colorless solid (27%, 251 mg, 470 µmol).

^{1}H NMR (600 MHz, DMSO-d_6, 25°C) δ = 7.95-7.89 (m, 4H, d, g), 7.88 (d, *J* = 2.2 Hz, 2H, i), 7.83 (d, *J* = 7.7 Hz, 2H, h), 7.76-7.72 (m, 3H, a, b), 7.55 (s, 2H, c), 7.54-7.48 (m, 4H, e, f) ppm. **^{13}C NMR** (151 MHz, DMSO-d_6, 25°C) δ = 166.97, 140.38, 140.19, 134.60, 133.02, 131.42, 130.32, 129.03, 128.99, 127.70, 127.60, 126.75, 126.53, 126.02, 121.86. **HRMS** (positive ESI-MS, ACN): m/z = 553.9539 ([M+Na$^+$], $C_{27}H_{17}Br_2NONa^+$, calc. 553.9549).

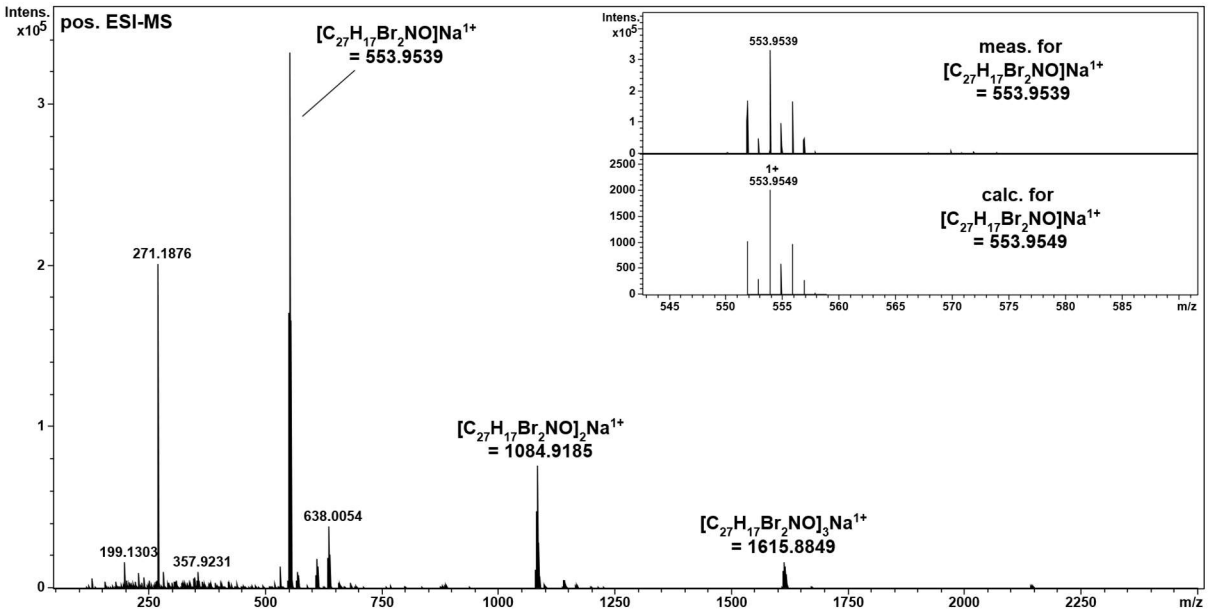

*Figure 3.58: Positive HRMS spectrum of precursor **S10** (ACN).*

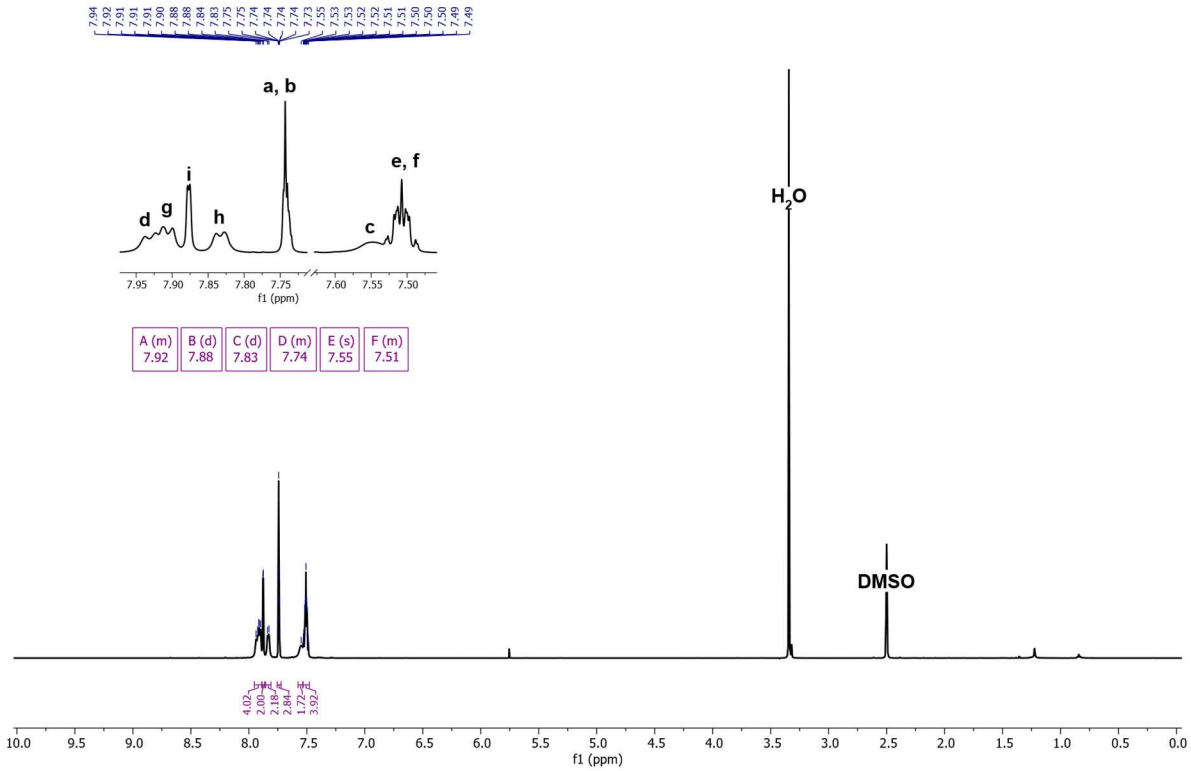

*Figure 3.59: ^{1}H NMR spectrum of the precursor **S10** (DMSO-d_6, 600 MHz, 25°C).*

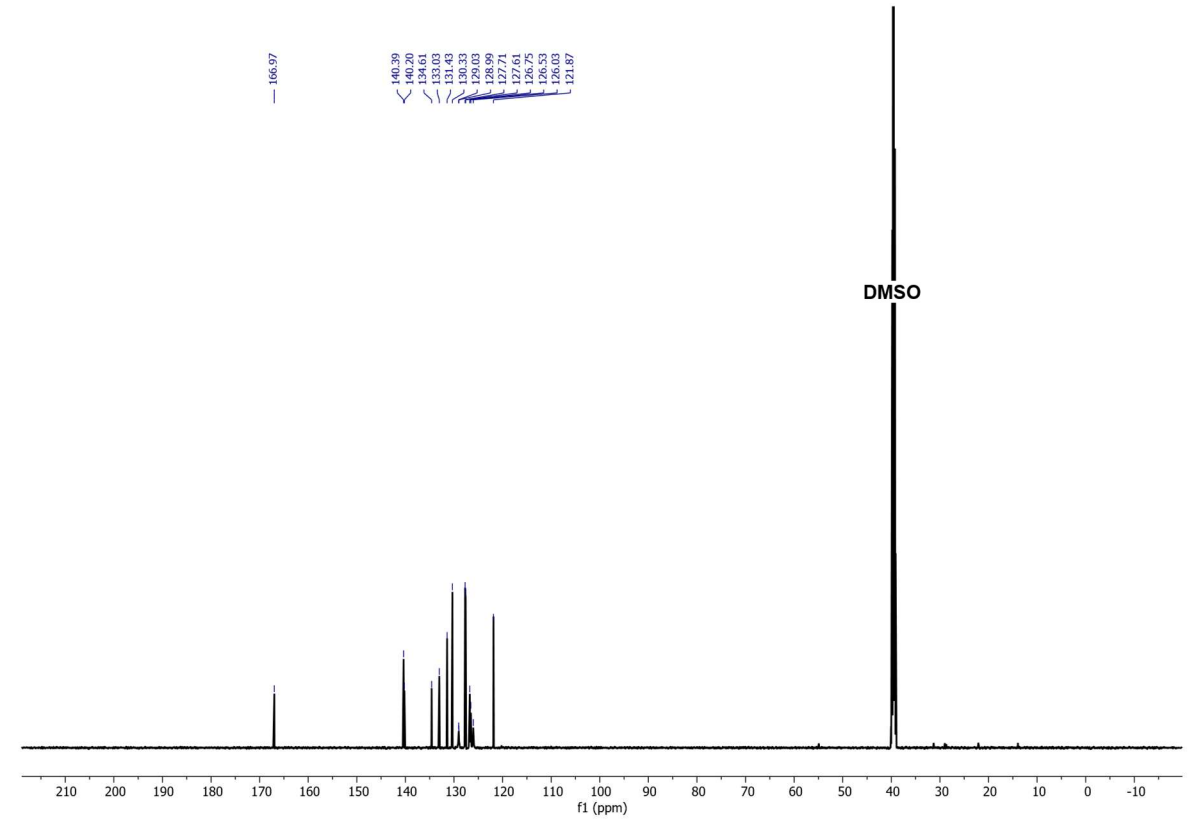

*Figure 3.60: ^{13}C NMR spectrum of precursor **S10** (DMSO-d_6, 151 MHz, 25°C).*

Synthesis of *N*,*N*-di(naphthalen-2-yl)-3,5-bis((trimethylsilyl)ethynyl)benzamide

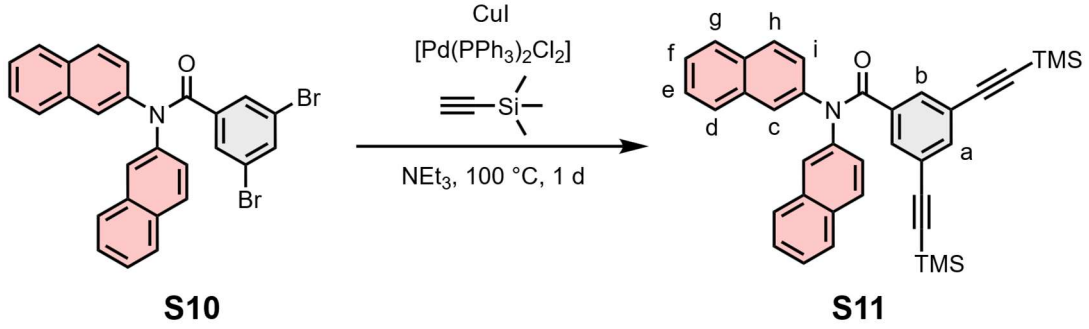

*Figure 3.61: The C-C SONOGASHIRA cross coupling of **S10** and TMS-acetylene to give precursor **S11**.*

S10 (50 mg, 94 µmol, 1 equiv.) and $[Pd(PPh_3)_2Cl_2]$ (6.61 mg, 9.4 µmol, 0.1 equiv.) were dissolved in 2 mL NEt_3. After three freeze pump thaws, CuI (1.8 mg, 9.4 µmol, 0.1 equiv.) and TMS-acetylene (54 µL, 376 µmol, 4 equiv.) were added sequentially. The reaction mixture was stirred at 100°C for 1 day under an argon atmosphere. Afterward, the reaction mixture was diluted with DCM, transferred in a separation funnel and washed with NH_4Cl and brine. The organic layer was dried with $MgSO_4$ and the solvent was evaporated. Column chromatography (silica, pentane/Et_2O 25:1) gives the product **S11** as a yellowish solid (45 mg, 79 µmol, 84%).

^{1}H NMR (500 MHz, DMSO-d_6, 25°C) δ = 7.95-7.88 (m, 4H, d, g), 7.85 (d, *J* = 2.2 Hz, 2H, i), 7.85-7.81 (m, 2H, h), 7.58 (d, *J* = 1.6 Hz, 2H, b), 7.56-7.47 (m, 6H, c, e, f), 7.37 (t, *J* = 1.5 Hz, 1H, a), 0.17 (s, 18H, methyl) ppm. **^{13}C NMR** (126 MHz, DMSO-d_6, 25°C) δ = 168.04, 140.66, 137.66, 135.31, 133.06, 131.69, 131.38, 128.92, 127.67, 127.58, 126.68, 126.44, 126.14, 122.43, 102.92, 96.16, 51.67 -0.35. **HRMS** (positive ESI-MS, ACN): m/z = 588.2086 ([M+Na$^+$], $C_{37}H_{35}NOSi_2Na^+$, calc. 588.2149).

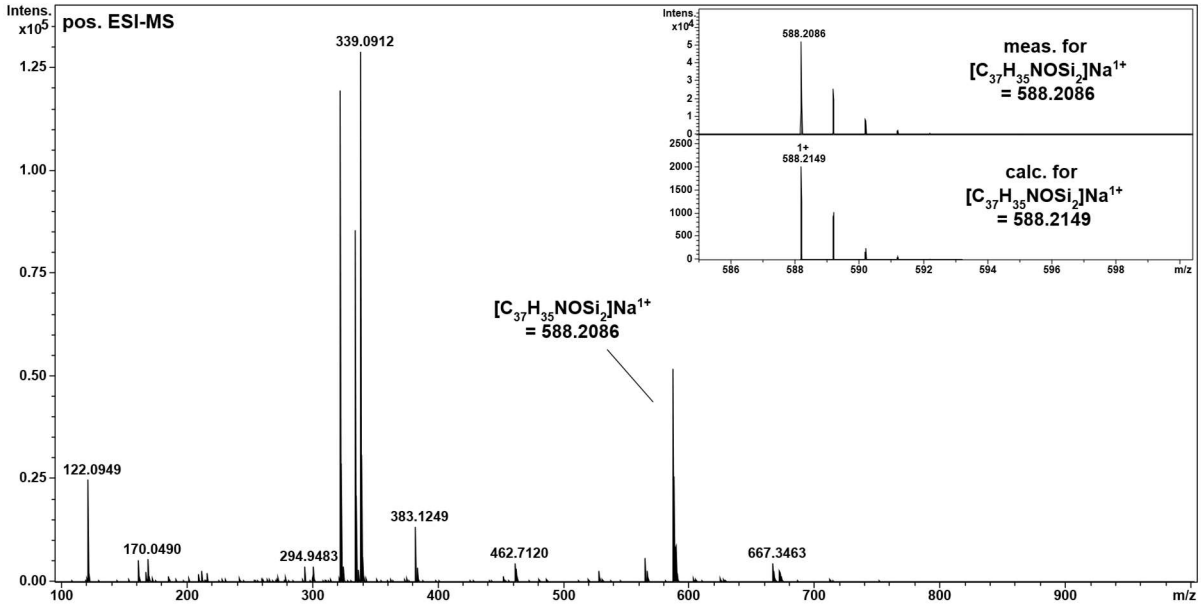

*Figure 3.62: Positive HRMS spectrum of precursor **S11** (ACN).*

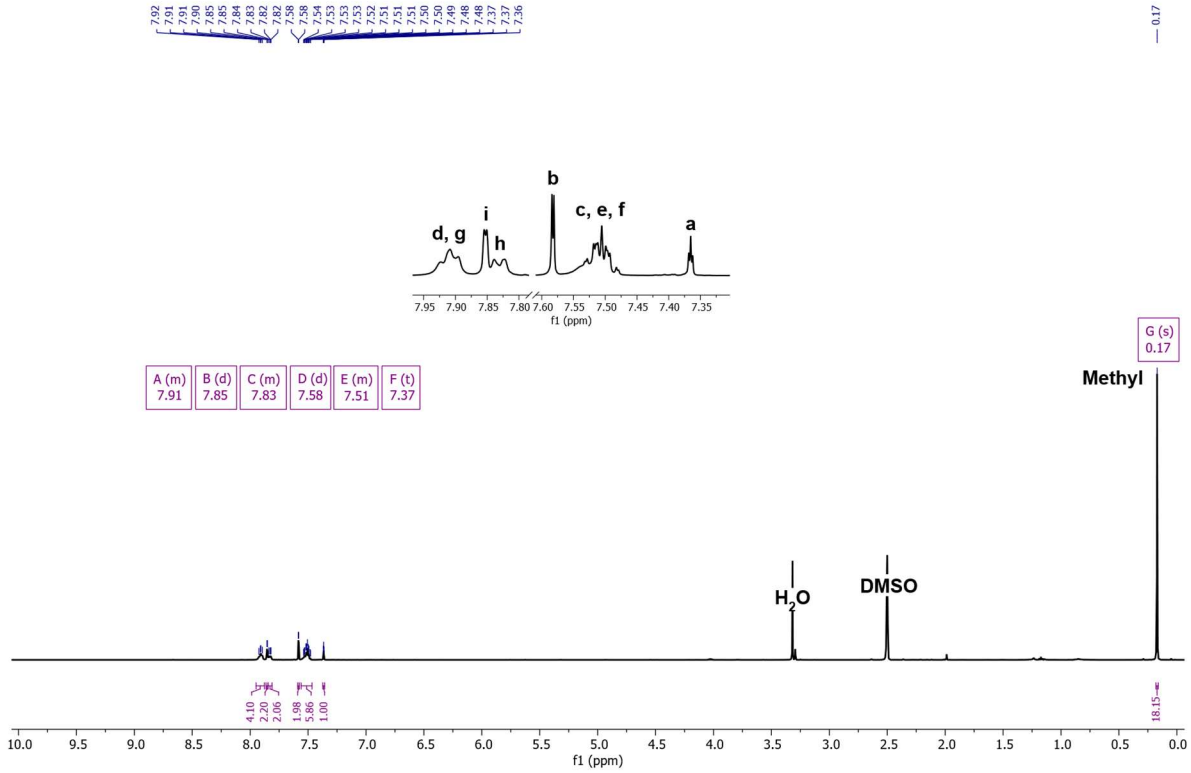

*Figure 3.63: ^{1}H NMR spectrum of precursor **S11** (DMSO-d_6, 500 MHz, 25°C).*

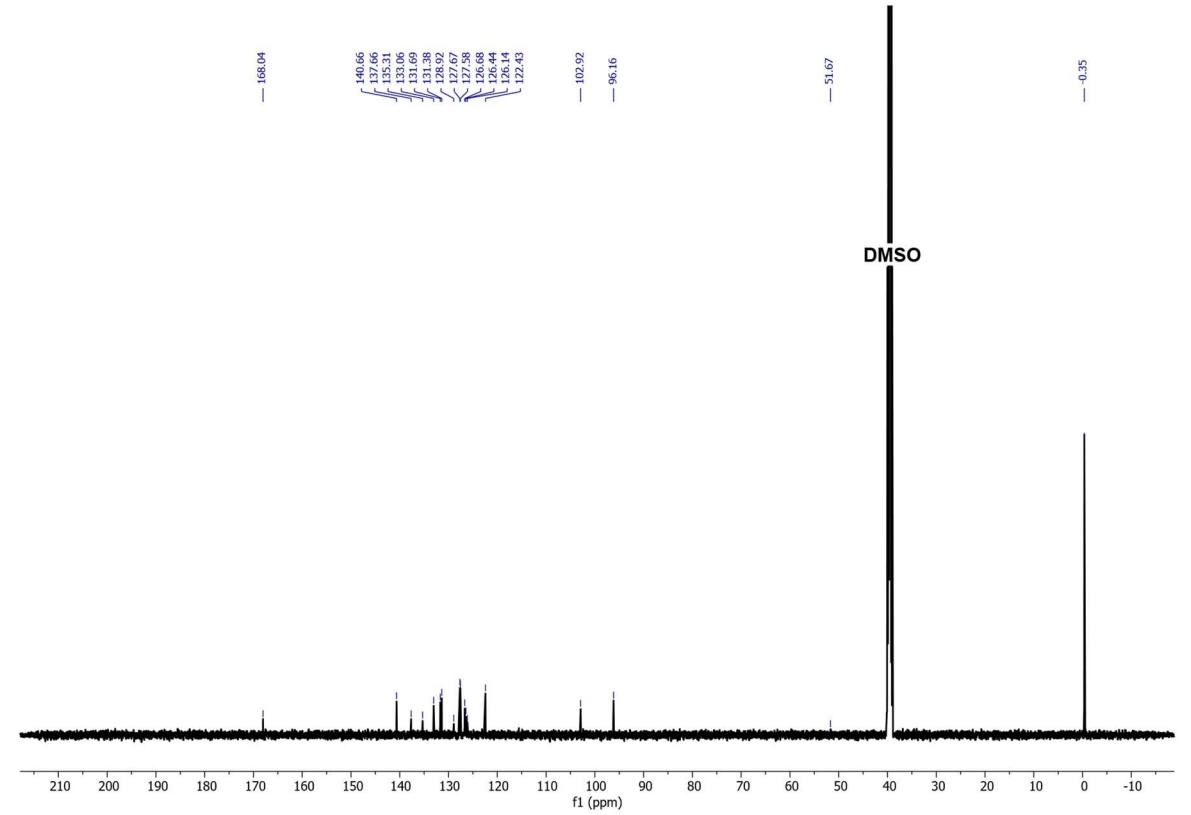

*Figure 3.64: ^{13}C NMR spectrum of precursor **S11** (DMSO-d_6, 126 MHz, 25°C).*

Synthesis of 3,5-diethynyl-*N*,*N*-di(naphthalen-2-yl)benzamide

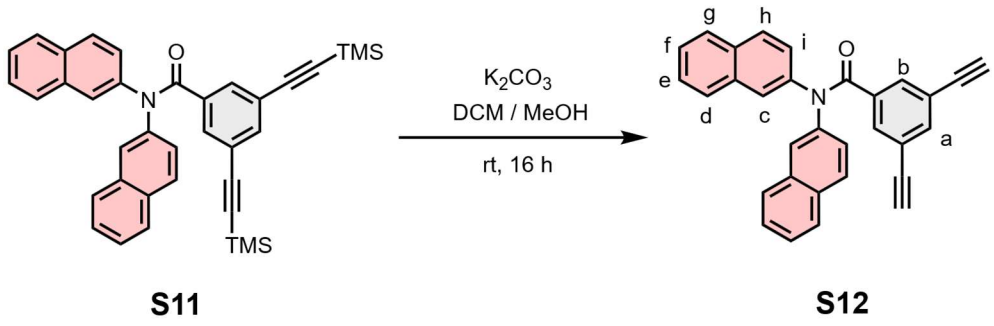

*Figure 3.65: Basic deprotection of precursor **S11** to give the ligand's backbone **S12**.*

Compound **S11** (45 mg, 79 µmol, 1 equiv.) was dissolved in a mixture of DCM and MeOH (1:1), then K_2CO_3 (66 mg, 477 µmol, 6 equiv.) was added to the stirring solution. The dispersion was stirred at room temperature overnight. Afterward, the reaction solution was diluted with DCM and washed with water (2x). The organic layer was dried with $MgSO_4$ and the solvent was evaporated under reduced pressure. Column chromatography (silica, pentane/EtOAc 80:1) gives the product **S12** as beige solid (25 mg, 59 µmol,75%).

^{1}H NMR (600 MHz, DMSO-d_6, 25°C) δ = 7.94-7.88 (m, 4H, d, g), 7.85 (d, *J* = 2.1 Hz, 2H, i), 7.83 (d, *J* = 7.5 Hz, 2H, h), 7.65 (d, *J* = 1.6 Hz, 2H, b), 7.56-7.47 (m, 6H, c, e, f), 7.44 (t, *J* = 1.6 Hz, 1H, a), 4.26 (s, 2H, j). **^{13}C NMR** (151 MHz, DMSO-d_6, 25°C) δ = 168.13, 140.59, 137.69, 135.53, 133.04, 131.87, 131.35, 128.98, 127.68, 127.59, 126.70, 126.46, 126.07, 122.02, 82.42, 81.50. **HRMS** (positive ESI-MS, ACN): m/z = 444.1350 [M+Na$^+$], [$C_{31}H_{19}NO$+Na]$^+$, calc. 444.1359.

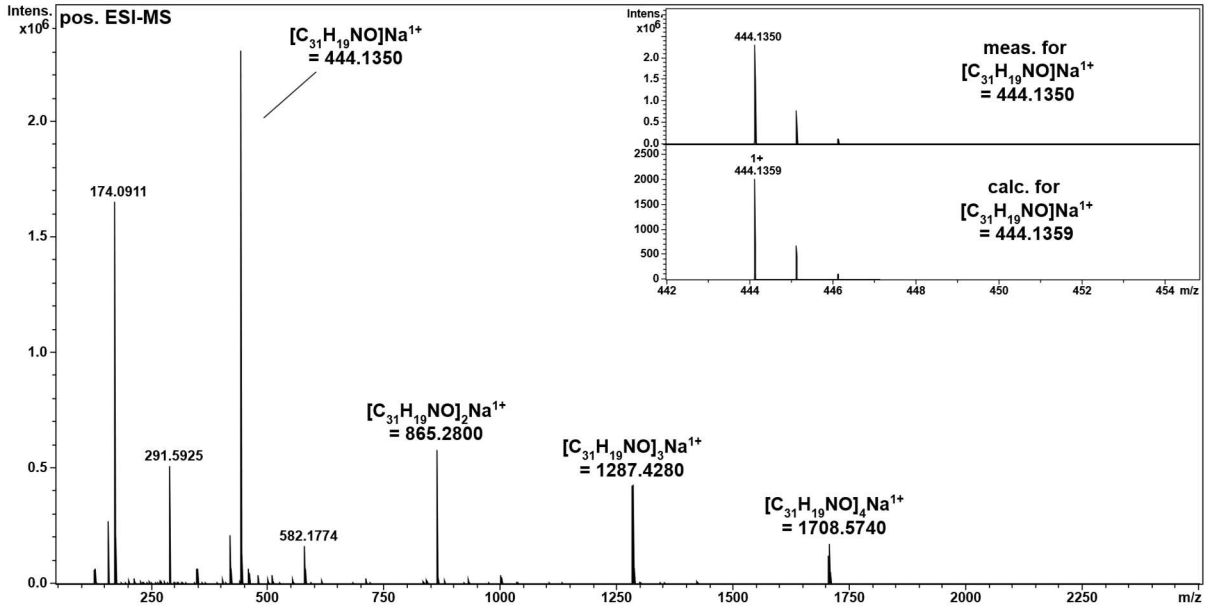

*Figure 3.66: Positive HRMS spectrum of the backbone **S12** (ACN).*

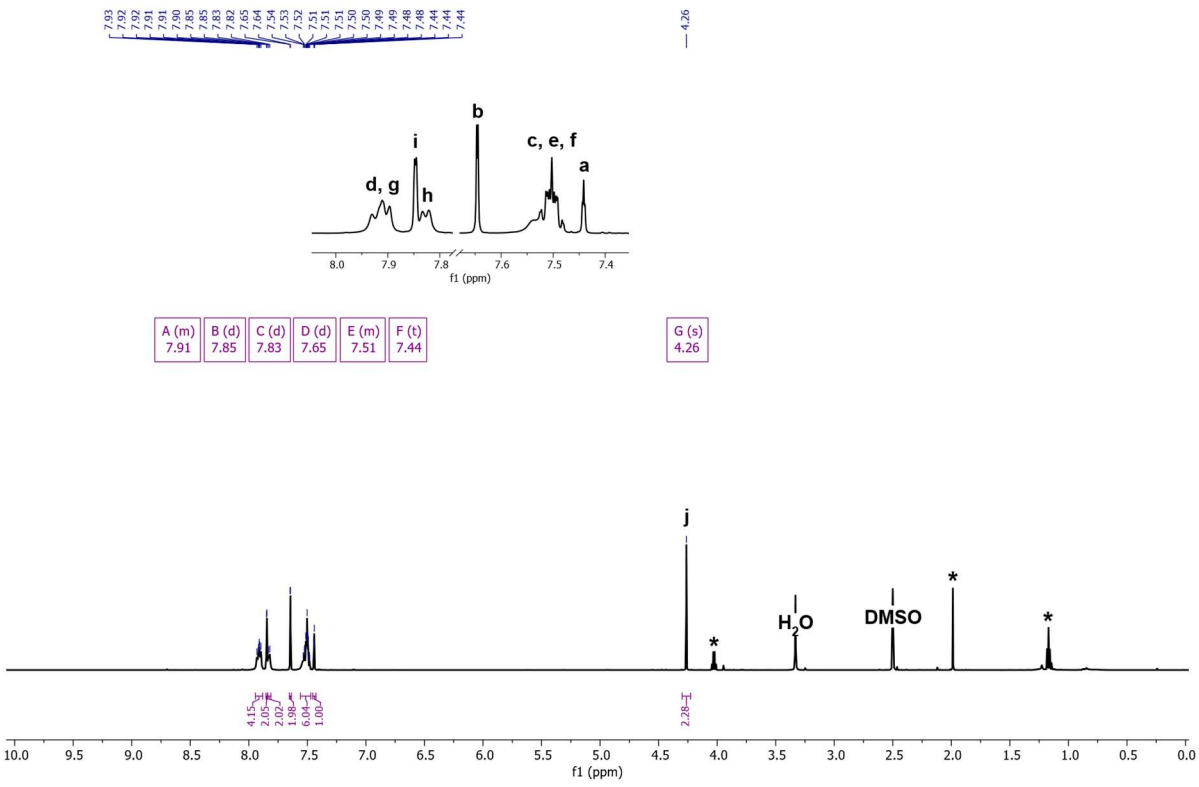

*Figure 3.67: ^{1}H NMR spectrum of the backbone **S12** (DMSO-d_6, 600 MHz, 25°C).*

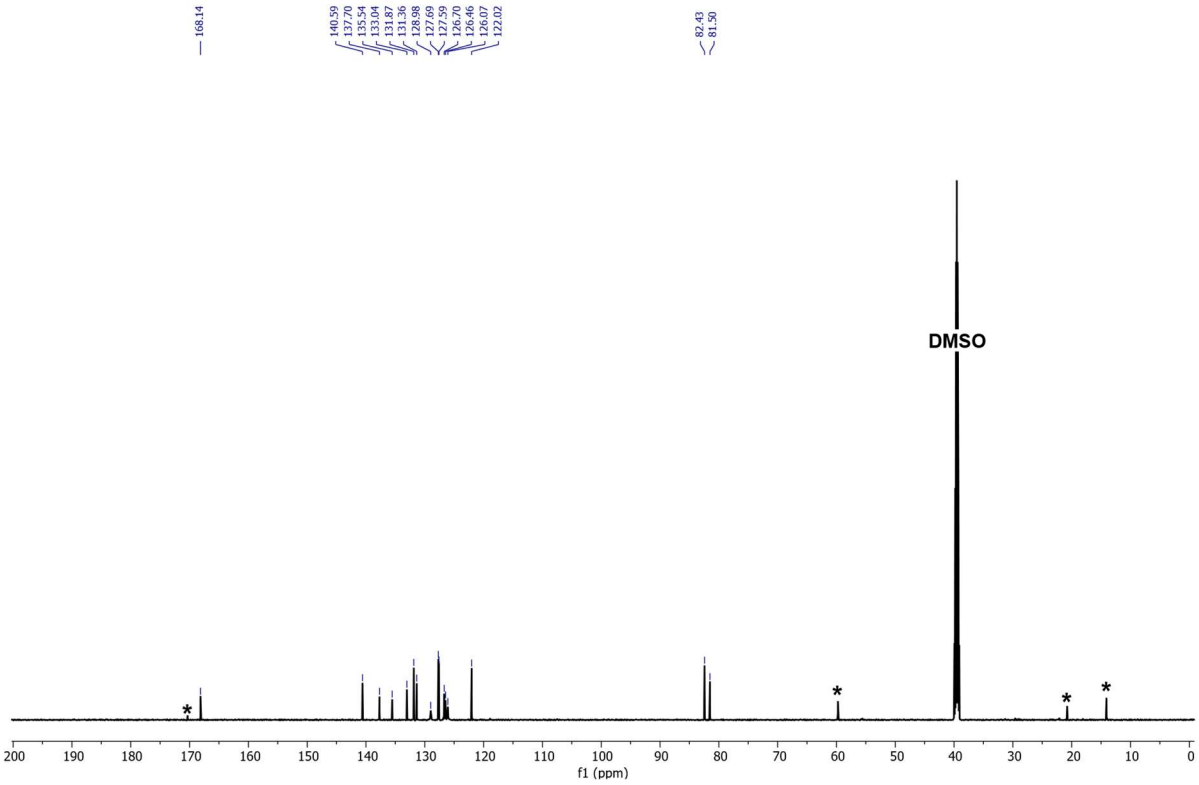

*Figure 3.68: ^{13}C NMR spectrum of the backbone **S12** (DMSO-d_6, 151 MHz, 25°C).*

Synthesis of the BOC protected ligand L^{N3}-H_2

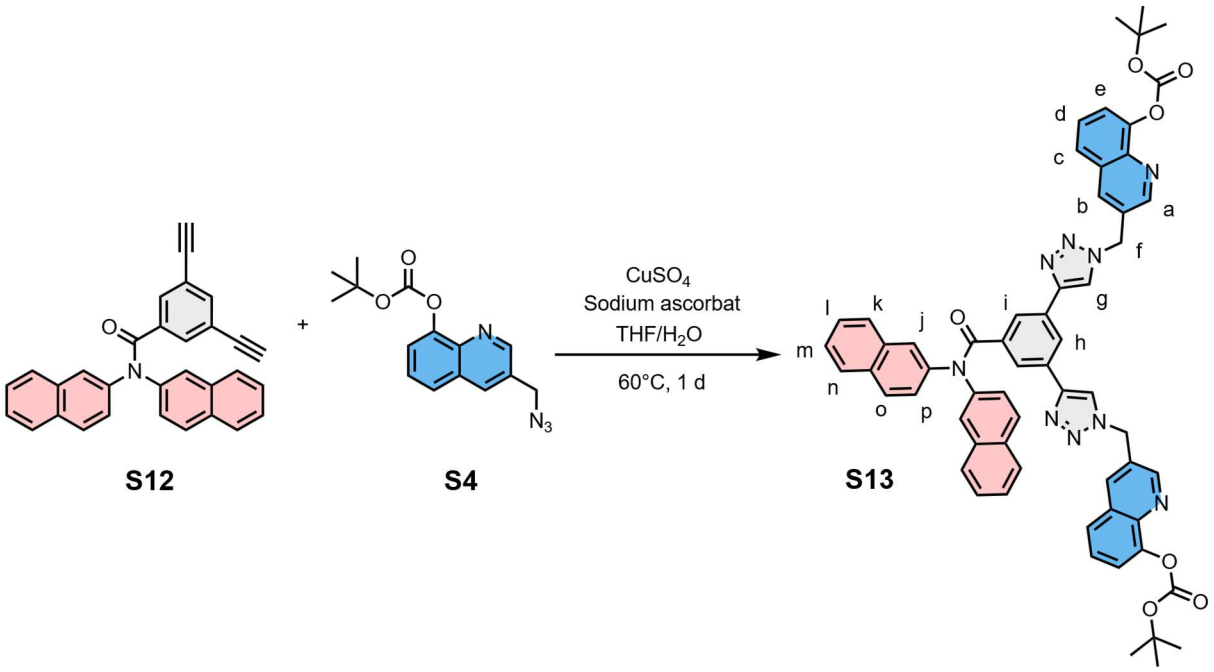

*Figure 3.69: 1,3-dipolar HUIGSEN cycloaddition of di-alkyne **S12** and azide **S4** gave the Boc-protected ligand **S13**.*

The azide **S4** (39.2 mg, 131 µmol, 2.2 equiv.) was transferred into a Schlenk tube and dissolved in THF. The solution was degassed for 20 min with argon. $CuSO_4$ (950 µg, 6 µmol, 0.1 equiv.) and sodium-ascorbate (47 mg, 237 µmol, 4 equiv.) were dissolved in small amounts of water and added sequentially. Backbone **S12** (25 mg, 59.3 µmol, 1 equiv.) was added under argon, the solution was heated to 60 °C and stirred for 16 h. The reaction solution was diluted with DCM and the organic layer was washed with EDTA (0.25 M), brine and saturated NH_4Cl solution. The aqueous layer was extracted with DCM (3x). The combined organic layers were dried with Na_2SO_4 and the solvent was evaporated under reduced pressure. Column chromatography (silica, DCM/MeOH gradient 0 % - 3 %) yielded the BOC-protected derivative **S13** as yellowish solid (42 mg, 41.1 µmol, 69%).

^{1}H NMR (600 MHz, DMSO-d_6, 25°C) δ = 8.95 (d, *J* = 2.2 Hz, 2H, a), 8.67 (s, 2H, g), 8.37 (d, *J* = 2.1 Hz, 2H, b), 8.22 (t, *J* = 1.6 Hz, 2H, h), 8.00 (d, *J* = 1.6 Hz, 2H, i), 7.92 (dd, *J* = 7.9, 1.8 Hz, 2H, c), 7.90-7.75 (m, 8H, k, l, m, n), 7.66-7.60 (m, 4H, d, e), 7.53 (d, *J* = 8.8 Hz, 2H, p), 7.43 (s, 4H, o, j), 5.89 (s, 4H, f), 1.49 (s, 18H, *t*-Bu) ppm. **^{13}C NMR** (151 MHz, DMSO-d_6, 25°C) δ = 169.69, 151.15, 150.59, 146.82, 145.72, 140.91, 140.05, 137.79, 135.41, 133.08, 131.25, 130.89, 129.60, 128.94, 128.48, 127.66, 127.51, 127.08, 126.61, 126.32, 126.20, 126.10, 124.70, 123.07, 122.26, 121.50, 83.05, 50.68, 27.26 ppm. **HRMS** (positive ESI-MS, ACN): m/z = 1044.3692, ([M+Na$^+$] $C_{61}H_{51}N_9O_7Na^+$, calc. 1044.3804).

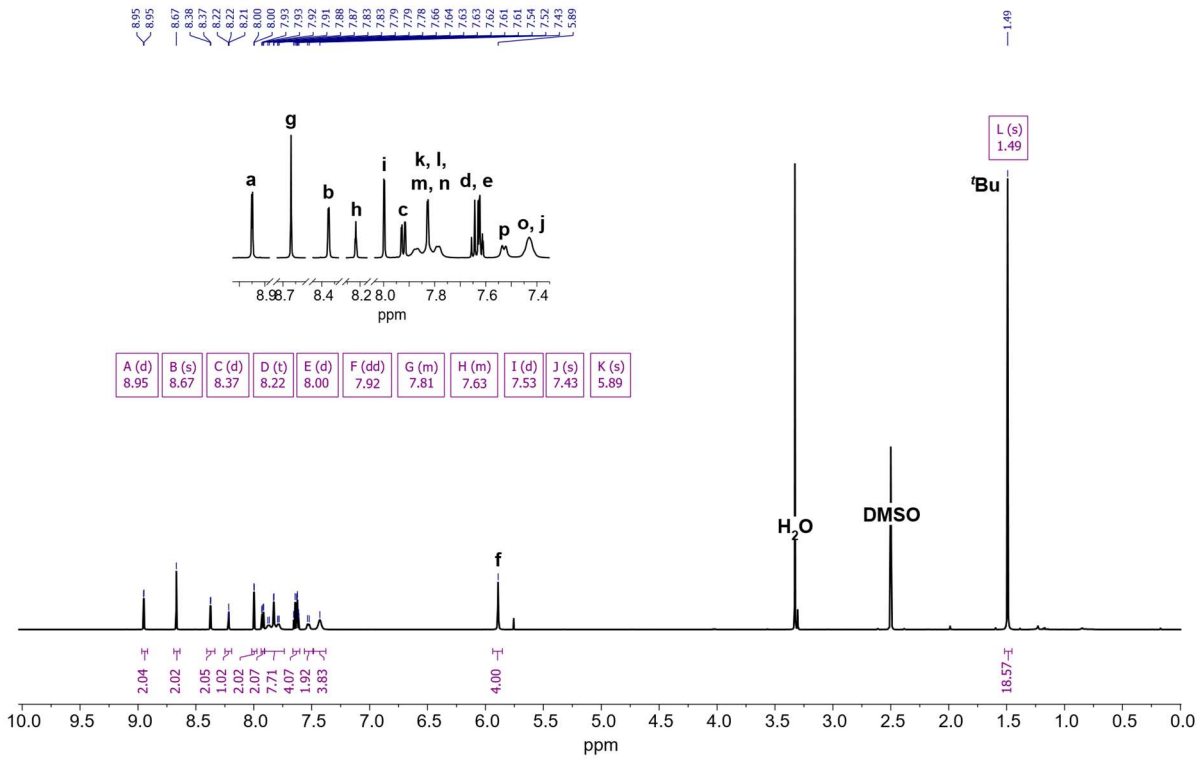

*Figure 3.70: ^{1}H NMR spectrum of the Boc-protected ligand **S13** (DMSO-d_6, 600 MHz, 25°C).*

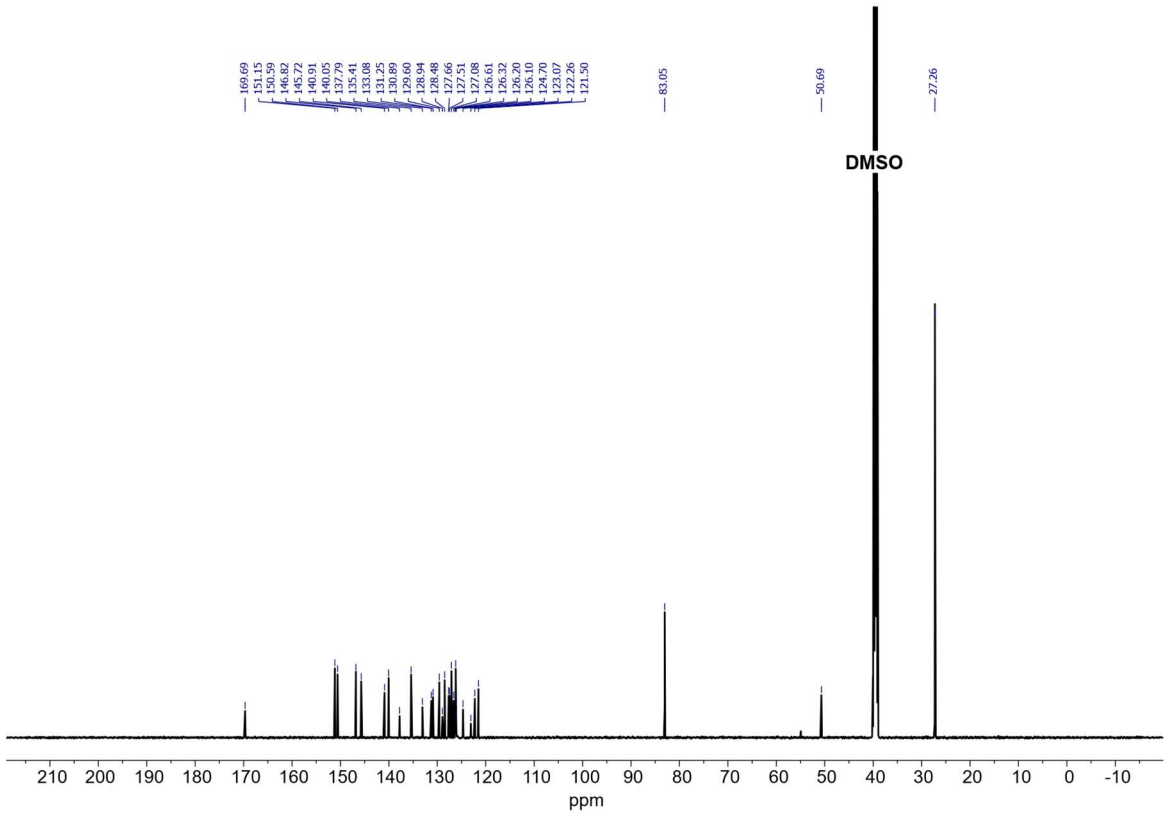

*Figure 3.71: ^{13}C NMR spectrum of the Boc-protected ligand **S13** (DMSO-d_6, 151 MHz, 25°C).*

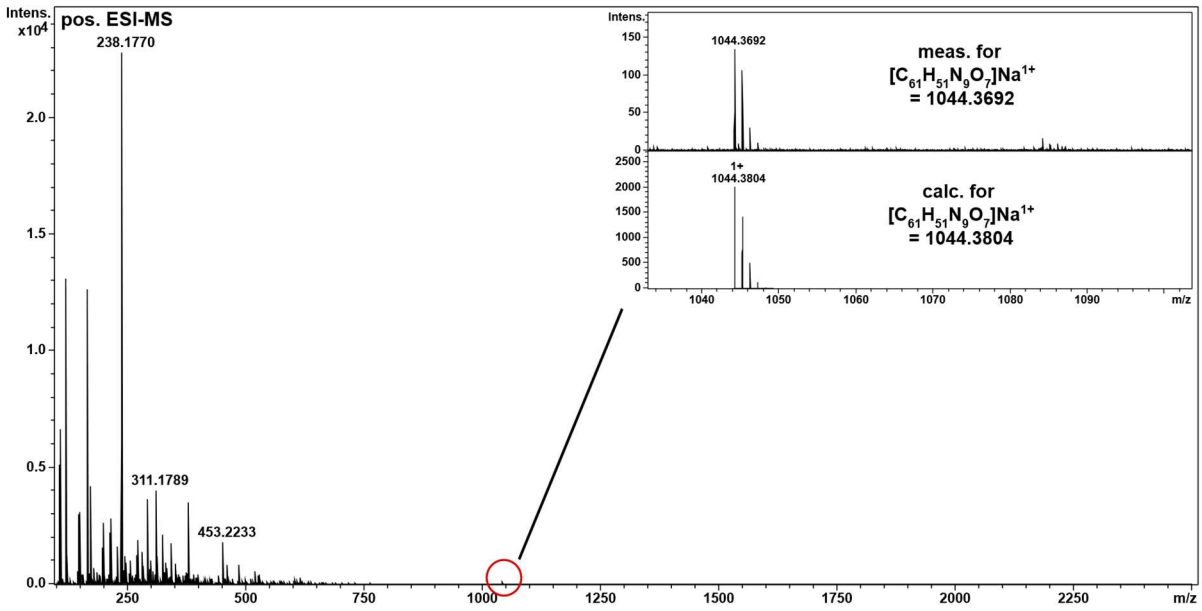

*Figure 3.72: Positive HRMS spectrum of the Boc-protected ligand **S13** (DCM).*

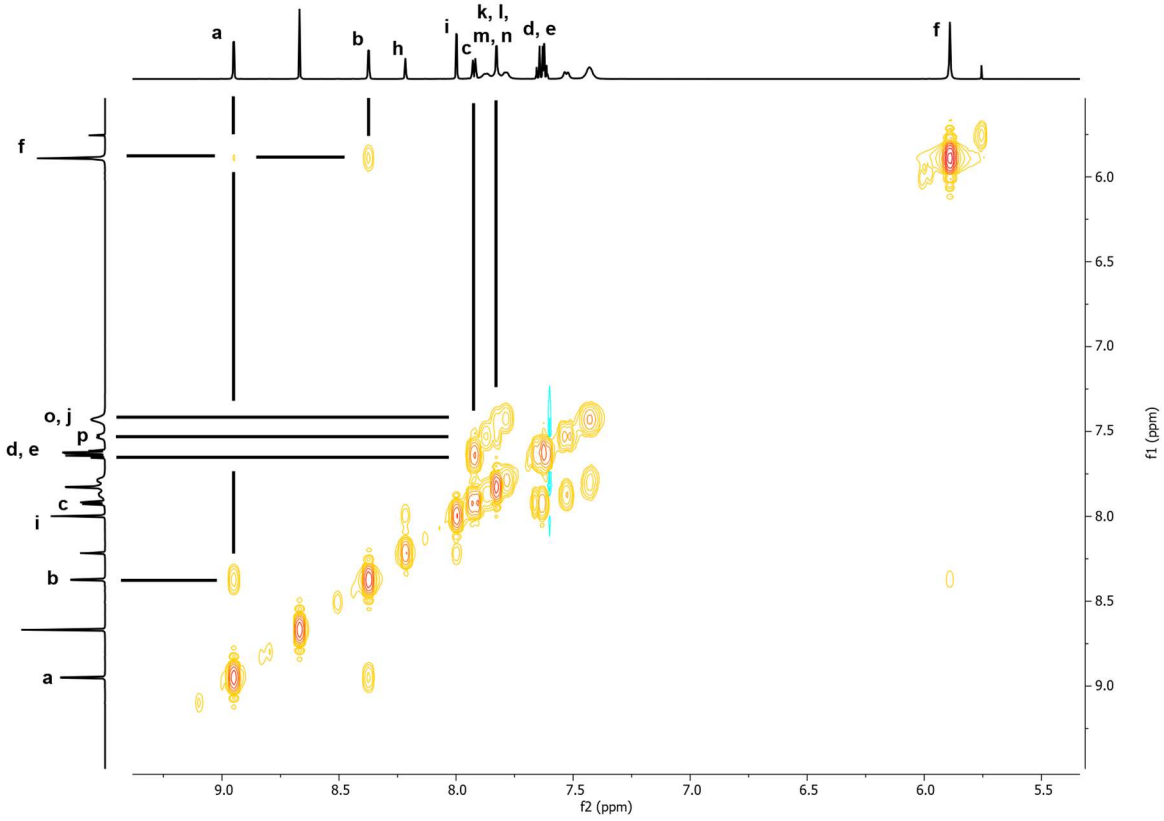

*Figure 3.73: ^{1}H COSY NMR spectrum of spectrum of the Boc-protected ligand **S13** (DMSO-d_6, 600 MHz, 25°C).*

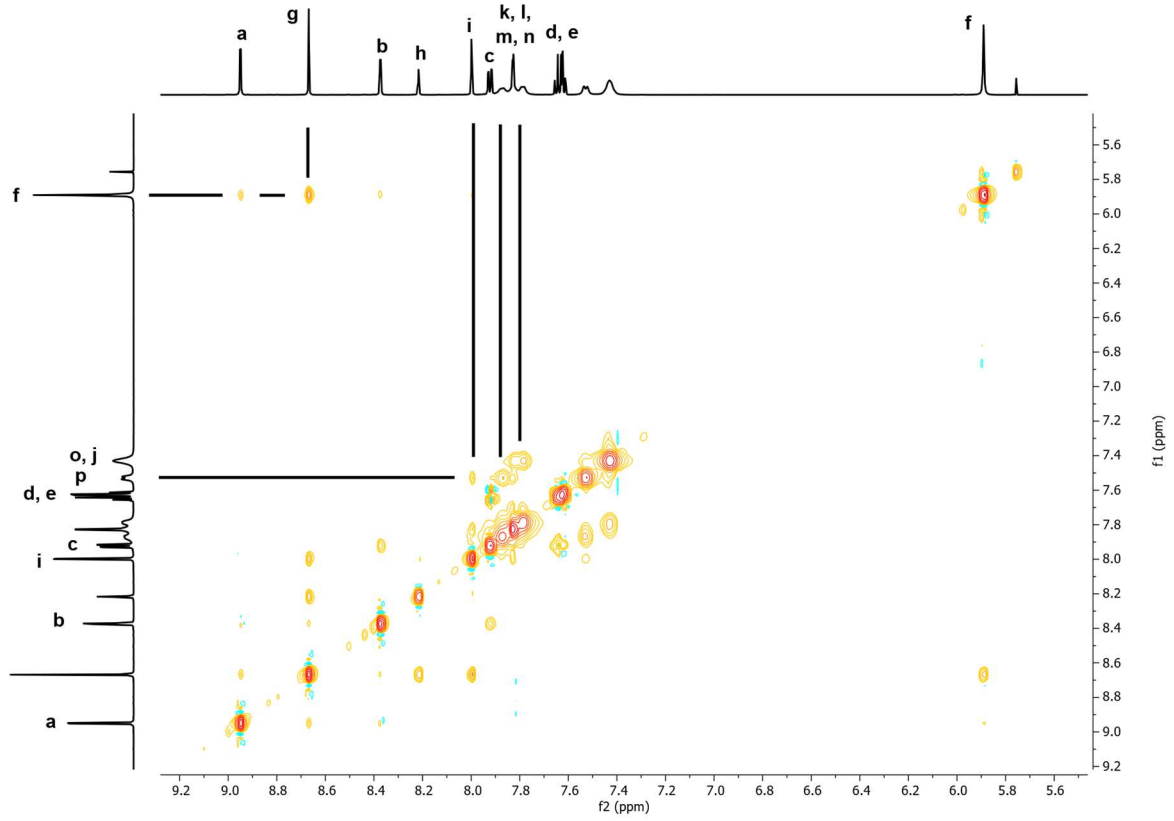

*Figure 3.74: ^{1}H NOESY NMR spectrum of spectrum of the Boc-protected ligand **S13** (DMSO-d_6, 600 MHz, 25°C).*

Synthesis of the ligand L^{N3}-H_2

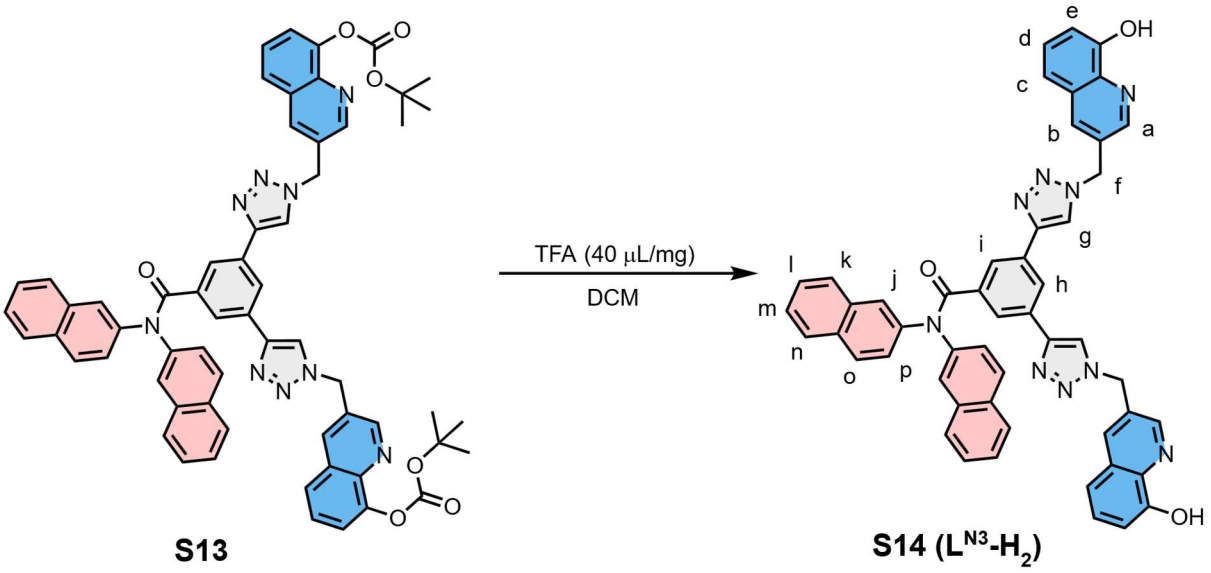

*Figure 3.75: Boc-deprotection of **S13** with TFA gave ligand **S14** (L^{N3}-H_2).*

The BOC-protected derivative **S13** (10 mg, 9.8 µmol, 1 equiv.) was dissolved in DCM and treated with TFA (40 µL/mg). After 1 h the reaction mixture was neutralized with sat. $NaHCO_3$. As soon as the reaction mixture reached a pH of around 7, der product **S14** precipitated as yellow solid. The reaction mixture was decantated and the yellow solid was washed with water. The yellow solid was redissolved in plenty of DCM, washed with brine and the organic layer was dried via Na_2SO_4. The solvent was evaporated until there was a residue organic layer present. Pouring Et_2O into the residue gives the ligand **S14** as a yellowish powder (98%, 7.9 mg, 9.6 µmol).

^{1}H NMR (700 MHz, DMSO-d_6, 25°C) δ = 9.94 (s, 2H, OH), 8.88 (d, *J* = 2.2 Hz, 2H, a), 8.64 (s, 2H, g), 8.26 (d, *J* = 2.1 Hz, 2H, b), 8.20 (t, *J* = 1.6 Hz, 1H, h), 7.98 (d, *J* = 1.6 Hz, 2H, i), 7.91-7.74 (m, 8H, k, l, m ,n), 7.52 (d, *J* = 8.6 Hz, 2H, p), 7.49-7.44 (m, 2H, d), 7.43 (s, 4H, o ,j), 7.39 (dd, *J* = 8.3, 1.3 Hz, 2H, c), 7.10 (dd, *J* = 7.6, 1.3 Hz, 2H, c), 5.87 (s, 4H, f) ppm. **^{13}C NMR** (151 MHz, DMSO-d_6, 25°C) δ = 169.7749, 152.1839, 147.2912, 145.7575, 140.9612, 138.3284, 137.9346, 135.5472, 133.1363, 131.3167, 130.9805, 129.4070, 129.0335, 128.6839, 127.7058, 127.5718, 126.6757, 126.3878, 126.1489, 124.7793, 123.0598, 122.3373, 118.1021, 116.8341, 114.8985, 113.2510, 50.5997 ppm. **HRMS** (positive ESI-MS, ACN): m/z = 411.6459 $[M+2H]^{2+}$, $[C_{51}H_{35}N_9O_3+2H]^{2+}$, calc. 411.6504.

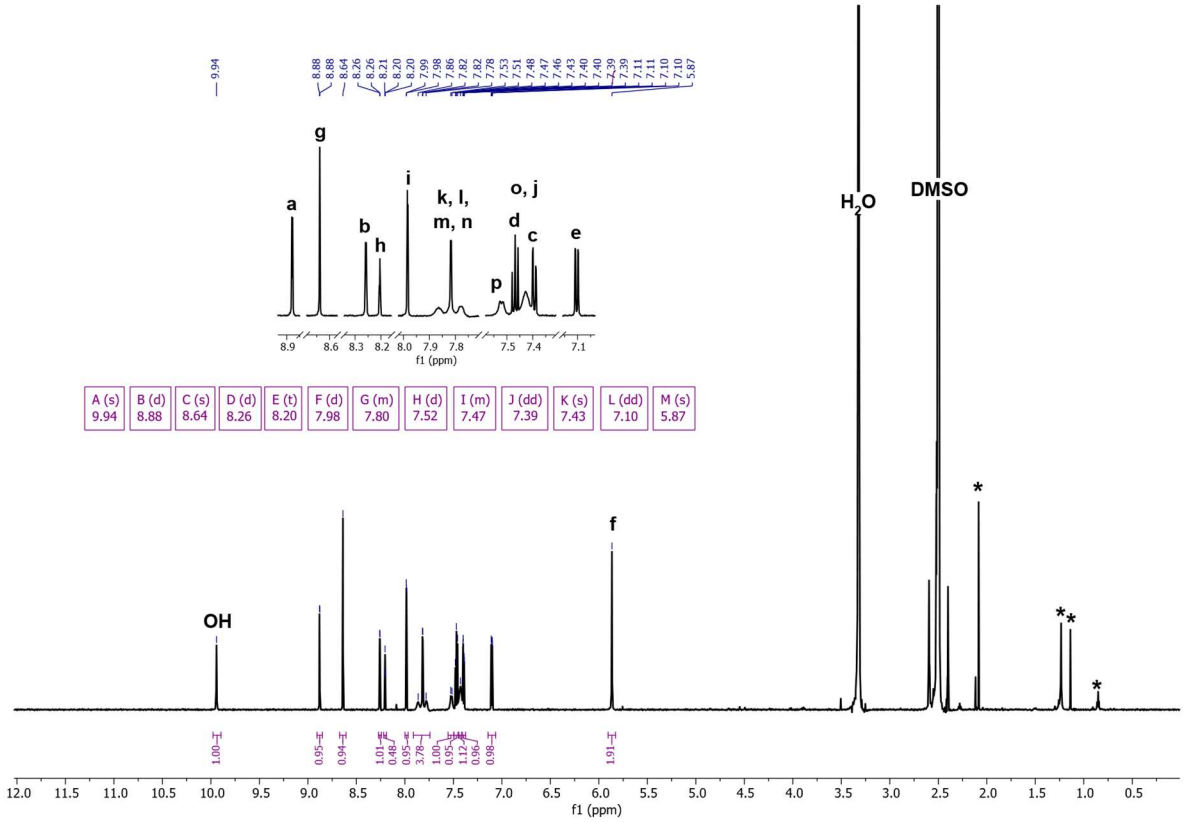

*Figure 3.76: ^{1}H NMR spectrum of ligand **S14** (L^{N3}-H_2) (DMSO-d_6, 600 MHz, 25°C).*

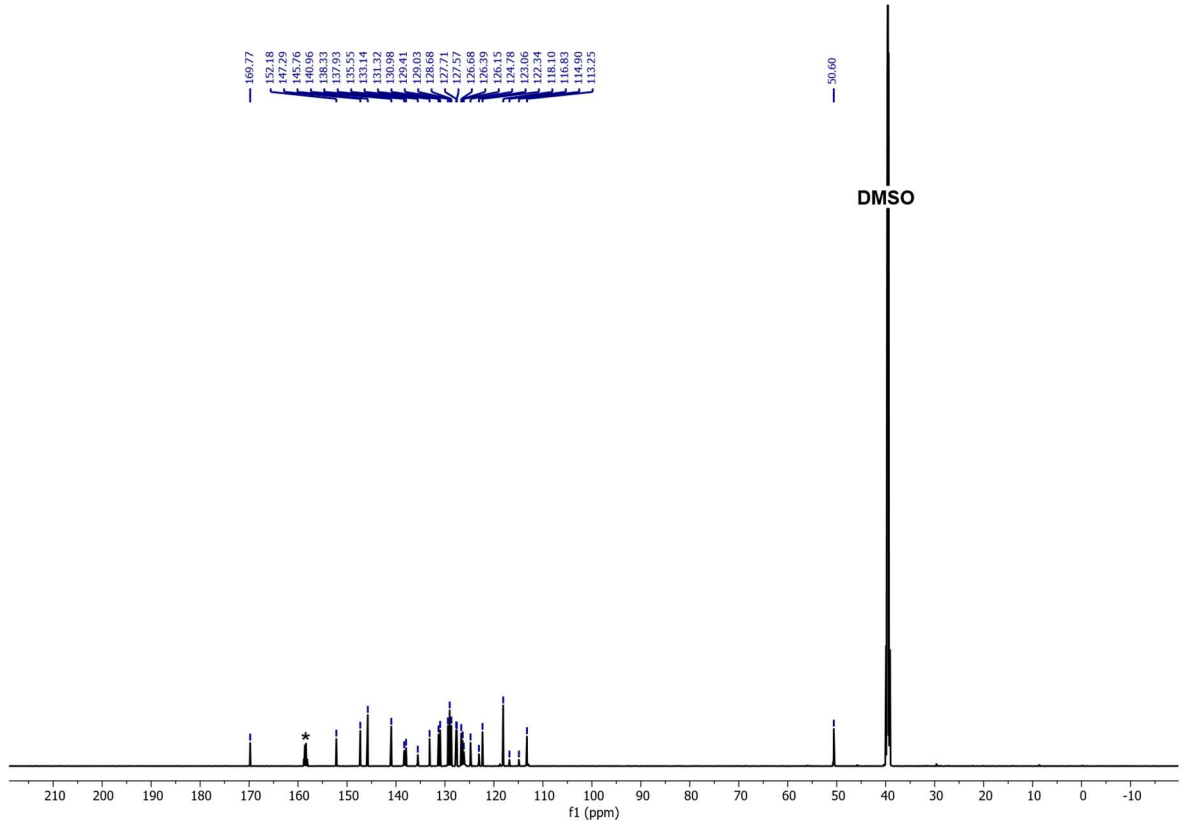

*Figure 3.77: ^{13}C NMR spectrum of ligand **S14** (L^{N3}-H_2) (DMSO-d_6, 151 MHz, 25°C).*

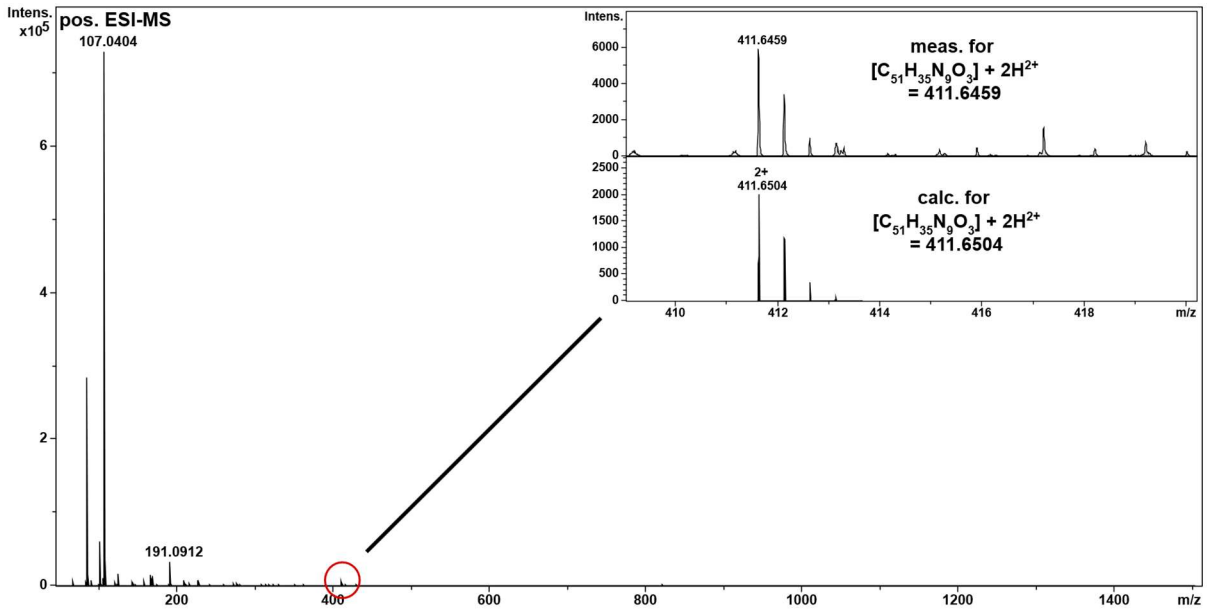

*Figure 3.78: Positive HRMS spectrum of ligand **S14** (L^{N3}-H_2) (DCM).*

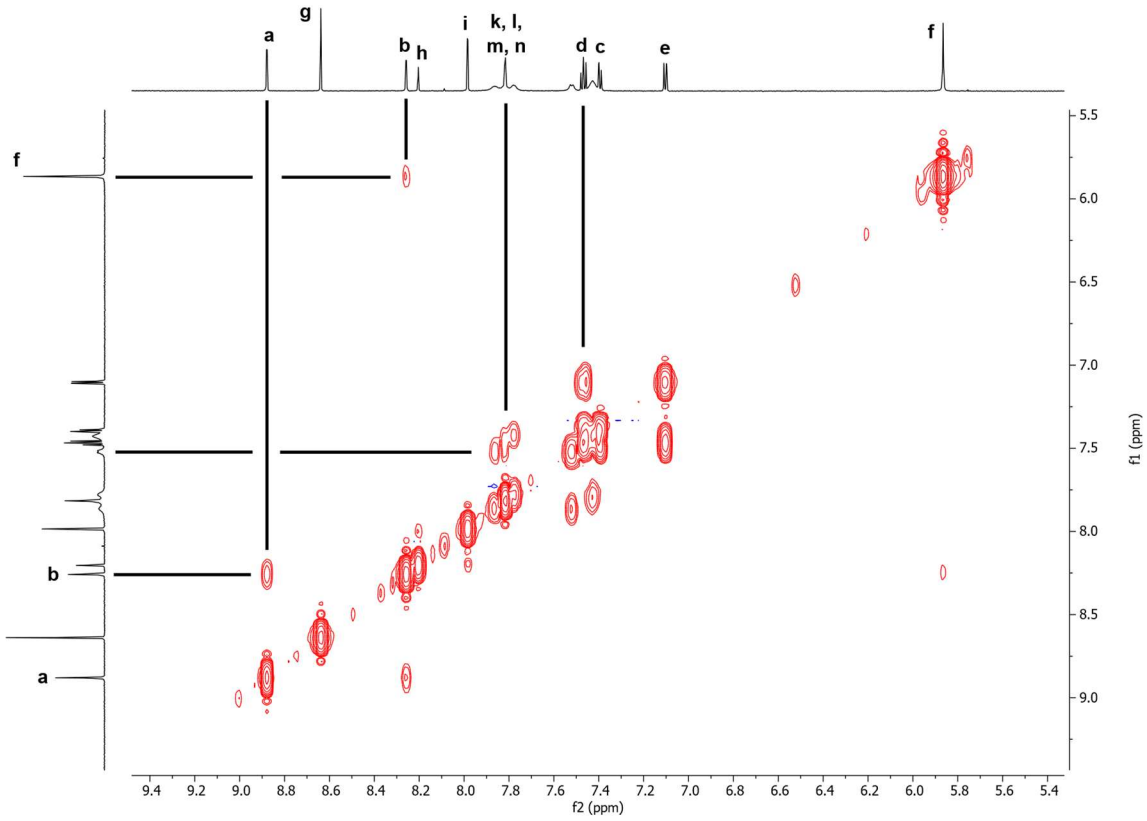

*Figure 3.79: ^{1}H COSY NMR spectrum of spectrum of ligand **S14** (L^{N3}-H_2) (DMSO-d_6, 600 MHz, 25°C).*

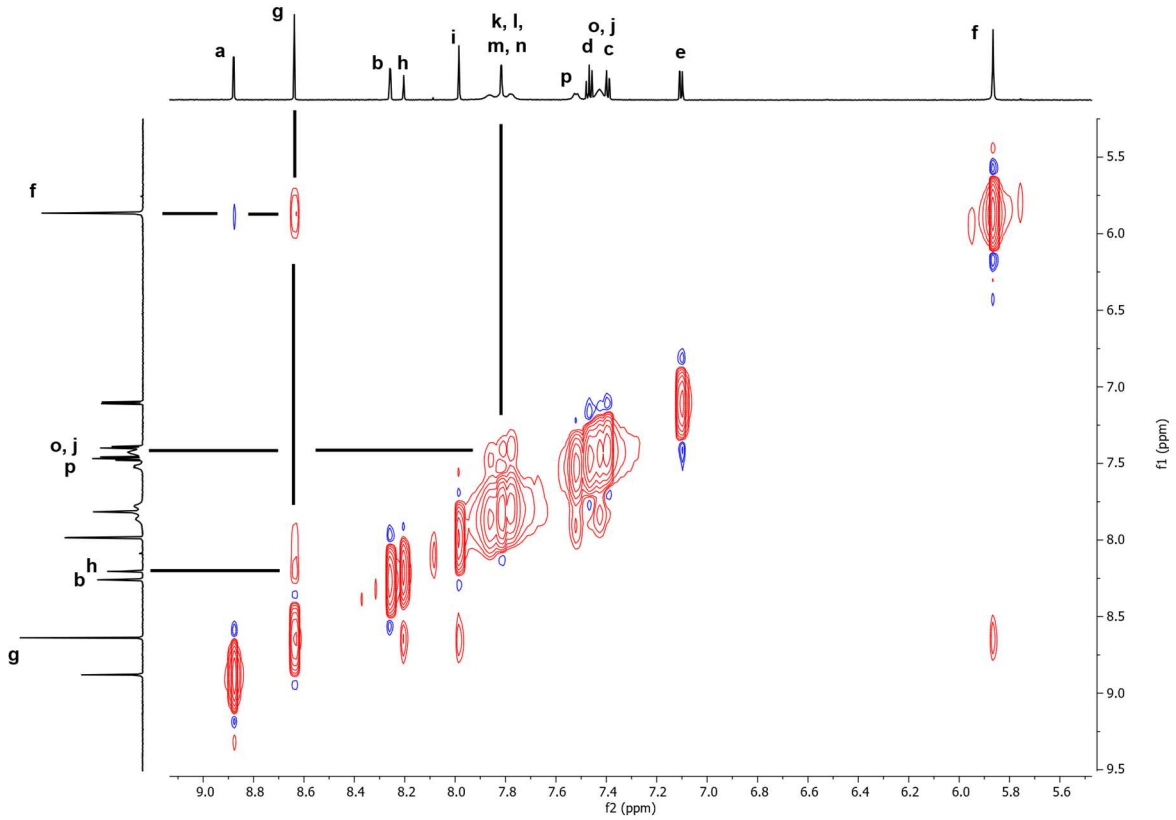

*Figure 3.80: ^{1}H NOESY NMR spectrum of spectrum of ligand **S14** (L^{N3}-H_2) (DMSO-d_6, 600 MHz, 25°C).*

3.7.8 Self-assembly of ligand L^{N3}-H_2 with $Zn(OAc)_2$

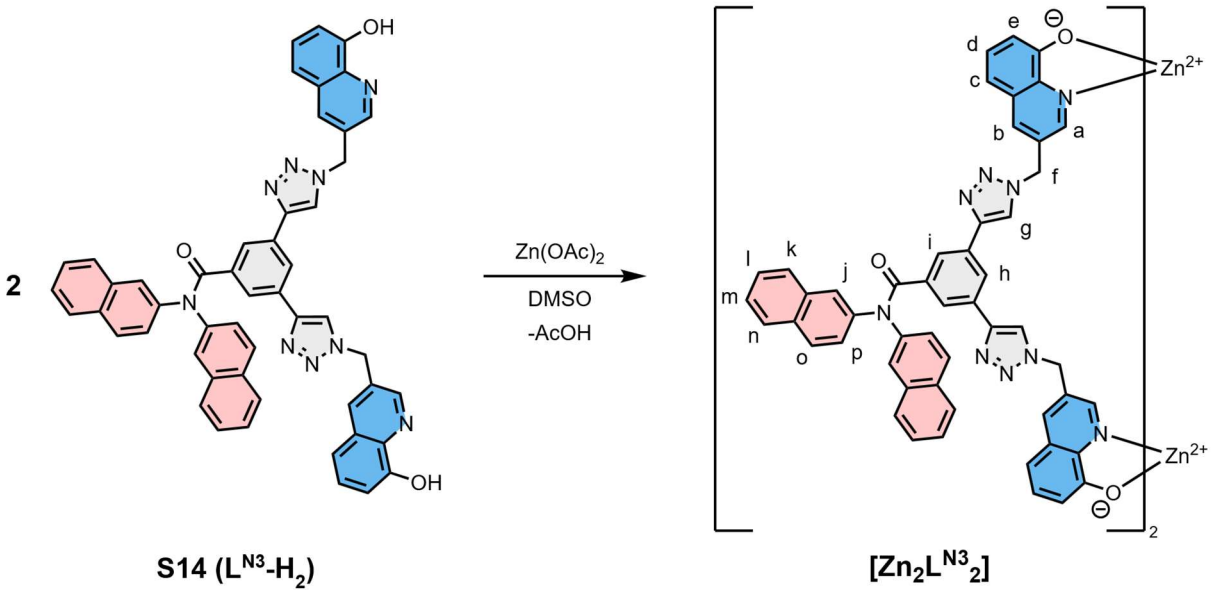

*Figure 3.81: Self-assembly of ligand **S14** (L^{N3}-H_2) and $Zn(OAc)_2$ in DMSO-d_6 in a 1:1 ratio.*

Ligand **S14** (L^{N3}-H_2) (1 equiv.) and $Zn(OAc)_2$ (1 equiv.) were dissolved separately in DMSO-d_6.The zinc acetate solution was added to the stirring ligand solution which resulted in a colour change to yellow. After 1 h the solvent as well as the by-product acetic acid were removed via lyophilization, which yields the complex **$[Zn_2L^{N3}_2]$** as a yellow solid with quantitative yield.

^{1}H NMR (600 MHz, DMSO-d_6, 25°C) δ = 8.56 (s, 2H, a), 8.51 (s, 2H, g), 8.35 (s, 2H, b), 8.06 (s, 1H, h), 7.98 (s, 2H, i), 7.90-7.67 (m, 8H, k, l, m ,n), 7.50 (d, *J* = 7.4 Hz, 2H, 2), 7.35 (t, *J* = 8.0 Hz, 2H, d), 7.31 (s, 4H, o, j), 6.86 (d, *J* = 7.9 Hz, 2H, c), 6.72 (d, *J* = 7.5 Hz, 2H, e), 5.83 (s, 4H, f) ppm. **HRMS** (positive ESI-MS, ACN): m/z = 1883.4068 ($[M+DMSO+Cl]^-$, $C_{102}H_{66}N_{18}O_6Zn_2(SO(CH_3)_2)Cl^-$, calc. 1883.3786).

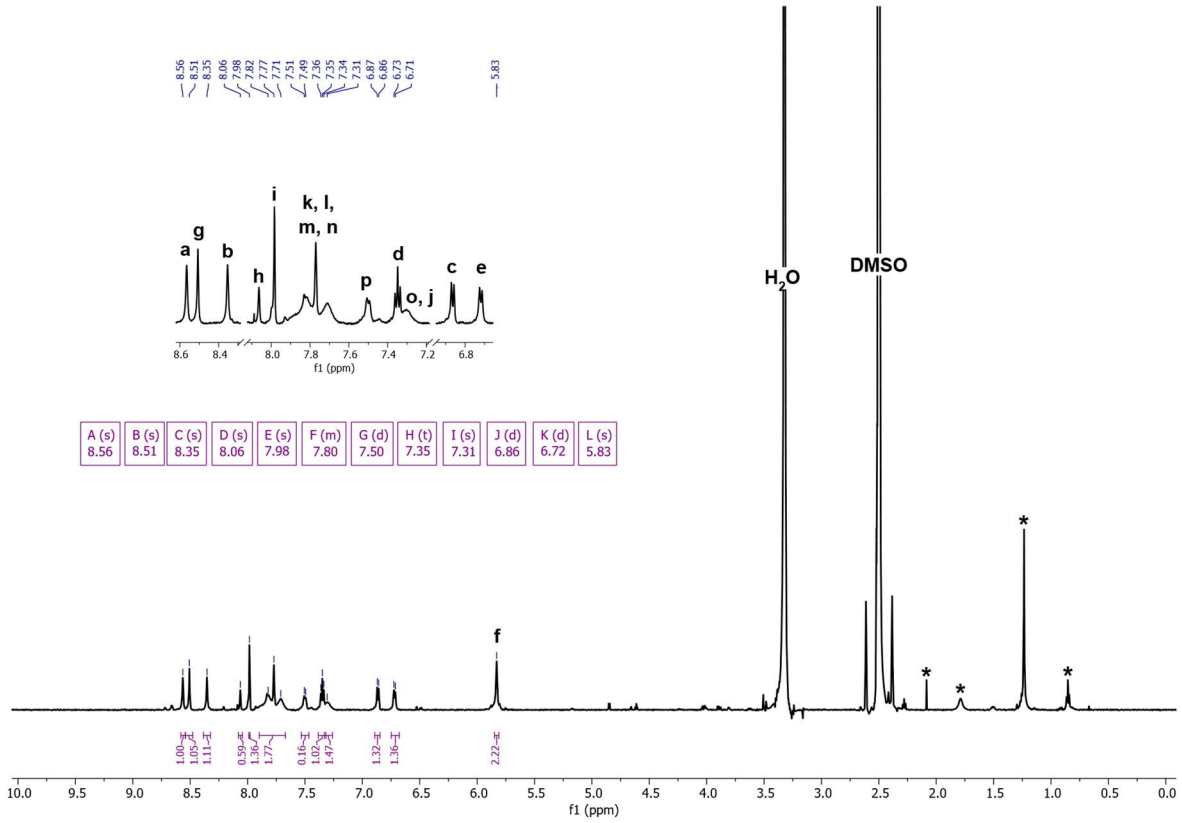

Figure 3.82: ^{1}H NMR spectrum of $[Zn_2L^{N3}{}_2]$ (DMSO-d_6, 600 MHz, 25°C).

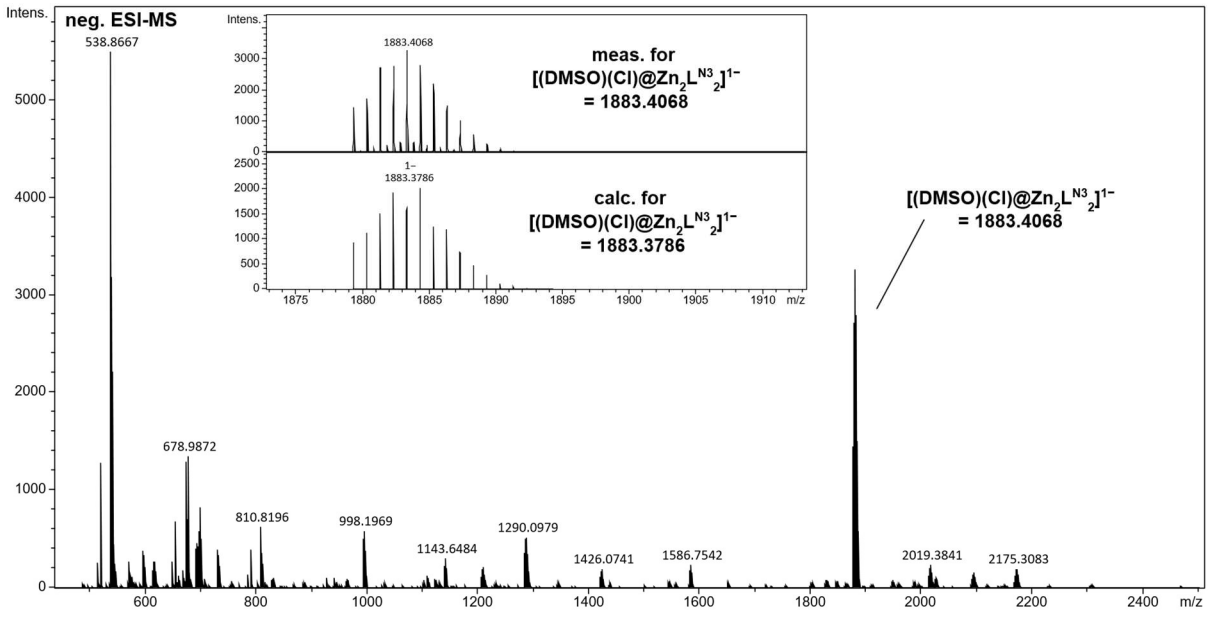

Figure 3.83: Negative ESI-MS spectrum of $[Zn_2L^{N3}{}_2]$ as adduct with DMSO and chloride in DMSO/ACN (1:9).

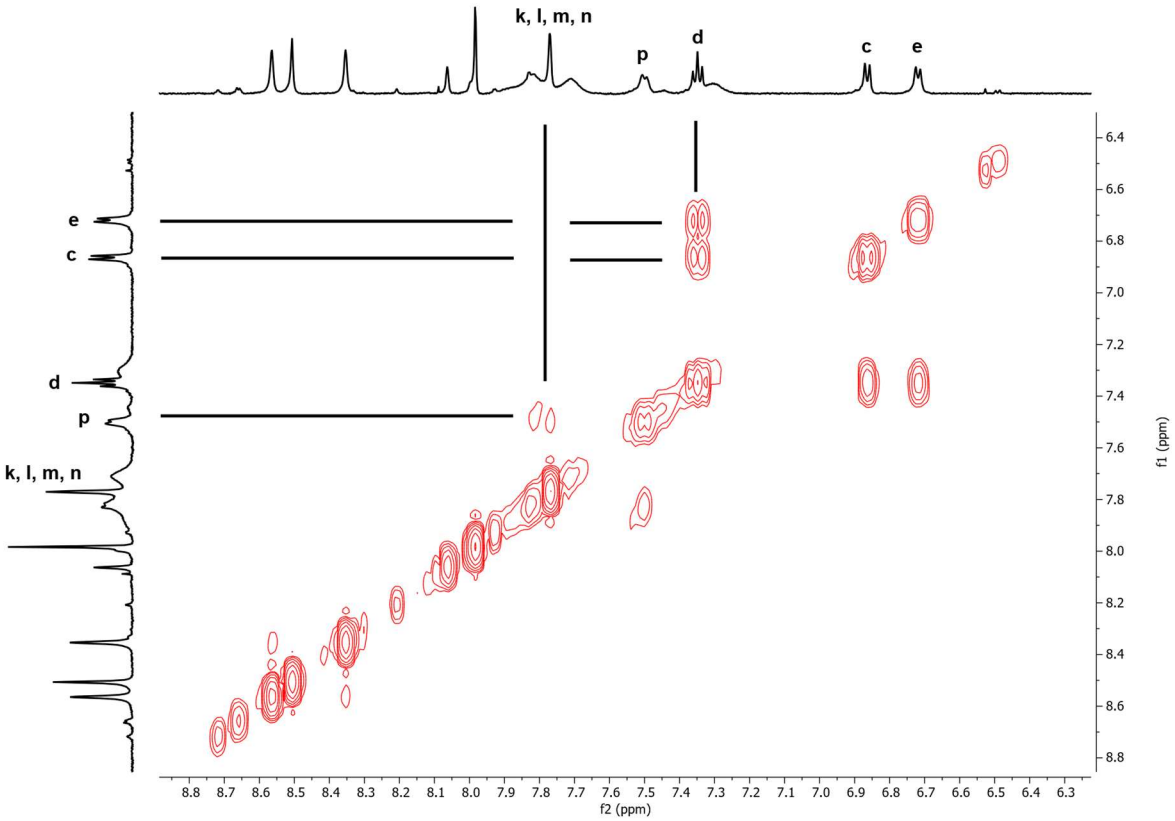

Figure 3.84: ^{1}H COSY NMR spectrum of complex $[Zn_2L^{N3}_2]$ (DMSO-d_6, 600 MHz, 25°C).

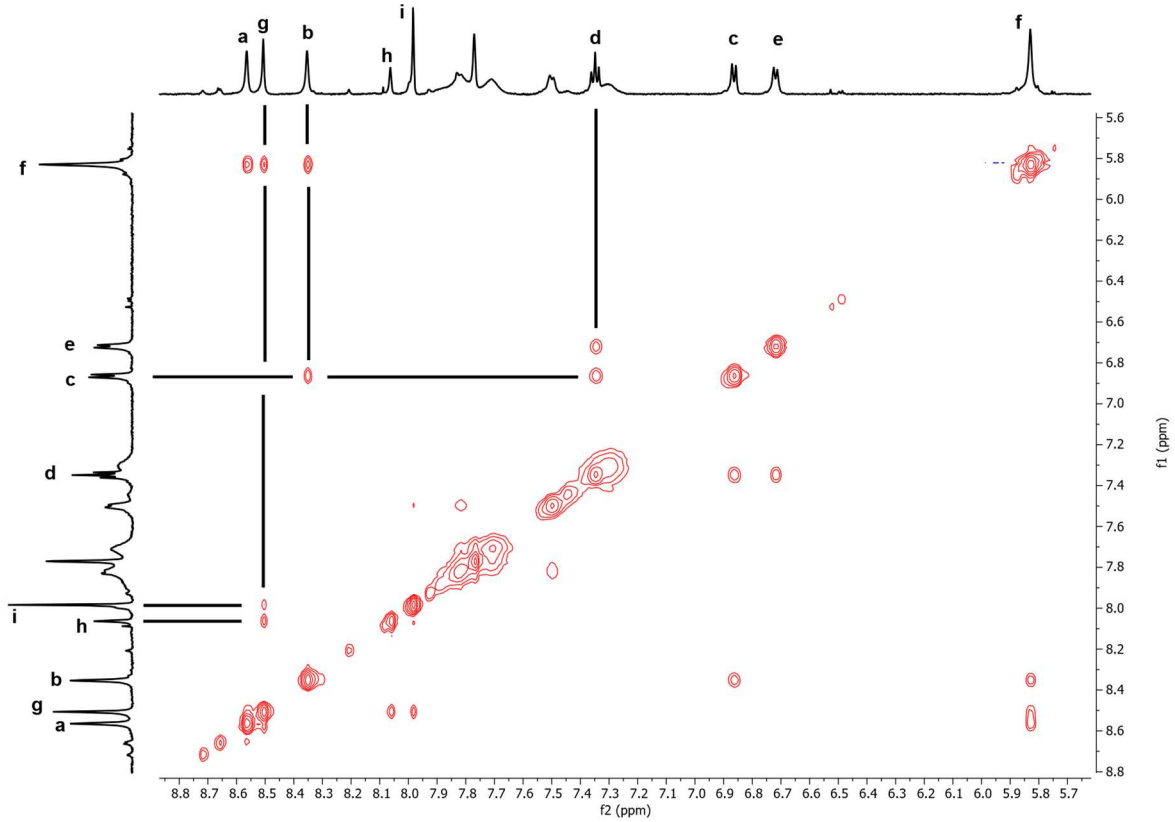

Figure 3.85: ^{1}H NOESY NMR spectrum of complex $[Zn_2L^{N3}_2]$ (DMSO-d_6, 600 MHz, 25°C).

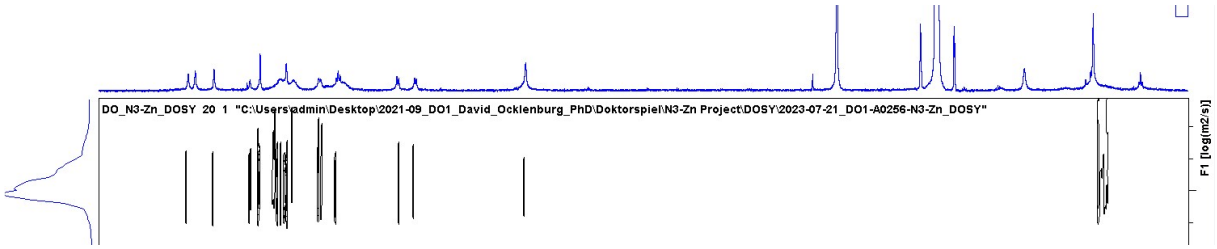

Figure 3.86: ^{1}H DOSY NMR spectrum of complex [$Zn_2L^{N3}_2$], D = 1.143 x 10^{-10} m^2 s^{-1}, r_H = 0.97 nm (DMSO-d_6, 500 MHz, 25°C).

Anion-Binding studies of [$Zn_2L^{N3}_2$] with TBA TP and TBA NP

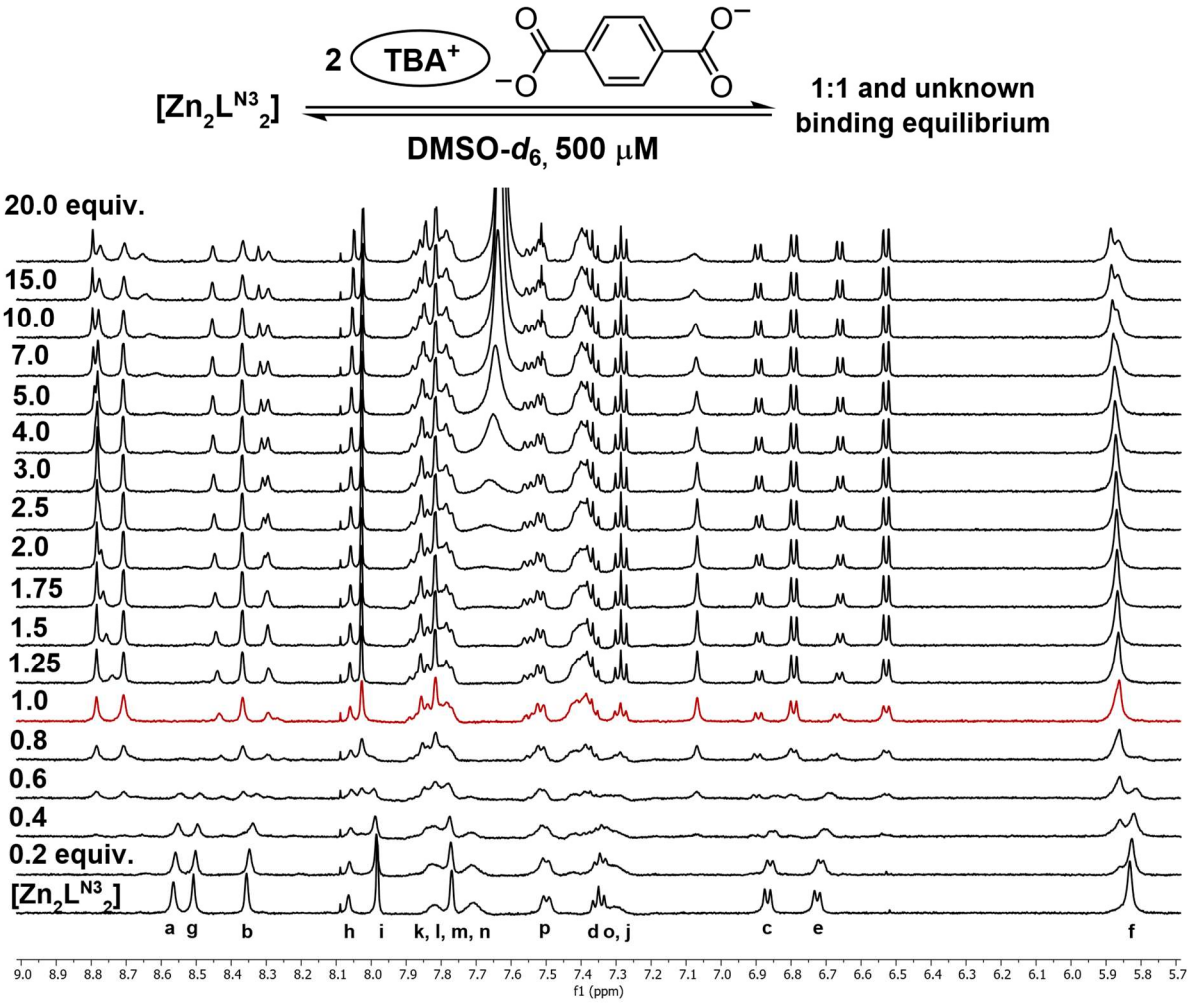

Figure 3.87: ^{1}H NMR titration of host [$Zn_2L^{N3}_2$] and TBA_2TP showing intermediate to slow binding fashion (DMSO-d_6, 500 MHz, 500 µM, 25°C).

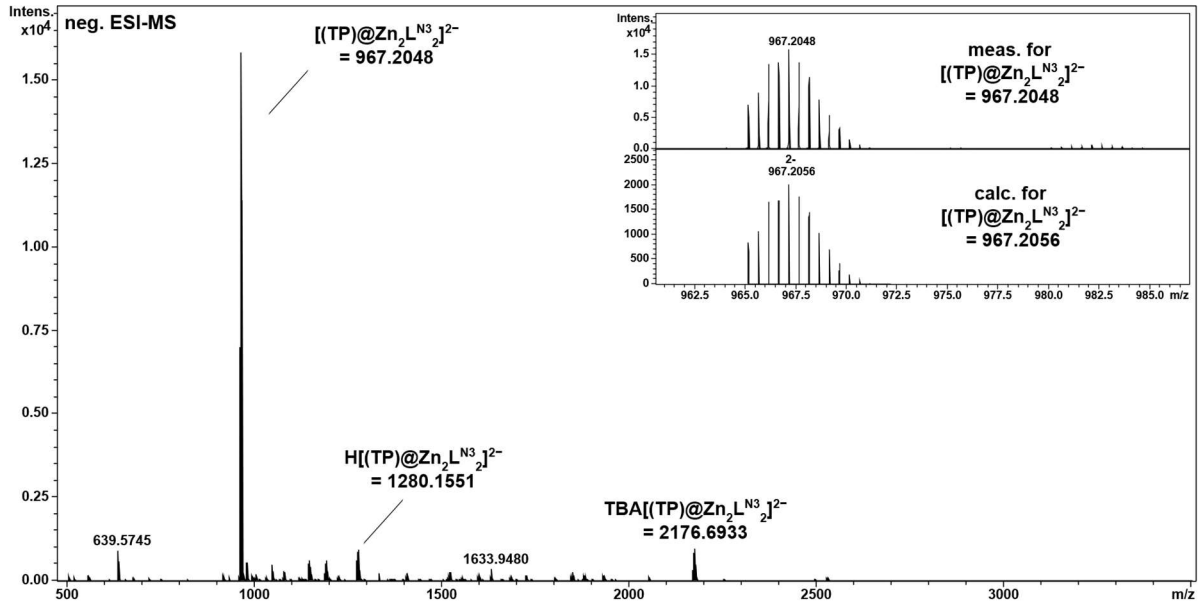

Figure 3.88: Negative ESI-MS spectrum of host-guest complex $[(TP)@Zn_2L^{N3}{}_2]^{2-}$ in DMSO/ACN (1:9).

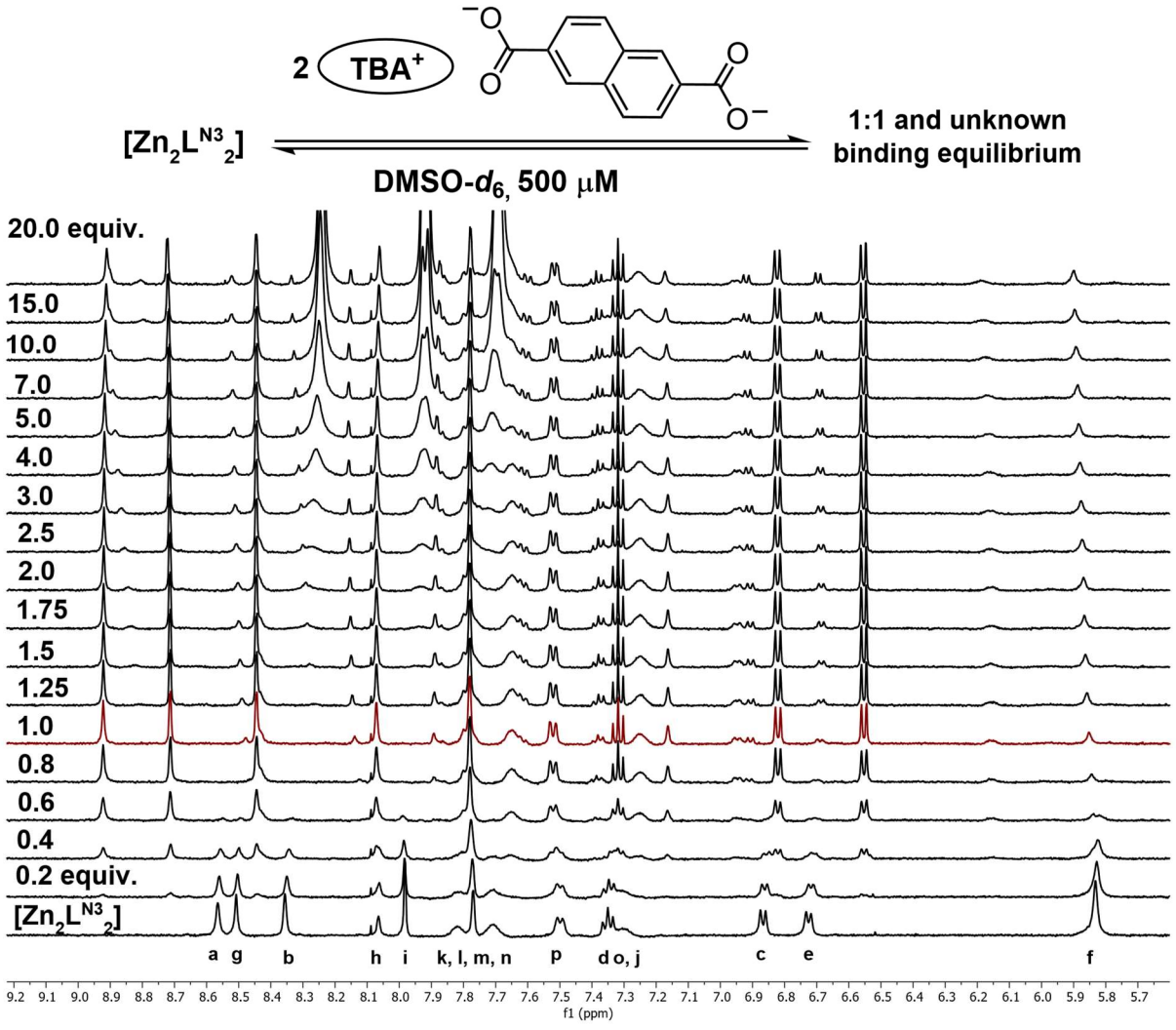

Figure 3.89: ^{1}H NMR titration of host $[Zn_2L^{N3}{}_2]$ and TBA_2NP showing intermediate to slow binding fashion (DMSO-d_6, 500 MHz, 500 µM, 25°C).

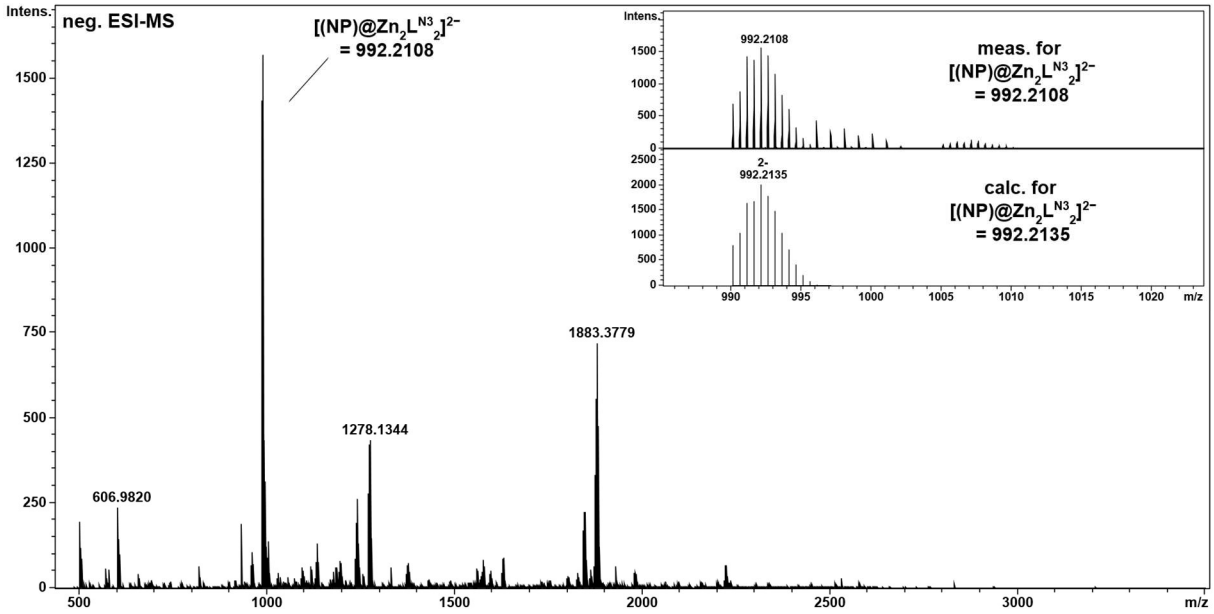

Figure 3.90: Negative ESI-MS spectrum of $[(NP)@Zn_2L^{N3}{}_2]^{2-}$.

3.7.9 Synthetic procedure of ligand L^{crown3}-H_2

Synthesis of methyl 3,5-dibromobenzoate **S15**

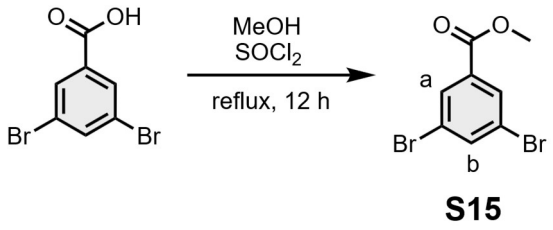

S15

*Figure 3.91: Esterification of 3,5-dibromobenzoic acid via acid chloride to obtain **S15**.*

The synthesis of compound **S15** is described in the literature, and was performed accordingly.[92] 3,5-dibromobenzoic acid (4.2 g, 15 mmol, 1 equiv.) was dissolved in $SOCl_2$ (5 mL) and refluxed for 4 h under argon atmosphere. Then, excess $SOCl_2$ was evaporated under reduced pressure and the residue was dissolved and refluxed in MeOH for additional 12 h. Afterward, the solvent was evaporated and the remaining white solid **S15** (98%, 4.3 g, 14.6 mmol) was washed with methanol.

^{1}H NMR (500 MHz, $CDCl_3$, 25°C) δ = 8.10 (d, *J* = 1.8 Hz, 2H, a), 7.85 (t, *J* = 1.8 Hz, 1H, b), 3.93 (s, 3H, OMe) ppm.

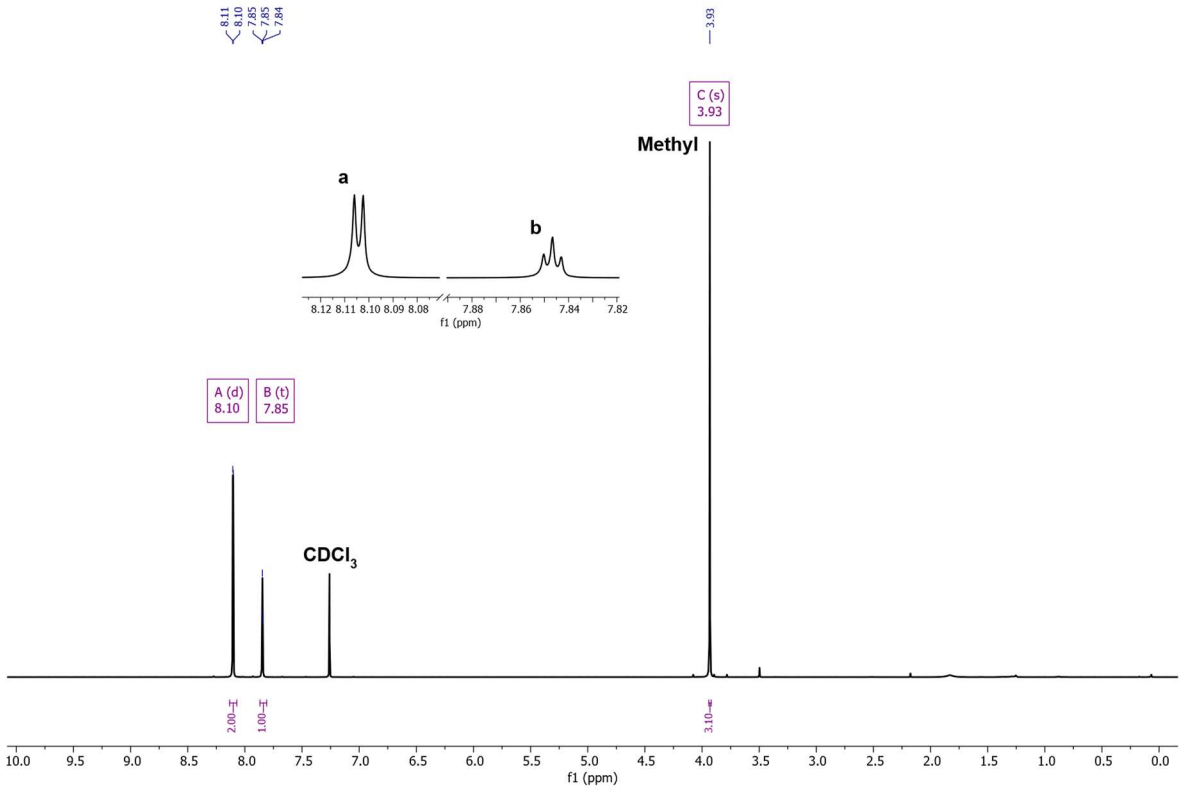

*Figure 3.92: ^{1}H NMR spectrum of precursor **S15** ($CDCl_3$, 500 MHz, 25°C).*

Synthesis of methyl 3,5-bis((trimethylsilyl)ethynyl)benzoate **S16**

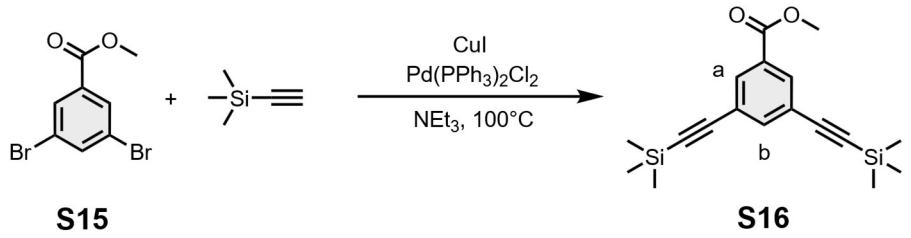

S15 **S16**

*Figure 3.93: The C-C SONOGASHIRA cross coupling of **S15** and TMS-acetylene to give precursor **S16**.*

The synthesis of **S16** is described in the literature, and was performed accordingly with small changes.[93] Compound **S15** (600 mg, 2 mmol, 1 equiv.), CuI (19.4 mg, 102 µmol, 0.05 equiv.) and $[Pd(PPh_3)_2Cl_2]$ (430 mg, 612 µmol, 0.3 equiv.) were suspended in dry Et_3N (15 mL). After three freeze-pump-thaws trimethylsilyl acetylene (1.4 mL, 10 mmol, 5 equiv.) was added and the reaction mixture was heated to 100°C and stirred for 16 h under argon atmosphere. The reaction mixture was cooled to room temperature and filtered through celite. The combined organic layers were washed with sat. NH_4Cl, dried with $MgSO_4$ and the solvent was evaporated with reduced pressure. Column chromatography gave **S16** as pale brown solid (89%, 600 mg, 1.8 mmol).

^{1}H NMR (500 MHz, $CDCl_3$, 25°C) δ = 8.04 (d, *J* = 1.6 Hz, 2H), 7.72 (t, 1.6 Hz, 1H), 3.91 (s, 3H), 0.24 (s, 18H).

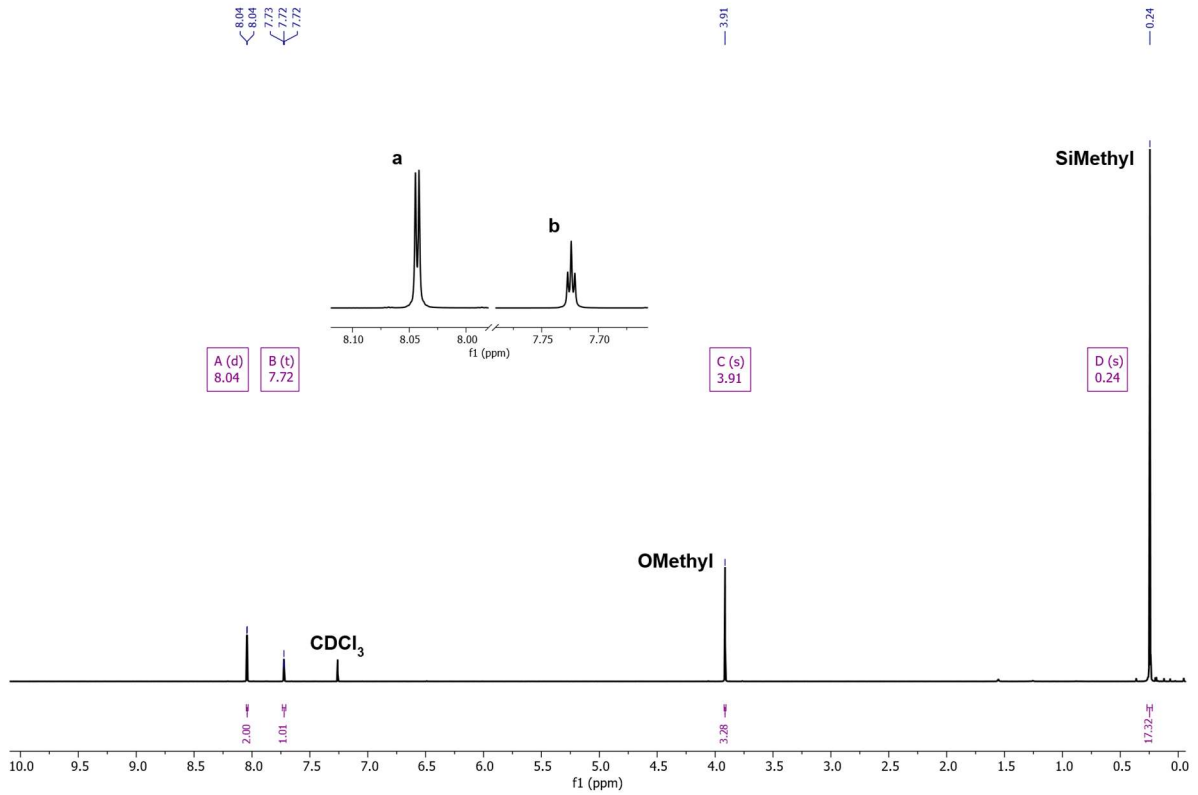

*Figure 3.94: ^{1}H NMR spectrum of precursor **S16** ($CDCl_3$, 500 MHz, 25°C).*

Synthesis of 3,5-diethynylbenzoic acid **S17**

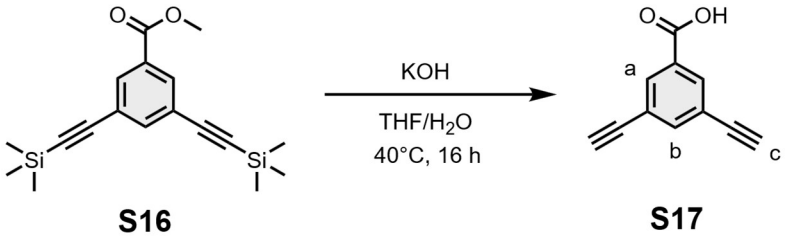

*Figure 3.95: Basic deprotection of the precursor **S16** to obtain di-alkyne **S17**.*

The synthesis of **S17** is described in the literature and was performed accordingly.[94] Reactant **S16** (250 mg, 760 µmol, 1 equiv.) was dissolved in dry THF (5 mL) and an aqueous solution (2 mL) of KOH (213 mg, 3.8 mmol, 5 equiv.) was added to the stirring solution. The reaction mixture was cooled to room temperature and the solvent was evaporated. The residue was dissolved in Et_2O (10 mL) and H_2O (5 mL). The mixture was neutralized with 1 M HCl. Afterward, the organic layer was separated and the aqueous layer was extracted with Et_2O (3x). The combined organic layers were dried with $MgSO_4$ and the solvent was evaporated to give the product **S17** as pale brown solid (69%, 90 mg, 529 µmol).

^{1}H NMR (400 MHz, $CDCl_3$, 25°C) δ = 8.18 (d, *J* = 1.6 Hz, 2H, a), 7.82 (t, *J* = 1.6 Hz, 1H, b), 3.16 (s, 2H, c).

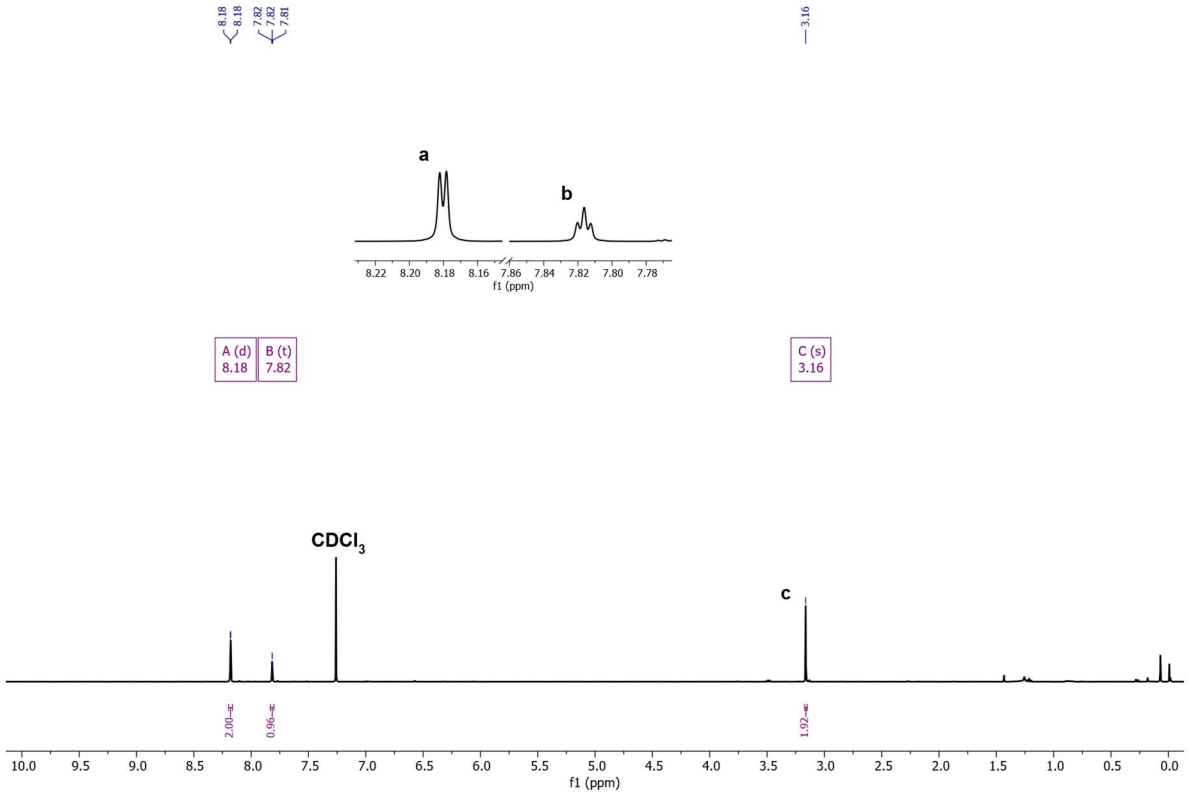

*Figure 3.96: ^{1}H NMR spectrum of di-alkyne **S17** ($CDCl_3$, 500 MHz, 25°C).*

Synthesis of (1,4,7,10,13-pentaoxacyclopentadecan-2-yl)methyl 3,5-diethynylbenzoate **S18**

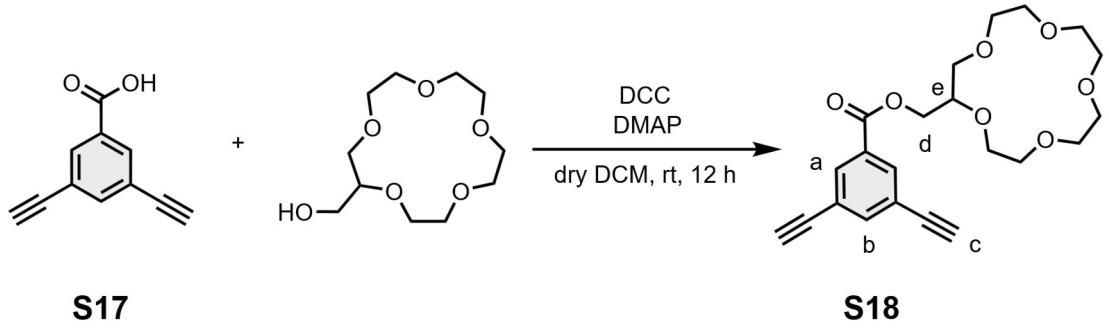

S17 **S18**

*Figure 3.97: Esterification of **S17** and crown-ether unit via DCC coupling to obtain the modified backbone **S18**.*

The carboxylic acid **S17** (105 mg, 617 µmol, 1 equiv.) was suspended in dry DCM (40 mL/g). Then, DCC (140 mg, 679 µmol, 1.1 equiv.) and the 15-crown-5 derivative ((1,4,7,10,13-pentaoxacyclopentadecan-2-yl)methanol) (158 µL, 740 µmol, 1.2 equiv.) were added to the reaction mixture sequentially. Afterward a catalytic amount of DMAP was added and the reaction mixture was stirred for 12 h at room temperature. The reaction mixture was filtered, and the filter cake was carefully washed with cold DCM. The organic layer was dried, and the solvent was evaporated. Column chromatography (DCM/MeOH gradient 0% to 1%) gives the product **S18** (60%, 150 mg, 372 µmol).

^{1}H NMR (500 MHz, $CDCl_3$, 25°C) δ = 8.10 (d, *J* = 1.6 Hz, 2H, a), 7.76 (t, *J* = 1.6 Hz, 1H, b), 4.48 (dd, *J* = 11.6, 4.1 Hz, 1H, d), 4.34 (dd, *J* = 11.6, 6.0 Hz, 1H, d'), 3.98 (qd, *J* = 5.8, 4.0 Hz, 1H, e), 3.91-3.77 (m, 3H, crown-ether), 3.76-3.62 (m, 15H, crown-ether), 3.14 (s, 2H, c) ppm. **^{13}C NMR** (126 MHz, $CDCl_3$, 25°C) δ = 164.99, 139.52, 133.41, 130.97, 123.13, 81.71, 79.12, 77.57, 71.37, 71.06, 70.96, 70.87, 70.7614, 70.72, 70.64, 70.55, 70.51, 65.48 ppm. **HRMS** (positive ESI-MS, ACN): m/z = 425.1593 ([M+Na]$^+$, $C_{22}H_{26}O_7Na^+$, calc. 425.1571).

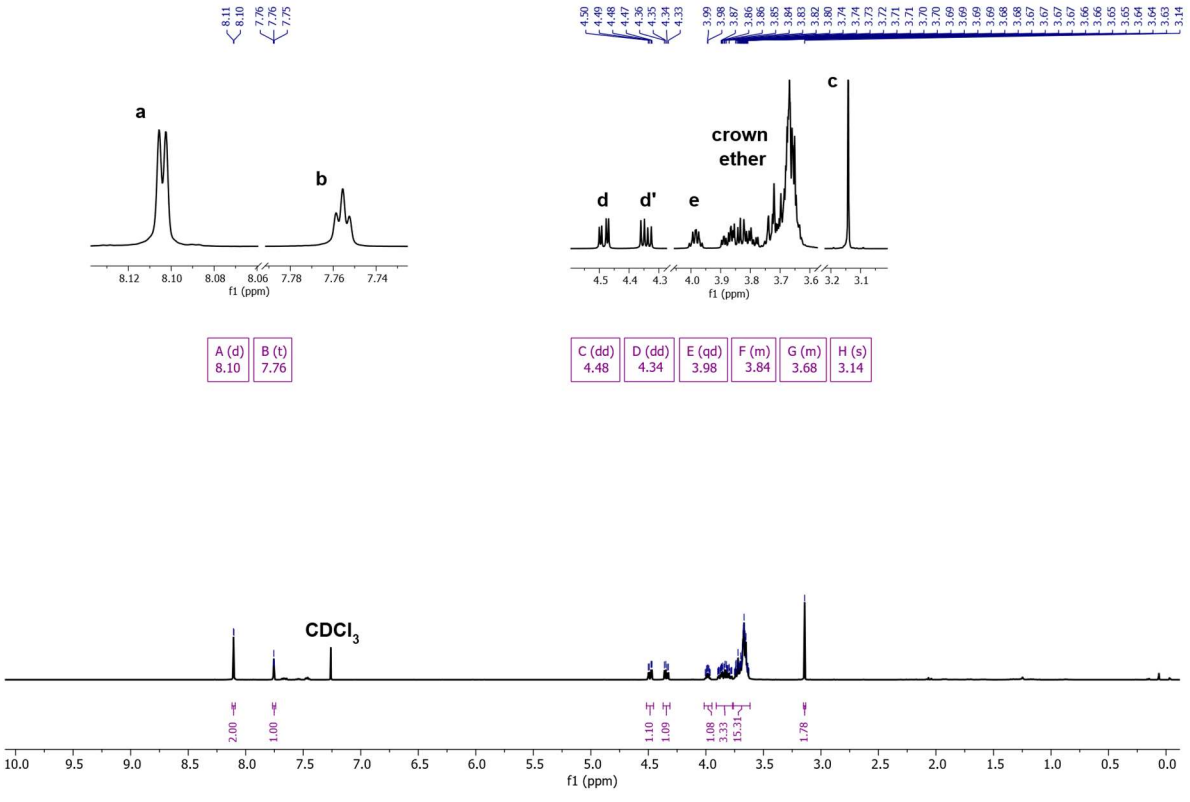

*Figure 3.98: ^{1}H NMR spectrum of the backbone **S18** ($CDCl_3$, 500 MHz, 25°C).*

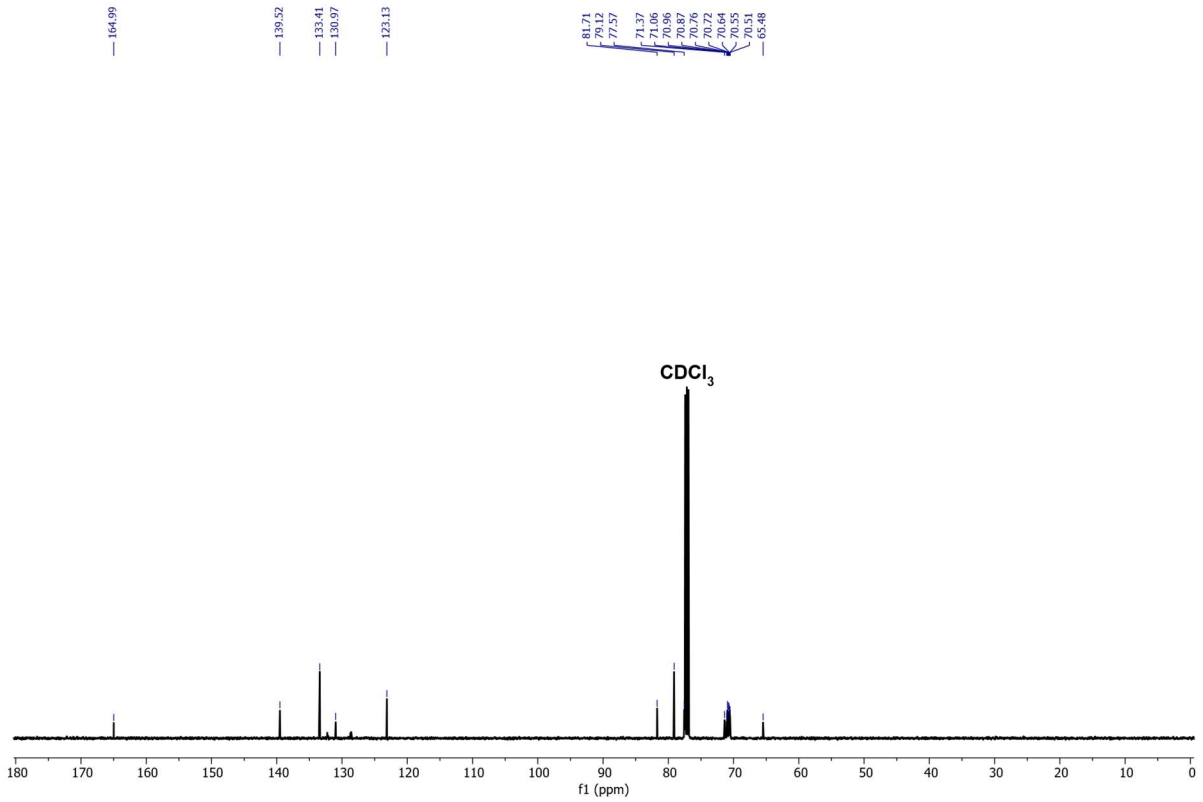

*Figure 3.99: ^{13}C NMR spectrum of backbone **S18** ($CDCl_3$, 126 MHz, 25°C).*

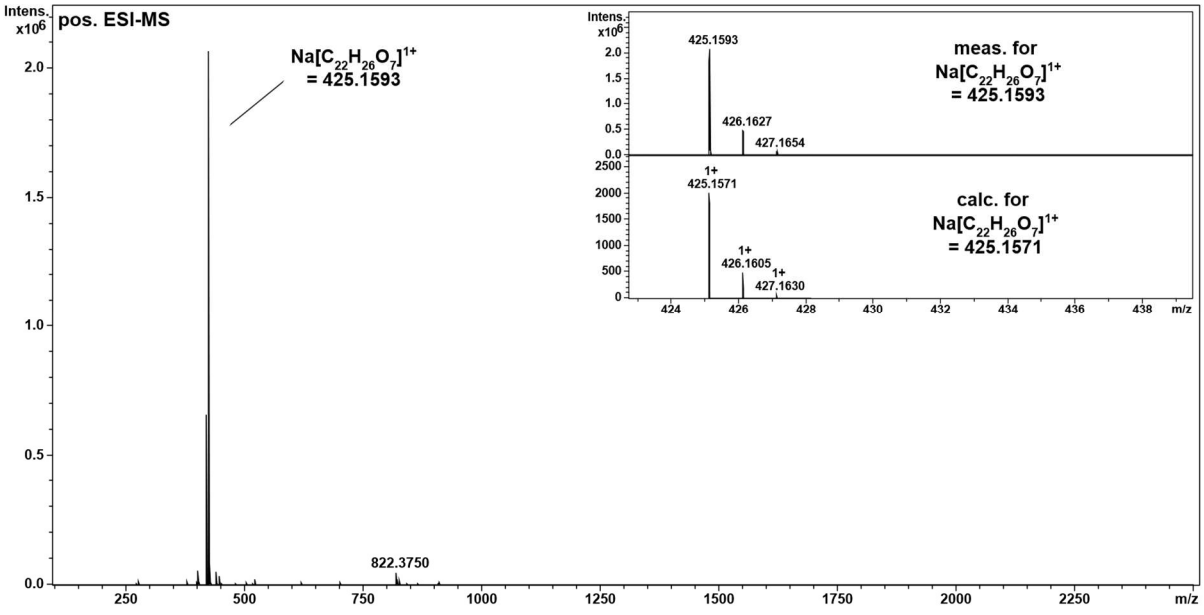

*Figure 3.100: Positive HR ESI-MS spectrum of backbone **S18** (DCM).*

Synthesis of ligand L^{crown3}-H_2

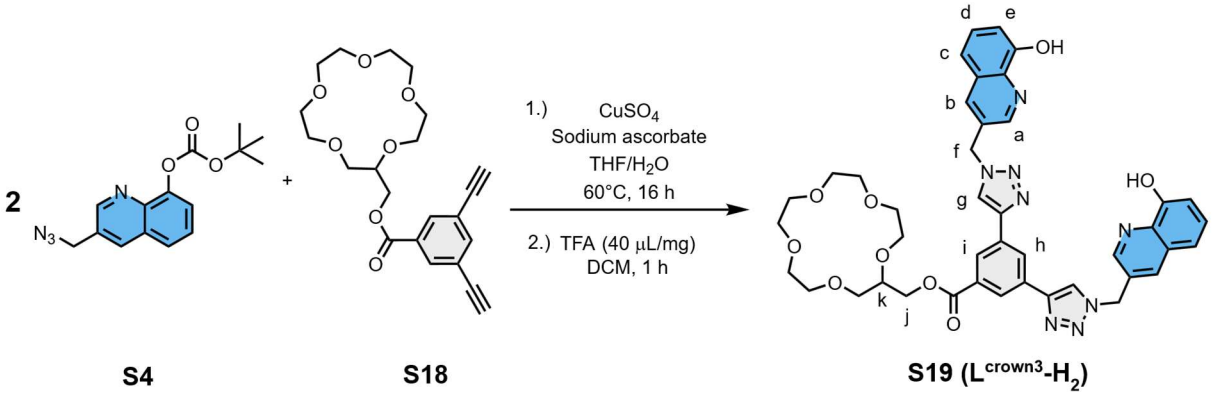

*Figure 3.101: 1,3-dipolar HUISGEN cycloaddition of backbone **S18** and azide **S4** gave the ligand **S19** (L^{crown3}-H_2).*

The azide **S4** (145 mg, 483 µmol, 2.2 equiv.) was transferred into a Schlenk tube and dissolved in THF. The solution was degassed for 20 min with argon. $CuSO_4$ (1.7 mg, 11 µmol, 0.05 equiv.) and sodium-ascorbate (174 mg, 878 µmol, 4 equiv.) were dissolved in small amounts of water and added sequentially. Backbone **S18** (106.9 mg, 265 µmol, 1.1 equiv.) was added under argon, the solution was heated to 60°C and stirred for 16 h. The reaction solution was diluted with DCM and the organic layer was washed with EDTA (0.25 M), brine and saturated NH_4Cl solution. The aqueous layer was extracted with DCM (3x). The combined organic layers were dried with Na_2SO_4 and the solvent was evaporated under reduced pressure. Column chromatography (silica, DCM/MeOH gradient 0 % - 5 %) yielded the Boc-protected derivative. The solvent was evaporated, redissolved in DCM and treated with TFA (40 µL/mg). After 1 h the reaction mixture was neutralized with sat. $NaHCO_3$ and the organic layer diluted with DCM. The yellow precipitate was dissolved in DCM. The aqueous layer was extracted with DCM (7x), washed with brine and the combined organic layers were dried via Na_2SO_4. The solvent was evaporated until there was a residue organic layer present. Pouring Et_2O into the residue gives the ligand **S19** (L^{crown3}-H_2) as a white solid (49%, 94.3 mg, 117.4 mmol).

^{1}H NMR (600 MHz, DMSO-d_6, 25°C) δ = 9.94 (s, 2H), 8.92 (d, *J* = 2.2 Hz, 2H), 8.90 (s, 2H), 8.57 (t, *J* = 1.7 Hz, 1H), 8.40 (d, *J* = 1.7 Hz, 2H), 8.30 (d, *J* = 2.2 Hz, 2H), 7.46 (t, *J* = 7.8 Hz, 2H), 7.40 (dd, *J* = 8.3, 1.4 Hz, 2H), 7.10 (dd, *J* = 7.5, 1.4 Hz, 2H), 5.93 (s, 4H), 4.45 (dd, *J* = 11.5, 3.8 Hz, 1H), 4.29 (dd, *J* = 11.5, 6.2 Hz, 1H), 3.93 (qd, *J* = 5.7, 3.8 Hz, 1H), 3.78-3.65 (m, 3H), 3.64-3.46 (m, 15H) ppm. **^{13}C NMR** (151 MHz, DMSO-d_6, 25°C) δ = 165.2333, 153.42, 148.22, 145.57, 138.06, 135.44, 131.91, 131.16, 129.14, 128.27, 128.19, 126.3358, 124.9204, 122.60, 117.82, 111.9557, 76.6024, 70.37, 70.07, 70.01, 69.90, 69.82, 69.69, 69.65, 69.58, 69.39, 64.95, 50.90 ppm. **HRMS** (positive ESI-MS, ACN): m/z = 825.2938 ($[M+Na]^+$, $C_{42}H_{42}N_8O_7Na^+$, calc. 825.2967).

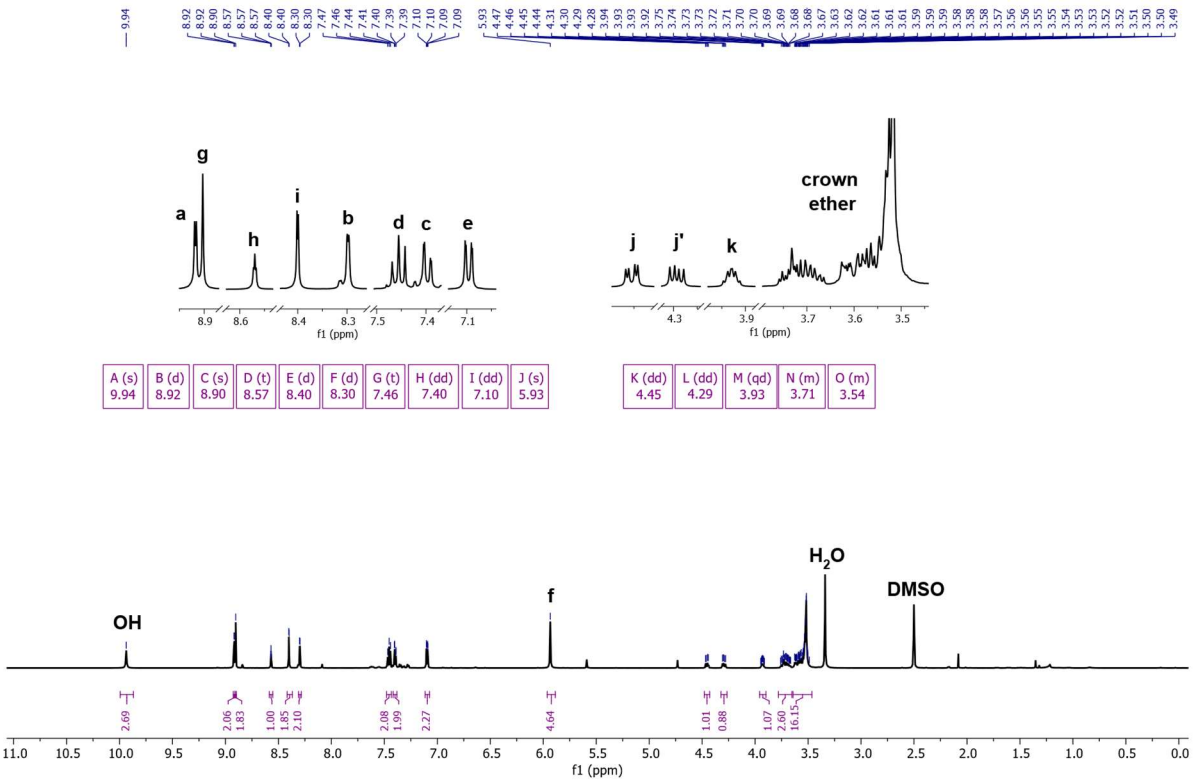

*Figure 3.102: ^{1}H NMR spectrum of the ligand **S19** (L^{crown3}-H_2). (DMSO-d_6, 600 MHz, 25°C).*

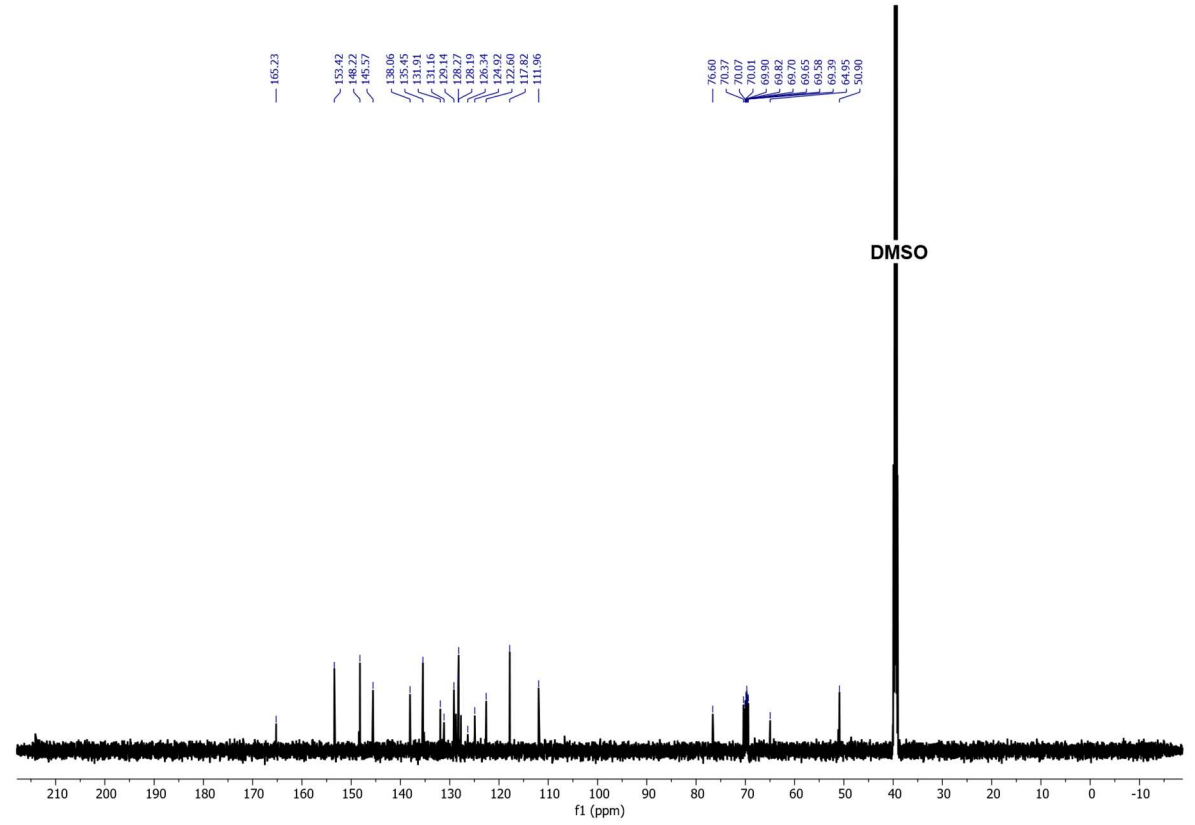

*Figure 3.103: ^{13}C NMR spectrum of the ligand **S19** (L^{crown3}-H_2) (DMSO-d_6, 151 MHz, 25°C).*

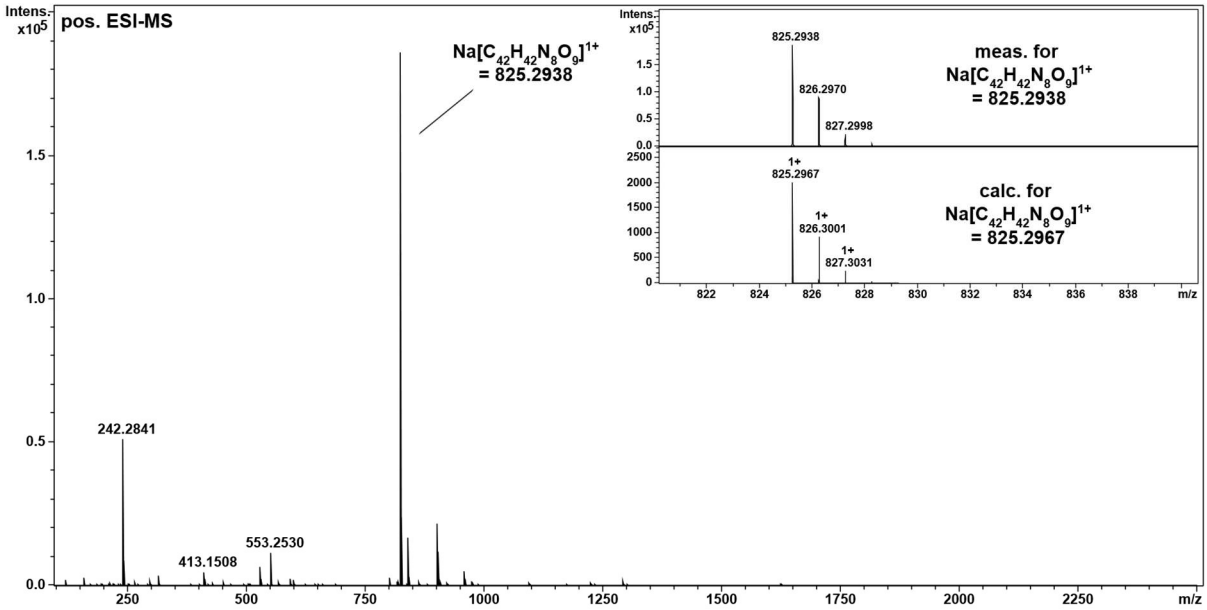

*Figure 3.104: Positive ESI-MS spectrum of the ligand **S19** (L^{crown3}-H_2) (DCM).*

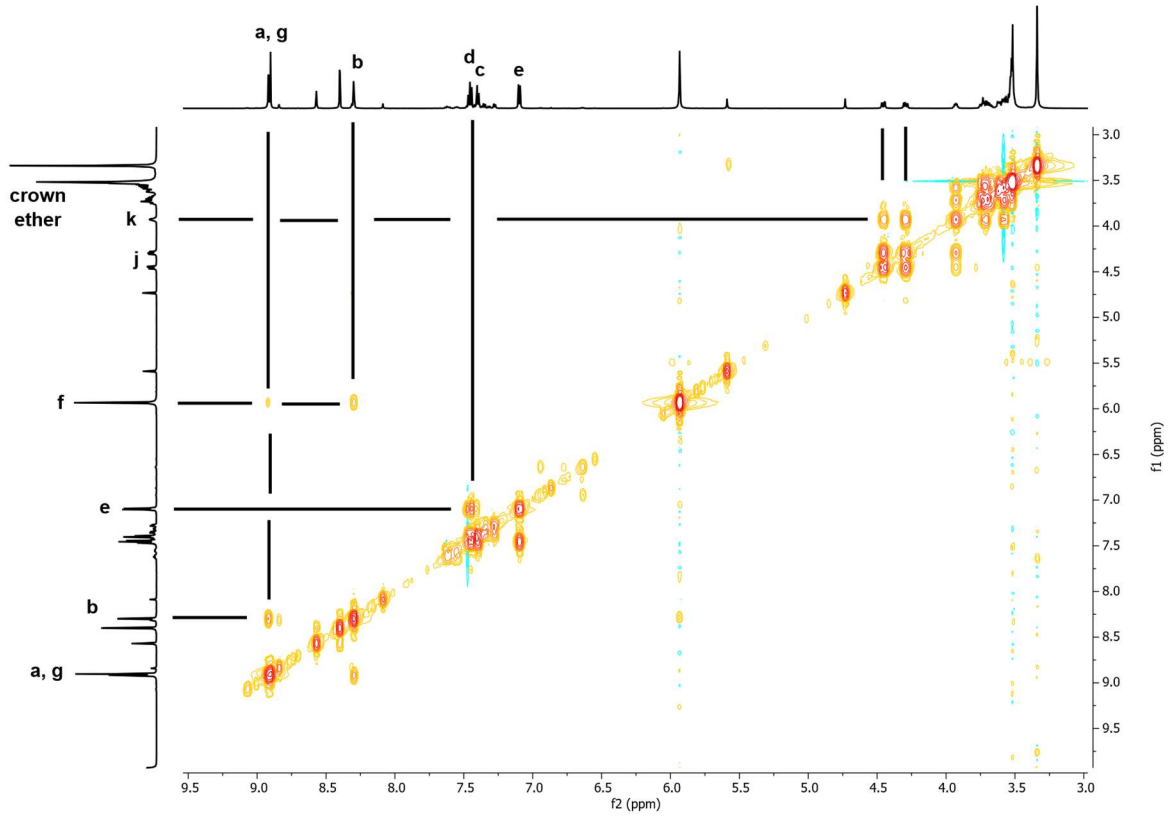

*Figure 3.105: ^{1}H COSY NMR spectrum of the ligand **S19** (L^{crown3}-H_2) (DMSO-d_6, 600 MHz, 25°C).*

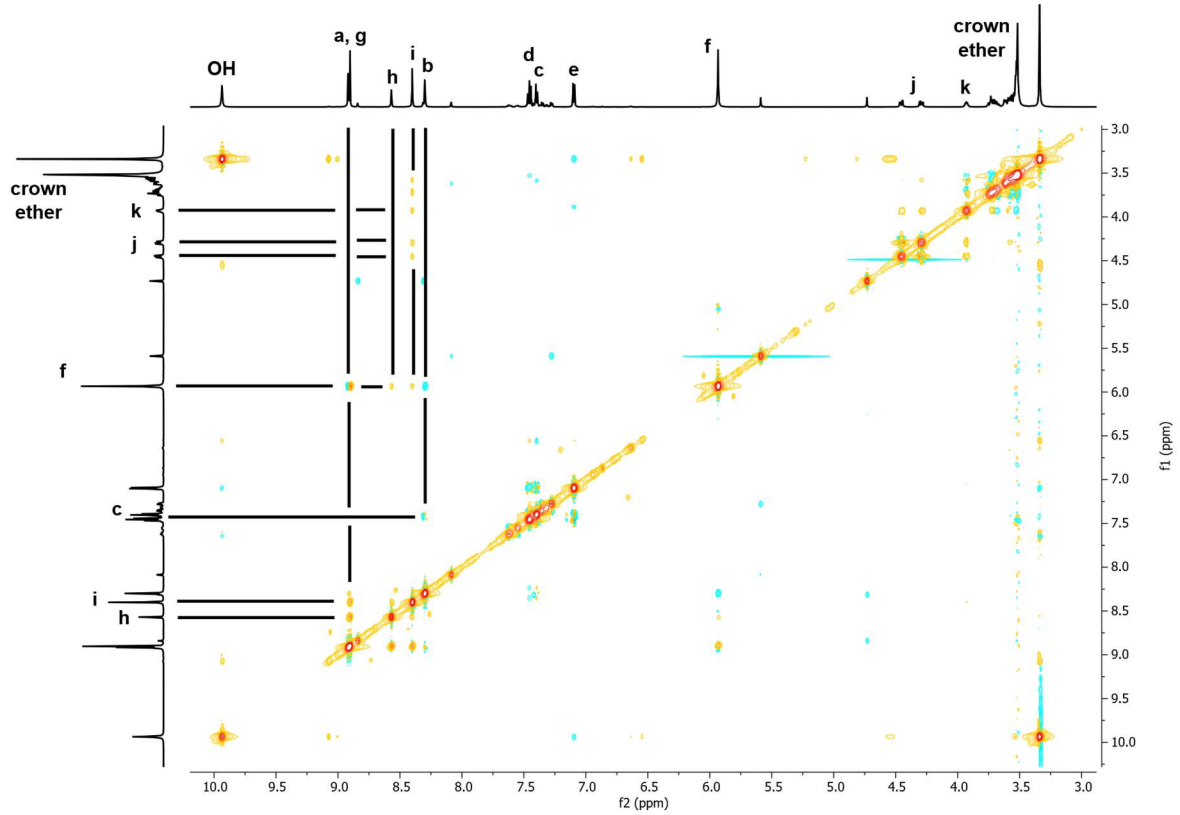

*Figure 3.106: ^{1}H NOESY NMR spectrum of the ligand **S19** (L^{crown3}-H_2) (DMSO-d_6, 600 MHz, 25°C).*

3.7.10 Self-assembly of ligand L^{crown3}-H_2 with $Zn(OAc)_2$

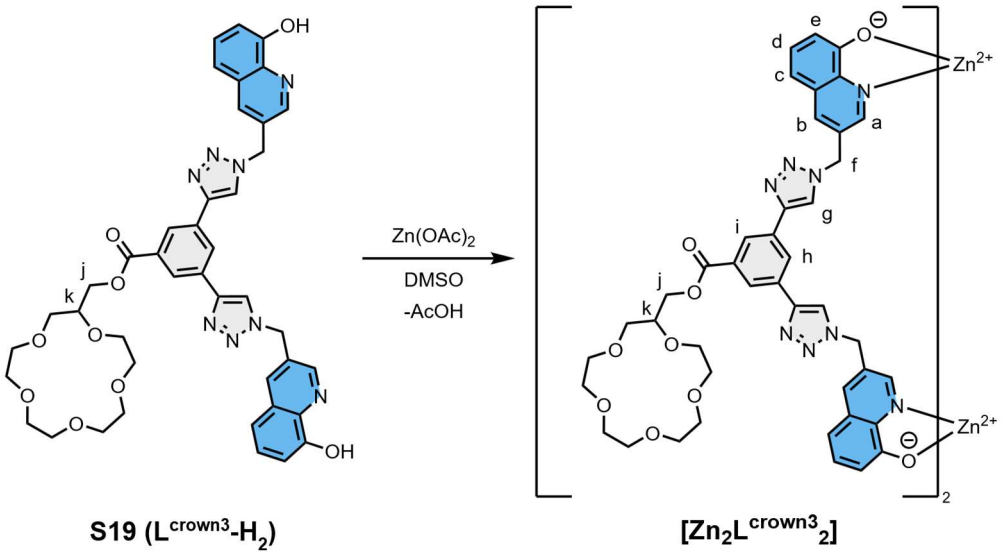

*Figure 3.107: Self-assembly of ligand **S19** (L^{crown3}-H_2) and $Zn(OAc)_2$ in DMSO-d_6 in a 1:1 ratio.*

Ligand **S19** (L^{crown3}-H_2) (5 mg, 6.23 µmol, 1 equiv.) and $Zn(OAc)_2$ (1.14 mg, 6.23 µmol, 1 equiv.) were dissolved separately in DMSO-d_6.The zinc acetate solution was added to the stirring ligand solution which resulted in a colour change to yellow. After 1 h the solvent as well as the by-product acetic acid were removed via lyophilization, which yields the complex $[Zn_2L^{crown3}{}_2]$ as a yellow solid with nearly quantitative yield (6.22 mg, 6.22 µmol, 99%).

^{1}H NMR (500 MHz, DMSO-d_6, 25°C) δ = 8.76 (s, 2H, a), 8.61 (s, 2H, b), 8.40 (s, 5H, g, h, i), 7.34 (t, *J* = 7.8 Hz, 2H, d), 6.87 (d, *J* = 8.0 Hz, 2H, c), 6.70 (d, *J* = 7.9 Hz, 2H, e), 5.92 (s, 4H, f), 4.44 (dd, *J* = 11.4, 4.1 Hz, 1H, j), 4.28 (dd, *J* = 11.4, 6.1 Hz, 1H, j'), 3.96-3.87 (m, 1H, k), 3.78-3.45 (m, 18H, crown ether) ppm. **HRMS** (negative ESI-MS, ACN): m/z = 901.1803 ($[M+2Cl]^{2-}$, $C_{84}H_{80}N_{16}O_{18}Zn_2Cl_2^-$, calc. 901.1892), 1767.3936 ($[M+Cl]^-$, $C_{84}H_{80}N_{16}O_{18}Zn_2Cl^-$, calc. 1767.4091).

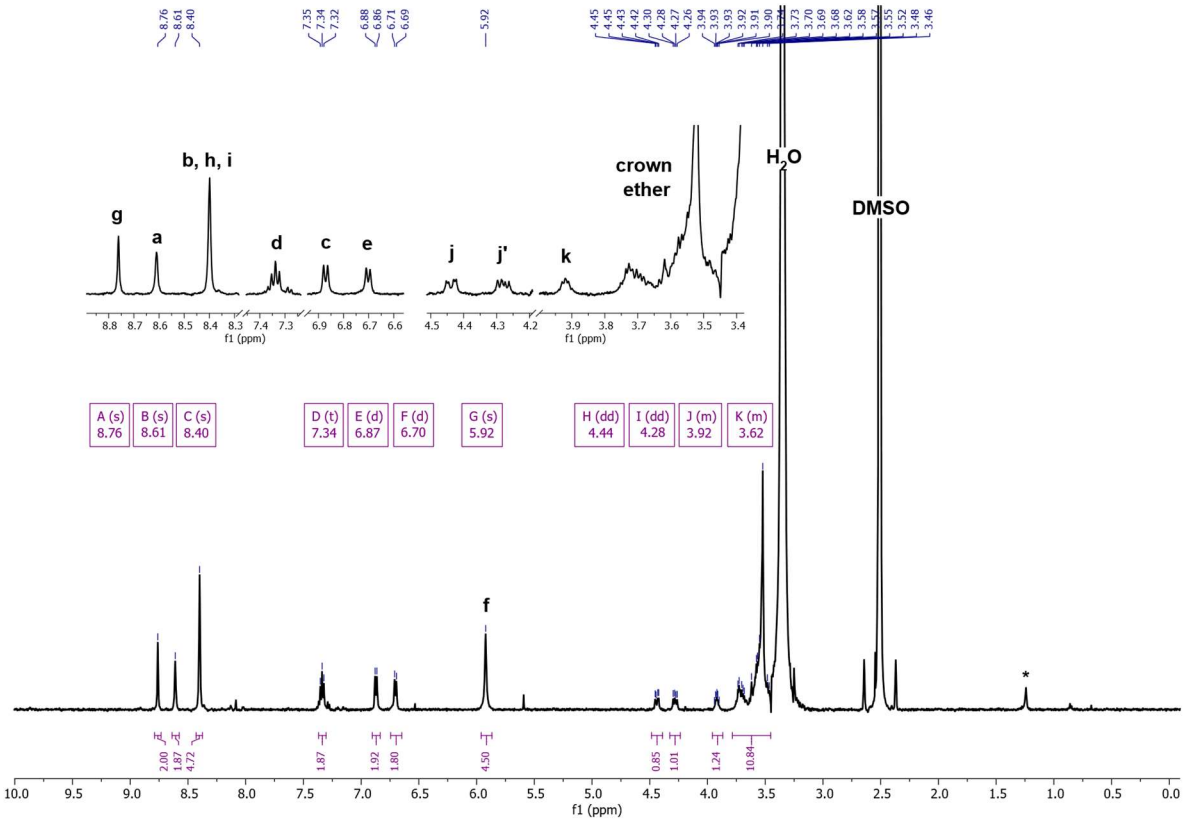

Figure 3.108: ^{1}H NMR spectrum of complex [$Zn_2L^{crown3}_2$] (DMSO-d_6, 600 MHz, 25°C).

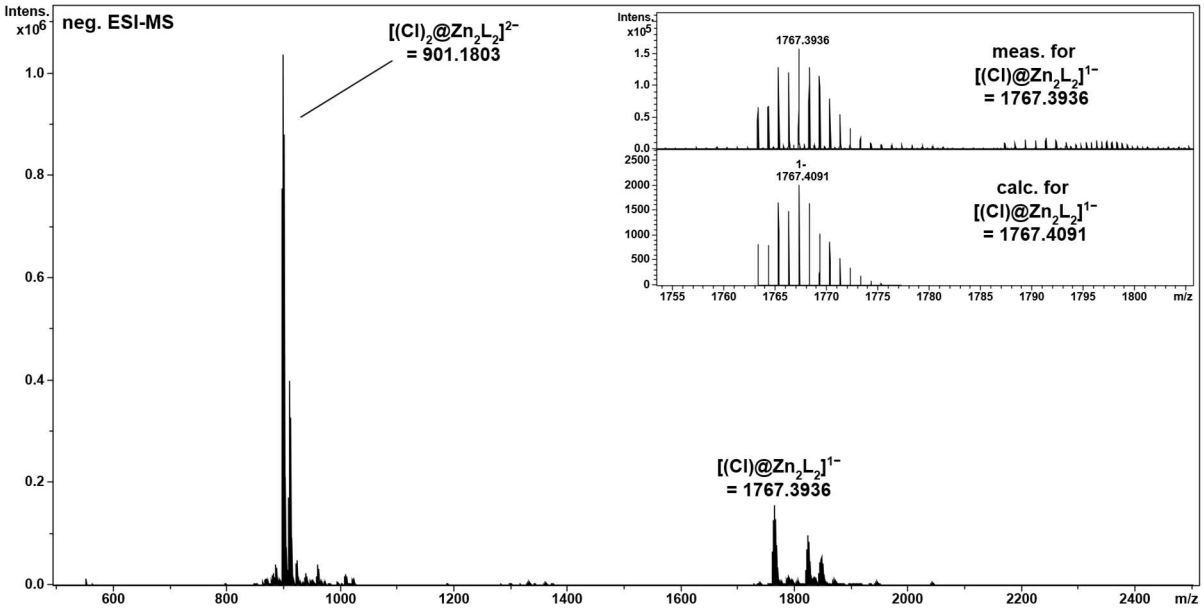

Figure 3.109: Negative ESI-MS spectrum of complex [$Zn_2L^{crown3}_2$] (DMSO/ACN 1:9).

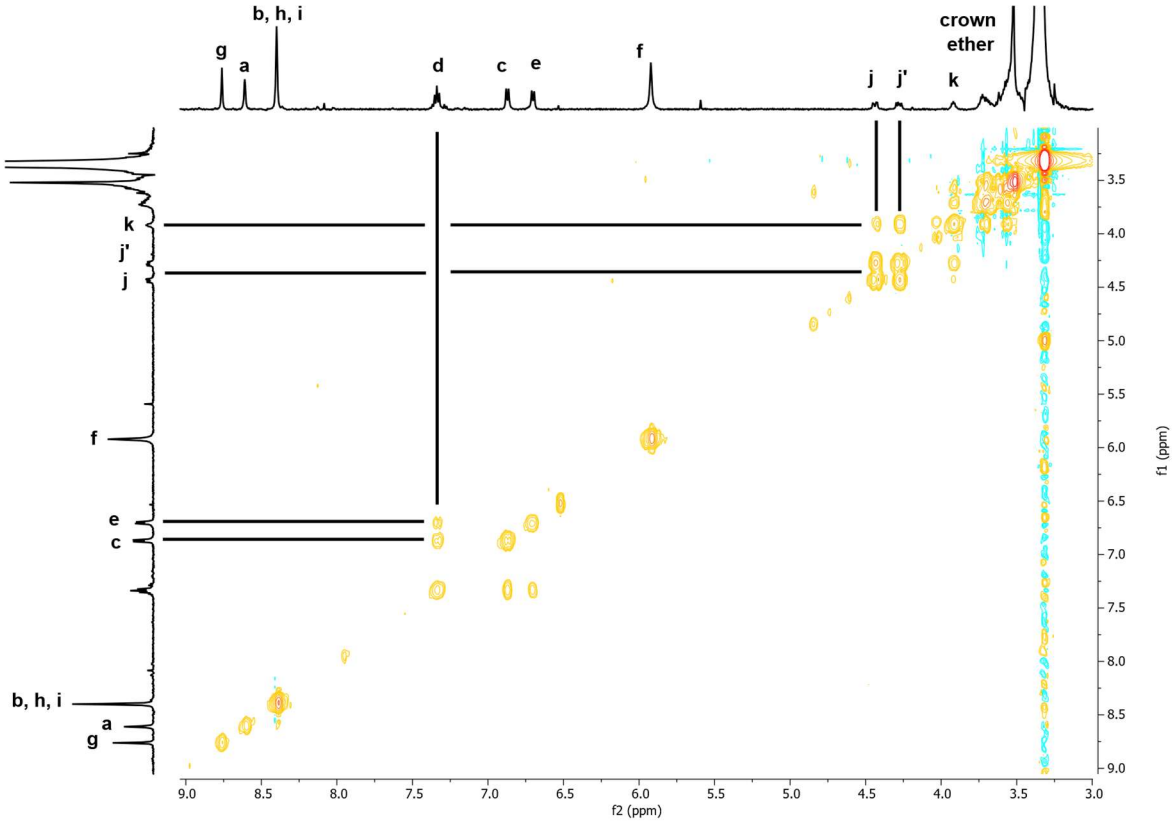

Figure 3.110: ^{1}H COSY NMR spectrum of complex [$Zn_2L^{crown3}_2$] (DMSO-d_6, 500 MHz, 25°C).

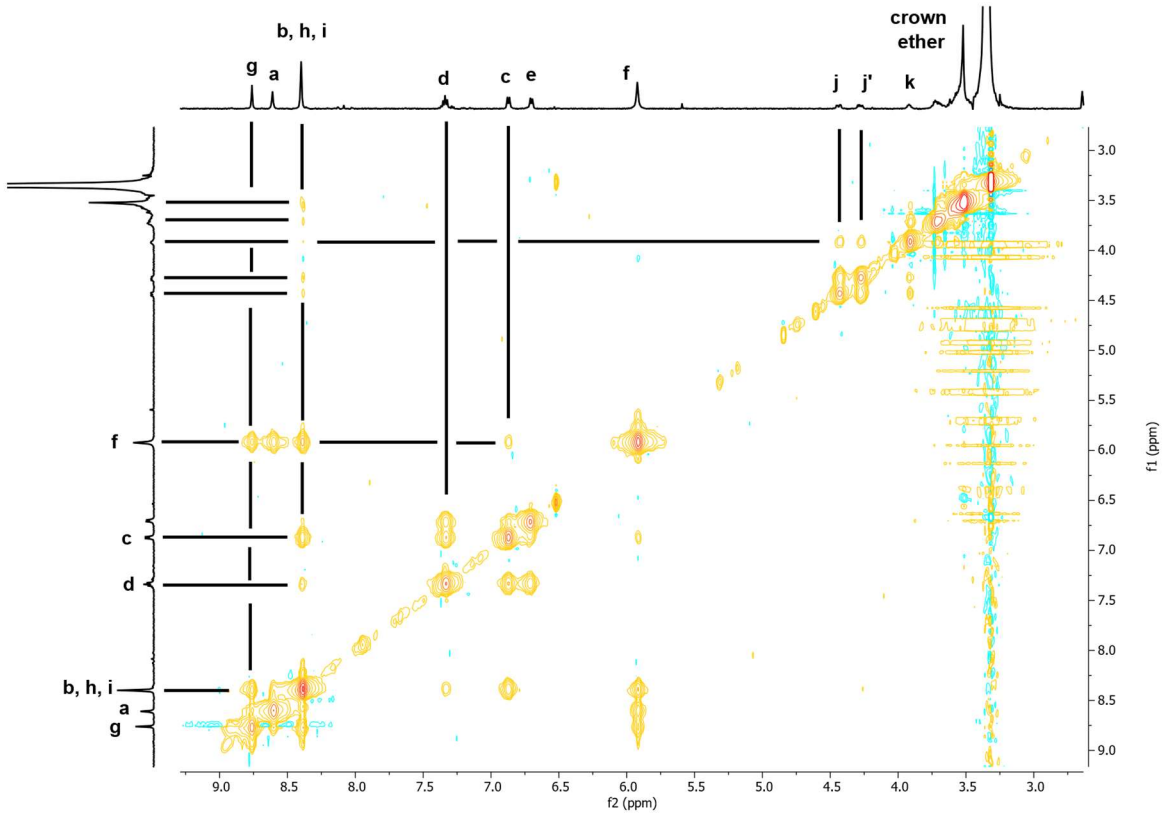

Figure 3.111: ^{1}H NOESY NMR spectrum of complex [$Zn_2L^{crown3}_2$] (DMSO-d_6, 500 MHz, 25°C).

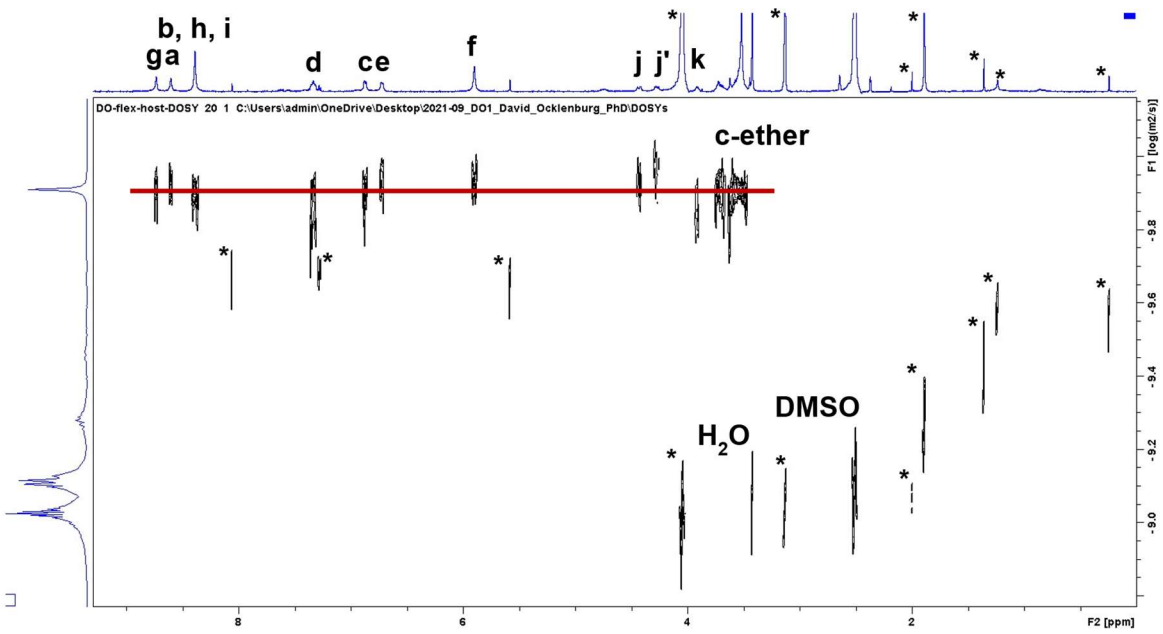

Figure 3.112: ^{1}H DOSY spectrum of complex $[Zn_2L^{crown3}{}_2]$, D = 1.201 x 10^{-10} m^2 s^{-1}, r_H = 0.92 nm (DMSO-d_6, 500 MHz, 25°C).

3.7.11 *Qualitative and quantitative binding studies of [Zn$_2$L$^{crown3}{}_2$]*

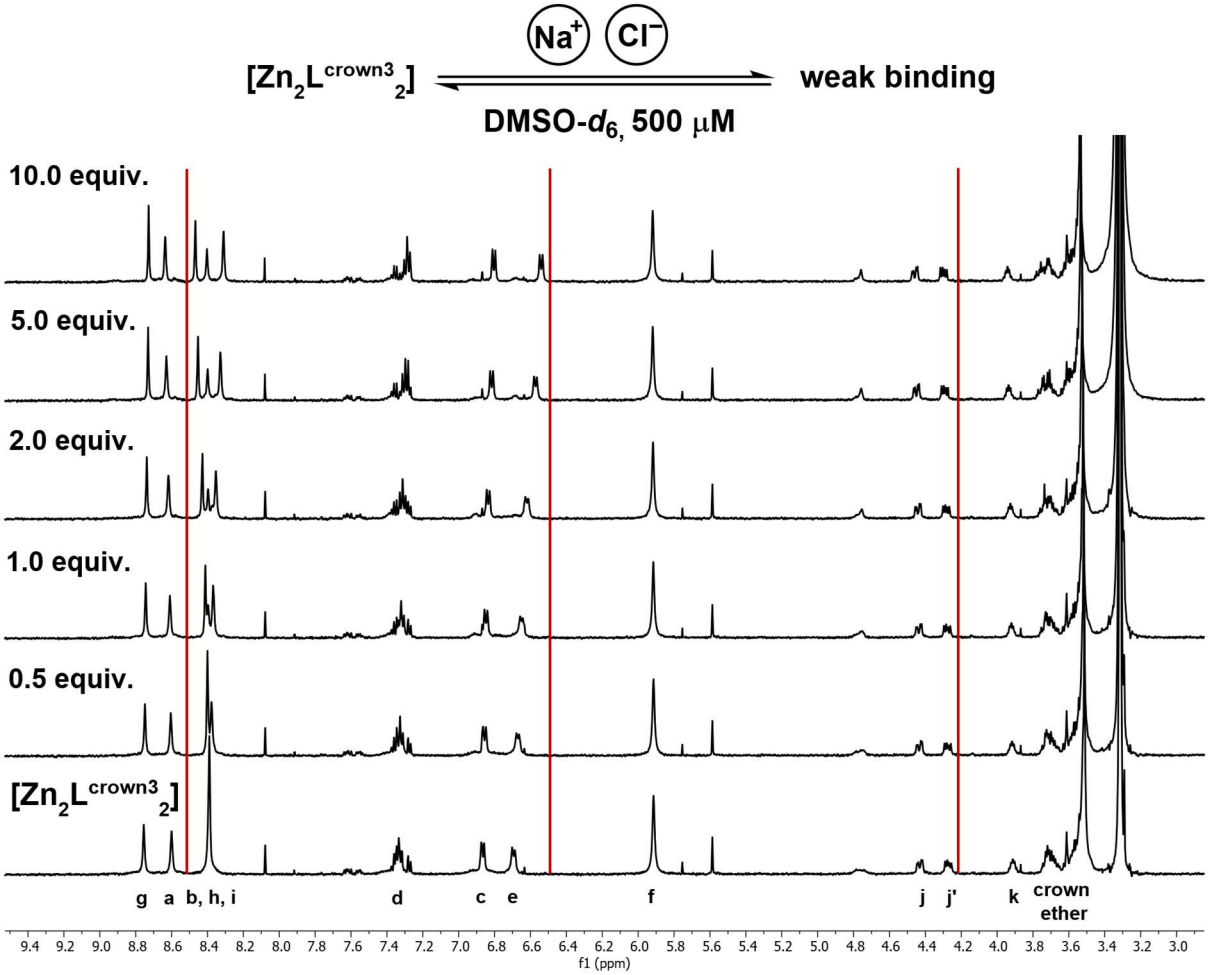

Figure 3.113: ^{1}H NMR test-titration of [Zn$_2$L$^{crown3}{}_2$] and ion pair NaCl (500 µM, DMSO-d$_6$, 500 MHz, 25°C).

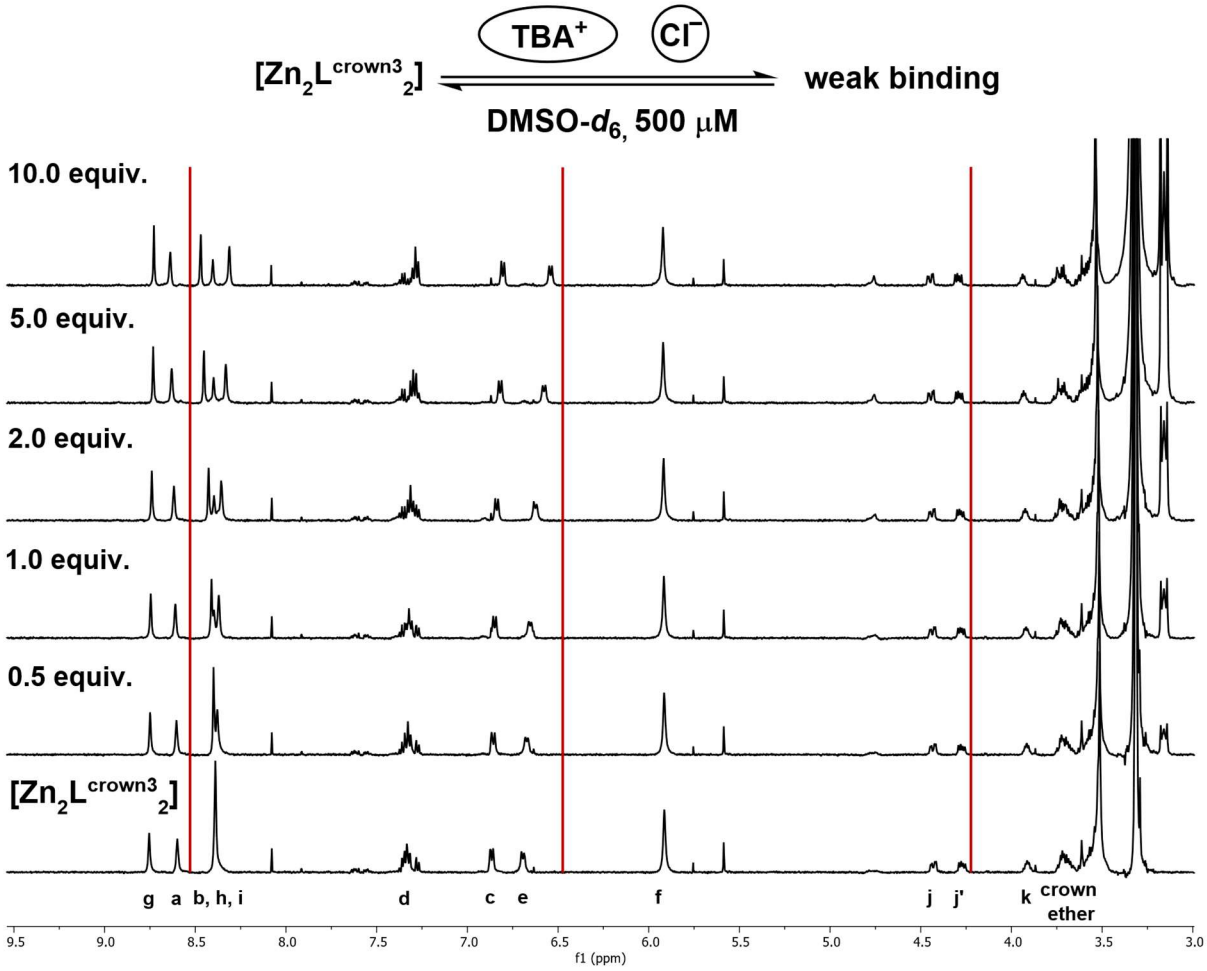

Figure 3.114: ^{1}H NMR test-titration of [$Zn_2L^{crown3}{}_2$].and TBA chloride (500 µM, DMSO-d_6, 500 MHz, 25°C).

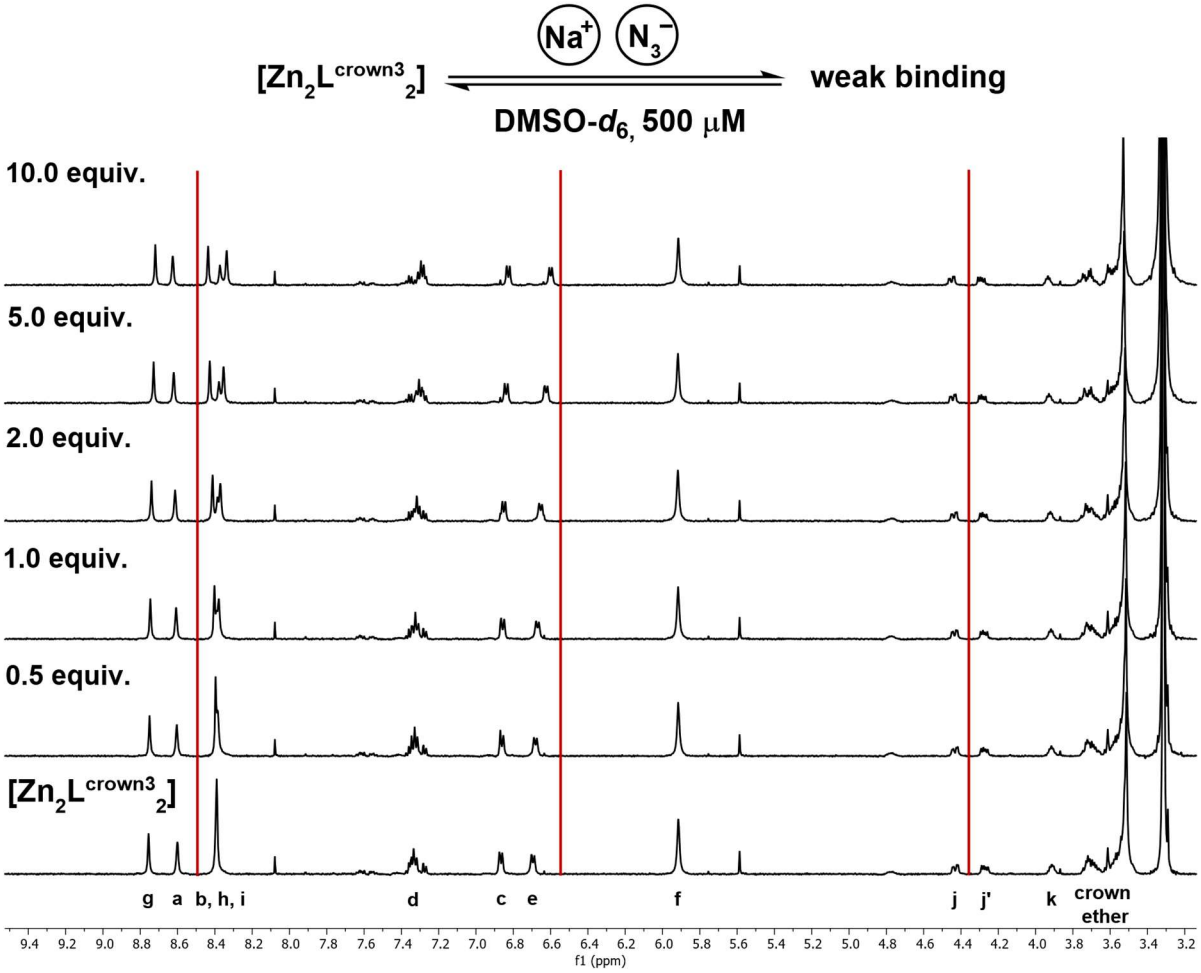

Figure 3.115: ^{1}H NMR test-titration of [$Zn_2L^{crown3}{}_2$].and ion pair NaN_3 (500 μM, DMSO-d_6, 500 MHz, 25°C).

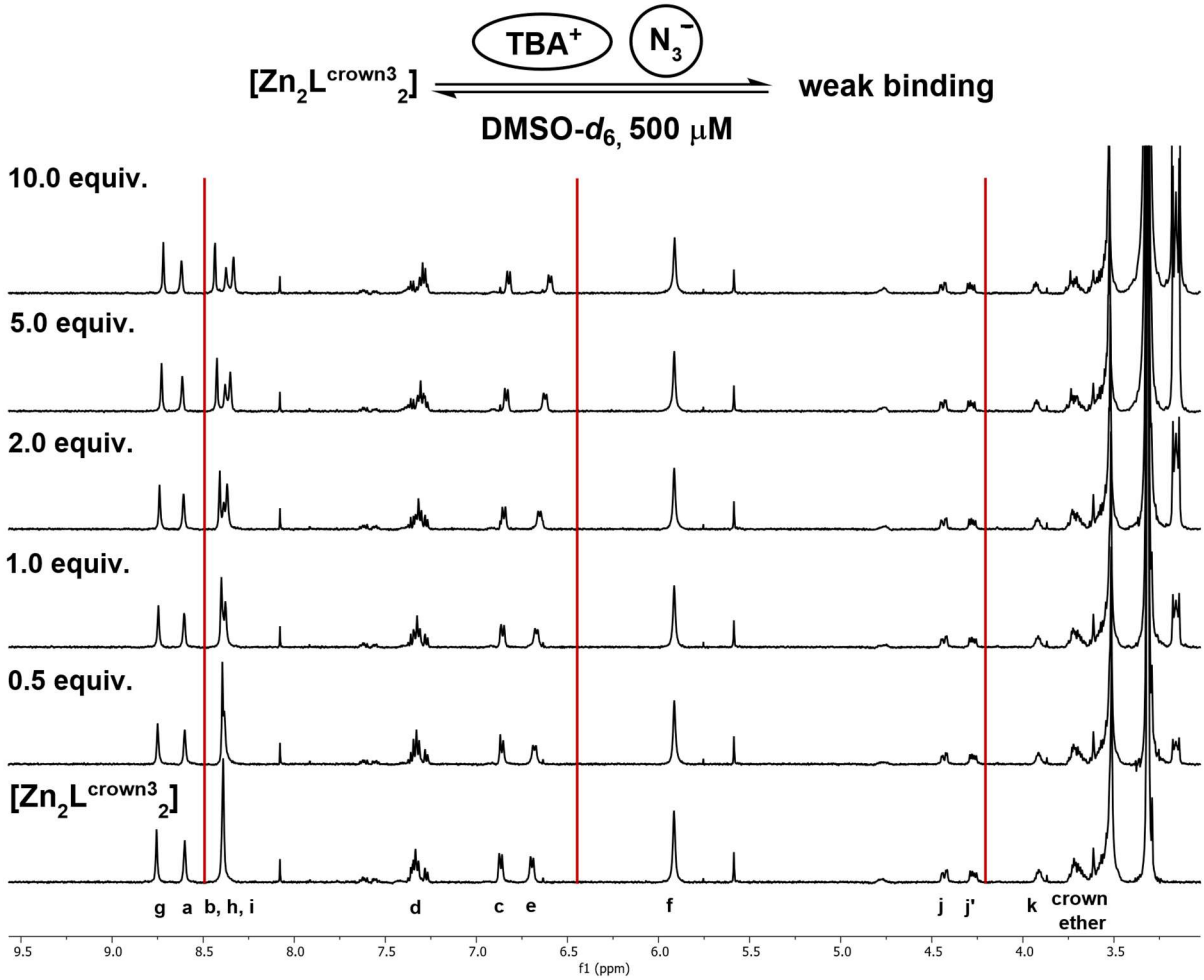

Figure 3.116: ^{1}H NMR test-titration of $[Zn_2L^{crown3}{}_2]$ and $TBAN_3$ (500 µM, DMSO-d_6, 500 MHz, 25°C).

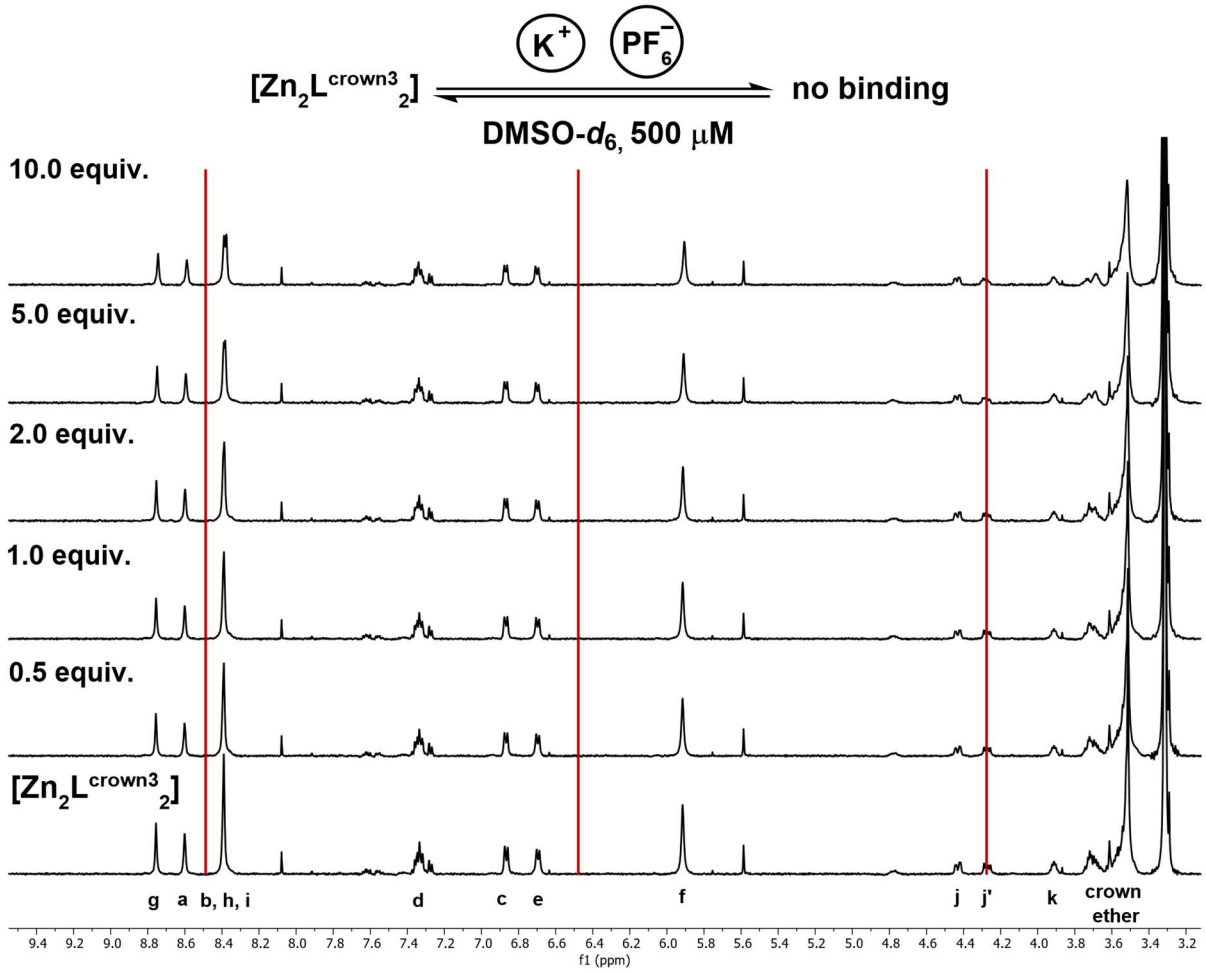

Figure 3.117: ^{1}H NMR test-titration of [$Zn_2L^{crown3}{}_2$] and KPF_6 (500 µM, DMSO-d_6, 500 MHz, 25°C).

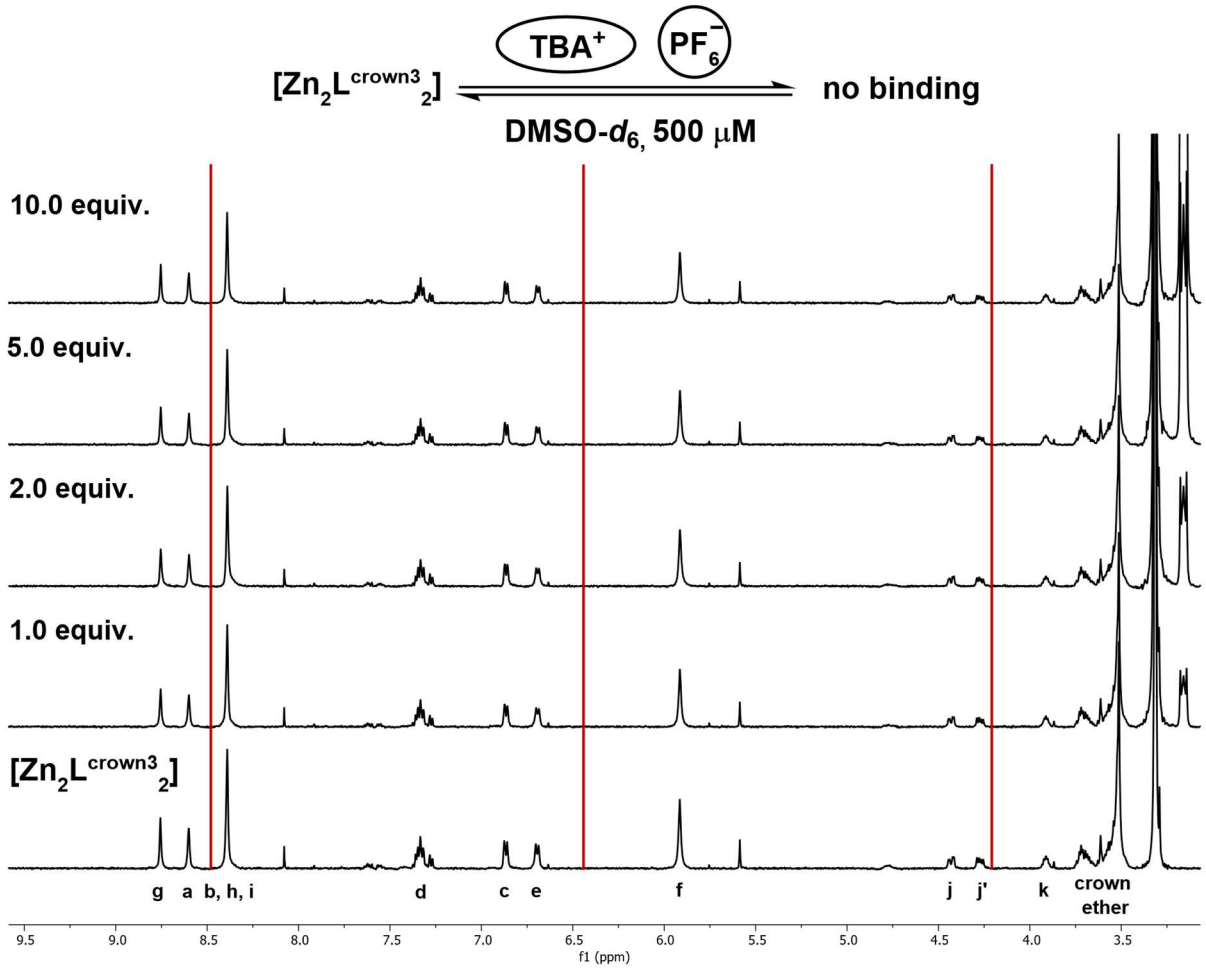

Figure 3.118: ^{1}H NMR test-titration of $[Zn_2L^{crown3}{}_2]$.and $TBAPF_6$ (500 µM, DMSO-d_6, 500 MHz, 25°C).

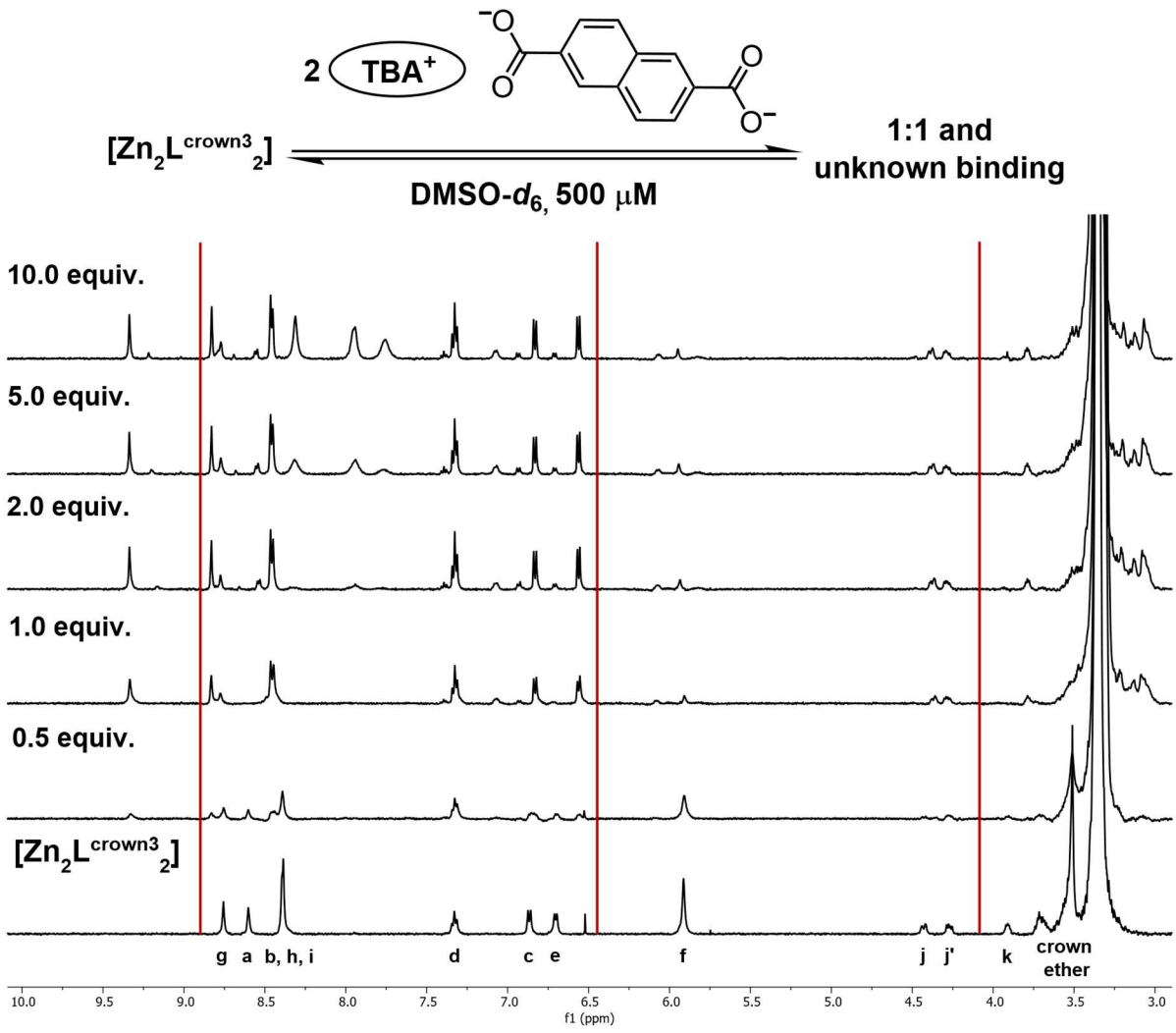

Figure 3.119: ^{1}H NMR test-titration of $[Zn_2L^{crown3}{}_2]$.and TBA_2NP (500 µM, DMSO-d_6, 500 MHz, 25°C).

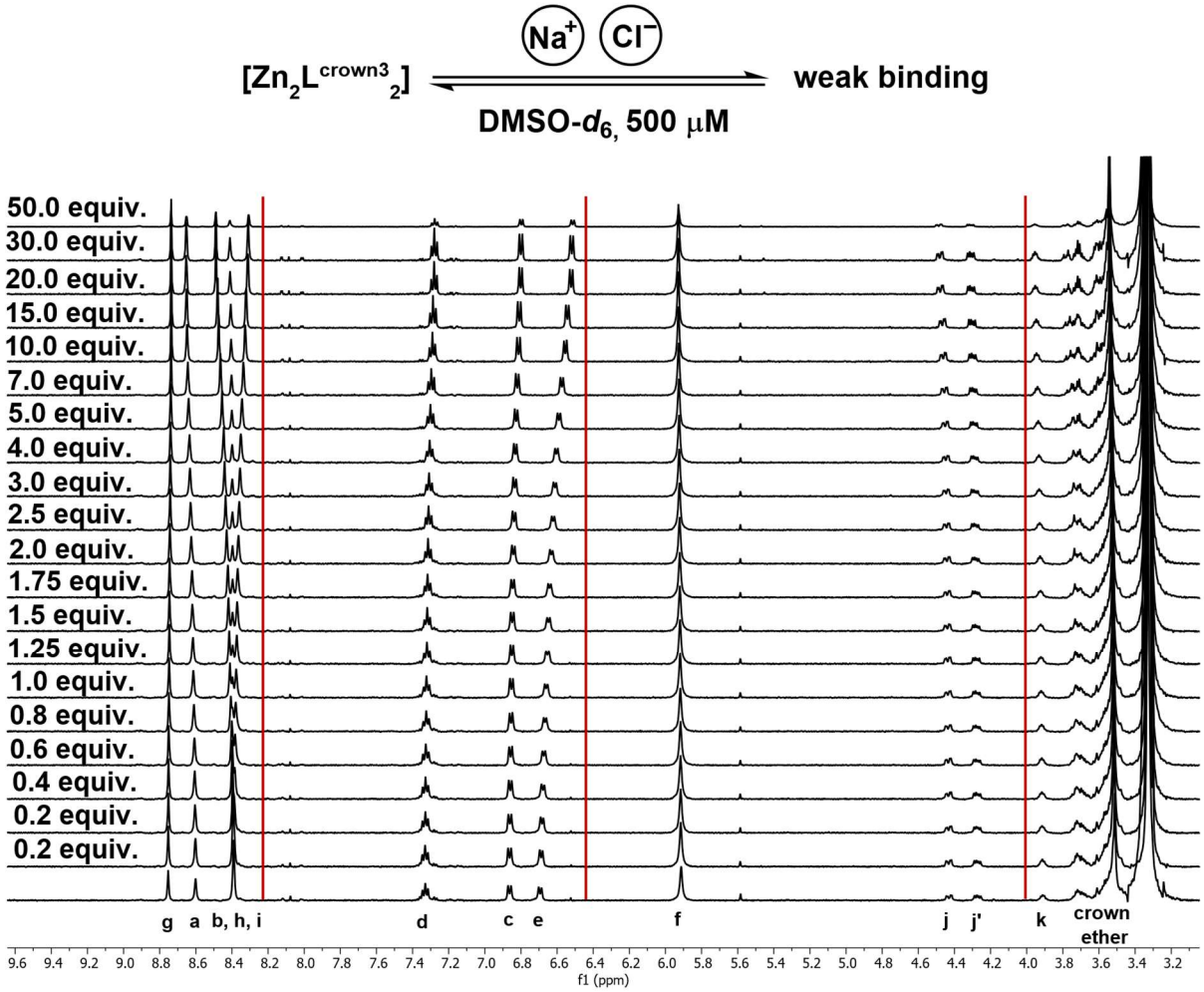

Figure 3.120: ^{1}H NMR fine-titration of [$Zn_2L^{crown3}{}_2$] and NaCl (500 µM, DMSO-d_6, 500 MHz, 25°C).

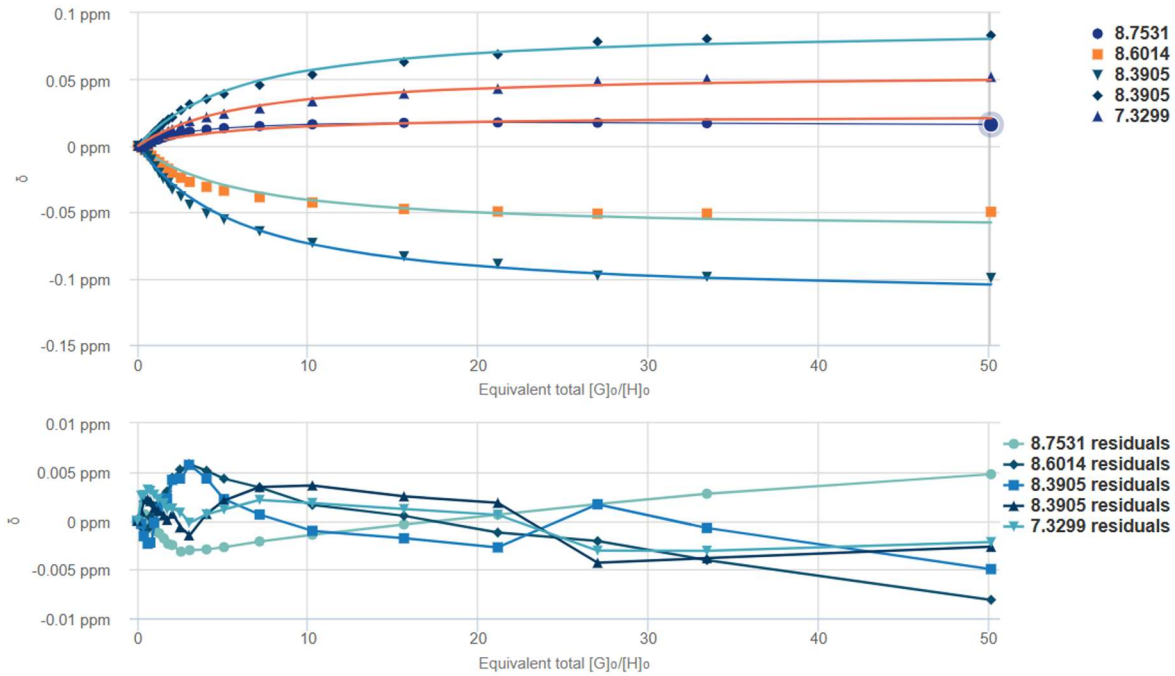

Parameter (bounds)	Optimised	Error	Initial
K (0 → ∞)	371.15 M^{-1}	± 2.5867 %	100.00 M^{-1}

Figure 3.121: Analysis of the titration data from (Figure 3.120) and determination of the binding constant of NaCl with BindFit.[91,85] The lack of inflection points is an indication for the formation of a 1:1 host–guest complex.

3.7.12 Computational Studies

DFT calculations $[(NP)@Zn_2L^{N3}{}_2]^{2-}$

The following relevant information was used in the input file's header for geometry optimization at ωB97-3c[95]/def2-SVP [96,97] level with ORCA 5.0.3[98,99]:

ωB97-3c def2-SVP Opt

%scf

MaxIter 1000

end

%maxcore 8000

%pal nprocs 10 end

%geom trust -0.1 end

*xyz -2 1

XYZ data for the optimized structure of **$[(NP)@Zn_2L^{N3}{}_2]^{2-}$**:

C	19.51484546709936	16.24550308607503	19.96245633681925
C	12.52215626948406	13.27253246627864	22.63296758611781
O	20.47228655257410	15.55079513346612	20.45097821076322
O	11.56412020958292	13.95187977512141	22.12910888774820
C	17.87546275662122	14.66237487995835	21.04628026759960
C	14.16019200058926	14.83917887212813	21.53071258267696
N	23.12506125332282	14.49987202071573	19.58861327104965
N	9.09017672827455	14.79992375970556	23.48389985000267
O	19.66299789613370	17.24698595113406	19.24729464322089
O	12.36469489872022	12.29264595602294	23.37970821964523
C	23.13081477465835	13.30974976228643	20.13468898395550
C	18.11275491187634	15.81234596071562	20.33005964179543
C	13.92253268962321	13.69020733784687	22.24869247788348
C	9.20520278154966	16.06472217257351	23.16645367776513
C	23.51057193216730	12.14588741603577	19.41349857752946
C	8.84413316498135	17.10567715397996	24.06285384119803
C	23.90181735122744	12.28921981350507	18.10228972758897
C	8.34474224858707	16.75961008178530	25.29731426013508
C	23.92143483024041	13.57566933765655	17.49157616594139

C	8.20476079760738	15.38985424704897	25.66241124601999
C	24.31853304710785	13.81274568694392	16.14740580986096
C	7.70804434733870	14.94362152262290	26.91752807590980
C	24.27679707470113	15.10712997470829	15.66552706567780
C	15.00890618569758	12.83926062338886	22.59603977243355
C	17.02314657784335	16.65559964627237	19.97081605179665
C	7.65136199908074	13.58387641604703	27.15870787480308
C	23.84946493233851	16.19911485563471	16.45546596460665
C	16.28816340207355	13.13751543090374	22.20293609843719
C	15.74523409966310	16.35325635236271	20.36205106880621
C	8.07281577099901	12.62328463393248	26.21064391153288
C	16.55623880384243	14.31577898231587	21.45085150934643
C	15.47853871395699	15.17870966373233	21.11961349954704
C	23.43984518144701	16.02452065169101	17.78430530524389
C	8.57387191068143	13.00419718772110	24.95827826457174
C	23.50007967606365	14.66360151987250	18.29376265469407
C	8.61574040402839	14.43498537681231	24.70175661974404
O	23.02643427626540	16.97533976965332	18.55896656721150
O	8.99024020020880	12.18534328209624	24.04759080140309
C	23.43021732317389	10.79556379613238	20.08545269058301
C	9.03421800204605	18.54572990680216	23.64682128534441
N	22.04491093856170	10.45607100154145	20.40042972394581
N	10.39808843296805	18.77769580109357	23.18220432397974
N	21.22832716593139	10.01600333750691	19.44851018629081
N	11.40398384370646	18.83936183114670	24.04930011440325
N	20.04715886592644	9.89238522429634	19.96211230594424
N	12.50305108331622	18.96316110100819	23.37704368491114
C	20.08261199830701	10.26788929260947	21.27200157720966
C	12.21790601046262	18.97046260472171	22.04407727285095
C	21.38253382648610	10.63829655427602	21.56337854316464
C	10.84744218097519	18.84874234133188	21.91033500356212
C	18.89172842629026	10.22818226670969	22.13873380066275
C	13.25461018708128	19.13171274607716	21.00976268087792

C	18.95739823983406	10.64687974872782	23.47273028613613
C	12.98045613824477	18.84514036221828	19.66736380971269
C	17.82652484500792	10.56432816703023	24.28786351490598
C	13.96154411763823	19.05359646013822	18.69509342893412
C	16.63016025405299	10.04839828469497	23.78120707303072
C	15.21329874028153	19.55975087679081	19.05650171855448
C	16.54597385656168	9.66146105563361	22.43895014137260
C	15.50330886322761	19.82600263771311	20.39929754584172
C	17.68147993730654	9.75370281255080	21.62796114178087
C	14.51904455557693	19.60490731876520	21.36799991737927
N	13.32677485571433	8.36918422937978	21.42887761897238
N	18.80760028533239	21.16748246787574	20.97058007098967
N	13.98013727234896	8.45108696188109	20.27418242260103
N	18.27817458875072	21.17754835280426	22.18982248155524
N	15.16295536481593	8.91773686287810	20.51729043518245
N	17.07770998905594	20.70059565280784	22.10746928488760
C	15.29136910922026	9.15312540894123	21.85401235181173
C	16.81163131786149	20.36483237218731	20.81350274464191
C	14.09493175257182	8.80176737722524	22.45299404190900
C	17.93875186826247	20.66241310678647	20.06809933628326
C	11.93942582170872	7.90782686923443	21.45918360816420
C	20.19186945397929	21.59925188903138	20.76849287046904
N	10.09963718900323	11.17078649916537	21.42900217961683
N	22.01428854403240	18.35166594417473	21.12314299686202
C	10.86717571551315	10.17191827552938	21.78819018524806
C	21.29540297280797	19.33555249540529	20.63995343228725
C	10.98880544736615	8.99116330857136	21.00809772061339
C	21.14781286462525	20.57127017719140	21.32226643064318
C	10.25730789959994	8.89500215728566	19.84758870423946
C	21.81687762622316	20.75085480409134	22.51018169538444
C	9.40554467360268	9.96311583852952	19.44187912682359
C	22.62337718738845	19.70578608345414	23.04469254424314
C	8.63155620723642	9.95383226135791	18.24973476250972

C	23.33414107374352	19.79915101648101	24.27257177946623
C	7.88144973007654	11.07224922690272	17.93991502254128
C	24.03771546137863	18.69554827441258	24.71453814747739
C	7.86061657232805	12.22313767284942	18.76074883815300
C	24.06676977745018	17.47732201754250	23.99680060072400
C	8.59842531688139	12.28545019619501	19.94890823183470
C	23.38439160191477	17.32930899201844	22.78391419933732
C	9.37160407387197	11.10170563356473	20.28146274356732
C	22.67097228864597	18.50017104809105	22.30557692758438
O	8.64615253700701	13.31906431124387	20.73274255652829
O	23.33209244272588	16.23181960772015	22.09395575994412
C	17.89589353453166	10.88934898617729	25.75499811616760
C	13.65529631825589	18.89487105082607	17.23087618698130
O	17.37161323408195	10.15140767225629	26.57697902131710
O	14.05125862945771	19.72300557767375	16.42342877687111
N	18.60815790491451	12.00000555254029	26.13645393979411
N	12.86314914312245	17.83858718255011	16.85015025266731
H	18.71040999864832	14.01787769427383	21.33066337539566
H	13.32702470419493	15.48904642534110	21.25362289203378
H	22.82032073601962	13.24248324986332	21.18419636146721
H	9.61042447019909	16.29081513212475	22.17340207675334
H	24.19633469646599	11.41347349039608	17.51461116460863
H	8.06232439568744	17.53598870307639	26.01592673534525
H	24.64497394915345	12.97738733475871	15.52262555913093
H	7.38718617647134	15.67292609025017	27.66581645743601
H	24.58163016146882	15.30191709028541	14.63161106774976
H	14.79093845443178	11.93945440644492	23.17223291277663
H	17.23667980600422	17.55611558881557	19.39265028915372
H	7.27114359231936	13.22904565998036	28.12278081624944
H	23.82628484486517	17.20829994836163	16.03364960314191
H	17.12105980948262	12.48215713475232	22.46392551312386
H	14.91071915361235	17.00289463598219	20.09681271338755
H	8.01998393807439	11.55640676171106	26.44737744724122

H	23.98753531783992	10.78439104179192	21.03241356547565
H	23.82819788171072	10.00701804600478	19.43424234229125
H	8.83725539623639	19.22571969215524	24.48569928885116
H	8.36401645731405	18.81389502586537	22.81761648313041
H	21.87213131119929	10.99876244963010	22.46581948402299
H	10.18077488096127	18.82093005232943	21.05065739558950
H	19.89924160866056	11.00815989166522	23.88630758305588
H	11.99327566118696	18.48221061602676	19.37728689778339
H	15.76615831472571	9.96443777654190	24.44485857516444
H	15.95337833013581	19.74928086104282	18.27547061632718
H	17.62581771359552	9.43694855162432	20.58619690112948
H	14.73237180568467	19.82983513810782	22.41353579413589
H	13.74488475620849	8.81212607955570	23.48328333311780
H	18.18399994872765	20.56338497205841	19.01272404097861
H	11.72899972307862	7.59943328216300	22.49258798800525
H	11.86744421817022	7.02547669820459	20.81052031748056
H	20.31764318134539	22.56960996922102	21.26615034388463
H	20.32829511380174	21.73726868163146	19.68750609390511
H	11.43772522678061	10.30663720119633	22.71208749546544
H	20.77616412208676	19.14199279121985	19.69687212408560
H	10.33159346682226	8.00187251086571	19.21848114965668
H	21.71846379050685	21.68928889934432	23.06562506816818
H	8.64697708133553	9.07527968848560	17.59955817301505
H	23.30471429303954	20.72913873719286	24.84615181779257
H	7.28461995285124	11.07775670925649	17.02155871361727
H	24.58689950230292	18.75512470873652	25.66029225086707
H	7.26511985229043	13.09461627196283	18.47225471912421
H	24.61967228736760	16.61920750472916	24.39052204584298
Zn	22.30321611730531	16.36471632394205	20.34458004339932
Zn	9.77711994000996	13.06253270383797	22.39724238832362
C	18.87587302233300	13.14609578459871	25.30517441325093
H	16.83775165635084	13.80604579689675	25.31190909282341
C	17.86241319400346	14.02212110236471	24.99822415397289

C	20.50026580999007	14.56680335812678	24.20637502188026
C	18.13913885186881	15.23479649661321	24.30352611360240
C	20.21417937285009	13.42065286093913	24.90507608044624
C	19.47473725395277	15.51286867514856	23.90858515478645
C	17.11825084270458	16.18601546608415	24.01031812190169
H	21.00254339691526	12.70833115982078	25.16216978387783
H	20.78042203725987	16.91364045795368	22.90315822121793
H	21.52131856143544	14.77860231120592	23.87335370553318
C	17.42491796657977	17.36447840170829	23.37518351784783
H	16.08723260120614	15.95865739149531	24.29705213591950
H	16.64048433627458	18.09295749466505	23.15389277190316
C	18.76302519318894	17.64166564628432	22.98320897268565
H	18.99083668594147	18.57848692702398	22.46867802634010
C	19.75997307004697	16.73314004859574	23.23461040811775
C	18.76855864202914	12.23416580630007	27.54780082847721
H	20.78692662485295	11.52851112050537	27.57654488434036
C	19.96482383820482	11.95610555446997	28.15701963478593
C	17.83496136234877	13.05018637026636	29.62561106028418
C	20.14673181410240	12.22462848640230	29.54617253258363
C	17.68713448792328	12.78911907650049	28.28796731786338
C	19.06836895641121	12.77809620953074	30.29110993370515
C	21.38001135046521	11.95387316723984	30.20805373859724
H	16.74476072722277	12.99889219002693	27.77594599151589
H	18.41793365417580	13.47370568747610	32.24595713029573
H	17.00701668632874	13.47433533934882	30.20166775242575
C	21.52843460123175	12.22292697066812	31.54818848442043
H	22.20607392591254	11.52875388865502	29.62973862962081
H	22.47820717370817	12.01173566793432	32.04823212038427
C	20.45117277602901	12.77658916529174	32.29268847909250
H	20.58294296818896	12.98708719145043	33.35807405658924
C	19.25098869982417	13.04695363624682	31.67887239180057
C	12.75684493274656	16.59131978332339	17.55921332380107
H	14.82179291870035	16.08855408465731	17.29329987745709

C	13.84930146687853	15.76596084470639	17.67502741537504
C	11.33873964787159	14.95285682044151	18.63982426264958
C	13.72135170974897	14.47735742226124	18.27098880875267
C	11.48414853416911	16.18322675397824	18.04996220509038
C	12.44901416697461	14.06280341042939	18.74659809268265
C	14.83046980203920	13.59023186907101	18.39899838069553
H	10.63533242007755	16.86551189766140	17.95143103204120
H	11.33906472188732	12.47940642288148	19.71319020749313
H	10.37281972106627	14.63663310691853	19.04612329055056
C	14.67009079561572	12.34945400404216	18.96712280574205
H	15.81294229392883	13.92190585440834	18.04975363036395
H	15.52572967237274	11.67609452040651	19.07301580588223
C	13.39431808532297	11.93447478763879	19.43662689991983
H	13.28042635981545	10.94619981861674	19.88881814628906
C	12.31344842827076	12.77300936773455	19.33027681230158
C	12.44014124593432	17.79026973725480	15.47567603354664
H	10.53584248659038	18.67094119327183	15.88720710351661
C	11.19666957966200	18.24925827560875	15.12485261391353
C	12.91981038279597	17.16513115582210	13.18886979238949
C	10.75799697077655	18.17720503961346	13.76981450804911
C	13.31655036738179	17.24021508440907	14.49919230813891
C	11.63023718911760	17.62878256112727	12.78831475627813
C	9.46813634039096	18.63709345484701	13.37289356857207
H	14.30272616918341	16.88531521655134	14.81025937997230
H	11.86591165986158	17.13575169864197	10.68333186651472
H	13.58884912443711	16.74746453751582	12.43063236295730
C	9.06865358205151	18.55212461402103	12.06020961212749
H	8.80209884288876	19.05709255721052	14.13275258251692
H	8.07659314693823	18.90559066204758	11.76426330620771
C	9.94040683574022	18.00536745488257	11.07900609413794
H	9.61051981287512	17.94361422088526	10.03780676053602
C	11.19017770499797	17.55600393135047	11.43449738258990

*

DFT calculations [(NP)@$Zn_2L^{mN3}{}_2]^{2-}$

The following relevant information was used in the input file's header for geometry optimization at ωB97-3c[95]/def2-SVP [96,97] level with ORCA 5.0.3[98,99]:

B97-3c def2-SVP Opt

%scf

MaxIter 1000

end

%maxcore 8000

%pal nprocs 10 end

%geom trust -0.1 end

*xyz -2 1

XYZ data for the optimized structure of **[(NP)@$Zn_2L^{mN3}{}_2]^{2-}$**:

C	19.514845	16.245503	19.962456
C	12.522156	13.272532	22.632968
O	20.472287	15.550795	20.450978
O	11.564120	13.951880	22.129109
C	17.875463	14.662375	21.046280
C	14.160192	14.839179	21.530713
N	23.125061	14.499872	19.588613
N	9.090177	14.799924	23.483900
O	19.662998	17.246986	19.247295
O	12.364695	12.292646	23.379708
C	23.130815	13.309750	20.134689
C	18.112755	15.812346	20.330060
C	13.922533	13.690207	22.248692
C	9.205203	16.064722	23.166454
C	23.510572	12.145887	19.413499
C	8.844133	17.105677	24.062854
C	23.901817	12.289220	18.102290
C	8.344742	16.759610	25.297314
C	23.921435	13.575669	17.491576
C	8.204761	15.389854	25.662411

C	24.318533	13.812746	16.147406
C	7.708044	14.943622	26.917528
C	24.276797	15.107130	15.665527
C	15.008906	12.839261	22.596040
C	17.023147	16.655600	19.970816
C	7.651362	13.583876	27.158708
C	23.849465	16.199115	16.455466
C	16.288163	13.137515	22.202936
C	15.745234	16.353256	20.362051
C	8.072816	12.623285	26.210644
C	16.556239	14.315779	21.450852
C	15.478539	15.178710	21.119613
C	23.439845	16.024521	17.784305
C	8.573872	13.004197	24.958278
C	23.500080	14.663602	18.293763
C	8.615740	14.434985	24.701757
O	23.026434	16.975340	18.558967
O	8.990240	12.185343	24.047591
C	23.430217	10.795564	20.085453
C	9.034218	18.545730	23.646821
N	22.044911	10.456071	20.400430
N	10.398088	18.777696	23.182204
N	21.228327	10.016003	19.448510
N	11.403984	18.839362	24.049300
N	20.047159	9.892385	19.962112
N	12.503051	18.963161	23.377044
C	20.082612	10.267889	21.272002
C	12.217906	18.970463	22.044077
C	21.382534	10.638297	21.563379
C	10.847442	18.848742	21.910335
C	18.891728	10.228182	22.138734
C	13.254610	19.131713	21.009763
C	18.957398	10.646880	23.472730

C	12.980456	18.845140	19.667364
C	17.826525	10.564328	24.287864
C	13.961544	19.053596	18.695093
C	16.630160	10.048398	23.781207
C	15.213299	19.559751	19.056502
C	16.545974	9.661461	22.438950
C	15.503309	19.826003	20.399298
C	17.681480	9.753703	21.627961
C	14.519045	19.604907	21.368000
N	13.326775	8.369184	21.428878
N	18.807600	21.167482	20.970580
N	13.980137	8.451087	20.274182
N	18.278175	21.177548	22.189822
N	15.162955	8.917737	20.517290
N	17.077710	20.700596	22.107469
C	15.291369	9.153125	21.854012
C	16.811631	20.364832	20.813503
C	14.094932	8.801767	22.452994
C	17.938752	20.662413	20.068099
C	11.939426	7.907827	21.459184
C	20.191869	21.599252	20.768493
N	10.099637	11.170786	21.429002
N	22.014289	18.351666	21.123143
C	10.867176	10.171918	21.788190
C	21.295403	19.335552	20.639953
C	10.988805	8.991163	21.008098
C	21.147813	20.571270	21.322266
C	10.257308	8.895002	19.847589
C	21.816878	20.750855	22.510182
C	9.405545	9.963116	19.441879
C	22.623377	19.705786	23.044693
C	8.631556	9.953832	18.249735
C	23.334141	19.799151	24.272572

C	7.881450	11.072249	17.939915
C	24.037715	18.695548	24.714538
C	7.860617	12.223138	18.760749
C	24.066770	17.477322	23.996801
C	8.598425	12.285450	19.948908
C	23.384392	17.329309	22.783914
C	9.371604	11.101706	20.281463
C	22.670972	18.500171	22.305577
O	8.646153	13.319064	20.732743
O	23.332092	16.231820	22.093956
C	17.895894	10.889349	25.754998
C	13.655296	18.894871	17.230876
O	17.371613	10.151408	26.576979
O	14.051259	19.723006	16.423429
N	18.608158	12.000006	26.136454
N	12.863149	17.838587	16.850150
H	18.710410	14.017878	21.330663
H	13.327025	15.489046	21.253623
H	22.820321	13.242483	21.184196
H	9.610424	16.290815	22.173402
H	24.196335	11.413473	17.514611
H	8.062324	17.535989	26.015927
H	24.644974	12.977387	15.522626
H	7.387186	15.672926	27.665816
H	24.581630	15.301917	14.631611
H	14.790938	11.939454	23.172233
H	17.236680	17.556116	19.392650
H	7.271144	13.229046	28.122781
H	23.826285	17.208300	16.033650
H	17.121060	12.482157	22.463926
H	14.910719	17.002895	20.096813
H	8.019984	11.556407	26.447377
H	23.987535	10.784391	21.032414

H	23.828198	10.007018	19.434242
H	8.837255	19.225720	24.485699
H	8.364016	18.813895	22.817616
H	21.872131	10.998762	22.465819
H	10.180775	18.820930	21.050657
H	19.899242	11.008160	23.886308
H	11.993276	18.482211	19.377287
H	15.766158	9.964438	24.444859
H	15.953378	19.749281	18.275471
H	17.625818	9.436949	20.586197
H	14.732372	19.829835	22.413536
H	13.744885	8.812126	23.483283
H	18.184000	20.563385	19.012724
H	11.729000	7.599433	22.492588
H	11.867444	7.025477	20.810520
H	20.317643	22.569610	21.266150
H	20.328295	21.737269	19.687506
H	11.437725	10.306637	22.712087
H	20.776164	19.141993	19.696872
H	10.331593	8.001873	19.218481
H	21.718464	21.689289	23.065625
H	8.646977	9.075280	17.599558
H	23.304714	20.729139	24.846152
H	7.284620	11.077757	17.021559
H	24.586900	18.755125	25.660292
H	7.265120	13.094616	18.472255
H	24.619672	16.619208	24.390522
Zn	22.303216	16.364716	20.344580
Zn	9.777120	13.062533	22.397242
C	18.875873	13.146096	25.305174
H	16.837752	13.806046	25.311909
C	17.862413	14.022121	24.998224
C	20.500266	14.566803	24.206375

C	18.139139	15.234796	24.303526
C	20.214179	13.420653	24.905076
C	19.474737	15.512869	23.908585
C	17.118251	16.186015	24.010318
H	21.002543	12.708331	25.162170
H	20.780422	16.913640	22.903158
H	21.521319	14.778602	23.873354
C	17.424918	17.364478	23.375184
H	16.087233	15.958657	24.297052
H	16.640484	18.092957	23.153893
C	18.763025	17.641666	22.983209
H	18.990837	18.578487	22.468678
C	19.759973	16.733140	23.234610
C	12.756845	16.591320	17.559213
H	14.821793	16.088554	17.293300
C	13.849301	15.765961	17.675027
C	11.338740	14.952857	18.639824
C	13.721352	14.477357	18.270989
C	11.484149	16.183227	18.049962
C	12.449014	14.062803	18.746598
C	14.830470	13.590232	18.398998
H	10.635332	16.865512	17.951431
H	11.339065	12.479406	19.713190
H	10.372820	14.636633	19.046123
C	14.670091	12.349454	18.967123
H	15.812942	13.921906	18.049754
H	15.525730	11.676095	19.073016
C	13.394318	11.934475	19.436627
H	13.280426	10.946200	19.888818
C	12.313448	12.773009	19.330277
H	18.720915	12.164613	27.128590
H	12.565643	17.804605	15.883466

*

DFT calculations [(NaCl)@$Zn_2L^{crown3}_2$]

The following relevant information was used in the input file's header for geometry optimization at ωB97-3c[95]/def2-SVP [96,97] level with ORCA 5.0.3[98,99]:

B97-3c def2-SVP Opt

%scf

MaxIter 1000

end

%maxcore 8000

%pal nprocs 10 end

%geom trust -0.1 end

*xyz 0 1

XYZ data for the optimized structure of **[(NaCl)@$Zn_2L^{crown3}_2$]**:

Zn	-0.5942489750	-3.7098931280	-0.6540154520
N	0.6721090250	9.9157708720	2.4407545480
C	-0.4020809750	9.6246138720	3.1705045480
H	-0.2356479750	9.0480418720	4.0970845480
C	-1.8682579750	10.7657418720	1.6193095480
H	-2.8715279750	11.0901878720	1.2948095480
C	-0.7335209750	11.1134578720	0.8263305480
C	-0.7996879750	11.8761948720	-0.3747574520
H	-1.7720869750	12.2490738720	-0.7321394520
C	0.3813170250	12.1269208720	-1.0804934520
H	0.3359240250	12.7157598720	-2.0122954520
C	1.6401090250	11.6444428720	-0.6488314520
H	2.5478430250	11.8542288720	-1.2379504520
C	1.7755750250	10.8723788720	0.5342735480
C	0.5438450250	10.6303468720	1.2858745480
O	2.9058150250	10.3876428720	0.9637905480
C	-2.9121819750	9.5897598720	3.6182535480
H	-2.7402579750	9.7791258720	4.6960335480
H	-3.8247019750	10.1325418720	3.3077475480
N	-3.1993689750	8.1535798720	3.4780315480

N	-3.9675089750	7.6973958720	2.4574995480
N	-3.9776019750	6.3869928720	2.5248905480
C	-3.2042869750	5.9744308720	3.5863305480
C	-2.6983399750	7.1213728720	4.2088685480
H	-2.0593499750	7.2805178720	5.0836145480
C	-2.9989479750	4.5576838720	3.9306455480
C	-2.1129039750	4.1989418720	4.9704945480
H	-1.5601579750	4.9690348720	5.5257035480
C	-1.9239159750	2.8444238720	5.3070505480
C	-2.6163959750	1.8358188720	4.6061925480
H	-2.4503989750	0.7873488720	4.8955425480
C	-3.5002029750	2.1747778720	3.5575325480
C	-3.6811729750	3.5383878720	3.2304055480
H	-4.3693469750	3.8103748720	2.4172405480
N	-5.1204639750	-0.7050521280	2.0400325480
N	-5.5162039750	0.3079658720	1.2302765480
N	-4.9823339750	1.4141168720	1.6914535480
C	-4.2254029750	1.1336568720	2.8072275480
C	-4.3143449750	-0.2449261280	3.0362495480
H	-3.8950159750	-0.9061181280	3.8021575480
C	-5.5482599750	-2.0860671280	1.7688675480
H	-6.6409049750	-2.0696701280	1.5916835480
H	-5.3604949750	-2.6591721280	2.6987245480
N	-2.7350959750	-3.4117491280	-0.3908294520
C	-3.4104379750	-2.8675881280	0.6166715480
H	-2.8204519750	-2.5292061280	1.4859855480
C	-4.8282159750	-2.7154551280	0.5899945480
C	-5.5179709750	-3.1822901280	-0.5278044520
H	-6.6159729750	-3.0879151280	-0.5792504520
C	-4.8200919750	-3.7877251280	-1.6179514520
C	-5.4448539750	-4.3004111280	-2.7918294520
H	-6.5400059750	-4.2523781280	-2.8945894520
C	-4.6426399750	-4.8551811280	-3.7941244520

H	-5.1210899750	-5.2584251280	-4.7026224520
C	-3.2306999750	-4.9188061280	-3.6932204520
H	-2.6349849750	-5.3604081280	-4.5083464520
C	-2.5452309750	-4.4193141280	-2.5563974520
C	-3.3872679750	-3.8620931280	-1.4983534520
O	-1.2462219750	-4.4350981280	-2.4204534520
Zn	2.7301920250	9.2101688720	2.6138155480
N	1.5365190250	-4.2015861280	-0.7906454520
C	2.4558850250	-3.8405551280	-1.6843164520
H	2.0966760250	-3.3304561280	-2.5952414520
C	3.8468370250	-4.0923871280	-1.4945534520
C	4.2443880250	-4.7588821280	-0.3366254520
H	5.3121830250	-4.9734551280	-0.1613364520
C	3.2842920250	-5.1665491280	0.6363425480
C	3.6084600250	-5.8506901280	1.8435755480
H	4.6575200250	-6.1026111280	2.0634455480
C	2.5786480250	-6.1798421280	2.7297365480
H	2.8237280250	-6.7086161280	3.6664235480
C	1.2249370250	-5.8545751280	2.4735545480
H	0.4409850250	-6.1238331280	3.2000095480
C	0.8338560250	-5.1687591280	1.2943035480
C	1.9080680250	-4.8396041280	0.3570395480
O	-0.3949949750	-4.8310711280	1.0232115480
C	4.8620690250	-3.6144401280	-2.5177854520
H	4.4487090250	-3.6605341280	-3.5436704520
H	5.7781430250	-4.2337201280	-2.4793394520
N	5.2860490250	-2.2232031280	-2.2876154520
N	6.2949160250	-1.9420171280	-1.4259324520
N	6.3982520250	-0.6361021280	-1.3494154520
C	5.4514450250	-0.0511541280	-2.1593844520
C	4.7273040250	-1.0816551280	-2.7712784520
H	3.8915950250	-1.0946801280	-3.4789874520
C	5.2809000250	1.4076078720	-2.2742994520

C	4.3208930250	1.9431698720	-3.1612424520
H	3.7169510250	1.2803268720	-3.7957274520
C	4.1045860250	3.3339948720	-3.2163554520
C	4.8636190250	4.2026918720	-2.4079034520
H	4.6516160250	5.2812508720	-2.4520554520
C	5.8441080250	3.6876188720	-1.5327864520
C	6.0398200250	2.2883778720	-1.4707004520
H	6.7835460250	1.8761958720	-0.7734994520
N	7.5423880250	6.2883448720	0.3516835480
N	7.9210400250	5.1648288720	1.0112365480
N	7.3700110250	4.1421558720	0.4001525480
C	6.6170570250	4.5902338720	-0.6614154520
C	6.7305860250	5.9849288720	-0.6981984520
H	6.3275960250	6.7517098720	-1.3686264520
C	7.9617540250	7.6122748720	0.8295765480
H	9.0048030250	7.5155438720	1.1858965480
H	7.9606480250	8.2839108720	-0.0527424520
N	4.8679970250	8.8155808720	2.6681675480
C	5.6707050250	8.3124168720	1.7342655480
H	5.1951280250	8.0050938720	0.7870365480
C	7.0762500250	8.1703668720	1.9320925480
C	7.6140460250	8.5989268720	3.1447755480
H	8.6979720250	8.5103018720	3.3301475480
C	6.7801200250	9.1673028720	4.1558925480
C	7.2506790250	9.6566858720	5.4082635480
H	8.3248270250	9.6099348720	5.6450065480
C	6.3284770250	10.1959658720	6.3104825480
H	6.6885220250	10.5833578720	7.2785295480
C	4.9401360250	10.2614348720	6.0345215480
H	4.2466930250	10.6901868720	6.7760075480
C	4.4039000250	9.7848848720	4.8104345480
C	5.3730170250	9.2399738720	3.8595335480
O	3.1351850250	9.8204158720	4.5031665480

C	2.9967650250	3.9227438720	-4.0336504520
C	-1.0265339750	2.4338338720	6.4350105480
O	-0.8871879750	1.2787378720	6.8172085480
O	2.6268600250	5.0874978720	-3.9541534520
O	-0.4113369750	3.5002658720	7.0098255480
O	2.4176280250	2.9989428720	-4.8470824520
C	1.1321590250	3.3160078720	-5.4249264520
H	0.9561630250	4.4063018720	-5.3329334520
H	1.1790120250	3.0529078720	-6.4992124520
C	0.0400680250	2.4829358720	-4.7050114520
C	-1.0298599750	3.3871358720	-4.0963114520
H	-1.4984649750	4.0194368720	-4.8879144520
H	-0.5355209750	4.0626258720	-3.3617974520
O	-2.0252629750	2.5891508720	-3.4549834520
C	-2.8827049750	3.3492118720	-2.5875064520
H	-3.2051569750	4.2881538720	-3.0936114520
H	-2.3195899750	3.6324288720	-1.6666644520
C	-4.1210939750	2.5431208720	-2.2049504520
H	-3.8319899750	1.4876858720	-1.9709054520
H	-4.5224279750	2.9645418720	-1.2600384520
O	-5.1943599750	2.6090458720	-3.1373184520
O	-0.6397319750	1.5502268720	-5.5474814520
C	0.1561230250	0.4976418720	-6.1086684520
H	0.8104430250	0.8711558720	-6.9289844520
H	0.8132890250	0.0469898720	-5.3268774520
C	-0.7989019750	-0.5413981280	-6.6634334520
H	-1.5140549750	-0.0429261280	-7.3566734520
H	-0.2312479750	-1.3073771280	-7.2407184520
O	-1.4913409750	-1.1511571280	-5.5664324520
C	-5.0628509750	1.8496468720	-4.3412594520
H	-5.8751039750	2.2243028720	-4.9969524520
C	-3.9207879750	-0.8769741280	-5.7813714520
H	-4.8436759750	-1.4359011280	-6.0635534520

C	-2.7230799750	-1.8074241280	-5.9042954520
H	-2.6815349750	-2.2308171280	-6.9320444520
H	-2.8365329750	-2.6501691280	-5.1895174520
C	1.8160270250	3.4130408720	8.1603605480
H	2.1609860250	3.3306348720	9.2208045480
C	2.5359670250	2.2983278720	7.4039705480
H	3.6240040250	2.3626268720	7.6373135480
H	2.1695300250	1.3109458720	7.7686145480
O	2.3098440250	2.4279868720	5.9981855480
C	3.0059870250	1.4537998720	5.2051935480
H	2.4727440250	1.4192248720	4.2336025480
H	2.9437170250	0.4447368720	5.6713965480
C	4.4624870250	1.8299818720	4.9696895480
H	5.0341680250	1.8520358720	5.9259435480
H	4.9388990250	1.0637128720	4.3135635480
O	4.4799070250	3.1156478720	4.3377995480
C	5.7801480250	3.7055078720	4.2062865480
H	6.5412550250	2.9349928720	3.9492305480
H	5.7104940250	4.4144518720	3.3561015480
C	6.2140620250	4.4550118720	5.4577055480
H	6.3044030250	3.7660808720	6.3314765480
H	7.2232830250	4.8939268720	5.2759355480
O	5.2638980250	5.4962378720	5.7254765480
C	5.6696960250	6.3930388720	6.7737315480
H	6.7796220250	6.4580938720	6.7789365480
C	1.9502980250	5.8312718720	8.3905975480
H	0.9083740250	6.1621078720	8.1727305480
O	2.2690050250	4.6615348720	7.6152055480
H	5.2895080250	7.4023568720	6.5049165480
H	2.0202840250	5.5950478720	9.4773445480
C	2.9080450250	6.9736238720	8.0642205480
H	3.0091230250	7.0913818720	6.9566285480
H	2.4352300250	7.9095498720	8.4299365480

C	5.1497650250	6.0074818720	8.1768005480
H	5.9809450250	6.0425288720	8.9103345480
H	4.7718340250	4.9592748720	8.1479455480
O	4.1736080250	6.9080088720	8.7097415480
C	0.2890160250	3.2900568720	8.2548465480
H	0.0366140250	2.2884128720	8.6562665480
H	-0.1030049750	4.0619338720	8.9470895480
H	-4.0958249750	2.0580438720	-4.8577204520
C	-5.2074559750	0.3225078720	-4.1315114520
H	-6.0435089750	-0.0810161280	-4.7442324520
H	-5.4590129750	0.1320078720	-3.0667764520
O	-4.0160429750	-0.4290281280	-4.4197814520
H	0.5617720250	1.9231888720	-3.8879764520
H	-3.8261159750	-0.0086251280	-6.4765774520
Na	-2.7723235006	1.0922338539	-4.8058588826
Na	3.7266960854	4.4017727805	6.5524700800
Cl	2.1892310250	7.3632068720	1.9781065480
Cl	0.0446339750	-1.8224398720	0.0088184520
C	-1.6941711408	9.9475253285	2.9122965789

*

4 Tailored Zn(II)-based metal organic cage for taming oxalate

4.1 Introduction

The charge-neutral $[Zn_2L_2]$ metal-organic container presented by VAN CRAEN is a receptor for aliphatic and aromatic dicarboxylates of various length. Nevertheless, the receptor showed limitations in forming distinct host-guest species with the shortest dicarboxylates: malonate and oxalate. Both dicarboxylates formed unknown species with VAN CRAEN'S $[Zn_2L_2]$ host in ^{1}H NMR titration experiments.[76] This was presumably because the metal-organic container is restricted in adjusting the distance between the two Zn(II) centers to selectively bind these dicarboxylates, combined with the inherently strong chelating effect of oxalate. MOCs are prone to be disassembled upon interaction with oxalate, as oxalate coordinates the metal centers and disrupts the integrity of the coordination around them.[100]

To overcome this limitation, the ligand's backbone design was modified to increase its degrees of freedom and allow adjustment of the Zn(II)-Zn(II) distance upon interaction with the competitive guests. The newly designed backbone was based on commercially available dipropargyl amine. In contrast to a rigid planar phenyl backbone, the nitrogen atom together with additional methylene groups introduced greater flexibility to the ligand's backbone. As a result, the self-assembled cage should ideally be able to adjust its Zn(II)-Zn(II) distance to accommodate malonate and oxalate binding without compromising its structural integrity. Nevertheless, introducing methylene groups into the backbone could reduce rigidity, but may lead to broad signals in the ^{1}H NMR spectrum of the self-assembled host, or even prevent the distinct formation of a new supramolecular architecture.

4.2 Synthesis of ligand L^{DB3}-H_2 and self-assembly

The synthetic pathway of ligand L^{DB3}-H_2 required fewer steps than those of the ligands described in the previous chapter (Figure 4.1). The synthesis of ligand L^{DB3}-H_2 began with a SCHOTTEN-BAUMANN reaction a) between the commercially available compounds dipropargyl amine and benzoyl chloride, which afforded the backbone *N*,*N*-di(prop-2-yn-1-yl)benzamide.[101] The synthesis b) of 3-(azidomethyl)quinolin-8-yl tert-butyl carbonate, the Boc protected coordination unit, involved five steps in total and was described in detail in chapter 1 (Figure 3.2). The final steps of the synthesis were a 1,3-dipolar azide-alkyne HUISGEN cycloaddition c) at 60°C and subsequent acidic deprotection d) of the Boc protecting groups with TFA. It was also possible to carry out the cycloaddition at 90°C, whereby the Boc protecting groups were cleaved without the need of an additional reaction step. The drawback in this case, however, was the requirement of a particularly laborious column purification.

The most important structural modification compared to the previously described ligand design was the incorporation of two additional methylene groups (signals h and h' in Figure 4.1) into the backbone, while omitting the phenyl ring and instead introducing a nitrogen atom. The signals corresponding to the additional methylene groups appeared as a doublet, which was due to a rotational barrier that was detectable on the ^{1}H NMR time scale under the given conditions. Upon heating the sample to 50°C, signals h and h' coalesced into a single signal (see chapter 4.6.4).

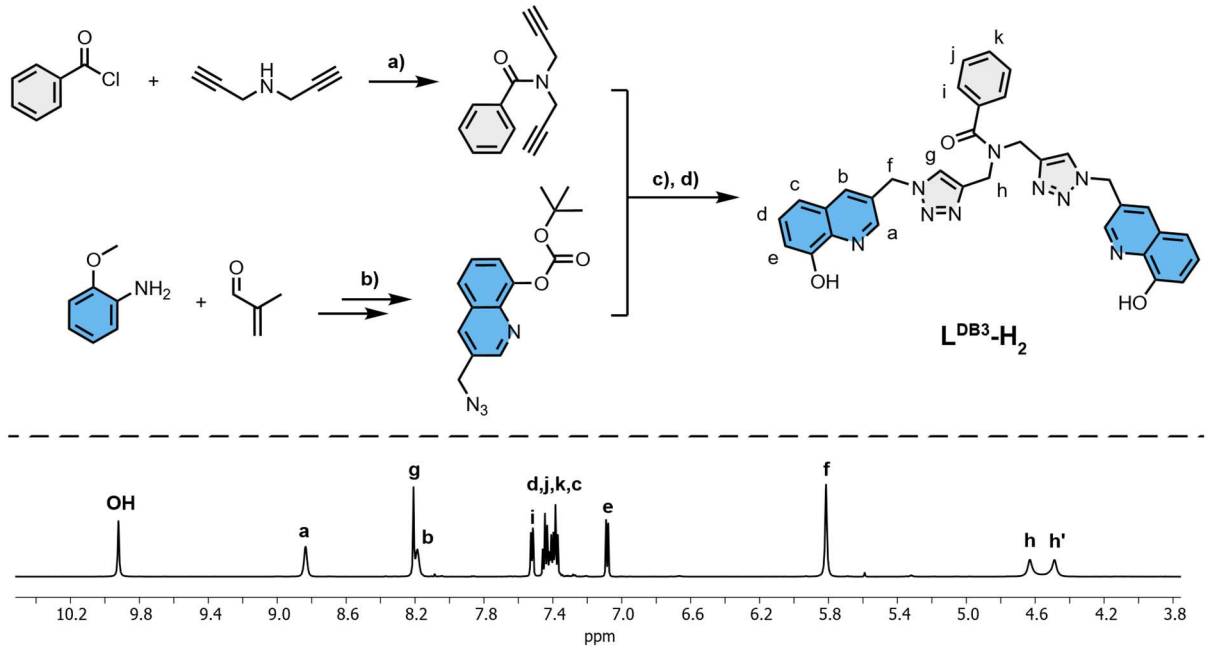

Figure 4.1: Top: Synthetic pathway ligand L^{DB3}-H_2, a) NEt_3, $CHCl_3$, rt, b) five steps, including a SKRAUP reaction among others, are described in detail in chapter 1, c) $CuSO_4$, Na-ascorbate, 60°C, d) TFA, DCM, rt. Bottom: ^{1}H NMR of ligand L^{DB3}-H_2 (DMSO-d_6, 500 MHz, 500 µM, 25°C).

The self-assembly of L^{DB3}-H_2 and $Zn(OAc)_2$ was performed in a ratio of 1:1 in DMSO-d_6, as it was expected to form an open $[Zn_2L_2]$ container. After stirring the solution for 1 h and to ensure reaching the thermodynamic minimum, the solution was heated at 70°C for 12 h, which afforded the same ^{1}H NMR spectrum as after 1 h of stirring at room temperature (Figure 4.2, b (ii)). Next, the solvent as well as the byproduct acetic acid were removed via lyophilization, which yielded a yellow powder in quantitative fashion. The ^{1}H NMR spectra of the self-assembled complex $[Zn_2L^{DB3}{}_2]$ showed a single set of signals (Figure 4.2 (b, (iii)). Upon coordination of the hydroxyquinolate units with Zn(II), the signals of proton a and g, as well as c and e, underwent highfield shifts, consistent with the previously described self-assemblies in chapter 1. Notably, the signal corresponding to proton g split into two signals, one of which overlapped with signal a, which indicated distinct chemical environment for the two triazole protons in each ligand under the given conditions. A possible cause for this behavior was a pronounced rotational barrier of the phenyl amide residue which was evident in both $[Zn_2L^{DB3}{}_2]$ and L^{DB3}-H_2 by the splitting of the neighboring methylene protons h and h'. In addition, signal f, corresponding to the methylene group linking the triazole and hydroxyquinolate moieties, also appeared as a doublet. Diastereotopic splitting of methylene groups is known for methylene groups in direct periphery of metal complex units. To resolve the overlap of signals a and g, VT ^{1}H NMR spectra were recorded. The ^{1}H NMR spectra of $[Zn_2L^{DB3}{}_2]$ in DMSO-d_6 at 90°C (Figure 4.2, b, (iii) and (iv)) showed that the signals corresponding to protons g and g' coalesced, while signals a and g appeared as individual singlets. With the interpretation of the VT ^{1}H COSY and VT ^{1}H NOESY NMR spectra at 90°C (see chapter 4.6.5), a clear assignment of each proton to its corresponding signal was possible.

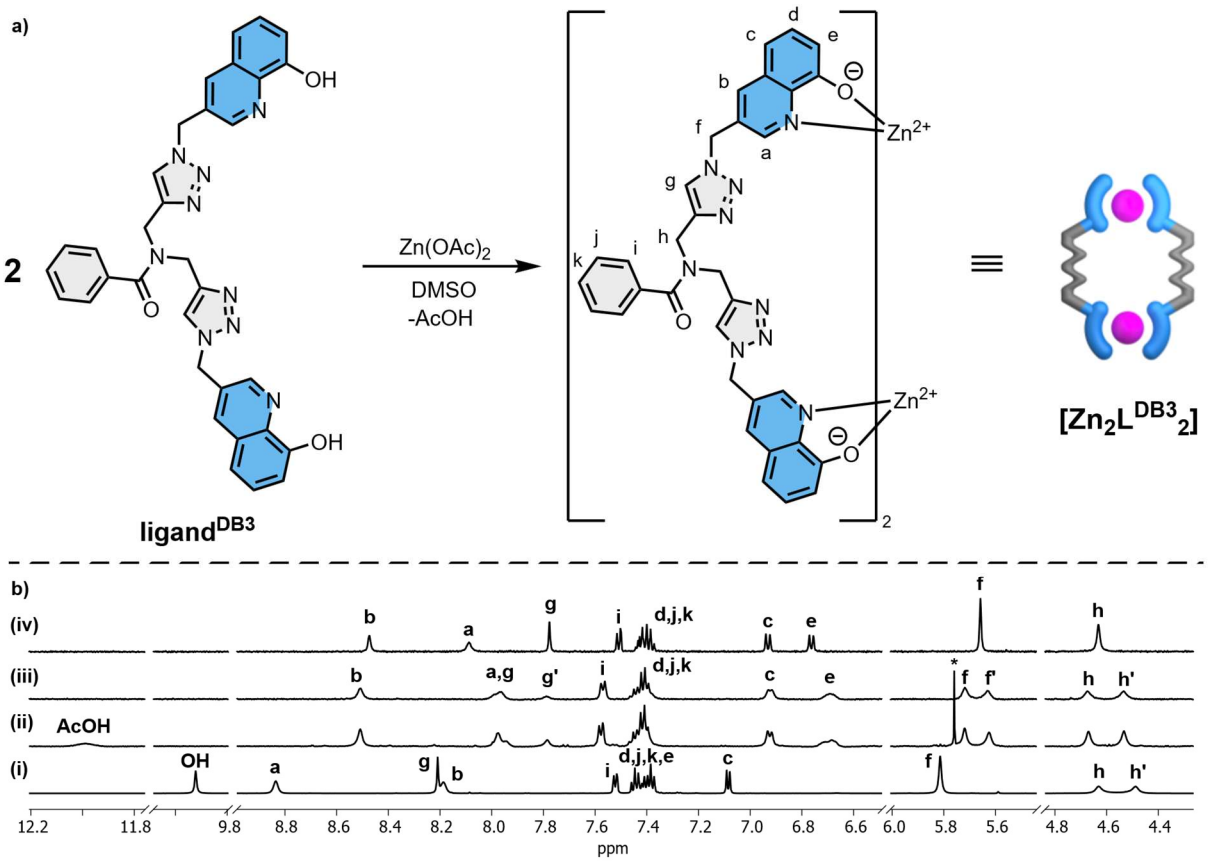

Figure 4.2: a) Self-assembly of ligand L^{DB3}-H_2 with $Zn(OAc)_2$ in DMSO-d_6 into the charge-neutral complex $[Zn_2L^{DB3}_2]$. b) ^{1}H NMR spectra of L^{DB3}-H_2 (i), the in situ self-assembly of $[Zn_2L^{DB3}_2]$ (ii), the lyophilized complex $[Zn_2L^{DB3}_2]$ (iii) and VT ^{1}H NMR spectrum of $[Zn_2L^{DB3}_2]$ at 90°C (iv) (i-iii, DMSO-d_6, 500 MHz, 500 µM, 25°C; iv, DMSO-d_6, 500 MHz, 500 µM, 90°C).

The formation of $[Zn_2L^{DB3}_2]$ was further confirmed by negative ESI-MS measurements (Figure 4.3). The spectrum showed a measured m/z value of 1257.2494 and an isotopic pattern consistent with the presence of two Zn(II) centers, which matched the calculated m/z value of 1257.2408 and the simulated isotopic pattern for the $[Cl@Zn_2L^{DB3}_2]^{1-}$ host-guest complex. The most intense m/z signal under the given conditions corresponded to a $[Cl@Zn_1L^{DB3}_1]^{1-}$ species.

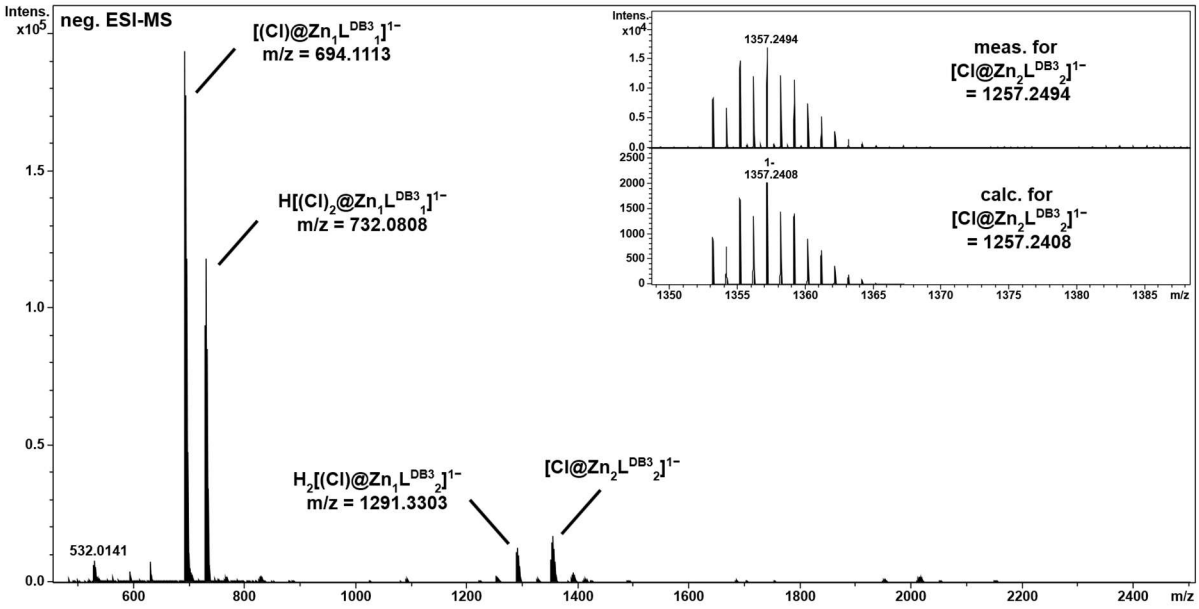

Figure 4.3: Negative HR-ESI-MS spectrum of $[Zn_2L^{DB3}{}_2]$ in DMSO/ACN (9:1) at 35°C.

As a noteworthy observation, preliminary test using the deprotected click product of non-functionalized dipropargyl amine as a ligand did not yield the clean self-assembly of a charge-neutral metal-organic assembly with $Zn(OAc)_2$. The modification with benzoyl chloride not only improved solubility but also shielded the secondary amine, which might otherwise serve as an additional coordination site.

4.3 Recognition experiments

To determine whether the charge-neutral host $[Zn_2L^{DB3}{}_2]$ could exploit the newly incorporated degrees of freedom to adjust its Zn(II)-Zn(II) distance to bind even the shortest dicarboxylates, several ^{1}H NMR test titrations were performed with dicarboxylates of varying lengths. The shortest dicarboxylate, oxalate, represented a challenging guest, as it readily forms complexes with various metal-cations.[102a,77,102b] Since metal-organic coordination cages rely on coordinative metal-ligand bonds, oxalate or other competitive anions, disrupt these interactions and cause the disassembly of the coordination cage. The undesired outcome is the formation of free ligand strands accompanied by simple metal oxalate complexes or unidentifiable mixture of aggregates. This issue has also been observed for VAN CRAEN'S charge-neutral $[Zn_2L_2]$ cage and provided the motivation for this project.

The recognition experiments of $[Zn_2L^{DB3}{}_2]$ began with aliphatic dicarboxylates of varying chain lengths in DMSO-d_6 at a concentration of 500 µM (Figure 4.4). Starting with the free host $[Zn_2L^{DB3}{}_2]$, a stepwise addition of each guest was carried out.

The test titration with the shortest dicarboxylate, oxalate (Figure 4.4, b)), revealed an intermediate binding event. Upon guest addition, the host signals performed a highfield shift and gradually lost intensity. After the addition of five equivalents TBA oxalate, a sharp single set of signals was observed. The species corresponded to the thermodynamic minimum of this specific host-guest arrangement, as it remained stable both upon heating to 90°C and after further addition of TBA oxalate. Signals a and g, which overlapped in the ^{1}H NMR of $[Zn_2L^{DB3}{}_2]$, split into three distinct signals. Two of these corresponded to the triazole protons of the ligand, while the remaining signal corresponds to proton a. This indicated different chemical environments for the triazole protons. This observation provided insight into the structural integrity of the formed host-guest complex and suggested that the conformation of the phenyl substituent on the ligand's backbone influenced the chemical shifts of the

triazole protons in the ^{1}H NMR. The formation of the two times negatively charged host-guest complex [(oxalate)@$Zn_2L^{DB3}_2$]$^{2-}$, as well as its structural characterization was provided by ESI-MS and 2D NMR spectroscopy (COSY, NOESY and DOSY). As the intermediate exchange behavior did not allow to calculate a binding constant from the ^{1}H NMR data, UV/Vis titrations were performed. Unfortunately, up to this point, it has not been possible to grown suitable single crystals of sufficient quality to obtain a solid-state structure of the oxalate host-guest complex [(oxalate)@$Zn_2L^{DB3}_2$]$^{2-}$. The structural information obtained from the NMR data provided a starting geometry for the DFT calculations. A detailed description of the host-guest complex [(oxalate)@$Zn_2L^{DB3}_2$]$^{2-}$ together with the experimental gathered data, as well as quantitative results are provided in the following section 4.4.

The subsequent ^{1}H NMR test titrations with dicarboxylates (Figure 4.4, c)-i)) of longer chain length also show 1:1 host-guest complexes, but consistently accompanied by the formation of another species.

The recognition experiment of host [$Zn_2L^{DB3}_2$] and TBA malonate (Figure 4.4, c) revealed fast exchange behavior during the initial steps of guest addition. After the addition of more than five equivalents of guest, the signals broaden and new signals appeared, which indicated the formation of a minor species alongside the major species. In this case, ESI-MS measurements did not provide a mass-to-charge ratio corresponding to the 1:1 host-guest complex [(malonate)@$Zn_2L^{DB3}_2$]$^{2-}$, presumably because the complex was not stable in the given ESI-MS conditions and dissociated during measurement.

The test titration of TBA succinate (Figure 4.4, d)) revealed the second cleanest formation of a 1:1 host-guest species in this experimental series of tested guests. Nevertheless, the host-guest complex [(succinate)@$Zn_2L^{DB3}_2$]$^{2-}$ was accompanied by a minor species. The signals of the free host underwent a highfield shift upon stepwise addition of TBA succinate. The formation of complex [(succinate)@$Zn_2L^{DB3}_2$]$^{2-}$ could further be proven in the gas phase by ESI-MS measurements (see chapter 4.6.6).

With increasing chain length of the TBA dicarboxylate guests, the ^{1}H NMR spectra of the recognition experiments became progressively more complex. The recognition experiment of host [$Zn_2L^{DB3}_2$] and TBA glutarate (Figure 4.4, e)) showed slow to fast intermediate guest exchange behavior upon stepwise addition of guest to the free host. After the addition of one equivalent of TBA glutarate signals underwent a shift, as well as new signals appeared. Upon addition of ten equivalents of guest the ^{1}H NMR spectra showed more than one distinct set of signals, which indicated the formation of two or more species in total. In contrast, negative ESI-MS measurements of [(glutarate)@$Zn_2L^{DB3}_2$]$^{2-}$ provided mass-to-charge ratios and isotopic pattern which fit to the calculated values (see chapter 4.6.6).

The recognition experiment of host [$Zn_2L^{DB3}_2$] and TBA adipate (Figure 4.4, f)) exhibited a transition from fast to slow guest exchange, as host signals shifted and new signals appeared in the ^{1}H NMR spectrum after the addition of only one equivalent of guest. This behavior was particularly evident for signals corresponding to protons f and h. Furthermore, signals c and e, corresponding to the peripheral protons of the hydroxyquinolate moiety, showed more than one set of signals after the addition of two equivalents, indicating the presence of multiple distinct species. This may arouse from the chain length of adipate being sufficient to curl outside of the receptor cavity, or from its acting as a linker between two host molecules. Another possible arrangement, supported by ESI-MS data alongside the 1:1 host-guest complex [(adipate)@$Zn_2L^{DB3}_2$]$^{2-}$, was a species which adipate coordinates to only one ligand and one Zn(II) ion. This species was observed as TBA adduct in the negative-mode ESI-MS measurement (see chapter 4.6.6).

The recognition experiment of host [$Zn_2L^{DB3}_2$] and TBA pimelate (Figure 4.4, g)) exhibited a slow exchange guest-behavior. After the addition of one equivalent of TBA pimelate signal intensity of the free host lowered, whereas a new set of signals appeared. After the addition of two equivalents and more, another set of signals appeared, which overlapped partially with the other signals, which was

presumably a formation of three distinct species at a time. Heating the sample to 70°C overnight did not influence the equilibrium. Nevertheless, it is highly probable that, among others, a 1:1 [(pimelate)@$Zn_2L^{DB3}{}_2]^{2-}$ complex was formed.

The recognition experiments with the two longest dicarboxylates, TBA suberate and TBA decanedioate (Figure 4.4, h) and i)), both exhibited intermediate binding behavior, transitioning from fast to slow exchange. Upon the addition of one equivalent of guest, the ^{1}H NMR spectra showed a shift of signals accompanied by the appearance of new signals. With further guest addition, the intensity of the initially shifted signals decreased, while a new set of signals appeared. ESI-MS measurements of both host-guest system confirmed the formation of 1:1 host-guest complexes of [(suberate)@$Zn_2L^{DB3}{}_2]^{2-}$ and [(decanedioate)@$Zn_2L^{DB3}{}_2]^{2-}$.

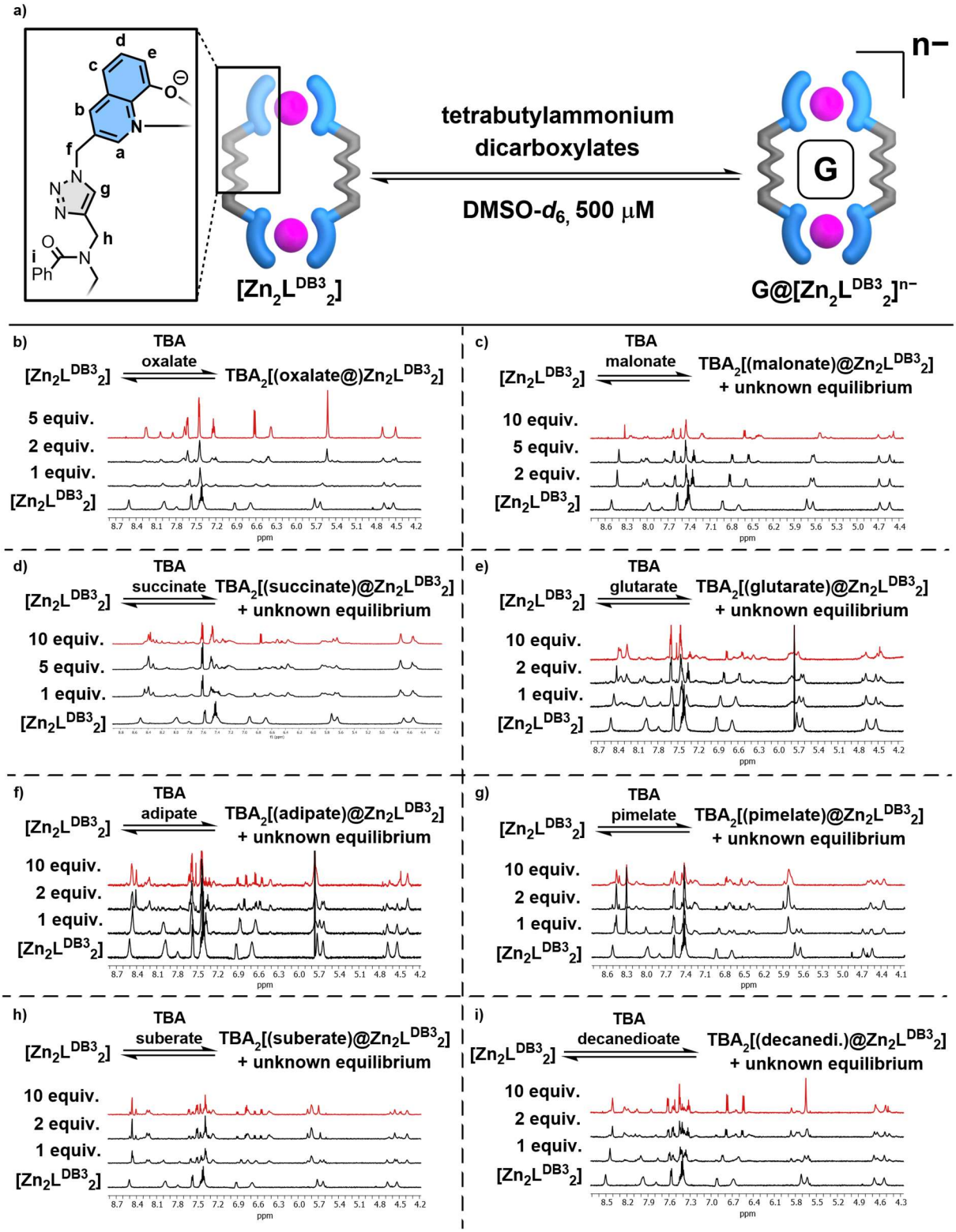

Figure 4.4: a) Host-guest equilibrium of $[Zn_2L^{DB3}{}_2]$ with tetrabutylammonium dicarboxylates. b)-i) ^{1}H NMR test titrations of $[Zn_2L^{DB3}{}_2]$ with TBA oxalate, -malonate, -succinate, -glutarate, -adipate, -pimelate, -suberate and -decanedioate (DMSO-d_6, 500 MHz, 500 μM, 25°C).

To explore the effects of the new modifications in $[Zn_2L^{DB3}{}_2]$ and its interactions with negatively charged species other than dicarboxylates, both inorganic and organic anions were tested. The first stage of

the investigation involved a series of ^{1}H NMR test titrations of TBA (pseudo-)halides and $[Zn_2L^{DB3}{}_2]$ in DMSO-d_6.

The test titration of TBA fluoride (Figure 4.5, b)) with $[Zn_2L^{DB3}{}_2]$ showed fast-exchange behavior with weak highfield shifts for the signals corresponding to the hydroxyquinolate peripheral protons c, d and e. The signals corresponding to proton a and g underwent shifts and overlapped. In addition, signals intensities of another minor species appeared upon further guest addition. This indicated no distinct binding of fluoride, whereas the data suggested a coordination of fluoride to the Zn(II) ions.

The test titration of TBA chloride (Figure 4.5, c)) with $[Zn_2L^{DB3}{}_2]$ also showed fast-exchange behavior, but without the formation of minor species forming upon guest addition. Signals d, c and e again displayed slight highfield shifts. The guest-exchange behavior of signals corresponding to protons a and g were comparable to that observed in the fluoride titration, although in this case the overlap was less pronounced. These observations likewise suggested the chloride ions to coordinate to the Zn(II) ions.

The ^{1}H NMR spectra of the test titrations of TBA bromide and iodide (Figure 4.5, d) and e)) with $[Zn_2L^{DB3}{}_2]$ showed no evidence of interaction between the host and the added guests. The TBA salts of pseudo halides azide and cyanide were also tested in a ^{1}H NMR test titration with host $[Zn_2L^{DB3}{}_2]$. (Figure 4.5, f) und g)). Stepwise addition of TBA azide to the host showed fast-exchange behavior with shifts comparable to those observed in the previous titrations with chloride and fluoride, though with even smaller highfield shifts. This observation indicated coordination to the Zn(II) centers or weak C-H anion hydrogen bonds.

The binding constant of $[Zn_2L^{DB3}{}_2]$ and the here presented (pseudo-)halides fluoride, chloride and azide were presumably low, as the observed shifts in the ^{1}H NMR titrations were small and the experiments were carried out in a competitive solvent. Attempting fine ^{1}H NMR titrations of e.g., $[Zn_2L^{DB3}{}_2]$ with TBA azide, gave poor quality curvature of the plotted data and inconclusive results.

In contrast, stepwise addition of TBA cyanide (Figure 4.5, g)) disrupted the integrity of the host $[Zn_2L^{DB3}{}_2]$. After the addition of 10 equivalents of TBA cyanide, the ^{1}H NMR spectrum showed signals corresponding to the free ligand L^{DB3}-H_2. Cyanide strongly coordinated to the Zn(II), thereby breaking the coordination bonds between the Zn(II) centers and the hydroxyquinolates.

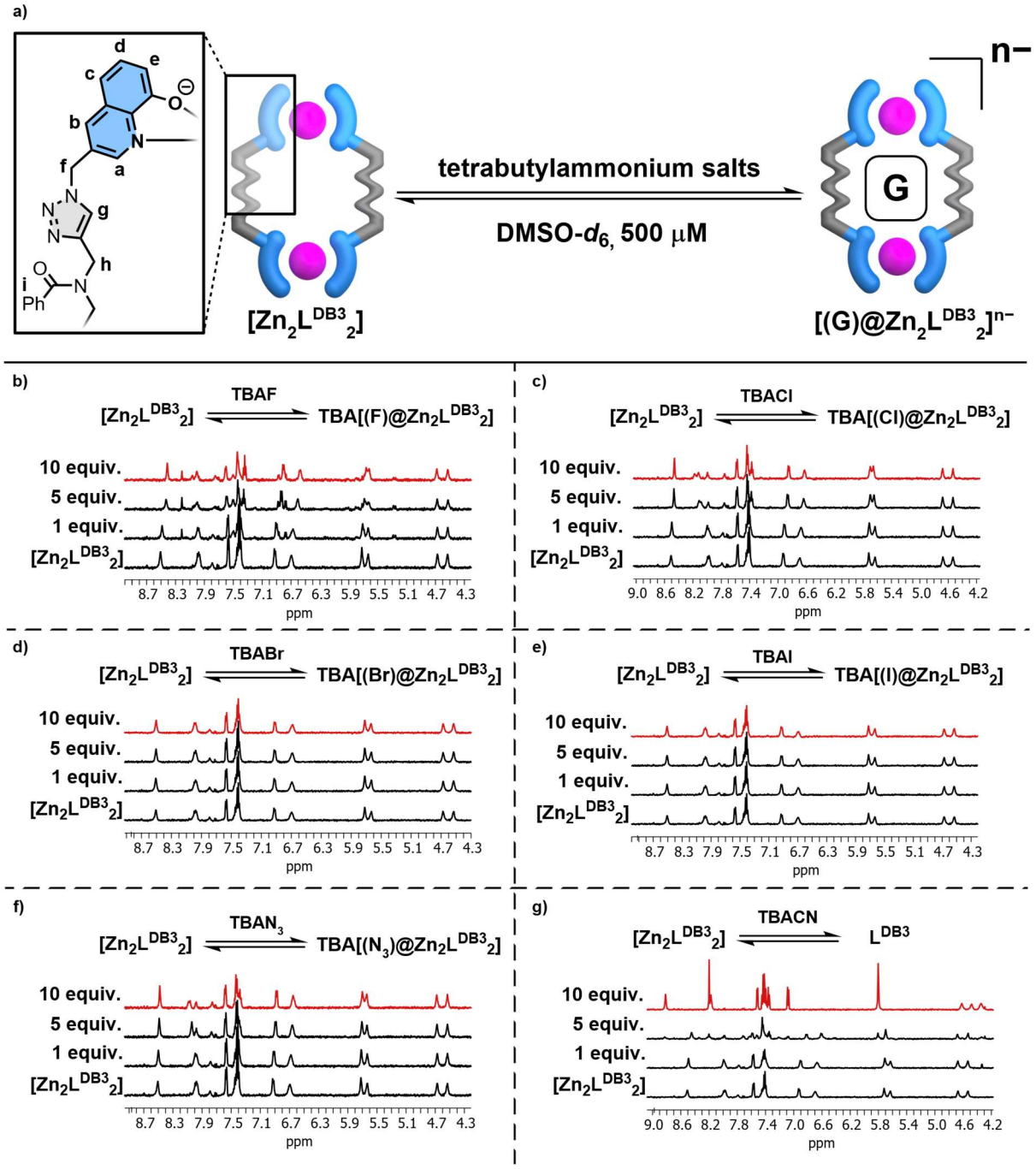

Figure 4.5: a) Host-guest equilibrium of [$Zn_2L^{DB3}_2$] with tetrabutylammonium (pseudo-)halides. b)-i) ^{1}H NMR test titrations of [$Zn_2L^{DB3}_2$] with TBA fluoride, -chloride, -bromide, -iodide, -azide and -cyanide (DMSO-d_6, 500 MHz, 500 µM, 25°C).

[$Zn_2L^{DB3}_2$] exhibited selective binding of oxalate but no distinct binding behavior with increasing chain lengths. Since the carboxylate moieties were known to coordinate to the Zn(II) centers, the small shifts observed in the experiments with inorganic anions motivated further investigation into the interactions between [$Zn_2L^{DB3}_2$] and monocarboxylates such as acetate and benzoate. Structurally more complex and chiral monocarboxylates, including (*S*)-2-(6-methoxynaphthalen-2-yl)propanoate (NPX^-) and 2-(4-isobutylphenyl)propanoate (IBU^-), which represent the carboxylate derivatives of the painkillers naproxen and ibuprofen, were also examined. The size difference among these monocarboxylate gave the question of whether the equilibrium corresponded to a 1:1 or 1:2 host-guest arrangement.

All ^{1}H NMR test-titrations of $[Zn_2L^{DB3}{}_2]$ with TBA monocarboxylates in DMSO-d_6 showed fast-exchange binding behavior (Figure 4.6, a)-f)). The signals corresponding to the peripheral protons of the hydroxyquinoline units, including proton b, performed a highfield shift. Interestingly the signal of proton e sharpened after the addition of 5 equivalents of guest in each case, which indicated a more defined chemical environment for proton e on the ^{1}H NMR time scale, consistent with coordination of the carboxylates to the Zn(II) centers. To quantify the fast-exchange behavior of $[Zn_2L^{DB3}{}_2]$ with the tested TBA monocarboxylates and to determine wheatear the host guest systems adopt a 1:1 or 1:2 arrangement, fine ^{1}H NMR titrations and ESI-MS analysis were conducted (chapter 4.4).

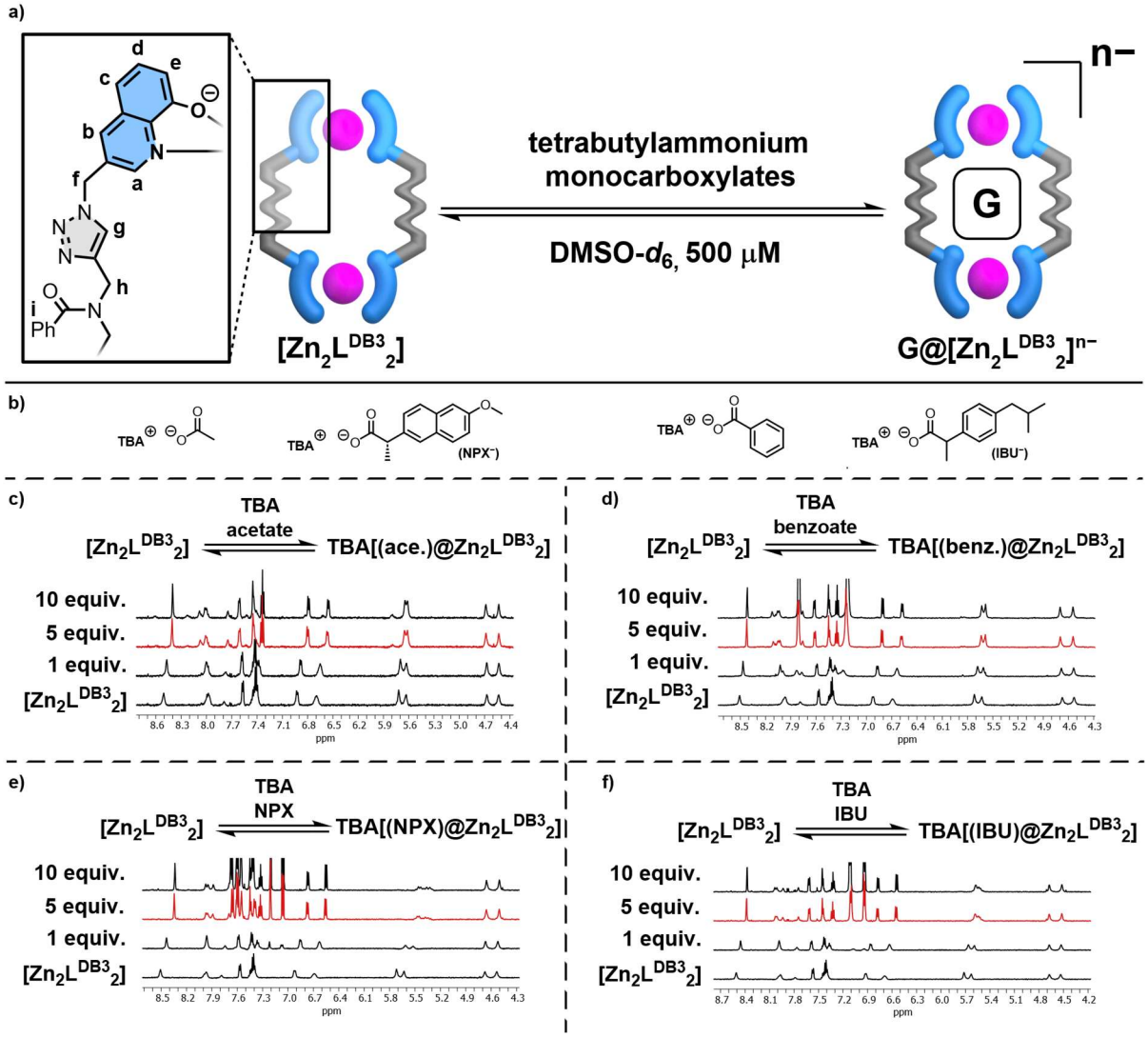

Figure 4.6: a) Host-guest equilibrium of $[Zn_2L^{DB3}{}_2]$ with tetrabutylammonium monocarboxylates. b) Structural formulars of TBA acetate, NPX$^-$, benzoate and IBU$^-$. c)-f) ^{1}H NMR test titrations of $[Zn_2L^{DB3}{}_2]$ with TBA acetate, benzoate, NPX$^-$ and IBU$^-$ (DMSO-d$_6$, 500 MHz, 500 µM, 25°C).

Recognizing that the LEWIS acid-base interactions between Zn(II) and the carboxylate moieties were the key recognition force, other inorganic multivalent salts were tested (Figure 4.7, a-d). The ^{1}H NMR titration experiment with sodium dithionite showed broadening of the signals, presumably due to the addition of 10% D_2O, which indicated no interaction.

The ^{1}H NMR titration of $[Zn_2L^{DB3}{}_2]$ with TBA phosphate showed a slow exchange guest-exchange behavior (Figure 4.7, d), with broadened signals presumably caused by coordinative interactions of the

phosphates with the Zn(II) centers. This observation suggested disruption of the structural integrity of $[Zn_2L^{DB3}{}_2]$. ^{1}H NMR titrations with TBA nitrate or sulfate show no significant binding (see chapter 4.6.6).

The most interesting observation was that after the addition of 20 equiv. TBA pyrophosphate the ^{1}H NMR titration showed a sharp single set of signals (Figure 4.7, c)). A ^{1}H NMR titration of ligand L^{DB3}-H_2 with TBA pyrophosphate revealed the same ^{1}H NMR spectrum after the addition of 40 equivalents (Figure 4.7, e)). Signals e and c merge in both experiments. Up to this point the ESI-MS data (see chapter 4.6.6) gave no clear insight into the interactions between $[Zn_2L^{DB3}{}_2]$ and TBA pyrophosphate.

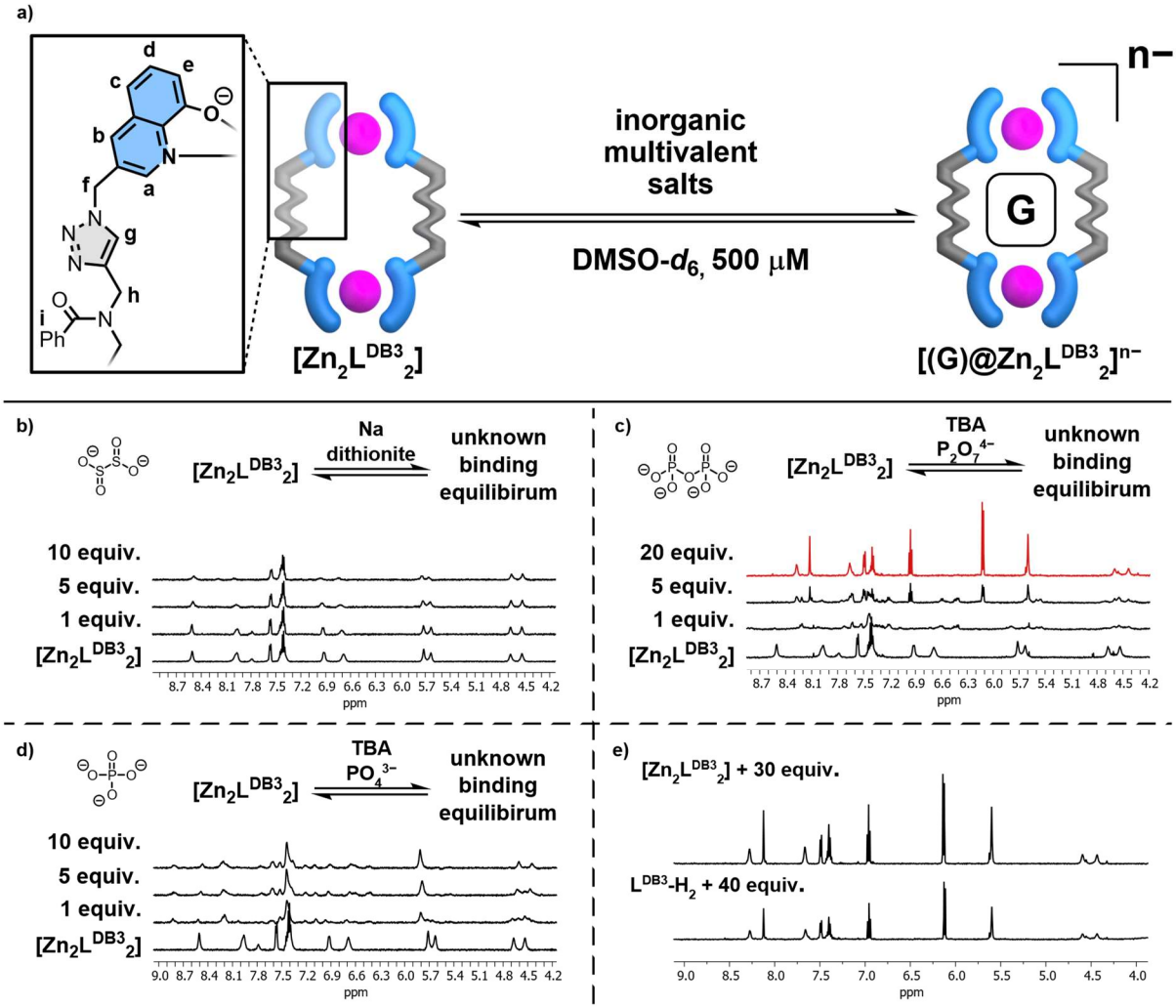

Figure 4.7: a) Host-guest equilibrium of $[Zn_2L^{DB3}{}_2]$ with inorganic multivalent salts.
b) ^{1}H NMR test titrations of $[Zn_2L^{DB3}{}_2]$ with sodium dithionite (DMSO-d_6/10% D_2O, 500 MHz, 500 µM, 25°C),
c) ^{1}H NMR test titrations of $[Zn_2L^{DB3}{}_2]$ with TBA pyrophosphate,
d) ^{1}H NMR test titrations of $[Zn_2L^{DB3}{}_2]$ with TBA phosphate, e) Comparison $[Zn_2L^{DB3}{}_2]$ with 30 equiv. TBA pyrophosphate and L^{DB3}-H_2 with 40 equiv. TBA pyrophosphate (c)-d): DMSO-d_6, 500 MHz, 500 µM, 25°C).

4.4 Taming oxalate, quantitative binding, competition experiments and NMR powered computational study

The qualitative ^{1}H NMR titrations of $[Zn_2L^{DB3}_2]$ showed that the receptor overcame the limitations of VAN CRAENS charge-neutral $[Zn_2L_2]$ host with respect to the selective binding of the shortest dicarboxylate, oxalate. Nevertheless, the intermediate guest exchange in the ^{1}H NMR with oxalate (Figure 4.8) prevented a quantitative determination of the binding constant *K*. To determine a binding constant *K* for oxalate, UV/Vis spectroscopy was used (Figure 4.8, b)-c)). The average binding constant for oxalate was log *K* = 4.39 ± 0.04, obtained by three independent UV/Vis titrations performed at varying concentrations (see chapter 4.6.7, data fitted with HypSpec2014[103]). The reported uncertainty represented the standard deviation of these measurements. Negative ESI-MS of $[Zn_2L^{DB3}_2]$ with 5 equivalents oxalate showed formation of a distinct 1:1 host-guest complex. The major signal of m/z = 705.1283 and its isotopic pattern matched with the calculated value m/z= 705.1263 of $[(oxalate)@Zn_2L_2]^{2-}$.

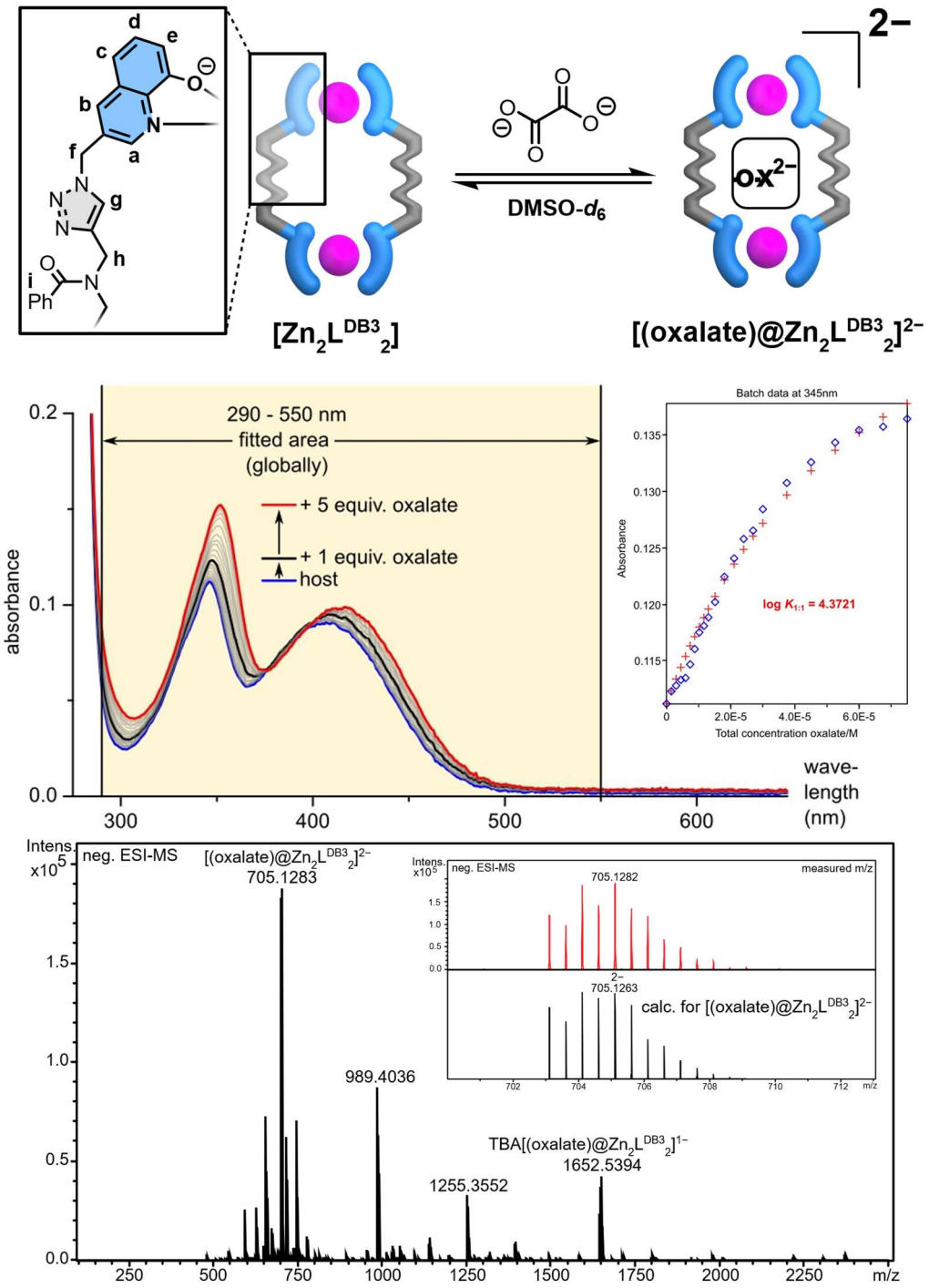

Figure 4.8: a) Host-guest equilibrium of $[Zn_2L^{DB3}_2]$ with tetrabutylammonium oxalate in DMSO-d_6. b) UV/Vis-titration of $[Zn_2L^{DB3}_2]$ with tetrabutylammonium oxalate (DMSO-d_6, d = 1 cm, 15 µM, 25°C), c) part of the HypeSpec2014 fit of the absorbance data between 290 nm and 550 nm assuming a 1:1 binding model, d) negative ESI-MS spectrum of $[Zn_2L^{DB3}_2]$ with 5 equivalents oxalate showing the formation of $[(oxalate)@Zn_2L^{DB3}_2]^{2-}$.

As already mentioned, up to this point, it was not possible to grow suitable single crystals to obtain solid-state structure of the host-guest complex $[(oxalate)@Zn_2L^{DB3}_2]^{2-}$. The structural information obtained from the 1D and 2D NMR data provided a starting geometry for the DFT calculations. The signals corresponding to the linking methylene group of the hydroxyquinolate and triazole showed diastereotopic splitting for the empty host $[Zn_2L^{DB3}_2]$, indicating the existence of a racemic ($\Delta\Delta/\Lambda\Lambda$) helicate. Upon oxalate binding these signals merged into a singlet, presumably due to the formation

of a *meso*-form. Further, ^{1}H NOESY NMR of the host-guest complex [(oxalate)@$Zn_2L^{DB3}{}_2$]$^{2-}$ revealed through-space contacts of the triazole protons g with the proton a of the hydroxyquinolate, which was next to the coordinating nitrogen atom of the hydroxyquinolate. This indicated that the proton g pointed towards the cavity. The geometry of the model was optimized (ORCA 5.0.3[98,99]) using ωB97X-D4/def2-SVP with implicit solvent (DMSO). The triazole moieties of each ligand adopted a nearly parallel orientation with a slight tilt compared to the horizontal axis which resulted in one short (Figure 4.9, left ligand: 2.2 Å, right ligand: 2.3 Å) and one longer proton g – proton a (left ligand: 2.8 Å, right ligand: 2.8 Å). In contrast, the calculated distance from the cross signals was roughly 2 Å for both contacts.

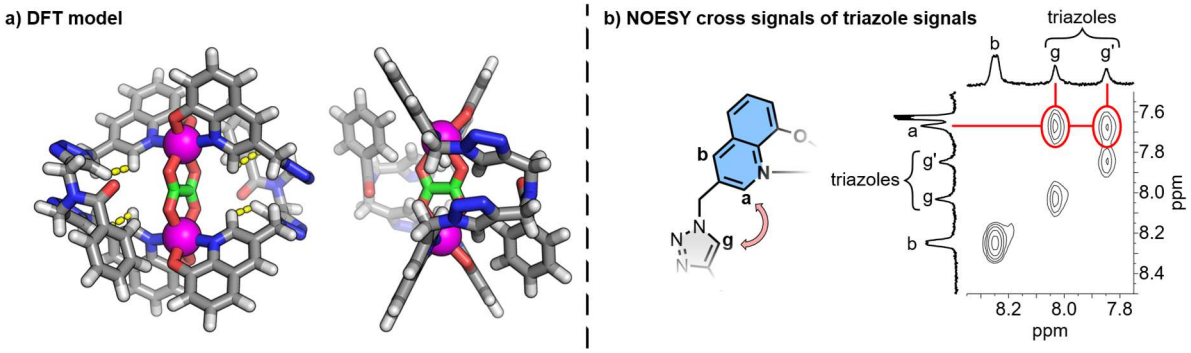

Figure 4.9: a) Optimized "meso-helicate" structure of [(oxalate)@$Zn_2L^{DB3}{}_2$]$^{2-}$ with oxalate chelating both Zn(II) centers, carbon atoms are shown in grey, nitrogen in blue, oxygen in red, hydrogen in white and Zn(II) is purple colored. (ωB97X-D4[104] def2-SVP[96,97], implicit solvation with DMSO[105], ORCA 5.0.3[98,99])
b) ^{1}H NOESY cross signals of protons g and a.

Based on previous investigations, the triazole units tend to rotate at ambient temperatures.[82,76] Consequently, dynamic tilting motions of the triazole units in upward and downward directions were expected. Molecular dynamics simulations (xTB 6.6.0[106,107]) supported this hypothesis (see chapter 4.6.9). Average distances between protons g and a of 2.6, 2.3, 2.3 and 2.4 Å were observed for the through-space interactions over a simulation timescale of 800 ps.

The ^{1}H NMR titrations with longer aliphatic chains showed no clear binding upon addition of these guests as TBA salts to [$Zn_2L^{DB3}{}_2$]. Broad regions and multiple sets of signals persisted even after the addition of a large excess of the respective analytes. Binding constant for these dicarboxylates were not determined due to the lack of clarity regarding the underlying binding equilibria and the exact speciation. Presumably because the host [$Zn_2L^{DB3}{}_2$] could not provide a suitable cavity size for these dicarboxylates in terms of the Zn(II)-Zn(II) distance and a selective formation of a 1:1 host-guest complex did not take place.

To circumvent the limitation that no binding constants were determined for the longer dicarboxylates, a qualitative comparison of the guest-binding tendencies was performed using a ^{1}H NMR competition experiment. Here, the behavior of [$Zn_2L^{DB3}{}_2$] with different combinations of analytes was investigated. The ^{1}H NMR spectra of all tested mixtures, dicarboxylates (oxalate to adipate) with and without monocarboxylates (acetate and benzoate), matched the spectrum of [(oxalate)@$Zn_2L^{DB3}{}_2$]$^{2-}$. The competition experiments demonstrated that the host [$Zn_2L^{DB3}{}_2$] binds oxalate selectively over all other guests studied.

The chemicals shift of the fast exchange behavior of both the (pseudo-)halides and the monocarboxylates were small. However, only the binding of [$Zn_2L^{DB3}{}_2$] with monocarboxylates was quantified, due to the previously mentioned limitations and the inconclusive plots obtained from the ^{1}H NMR fine titration with TBA chloride and azide. Plotting the chemical shifts of the fine ^{1}H NMR titrations gave binding constants for the monocarboxylates (Figure 4.11, see SI). The titrations for

acetate and benzoate were performed three times, the titrations of NPX^- and IBU^- two times. The binding constants for acetate (log K = 3.44 ± 0.34), benzoate (log K = 3.33 ± 0.19), NPX^- (log K = 3.36 ± 5.6%) and IBU^- (log K = 3.37 ± 5.8%) were a magnitude lower compared to oxalate binding. The ^{1}H NMR titration data for all monocarboxylates suggests 1:1 host-guest binding, as no inflection point was observed. Furthermore, negative ESI-MS (Figure 4.10) supported the argument for 1:1 host-guest assemblies. The calculated m/z values for each host-guest complex matched with the experimentally measured m/z values and confirm the formation of 1:1 host-guest complexes of $[(acetate)@Zn_2L^{DB3}{}_2]^{1-}$, $[(benzoate)@Zn_2L^{DB3}{}_2]^{1-}$, $[(NPX)@Zn_2L^{DB3}{}_2]^{1-}$ and $[(IBU)@Zn_2L^{DB3}{}_2]^{1-}$ in the gas phase.

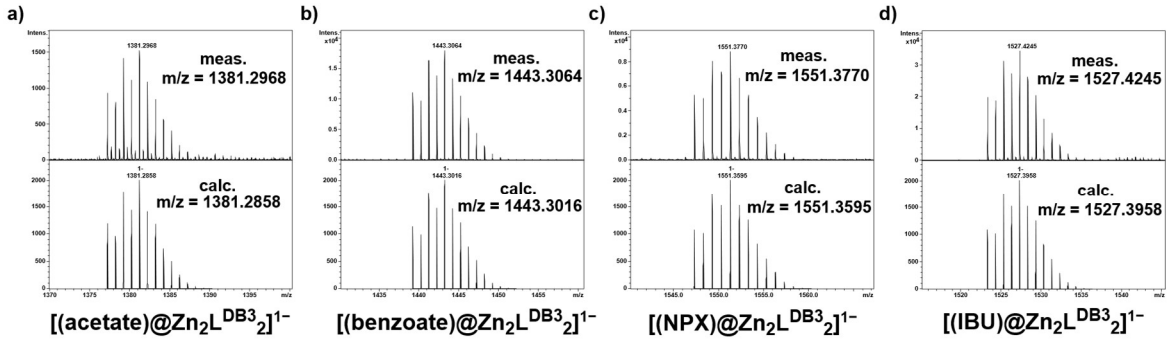

Figure 4.10: Excerpt from the negative ESI-MS spectrum of a) $[(acetate)@Zn_2L^{DB3}{}_2]^{1-}$, b) $[(benzoate)@Zn_2L^{DB3}{}_2]^{1-}$, c) $[(NPX)@Zn_2L^{DB3}{}_2]^{1-}$ and d) $[(IBU)@Zn_2L^{DB3}{}_2]^{1-}$. Showing a 1:1 host-guest complex formation for each spectrum.

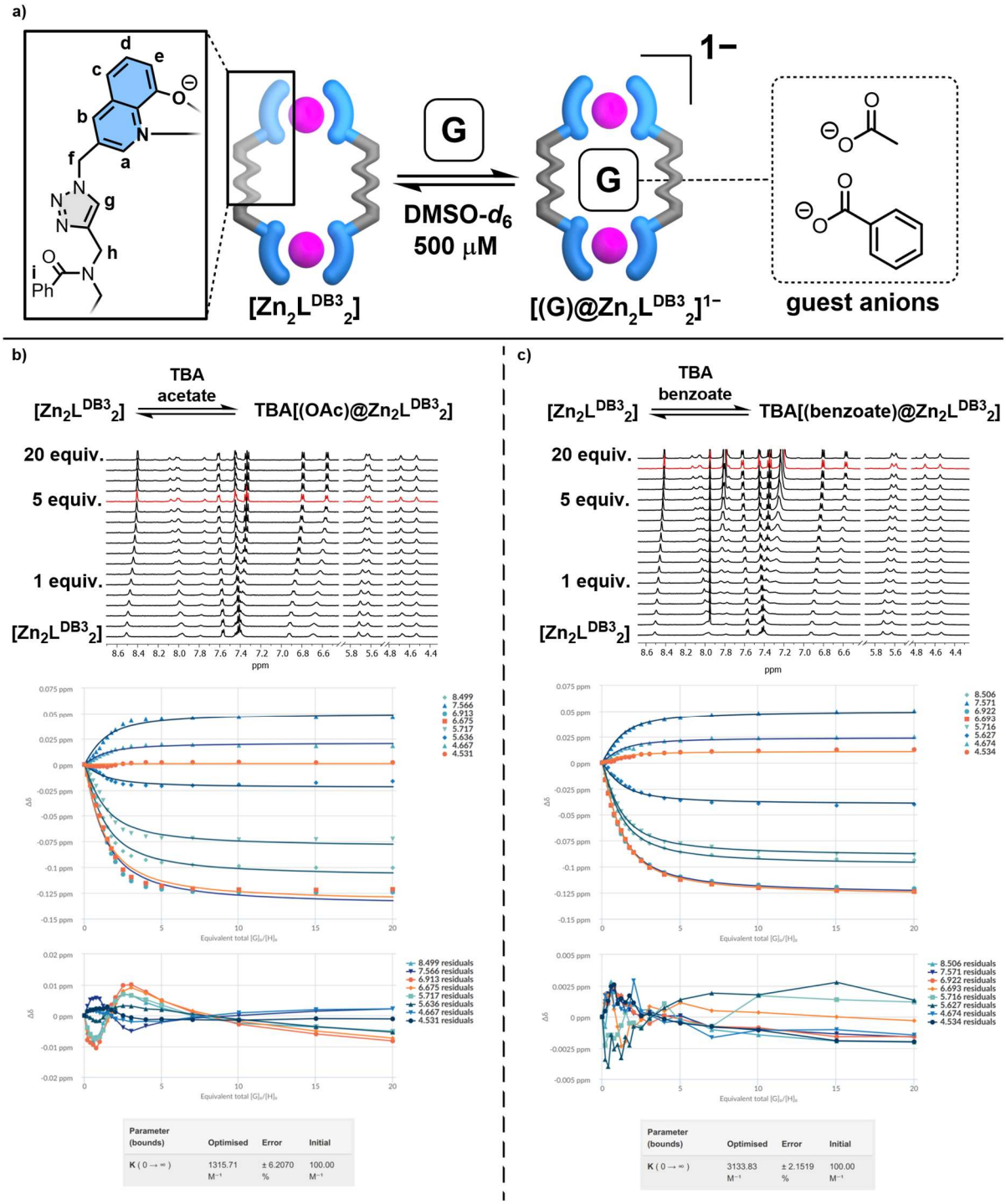

Figure 4.11: a) Host-guest formation of $[Zn_2L^{DB3}{}_2]$ with TBA acetate and TBA benzoate in DMSO-d_6. b-c) Fine ^{1}H NMR titration of $[Zn_2L^{DB3}{}_2]$ with TBA acetate (b), DMSO-d_6, 500 MHz, 500 µM 25°C) and benzoate (c), DMSO-d_6, 500 MHz, 500 µM 25°C), BindFit[91,85] plot of selected signals from the fine ^{1}H titrations and the resulting binding constants K.

4.5 Conclusion and Outlook

The new ligand L^{DB3}-H_2 successfully addressed the limitations of VAN CRAEN'S charge-neutral $[Zn_2L_2]$ cage regarding the discrete binding of short carboxylates. The introduction of a flexible dipropargyl amine-based backbone, incorporating two additional methylene units and a central nitrogen atom, enabled increased conformational freedom and adjustable Zn(II)-Zn(II) distance during guest binding. Despite the reduced rigidity associated with this modification, the self-assembly with $Zn(OAc)_2$ yielded the desired chare-neutral complex $[Zn_2L^{DB3}{}_2]$, as confirmed by NMR and ESI-MS data.

Recognition studies revealed that $[Zn_2L^{DB3}{}_2]$ exhibited distinct and selective binding toward oxalate, forming a well-defined 1:1 host-guest complex, while longer dicarboxylates showed less specific or multiple binding equilibria. The oxalate complex remained intact under competitive conditions and demonstrated selective binding of oxalate, highlighting the structural adaptability of the flexible cage. In contrast, monocarboxylates displayed weaker binding affinities, and multivalent inorganic anions such phosphate and pyrophosphate led to partial or complete disruption, consistent with Zn(II)-anion interactions.

Although the crystallization of $[Zn_2L^{DB3}{}_2]$ and its host-guest complexes remained unsuccessful, solution-state studies, supported by computational analyses, provided a detailed structural model of the $[(oxalate)@Zn_2L^{DB3}{}_2]^{2-}$ host-guest complex. The system thus represented a rare example of a charge-neutral Zn(II)-based container capable of accommodating short, highly coordinating anions without disassembly.

The demonstrated flexibility and binding selectivity of $[Zn_2L^{DB3}{}_2]$ open promising avenues for future investigations. Modifications of the ligand backbone may allow fine-tuning of the Zn(II)-Zn(II) distance and cavity polarity to achieve discrimination between anions of similar size and charge. Furthermore, the robust yet adaptive coordination motif suggests potential applications in anion sensing, selective separation, or catalytic transformations where reversible anion binding plays a crucial role. Integrating chiral or redox active functionalities into the flexible backbone could further extend the utility of this system toward enantioselective recognition or stimuli-responsive supramolecular catalysis.

4.6 Experimental Part

4.6.1 General Information

All experiments were performed under argon atmosphere, when necessary. Chemicals and solvents were purchased from Sigma Aldrich, Acros Organics, Carl Roth, TCI Europe, VWR and ABCR. Dry solvents were purchased or purified with absorbent-filled columns in a solvent purification system (SPS). Monitoring of reactions were performed with thin layer chromatography using silica coated aluminium plates (Merck, silica 60, fluorescence indicator F_{254}, thickness 0.25 mm). For column chromatography, silica (Merck, silica 60, 0.02-0.063 mesh ASTM) was used as the stationary phase. UV-Vis spectra were obtained using a DAD HP-8453 UV-Vis spectrometer. High resolution Electrospray ionization (ESI) mass spectra were obtained using a Bruker ESI timsTOF (trapped ion mobility-time of flight) and Compact mass spectrometers (positive and negative mode). Samples were diluted with HPLC-grade acetonitrile. NMR spectra were recorded on Bruker AVANCE III 500, 600 and 700 MHz spectrometers. Chemical shifts were reported in ppm with residual solvent as reference: DMSO-d_6 (2.50 ppm for ^{1}H, 39.52 ppm for ^{13}C), $CDCl_3$ (7.26 ppm for ^{1}H, 77.16 ppm for ^{13}C) and DMF-d_7 (8.03 ppm for ^{1}H). Abbreviations for signal multiplicity in the ^{1}H NMR spectra were indicated as: s, singlet; d, doublet; t, triplet; dd, doublets of doublets; m, multiplet; b, broad.

4.6.2 Deprotonation of carboxylic acids

Oxalic, malonic, succinic, glutaric, adipic, pimelic, suberic, decanedioic, malic, terephthalic and 2,6-naphthalenedicarboxylic acid were commercially obtained from chemPUR and Merck (Sigma-Aldrich). Ibuprofen and Naproxen were purchased at merck. The (di)carboxylic acids were dissolved in a small amount of MeOH (up to 5 mL), and one or two equivalents of TBA-hydroxide (1 M in MeOH) were added, depending on whether it was a mono- or dicarboxylic acid. Afterward, the mixture was vortexed for 30 min and the solvent was evaporated. A small amount of water (1-2 mL) was added to the remaining slurry residue to assist the final lyophilization process. The TBA-dicarboxylates were used without further purification. The TBA-salts of fluoride, chloride, bromide, iodide, cyanide, azide, nitrate, phosphate, pyrophosphate, acetate and benzoate were commercially available. Bicarbonate was obtained as a TEA-salt, dithionite as a sodium salt.

4.6.3 Titration procedure

All preliminary qualitative NMR binding studies were performed at 500 µM in DMSO-d_6 with a Bruker NEO 500. All quantitative binding studies were performed dilution corrected. Binding constants were determined by ^{1}H NMR titration experiments, if not mentioned differently. The obtained data was fitted by BindFit[91,85]. The binding constant for oxalate was obtained by performing UV-Vis titrations (Hellma 10 mm x 10 mm QS cuvettes, room temperature) because of the intermediate-like exchange behavior in the NMR. Therefore, the absorbance between 290 nm and 550 nm was fitted globally with the program HypSpec2014[103] Errors were estimated by repeating the NMR and UV-Vis titration experiments three times.

4.6.4 Synthetic procedure of ligand L^{DB3}-H_2

Synthesis of *N*,*N*-di(prop-2-yn-1-yl)benzamide

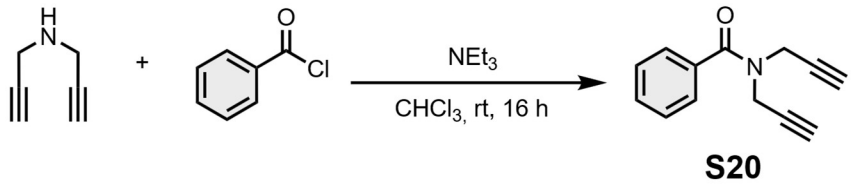

Figure 4.12: Synthesis of the backbone via a SCHOTTEN-BAUMANN reaction.

The synthesis of *N,N*-di(prop-2-yn-1-yl)benzamide (**S20**) is described in the literature and was followed with small changes.[101] Dipropargylamine (1.11 mL, 10.74 mmol, 3 equiv.) was dissolved in chloroform (50 mL) and triethylamine (1.49 mL, 10.74 mmol, 3 equiv.) was added. After 5 min of stirring benzoyl chloride (0.41 mL, 3.58 mmol, 1 equiv.) was added slowly and the reaction mixture was stirred overnight at 70°C. Then the reaction mixture was quenched with water. Afterward, the aqueous layer was extracted with chloroform (3x). The combined organic layers were dried ($MgSO_4$) and the solvent was evaporated under reduced pressure. Column chromatography (silica, pentane/EtOAc 9:1) gives *N,N*-di(prop-2-yn-1-yl)benzamide (**S20**) as a yellowish oil, which crystallized in the fridge (95%, 668.9 mg, 3.39 mmol).

^{1}H NMR (500 MHz, $CDCl_3$, 25°C): δ = 7.57-7.53 (m, 2H), 7.50-7.40 (m, 3H), 4.47 (br. s, 2H), 4.21 (br. s, 2H), 2.32 (br. s, 2H) ppm.

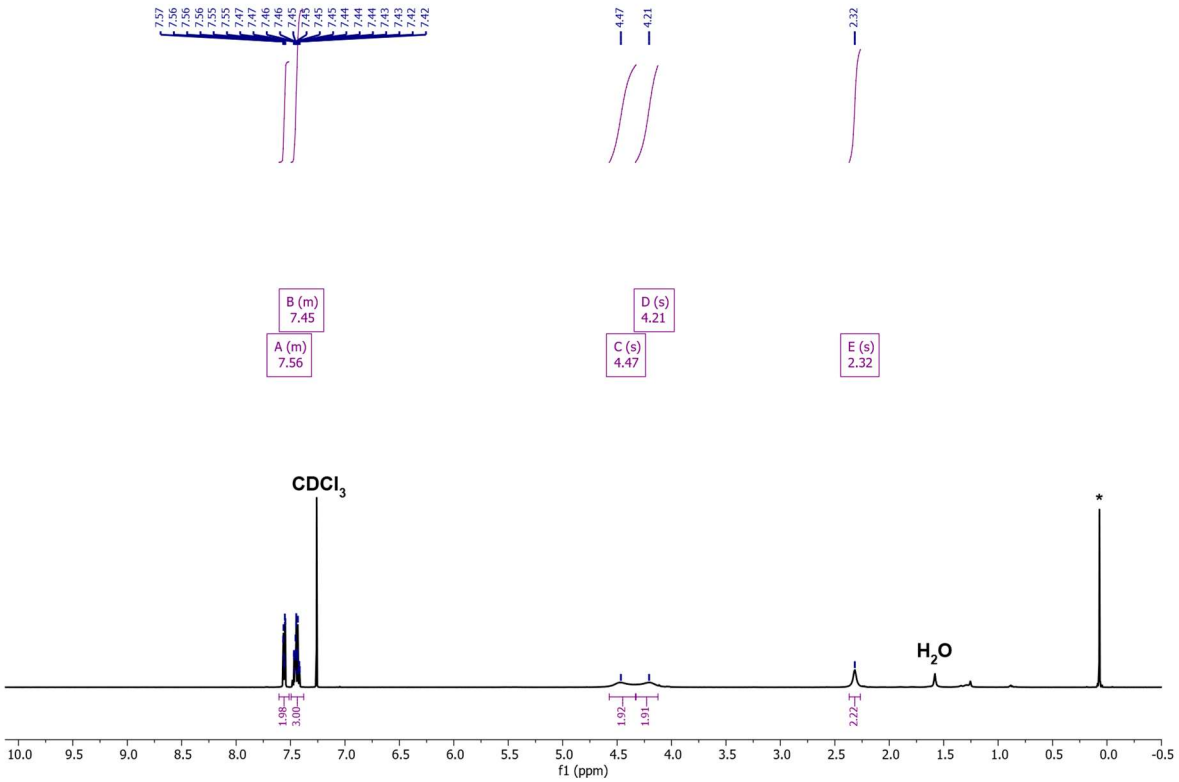

*Figure 4.13: ^{1}H NMR of the backbone **S20** (DMSO-d_6, 500 MHz, 25°C).*

Synthesis of the Boc-protected ligand L^{DB3}-H_2

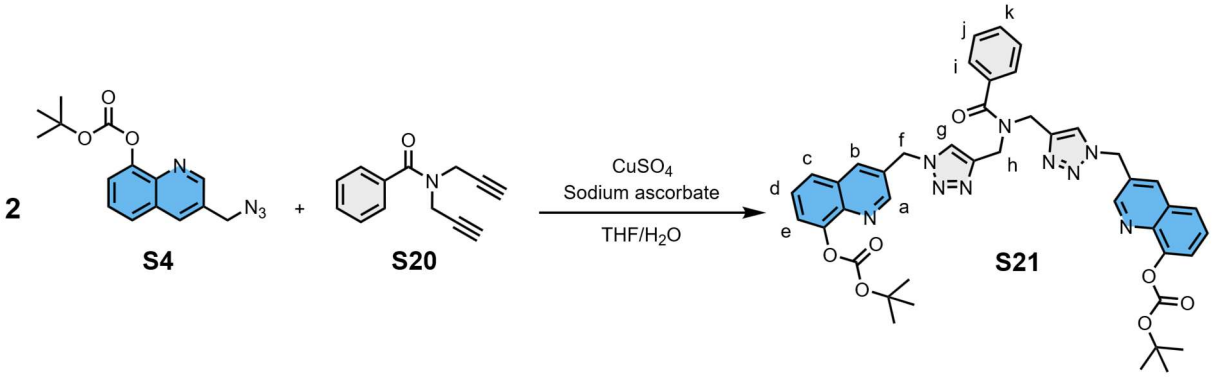

*Figure 4.14: Cu(I) catalyzed 1,3-dipolar HUISGEN cycloaddition between azide **S4** and backbone **S20** to synthesize the Boc-protected ligand **S21**.*

S4 (183.15 mg, 609.9 µmol, 2.2 equiv.) was dissolved in THF and transferred into a pressure tube. The solution was degassed for 20 min with argon. $CuSO_4$ (2.2 mg, 13.8 µmol, 0.05 equiv.) and sodium-ascorbate (27.4 mg, 138.6 µmol, 0.5 equiv.) were dissolved in water and added sequentially. Compound **S20** (54.7 mg, 277.2 µmol, 1 equiv.) was added under argon and the solution was heated to 60°C and stirred for 16 h. The reaction solution was diluted with dichloromethane and the organic layer was washed with EDTA (0.25 M), brine and sat. NH_4Cl solution. The aqueous layer was extracted with dichloromethane (3x). The combined organic layers were dried (Na_2SO_4) and the solvent was evaporated under reduced pressure. Column chromatography (silica, DCM/MeOH 0 to 4%) gives the BOC-protected ligand **S21** as white solid (142.4 mg, 178.5 µmol, 64%).

^{1}H NMR (600 MHz, DMSO-d_6, 25°C): δ = 8.90 (s, 2H, g), 8.30 (s, 2H, b), 8.23 (s, 2H, a), 7.91 (dd, 2H, *J* = 7.8, 1.8 Hz, c), 7.61 (m, 4H, d, e), 7.52 (m, 2H, i), 7.41 (m, 3H, j and k), 5.83 (s, 4H, f), 4.64 (s, 2H, h), 4.49 (s, 2H, h'), 1.48 (s, 18H, *t*Bu). **^{13}C NMR** (151 MHz, DMSO-d_6, 25°C) δ = 170.49, 151.14, 150.45, 146.80, 139.94, 135.85, 135.07, 129.62, 128.44, 128.32, 127.03, 126.87, 126.13, 124.10, 121.38, 83.03, 50.37, 40.05, 39.93, 39.79, 39.65, 39.52, 39.38, 39.24, 39.10, 30.68, 27.23. **HRMS** (positive ESI-MS, ACN acidified): m/z = 820.3174 ($[M+Na]^+$, $C_{43}H_{43}N_9O_7Na^+$, calc. 820.3178), 836.2912 ($[M+K]^+$, $C_{33}H_{27}N_9O_3K^+$, calc. 836.2917).

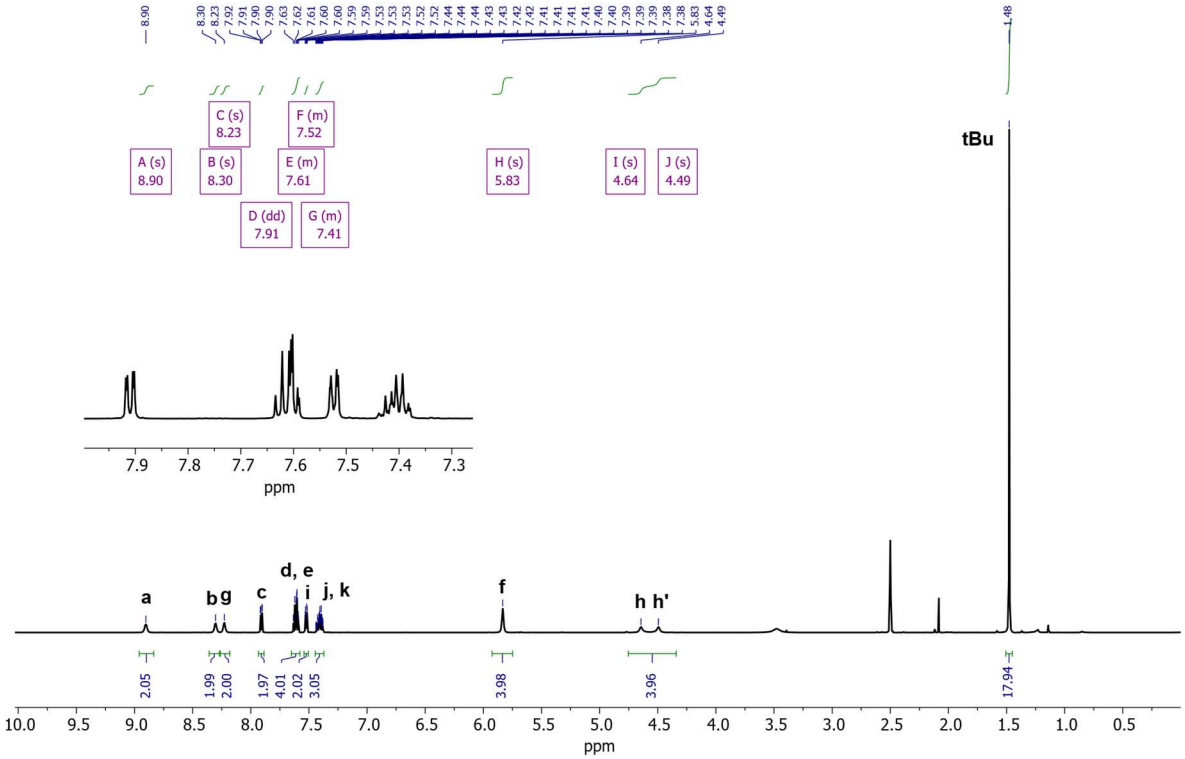

*Figure 4.15: ^{1}H NMR of the Boc-protected ligand **S21** (DMSO-d_6, 600 MHz, 25°C).*

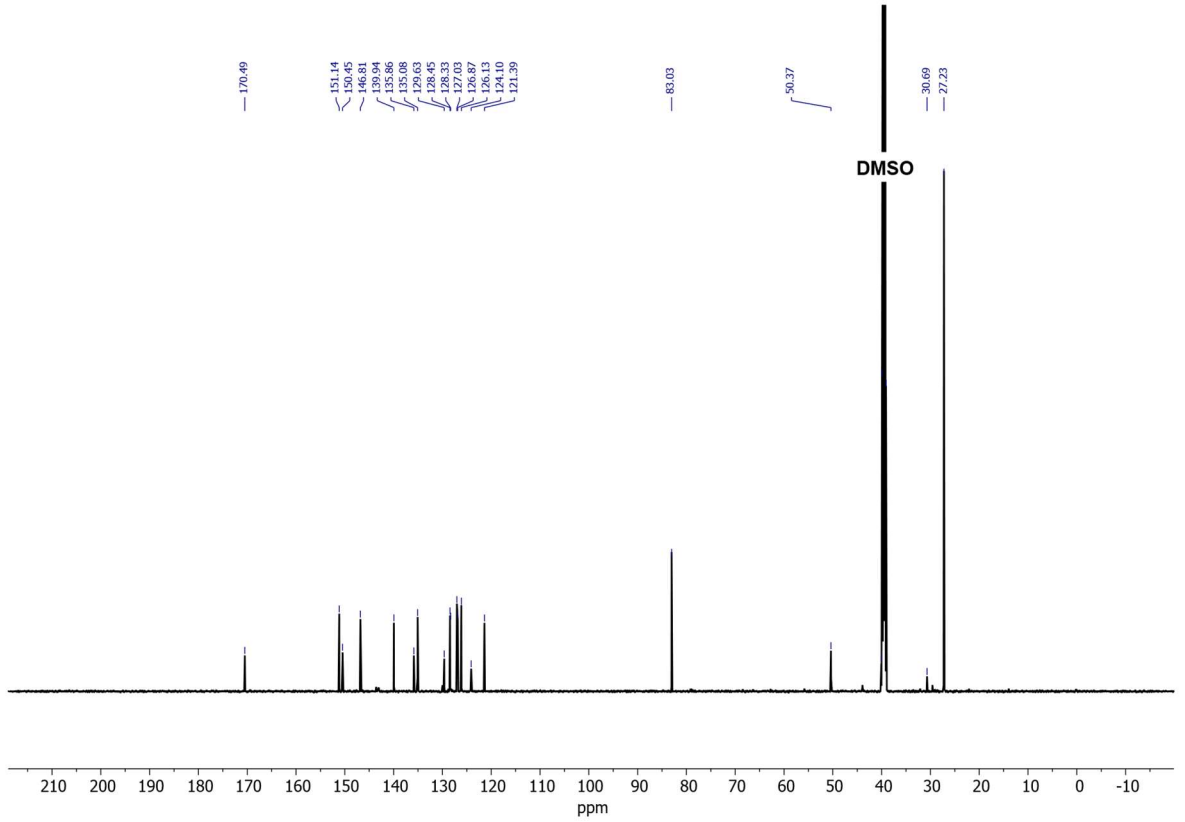

*Figure 4.16: ^{13}C NMR of the Boc-protected ligand **S21** (DMSO-d_6, 151 MHz, 25°C).*

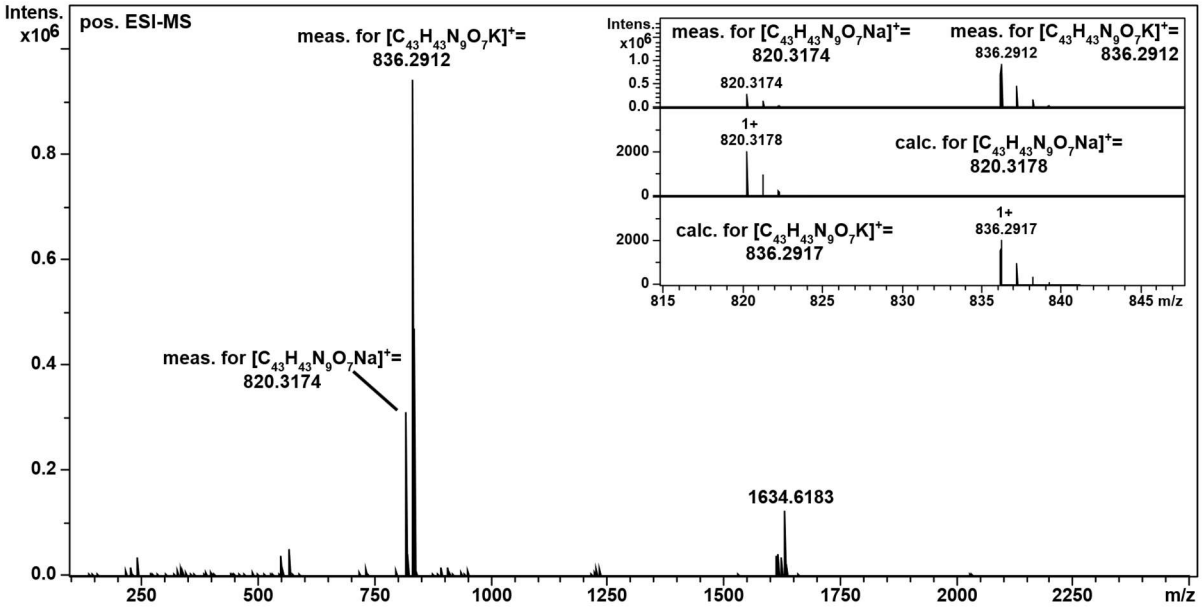

*Figure 4.17: Positive HR-ESI-MS spectrum (ACN) of the Boc-protected ligand **S21**.*

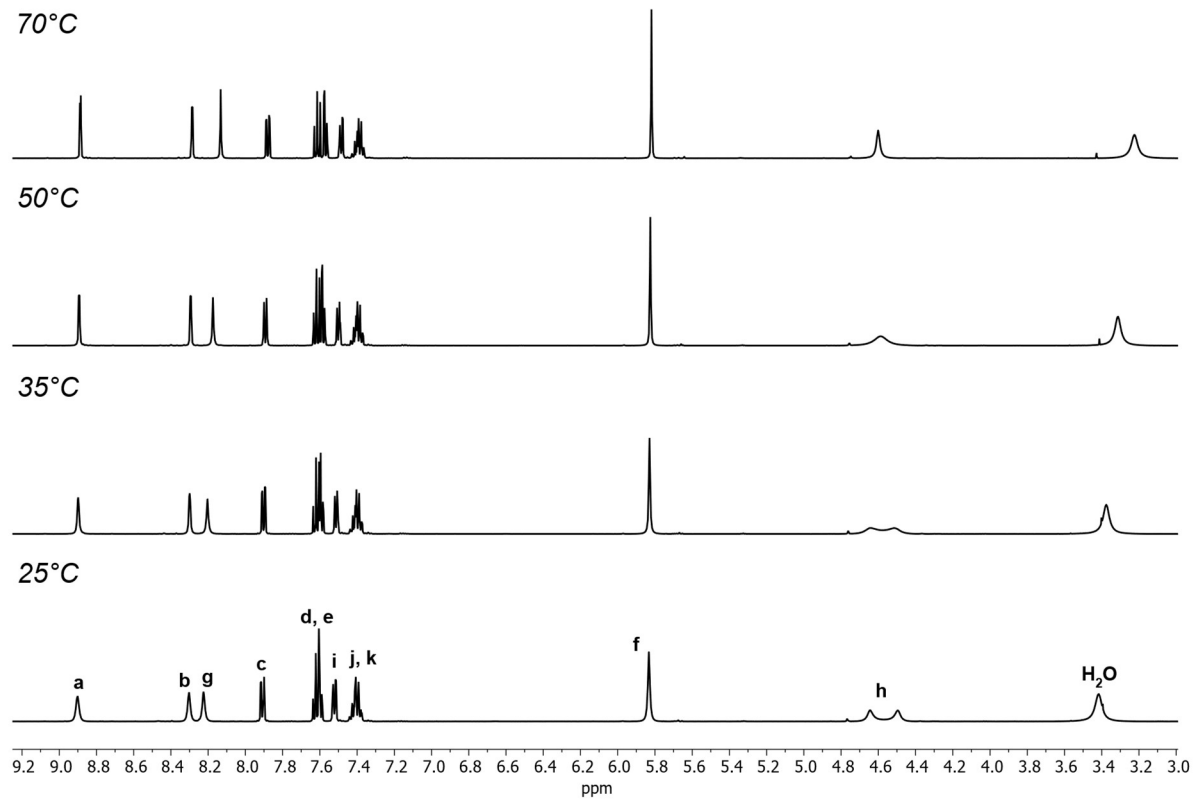

*Figure 4.18: VT ^{1}H NMR of the Boc-protected ligand **S21** (L^{DB3}-H_2) (DMSO-d_6, 500 MHz, 25°C to 70°C).*

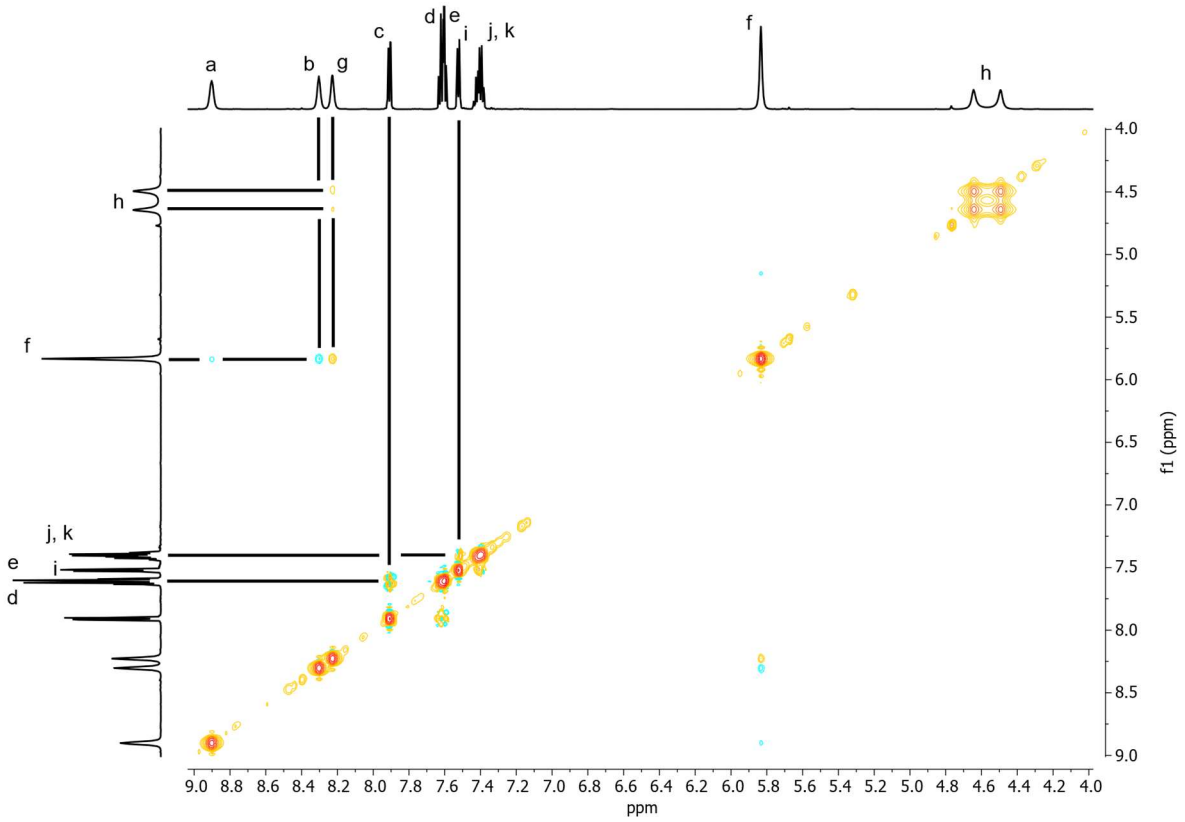

*Figure 4.19: ^{1}H NOESY of the Boc-protected ligand **S21** (DMSO-d_6, 600 MHz, 25°C).*

Synthesis of ligand L^{DB3}-H_2

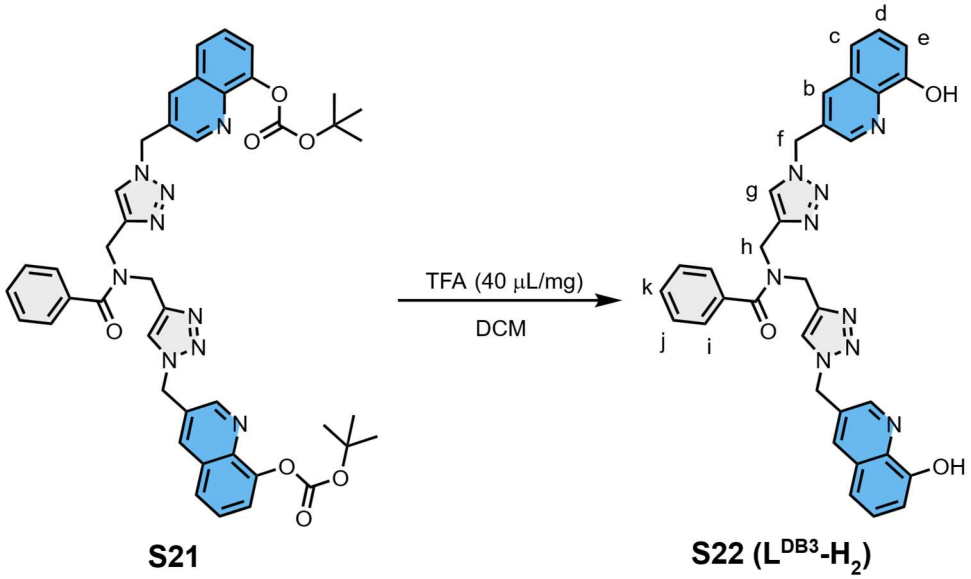

*Figure 4.20: Cleavage of the Boc-groups with TFA to obtain ligand **S22** (L^{DB3}-H_2).*

Compound **S21** (105 mg, 131.6 µmol, 1 equiv.) was dissolved in DCM and treated with TFA (40 µL/mg). After 1 h the reaction mixture was neutralized with sat. $NaHCO_3$ and the organic layer diluted with DCM. The aq. layer was extracted with DCM (7x), washed with brine and the organic layers were dried (Na_2SO_4). The solvent was evaporated until there was a residue organic layer present. Pouring Et_2O into the residue gave the ligand **S22** (L^{DB3}-H_2) as a white powder (99%, 90.12 mg, 131.4 µmol).

^{1}H NMR (600 MHz, DMSO-d_6, 25°C): δ = 9.92 (s, 2H, OH), 8.84 (s, 2H, a), 8.21 (s, 2H, g), 8.19 (s, 2H, b), 7.52 (d, *J* = 6.9 Hz, 2H, i), 7.46-7.37 (m, 7H, j, k, d, c), 7.09 (d, *J* = 7.5 Hz, 2H, e), 5.81 (s, 4H, f), 4.63 (s, 2H, h), 4.49 (s, 2H, h') ppm. **^{13}C NMR** (151 MHz, DMSO-d_6, 25°C): δ = 170.50, 153.40, 148.07, 143.27, 137.96, 135.84, 135.10, 129.66, 129.48, 128.35, 128.23, 128.16, 126.88, 123.98, 117.77, 111.88, 50.51, 43.91 ppm. **HRMS** (positive ESI-MS, ACN, acidified): m/z = 598.2339 ($[M+H]^+$, $C_{33}H_{28}N_9O_3^+$, calc. 598.2310), 620.2112 ($[M+Na]^+$, $C_{33}H_{27}N_9O_3Na^+$, calc. 620.2129).

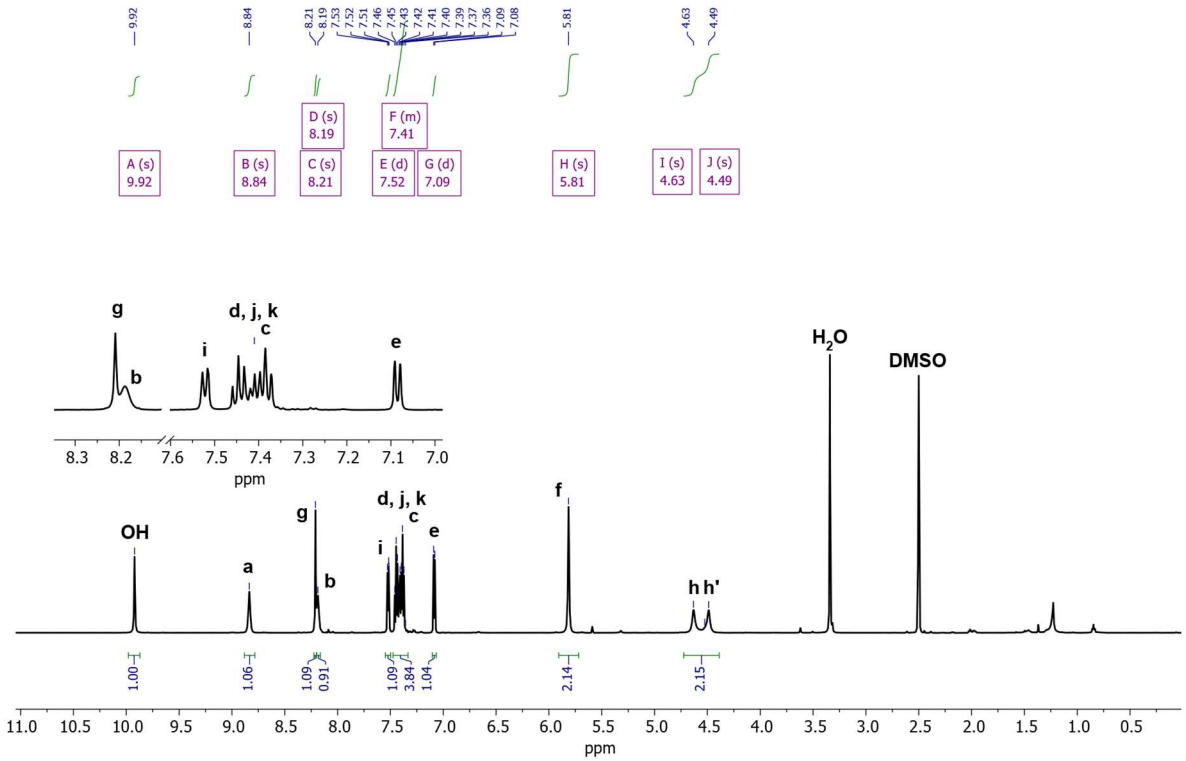

*Figure 4.21: ^{1}H NMR spectrum of ligand **S22** (L^{DB3}-H_2) (DMSO-d_6, 600 MHz, 25°C).*

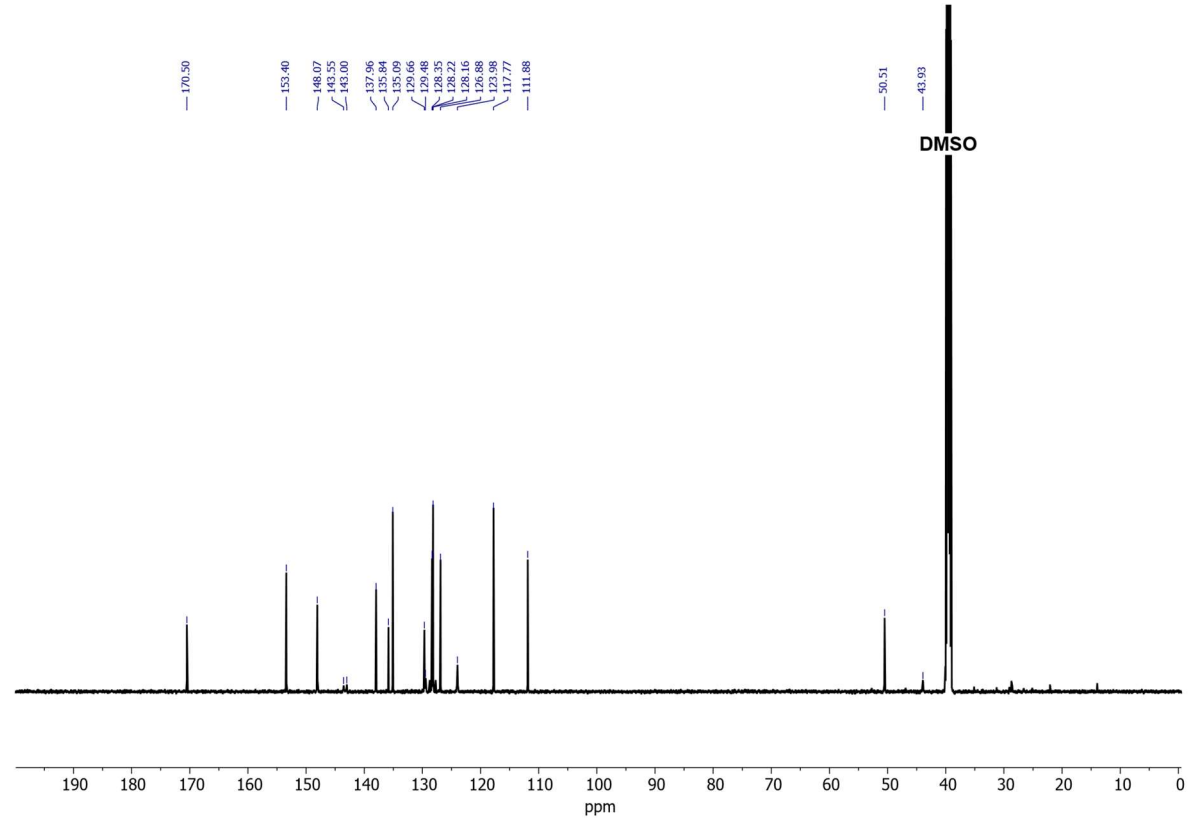

*Figure 4.22: ^{13}C NMR spectrum of ligand **S22** (L^{DB3}-H_2) (DMSO-d_6, 151 MHz, 25°C).*

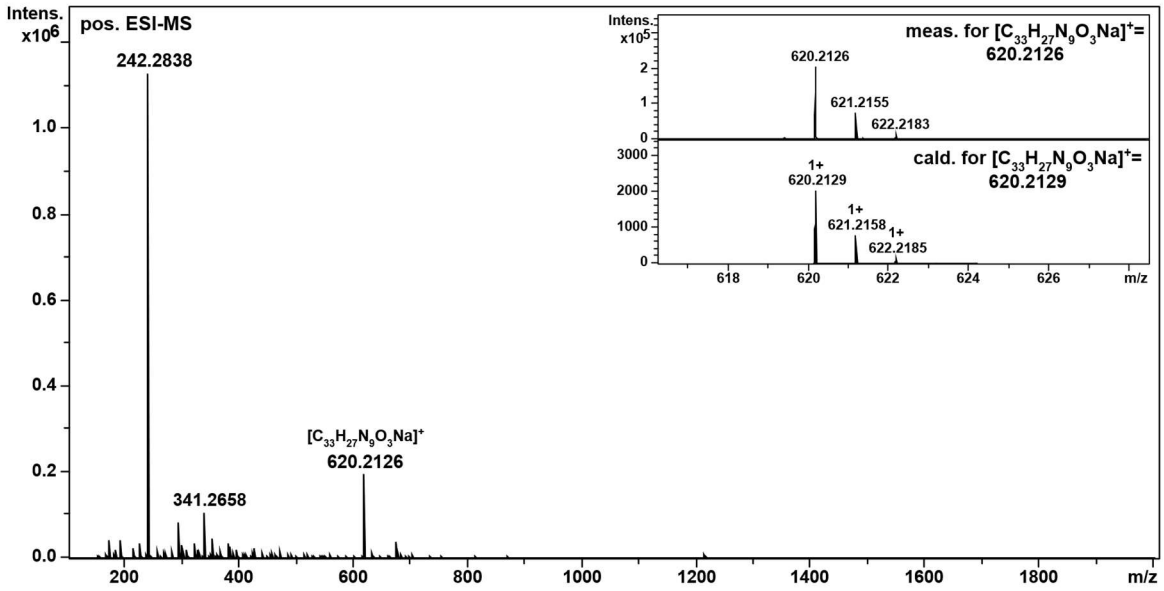

*Figure 4.23: Positive HR-ESI-MS spectrum (ACN) of ligand **S22** (L^{DB3}-H_2).*

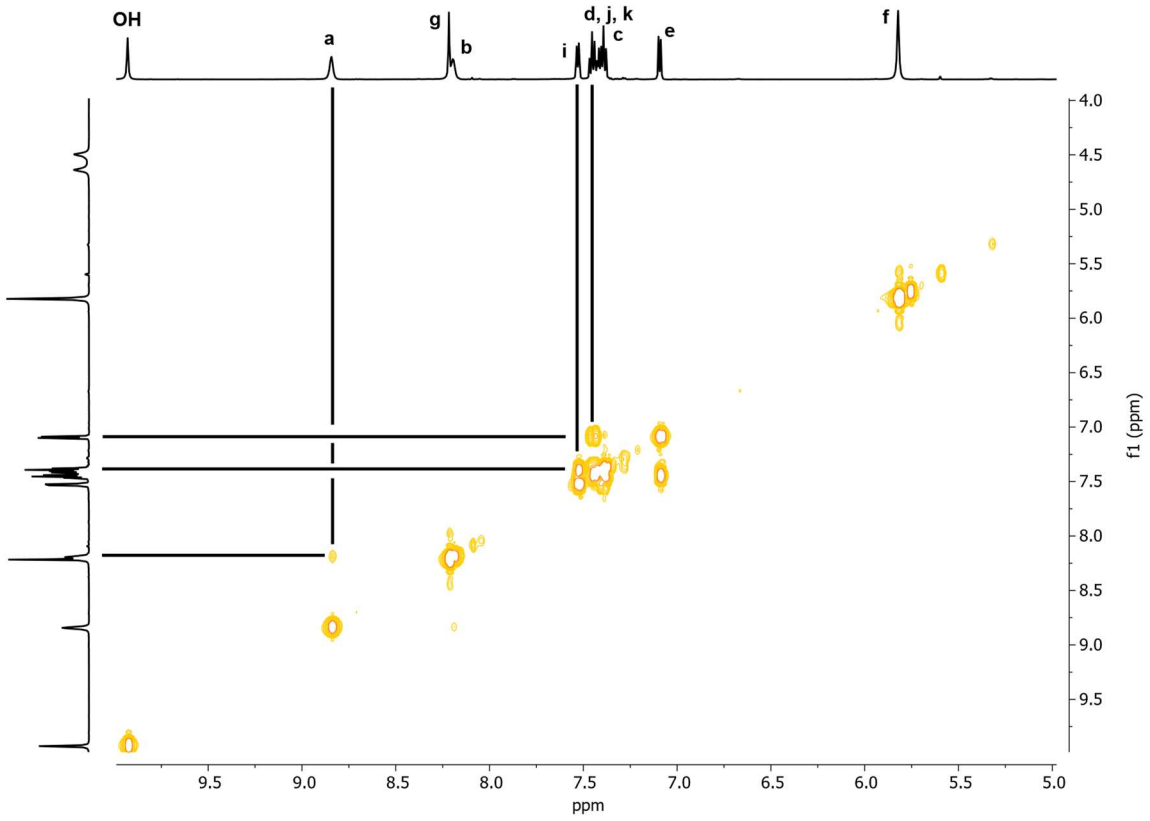

*Figure 4.24: ^{1}H COSY spectrum of ligand **S22** (L^{DB3}-H_2) (DMSO-d_6, 600 MHz, 25°C).*

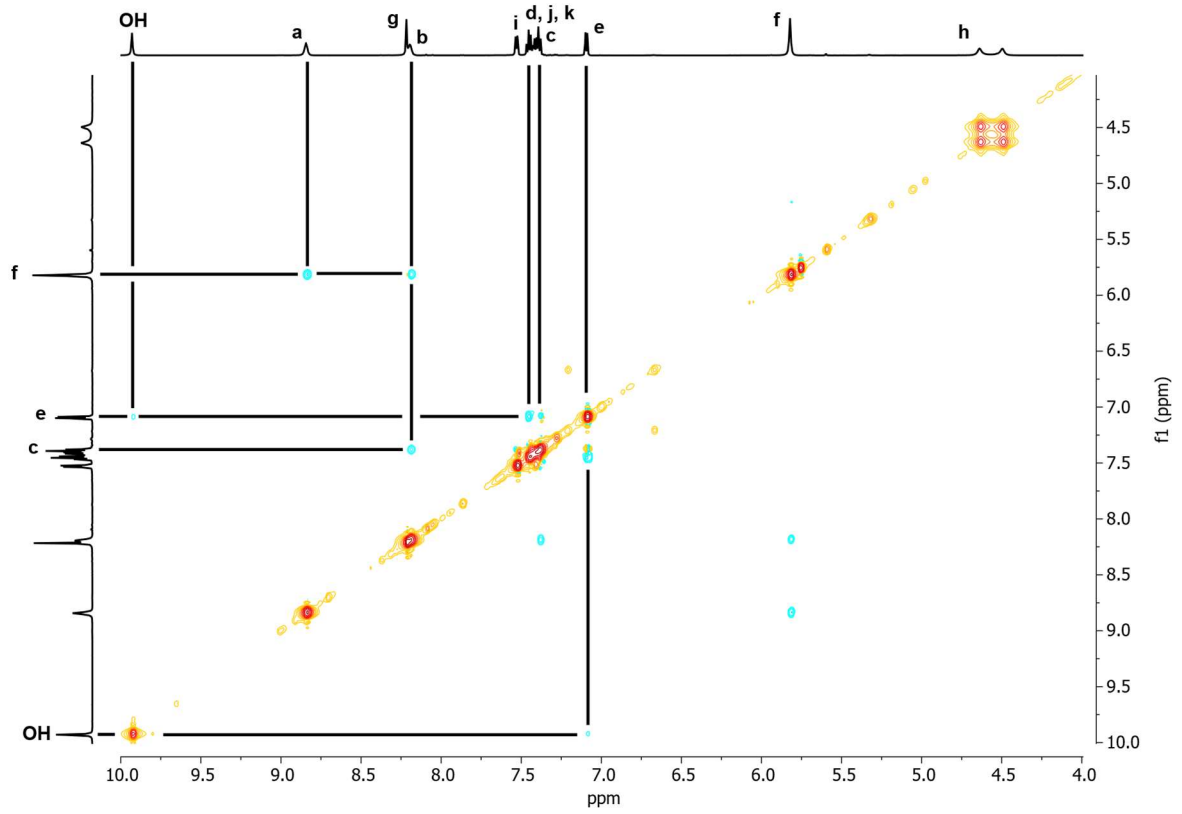

*Figure 4.25: ^{1}H NOESY spectrum of ligand **S22** (L^{DB3}-H_2) (DMSO-d_6, 600 MHz, 25°C).*

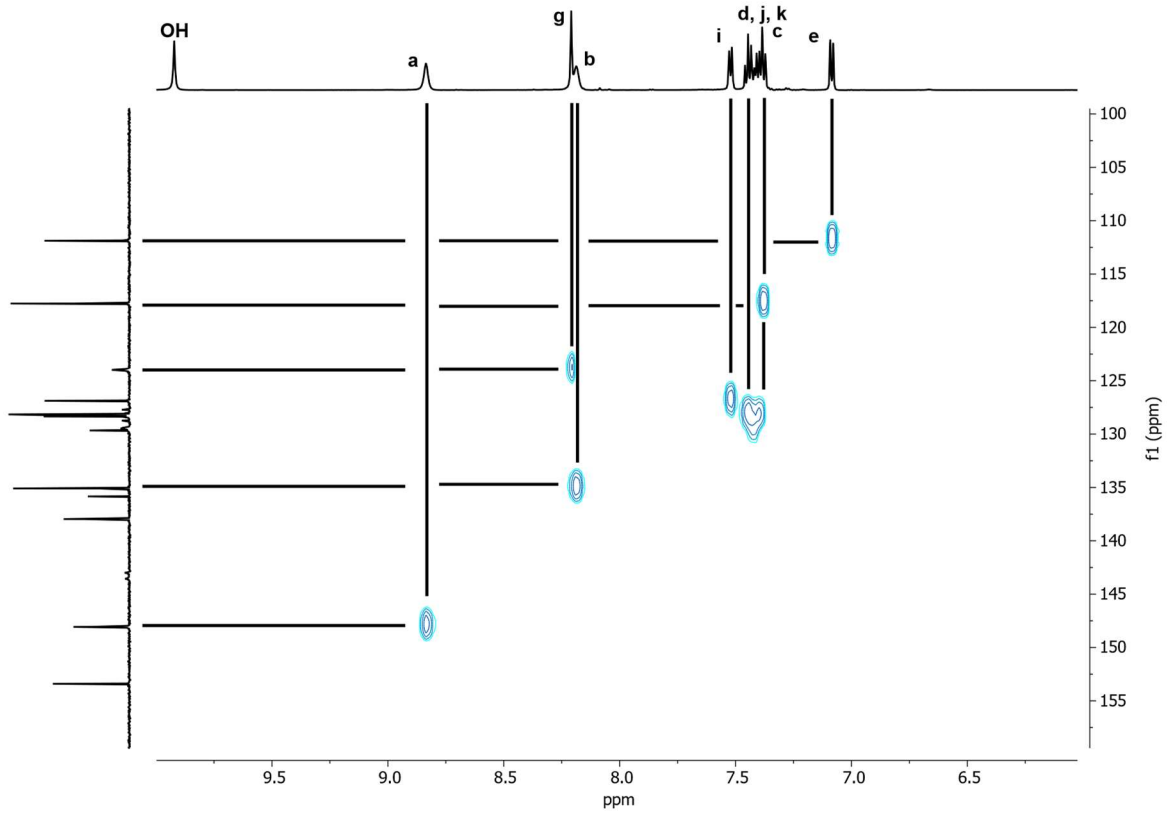

*Figure 4.26: HSQC NMR spectrum of ligand **S22** (L^{DB3}-H_2) (DMSO-d_6, 600 MHz, 25°C).*

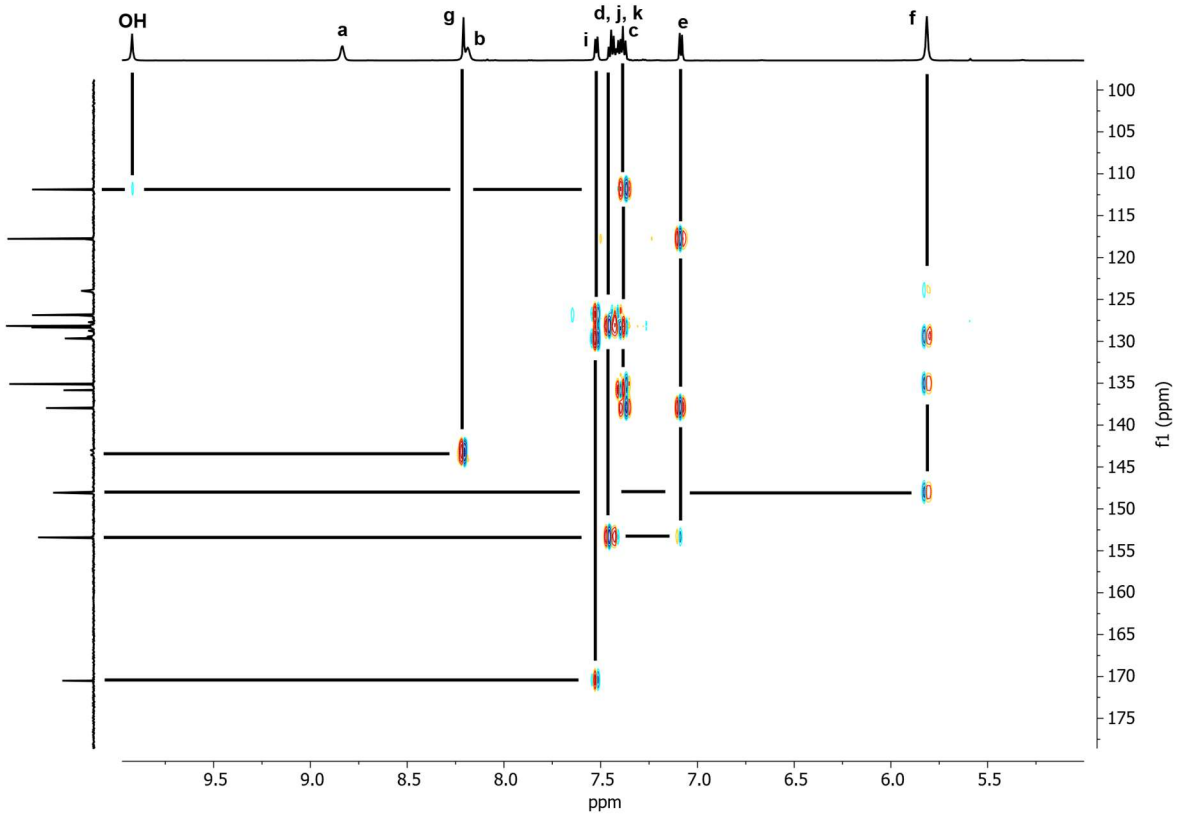

*Figure 4.27: HMBC NMR spectrum of ligand **S22** (L^{DB3}-H_2) (DMSO-d_6, 600 MHz, 25°C).*

4.6.5 *Self-assembly of ligand L^{DB3}-H_2 and $Zn(OAc)_2$*

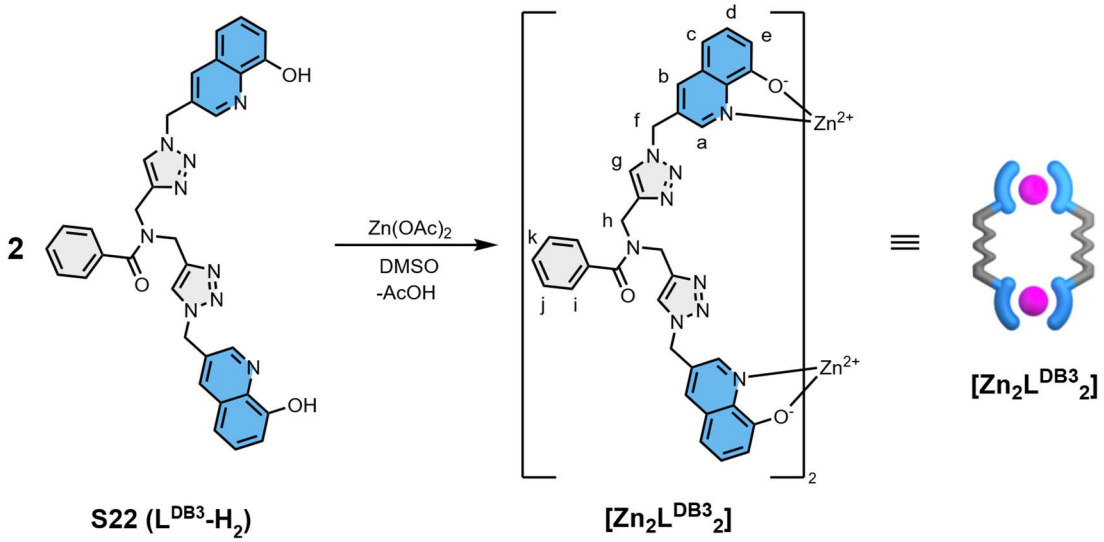

*Figure 4.28: Self-assembly of ligand **S22** (L^{DB3}-H_2) and $Zn(OAc)_2$ in DMSO, forming a charge-neutral $[Zn_2L^{DB3}_2]$ host-complex.*

Ligand **S22** (L^{DB3}-H_2) (1 eq.) and $Zn(OAc)_2$ (1 equiv.) were dissolved in DMSO (500 µM). The $Zn(OAc)_2$ solution was added to the stirring ligand solution which results in a color change to yellow. The solution was stirred for 16 h and the solvent as well as the byproduct acetic acid were removed via lyophilization, which gives the complex as a yellow solid. The complex is suspended and washed with MeOH for further purification. The mixture is centrifuged and the solvent is removed by decantation. This cleaning process is repeated twice. The resulting precipitate was again dissolved in DMSO which was removed via lyophilization to give the clean complex as a yellow solid in a quantitative fashion.

^{1}H NMR (500 MHz, DMSO-d_6, 25°C): δ = 8.51 (s, 2H, b), 7.97 (s, 3H, a, g), 7.78 (s, 1H, g'), 7.57 (d, *J* = 7.2 Hz, 2H, i), 7.47-7.36 (m, 5H, d, j, k), 6.92 (d, *J* = 6.9 Hz, 2H, c), 6.69 (s, 2H, e), 5.72 (s, 2H, f), 5.63 (s, 2H, f'), 4.67 (s, 2H, h), 4.53 (s, 2H, h') ppm. **HRMS** (negative ESI-MS, ACN/DMSO): m/z = 1357.2493 ($[M+Cl]^-$, $[(Cl)@Zn_2L^{DB3}_2]^-$, $[(Cl)@(C_{33}H_{25}N_9O_3)_2Zn_2]^-$, calc. 1357.2408).

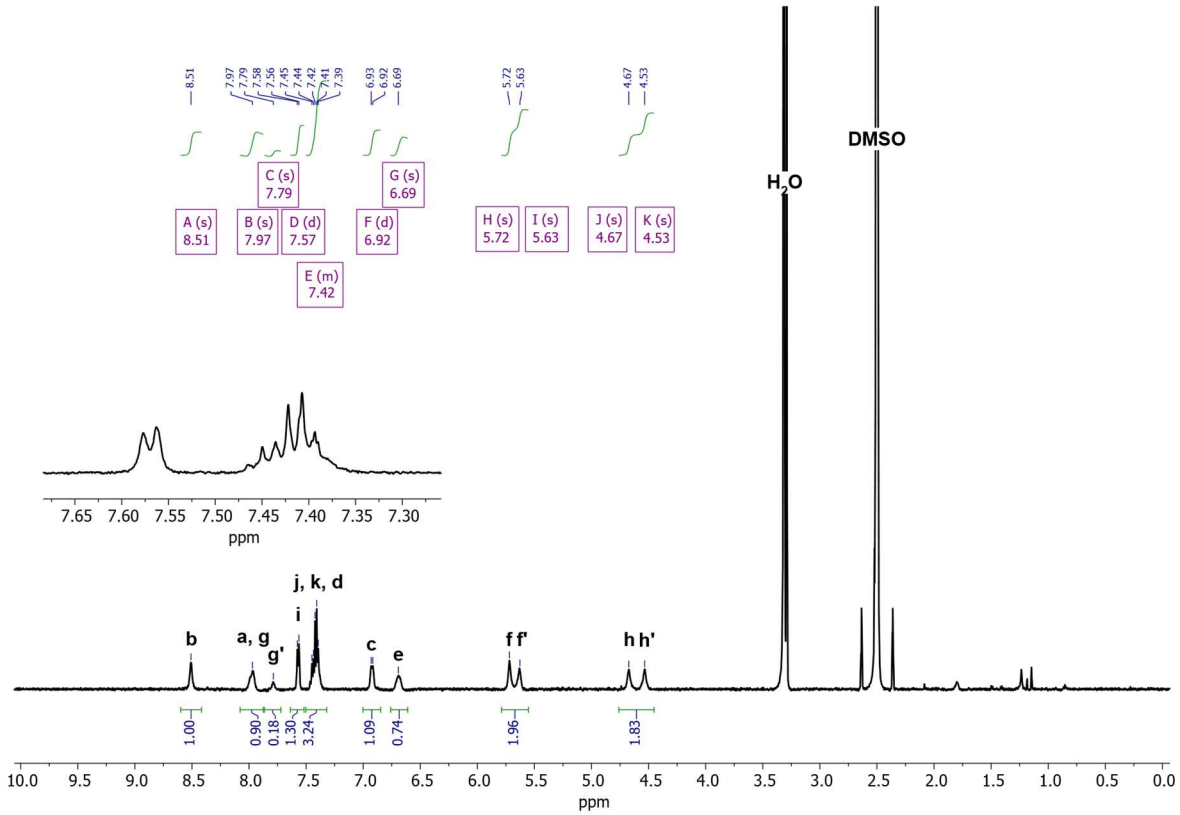

Figure 4.29: ^{1}H NMR spectrum of host-complex $[Zn_2L^{DB3}{}_2]$ (DMSO-d_6, 600 MHz, 25°C).

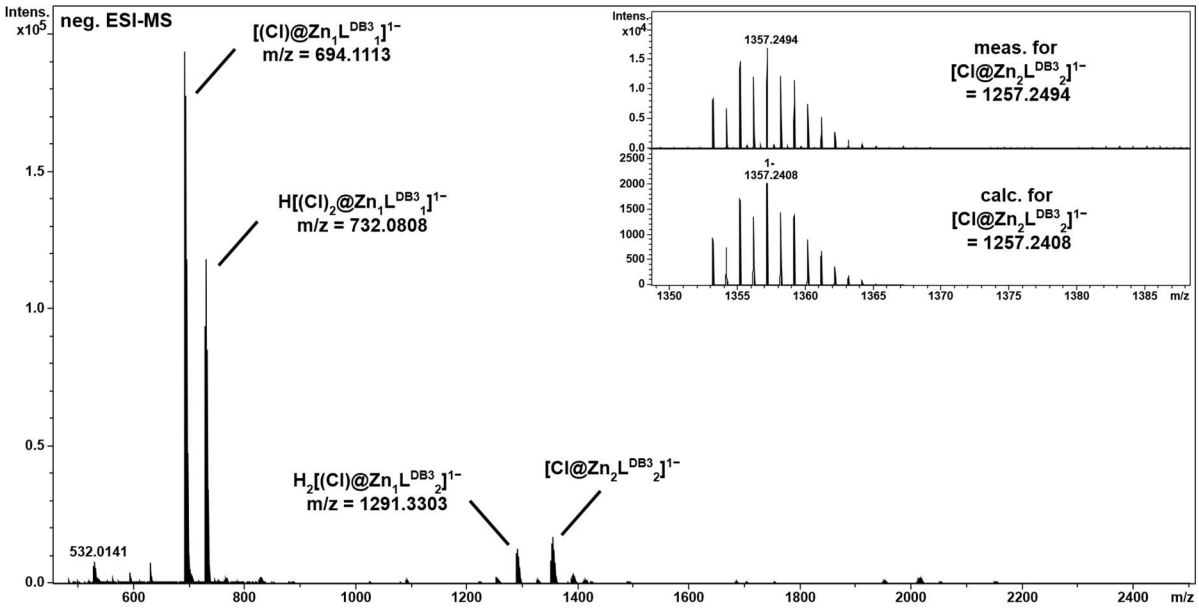

Figure 4.30: Negative HR-ESI-MS spectrum of $[(Cl)@Zn_2L^{DB3}{}_2]^-$ in DMSO/ACN (1:9).

Variable temperature ^{1}H NMR studies between 25°C and 90°C (Figure 4.31) and ^{1}H NOESY as well as COSY and NOESY measurements (Figure 4.32, Figure 4.33) at 90°C were conducted, as some signals overlap at room temperature. The combination of 1D and 2D NMR-experiments at elevated temperatures made clear signal assignment possible.

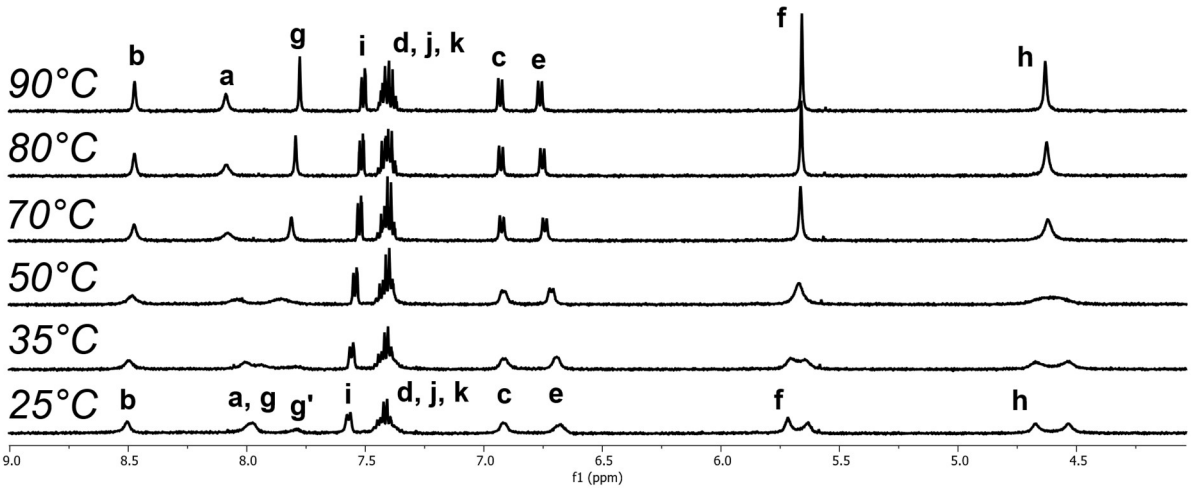

Figure 4.31: VT ^{1}H NMR of [$Zn_2L^{DB3}_2$] (DMSO-d_6, 500 MHz, 25°C to 90°C).

^{1}H NMR (500 MHz, DMSO-d_6, 90°C): δ = 8.47 (s, 2H, b), 8.09 (s, 2H, a), 7.78 (s, 2H, g), 7.51 (dd, *J* = 8.0, 1.4 Hz, 2H, i), 7.44-7.36 (m, 5H, d, j, k), 6.93 (d, *J* = 7.9 Hz, 2H, c), 6.76 (d, *J* = 7.8 Hz,2, e), 5.66 (s, 4H, f), 4.63 (s, 4H, h) ppm.

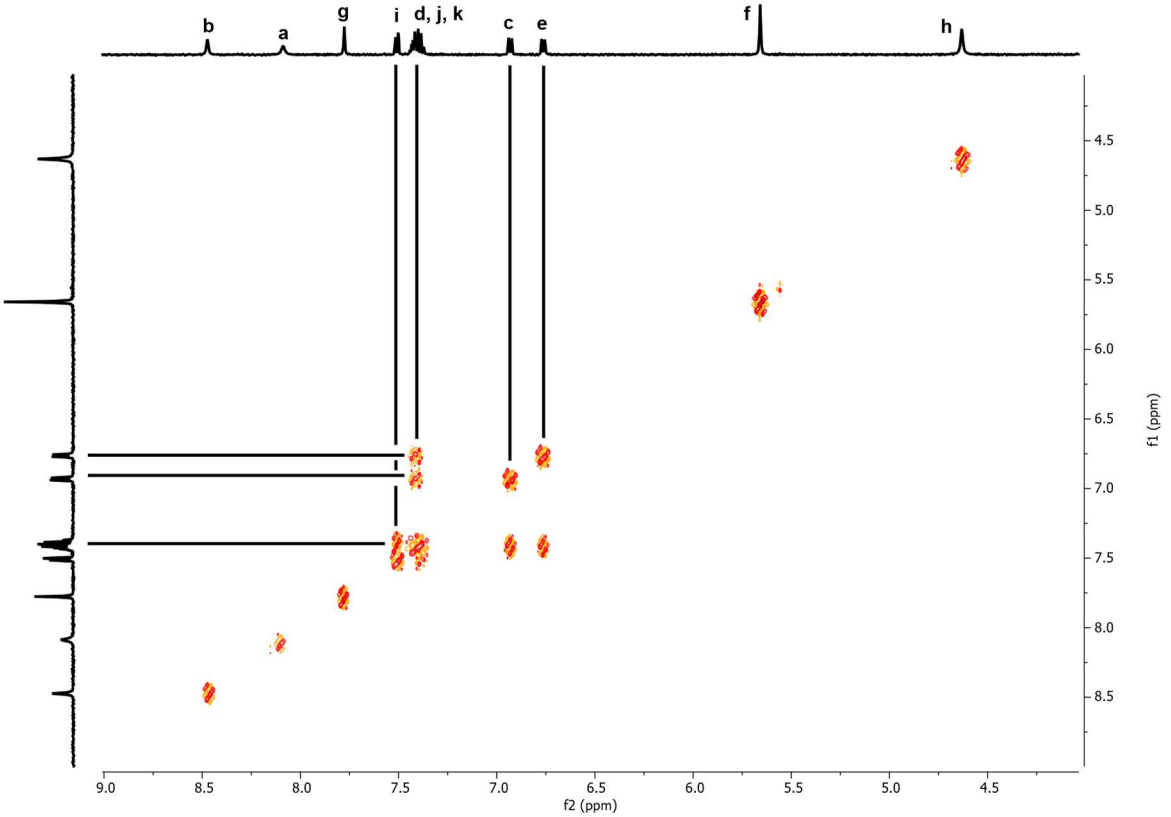

Figure 4.32: ^{1}H COSY spectrum of host-complex [$Zn_2L^{DB3}_2$] (DMSO-d_6, 500 MHz, 90°C).

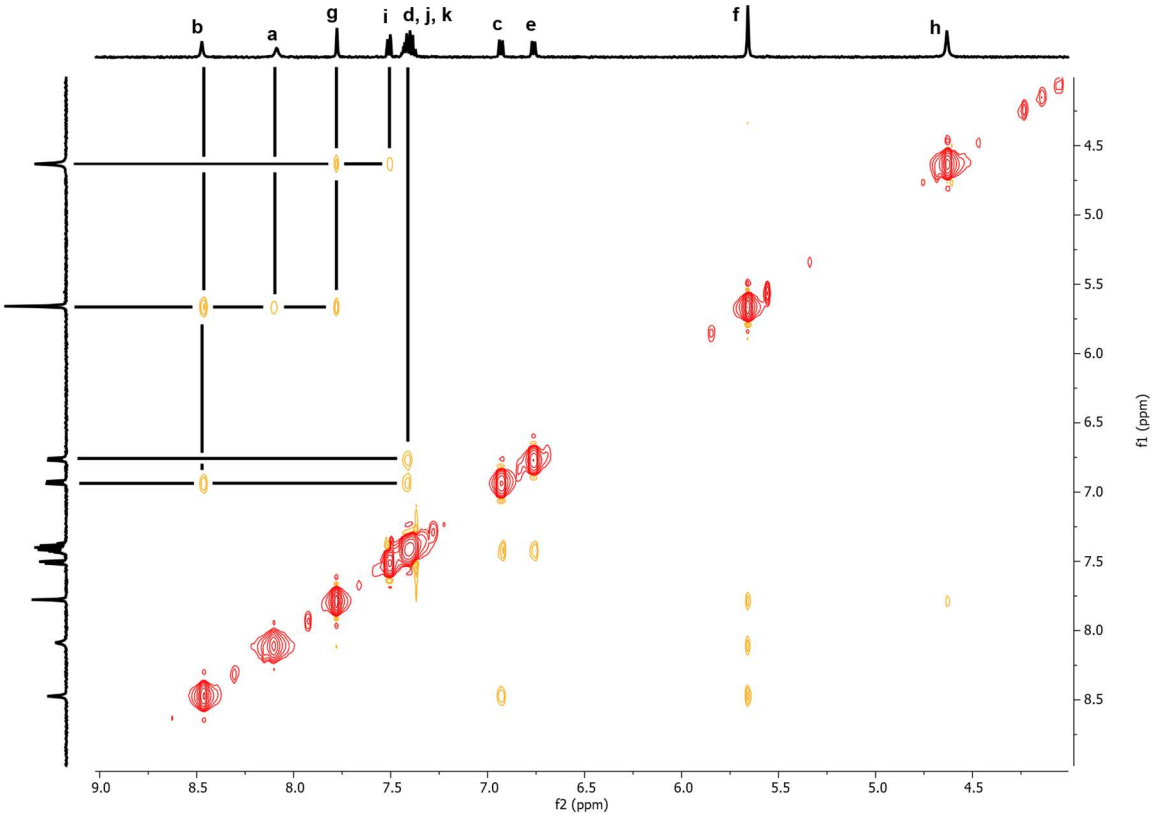

Figure 4.33: ^{1}H NOESY spectrum of host-complex $[Zn_2L^{DB3}{}_2]$ (DMSO-d_6, 500 MHz, 90°C).

4.6.6 Qualitative anion binding studies of host-complex $[Zn_2L^{DB3}{}_2]$

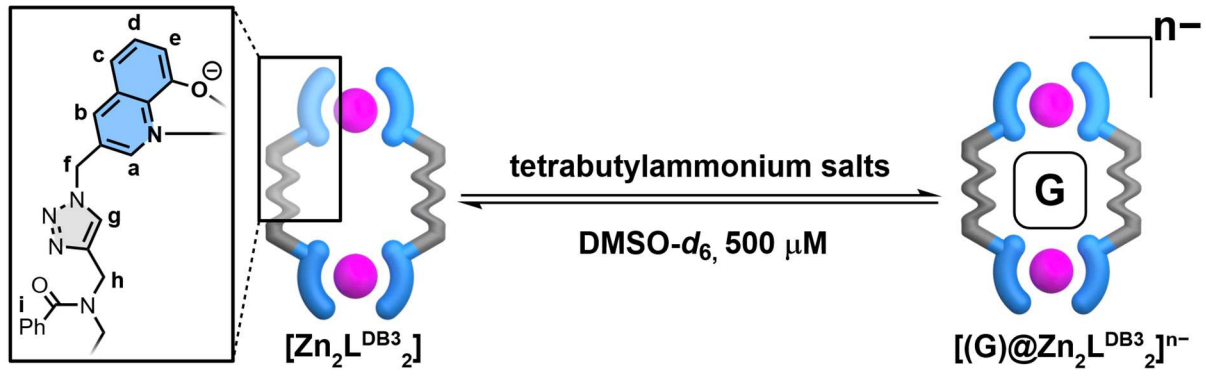

Figure 4.34: Host-complex $[Zn_2L^{DB3}{}_2]$ was tested with several mono- or di-anions as tetrabutylammonium salts.

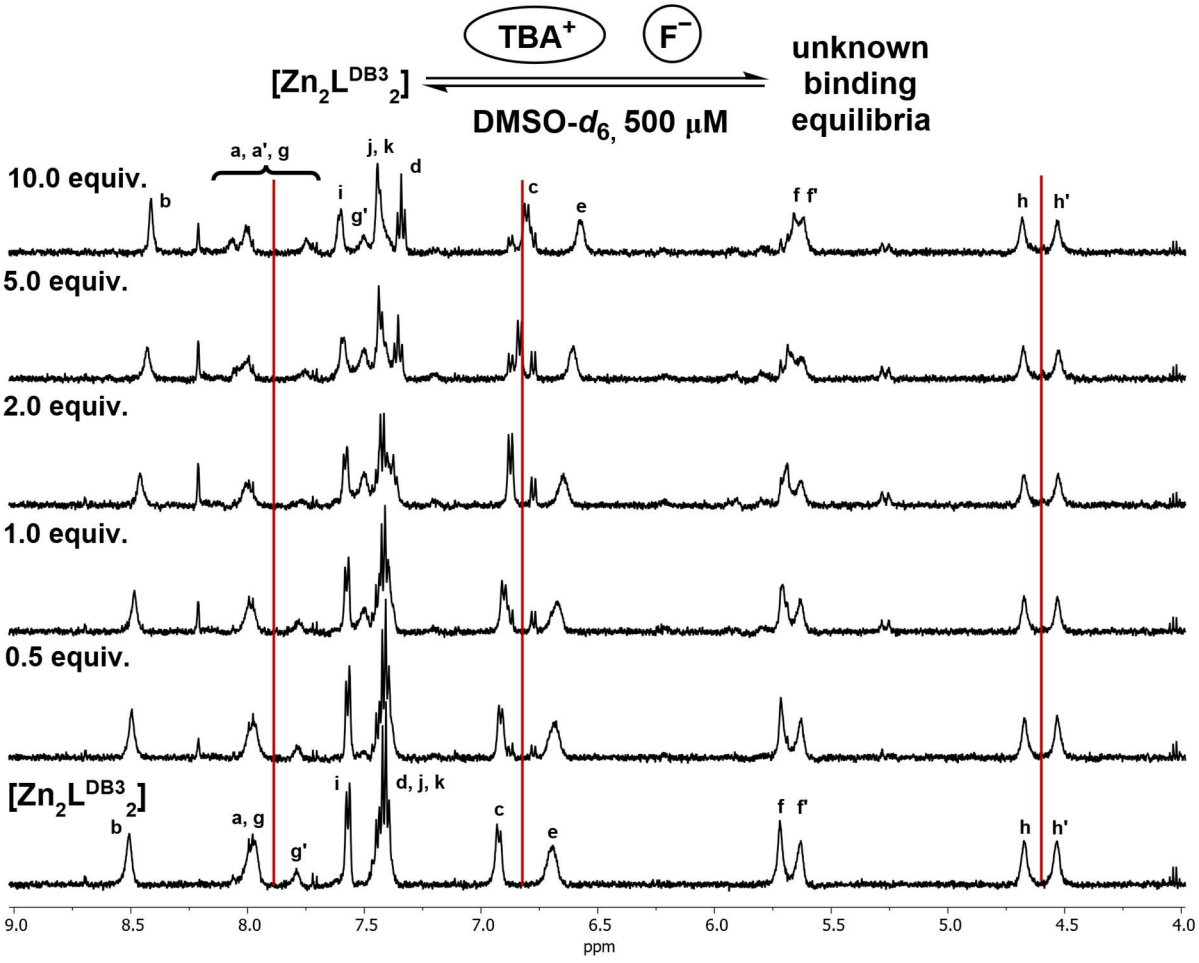

Figure 4.35: ^{1}H NMR test-titration of host-complex $[Zn_2L^{DB3}{}_2]$ and TBA fluoride as guest (DMSO-d_6, 500 MHz, 500 µM, 25°C).

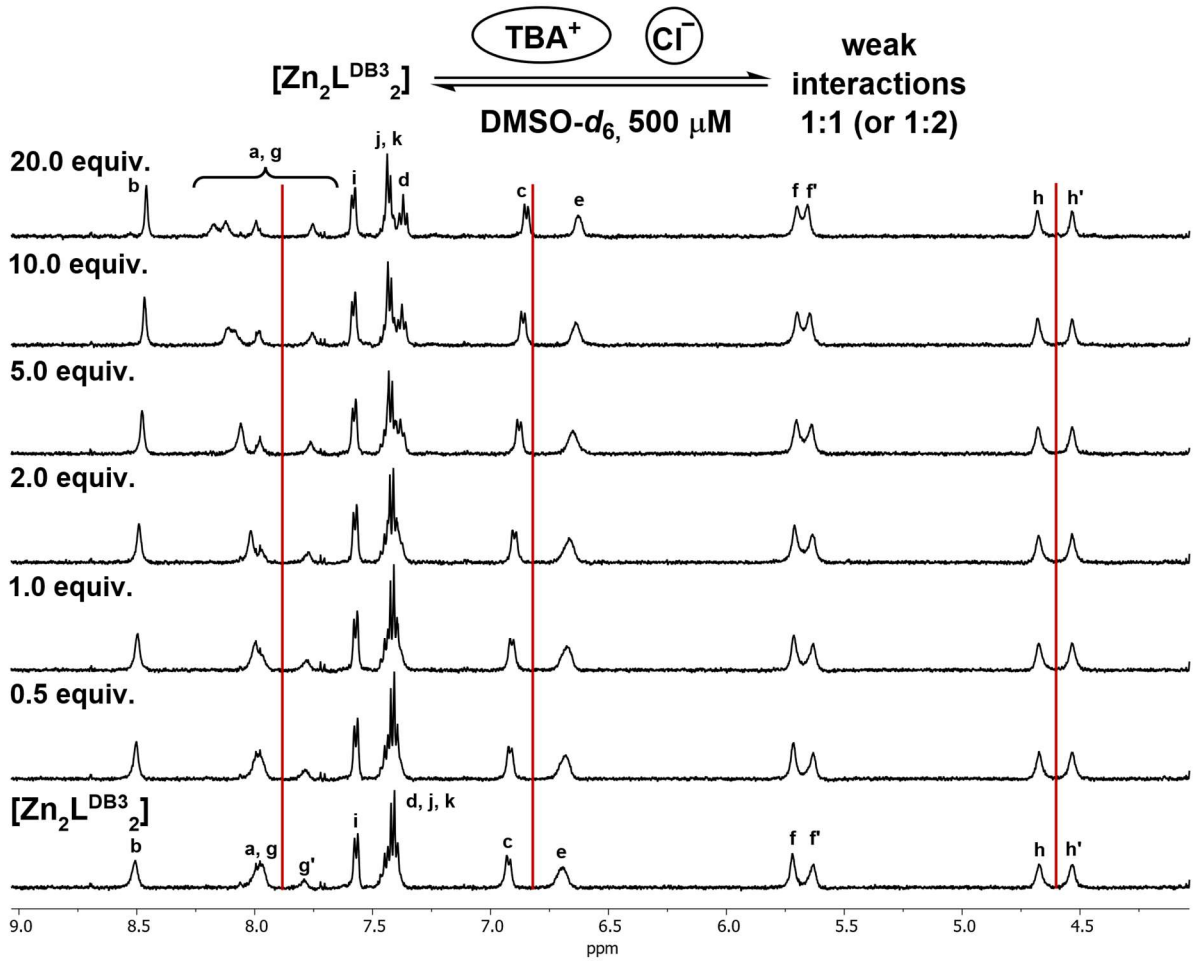

Figure 4.36: ^{1}H NMR test-titration of host [$Zn_2L^{DB3}{}_2$] and TBA chloride as guest (DMSO-d_6, 500 MHz, 500 μM, 25°C).

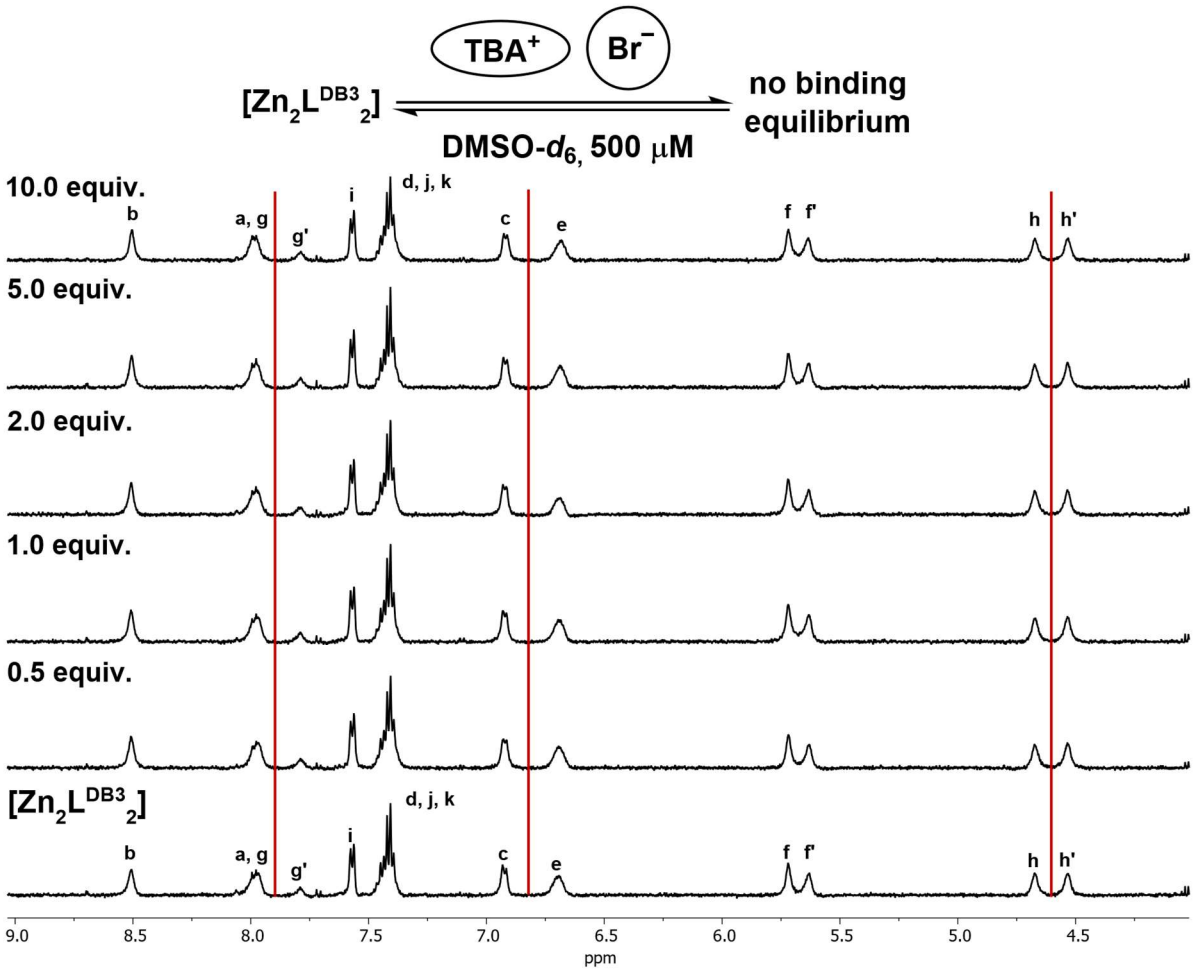

Figure 4.37: ^{1}H NMR test-titration of host [$Zn_2L^{DB3}{}_2$] and TBA bromide (DMSO-d_6, 500 MHz, 500 μM, 25°C).

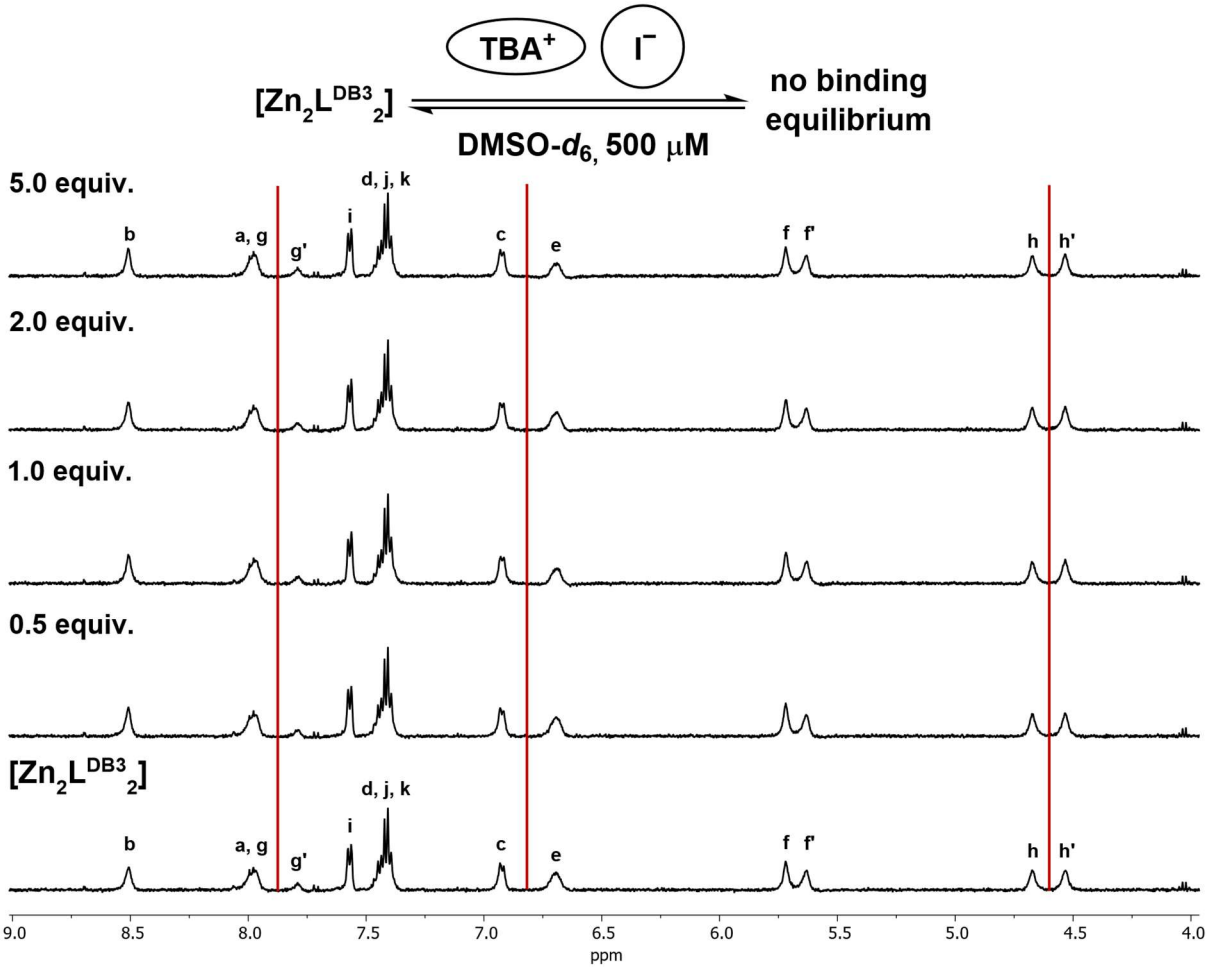

Figure 4.38: ^{1}H NMR test-titration of host [$Zn_2L^{DB3}{}_2$] and TBA iodide as guest (DMSO-d_6, 500 MHz, 500 µM, 25°C).

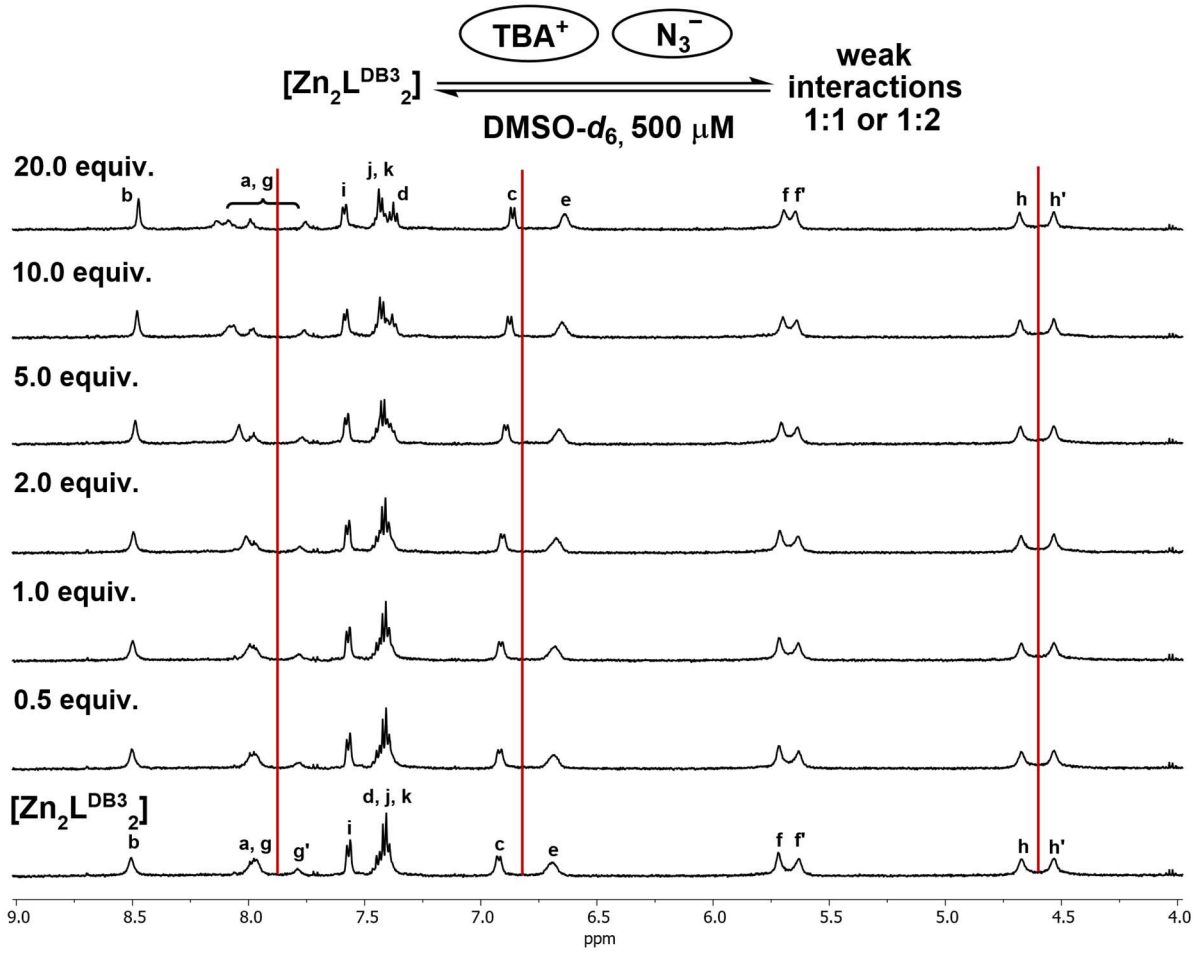

Figure 4.39: ^{1}H NMR test-titration of host $[Zn_2L^{DB3}{}_2]$ and TBA azide as guest (DMSO-d_6, 500 MHz, 500 μM, 25°C).

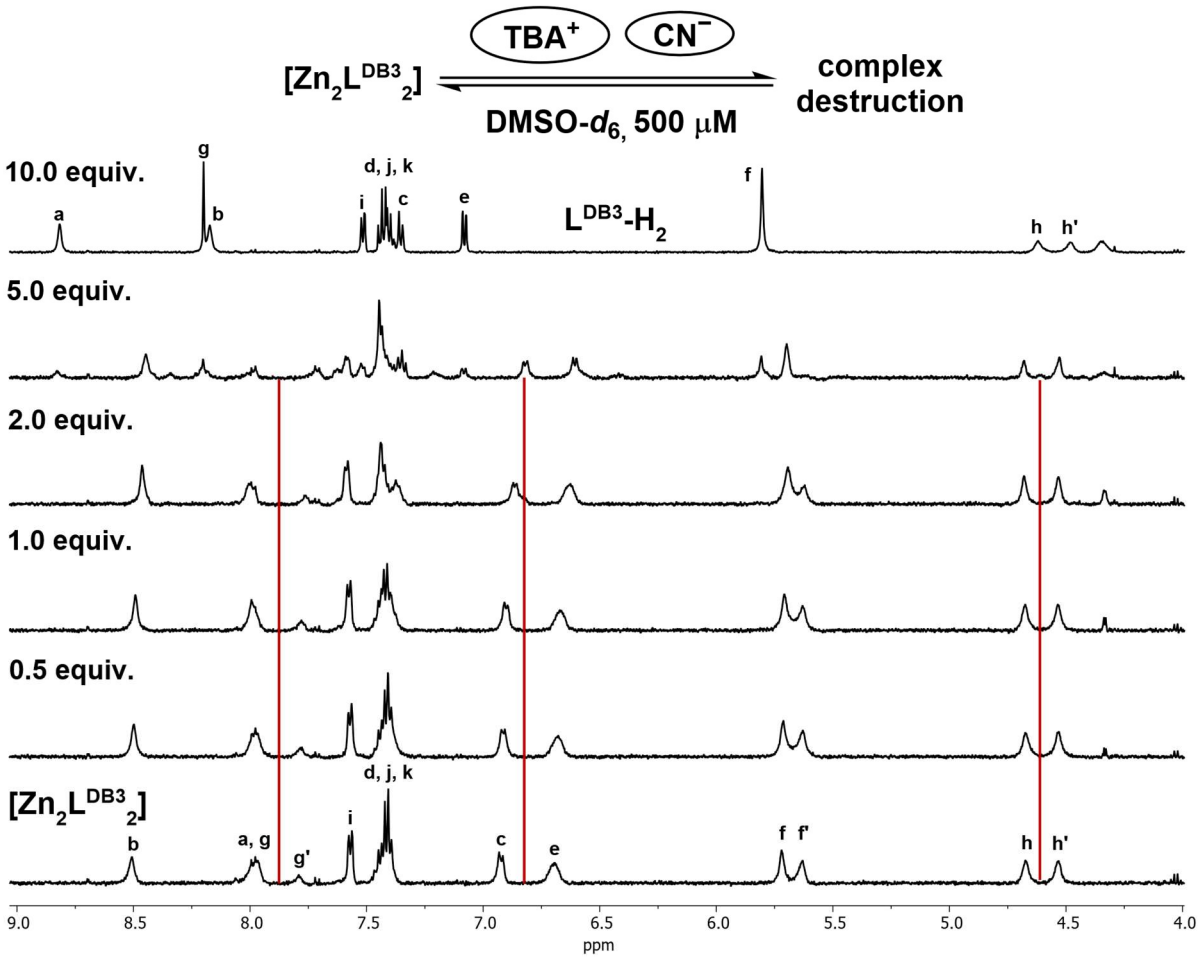

Figure 4.40: ^{1}H NMR test-titration of host $[Zn_2L^{DB3}{}_2]$ and TBA cyanide as guest (DMSO-d_6, 500 MHz, 500 μM, 25°C). After the addition of 10 equiv. TBACN, the ^{1}H NMR signals correspond to the free ligand L^{DB3}-H_2.

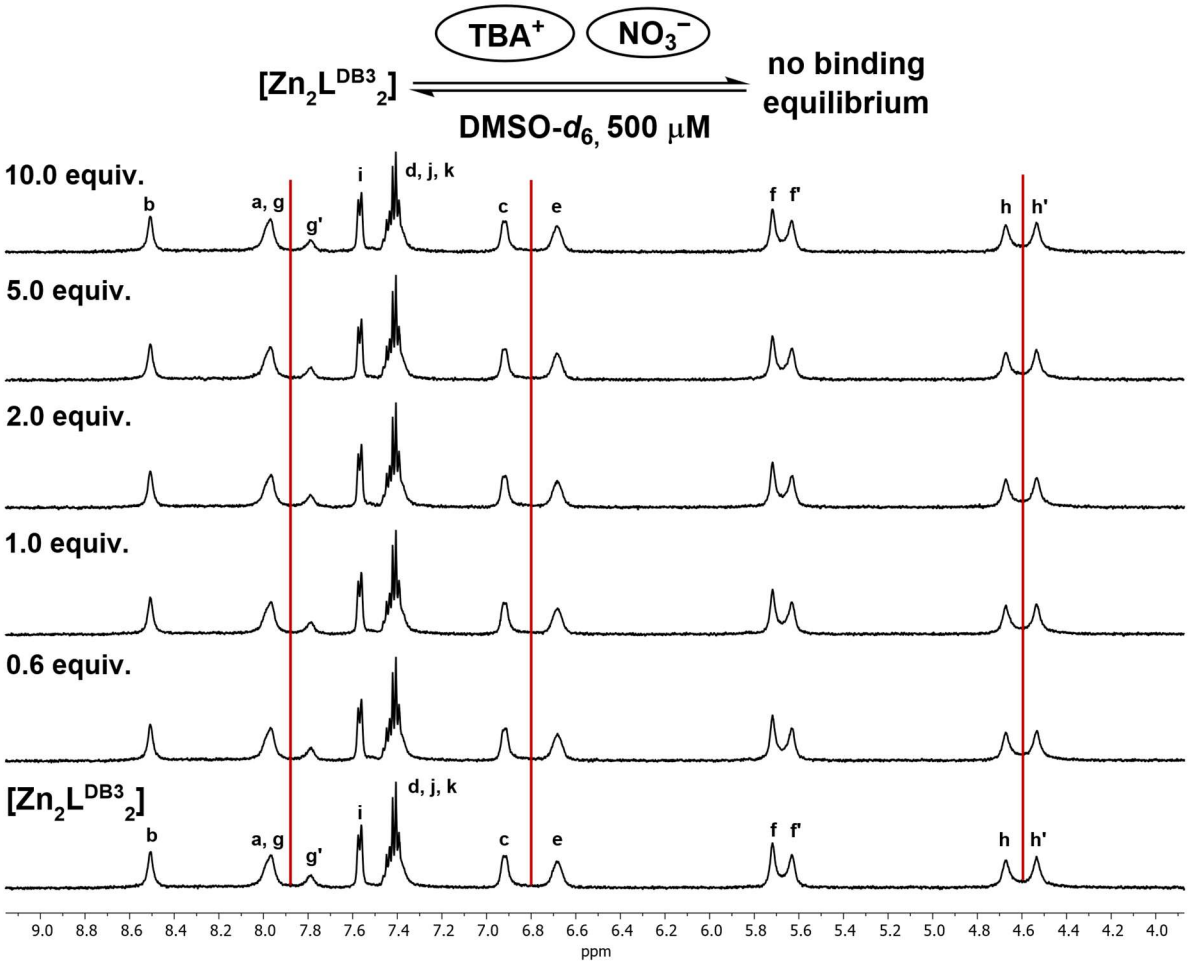

Figure 4.41: ^{1}H NMR test-titration of host [$Zn_2L^{DB3}{}_2$] and TBA nitrate as guest (DMSO-d_6, 500 MHz, 500 µM, 25°C).

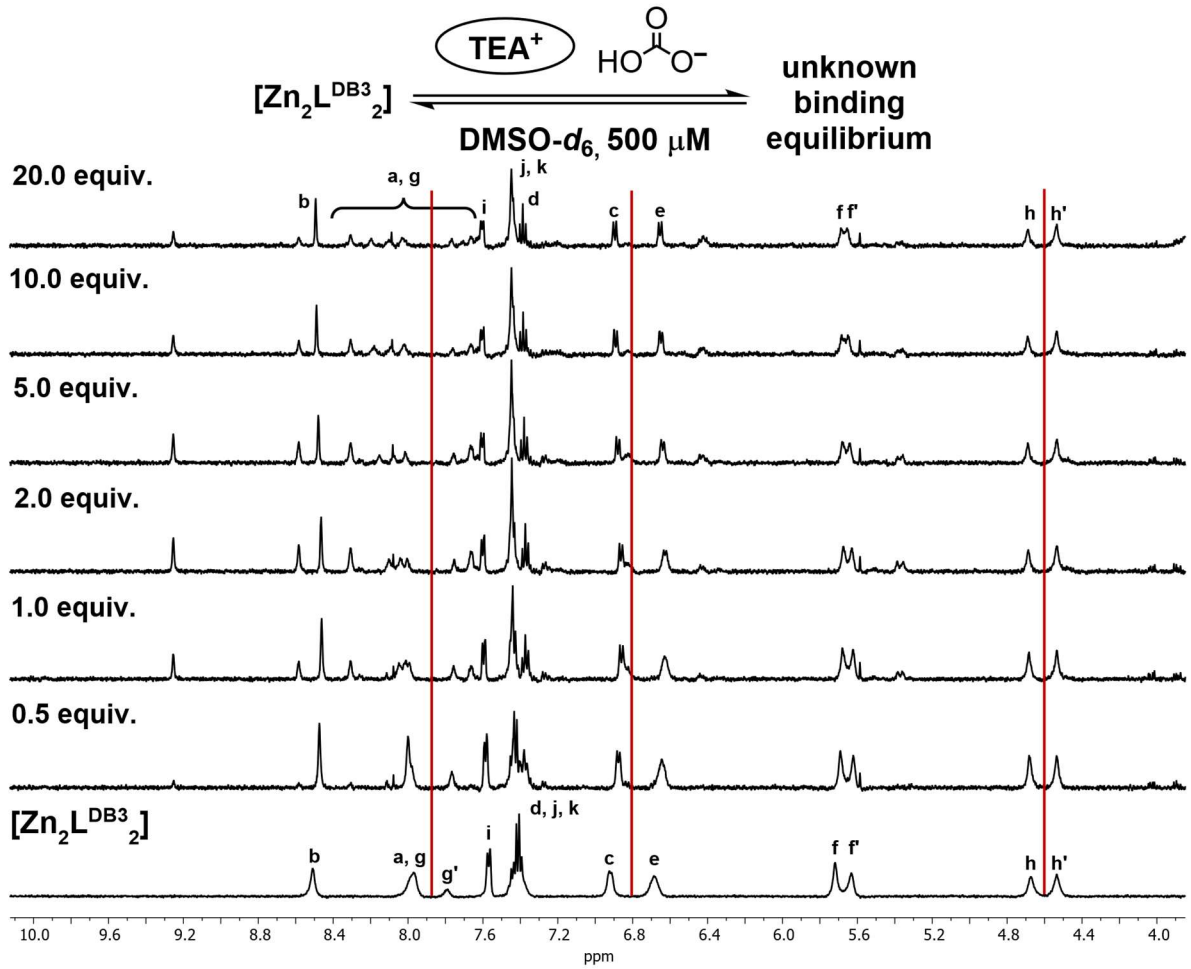

Figure 4.42: ^{1}H NMR test-titration of host [$Zn_2L^{DB3}_2$] and TEA bicarbonate (DMSO-d_6, 500 MHz, 500 μM, 25°C).

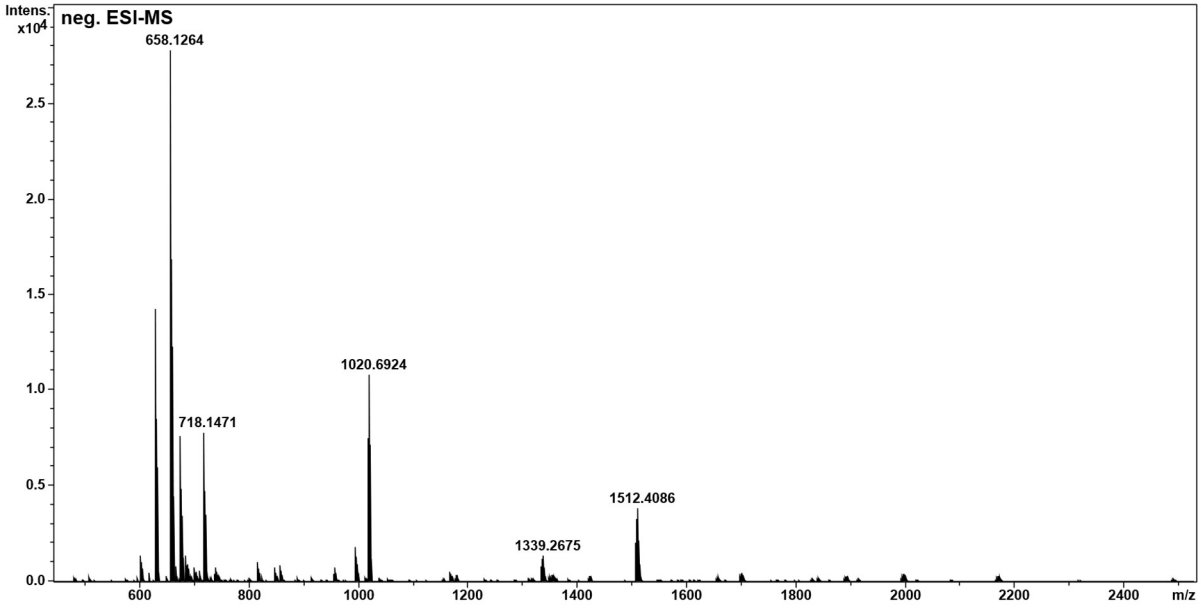

Figure 4.43: Negative HR-ESI-MS spectrum of [$Zn_2L^{DB3}_2$] and TEA bicarbonate (ACN/DMSO 9:1, 100 μM).

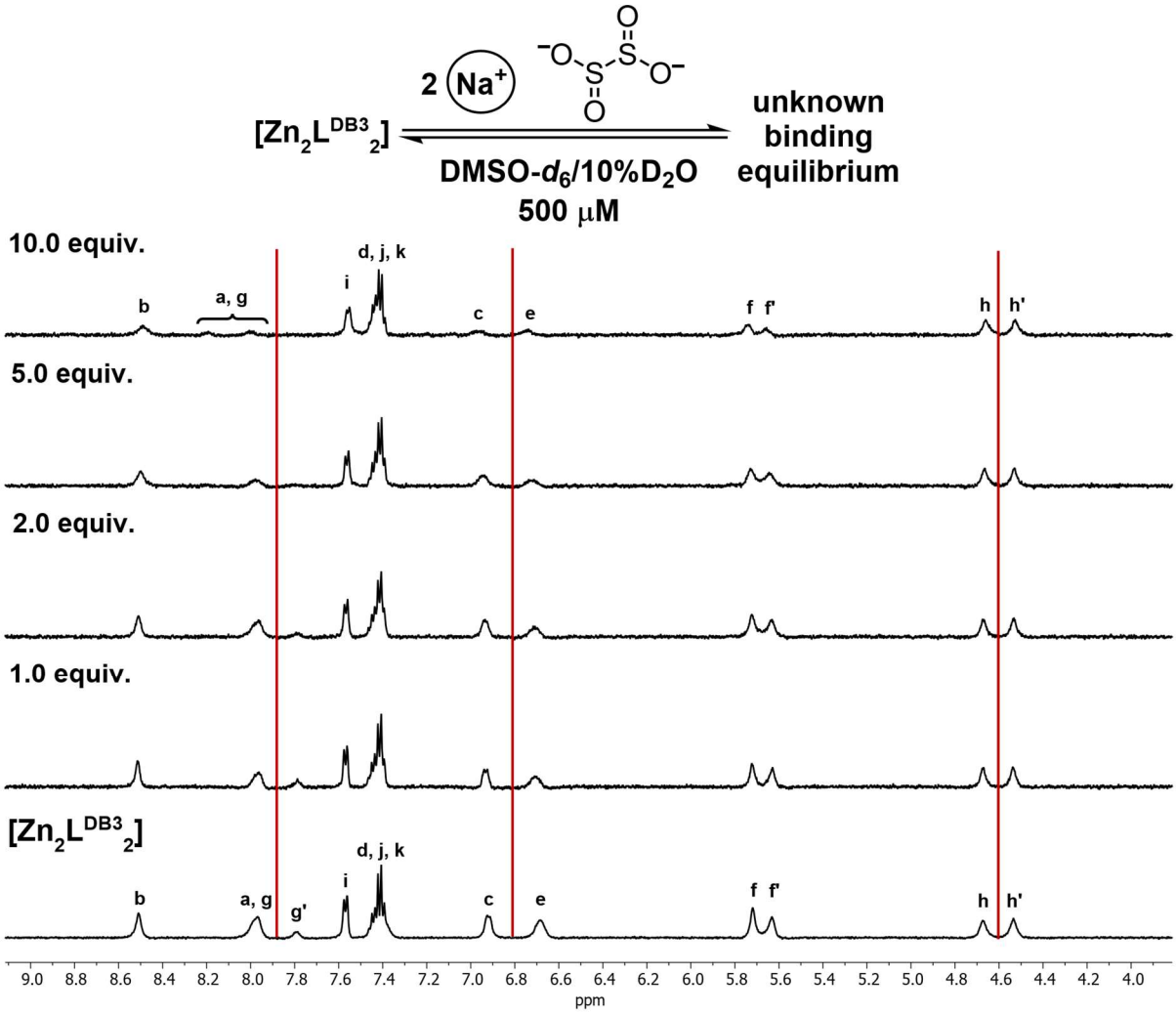

Figure 4.44: ^{1}H NMR test-titration of host $[Zn_2L^{DB3}{}_2]$ and sodium dithionite (DMSO-d_6/10%H_2O), 500 MHz, 500 μM, 25°C).

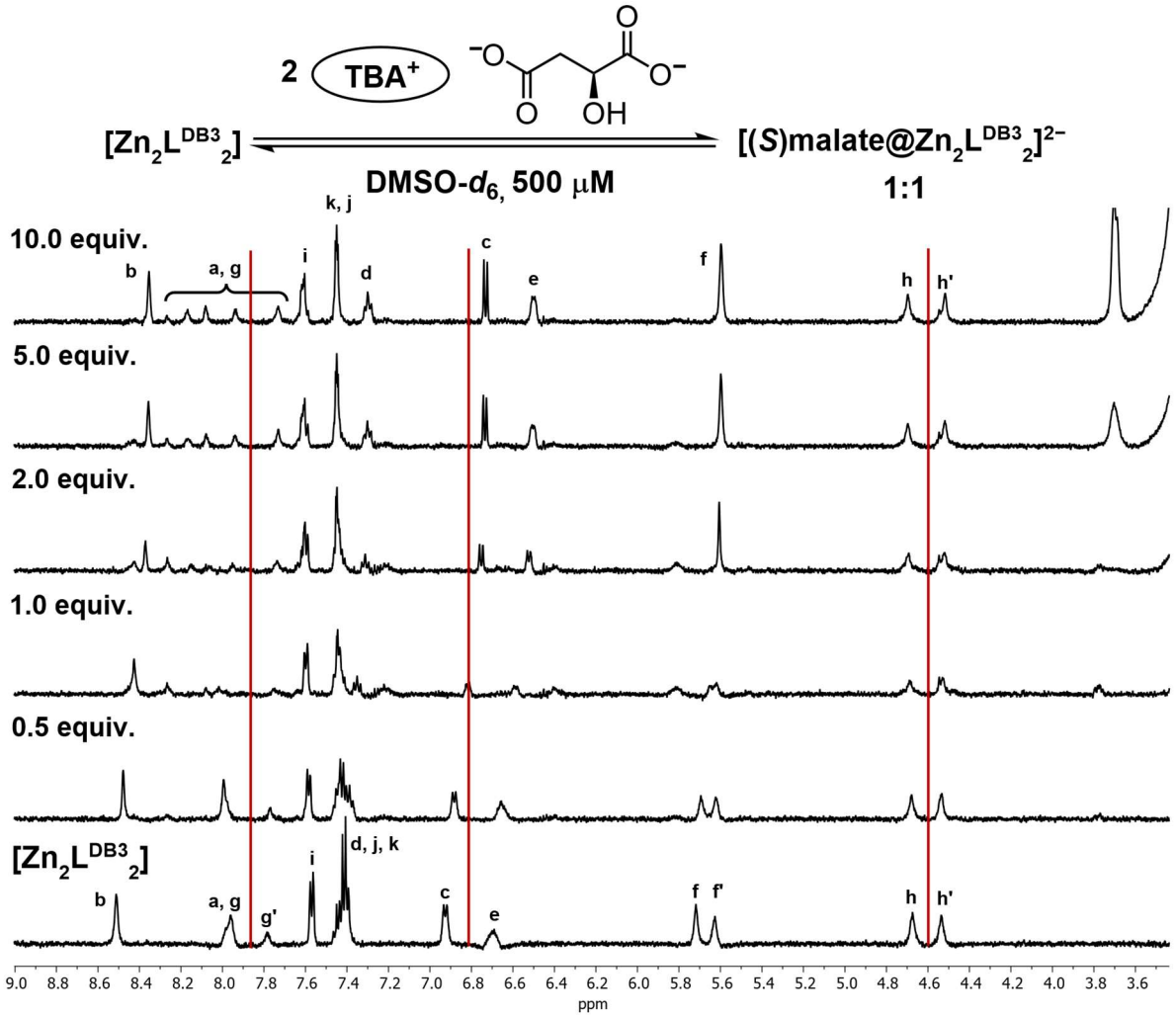

Figure 4.45: ^{1}H NMR test-titration of host [$Zn_2L^{DB3}_2$] and TBA malate (DMSO-d_6, 500 MHz, 500 µM, 25°C).

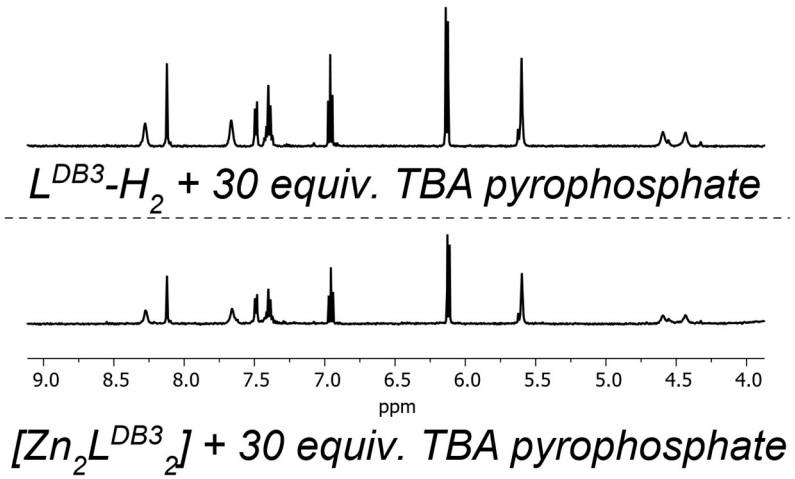

*Figure 4.46: Comparison of [$Zn_2L^{DB3}_2$] and ligand **S22** (L^{DB3}-H_2), each treated with 30 equiv. of TBA pyrophosphate (DMSO-d_6, 500 MHz, 500 µM, 25°C).*

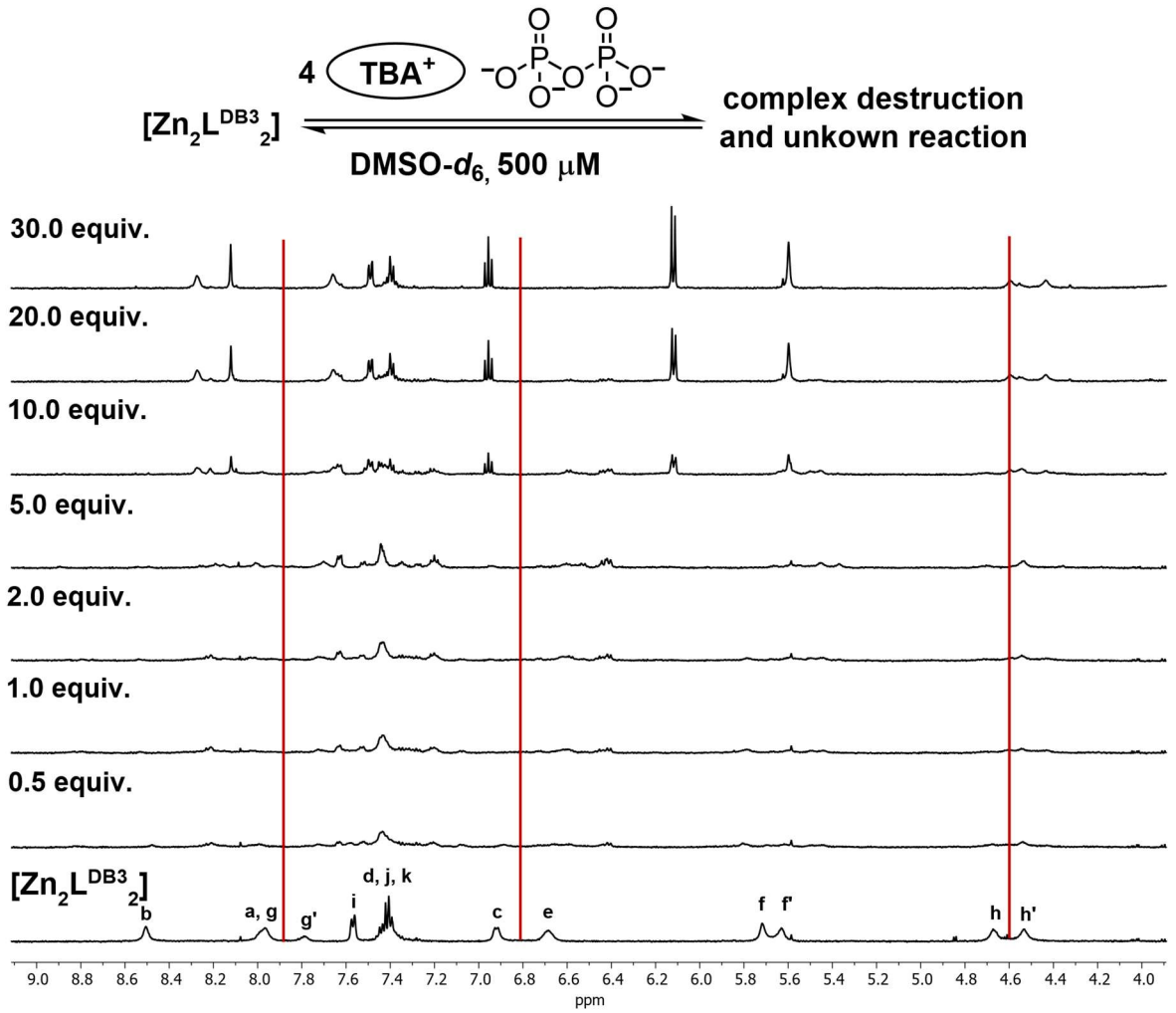

Figure 4.47: ^{1}H NMR test-titration of host [$Zn_2L^{DB3}{}_2$] and TBA pyrophosphate (DMSO-d_6, 500 MHz, 500 µM, 25°C).

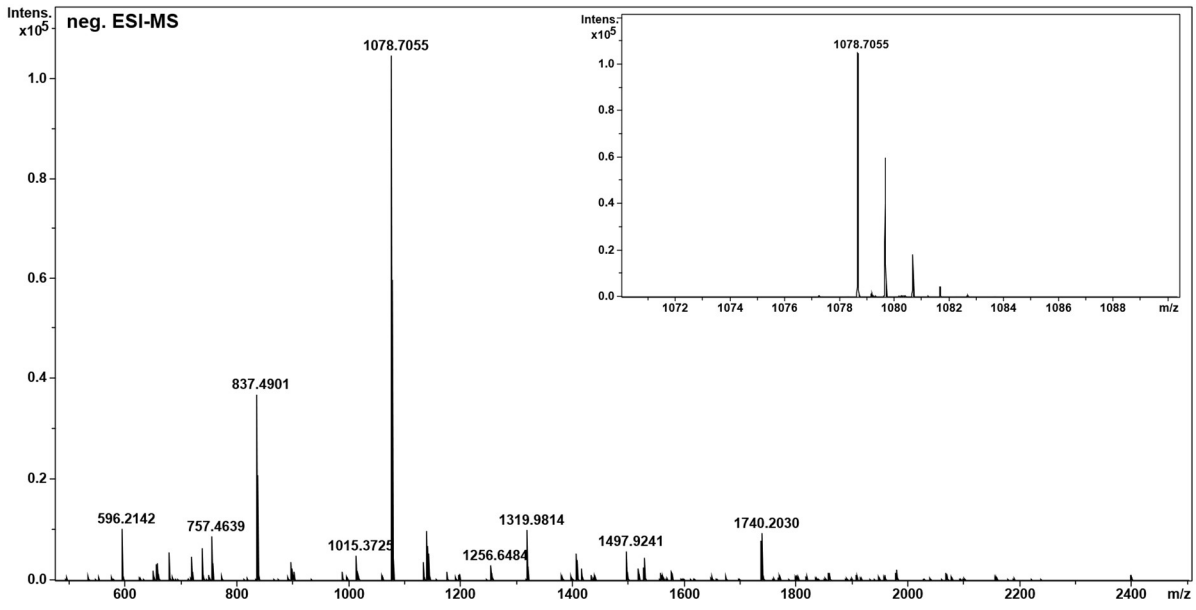

Figure 4.48: Negative HR-ESI-MS spectrum of [$Zn_2L^{DB3}{}_2$] and TBA pyrophosphate (ACN/DMSO 9:1, 100 µM).

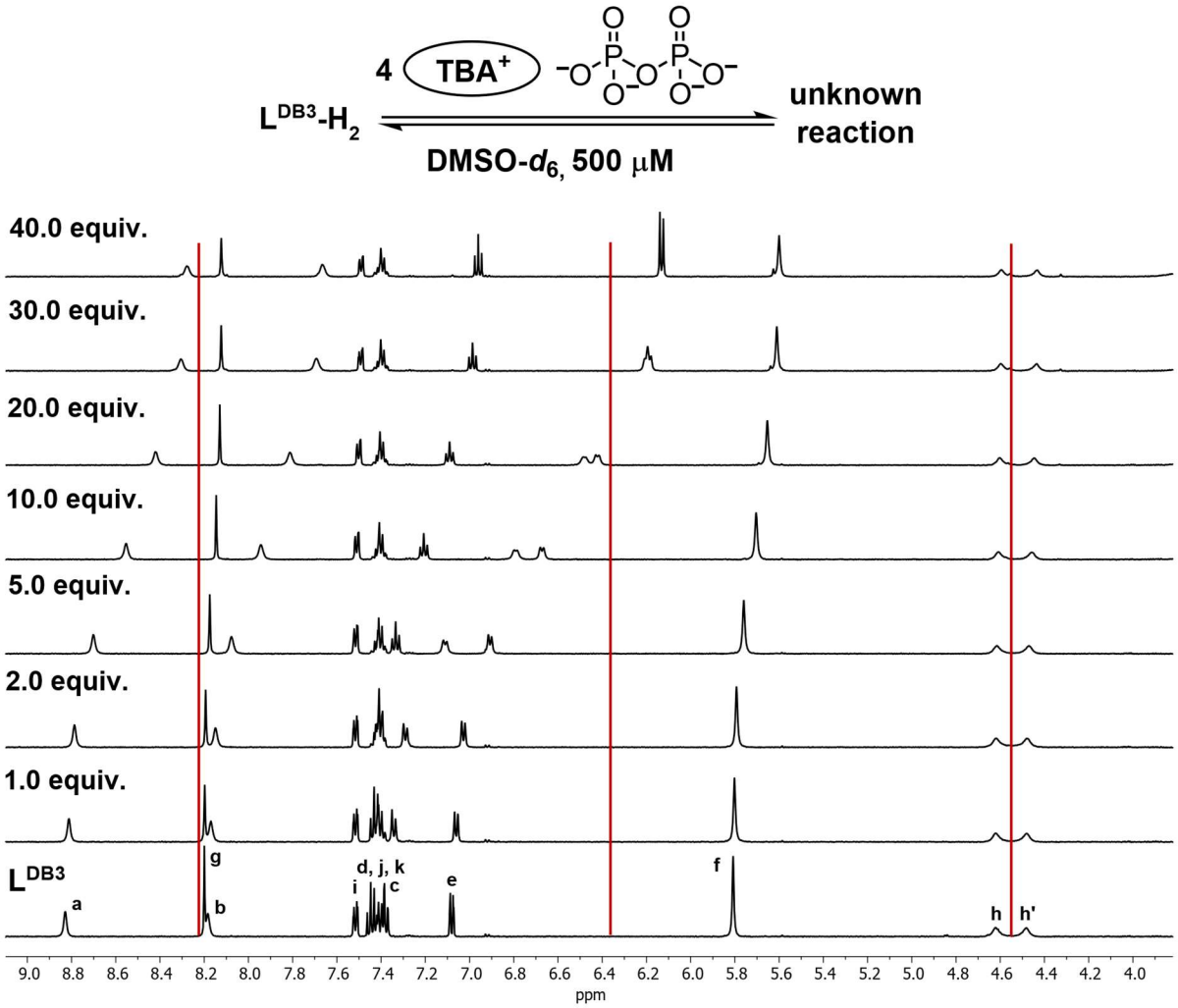

*Figure 4.49: ^{1}H NMR test-titration of ligand **S22** (L^{DB3}-H_2) and TBA pyrophosphate (DMSO-d_6, 500 MHz, 500 μM, 25°C).*

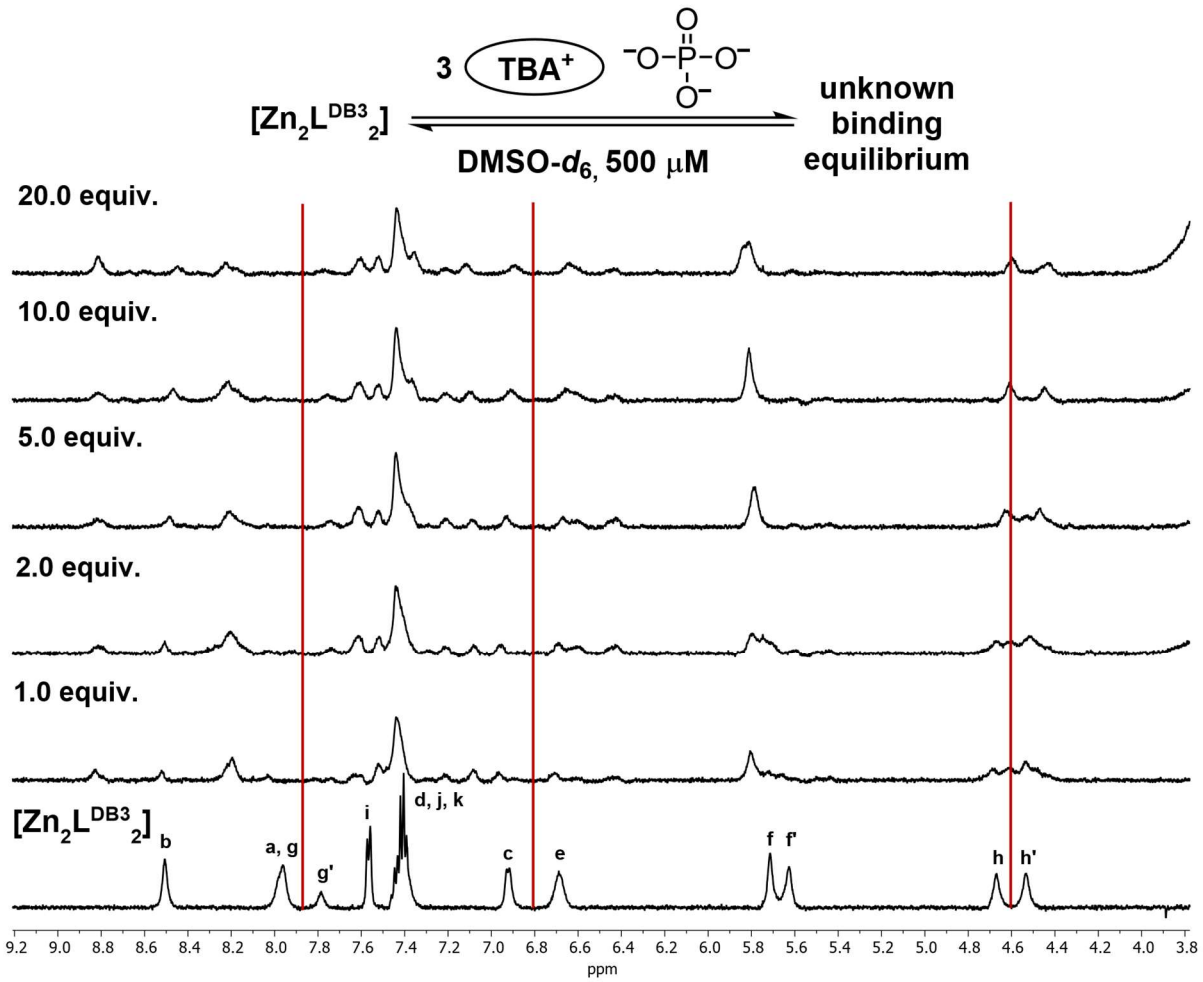

Figure 4.50: ^{1}H NMR test-titration of host [$Zn_2L^{DB3}{}_2$] and TBA phosphate (DMSO-d_6, 500 MHz, 500 μM, 25°C).

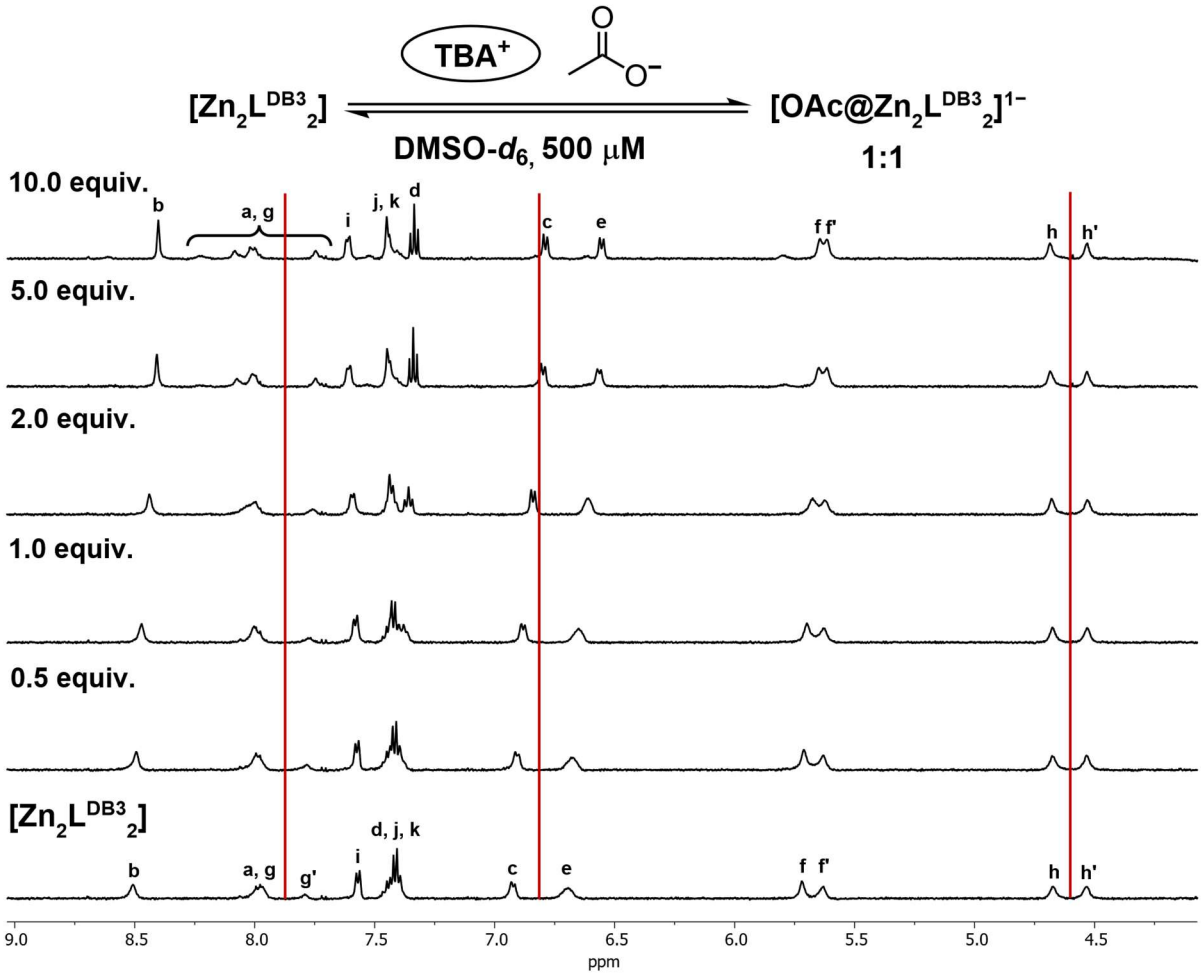

Figure 4.51: ^{1}H NMR test-titration of host [$Zn_2L^{DB3}_2$] and TBA acetate (DMSO-d_6, 500 MHz, 500 µM, 25°C).

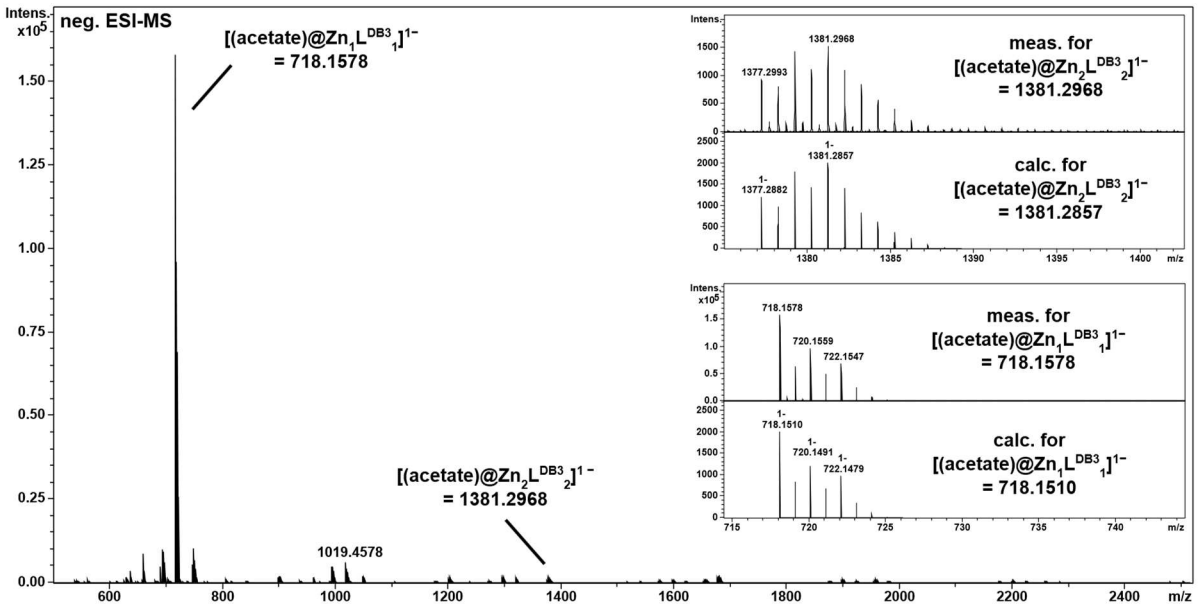

Figure 4.52: Negative HR-ESI-MS spectrum of [$Zn_2L^{DB3}_2$] and TBA acetate (ACN/DMSO 9:1, 100 µM).

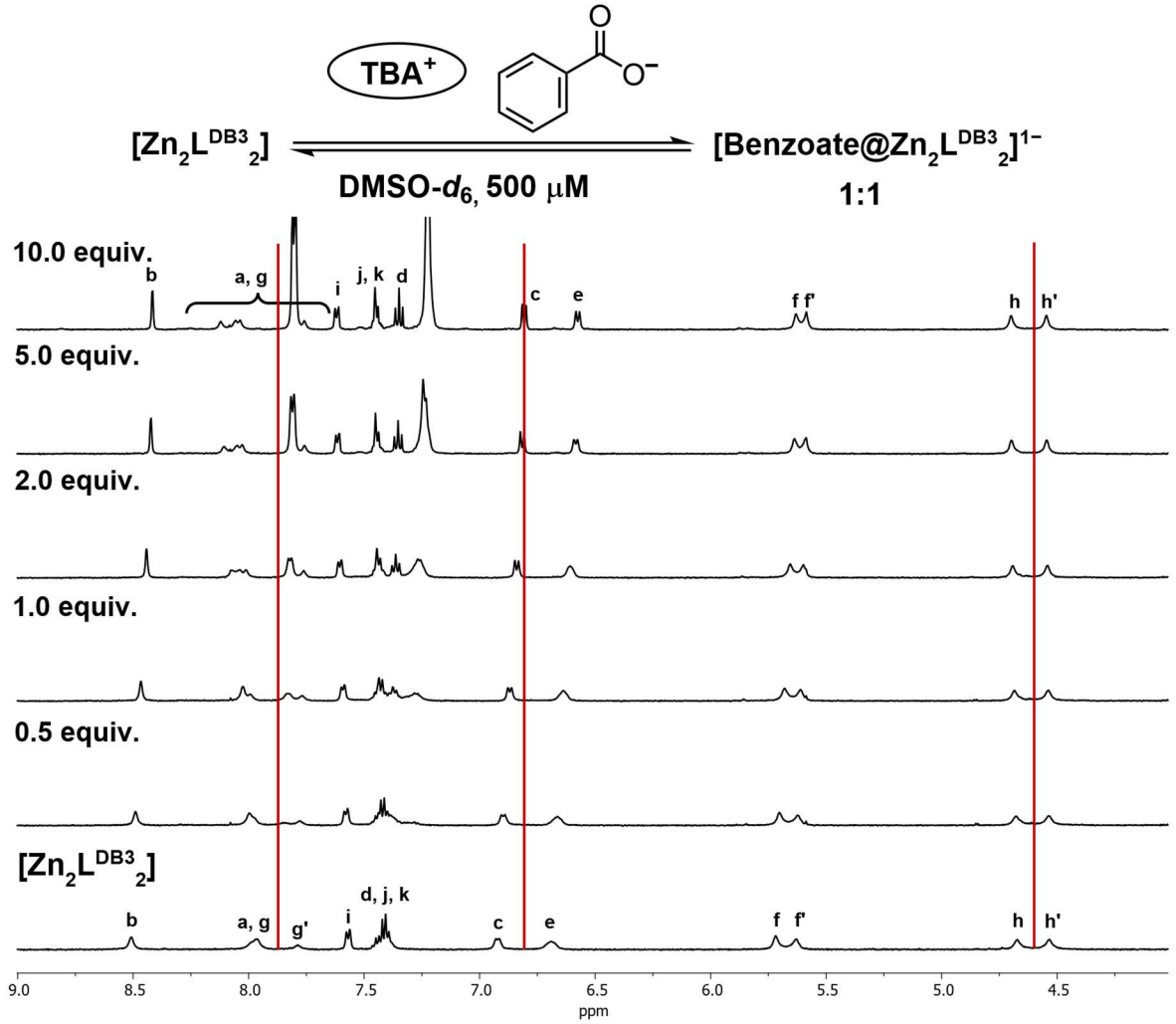

Figure 4.53: ^{1}H NMR test-titration of host $[Zn_2L^{DB3}{}_2]$ and TBA benzoate (DMSO-d_6, 500 MHz, 500 μM, 25°C).

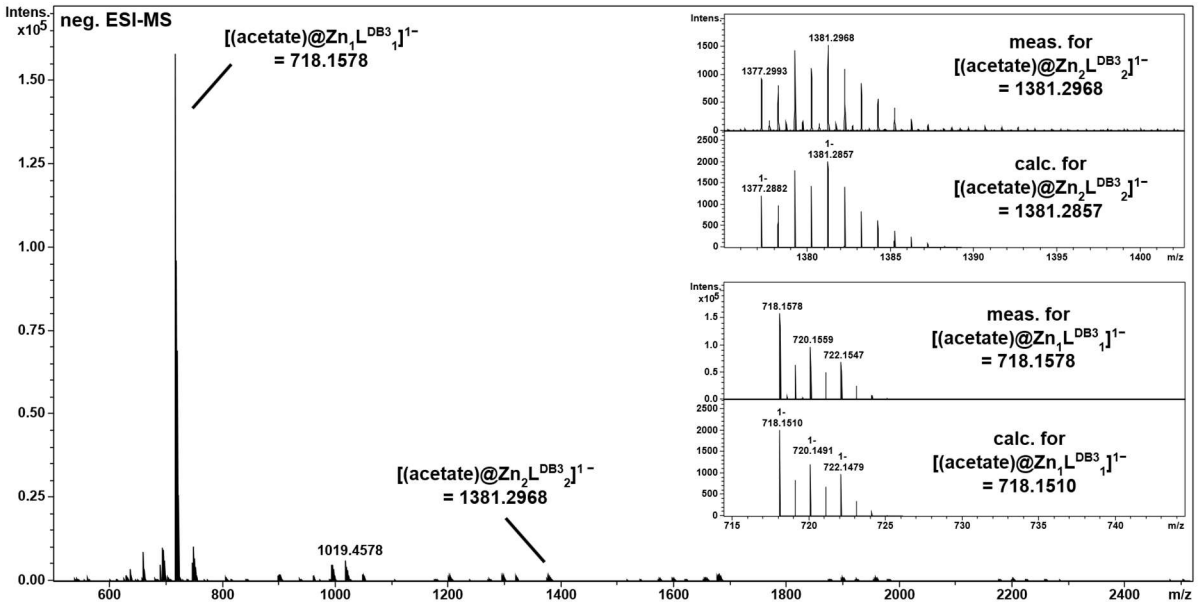

Figure 4.54: Negative HR-ESI-MS spectrum of $[Zn_2L^{DB3}{}_2]$ and TBA benzoate (ACN/DMSO 9:1, 100 μM).

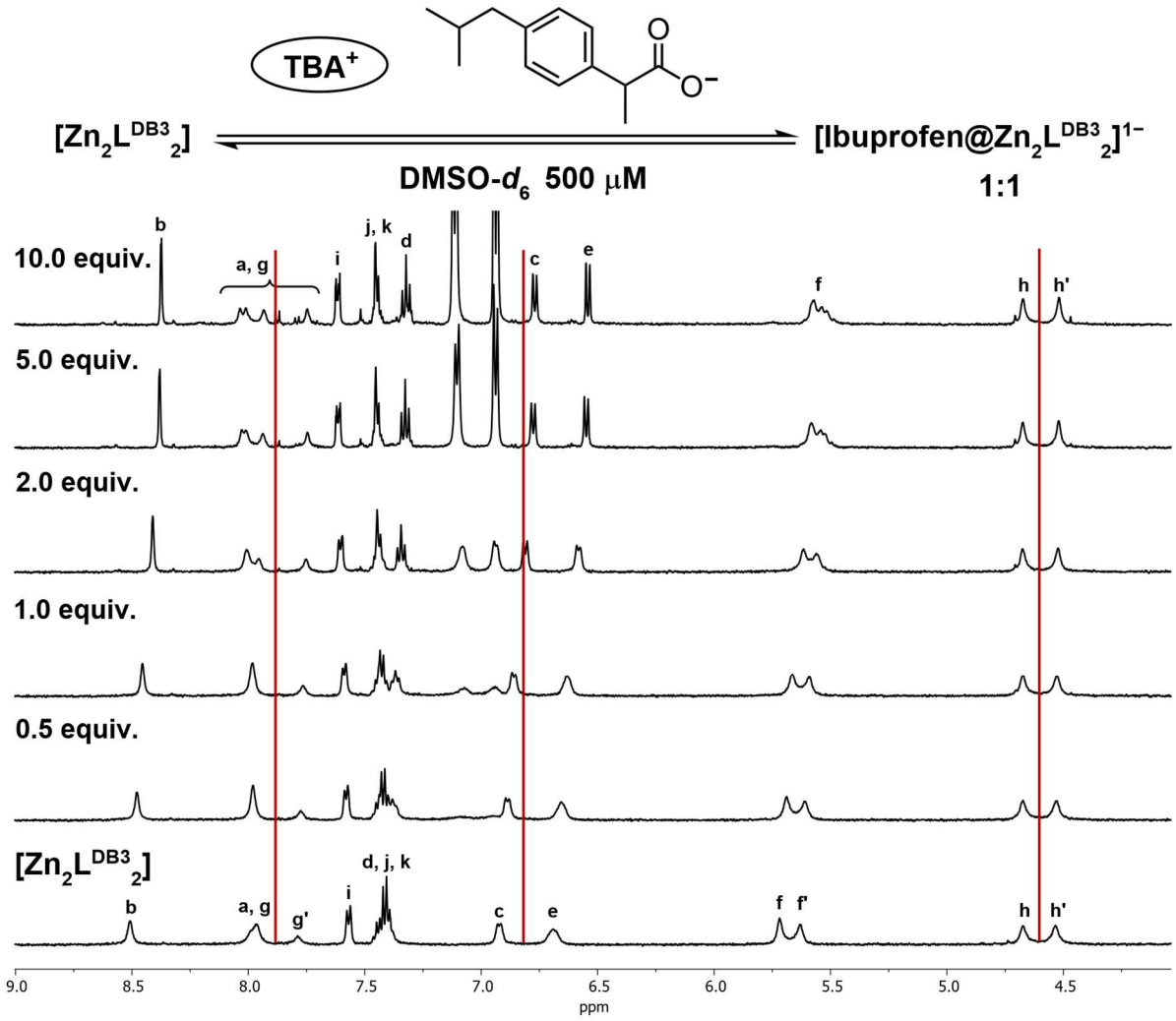

Figure 4.55: ^{1}H NMR test-titration of host [$Zn_2L^{DB3}_2$] and TBA ibuprofen (DMSO-d_6, 500 MHz, 500 µM, 25°C).

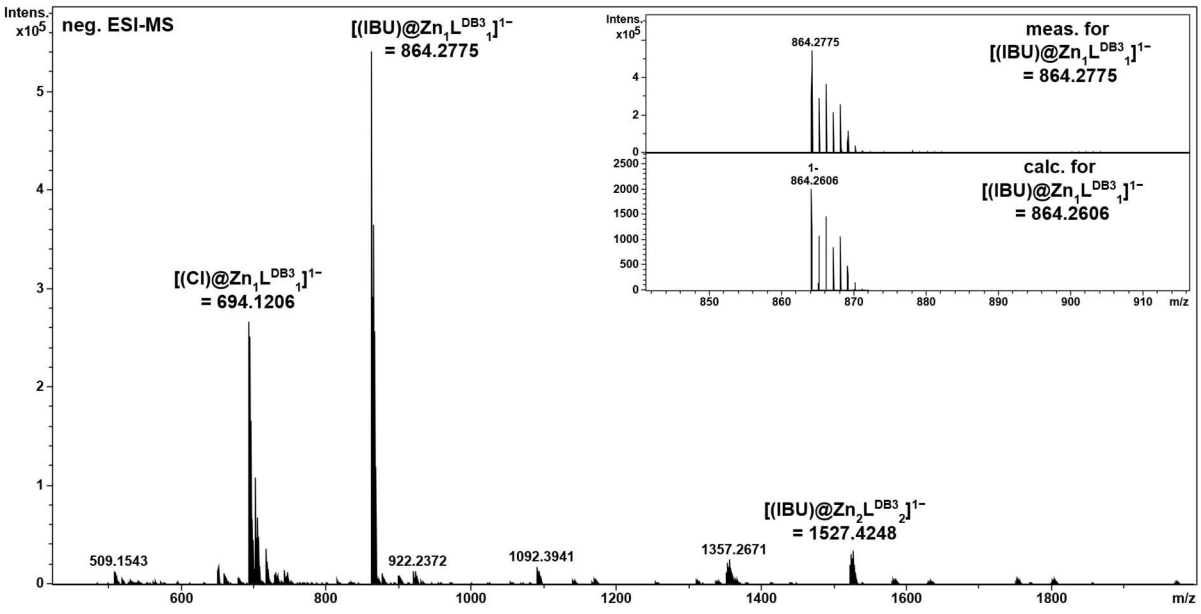

Figure 4.56: Negative HR-ESI-MS spectrum of [$Zn_2L^{DB3}_2$] and TBA ibuprofen (ACN/DMSO 9:1, 100 µM).

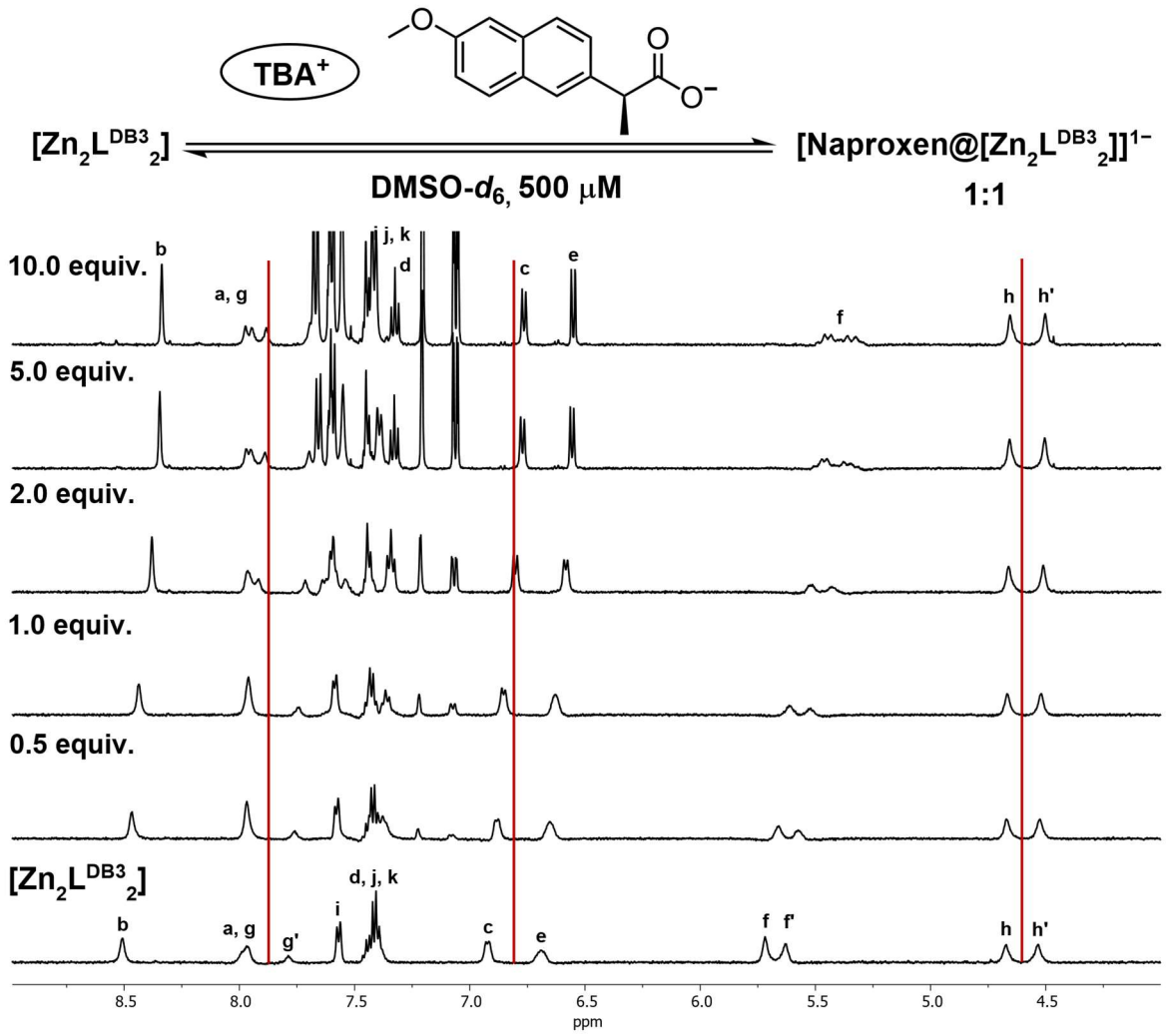

Figure 4.57: ^{1}H NMR test-titration of host [$Zn_2L^{DB3}{}_2$] and TBA naproxen (DMSO-d_6, 500 MHz, 500 μM, 25°C).

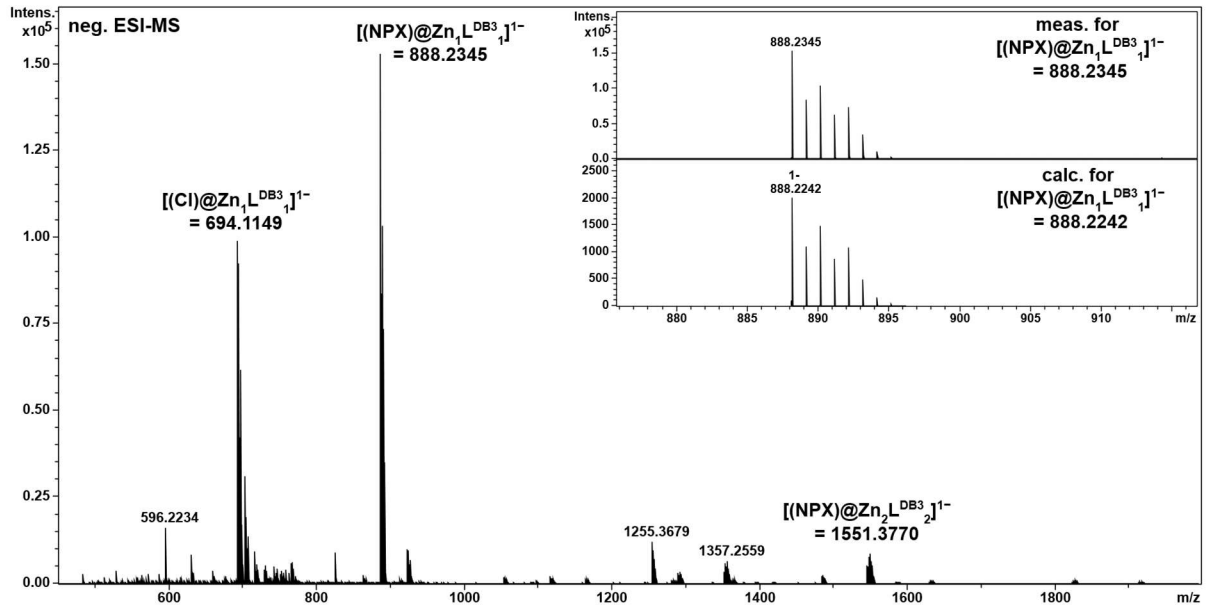

Figure 4.58: Negative HR-ESI-MS spectrum of [$Zn_2L^{DB3}{}_2$] and TBA naproxen (ACN/DMSO 9:1, 100 μM).

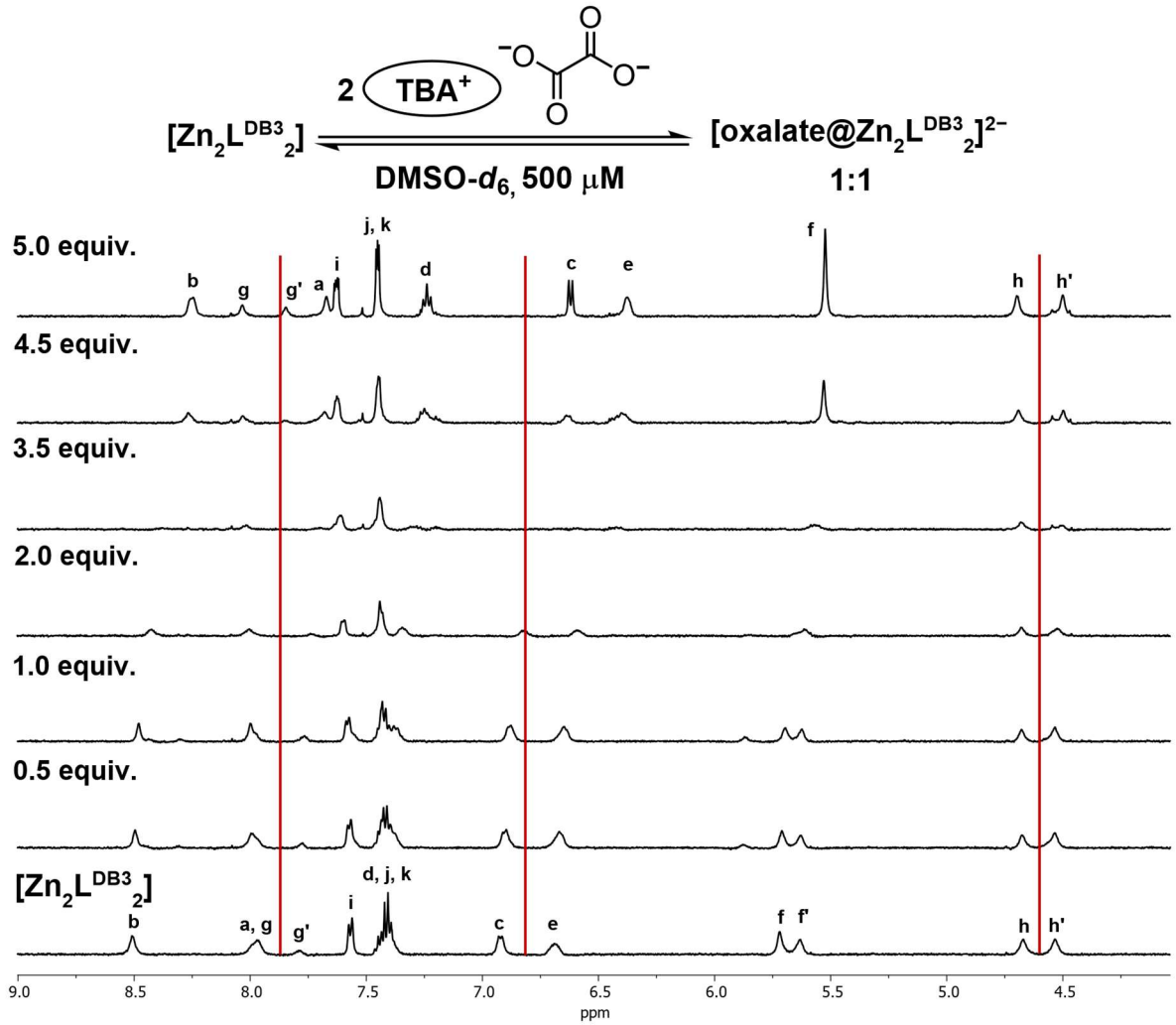

Figure 4.59: ^{1}H NMR test-titration of host [$Zn_2L^{DB3}_2$] and TBA oxalate (DMSO-d_6, 500 MHz, 500 μM, 25°C).

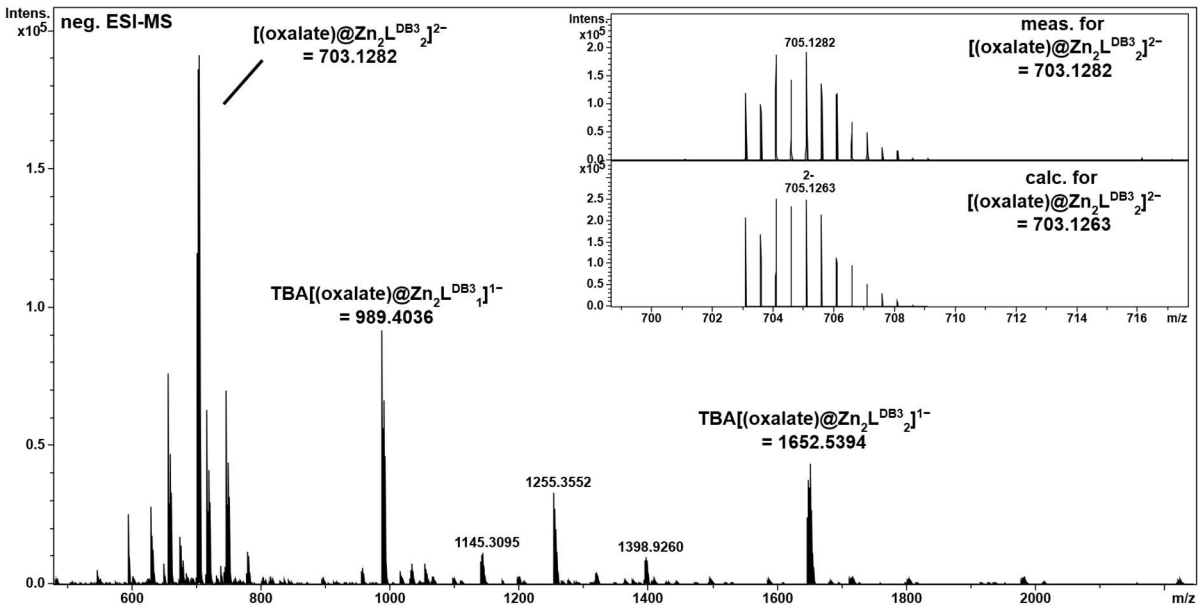

Figure 4.60: Negative HR-ESI-MS spectrum of [$Zn_2L^{DB3}_2$] and TBA oxalate (ACN/DMSO 9:1, 100 μM).

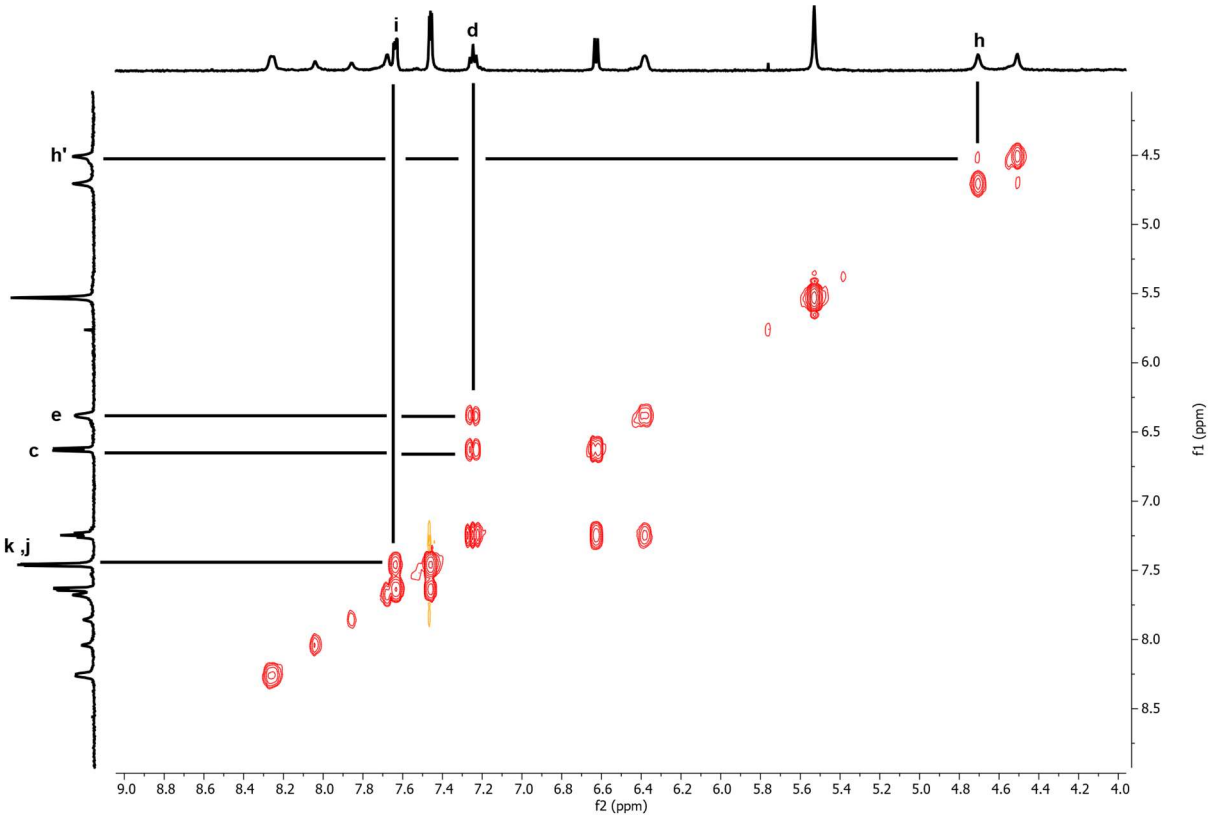

Figure 4.61: ^{1}H COSY spectrum of [(oxalate)@$Zn_2L^{DB3}{}_2$]$^{2-}$ (DMSO-d_6, 500 MHz, 25°C).

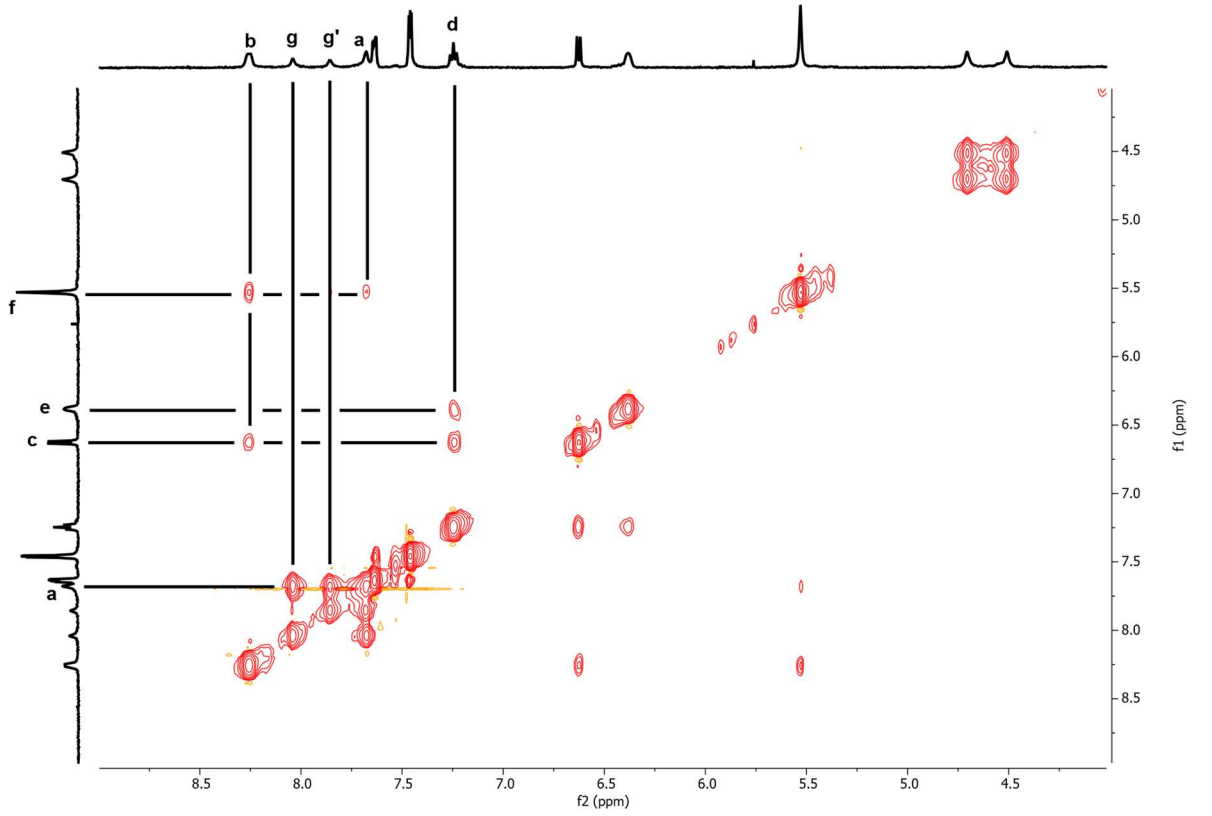

Figure 4.62: ^{1}H NOESY spectrum of [(oxalate)@$Zn_2L^{DB3}{}_2$]$^{2-}$ (DMSO-d_6, 500 MHz, 25°C).

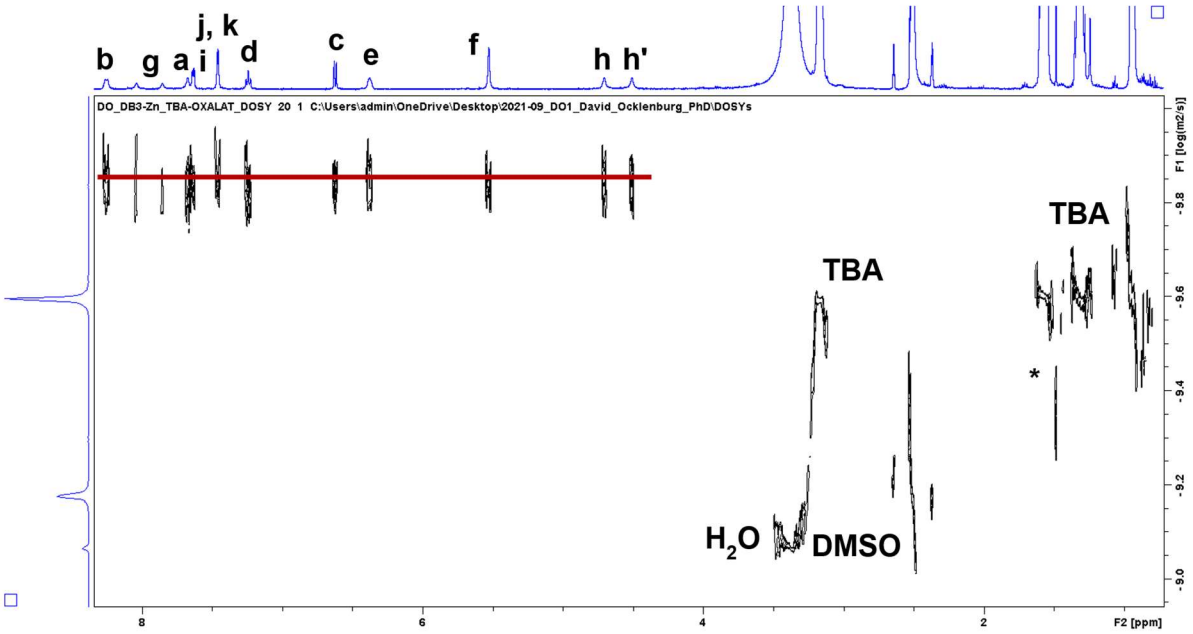

Figure 4.63: ^{1}H DOSY spectrum of $[(oxalate)@Zn_2L^{DB3}{}_2]^{2-}$, D = 1.449 x 10^{-10} m^2 s^{-1}, r_H = 0.76 nm (DMSO-d_6, 500 MHz, 25°C).

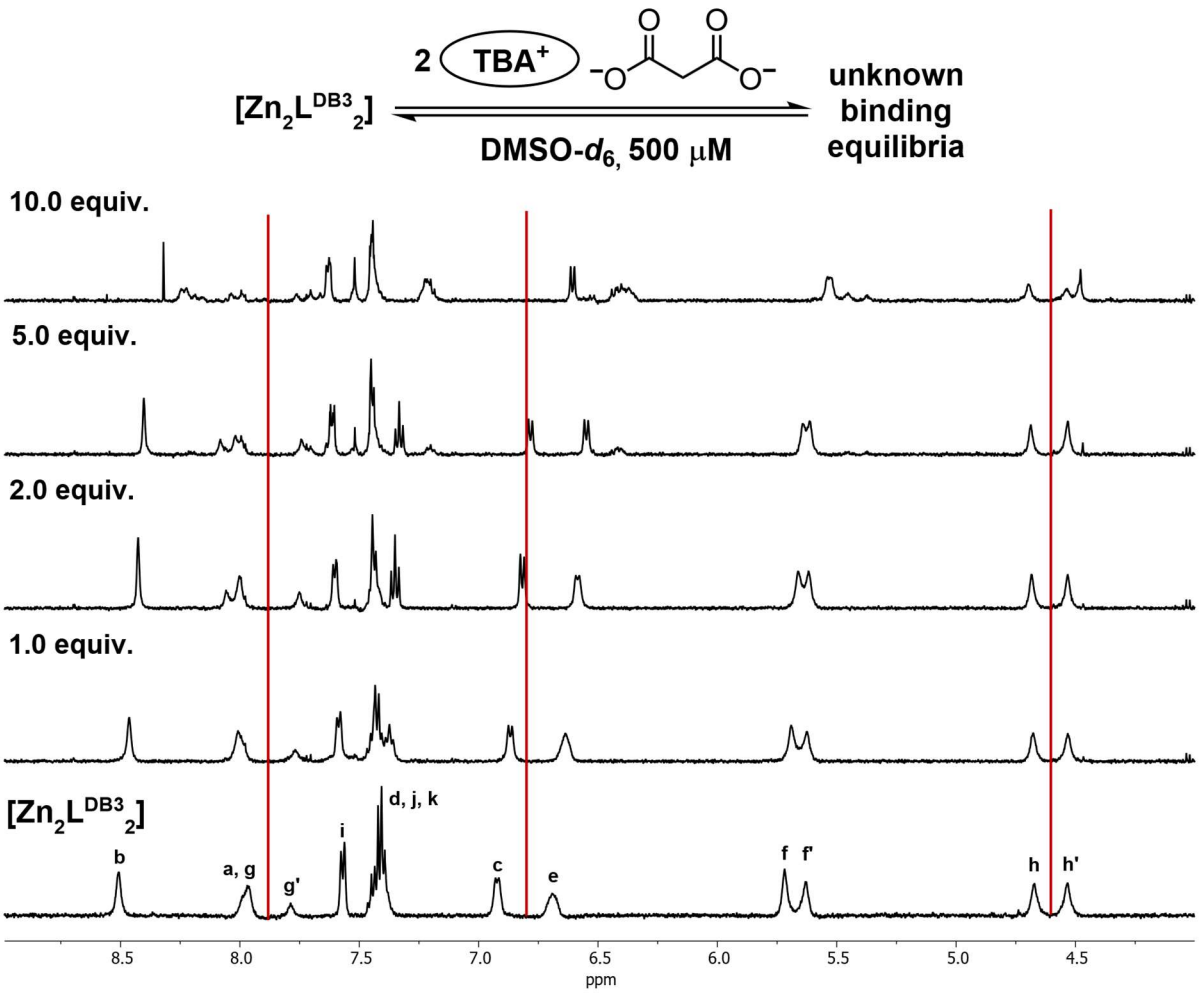

Figure 4.64: ^{1}H NMR test-titration of host [$Zn_2L^{DB3}{}_2$] and TBA malonate (DMSO-d_6, 500 MHz, 500 μM, 25°C).

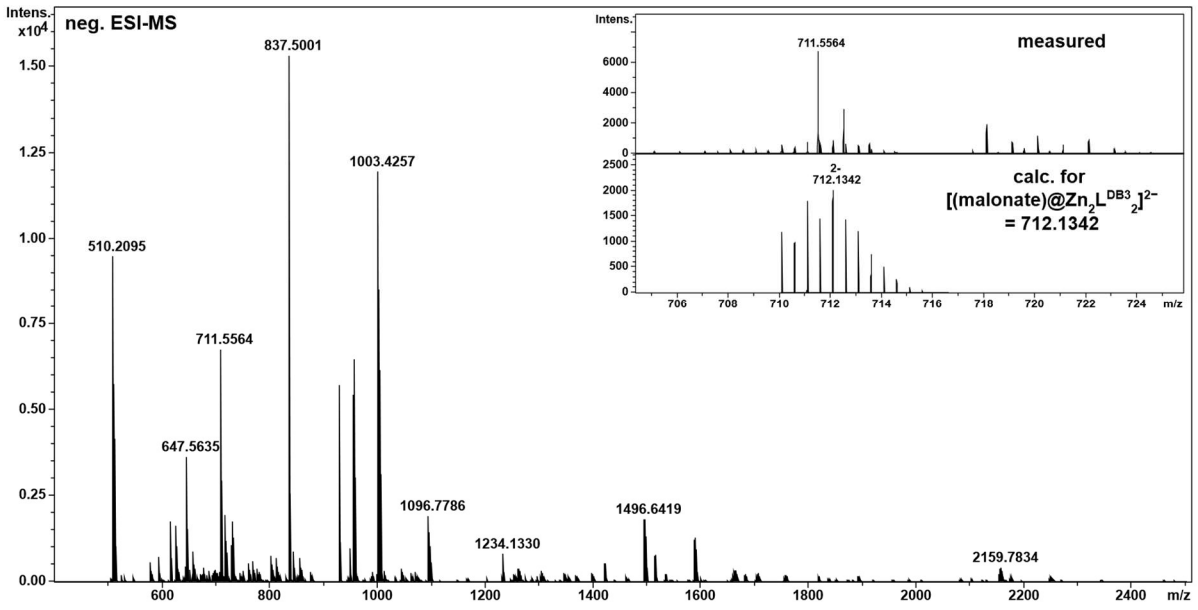

Figure 4.65: Negative HR-ESI-MS spectrum of [$Zn_2L^{DB3}{}_2$] and TBA malonate (ACN/DMSO 9:1, 100 μM).

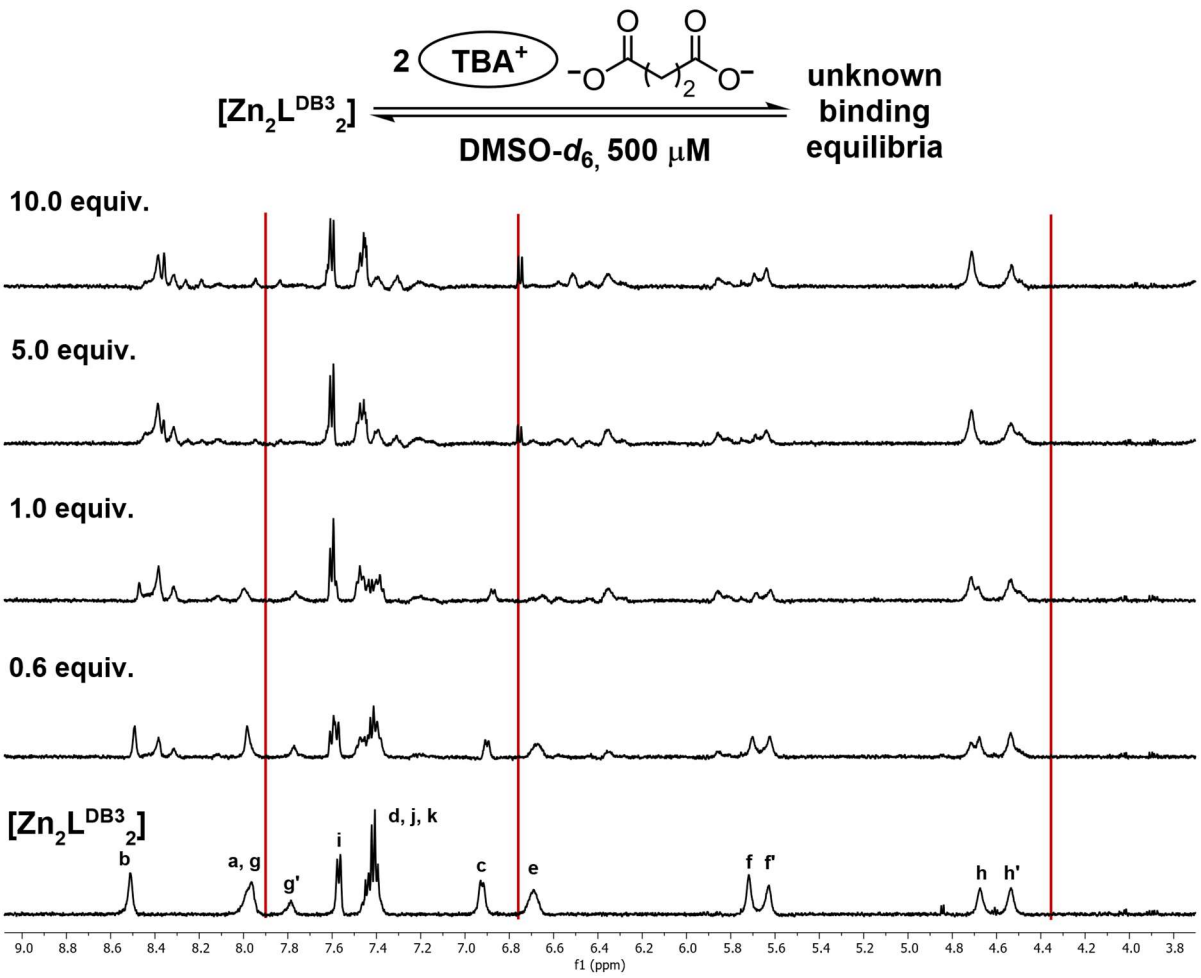

Figure 4.66: ^{1}H NMR test-titration of host [$Zn_2L^{DB3}_2$] and TBA succinate (DMSO-d_6, 500 MHz, 500 μM, 25°C).

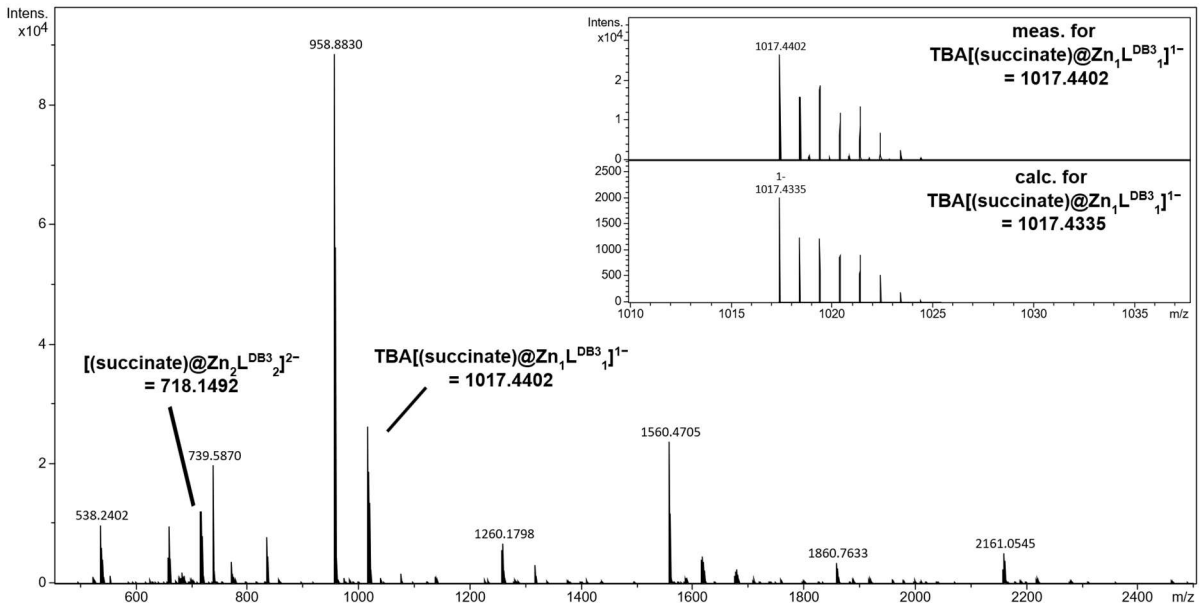

Figure 4.67: Negative HR-ESI-MS spectrum of [$Zn_2L^{DB3}_2$] and TBA succinate (ACN/DMSO 9:1, 100 μM).

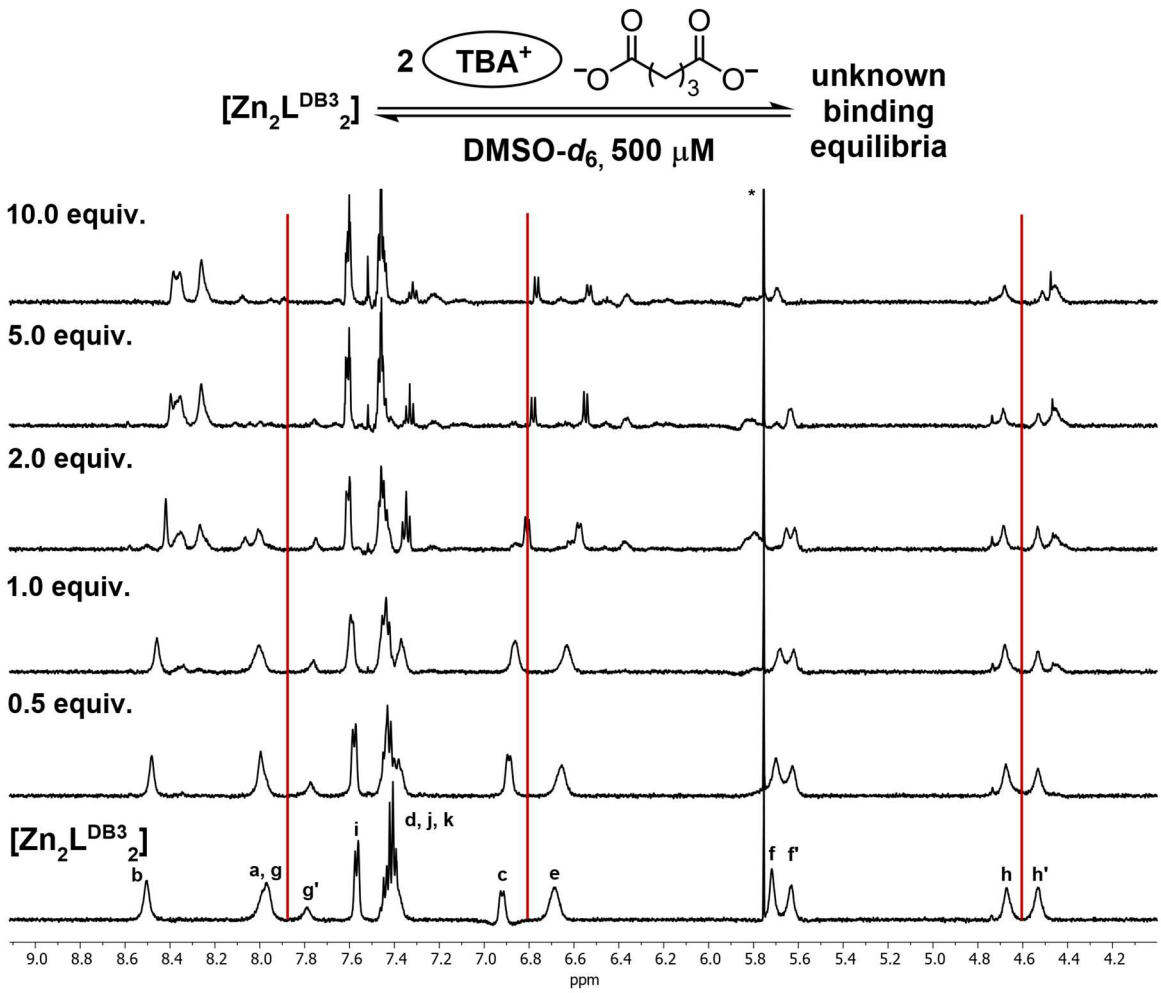

Figure 4.68: ^{1}H NMR test-titration of host [$Zn_2L^{DB3}{}_2$] and TBA glutarate (DMSO-d_6, 500 MHz, 500 μM, 25°C).

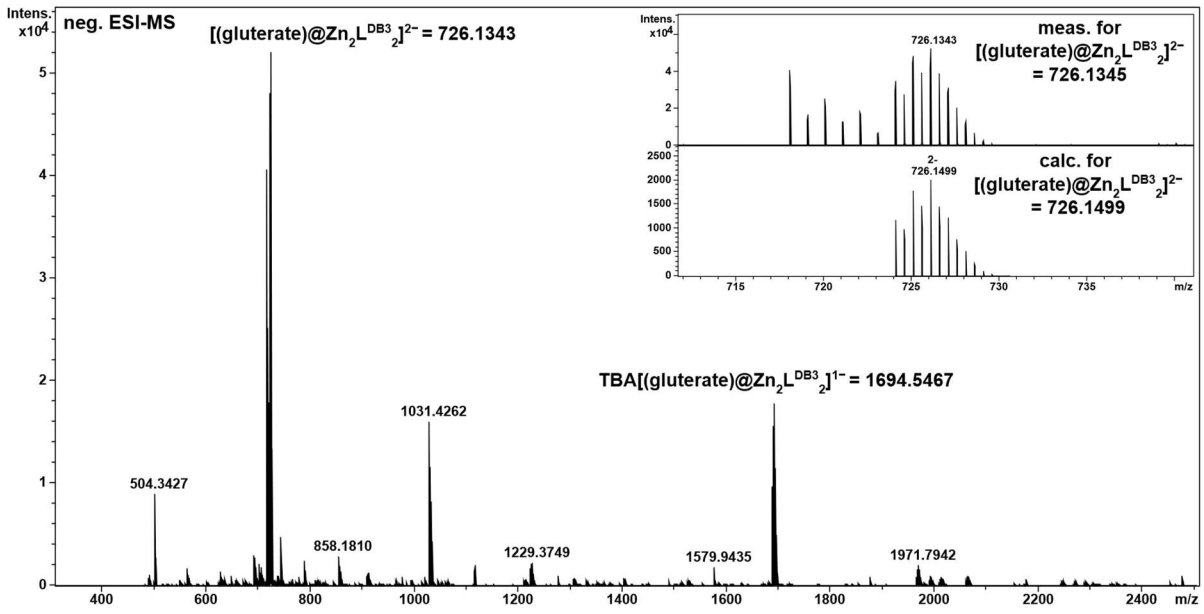

Figure 4.69: Negative HR-ESI-MS spectrum of [$Zn_2L^{DB3}{}_2$] and TBA glutarate (ACN/DMSO 9 to 1, 100 μM).

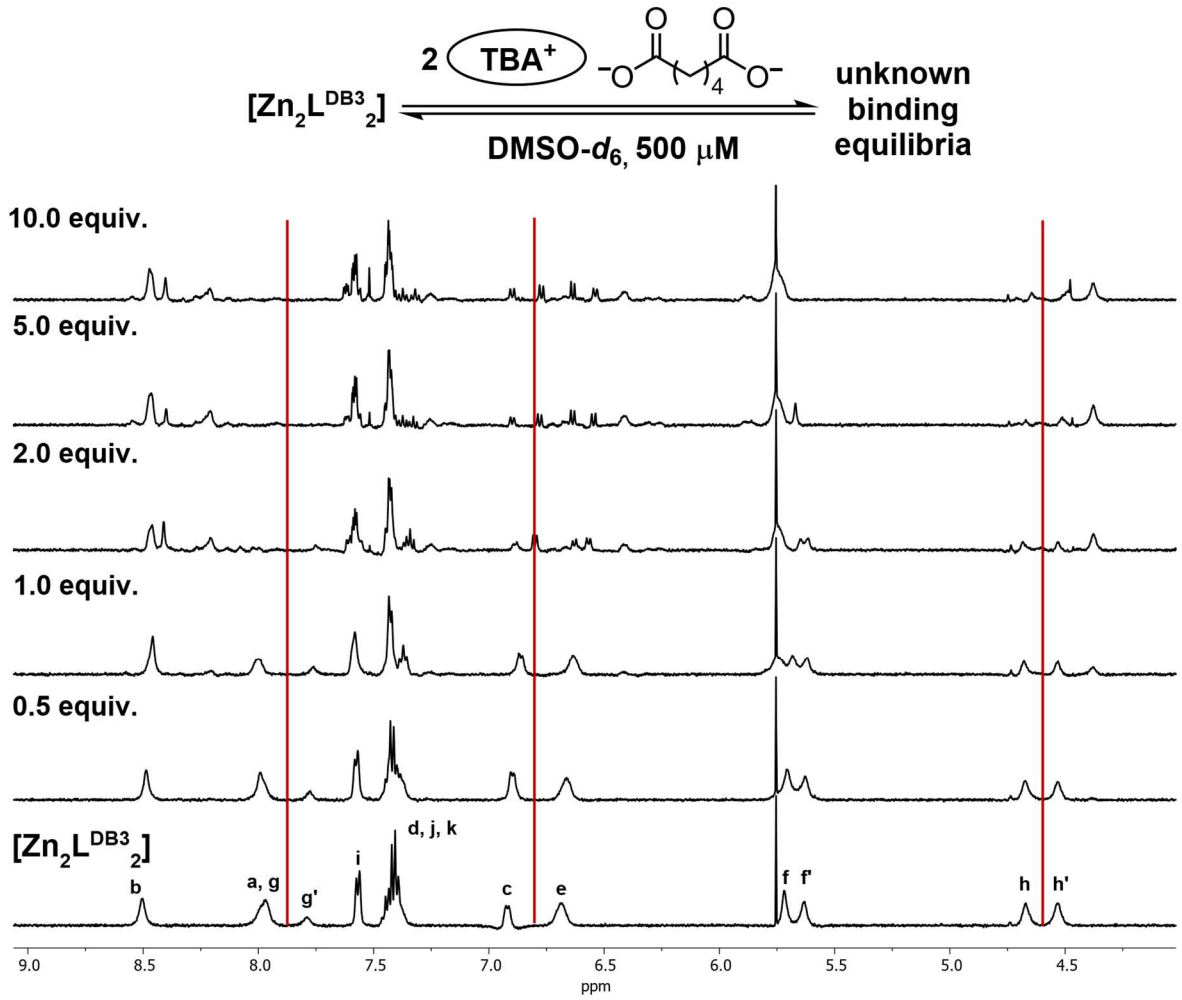

Figure 4.70: ^{1}H NMR test-titration of host [$Zn_2L^{DB3}_2$] and TBA adipate (DMSO-d_6, 500 MHz, 500 µM, 25°C).

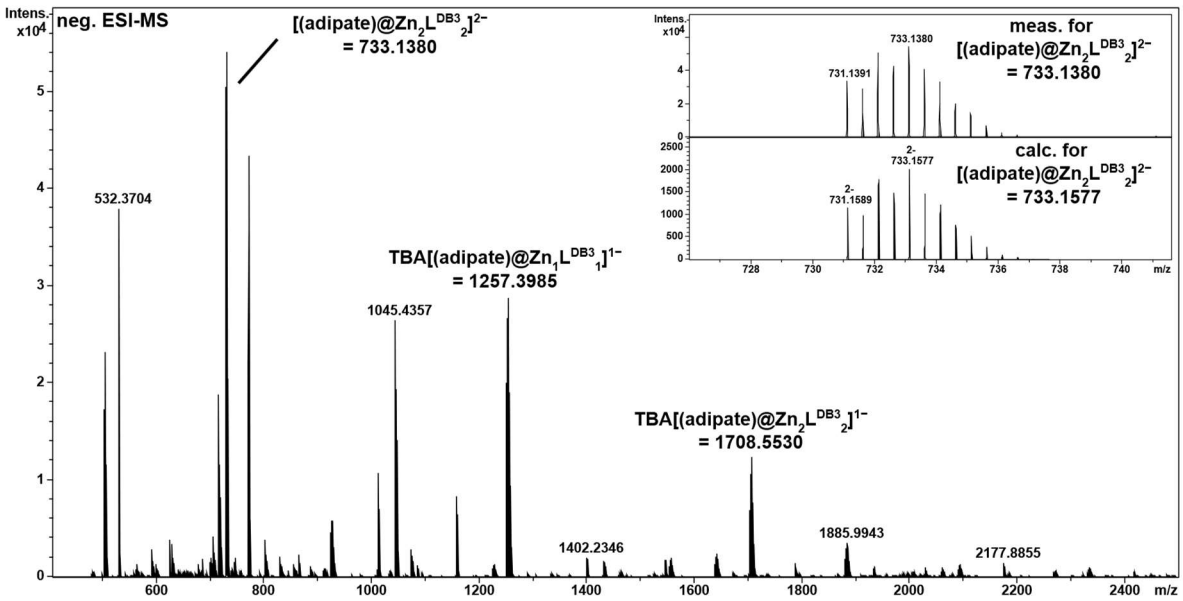

Figure 4.71: Negative HR-ESI-MS spectrum of [$Zn_2L^{DB3}_2$] and TBA adipate (ACN/DMSO 9:1, 100 µM).

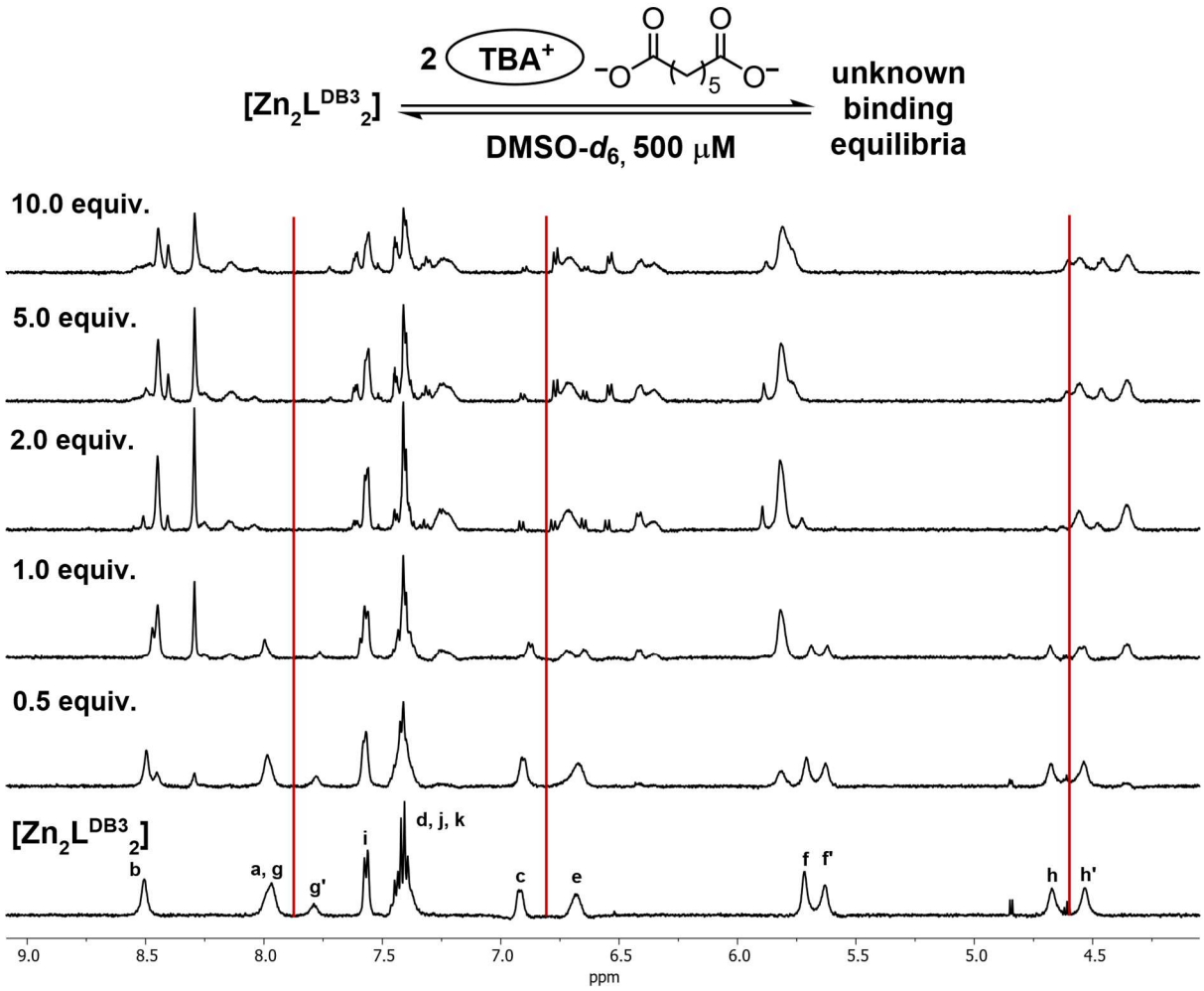

Figure 4.72: ^{1}H NMR test-titration of host $[Zn_2L^{DB3}{}_2]$ and TBA pimelate (DMSO-d_6, 500 MHz, 500 µM, 25°C).

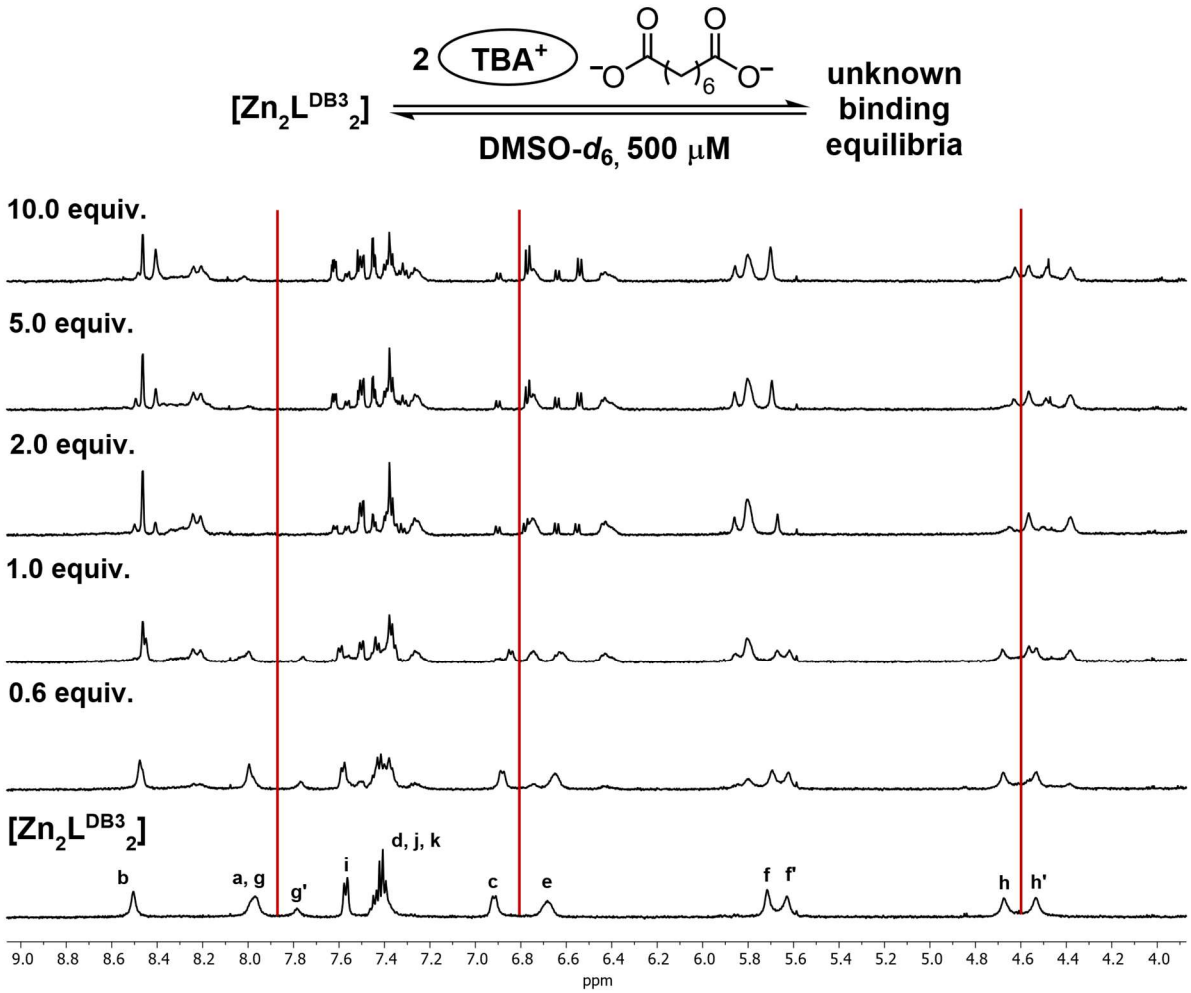

Figure 4.73: ^{1}H NMR test-titration of host [$Zn_2L^{DB3}{}_2$] and TBA octanedioate (DMSO-d_6, 500 MHz, 500 μM, 25°C).

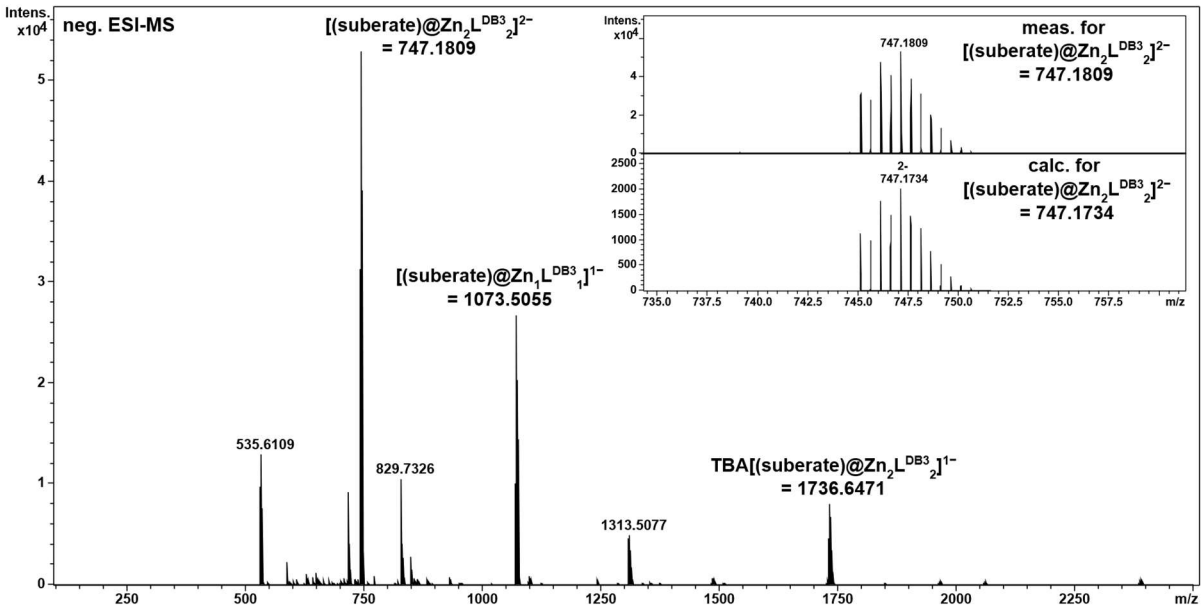

Figure 4.74: Negative HR-ESI-MS spectrum of [$Zn_2L^{DB3}{}_2$] and TBA octanedioate (ACN/DMSO 9:1, 100 μM).

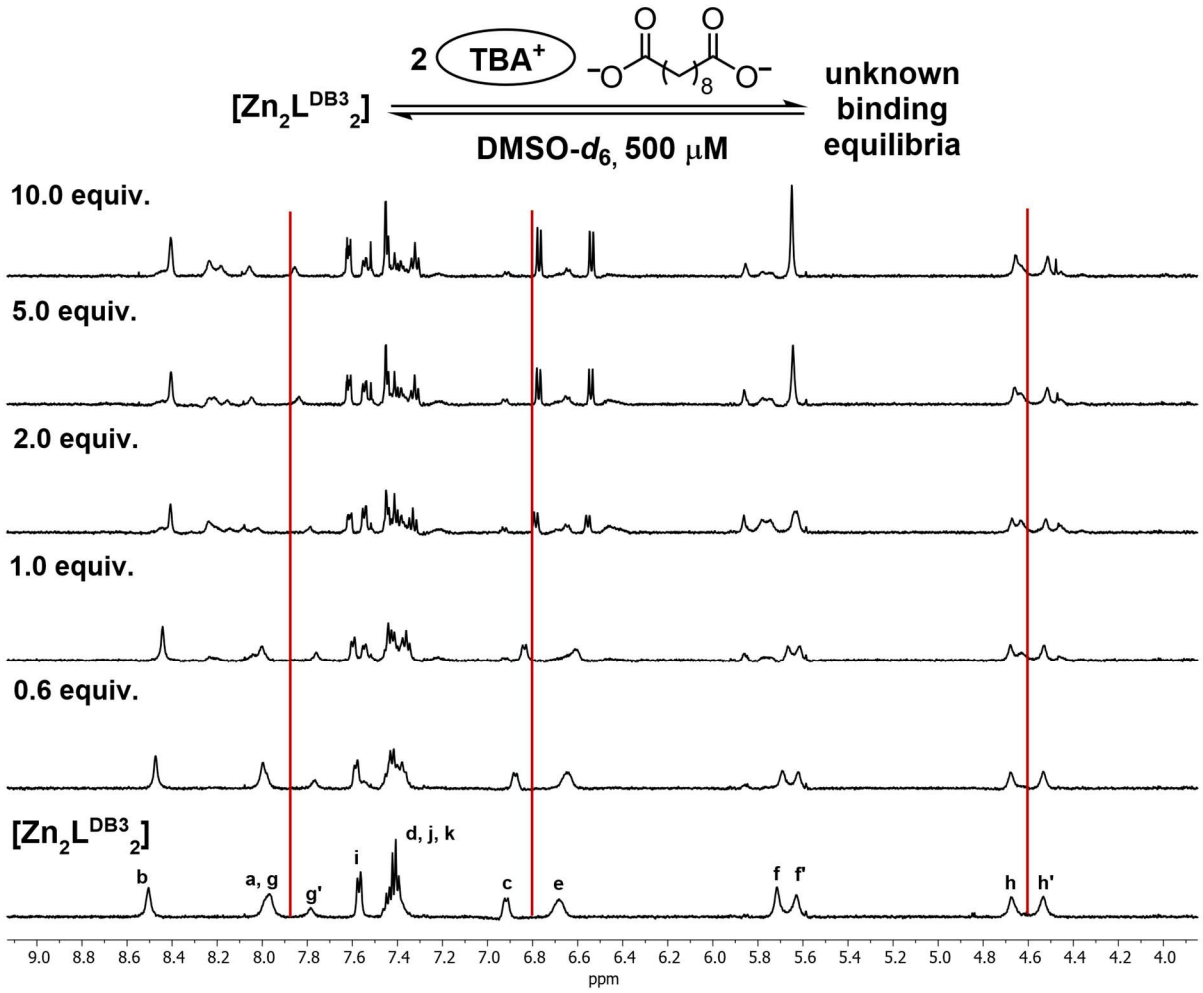

Figure 4.75: ^{1}H NMR test-titration of host [$Zn_2L^{DB3}_2$] and TBA decanedioate (DMSO-d_6, 500 MHz, 500 µM, 25°C).

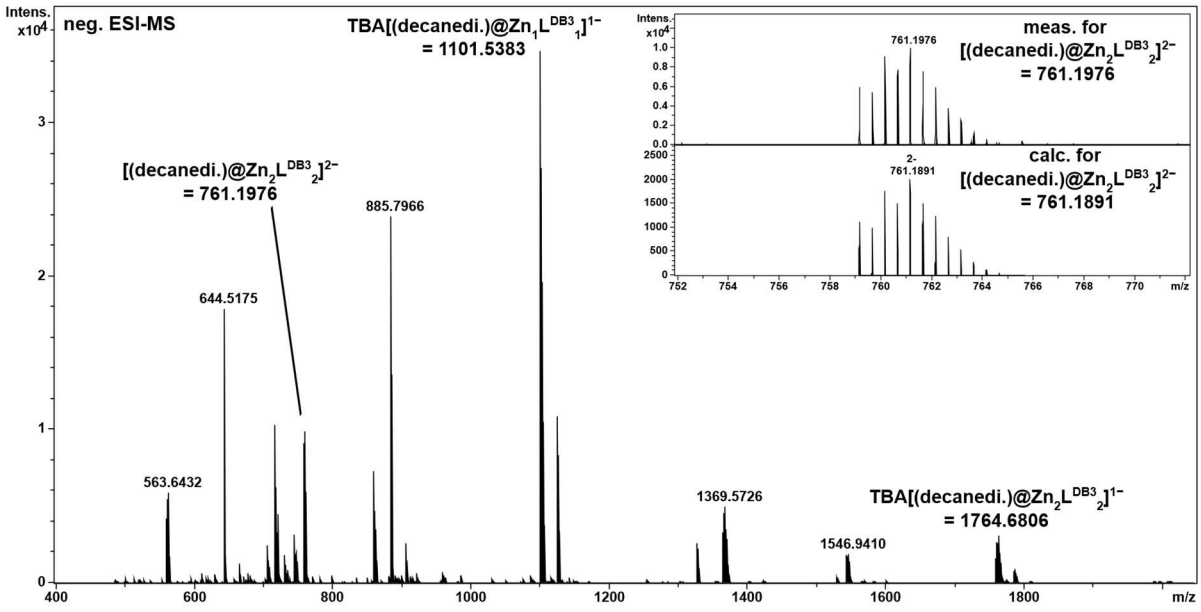

Figure 4.76: Negative HR-ESI-MS spectrum of [$Zn_2L^{DB3}_2$] and TBA decanedioate (ACN/DMSO 9 to 1, 100 µM).

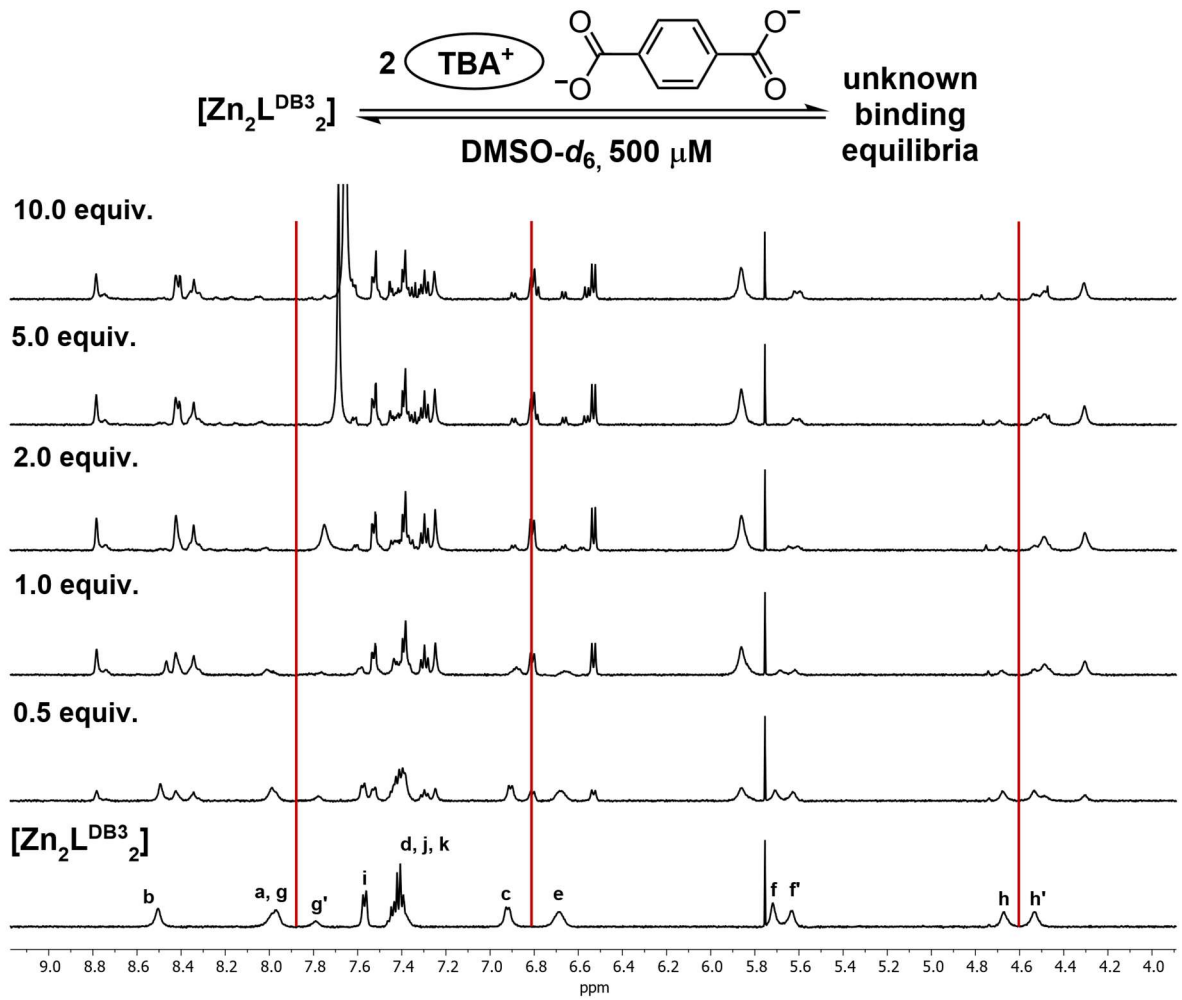

Figure 4.77: ^{1}H NMR test-titration of host [$Zn_2L^{DB3}{}_2$] and TBA_2TP (DMSO-d_6, 500 MHz, 500 µM, 25°C).

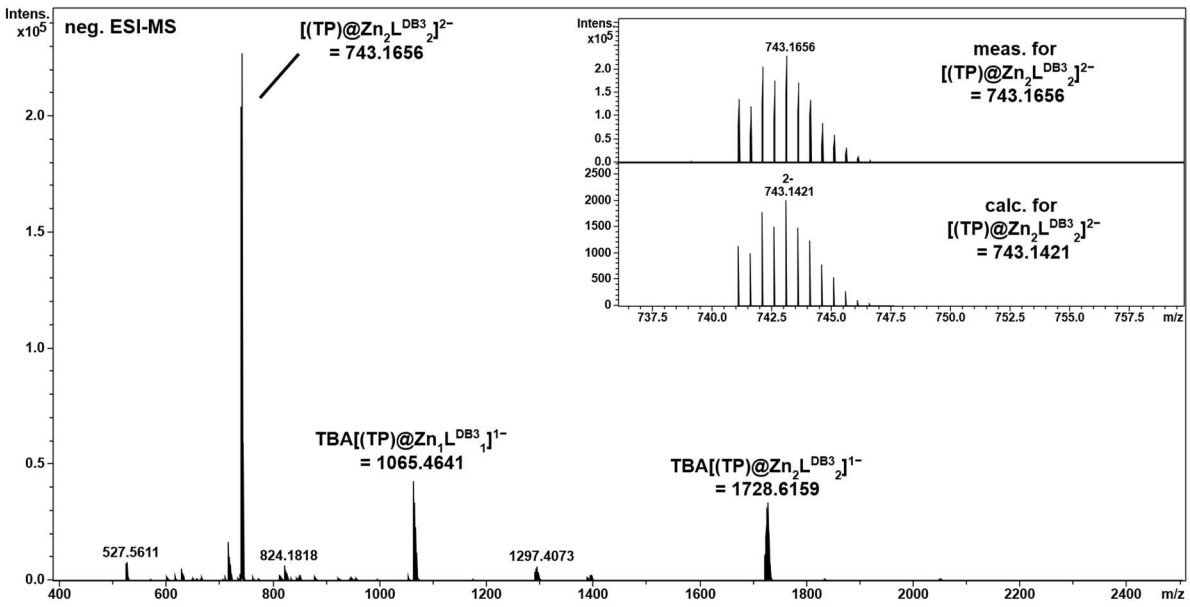

Figure 4.78: Negative HR-ESI-MS spectrum of [$Zn_2L^{DB3}{}_2$] and TBA_2TP (ACN/DMSO 9 to 1, 100 µM).

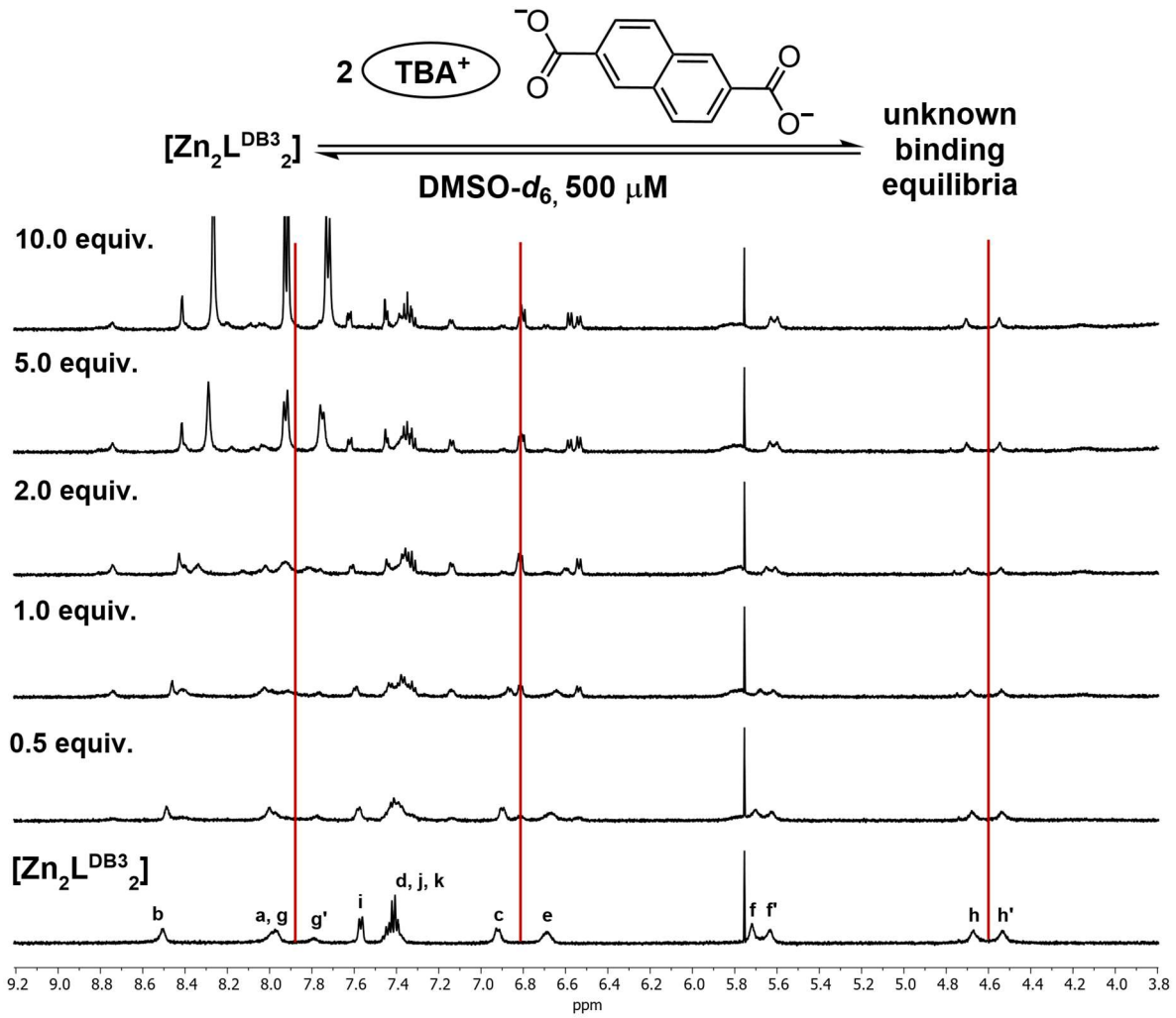

Figure 4.79: ^{1}H NMR test-titration of host $[Zn_2L^{DB3}{}_2]$ and TBA_2NP (DMSO-d_6, 500 MHz, 500 µM, 25°C).

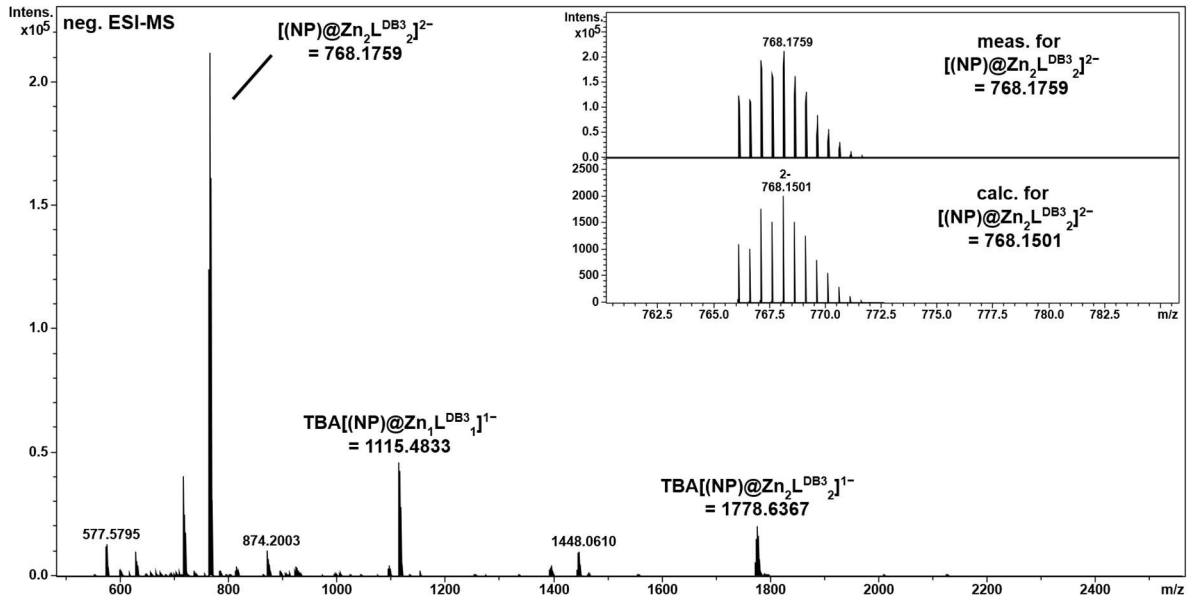

Figure 4.80: Negative HR-ESI-MS spectrum of $[Zn_2L^{DB3}{}_2]$ and TBA_2NP (ACN/DMSO 9:1, 100 µM).

4.6.7 Quantitative binding studies:

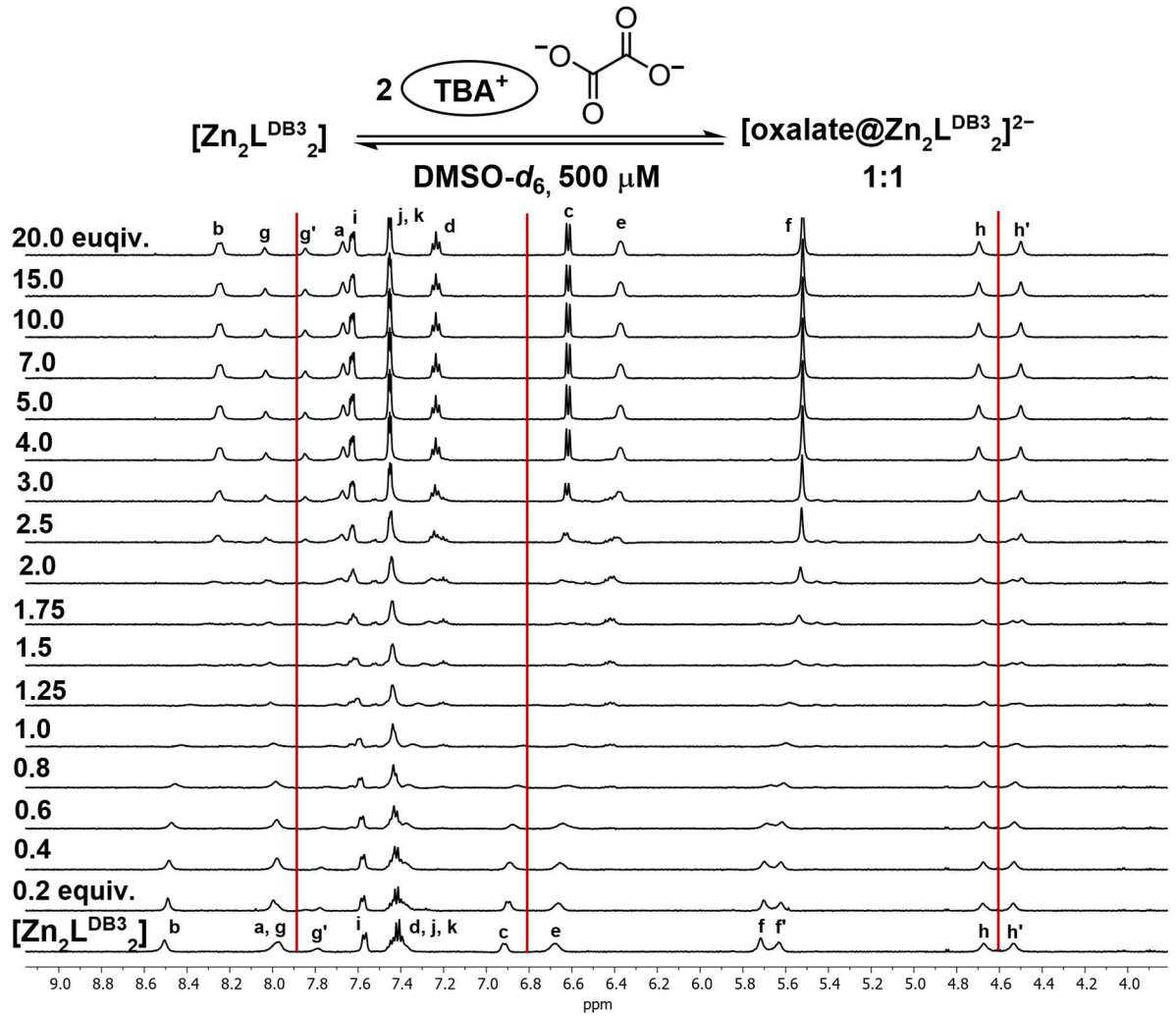

Figure 4.81: ^{1}H NMR titration of host [$Zn_2L^{DB3}{}_2$] and TBA oxalate showing intermediate binding fashion (DMSO-d_6, 500 MHz, 500 µM, 25°C).

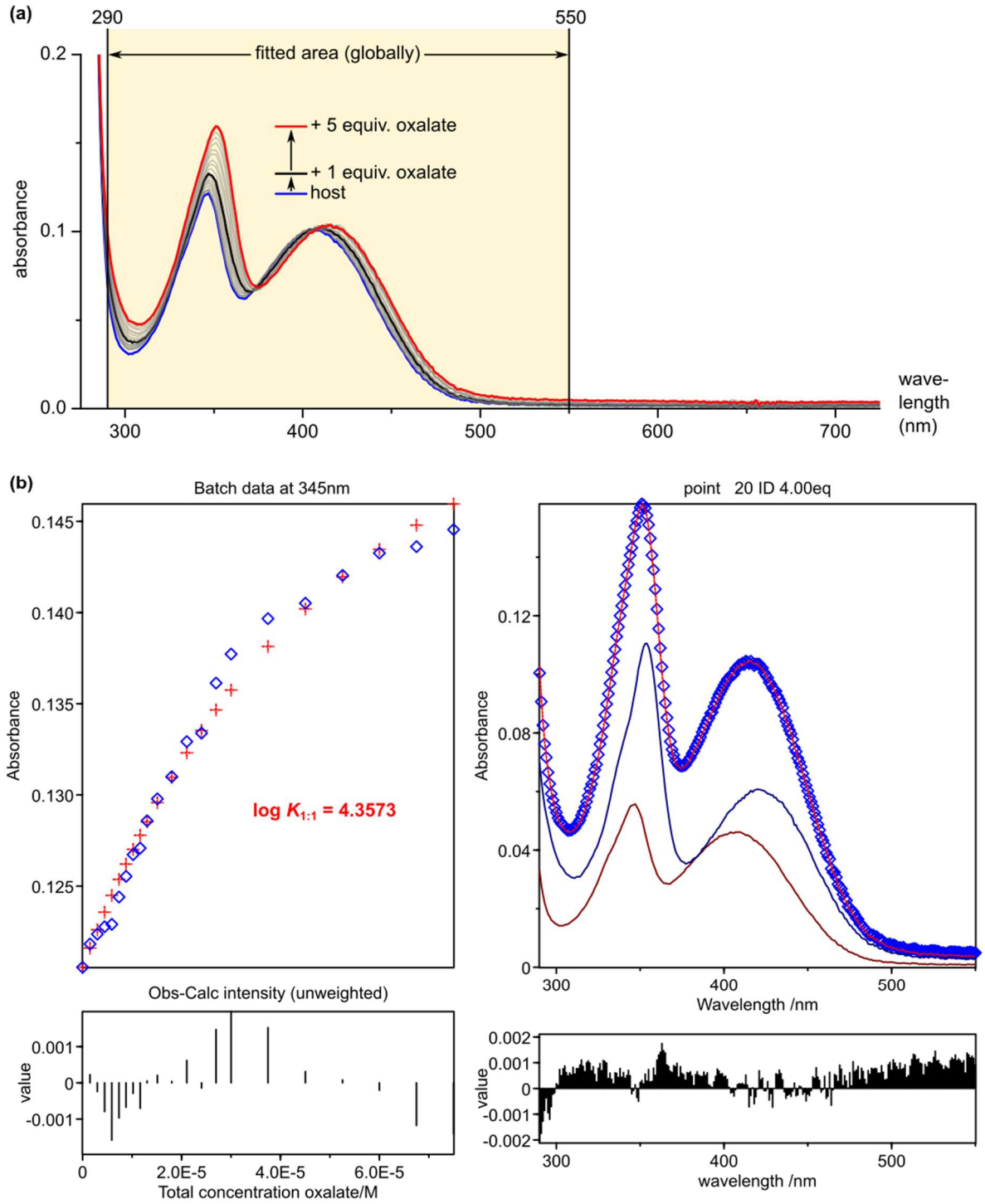

Figure 4.82: a) First UV-Vis titration (15 µM, l = 1 cm, DMSO-d_6) of [$Zn_2L^{DB3}{}_2$] with TBA oxalate. b) HypSpec2014[103] result of fitting the absorbance data in the area between 290 nm and 550 nm by applying a 1:1 binding model.

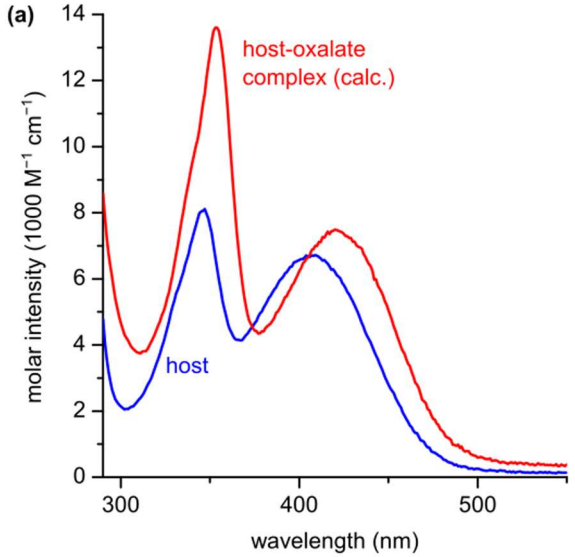

(b)

HypSpec refinement output. Version number 1.2.35

Converged in 5 iterations with sigma = 1.2198E-03

Log beta (L2Zn2)oxalate	value	standard deviation
	4.3573	0.0074

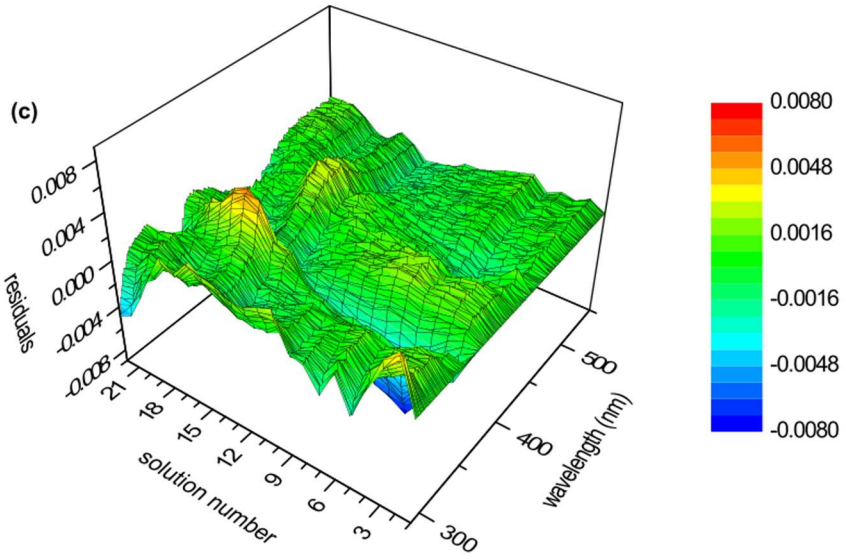

Figure 4.83: Additional information about the fitting result of the first titration shown in Figure 4.82. a) Molar intensity of the involved absorbing species. b) Information about the fitting process. c) Residual map = Difference between measured and calculated (fitted) data.

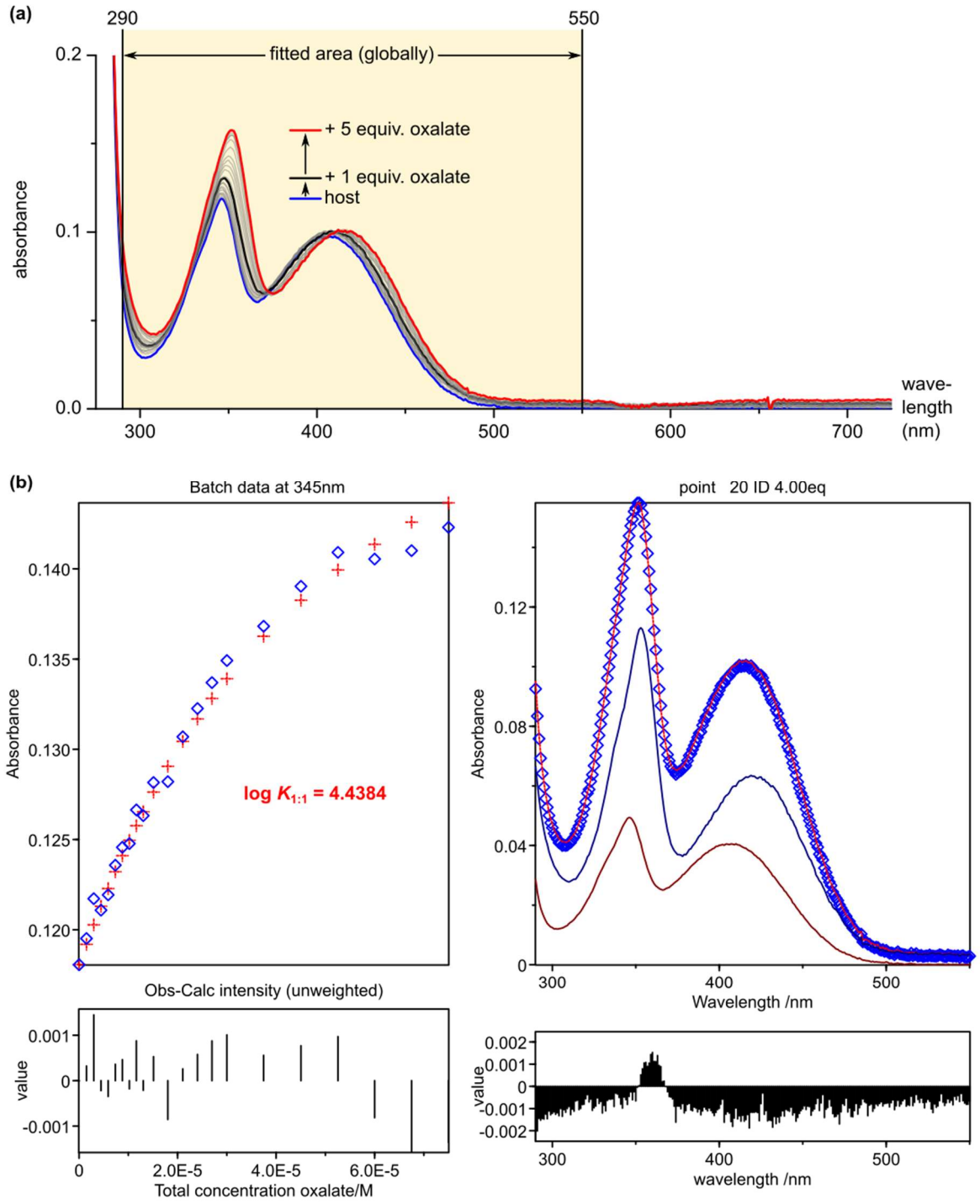

Figure 4.84: a) Second UV-Vis titration (15 µM, l = 1 cm, DMSO-d_6) of $[Zn_2L^{DB3}{}_2]$ with TBA oxalate. b) HypSpec2014[103] result of fitting the absorbance data in the area between 290 nm and 550 nm by applying a 1:1 binding model.

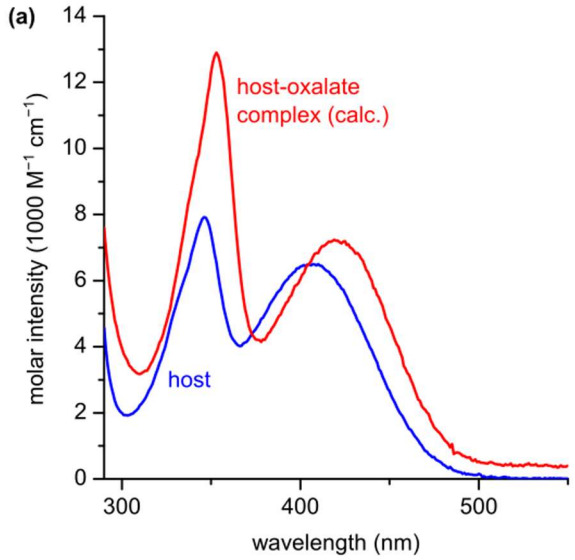

(b)

HypSpec refinement output. Version number 1.2.35

Converged in 4 iterations with sigma = 1.5707E-03

Log beta (L2Zn2)oxalate	value	standard deviation
	4.4384	0.0095

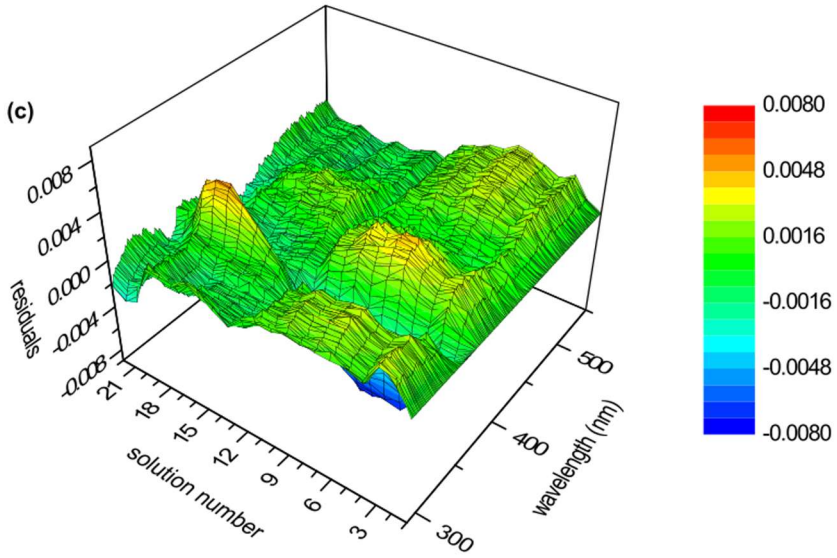

Figure 4.85: Additional information about the fitting result of the second titration shown in Figure 4.84. a) Molar intensity of the involved absorbing species. b) Information about the fitting process. c) Residual map = Difference between measured and calculated (fitted) data.

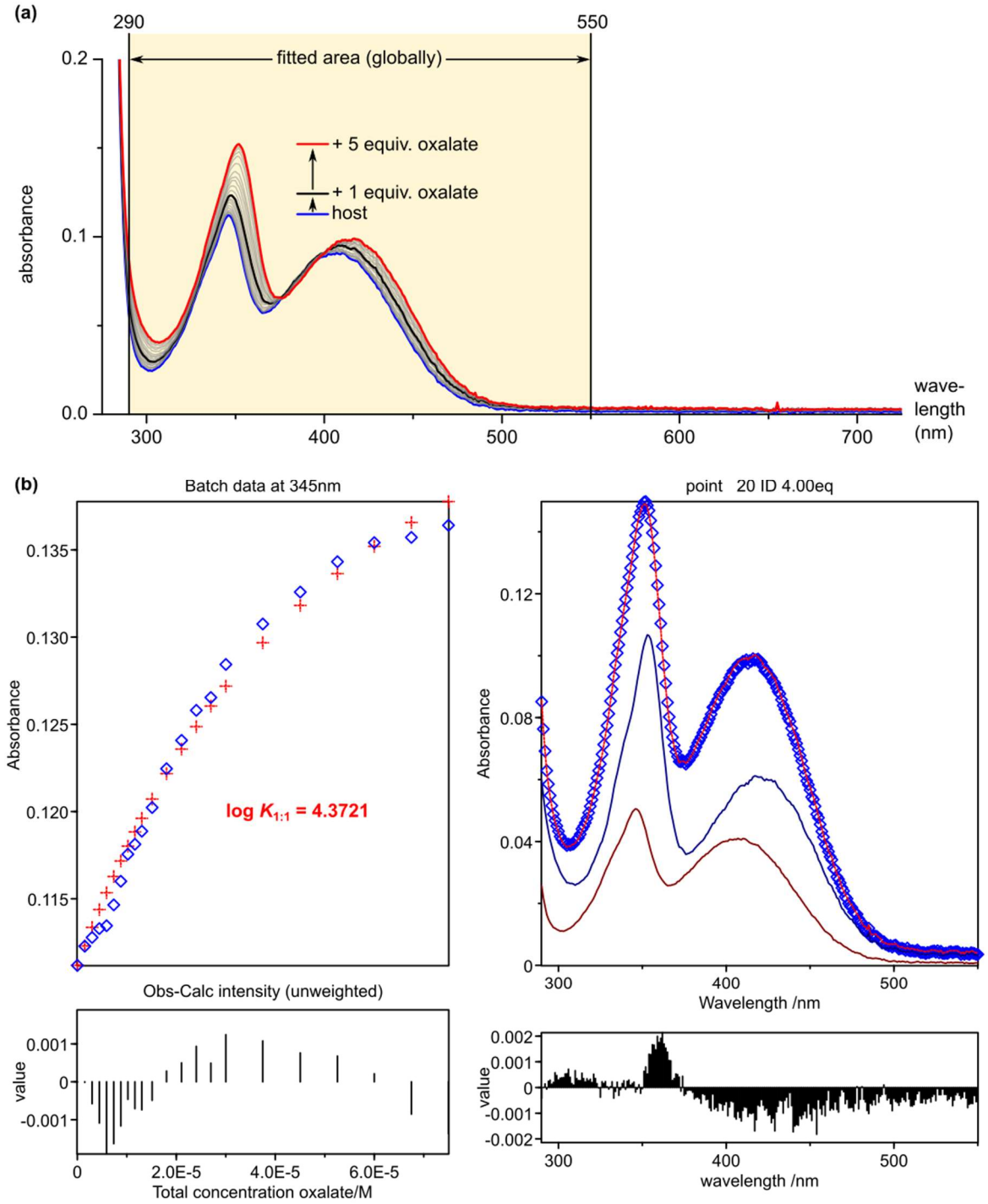

Figure 4.86: a) Third UV-Vis titration (15 µM, l = 1 cm, DMSO-d_6) of [$Zn_2L^{DB3}{}_2$] with TBA_2oxalate. b) HypSpec2014[103] result of fitting the absorbance data in the area between 290 nm and 550 nm by applying a 1:1 binding model.

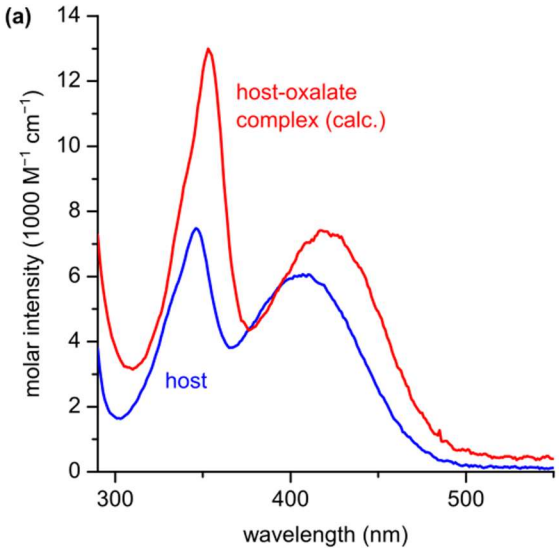

(b)

HypSpec refinement output. Version number 1.2.35

Converged in 5 iterations with sigma = 1.2073E-03

Log beta (L2Zn2)oxalate	value	standard deviation
	4.3721	0.0072

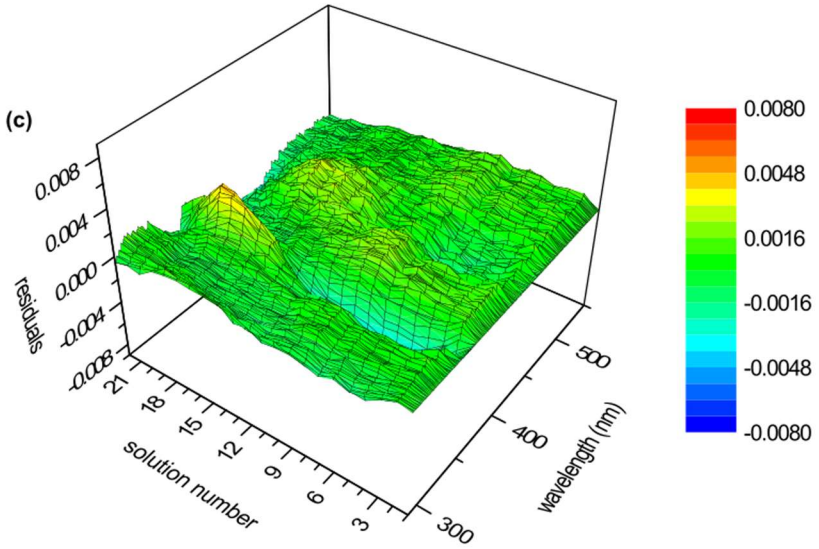

Figure 4.87: Additional information about the fitting result of the third titration shown in Figure 4.86. a) Molar intensity of the involved absorbing species. b) Information about the fitting process. c) Residual map = Difference between measured and calculated (fitted) data.

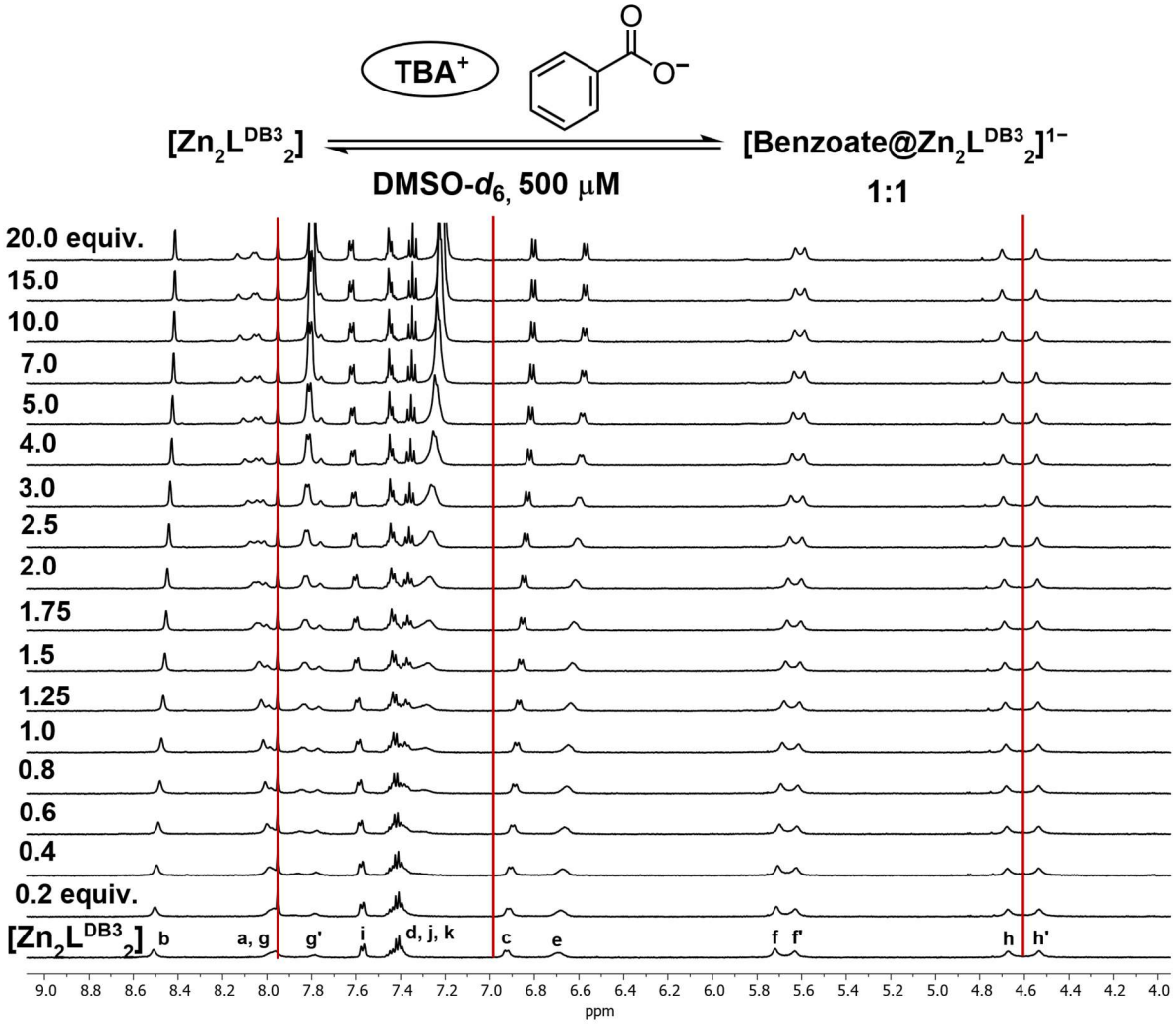

Figure 4.88: ^{1}H NMR titration of host [$Zn_2L^{DB3}_2$] and TBA benzoate showing fast binding fashion (DMSO-d_6, 500 MHz, 500 μM, 25°C).

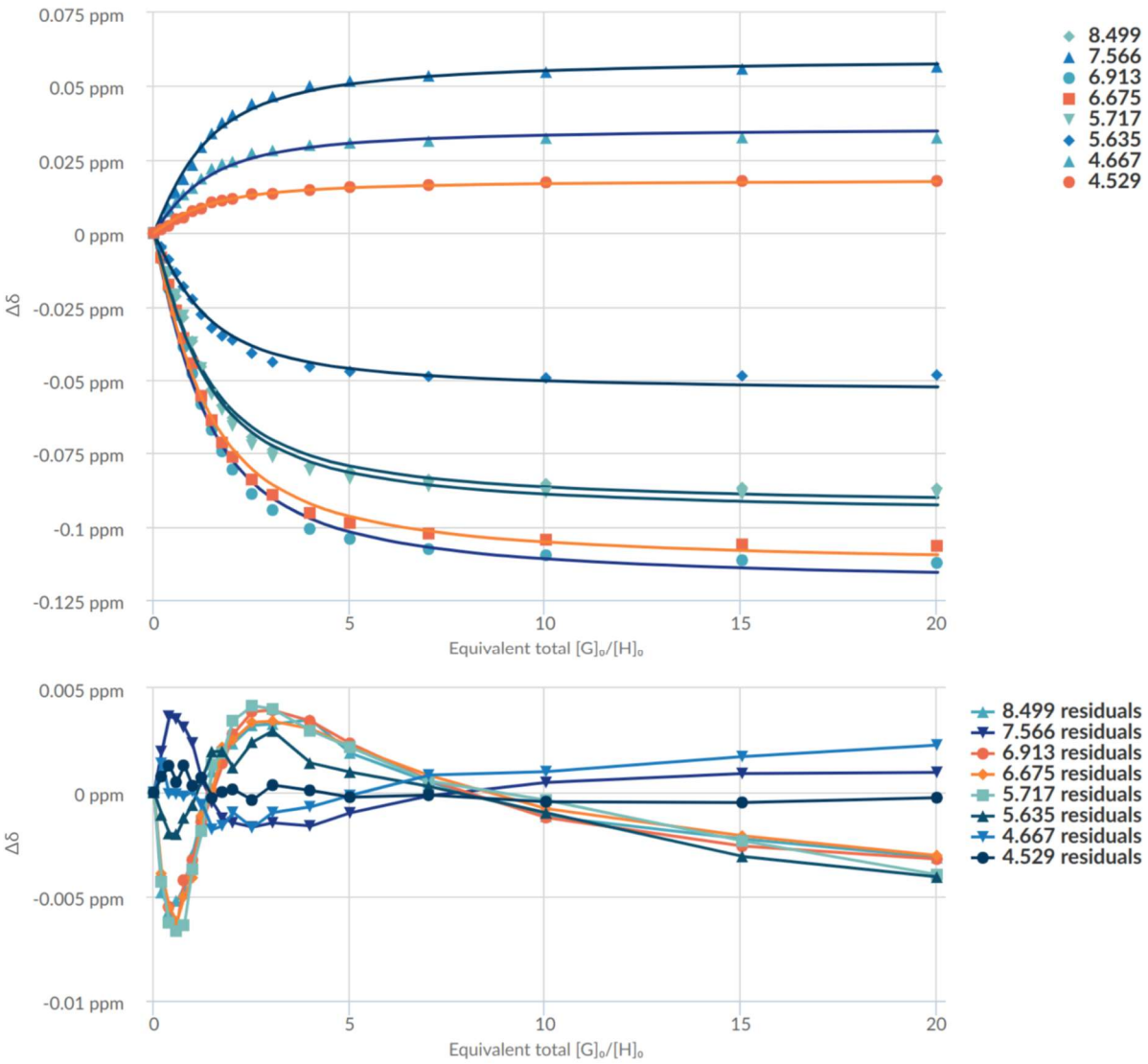

Parameter (bounds)	Optimised	Error	Initial
K (0 → ∞)	1337.73 M^{-1}	± 3.8996 %	100.00 M^{-1}

Figure 4.89: Analysis of the titration data from Figure 4.88 and determination of the binding constant of benzoate with BindFit[91,85]. The lack of inflection points is an indication for the formation of a 1:1 host–guest complex.

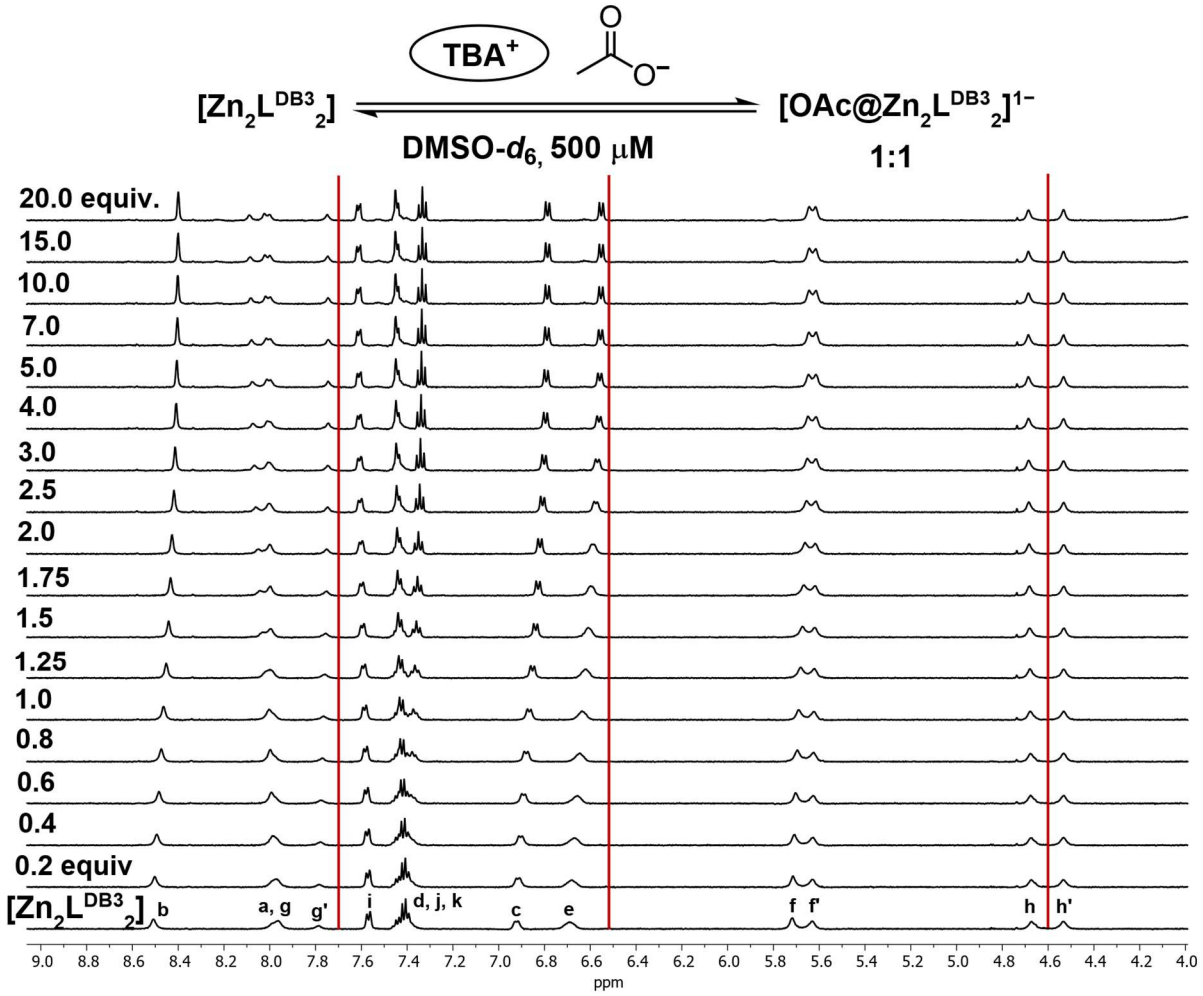

Figure 4.90: ^{1}H NMR titration of host $[Zn_2L^{DB3}{}_2]$ and TBA acetate showing fast binding fashion (DMSO-d_6, 500 MHz, 500 µM, 25°C).

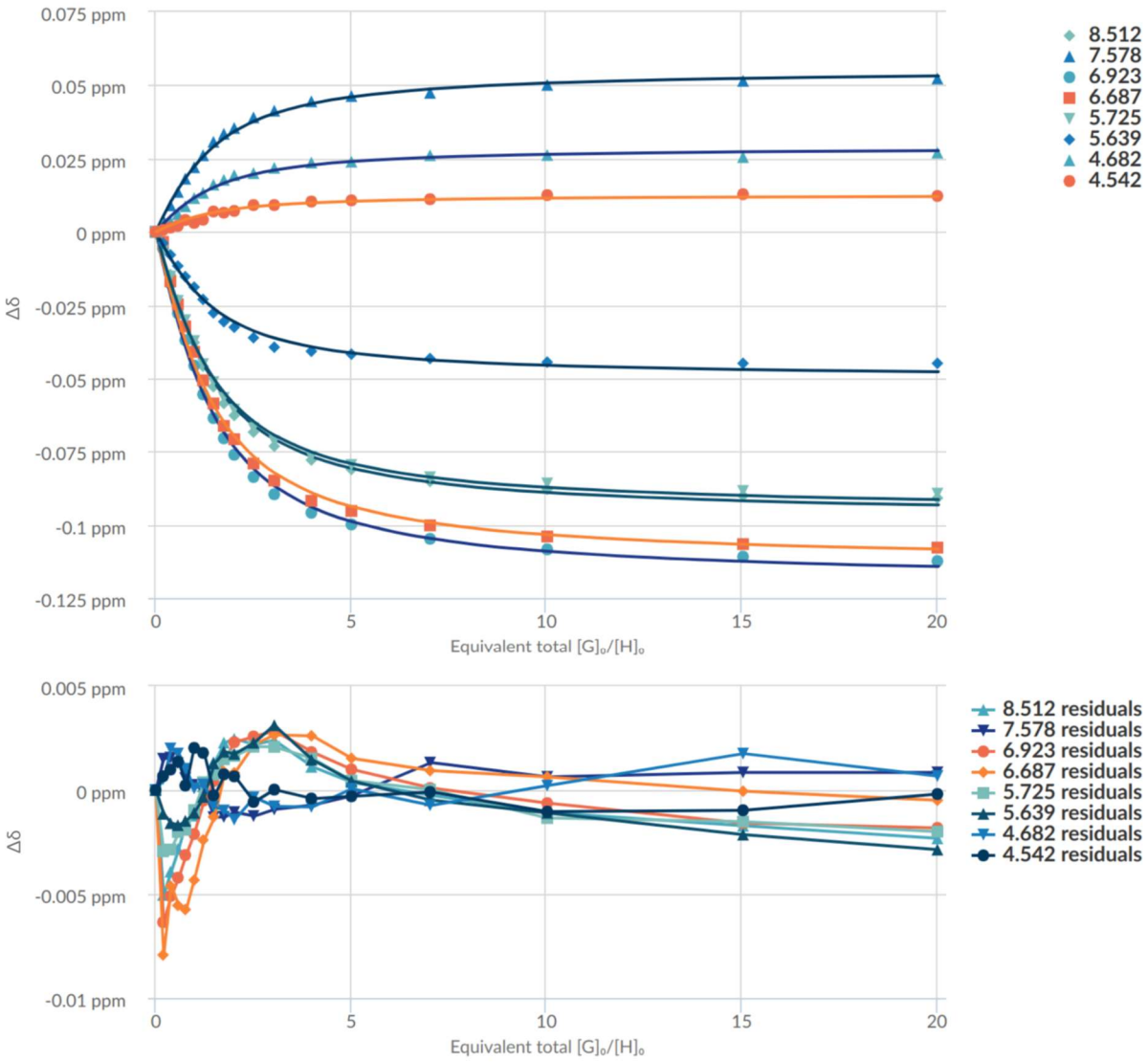

Parameter (bounds)	Optimised	Error	Initial
K (0 → ∞)	2304.49 M^{-1}	± 2.9269 %	100.00 M^{-1}

Figure 4.91: Analysis of the titration data from Figure 4.90 and determination of the binding constant of acetate with BindFit[91,85]. The lack of inflection points is an indication for the formation of a 1:1 host–guest complex.

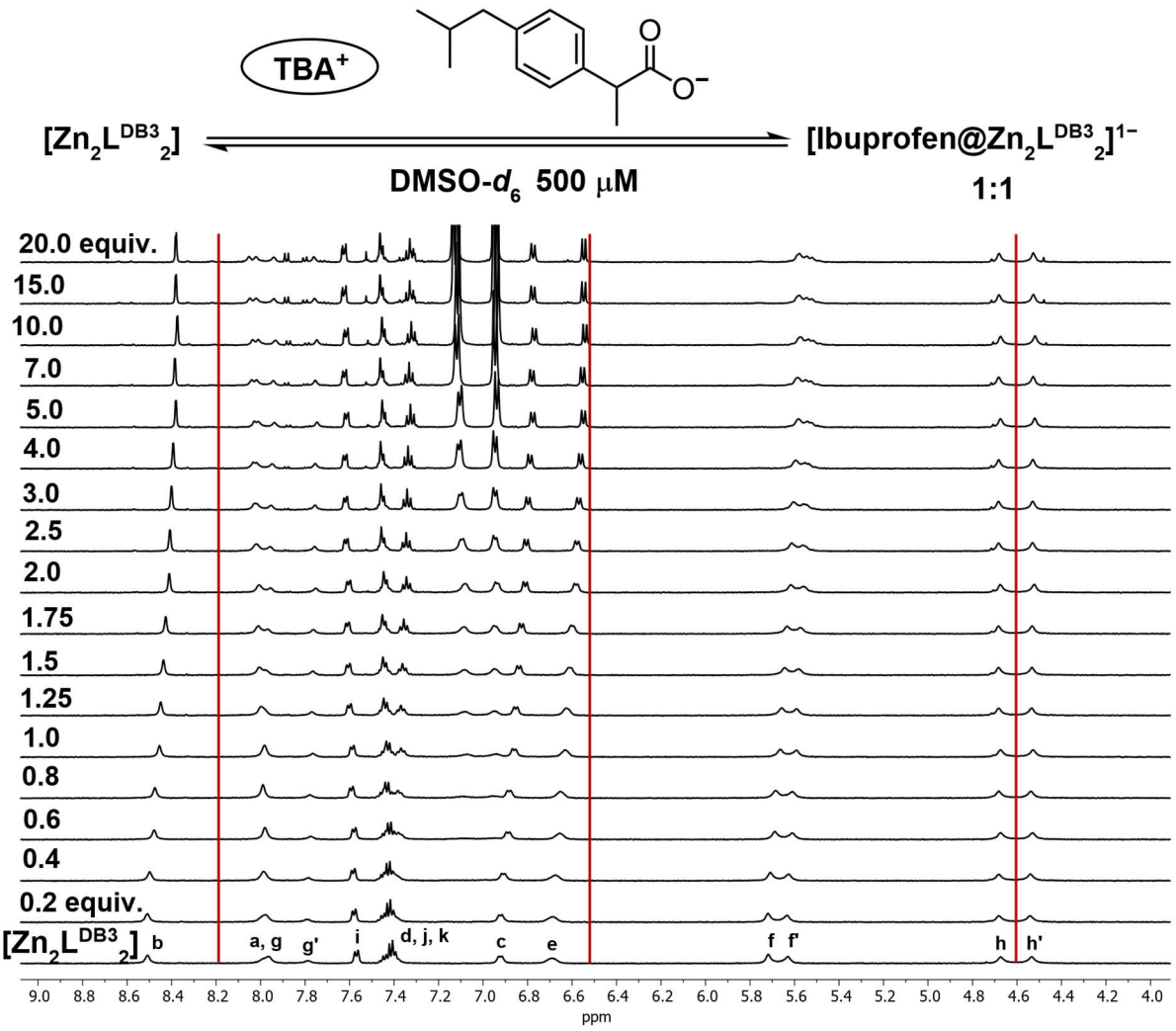

Figure 4.92: ^{1}H NMR titration of host [$Zn_2L^{DB3}_2$] and TBA ibuprofen showing fast binding fashion (DMSO-d_6, 500 MHz, 500 µM, 25°C).

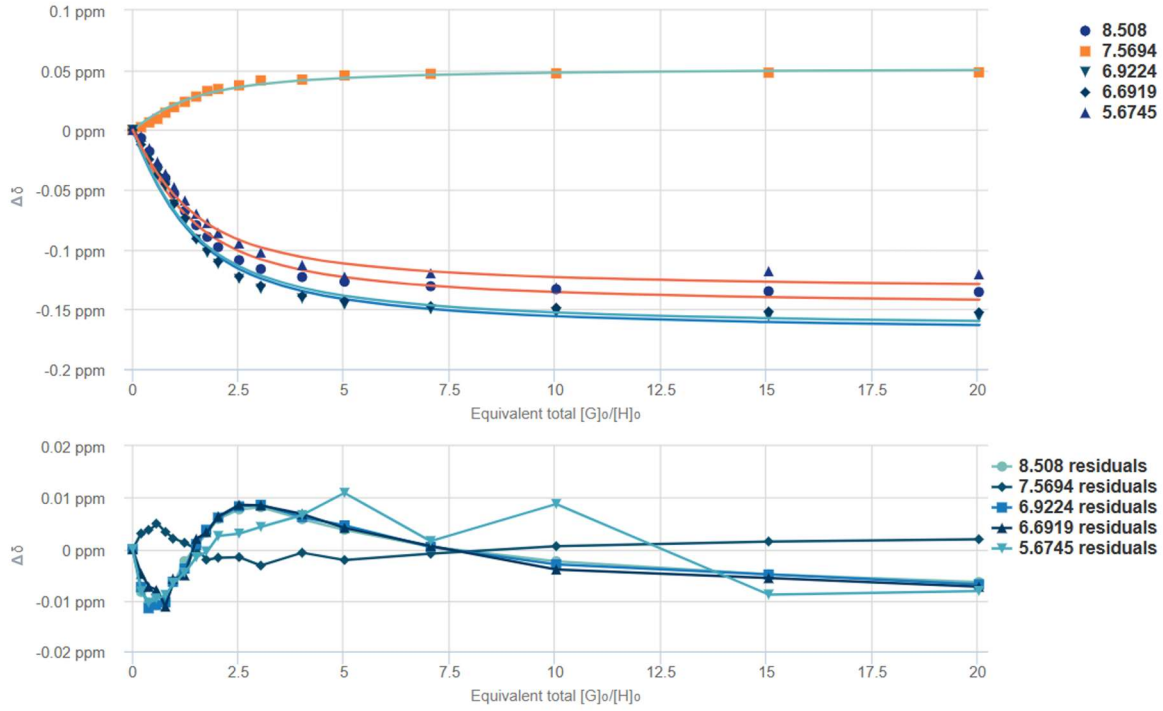

Parameter (bounds)	Optimised	Error	Initial
K (0 → ∞)	2347.05 M^{-1}	± 5.7944 %	100.00 M^{-1}

Figure 4.93: Analysis of the titration data from Figure 4.92 and determination of the binding constant of ibuprofen-anion with BindFit[91,85]. The lack of inflection points is an indication for the formation of a 1:1 host-guest complex.

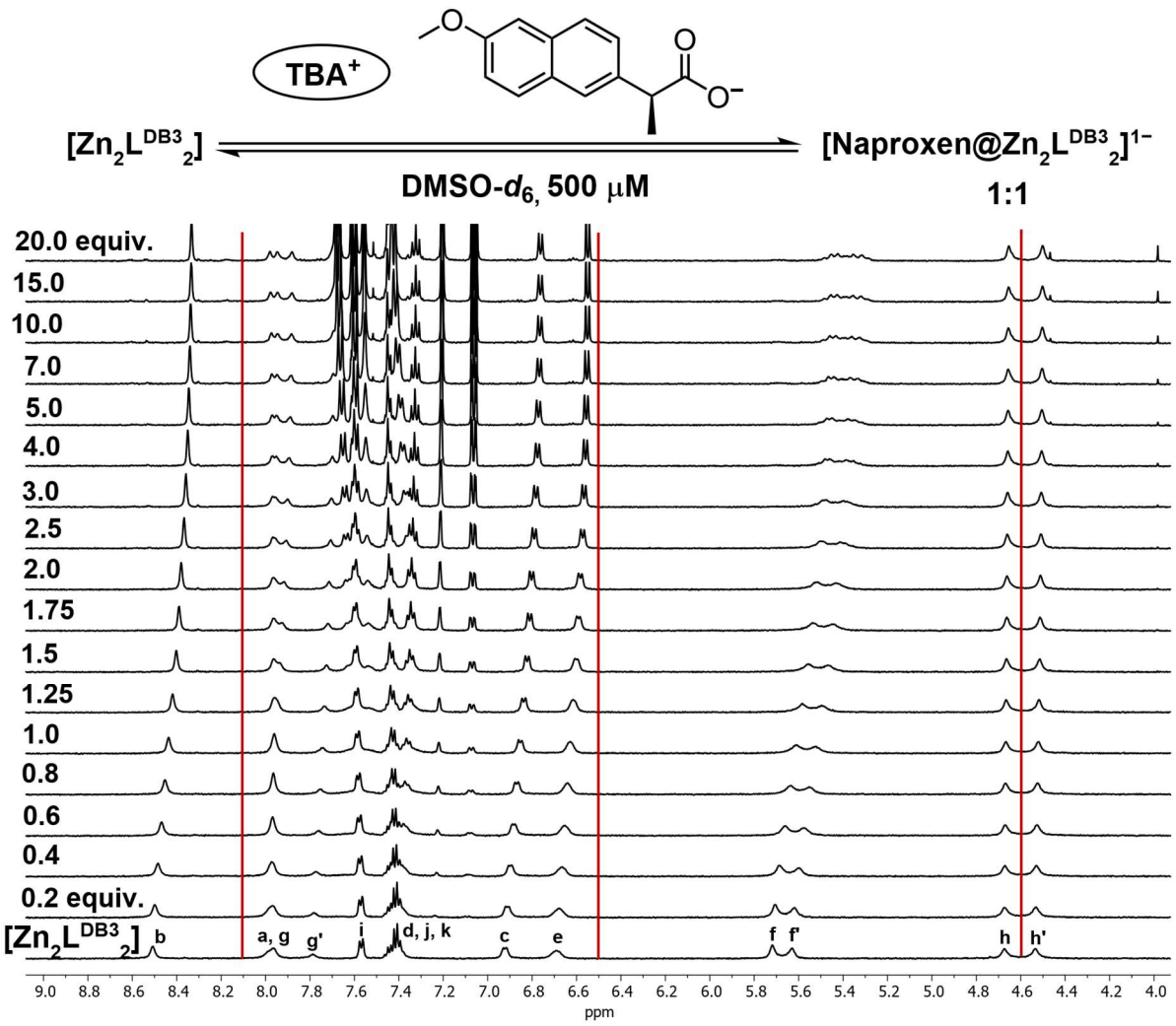

Figure 4.94: ^{1}H NMR titration of host [$Zn_2L^{DB3}_2$] and TBA naproxen showing fast binding fashion (DMSO-d_6, 500 MHz, 500 µM, 25°C).

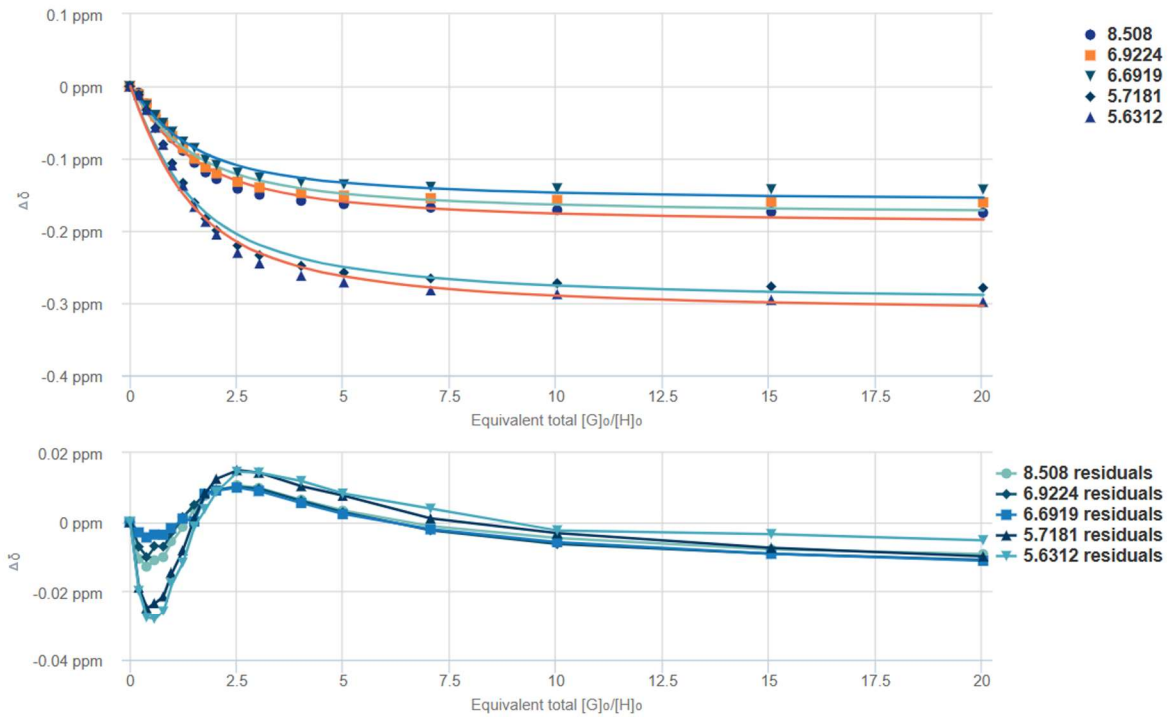

Parameter (bounds)	Optimised	Error	Initial
K (0 → ∞)	2312.02 M^{-1}	± 5.5792 %	100.00 M^{-1}

Figure 4.95: Analysis of the titration data from Figure 4.94 and determination of the binding constant of naproxen-anion with BindFit[91,85]. The lack of inflection points is an indication for the formation of a 1:1 host-guest complex.

4.6.8 Computational Studies - DFT calculations

The following relevant information was used in the input file's header for geometry optimization at the ωB97X-D4[104]/def2-SVP[97,96] level of theory in DMSO (CPCM solvent model applied)[105] with ORCA 5.0.3[99,98]:

wB97X-D4 def2-SVP Opt SlowConv CPCM(DMSO)

%scf autoTRAH false end

%geom trust -0.1 end

XYZ data for the optimized structure of **[(oxalate)@$Zn_2L^{DB3}{}_2$]$^{2-}$** (148 atoms):

Zn -0.93367875677014 -0.58884770834741 2.39795959006068
Zn -0.06926467533533 0.62419665728443 -2.94789640248994
N -4.52067877950102 -3.73008890077641 -3.50707552074735
C -3.31798389779962 -4.28340071235272 -3.77495993786396
C -3.49799612730424 -5.62861413700259 -3.50518717502345
N -4.78661222823198 -5.80211216825522 -3.11197331725856
N -5.39210093935631 -4.65589643469184 -3.11469070600186
H -2.46162073319020 -3.70736848470541 -4.11536244351257
C -2.49397132616693 -6.74913154794813 -3.48502987162263
N -1.58862726438806 -6.67665104074622 -2.33013925232568
C -2.08876925128409 -7.21040816019347 -1.06485430637347
C -3.19775091501647 -6.38662425809139 -0.47404505162618
N -4.36467319371413 -6.93531136152493 -0.04774085017641
N -5.18092731008885 -5.98806427774355 0.29837294259576
N -4.56539090662876 -4.82573049697387 0.10203882944245
C -3.31315710743704 -5.01606143840465 -0.37045933740940
H -2.63592222426217 -4.20526311941864 -0.62492520888366
H -1.91350962034339 -6.75598610715602 -4.41298142848800
H -3.03530657874238 -7.70344062187541 -3.42834895445985
H -2.47303166362516 -8.22594984487071 -1.23902428283927
H -1.23862351522437 -7.27598174641636 -0.37346882393036
H -5.05206390711395 -0.93960334004970 -5.89938454791848
C -4.19195389430248 -0.67656067096353 -5.27493712434560
N -2.03519530519126 0.01339250941656 -3.67613930726644
C -3.96557797527162 -1.34575586546023 -4.09329683968309
C -3.35188867938956 0.39878348575177 -5.67719898123670
C -2.28973268454727 0.73432434429129 -4.80259956673827
C -2.82519362398606 -0.97388360277483 -3.32493474265028
C -3.56231172579797 1.15920812541033 -6.85877217030538
C -2.72937621778813 2.23403571587371 -7.10709824874111
C -1.69157650691337 2.60454274525236 -6.22518167476875
C -1.43501749159473 1.89124503325220 -5.04233020108132
H -1.06622580357468 3.47528246680972 -6.44464951673436
H -4.37732646986262 0.89325053517625 -7.53672624621493
H -2.88161541715874 2.83155045874358 -8.01264500838603
O -0.53124768273885 2.20903762817837 -4.18137535720043
H -2.57568968369662 -1.50606691364277 -2.39900223023329
C -4.97718675355251 -2.33756677472181 -3.57677854849500
H -5.86927921532921 -2.32260210377753 -4.21672288943439
H -5.28875429668059 -2.04681794573864 -2.56278199112074

C -0.56648608497969 -5.76757420518890 -2.25906977798874
O -0.13444062548883 -5.35752137770502 -1.18668326953503
C 0.04285382201172 -5.29898402476413 -3.55124811401517
C 1.24983680244517 -4.36841478045253 -5.89285529461487
C 0.25155599116914 -3.92758738613271 -3.73513323344282
C 0.47235645586548 -6.20696190536171 -4.52742075801221
C 1.08352519826497 -5.74179131112606 -5.69256054048437
C 0.83241230721375 -3.46020989391899 -4.91610554304503
H -0.04393897327654 -3.21892517012178 -2.95479950681239
H 0.33531582472376 -7.28112870920824 -4.37162799557041
H 1.42656719264085 -6.45465512203522 -6.44806033286389
H 0.94502991588175 -2.38011319517458 -5.05320413407721
H 1.71303654624980 -4.00352344380824 -6.81484381293666
H -6.40953779561769 -2.97653687635630 2.72592580631228
C -5.43690945822603 -2.49763895803003 2.57081141551916
N -2.96862908801822 -1.29323692475654 2.17961091354218
C -4.73842189307452 -2.70870983115492 1.40394851253666
C -4.91626141798023 -1.64205875429601 3.58241890266455
C -3.65084992805393 -1.05742130089168 3.33137906759340
C -3.48166056703157 -2.06269123809089 1.25110780345751
C -5.59658667494971 -1.34860571042920 4.79552573241706
C -4.99861653931311 -0.48713417323866 5.69571656470541
C -3.73952243371219 0.10656296292474 5.45534667281731
C -3.01618100872720 -0.15386605148077 4.28075610379829
H -3.30099295240911 0.78241443350841 6.19601403817566
H -6.57295571744910 -1.79893877440009 4.99232459318002
H -5.51557712871085 -0.25092079706744 6.63221933459017
O -1.86790530977329 0.36167805849456 3.99773772677239
H -2.89009526525607 -2.18822344942323 0.33862941824836
C -5.29094313144698 -3.57191482413796 0.29578862479690
H -6.32831758755653 -3.85727046517375 0.50742889055152
H -5.27342711749114 -3.02806194192028 -0.65830488878342
C -0.68251631825129 0.76418706924993 -0.13304328717381
C -0.32029268764360 -0.72928100271923 -0.41699671693469
O -0.98298532371240 1.05556322945429 1.04833637438270
O -0.01927125881791 -1.02061464449044 -1.59823040676662
O -0.62584921444128 1.55436192870161 -1.10130381512491
O -0.37754864582235 -1.51953544180416 0.55118010722422
N 3.56350675201979 4.86234840536794 -0.64975219847575
C 2.31121317185744 5.05409492984201 -0.17807096077325
C 2.19780835162494 6.42473502752452 -0.07324702343849
N 3.36547367764294 6.97212462491069 -0.49920075359840
N 4.18071973927615 6.02394989046345 -0.84517887539743
H 1.63259734208133 4.24411030012083 0.07535837618212
C 1.08969074907056 7.24948919308567 0.51783059545165
N 0.58819757310111 6.71481345031636 1.78219541707440
C 1.49282956099181 6.78514379988421 2.93775475738630
C 2.49622205808843 5.66403627967495 2.95723995892337
N 3.78529139796376 5.83745387262913 2.56546046817541
N 4.39028894727866 4.69097137092850 2.56732609977253
N 3.51817046254612 3.76513813753266 2.95807725913780
C 2.31554448065607 4.31867507583369 3.22575431033204

H 1.45869911113864 3.74261771056175 3.56486304376901
H 0.24002336178650 7.31704468624373 -0.17396536152409
H 1.47525756032396 8.26428218928484 0.69345999630463
H 2.03479936533633 7.73918996161840 2.88268366919910
H 0.91168093131114 6.79118559838556 3.86529847784876
H 5.40634097480985 3.01427005539017 -3.27367545508959
C 4.43390520265713 2.53494312498283 -3.11868565663779
N 1.96604694576111 1.32945068728304 -2.72772647775311
C 3.73565531053956 2.74485016833085 -1.95148168095806
C 3.91324040914483 1.67996390436120 -4.13079307627370
C 2.64809621257365 1.09470681743284 -3.87983627504628
C 2.47913851935650 2.09831614893780 -1.79879486759208
C 4.59327091728685 1.38778030065189 -5.34438043138709
C 3.99523375184634 0.52705269991340 -6.24521235493986
C 2.73645179323474 -0.06735849389745 -6.00488779171646
C 2.01353193913805 0.19170022646033 -4.82977827243772
H 2.29776460943134 -0.74247803795826 -6.74612646042036
H 5.56933657043331 1.83876765489968 -5.54118572165942
H 4.51204219513420 0.29168898158884 -7.18201073152806
O 0.86548332300867 -0.32453326298306 -4.54683664837855
H 1.88780018821996 2.22315456583550 -0.88602807410948
C 4.28785780813109 3.60753925957228 -0.84276354602803
H 5.32584585504631 3.89170208337183 -1.05298023237591
H 4.26830632684831 3.06382611258728 0.11136713074906
C -0.43451359101835 5.80651777599450 1.70926104408458
O -0.86680320579932 5.39894963088528 0.63603764247203
C -1.04548119938129 5.33729685372655 3.00043087728880
C -2.25427870513656 4.40571916982114 5.34067870293969
C -1.25391788707293 3.96578743126551 3.18374768743240
C -1.47578653539316 6.24487584820454 3.97660856505844
C -2.08784710879208 5.77919230846125 5.14108075210532
C -1.83564842837869 3.49789344608187 4.36409912600263
H -0.95704804957329 3.25738155885302 2.40370989310947
H -1.33785025083110 7.31906310385291 3.82169012513271
H -2.43196078611992 6.49175096884422 5.89638053671408
H -1.94778852214029 2.41769015980090 4.50091648438515
H -2.71810971460513 4.04042987684873 6.26219441642064
H 4.04850828173065 0.97522237906827 5.34968046122017
C 3.18844308778426 0.71203938172242 4.72523211179342
N 1.03166259266578 0.02187264300300 3.12649493874829
C 2.96225429216649 1.38082262347403 3.54332532535173
C 2.34807260252940 -0.36291901934668 5.12787190129975
C 1.28596609627102 -0.69860000485486 4.25329681303611
C 1.82189771847516 1.00885210613240 2.77495886367758
C 2.55803813239885 -1.12280900888736 6.30987797667509
C 1.72497033339156 -2.19748459025095 6.55840436618104
C 0.68736091555407 -2.56827508766427 5.67637541915891
C 0.43108729779701 -1.85533057254182 4.49326443727757
H 0.06192952959273 -3.43891896154592 5.89599968248713
H 3.37287705579734 -0.85662400878842 6.98795336331831
H 1.87686425271880 -2.79458357618981 7.46428244376339
O -0.47253777549419 -2.17324230677809 3.63220657922956

H 1.57291952778093 1.54049464837625 1.84855623606059
C 3.97393438075058 2.37231964561978 3.02639471901246
H 4.86664519753088 2.35655712463409 3.66544608467956
H 4.28429045776948 2.08189103291721 2.01193231750125

4.6.9 Molecular Dynamics Simulations

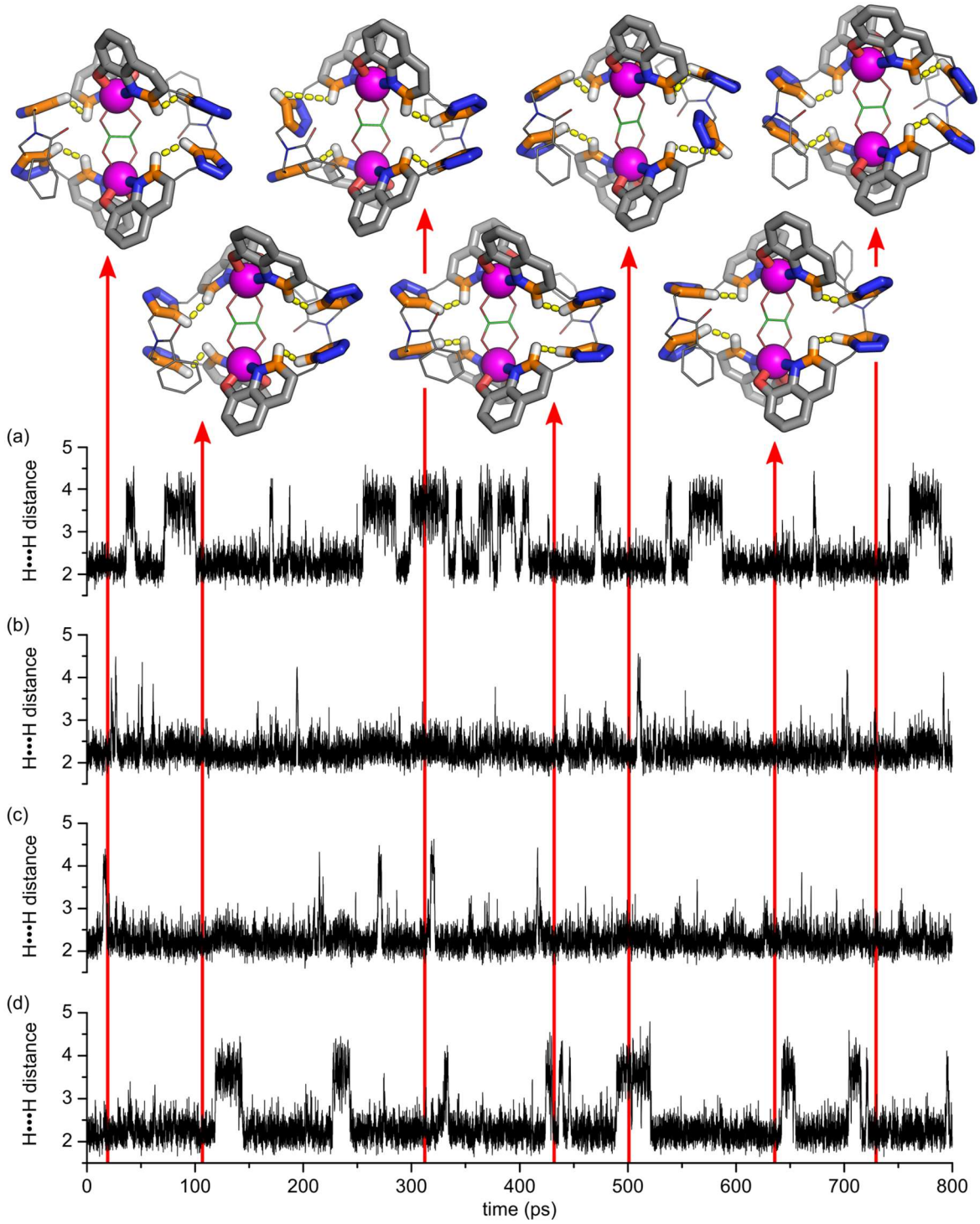

Figure 4.96: Distance between the triazole proton and the proton in 2-position of the quinolate unit, for all four contacts marked with yellow dashes (a: up left, b: up right, c: down left, and d: down right). Seven snapshots elucidate the possible triazole rotations which take place at 25°C (xTB 6.6.0[106,107], see relevant information regarding the set-up on the next page).

The following command line was used to start the MD simulation with a prior geometry optimization (below with "...." as placeholder for the file names):
xtb "input-file".xyz --chrg -2 --cosmo dmso --omd --input "control-file".ctrl --parallel 20 > "output-file".out
The control file contained the following information about the simulation time (800 ps) and the applied constraints for the hydroxyquinolate-zinc coordination bonds (oxalate-zinc coordination bonds were not constrained):

```
$md
time=800
$end
$constrain
atoms: 1, 56
atoms: 1, 68
atoms: 1, 132
atoms: 1, 144
atoms: 2, 24
atoms: 2, 36
atoms: 2, 100
atoms: 2, 112
                $end
```

5 Guest-templated formation of tri- and hexanuclear Zn(II)-based host-guest complexes and guest induced transformation

5.1 Introduction

The supramolecular hosts presented in chapter 1 and 2 displayed charge-neutral metal organic cages with rather open cavity windows. To explore the horizon of the design principles used in chapter 2 and to control the self-assembly of charge-neutral metal organic architectures with higher nuclearity and confinement, the idea of using tripropargyl amine suggested itself very clearly. By simply adding a further methylene linked terminal alkyne, a tripodal bis-bidentate ligand L^{TP3}-H_3 could be synthesized within two steps. Not taking the five steps-synthesis of the hydroxyquinolate unit into account. The commercially available tripropargyl amine was supposed to be clicked with the hydroxyquinoline, deprotected and then it was aimed to self-assemble into charge-neutral [Zn_3L_2] complexes with a cavity, capable of using its LEWIS acidic Zn(II) centers and the free electron pairs of the two central tertiary amines in the backbone as recognition units.

5.2 Synthesis of ligand L^{TP3}-H_3 and self-assembly

The synthesis of ligand L^{TP3}-H_3 began with the preparation of the coordination unit. The synthesis of the Boc-protected 8-hydroxyquinolate-coordination unit was described in detail in chapter 1 (Figure 3.2). The 1,3-dipolar azide-alkyne HUISGEN cycloaddition a) of tripropargyl amine and the hydroxyquinolate with the following acidic Boc-deprotection b) (Figure 5.1) gave ligand L^{TP3}-H_3 as white powder in a moderate yield of 57%. Full characterization of the tripodal ligand L^{TP3}-H_3 and synthetic protocols are given in the experimental part associated with this chapter (Chapter 5.6).

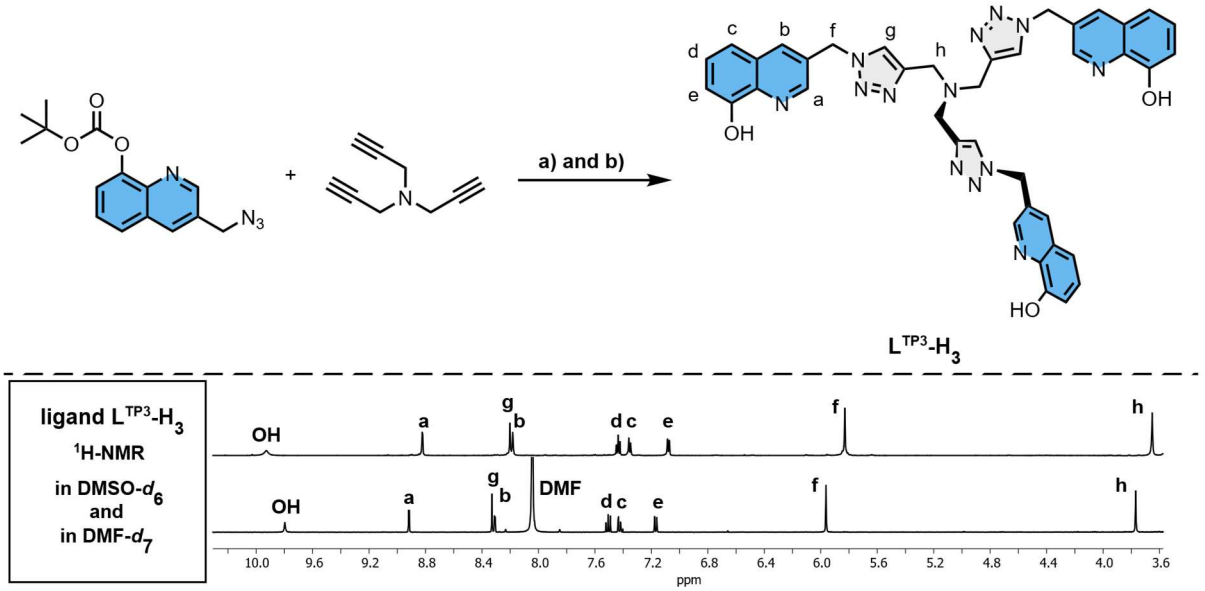

Figure 5.1: Top: Synthesis of the tripodal bis-bidentate ligand L^{TP3}-H_3. a) $CuSO_4$, Na-ascorbate, THF/H_2O, 60°C; b) TFA, DCM, rt. Bottom: ^{1}H NMR spectra of ligand L^{TP3}-H_3 in DMSO-d_6 (600 MHz, 500 µM, 25°C) and in DMF-d_7 (500 MHz, 500 µM, 25°C).

The self-assembly of ligand L^{TP3}-H_3 with $Zn(OAc)_2$ was performed in a 2:3 ratio in DMSO, which resulted in the formation of a yellow precipitate. Subsequent lyophilization of the solvent and the byproduct acetic acid yielded a weakly soluble yellow powder in quantitative yield. ^{1}H NMR experiments of the suspended powder showed both broad signals in DMSO-d_6 and sharp signals in DMF-d_7 (Figure 5.2). Both NMR-samples were heated at 70°C for 4 h prior to each ^{1}H NMR measurement.

The broad signals in DMSO-d_6, together with the increased conformational flexibility of the tripodal ligand, indicated the formation of aggregated species or coordination polymers rather than a discrete supramolecular assembly. When the sample is analyzed in DMSO-d_6 with an increased number of scans

(72), the signals appear shaper but remain too numerous to correspond to a single defined species, further supporting the absence of a discrete self-assembled trinuclear complex. This was further confirmed by 2D ^{1}H DOSY NMR (see SI, Figure 5.28), which gave a diffusion coefficient of $D = 3.554 \times 10^{-10}$ m^2 s^{-1} and consequently, with the assumption that a spherical species formed, a hydrodynamic radius of 0.31 nm. This observation indicated the formation of a weakly soluble $[Zn_1L_1]$ species, rather than a trinuclear assembly.

In contrast, the ^{1}H NMR spectrum in DMF-d_7 displayed sharp signals, which suggested the formation of a discrete self-assembly, although complete solubility is not achieved under the given conditions. Upon coordination to Zn(II), the methylene protons linking the hydroxyquinoline and triazole moieties, as well as of the vicinal N-CH_2 protons, lost their magnetic equivalence. In the free ligand L^{TP3}-H_3, rapid rotation about the C-C bond resulted in an averaged environment and a singlet signal in the ^{1}H NMR spectrum. After complexation, coordination of the hydroxyquinolate unit to Zn(II) restricts this rotation and created an asymmetric environment for the two methylene protons, which resulted in diastereotopicity. This led to mutual spin-spin coupling and the appearance of an AB pattern, which resulted in a quartet-like signal in the ^{1}H NMR spectrum.

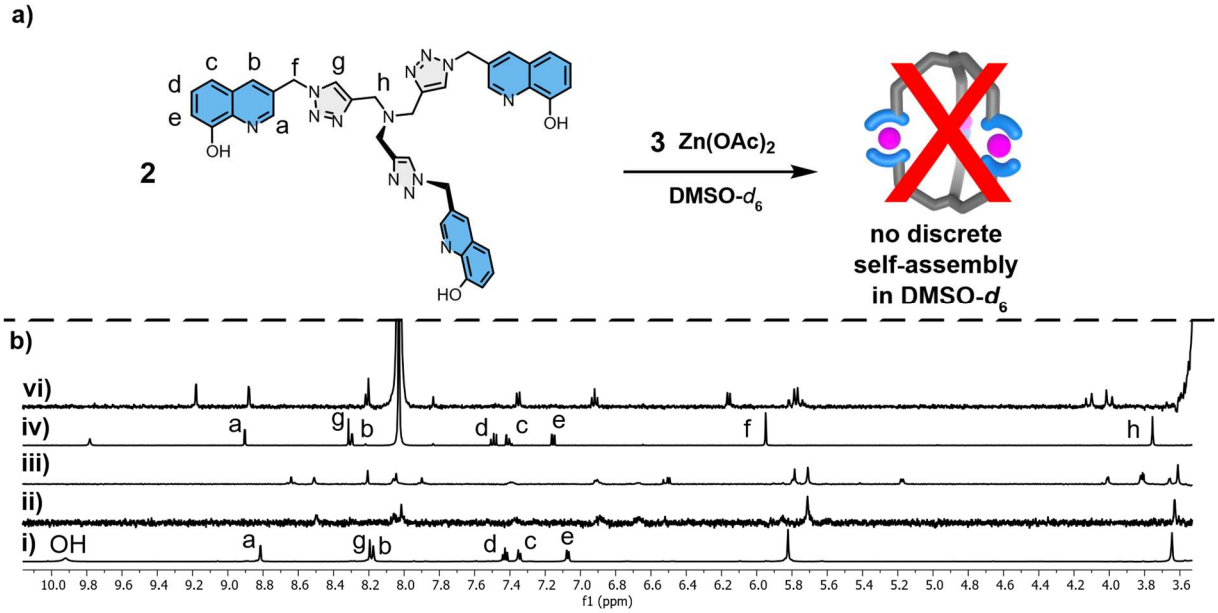

Figure 5.2: a) Self-assembly of the tripodal bis-bidentate ligand L^{TP3}-H_3 with $Zn(OAc)_2$ in a 2:3 ratio. b) ^{1}H NMR experiments of the self-assembly. i) Ligand L^{TP3}-H_3 (500 MHz, 500 µM, 25°C), ii) self-assembly in DMSO-d_6 (16 scans, 500 MHz, 500 µM, 25°C), iii) self-assembly in DMSO-d_6 (72 scans, 500 MHz, 500 µM, 25°C), iv) ligand L^{TP3}-H_3 in DMF-d_7 (500 MHz, 500 µM, 25°C) and vi) self-assembly in DMF-d_7 (600 MHz, 500 µM, 25°C).

The poor solubility of the material in both DMSO-d_6 and DMF-d_7, combined with the absence of a clearly observable discrete self-assembly in DMSO-d_6 and the high cost of DMF-d_7, posed a significant obstacle to the continuation of the project. The preparation of a single NMR-sample (500 µL of DMF-d_7) costs approximately 50 €. Negative ESI-MS experiments showed m/z values, which corresponded to a $[Zn_1L_1]^-$ species (see SI, Figure 5.27). All crystallization attempts resulted in precipitation of an amorphous solid. Although the ^{1}H NMR spectrum of the resulting yellow powder displayed a single set of signals in DMF-d_7, further 2D NMR experiments of the charge-neutral $[Zn_{1.5xn}L_n]$ species were hampered by its low solubility. Consequently, the discrete self-assembly of a $[Zn_{1.5xn}L_n]$ species could not be unequivocally confirmed. Nevertheless, the implementation of established self-assembly strategies for supramolecular architectures made this project a particularly rewarding and stimulating scientific journey.

5.3 Guest driven self-assembly of $[Zn_3L_2]$ and $[Zn_6L_4]$ supramolecular architectures

As the tripodal ligand L^{TP3}-H_3 did not self-assemble with $Zn(OAc)_2$ in DMSO-d_6 on its own, tetrabutylammonium tricarboxylates were employed as templates to initiate a discrete self-assembly. Several tetrabutylammonium (TBA) tricarboxylates were tested, including those of benzo[1,2-*b*:3,4-*b*':5,6-*b*'']trithiophene-2,5,8-tricarboxylic acid (BTT^{3-}), trimesic acid (TRI^{3-}) and 1,3,5-cis,cis-cyclohexanetricarboxylic acid (CYC^{3-}).

To investigate if the tricarboxylates could serve as templates, the statistical $[Zn_{1.5xn}L_n]$ complex was suspended in DMSO-d_6. Next, one equivalent of the TBA salts, dissolved in DMSO-d_6, was added in two steps, with the sample heated to 80°C for 10 min after each addition prior to recording a ^{1}H NMR spectrum.

5.3.1 Guest driven self-assembly TBA BTT

In the case of TBA BTT, the ^{1}H NMR spectrum showed a single set of signals appearing along with a minor species after the addition of 0.5 equivalents of TBA BTT (Figure 5.3, b); ii)). Upon addition of a total of 1 equivalent of TBA BTT, the intensity of the signals increased accordingly, which indicated slow exchange behavior (Figure 5.3, b); iii)) and the self-assembly of a single host-guest species, $[(BTT)@Zn_3L_2]^{3-}$. The signals corresponding to the peripheral protons of the hydroxyquinolate units were sharp (Figure 5.3, b) [iii) signals b-d]), whereas signal a was split, as well as signal g, which corresponded to the triazole proton. The signals of the methylene linkers (f, f' and h, h') appeared split and broadened, with the inner methylene protons (h and h') exhibiting a highfield shift (see 5.3.1, Figure 5.32). The signals corresponding to proton a and g are individually split, as the integrity of the BTT guest, in particular the orientation of the thiophene moieties, induced distinct chemical environments for the two a protons bound to the two coordinating hydroxyquinolate units. This splitting could be attributed to a reduction in overall molecular symmetry and restricted rotational freedom within the complex at the given conditions. The ^{1}H VT NMR spectrum of the host-guest complex $[(BTT)@Zn_3L_2]^{3-}$ at 55°C showed that the signals corresponding to protons a, g and f each sharpened and merged individually, which reflected increased molecular dynamics. At 90°C, all signals in the ^{1}H VT NMR spectrum broaden significantly, which indicated a loss of structural integrity under the given conditions (see 5.3.1, Figure 5.33). Further addition of TBA BTT resulted in increased signal intensities corresponding to the free TBA salt. To assign the signals in the ^{1}H NMR spectrum to their corresponding protons and to confirm the guest-driven self-assembly of a single species, several 2D NMR (see 5.3.1) and ESI-MS experiments were performed. The ^{1}H DOSY NMR (see 5.3.1, Figure 5.41) confirmed the formation of a single species with a D = 9.005 x 10^{-11} m^2 s^{-1}, which gave a r_H = 1.22 nm. These observations together with the partially broad signals in the ^{1}H NMR indicated, that the structure might be strained because of the size and shape of the encapsulated guest. The negative ESI-MS spectrum (Figure 5.3, c)) of the same ^{1}H NMR sample exhibited a signal with a m/z value of 676.4049, which matched the calculated m/z value of 676.4046 and the calculated isotopic pattern of the self-assembled host-guest complex $[(BTT)@Zn_3L_2]^{3-}$. These results indicated the successful guest-driven self-assembly of a trinuclear complex $[(BTT)@Zn_3L_2]^{3-}$ in DMSO-d_6.

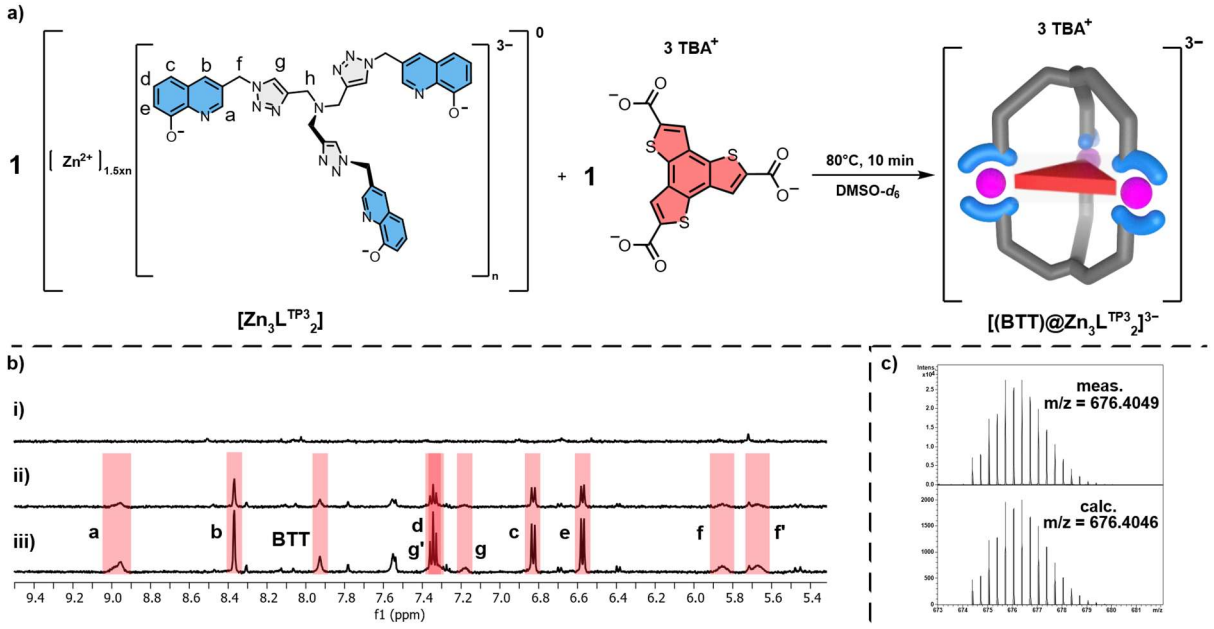

Figure 5.3: a) Guest-driven self-assembly of $[Zn_{1.5xn}L_n]$ and TBA BTT in a 1:1 ratio in DMSO-d_6. b) ^{1}H NMR two-step titration of $[Zn_{1.5xn}L_n]$ and TBA BTT. i) ^{1}H NMR of the suspended statistical $[Zn_{1.5xn}L_n]$ complex in DMSO-d_6 (500 MHz, 500 µM 25°C), ii) ^{1}H NMR of $[(BTT)@Zn_3L_2]^{3-}$ upon addition of 0.5 equiv. of TBA BTT and heating the sample for 10 min at 80°C. (DMSO-d_6, 500 MHz, 500 µM, 25°C), iii) ^{1}H NMR of $[(BTT)@Zn_3L_2]^{3-}$ upon addition of 1 equiv. of TBA BTT and heating the sample for 10 min at 80°C. (DMSO-d_6, 500 MHz, 500 µM, 25°C). c) measured negative ESI-MS spectrum and calculated spectrum of $[(BTT)@Zn_3L_2]^{3-}$.

So far, all crystalline material obtained from slow vapor diffusion of various solvents into a solution of $[(BTT)@Zn_3L_2]^{3-}$ in DMSO or DMF has proven unsuitable for X-ray diffraction analysis. Nevertheless, based on the information obtained from 2D NMR experiments (COSY, NOESY, HSQC and HMBC) and previously established solid-structures derived from our proven design principles, a structural model of the host-guest complex $[(BTT)@Zn_3L_2]^{3-}$ could be proposed. The computational host-guest structures were optimized using the r2SCAN-3c basis set with constrained coordination spheres around the Zn(II) centers (Figure 5.4). The resulting model displayed a C_3-symmetric, sandwich-type complex in which two hydroxyquinolate units from each ligand, together with one carboxylate unit of the BTT^{3-} guest, coordinate to a single Zn(II) center, forming a distorted trigonal-bipyramidal coordination sphere around each Zn(II) center. As mentioned, the orientation of the thiophene moieties of the guest BTT^{3-} had a significant influence on the chemical environment of the protons a and g. In the optimized structure, the closer proximity of the sulfur atoms to one rim of the ligands, and consequently to the a and g protons, clearly affected their local chemical and magnetic environment. Furthermore, the calculated model of $[(BTT)@Zn_3L_2]^{3-}$ showed the guest BTT^{3-} to be slightly bent, suggesting a certain degree of structural strain resulting from the imperfect fit between the guest and the encapsulating supramolecular environment. This distortion likely affected the overall electronic and magnetic environment of the assembly and may account for the partially broadened and split signals observed in the ^1H NMR spectrum.

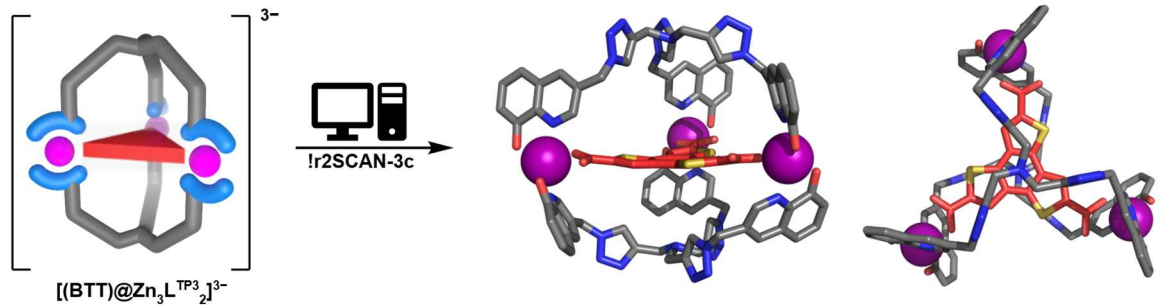

Figure 5.4: Structural information of $[(BTT)@Zn_3L_2]^{3-}$ from 2D NMR experiments funneled into a model for the host-guest complex with the basis set r2SCAN-3c, carbon atoms are shown in grey, nitrogen in blue, oxygen in red, and Zn(II) is purple colored.

5.3.2 Guest driven self-assembly TBA TRI

The guest-driven self-assembly of the statistical [$Zn_{1.5xn}L_n$] complex and TBA TRI (Figure 5.5, a)) exhibited a different behavior compared to the previous host-guest system. After the addition of 0.5 equivalents of TBA TRI to the suspended statistical [$Zn_{1.5xn}L_n$] complex in DMSO-d_6 and subsequent heating of the sample at 80°C for 10 min, two distinct sets of signals were present in the ^{1}H NMR spectrum (Figure 5.5, b; ii)): one single set of signals, and a double set of signals. The signals corresponding to the aromatic protons of the second assembly appeared as a double set of signals, whereas those of the methylene linkers were split into four distinct signals. This observation indicated the presence of two discrete host-guest complexes, one exhibiting higher symmetry and the other lower symmetry. Upon addition of a total of one equivalent of TBA TRI, the double set of signals disappeared, while the intensity of the single set of signals increased, which suggested slow exchange behavior and a preferential formation of the higher symmetry host-guest species in solution (Figure 5.5, b; iii)). The signals in the ^{1}H NMR corresponding to the aromatic protons of the self-assembled host-guest complex appeared sharp and well defined, compared to the partially broadened and split signals of host-guest complex [(BTT)@Zn_3L_2]$^{3-}$. Suggesting a more ridged assembly overall and that TRI was a better fit for the guest-driven self-assembly of [$Zn_{1.5xn}L_n$]. Further addition of TBA TRI resulted in increased signal intensities corresponding to the free TBA salt. The interpretation of the 2D NMR experiments (see 5.3.2) and the assignment of the ^{1}H NMR signals to the corresponding protons suggested the formation of a single species of high symmetry. The ^{1}H DOSY NMR (see chapter 5.3.2, Figure 5.56) confirmed the formation of a single species with a D = 9.142 x 10^{-11} m^2 s^{-1} and a hydrodynamic radius of r_H = 1.20 nm. Negative ESI-MS experiments (Figure 5.5, c) of a 1:1 mixture of [$Zn_{1.5xn}L_n$] and TBA TRI exhibited a signal with a m/z value of 619.7664, which matched the calculated m/z value of 619.7662 and the calculated isotopic pattern of a. [(TRI)@Zn_3L_2]$^{3-}$ species. The combination of the gathered information from the NMR data together with the observations of the ESI-MS spectrum indicated that it was possible to control the self-assembly of a trinuclear host-guest complex [(TRI)@Zn_3L_2]$^{3-}$ in DMSO-d_6.

As the formation of the double set of signals in the ^{1}H NMR could not be controlled under the given conditions, the identification of this host-guest species remained challenging. Nevertheless, negative ESI-MS experiments of a 2:1 mixture of [$Zn_{1.5xn}L_n$] and TBA TRI revealed a signal with an isotopic pattern and a m/z value of 1171.2024, which matched the calculated isotopic pattern and m/z value of 1171.2008, consistent with the guest-driven self-assembly of a hexanuclear [(TRI)@Zn_6L_4]$^{3-}$ species (see 5.3.2, Figure 5.50). Great!

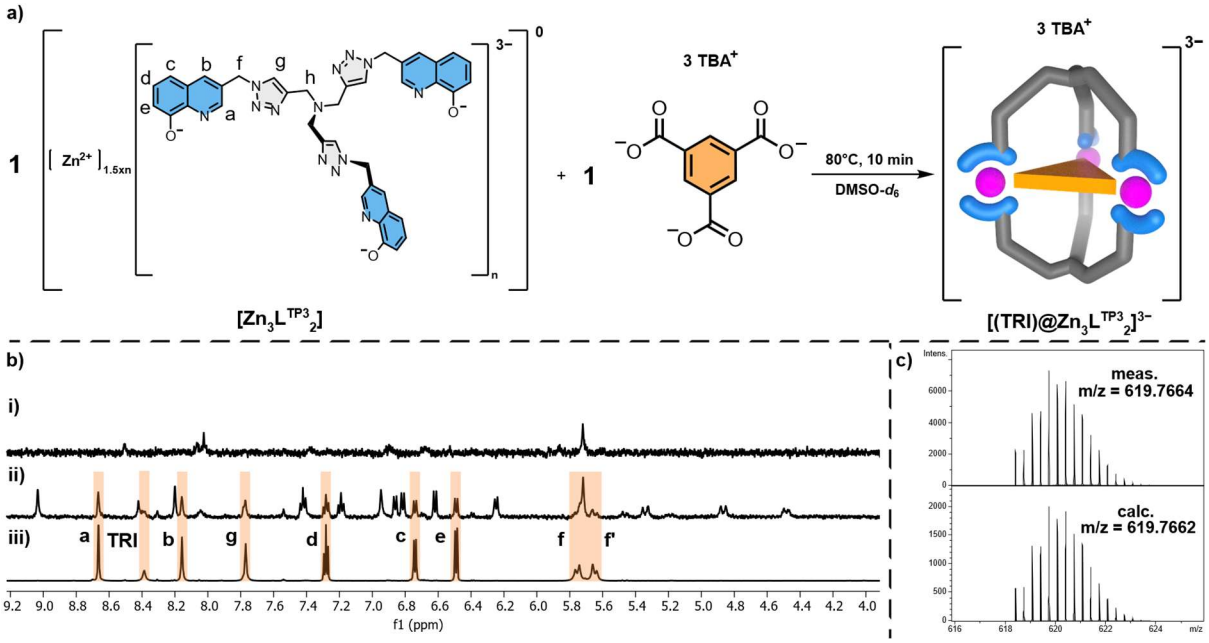

Figure 5.5: a) Guest-driven self-assembly of $[Zn_{1.5xn}L_n]$ and TBA TRI in a 1:1 ratio in DMSO-d_6. b) ^{1}H NMR two-step titration of $[Zn_{1.5xn}L_n]$ and TBA TRI. i) ^{1}H NMR of the suspended statistical $[Zn_{1.5xn}L_n]$ complex in DMSO-d_6 (500 MHz, 500 µM 25°C), ii) ^{1}H NMR of $[(TRI)@Zn_3L_2]^{3-}$ upon addition of 0.5 equiv. of TBA TRI and heating the sample for 10 min at 80°C. (DMSO-d_6, 500 MHz, 500 µM, 25°C), iii) ^{1}H NMR of $[(TRI)@Zn_3L_2]^{3-}$ upon addition of 1 equiv. of TBA TRI and heating the sample for 10 min at 80°C. (DMSO-d_6, 500 MHz, 1 mM, 25°C). c) measured negative ESI-MS spectrum and calculated spectrum of $[(TRI)@Zn_3L_2]^{3-}$.

In the case of $[Zn_{1.5xn}L_n]$ and TBA TRI, slow-vapor diffusion crystallization gave yellow single crystals suitable for X-ray diffraction analysis. For this, host-guest mixtures of $[Zn_{1.5xn}L_n]$ and an excess of TBA TRI were prepared in DMSO and in DMF, respectively, and heated at 80°C for 10 min. Slow-vapor diffusion of the anti-solvent's benzene or dioxane into the DMSO solution and *tert*-butyl methyl ether into the DMF solution, gave yellow crystals that grew at the phase boundary between the two solvents, adhering to the inner wall of the inner tube.

X-ray diffraction analysis of the yellow single-crystals from both mother-solvents revealed a hexanuclear $[(TRI)@Zn_6L_4]^{3-}$ species present in the solid state, presenting an onion-like structure. In the solid state, the more confined, onion-like supramolecular structure is thermodynamically preferred compared to the trinuclear $[(TRI)@Zn_3L_2]^{3-}$ species, as it maximizes non-covalent interactions and minimizes void space between the crystal lattice. Although the dataset from crystals grown out of DMF was incomplete, it was nevertheless sufficient enough to confirm the onion-type structure of $[(TRI)@Zn_6L_4]^{3-}$. In contrast, the dataset obtained from crystals grown from DMSO was of adequate quality for full refinement (in the future) and unambiguously confirms the connectivity of the supramolecular assembly. Unfortunately, the full refinement of the crystal structure is lacking. So, I decided to take the preliminary XRD-data, and ran a calculation with the basis set ωB97-3c def2-SVP to generate a computational model for the illustration of the hexanuclear host-guest complex $[(TRI)@Zn_6L_4]^{3-}$.

The onion-type $[(TRI)@Zn_6L_4]^{3-}$ assembly consisted of three binuclear Zn(II)clusters, each coordinated by four hydroxyquinolate units and bridged by one carboxylate substituent of the trimesate guest, which resulted in an distorted octahedral coordination-sphere around each Zn(II) cation. In the binuclear Zn(II) clusters, the hydroxyquinolate units of the ligands forming the outer shell of the onion coordinated axially to the Zn(II)-Zn(II) plane through their nitrogen atoms to one of the two Zn(II) cations, while the oxygen atoms of the same hydroxyquinolates coordinated both metal centers, thereby bridging the Zn(II) cations within the cluster. The two hydroxyquinolates units of the ligand forming the inner shell each chelate one of the two Zn(II) cations within the cluster, lied equatorial in

the Zn(II)-Zn(II) plane and oriented perpendicular to the hydroxyquinolates of the outer-shell ligands. The trianionic trimesate guest occupies the center of the structure, with each of its carboxylate groups oriented toward a distinct binuclear Zn(II) cluster, wherein each oxygen atom coordinated to one of the two Zn(II) cations within the cluster. ^{1}H DOSY NMR spectroscopy further confirmed the formation of the onion-type structure in solution. The double set of signals gave a diffusion coefficient of D = 9.183 x 10^{-11} m^2 s^{-1} and a hydrodynamic radius of r_H = 1.19 nm (see chapter 5, Figure 5.63), consistent with the top-to-bottom distance of 18.4 Å (distance between tripropargyl amine nitrogen atom to tripropargyl amine nitrogen atom of the outer shell) observed in the onion-type structure of $[(TRI)@Zn_6L_4]^{3-}$. As the hexa- and trinuclear species are coexisting in DMSO-d_6, the diffusion coefficients of both can be compared in one sample (see chapter 5, Figure 5.63). In this ^{1}H DOSY measurement the diffusion coefficient and corresponding hydrodynamic radius appeared to be D = 1.096 x 10^{-10} m^2 s^{-1} and r_H = 1.00 nm for the trinuclear $[(TRI)@Zn_3L_2]^{3-}$.

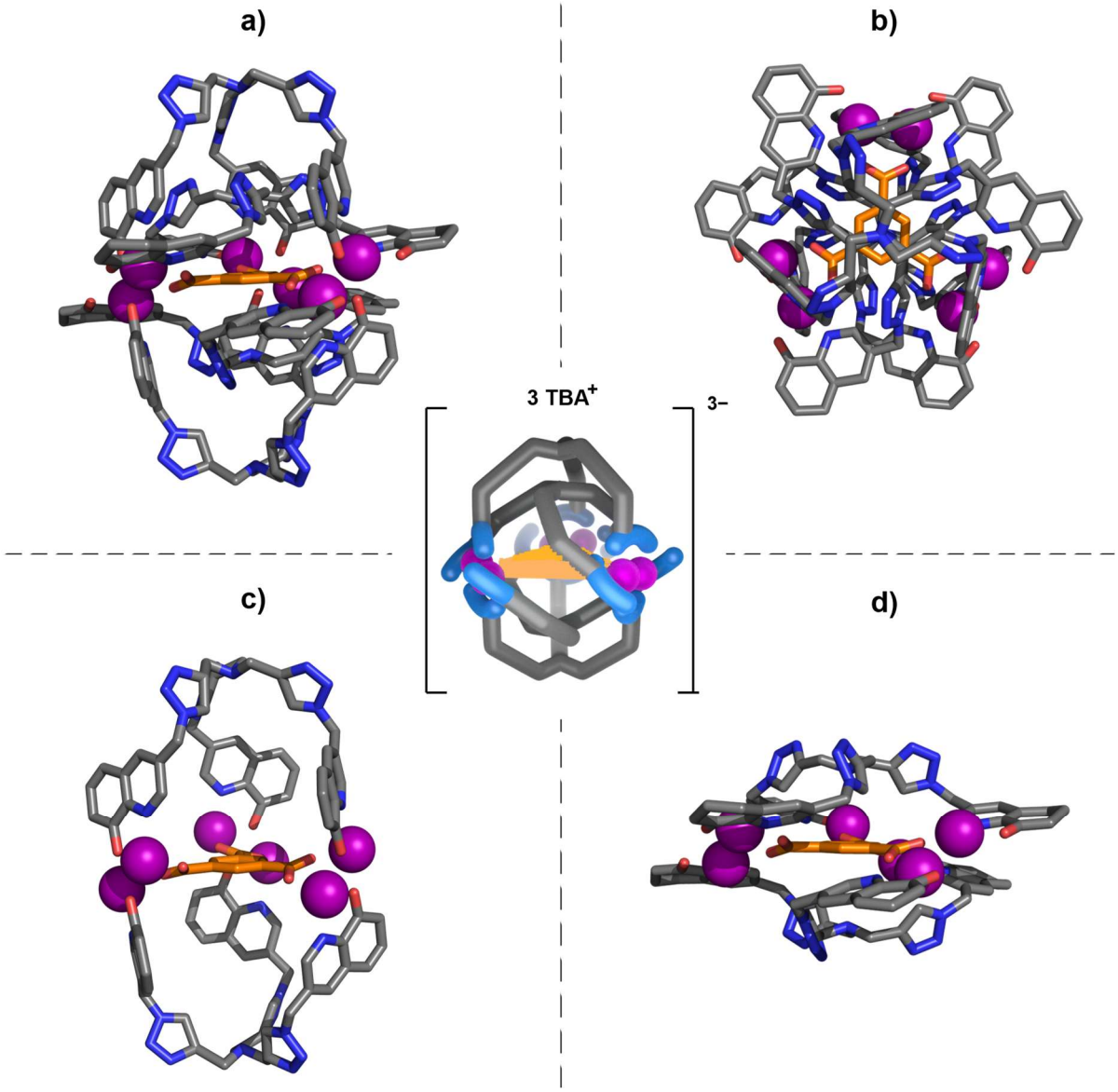

Figure 5.6: Calculated model from preliminary XRD-data and excerpts of complex $[(TRI)@Zn_6L_4]^{3-}$; carbon atoms are shown in grey, nitrogen in blue, oxygen in red, and Zn(II) is purple colored. The guest TRI^{3-} is shown in orange. a) Side-view of the calculated model-structure of the hexanuclear onion-type complex $[(TRI)@Zn_6L_4]^{3-}$. b) Top-to-bottom view of the onion-type complex $[(TRI)@Zn_6L_4]^{3-}$. c) Excerpt of the outer-shell assembly of the onion-type structure. d) Excerpt of the inner-shell assembly of the onion-type structure.

Nevertheless, as suitable single crystals for X-ray diffraction analysis of the trinuclear host-guest complex $[(TRI)@Zn_3L_2]^{3-}$ has not been obtained yet, DFT calculations were performed to model a molecular structure of the guest-driven self-assembly, based on the information obtained from 2D NMR experiments (COSY, NOESY, HSQC and HMBC) and previously established solid-structures derived from our proven design principles. The computational host-guest structures were optimized using the r2SCAN-3c basis set with constrained coordination spheres around the Zn(II) centers (Figure 5.7). The resulting model displayed a C_3-symmetric, sandwich-type complex in which two hydroxyquinolate units from each ligand, together with one carboxylate unit of the trimesate guest, coordinate to a single Zn(II) center, forming a distorted trigonal-bipyramidal coordination sphere around each Zn(II) center. In the optimized structure, the trimesate guest occupied the center of the host-guest assembly, symmetrically encapsulated between the upper and lower ligands, which formed a confined supramolecular architecture with well-defined voids between the ligands and the central trimesate guest. Compared to the BTT^{3-} guest, trimesate is smaller and therefore represented a better geometrical fit within the host cavity, as evidenced by the more defined ^1H NMR spectrum and supported by the calculated model.

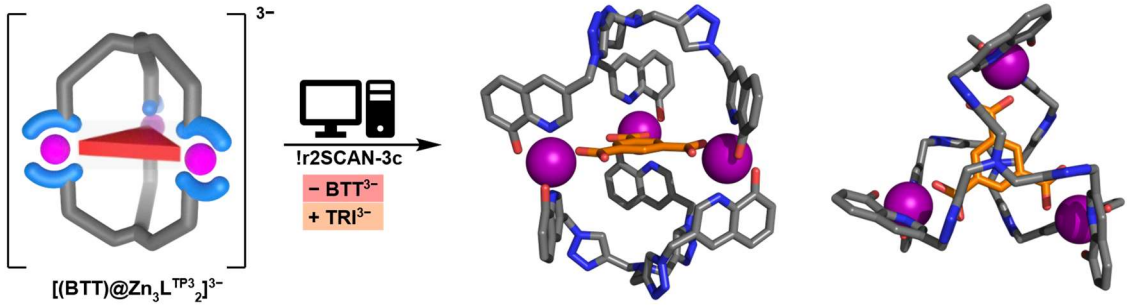

Figure 5.7: Structural information of $[(TRI)@Zn_3L_2]^{3-}$ from 2D NMR experiments funneled into a model for the host-guest complex with the basis set r2SCAN-3c, carbon atoms are shown in grey, nitrogen in blue, oxygen in red, and Zn(II) is purple colored.

To investigate if the voids between backbone and trimesate guest could be occupied by small cations, ^1H NMR titration experiments of the trinuclear species with lithium triflate and sodium tetrafluoroborate in DMSO-d_6 exhibited, although the shifts were small, fast guest exchange behavior. Up to this point every experimental (slow-vapor diffusion, recrystallization) and/or analytical (positive and negative ESI-MS) attempt to understand the stoichiometry and intermolecular interactions between the small cationic guests and the host-guest complex failed. The observed host-guest interactions in the ^1H NMR titration experiment between the cationic guests and the trinuclear complex $[(TRI)@Zn_3L_2]^{3-}$ occurred presumably due to attractive electronic interactions. The fact that DMSO-d_6 coordinates small cations like lithium and sodium together with the small shifts allows to assume the bindings constants to be low and a plot of the titration data is not included.

5.3.3 Guest driven self-assembly TBA CYC

The guest-driven self-assembly of $[Zn_{1.5xn}L_n]$ and TBA CYC in DMSO-d_6 reassembled a clean transformation (Figure 5.8, a)). The two-step titration of the in DMSO-d_6 suspended complex $[Zn_{1.5xn}L_n]$ and TBA CYC was carried out as in the previous cases and exhibited a slow-exchange behavior (Figure 5.8, b)). Upon addition of 0.5 equivalents of TBA CYC the ^{1}H NMR spectrum showed a double set of signals for the aromatic protons and a quadruple set of signals for the methylene linkers (Figure 5.8, b); iii)). The addition of one equivalent in total increased the signal intensity in the ^{1}H NMR spectrum. These observations, considering the observations from the previous guest-driven self-assembly, indicated the formation of a low symmetry hexanuclear $[(CYC)@Zn_6L_4]^{3-}$ host-guest assembly. Which led to the assumption, that TBA CYC drove the self-assembly into an onion-type architecture. One set of signals corresponded to the inner core (signals a - h), while the other set corresponded the outer shell (signals a# - h#) of the host-guest complex of $[(CYC)@Zn_6L_4]^{3-}$. In this structure, the equatorial carboxylate units of the cyclohexane tricarboxylate guest coordinated to and bridged the binuclear Zn(II) centers, just like in the previous case. The vicinal axial protons of the carboxylates were expected to exhibit NOE contacts exclusively with the inner core of the onion-type architecture. The ^{1}H NOESY NMR spectrum of $[(CYC)@Zn_6L_4]^{3-}$ revealed NOE contacts of proton a and g with the axial protons of the cyclohexane tricarboxylate guest (Figure 5.8, c)). This indicated that protons a and g were corresponding to the inner shell of the host-guest complex. The negative ESI-MS spectrum of a 1:1 mixture of $[Zn_{1.5xn}L_n]$ and TBA CYC in DMSO-d_6 (Figure 5.8, d)) exhibited matching m/z values and isotopic patterns corresponding to a trinuclear $[(CYC)@Zn_3L_2]^{3-}$ and the expected hexanuclear $[(CYC)@Zn_6L_4]^{3-}$ species.

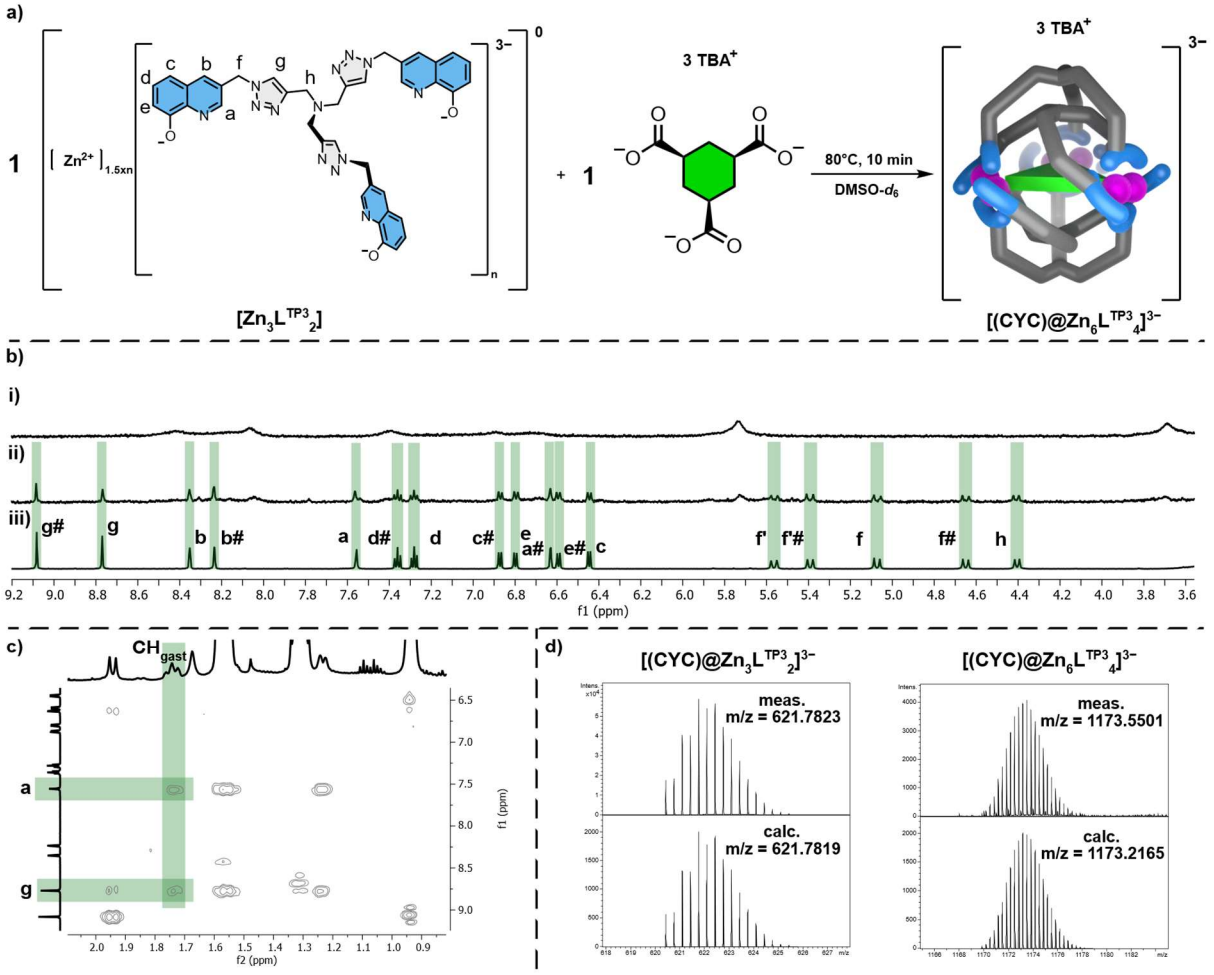

Figure 5.8: a) Guest-driven self-assembly of $[Zn_{1.5xn}L_n]$ and TBA CYC in a 1:1 ratio in DMSO-d_6. b) ^{1}H NMR two-step titration of $[Zn_{1.5xn}L_n]$ and TBA CYC. i) ^{1}H NMR of the suspended $[Zn_{1.5xn}L_n]$ complex in DMSO-d_6 (500 MHz, 500 µM 25°C), ii) ^{1}H NMR of $[(CYC)@Zn_6L_4]^{3-}$ upon addition of 0.5 equiv. of TBA CYC and heating the sample for 10 min at 80°C. (DMSO-d_6, 500 MHz, 500 µM, 25°C), iii) ^{1}H NMR of $[(CYC)@Zn_6L_4]^{3-}$ upon addition of 1 equiv. of TBA TRI and heating the sample for 10 min at 80°C. (DMSO-d_6, 500 MHz, 500 µM, 25°C). c) Excerpt from the ^{1}H NOESY spectrum of $[(CYC)@Zn_6L_4]^{3-}$, highlighting the NOE contact between protons a and g respectively with the axial proton of the CYC^{3-} guest. d) measured negative ESI-MS spectra and calculated spectra of complexes $[(CYC)@Zn_3L_2]^{3-}$ and $[(CYC)@Zn_6L_4]^{3-}$.

Slow-vapor crystallization of a mixture of $[Zn_{1.5xn}L_n]$ and an excess of TBA CYC, dissolved in DMF with *tert*-butyl methyl ether as anti-solvent, yielded yellow single-crystalline plates suitable for X-ray diffraction analysis. The crystal-structure revealed a C_3-symmetric hexanuclear onion-type structure $[(CYC)@Zn_6L_4]^{3-}$ (Figure 5.9, a) and b)), comparable with the solid-state structure of $[(TRI)@Zn_6L_4]^{3-}$. The 1,3,5-*cis*,*cis*-cyclohexantricarboxylate guest occupied the center of the supramolecular architecture, with each of its three carboxylate units coordinating to and bridging the two Zn(II) cations within a distinct binuclear Zn(II) cluster. In the binuclear Zn(II) clusters, the hydroxyquinolate units of the ligands forming the outer shell of the onion-type architecture coordinated axially to the Zn(II)-Zn(II) plane through their nitrogen atoms to one of the two Zn(II) cations , while the oxygen atoms of the same hydroxyquinolates bridged both Zn(II) cations within the binuclear cluster (Figure 5.9, a) and b)). The two hydroxyquinolates units of the ligands forming the inner shell each chelated one of the two Zn(II) cations, lying equatorial within the Zn(II)-Zn(II) plane and oriented perpendicular to the hydroxyquinolates of the outer-shell ligands (Figure 5.9, a) and b)). As a result, each Zn(II)center adopted a distorted octahedral coordination geometry. Moreover, the solid-state structure of $[(CYC)@Zn_6L_4]^{3-}$ confirmed the previous 2D NMR observations, confirming that the signals a and g in the ^{1}H NMR spectrum of $[(CYC)@Zn_6L_4]^{3-}$ correspond to protons of the inner-shell ligands (Figure

5.9, c)). ^{1}H DOSY NMR experiments showed the formation of a single species with a diffusion coefficient of D = 1.156 x 10^{-10} m^2 s^{-1} and a hydrodynamic radius of r_H = 0.95 nm, consistent with the top-to-bottom distance of 18.4 Å in the crystal-structure of the onion. Unfortunately, full refinement of the onion-type structure of $[(CYC)@Zn_6L_4]^{3-}$ is lacking, nevertheless, the XRD-data was partially refined and unambiguously confirms the connectivity of the supramolecular assembly.

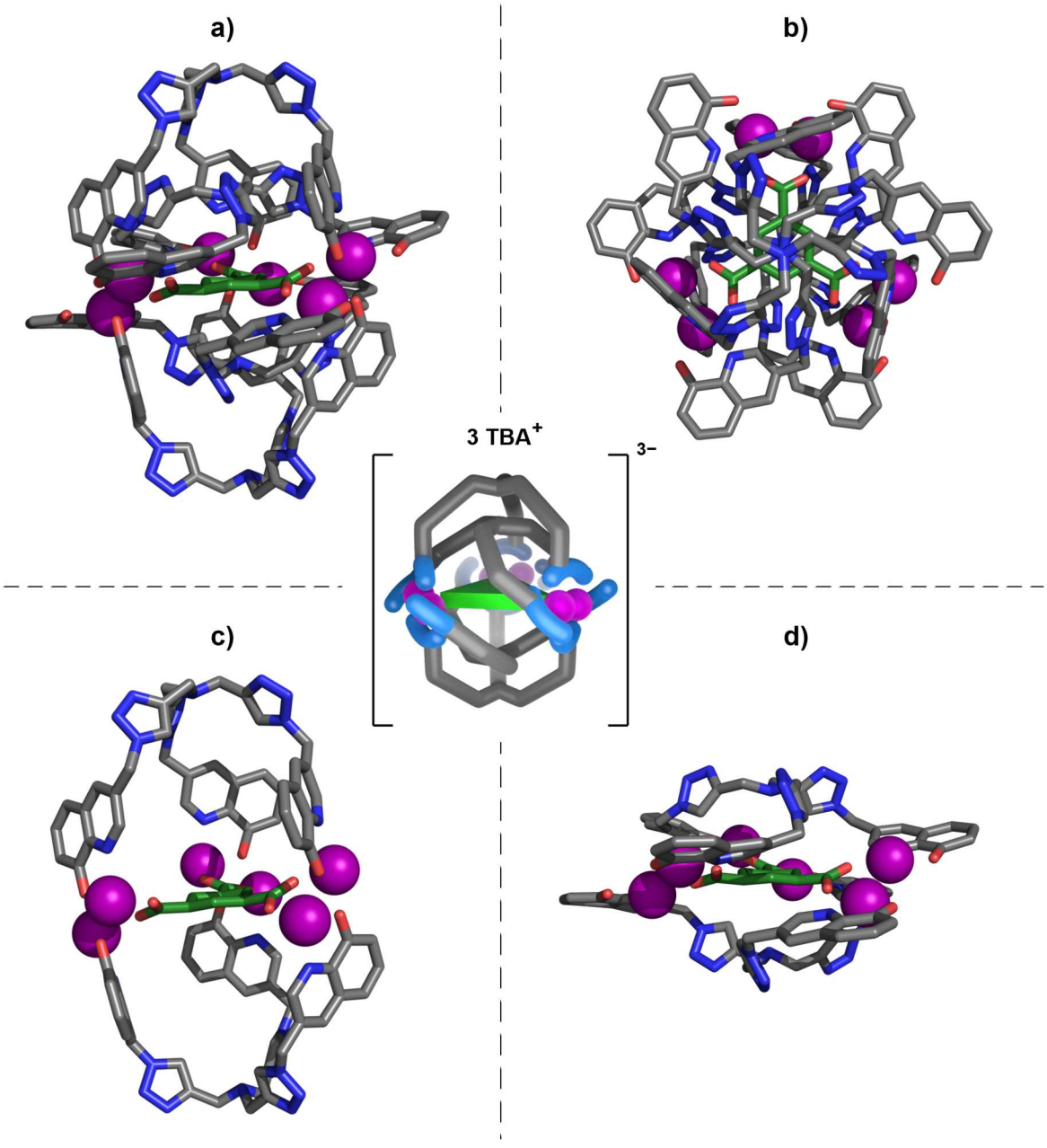

Figure 5.9: Preliminary XRD-structure and excerpts of complex $[(CYC)@Zn_6L_4]^{3-}$; carbon atoms are shown in grey, nitrogen in blue, oxygen in red, and Zn(II) is purple colored. The guest CYC is shown in green. a) Side-view of the XRD-structure of the hexanuclear onion-type complex $[(CYC)@Zn_6L_4]^{3-}$. b) Top-to-bottom view of the onion-type complex $[(CYC)@Zn_6L_4]^{3-}$. c) Excerpt of the outer-shell assembly of the onion-type structure. d) Excerpt of the inner-shell assembly of the onion-type structure.

The observation and confirmation of the hexanuclear onion-type architecture and its binuclear Zn(II)clusters in the solid-state, as well as in solution and the gas phase, represented a remarkable finding. However, the single crystals of the onion-type complex $[(CYC)@Zn_6L_4]^{3-}$ were obtained from DMF, whereas the solution-state analysis was conducted in DMSO-d_6. The same holds true for the onion-type complex $[(TRI)@Zn_6L_4]^{3-}$, with the distinction that suitable single crystals for X-ray analysis

were successfully grown from DMSO in this case. To complete the overall picture and ensure consistency between solid- and solution-state characterization, additional investigations of the guest-driven self-assembly of $[(CYC)@Zn_6L_4]^{3-}$ in DMF-d_7 is therefore both reasonable and necessary.

5.3.4 Solution-State analysis of [(CYC)@Zn_6L_4]$^{3-}$ and [(TRI)@Zn_6L_4]$^{3-}$ in DMF-d_7.

The guest-driven self-assembly of [$Zn_{1.5xn}L_n$] and TBA CYC in DMF-d_7 exhibited behavior comparable to that observed in DMSO-d_6 (Figure 5.10, a)). In the ^{1}H NMR experiment of [$Zn_{1.5xn}L_n$] and TBA CYC in DMF-d_7, the addition of 0.5 equivalents of the guest to the suspended statistical [$Zn_{1.5xn}L_n$] complex solution and heating to the sample to 80°C for 10 min, drove the self-assembly into the hexanuclear species, as evidenced by the appearance of a double-set of signals in the ^{1}H NMR spectrum (Figure 5.10, b); ii)). The addition of one equivalent of the guest TBA CYC showed the exclusive formation of the hexanuclear species (Figure 5.10, b); iii)). To further confirm the self-assembly of the onion-type structure, NOE cross-peaks were observed between signals corresponding to proton a and a#, which were part of ligands of the inner and outer shells, respectively (Figure 5.10, c)). This NOE contact provided direct evidence for the formation of binuclear Zn(II) clusters and thus supported the presence of the characteristic onion-type supramolecular architecture in solution.

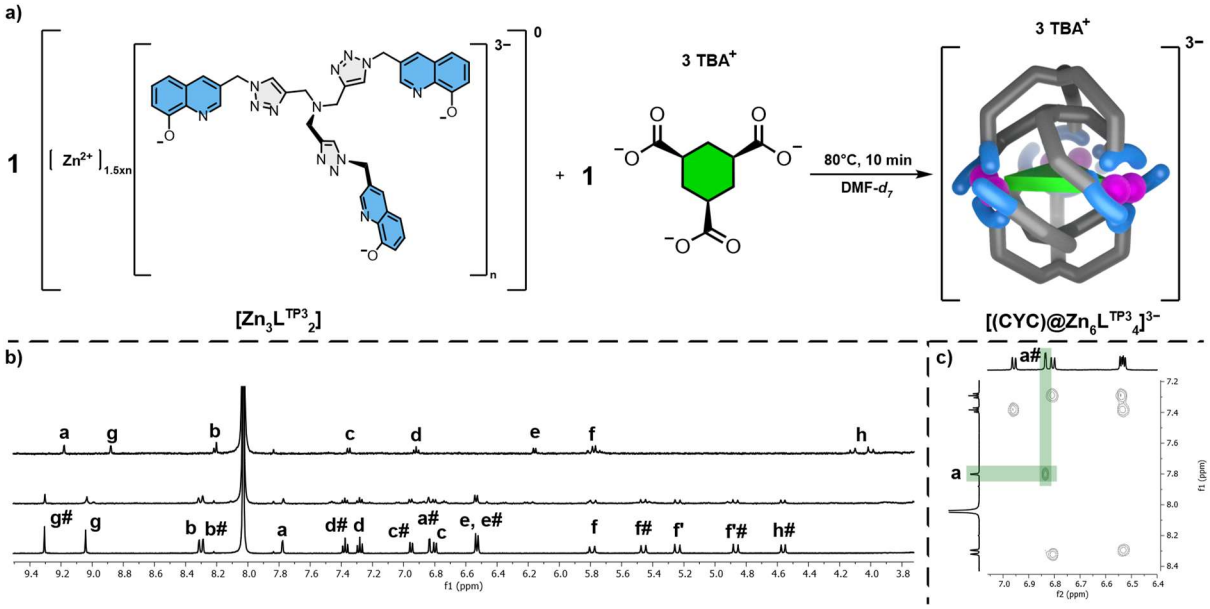

Figure 5.10: a) Guest driven self-assembly of [$Zn_{1.5xn}L_n$] and TBA CYC in DMF-d_7. b) ^{1}H NMR spectra of the two-step titration and heating the sample for 10 min at 80°C after each addition (DMF-d_7, 500 MHz, 500 µM, 25°C). c) Excerpt on the ^{1}H NOESY spectrum, visualization of the NOE cross-peak between proton a and a#.

The NMR solution state analysis of the hexanuclear species $[(TRI)@Zn_6L_4]^{3-}$ with a clear signal assignment in DMF-d_7 was hampered because of overlapping signals, which corresponded to the host-guest complex and the DMF-d_7 signal at 8.03 ppm, as well as water (see chapter 5.3.4, Figure 5.61, Figure 5.62). Nevertheless, negative ESI-MS experiments of complex $[Zn_{1.5xn}L^{TP3}{}_n]$ and 0.5 equiv. of TBA TRI gave a measured m/z value of 1171.2059 which matched the calculated m/z value of 1171.2008 for the hexanuclear species. The same hold true for the trinuclear species $[(TRI)@Zn_3L_2]^{3-}$ after adding an excess of TBA TRI to the mixture. The addition of >1 equiv. of TBA TRI to a suspended solution of $[Zn_{1.5xn}L^{TP3}{}_n]$ with subsequent heating to 80°C over 10 min led to a single set of signals in the ^{1}H NMR spectrum, but unfortunately also in this case the solution state analysis in DMF-d_7 is hampered due to broad and overlapping signals. Nevertheless, negative ESI-MS could prove the trinuclear species $[(TRI)@Zn_3L_2]^{3-}$ in the gas phase. The measurement gave a m/z value of 619.7685, which matched the calculated m/z value of 619.7662 for the trinuclear host-guest complex $[(TRI)@Zn_3L_2]^{3-}$. Besides the overlapping signals in the ^{1}H NMR and a missing clear signal assignment for both, the tri- and hexanuclear species in DMF-d_7, these observations indicated that it is possible to control the formation of the trinuclear species and the hexanuclear species in DMF-d_7 with the induce-fit character of the guest TRI^{3-}.

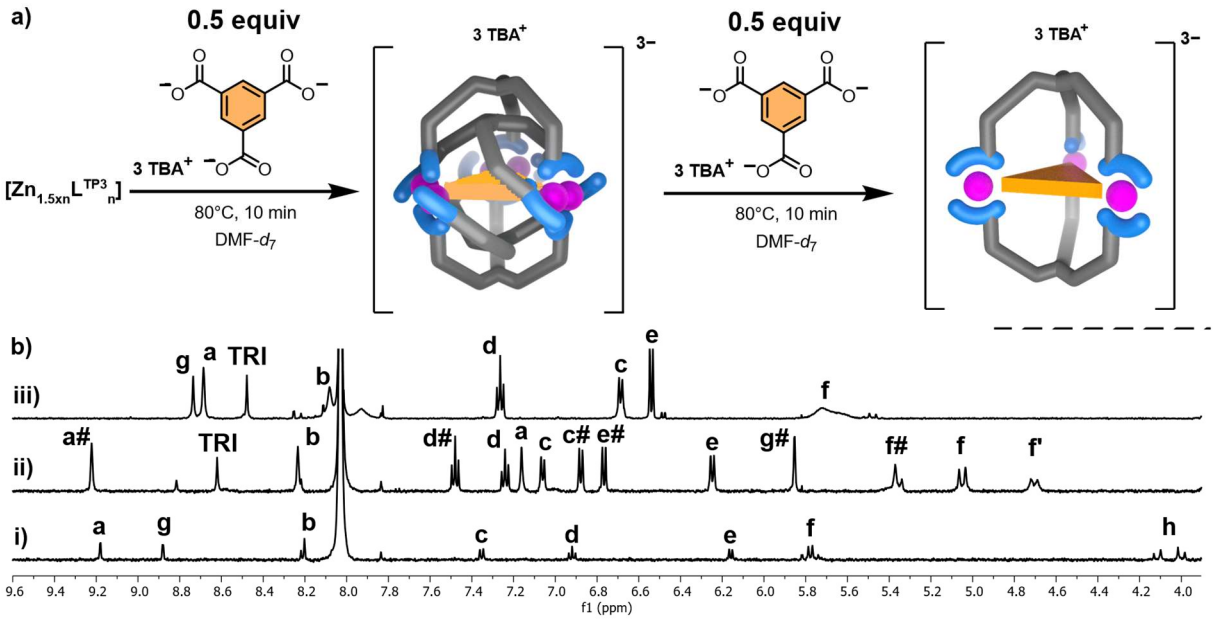

Figure 5.11: a) $[Zn_{1.5xn}L^{TP3}{}_n]$ templated into the hexanuclear onion-type structure and subsequent transformation into the trinuclear species. b) ^{1}H NMR spectra of i) suspended complex $[Zn_{1.5xn}L^{TP3}{}_n]$, ii) hexanuclear $[(TRI)@Zn_6L^{TP3}{}_4]^{3-}$ onion-type structure, iii) trinuclear $[(TRI)@Zn_3L^{TP3}{}_2]^{3-}$ species (DMF-d_7, 500 MHz, 500 µM, 25°C). After each addition the sample was heated for 10 min at 80°C.

5.3.5 Guest driven self-assembly TBA BtA

Analysis of the induced-fit self-assembly of the previously studied tricarboxylates already exhibited limitations with respect to the size and shape of the tricarboxylate template. The observation that TRI^{3-} and CYC^{3-} form rather rigid assemblies, and that BTT^{3-} is already slightly too large but still accommodated, suggested the introduction of an additional methylene linker between the phenyl ring and the carboxylate groups of trimesate (Figure 5.12, a). In the ^{1}H NMR investigations the 2,2',2''- (benzene-1,3,5-triyl)triacetate guest BtA^{3-} behaved similar to CYC^{3-}. The ^{1}H NMR of the host-guest complex $[(BtA)@Zn_6L_4]^{3-}$ showed a double set of signals for the corresponding aromatic protons, whereas the protons of the aliphatic linkers were split into eight doublets (Figure 5.12, b). This observation indicated the formation of the onion-type structure in DMSO-d_6. Further, the characteristic NOE contact between proton a and a# was observed in the ^{1}H NOESY NMR spectrum, as observed before in the ^{1}H NOESY spectra of $[(TRI)@Zn_6L_4]^{3-}$ and $[(CYC)@Zn_6L_4]^{3-}$. The same NOESY spectrum gave the indication that proton a corresponds to the inner shell assembly of the onion-structure, as the corresponding signal revealed a NOE contact with the signal corresponding to the aromatic proton of the guest BtA^{3-}, which is located in the center of the architecture (Figure 5.12, c). ^{1}H DOSY NMR spectroscopy showed a diffusion coefficient of D = 1.319 x 10^{-10} m^2 s^{-1}, which gave a hydrodynamic radius of r_H = 0.83 nm using the STOCKES-EINSTEIN equation, which is in line with the top-to-bottom distance (18.4 Å) of the $[(CYC)@Zn_6L_4]^{3-}$ host-guest complex in the solid-state structure. The negative ESI-MS investigations showed a m/z value of 633.7761, which matched the calculated m/z value of 633.7781 for a trinuclear $[(BtA)@Zn_3L_2]^{3-}$ host-guest complex (Figure 5.12, d).

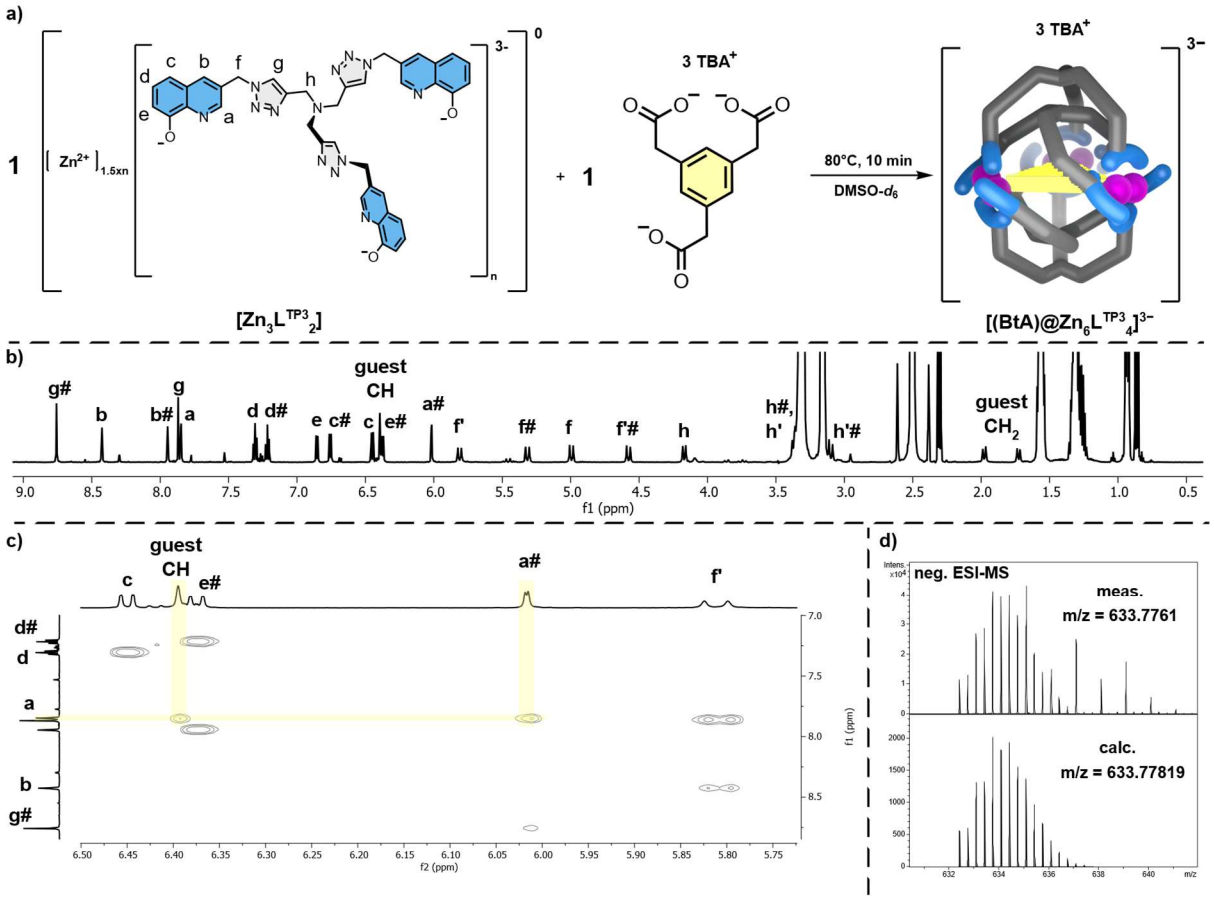

Figure 5.12: a) Guest driven self-assembly of $[Zn_{1.5xn}L^{TP3}{}_n]$ and TBA BtA in DMSO-d_6. b) ^{1}H NMR spectrum of the onion-type structure $[(BtA)@Zn_6L_4]^{3-}$ with prior heating of the sample for 10 min at 80°C after the addition of 1 equiv. BtA^{3-} (DMSO-d_6, 500 MHz, 500 µM, 25°C). c) Excerpt on the ^{1}H NOESY spectrum, visualization of the NOE cross-peak between proton a and a#, as well as between the aromatic proton of the guest and the proton a. d) Isotopic pattern and m/z values of the measured and calculated ESI-MS spectrum of $[(BtA)@Zn_3L_2]^{3-}$.

Unfortunately, all crystallization attempts for the host-guest complex $[(BtA)@Zn_6L_4]^{3-}$ failed. Nevertheless, from the previous obtained crystal-data and calculated models of $[(TRI)@Zn_6L_4]^{3-}$ and $[(CYC)@Zn_6L_4]^{3-}$, a PM6 model of the onion structure could be obtained. Starting from the previous calculated model of $[(TRI)@Zn_6L_4]^{3-}$, one additional methylene linker was implemented between the phenyl-ring and the respective three carboxylate units, to generate a starting geometry of the onion-type structure with 2,2',2''-(benzene-1,3,5-triyl)triacetate guest BtA^{3-} in the center of the structure.

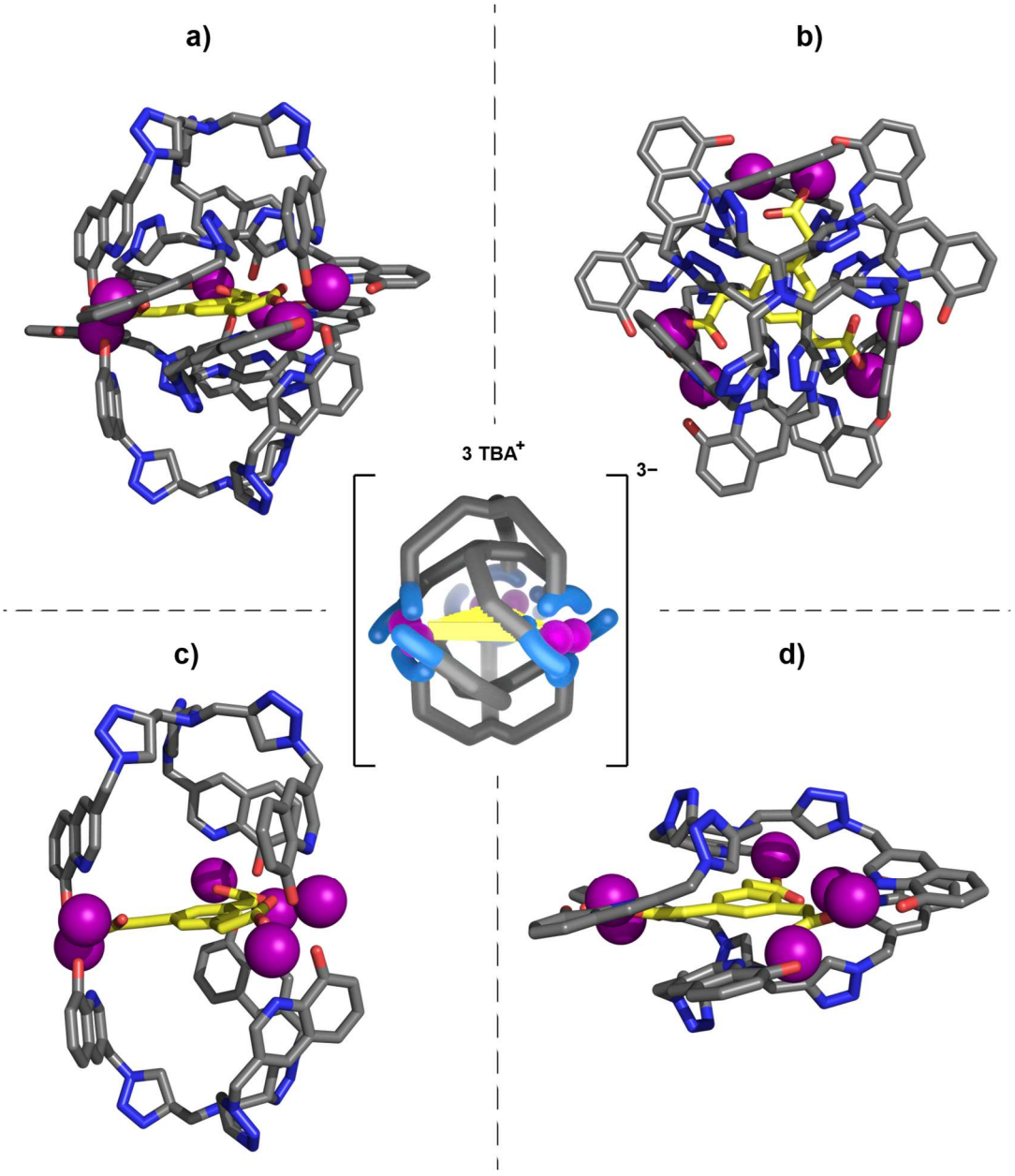

Figure 5.13: Figure 5.14: PM6 model-structure and excerpts of complex $[(BtA)@Zn_6L_4]^{3-}$; carbon atoms are shown in grey, nitrogen in blue, oxygen in red, and Zn(II) is purple colored. The guest BtA^{3-} is shown in green. a) Side-view of the XRD-structure of the hexanuclear onion-type complex $[(BtA)@Zn_6L_4]^{3-}$. b) Top-to-bottom view of the onion-type complex $[(BtA)@Zn_6L_4]^{3-}$. c) Excerpt of the outer-shell assembly of the onion-type structure. d) Excerpt of the inner-shell assembly of the onion-type structure.

5.4 Qualitative investigation of guest binding and kinetic investigation

The limited solubility of the host complex [$Zn_{1.5xn}L_n$] posed significant challenges for the quantitative determination of binding constants, as all attempts to employ UV-Vis and ITC titrations proved unsuccessful. To gain initial qualitative insights into the relative binding affinities of the investigated guests, a series of competition experiments were conducted (Figure 5.15). At first, the complex [$Zn_{1.5xn}L^{TP3}{}_n$] was suspended in DMSO-d_6, then 1 equiv. BTT^{3-} was added at room temperature and heated to 80°C for 10 min. Prior ^{1}H NMR competition analysis revealed BTT^{3-} to be the guest with the lowest binding affinity. The preorganized complex [(BTT)@Zn_3L_2]$^{3-}$ now could exchange its guest with 1 equiv. TRI^{3-} at room temperature, forming the trinuclear complex [(TRI)@Zn_3L_2]$^{3-}$. This guest-exchange process (BTT^{3-} → TRI^{3-}) took place within five minutes in the given conditions. Heating the sample to 80°C accelerated the guest exchange process. Adding an equimolar amount of TBA CYC to the sample and recording a ^{1}H NMR spectrum right after the addition showed the same trinuclear species together with a new set of signals in low intensity. After more than 4 h the guest induced transformation by CYC^{3-} to the hexanuclear species [(CYC)@Zn_6L_4]$^{3-}$ was completed. Follow up experiments with BtA^{3-} showed a similar qualitative binding strength as BTT^{3-}. These experiments revealed the following binding affinity trend: CYC^{3-} > TRI^{3-} > BtA^{3-} ≈ BTT^{3-}

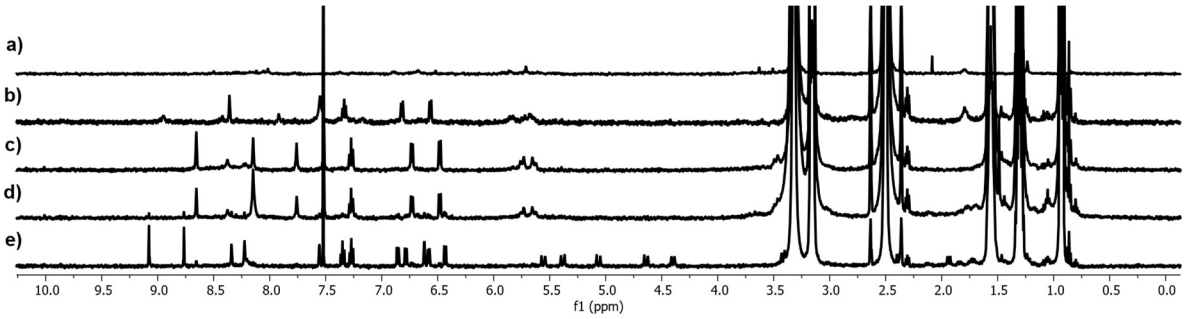

Figure 5.15: Qualitative ^{1}H NMR investigations of the binding affinities for [$Zn_{1.5xn}L^{TP3}{}_n$] and the guests CYC^{3-}, TRI^{3-} and BTT^{3-}. a) Suspended [$Zn_{1.5xn}L^{TP3}{}_n$] complex in DMSO-d_6. b) After the addition of 1 equiv. of BTT^{3-} and additional heating to 80°C for 10 min. c) After the addition of 1 equiv. TRI^{3-} and heating to 80°C for 10 min. d) Five minutes after the addition of 1 equiv. CYC^{3-}. e) After the addition of CYC^{3-}, the sample was kept for four hours at 25°C (DMSO-d_6, 500 MHz, 500 µM, 25°C).

A one-pot experiment illustrated the high binding affinity of the guest CYC^{3-}. In this experiment, the host was suspended in DMSO-d_6 and an equimolar mixture of all guest molecules was added simultaneously. The sample was heated to 85°C prior to the ^{1}H NMR measurement. The signals in the ^{1}H NMR spectra of the mixture exhibited a clean guest-driven self-assembly of the hexanuclear onion-type complex [(CYC)@Zn_6L_4]$^{3-}$ (Figure 5.16).

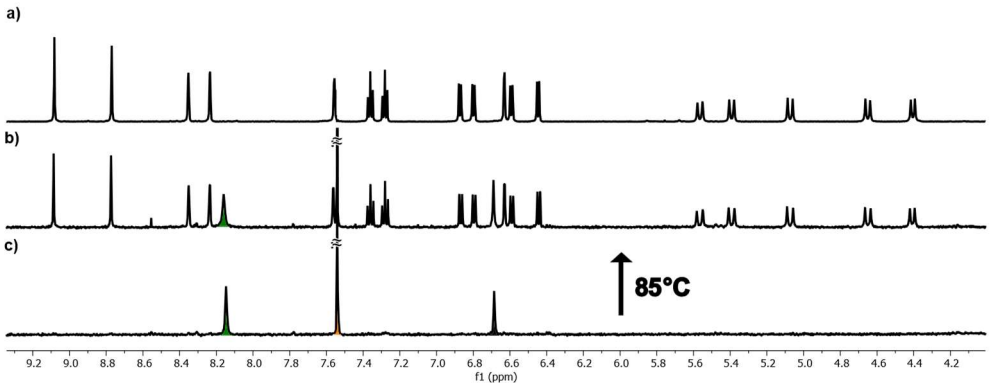

Figure 5.16: One pot experiment. a) reference ^{1}H NMR spectrum of [(CYC)@$Zn_6L^{TP3}{}_4$]$^{3-}$, b) ^{1}H NMR spectrum of an equimolar (1 equiv. each) mixture of TBA BTT, -TRI and -CYC + the suspended [$Zn_{1.5xn}L^{TP3}{}_n$] complex, after heating to 85°C for 10 min, c) ^{1}H NMR spectrum of an equimolar (1 equiv. each) mixture of TBA BTT, -TRI and -CYC + the suspended [$Zn_{1.5xn}L^{TP3}{}_n$] complex, prior to heating (DMSO-d_6, 500 MHz, 500 µM, 25°C).

The demonstrated ^{1}H NMR competitions experiments showed that the guest BTT^{3-} of $[(BTT)@Zn_3L_2]^{3-}$ was readily displaced by TRI^{3-} within five minutes at room temperature to form $[(TRI)@Zn_3L_2]^{3-}$, whereas the exchange of TRI^{3-} with CYC^{3-} and its corresponding transformation from a tri- to the hexanuclear host-guest assembly $[(CYC)@Zn_6L_4]^{3-}$ (equation 4) required more than 4 h under identical conditions.

Equation 4

$$2\,[(\mathrm{TRI})@\mathrm{Zn_3L_2}]^{3-} + CYC^{3-} \rightarrow [(\mathrm{CYC})@\mathrm{Zn_6L_4}]^{3-} + TRI^{3-}$$

To investigate this phenomenon, a kinetic evaluation of the guest exchange $TRI^{3-} \rightarrow CYC^{3-}$ was performed. Considering the host-guest system $[(TRI)@Zn_3L_2]^{3-}$ and CYC^{3-} as the reactants A and B, and assuming that only a single species is formed while neglecting that the stoichiometric requirement of two equivalents of $[(TRI)@Zn_3L_2]^{3-}$ are necessary for the transformation, we define the process as guest exchange. Under these assumptions, the equilibrium can be described as a pseudo second-order reaction (equation 5).[108]

Equation 5

$$\mathrm{A} + \mathrm{B} \xrightarrow{k} \mathrm{AB}$$

The course of this pseudo second-order guest exchange was observed via ^{1}H NMR spectroscopy and conducted at five different temperatures (25, 30, 35, 40 and 45°C). The rate constant k for each temperature was determined via the fully integrated rate law of a second-order reaction (equation 6), where each temperature has the same initial concentration $[A]_0$.

Equation 6

$$\frac{1}{[\mathrm{A}]} = kt + \frac{1}{[\mathrm{A}]_0}$$

A plot of the reciprocal of the current state concentration $[A]^{-1}$ against the initial time t together with a linear regression gives a slope with the value of the rate constant k.

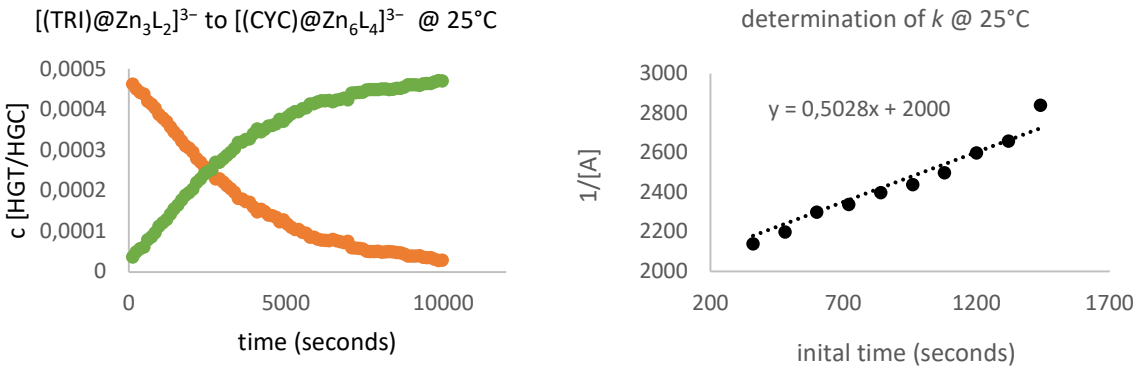

Figure 5.17: Left: Plot of the time-dependent ^{1}H NMR experiment showing the guest-induced transformation of the hexanuclear complex at 25°C. Green data points correspond to the concentration of complex $[(CYC)@Zn_6L_4]^{3-}$ (HGC) at a given time, while orange data points represent the concentration of $[(TRI)@Zn_3L_2]^{3-}$ (HGT). Right: Linear fit of the initial seconds of the guest exchange used to determine the rate constant at 25°C.

To determine the value of the activation energy ΔE_A of the guest-exchange process, the natural logarithm of k was plotted as a function of the reciprocal of the temperature T^{-1} in agreement with the ARRHENIUS equation (equation 7). The value of ΔE_A was then obtained from the slope of the resulting linear regression.[108]

Equation 7

$$\ln k = \frac{-E_A}{R}\left(\frac{1}{T}\right) + \ln A$$

The value of the activation energy ($\Delta E_A = 104.3\ kJ\ mol^{-1}$) was then obtained from the slope of the resulting linear regression. In addition to the Arrhenius plot, the EYRING plot allowed to determine the entropy of the transition state ($\Delta S^{\ddagger} = 78.2\ J\ mol\ K^{-1}$) and the activation enthalpy ($\Delta H^{\ddagger} = 97.8\ kJ\ mol^{-1}$) and thus an activation GIBBS free energy ($\Delta G^{\ddagger} = 74.5\ kJ\ mol^{-1}$) at 25°C. The EYRING plot describes the free energy of a transition state.[109] To determine the values, the natural logarithm of $\frac{k}{T}$ was plotted as a function of the reciprocal of the temperature T^{-1}. The EYRING equation in its straight linear form then gave the values for the transition state (equation 8).

Equation 8

$$\ln\left(\frac{k}{T}\right) = -\frac{\Delta H^{\ddagger}}{R}\left(\frac{1}{T}\right) + \ln\left(\frac{k_B}{h}\right) + \left(\frac{\Delta S^{\ddagger}}{R}\right)$$

These two plots provided mechanistical insight into the guest-exchange process. The interpretation of the activation energy, together with the positive entropy of the transition state, indicated an associative-dissociative exchange mechanism, in which the incoming guest interacts rapidly with the host before the complete release of the departing guest. The high activation barrier and the positive entropic contribution reflect the requirement for partial dissociation and structural reorganization of the supramolecular assembly during the guest-exchange transformation.

5.5 Conclusion and Outlook

In this chapter, the tripodal bis-bidentate ligand L^{TP3}-H_3, derived from tripropargyl amine, was designed to expand the structural diversity of charge-neutral supramolecular architectures. The ligand introduced a flexible backbone with a tertiary amine center, providing both adaptability and potential internal recognition sites. While direct self-assembly with $Zn(OAc)_2$ in DMSO-d_6 led to poorly defined aggregates, sharper NMR signals in DMF-d_7 indicated the formation of discrete species.

To control the assembly, guest-driven self-assembly was employed using tricarboxylate anions as templates. Depending on the guest geometry, the system formed either trinuclear $[(BTT)@Zn_3L_2]^{3-}$ and $[(TRI)@Zn_3L_2]^{3-}$ or hexanuclear onion-type complexes $[(TRI)@Zn_6L_4]^{3-}$, $[(CYC)@Zn_6L_4]^{3-}$ and $[(BtA)@Zn_6L_4]^{3-}$. The thiophene-based guest BTT^{3-} induced a distorted, strained complex with broad NMR signals, whereas the smaller trimesate guest yielded a more symmetric and rigid assembly. Crystallographic analysis confirmed the hexanuclear onion-type structure for both TRI^{3-} and CYC^{3-} guests, consisting of three binuclear Zn(II) clusters. NOE contacts between inner- and outer-shell ligands further confirmed the onion-type architecture in solution.

Competition experiments gave a qualitative determination of the binding affinity order for the three guests. With BTT^{3-} and BtA^{3-} being displaced by TRI^{3-} within minutes, while the guest induced transformation from TRI^{3-} to CYC^{3-} required several hours. Kinetic analysis revealed a pseudo-second-order transformation, indicating an associative-dissociative exchange mechanism involving partial reorganization of the assembly.

Overall, this study demonstrated that guest temptation effectively controls the nuclearity, symmetry and topology of charge-neutral Zn(II) complexes. Guest geometry dictated not only the structures but also the kinetics of transformation between assemblies.

The modular adaptive nature of these host-guest systems makes them attractive for further studies on cooperative binding., anion recognition and templated catalysis. Their dynamic transformations and confined cavities may inspire stimuli-responsive materials, molecular encapsulation or nanoreactors, providing a bridge between fundamental supramolecular design and potential applications.

5.6 Experimental Part

5.6.1 General information

Chemicals and solvents were purchased from Sigma Aldrich, Acros Organics, Carl Roth, TCI Europe, VWR and ABCR. Monitoring of reactions were performed with thin layer chromatography using silica coated aluminium plates (Merck, silica 60, fluorescence indicator F_{254}, thickness 0.25 mm). For column chromatography, silica (Merck, silica 60, 0.02-0.063 mesh ASTM) was used as the stationary phase. High resolution Electrospray ionization (ESI) mass spectra were obtained using a Bruker ESI timsTOF (trapped ion mobility-time of flight) and Compact mass spectrometers (positive and negative mode). Samples were diluted with HPLC-grade acetonitrile. NMR spectra were recorded on Bruker AVANCE III 500, 600 and 700 MHz spectrometers. Chemical shifts were reported in ppm with residual solvent as reference: DMSO-d_6 (2.50 ppm for ^{1}H, 39.52 ppm for ^{13}C), $CDCl_3$ (7.26 ppm for ^{1}H, 77.16 ppm for ^{13}C) and DMF-d_7 (8.03 ppm for ^{1}H). Abbreviations for signal multiplicity in the ^{1}H NMR spectra were indicated as: s, singlet; d, doublet; t, triplet; dd, doublets of doublets; m, multiplet; b, broad.

5.6.2 Deprotonation of tri-carboxylic acids

The tricarboxylic acids were dissolved in a small amount of MeOH (up to 5 mL), and three equivalents of TBA hydroxide (1 M in MeOH) were added. Afterward, the mixture was vortexed for 30 min and the solvent was evaporated. A small amount of water (1-2 mL) was added to the remaining slurry residue to assist the final lyophilization process. The TBA tricarboxylates were used without further purification.

5.6.3 General procedure of guest driven self-assembly

$[Zn_{1.5xn}L^{TP3}{}_n]$ (1 equiv.) was suspended in DMSO-d_6 or DMF-d_7 (500 µM, 500 µL), transferred to an NMR-tube and titrated with a solution of a TBA tricarboxylate (5 µL, 50 mmol, DMSO-d_6, 1 equiv.). Before the acquisition of the ^{1}H NMR data at 25°C, each titration step was heated at 80°C for 10 min.

5.6.4 Synthetic procedure of ligand L^{TP3}-H_3

The azide **S4** was prepared in five steps (Figure 5.18) according to the synthetic route described in the previous chapter (chapter 3.7.4).

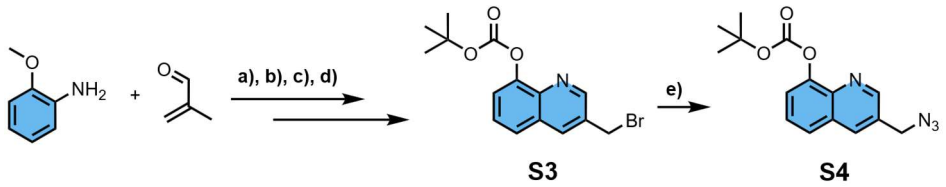

*Figure 5.18: A simplified representation of the five-step synthesis route for the preparation of the azide **S4**. a) SKRAUP-type reaction, b) methoxy cleavage, c) Boc-protection, d) radical bromination, e) nucleophilic substitution.*

Next, the azide **S4** was *clicked* with tripropargyl amine in a 1:3 ratio and the resulting product treated with TFA to cleave the BOC groups (Figure 5.19).

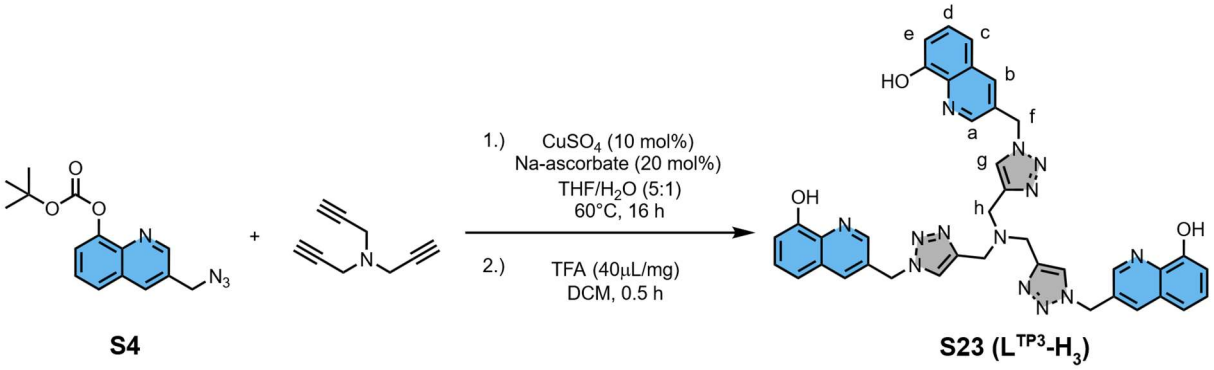

*Figure 5.19: The copper(I)-catalyzed click reaction of **S4** and tripropargylamine with subsequent deprotection of the BOC protecting groups, which gave the ligand **S23** (L^{TP3}-H_3).*

The azide **S4** (183.15 mg, 609.9 µmol, 3.2 equiv.) was transferred into a Schlenk tube and dissolved in THF. The solution was degassed for 20 min with argon. $CuSO_4$ (3 mg, 19.1 µmol, 0.1 equiv.) and sodium-ascorbate (15.1 mg, 76.2 µmol, 0.4 equiv.) were dissolved in small amounts of water and added sequentially. Tripropargylamine (27 µL, 190.6 µmol, 1 equiv.) was added under argon, the solution was heated to 60 °C and stirred for 16 h. The reaction solution was diluted with DCM and the organic layer was washed with EDTA (0.25 M), brine and saturated NH_4Cl solution. The aqueous layer was extracted with DCM (3x). The combined organic layers were dried with Na_2SO_4 and the solvent was evaporated under reduced pressure. Column chromatography (silica, DCM/MeOH gradient 0 % - 3 %) yielded the BOC-protected derivative. The solvent was evaporated, redissolved in DCM and treated with TFA (40 µL/mg). After 1 h the reaction mixture got neutralized with sat. $NaHCO_3$ and the organic layer diluted with DCM. The aqueous layer was extracted with DCM (7x), washed with brine and the organic layers were dried via Na_2SO_4. The solvent was evaporated until there was a residue organic layer present. Pouring Et_2O into the residue gives the ligand **S23** (L^{TP3}-H_3) as a white powder (57%, 79.4 mg, 108.5 µmol).

^{1}H NMR (500 MHz, DMSO-d_6, 25°C): δ = 9.91 (s, 3H, OH), 8.82 (d, *J* = 2.1 Hz, 3H, a), 8.20 (s, 3H, g), 8.18 (d, *J* = 2.2 Hz, 3H, b), 7.43 (t, *J* = 7.9 Hz, 3H, d), 7.36 (dd, *J* = 1.3 Hz, 3H, c) 7.07 (dd, *J* = 7.5 Hz, 3H, e), 5.83 (s, 6H, f), 3.65 (s, 6H, h) ppm. **^{13}C NMR** (151 MHz, DMSO-d_6, 25°C): δ = 153.85, 148.48, 144.30, 138.40, 135.46, 130.07, 128.69, 128.64, 124.86, 118.21, 112.35, 50.92, 47.47 ppm. **HRMS** (negative ESI-MS, ACN/DMSO 98:2, 30°C): m/z = 730.2700 ($[M-H]^-$, $C_{39}H_{32}N_{13}O_3^-$, calc. 730.2757).

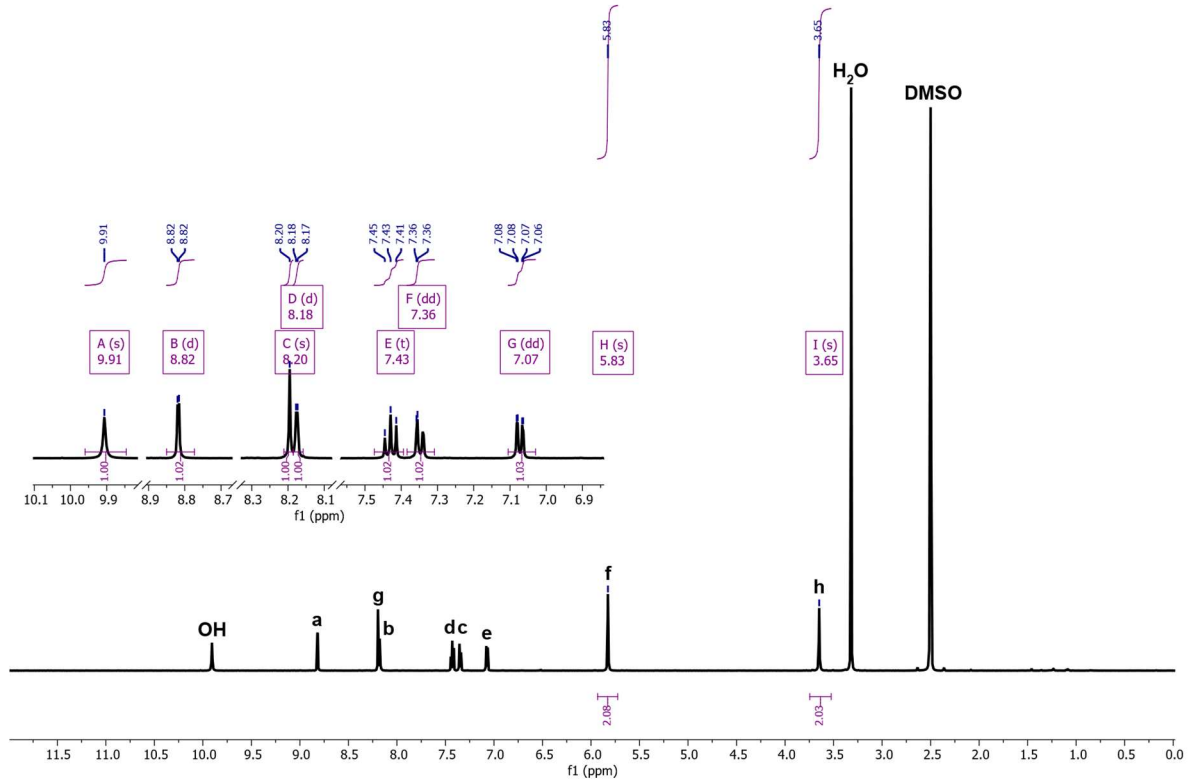

*Figure 5.20: ^{1}H NMR of ligand **S23** (L^{TP3}-H_3) (DMSO-d_6, 500 MHz, 25°C).*

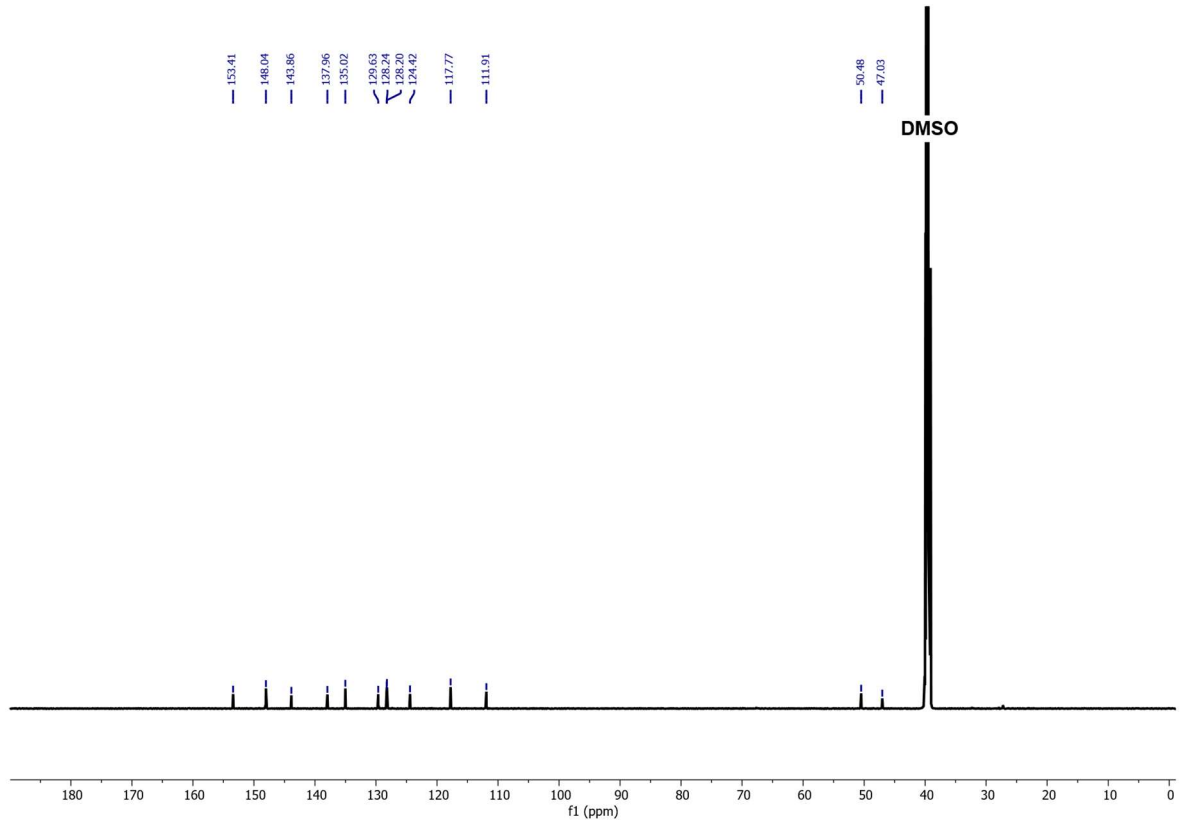

*Figure 5.21: ^{13}C NMR of ligand **S23** (L^{TP3}-H_3) (DMSO-d_6, 151 MHz, 25°C).*

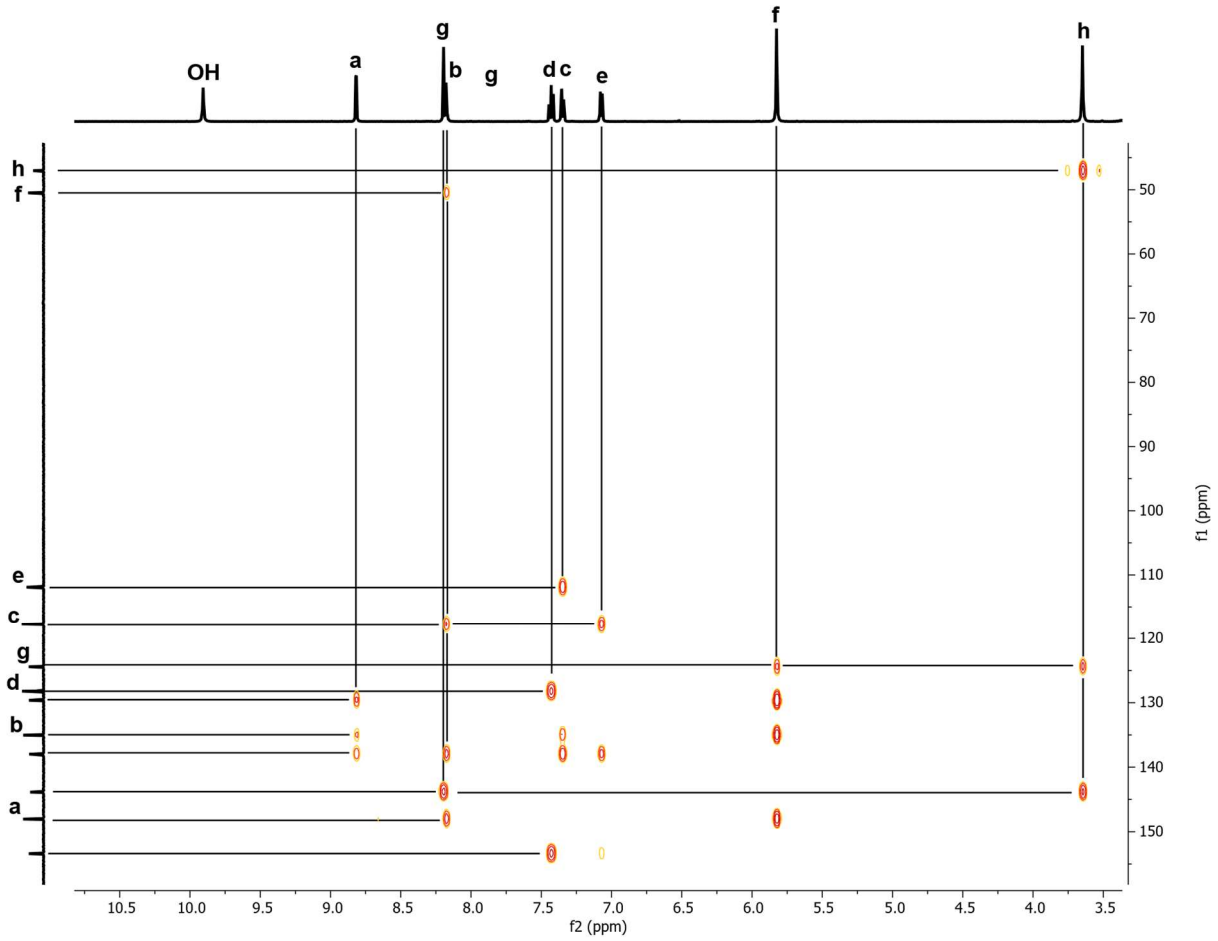

*Figure 5.22: HMBC NMR of ligand **S23** (L^{TP3}-H_3) (DMSO-d_6, 600 MHz, 25°C).*

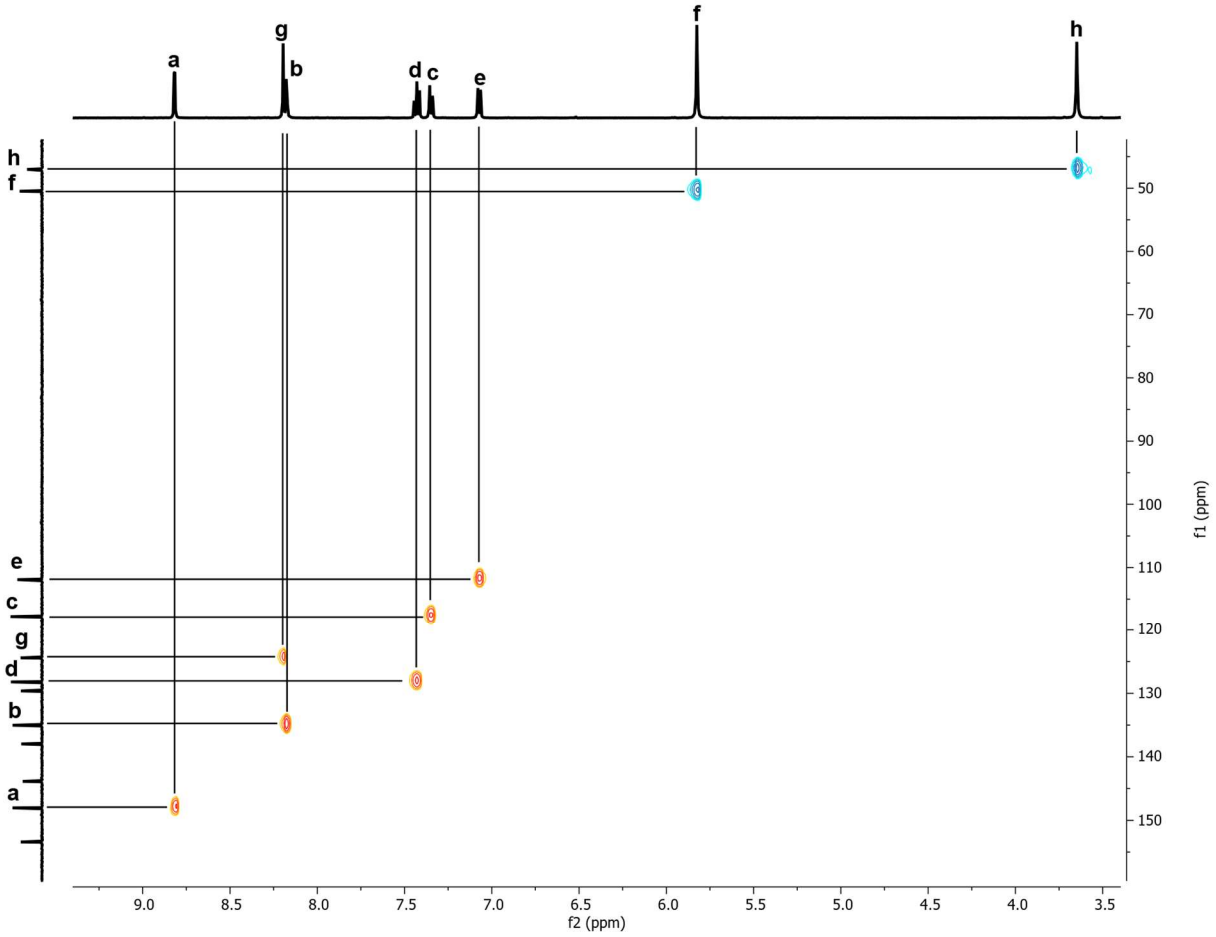

*Figure 5.23: HSQC NMR of ligand **S23** (L^{TP3}-H_3) (DMSO-d_6, 600 MHz, 25°C).*

5.6.5 *Self-assembly of ligand L^{TP3}-H_3 with $Zn(OAc)_2$*

Then, the ligand **S23** (L^{TP3}-H_3) was self-assembled with $Zn(OAc)_2$ in DMSO-d_6 (Figure 5.24) and in DMF-d_7 (Figure 5.29) in a 2:3 ratio.

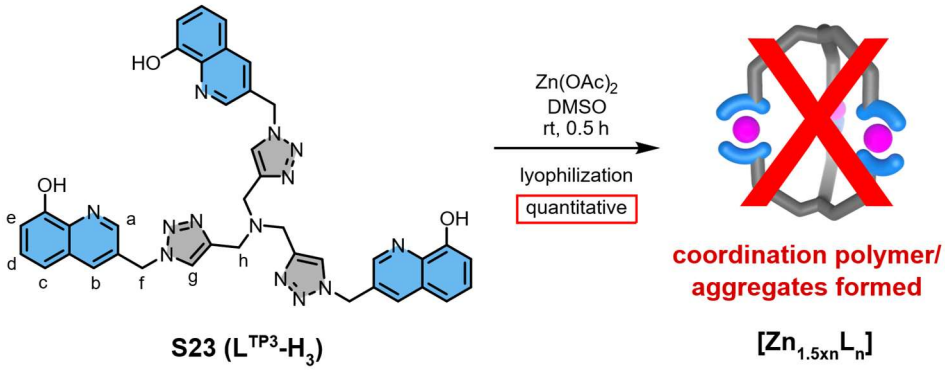

*Figure 5.24: Self-assembly of ligand **S23** (L^{TP3}-H_3) and $Zn(OAc)_2$ in a 2:3 ratio in DMSO-d_6 at 25°C. Forming a weakly soluble aggregate.*

Ligand **S23** (L^{TP3}-H_3) (1 equiv.) and $Zn(OAc)_2$ (1.5 equiv.) were dissolved separately in DMSO-d_6.The zinc acetate solution was added to the stirring ligand solution which resulted in a colour change to yellow. The reaction solution was allowed to stir for 2 h, observing precipitation. The solvent as well as the by-product acetic acid were removed via lyophilization, which yields the complex as a yellow solid. The complex is suspended and washed with methanol for further purification. The mixture was centrifuged and the solvent was removed via decantation. This cleaning process was repeated twice but with Et_2O. The resulting precipitate was again dissolved in DMSO which was removed via lyophilization to give the clean complex as a yellow solid in quantitative fashion. Full ^{1}H NMR signal-assignment of the different species shown in the ^{1}H NMR spectrum was not successful. ESI-MS spectrometry did not show m/z values corresponding to the formation of a $[Zn_{1.5xn}L^{TP3}{}_n]$ species, but a $[Zn_1L^{TP3}{}_1]^-$ species. All crystallization attempts resulted in precipitation of an amorphous solid.

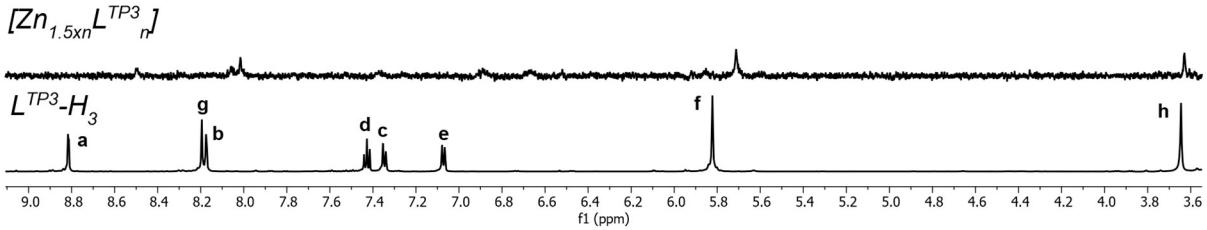

*Figure 5.25: ^{1}H NMR spectra of the self-assembly of ligand **S23** (L^{TP3}-H_3) with $Zn(OAc)_2$ in a 2:3 ratio (DMSO-d_6, 500 MHz, 25°C).*

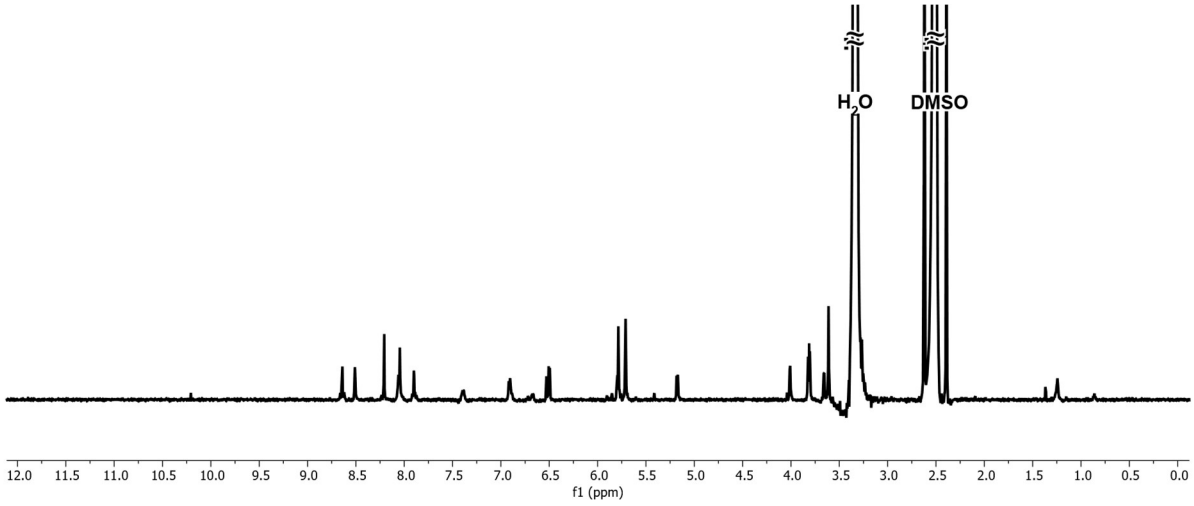

Figure 5.26: ^{1}H NMR spectrum of [$Zn_{1.5xn}L^{TP3}{}_{n}$] suspension (DMSO-d_6, 600 MHz, 25°C, 72 scans).

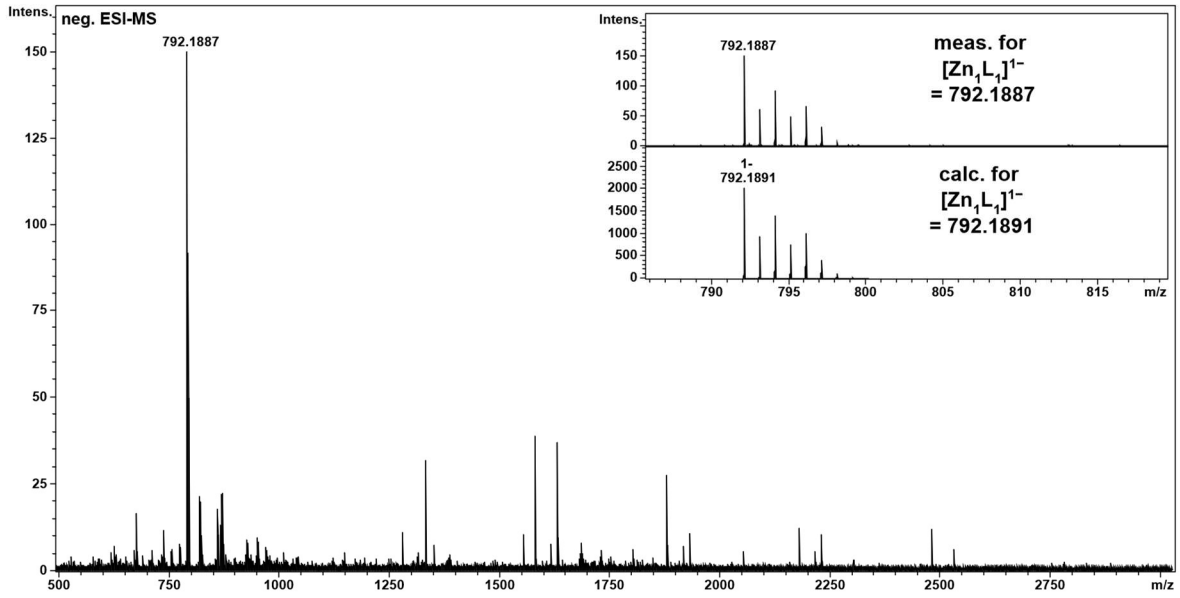

Figure 5.27: Negative ESI MS spectrum of a [$Zn_{1.5xn}L^{TP3}{}_{n}$] suspension in DMSO-d_6.

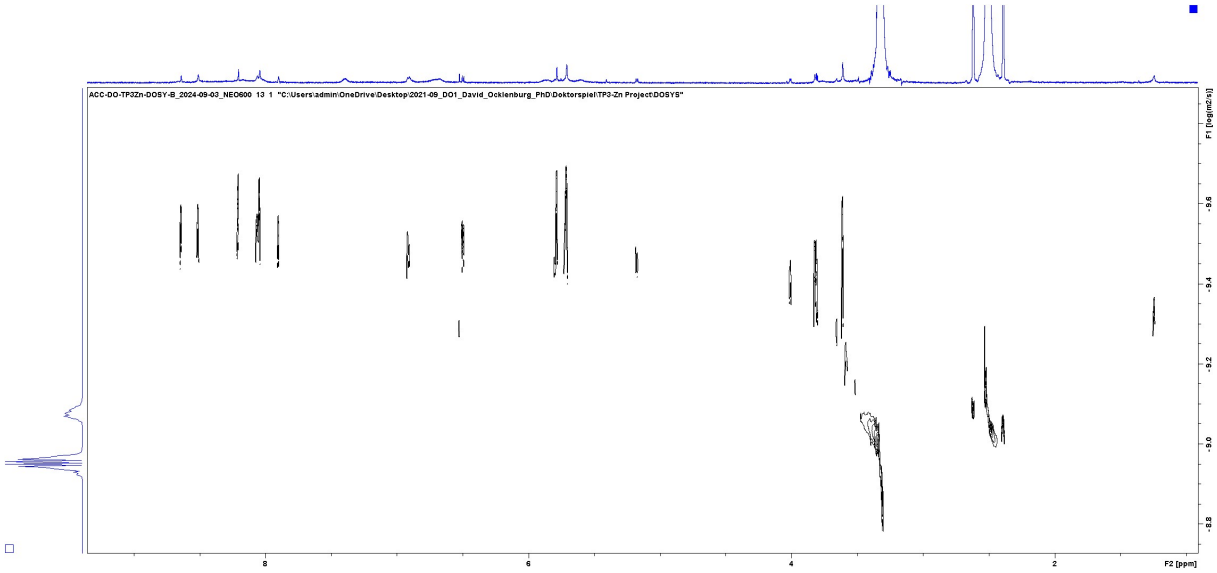

*Figure 5.28: ^{1}H DOSY NMR spectrum of complex formation of ligand **S23** (L^{TP3}-H_3) with $Zn(OAc)_2$ (2:3) in DMSO-d_6 at 25 °C. After addition of $Zn(OAc)_2$, the sample was heated at 70°C for 16 h, D = 3.355 x 10^{-10} m^2 s^{-1}, r_H = 0.33 nm. (DMSO-d_6, 600 MHz, 25°C)*

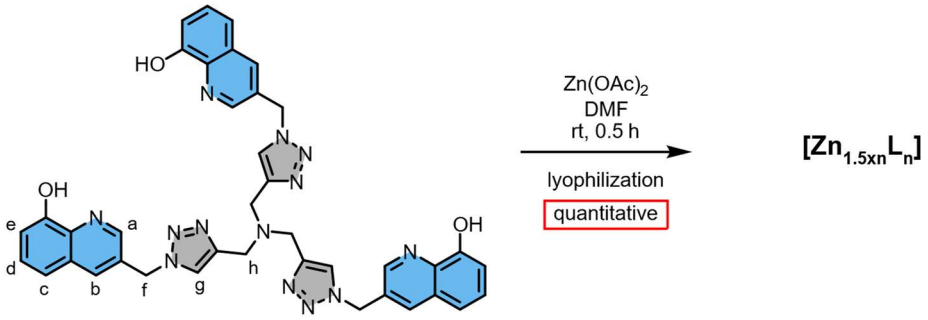

*Figure 5.29: Complex formation of ligand **S23** (L^{TP3}-H_3) with $Zn(OAc)_2$ (2:3) in DMF-d_7 at 25°C, forming an observable $[Zn_1L^{TP3}{}_1]^-$ complex. After addition of $Zn(OAc)_2$, the sample was heated at 70°C for 16 h.*

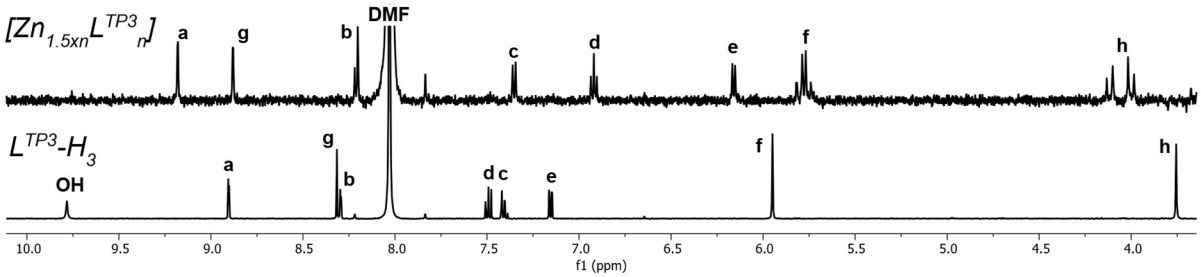

*Figure 5.30: ^{1}H NMR spectra of complex formation of ligand **S23** (L^{TP3}-H_3) with $Zn(OAc)_2$ (2:3) in DMF-d_7. After addition of $Zn(OAc)_2$, the sample was heated at 70°C for 16 h. (DMF-d_7, 500 MHz, 25°C)*

5.6.6 Guest-induced host-guest formations

According to the general procedure of the host-guest complex formation, the suspended [$Zn_{1.5xn}L^{TP3}{}_n$] (1 equiv.) was treated with TBA BTT (1 equiv.) and was then heated for 10 min at 70°C. ^{1}H NMR showed the formation of [(BTT)@$Zn_3L^{TP3}{}_2$]$^{3-}$ and a minor species.

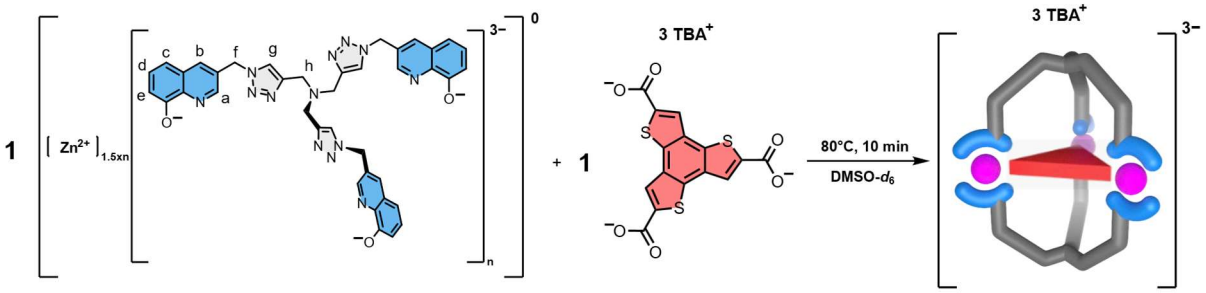

Figure 5.31: Templated self-assembly of the weakly soluble [$Zn_{1.5nx}L^{TP3}{}_n$] aggregate with TBA BTT in DMSO in a 1 to 1 ratio in DMSO-d_6 into a negatively charged host-guest complex [(BTT)@Zn_3L_2]$^{3-}$.

^{1}H NMR (500 MHz, DMSO-d_6, 25°C): δ = 8.95 (s, 6H, a), 8.36 (s, 6H, b), 7.93 (s, 3H, guest), 7.34 (m, 7H, d, g), 7.17 (s, 3H, g'), 6.82 (d, *J* = 7.0 Hz, 6H, c), 6.57 (d, *J* = 8.3 Hz, 6H, e), 5.85 (s, 6H, f), 5.66 (s, 6H, f'), 2.80 (d, *J* = 31.1 Hz, 6H, h), 1.05 (m, 6H, h', the signals are overlapping with TBA) ppm. **^{13}C NMR** (151 MHz, DMSO-d_6, 25°C): δ = 166.6026, 164.0436, 144.7216, 143.2078, 142.0805, 140.2326, 137.7527, 134.8444, 131.1762, 130.5965, 129.1517, 123.8809, 122.5675, 120.5020, 111.6373, 107.3834, 50.7000, 46.3082 ppm. **HRMS** (negative ESI-MS, ACN/DMSO 80:20, 30°C): m/z = 676.4049 [($C_{15}H_3O_6S_3$)@($C_{39}H_{31}N_{13}O_3$)$_2$$Zn_3$]$^{3-}$, calc. 676.4046.

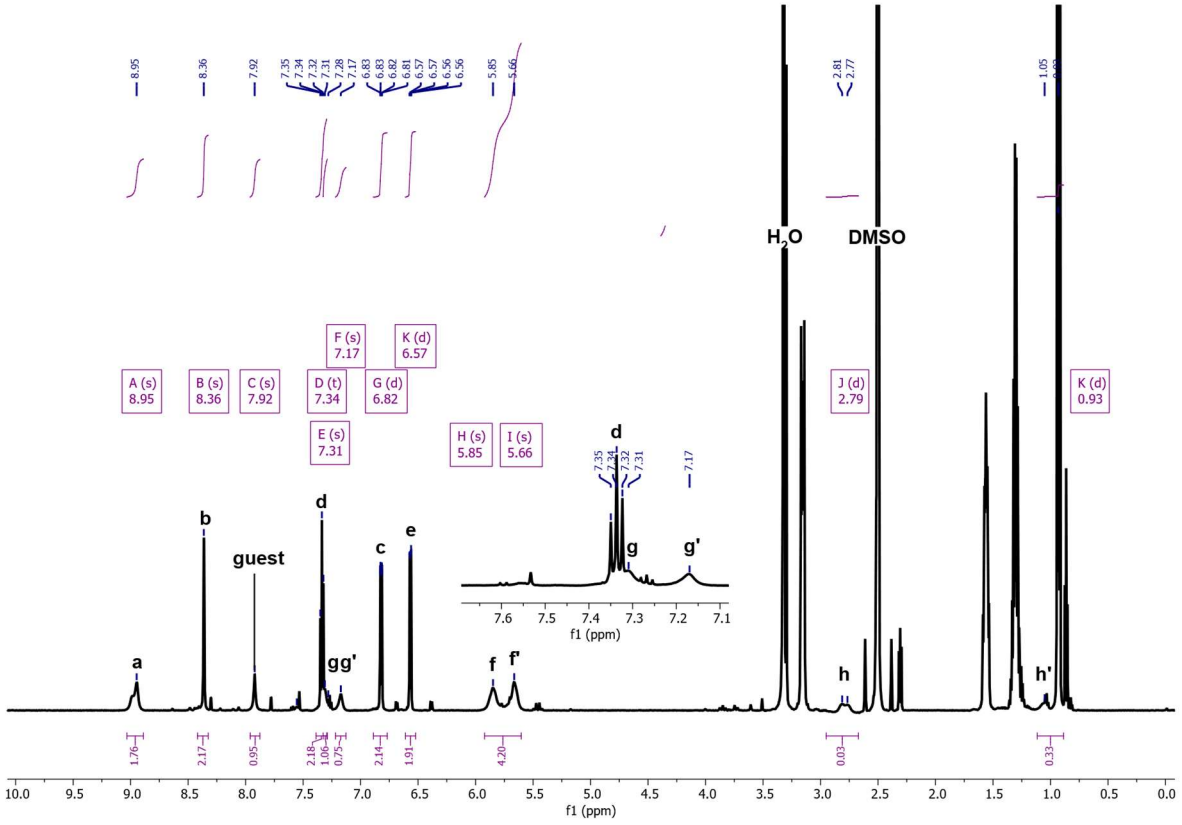

Figure 5.32: ^{1}H NMR spectrum of [(BTT)@ $Zn_3L^{TP3}{}_2$]$^{3-}$ (1 mM, 500 MHz, DMSO-d_6, 25°C).

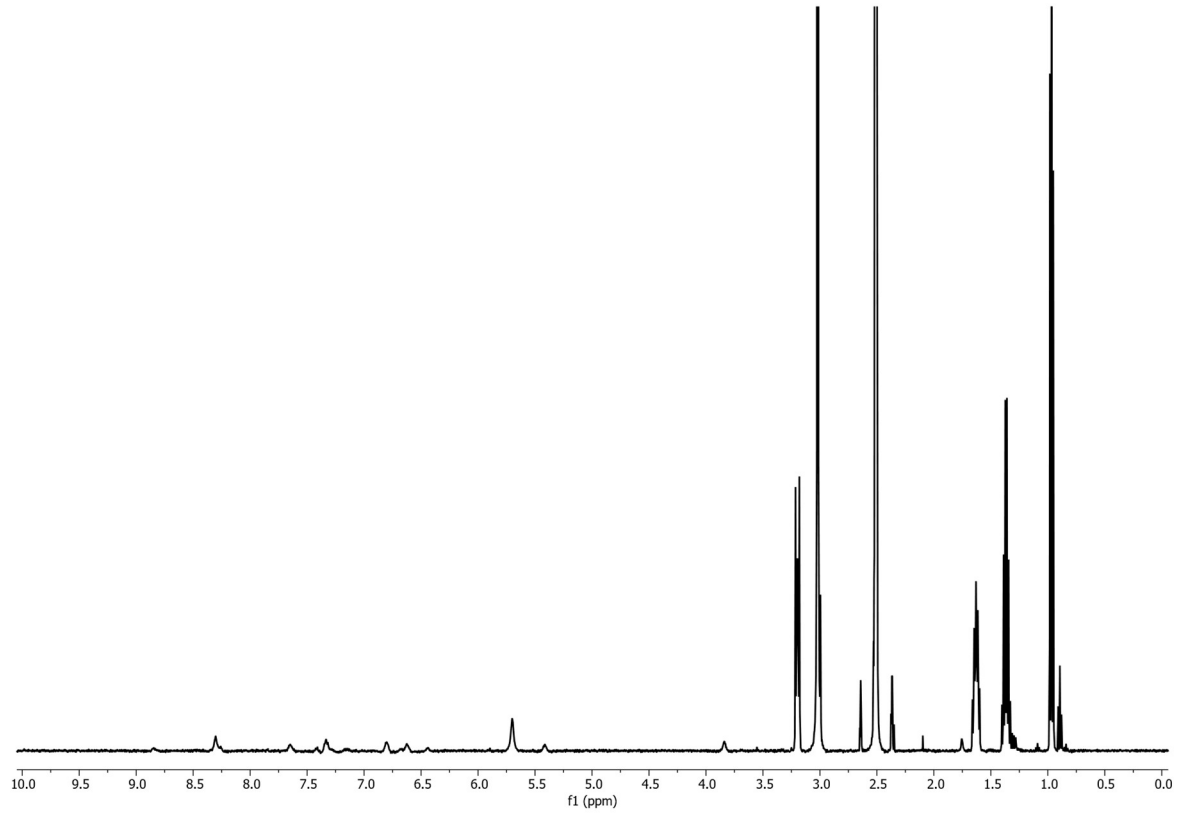

Figure 5.33: ^{1}H VT NMR spectrum of [(BTT)@ $Zn_3L^{TP3}{}_2]^{3-}$ (1 mM, 500 MHz, DMSO-d_6, 90°C).

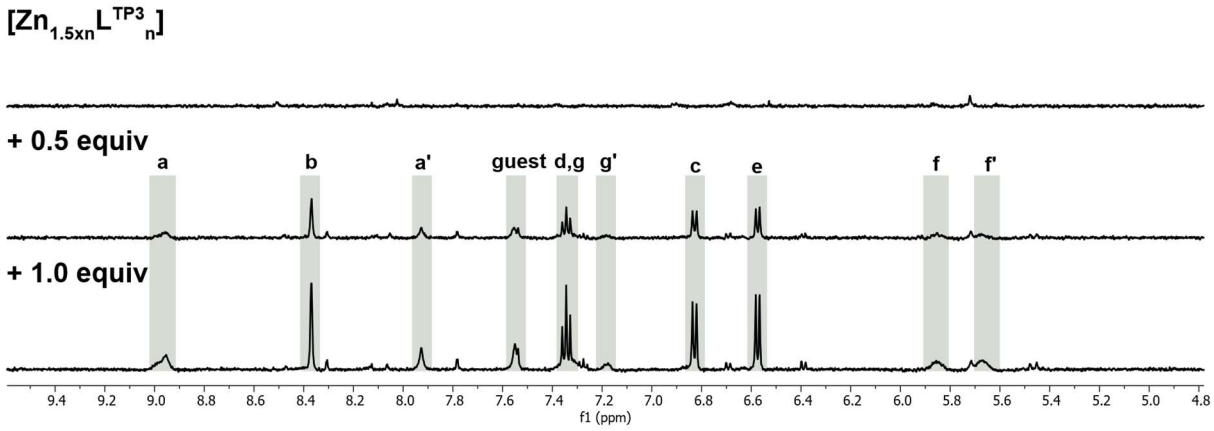

Figure 5.34: ^{1}H NMR spectra of a two-step titration showing exclusively the self-assembly of [(BTT)@ $Zn_3L^{TP3}{}_2]^{3-}$ (DMSO-d_6, 500 MHz, 25°C).

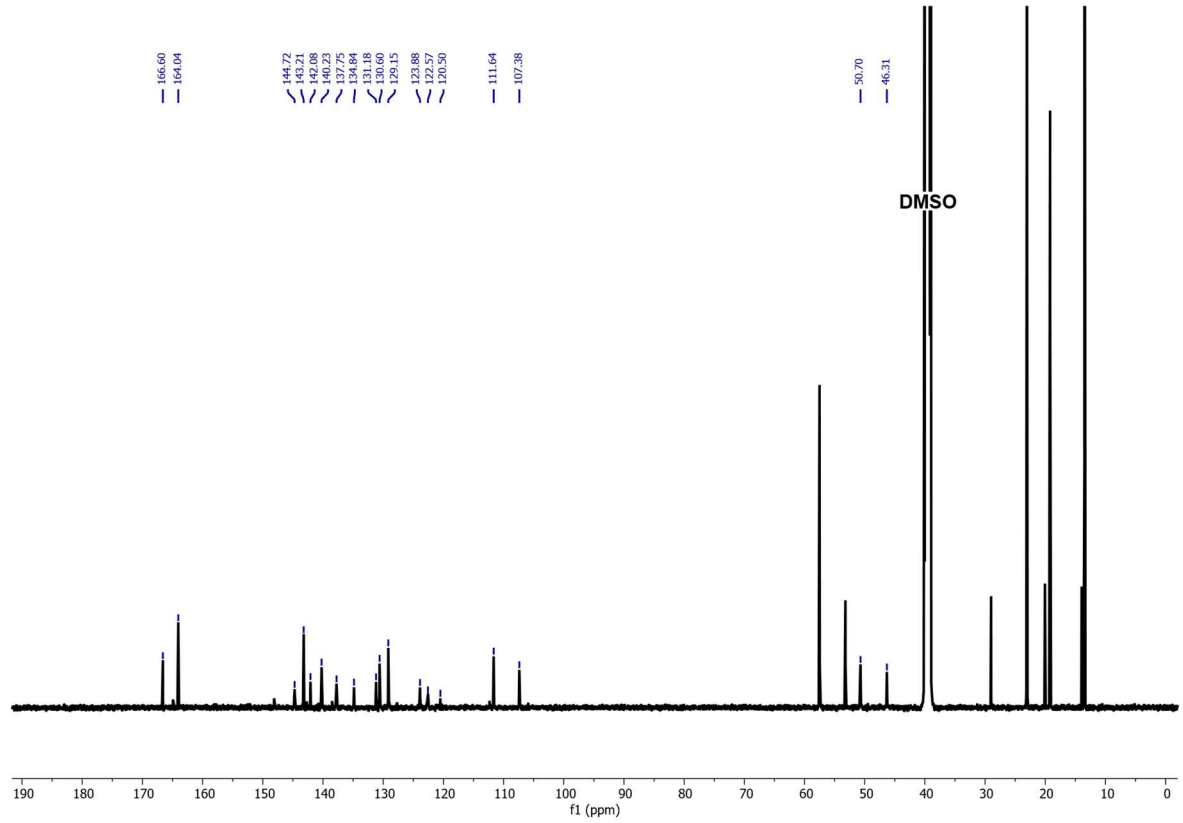

Figure 5.35: ^{13}C NMR spectrum of [(BTT)@ $Zn_3L^{TP3}{}_2]^{3-}$ (1 mM, 151 MHz, DMSO-d_6, 25°C).

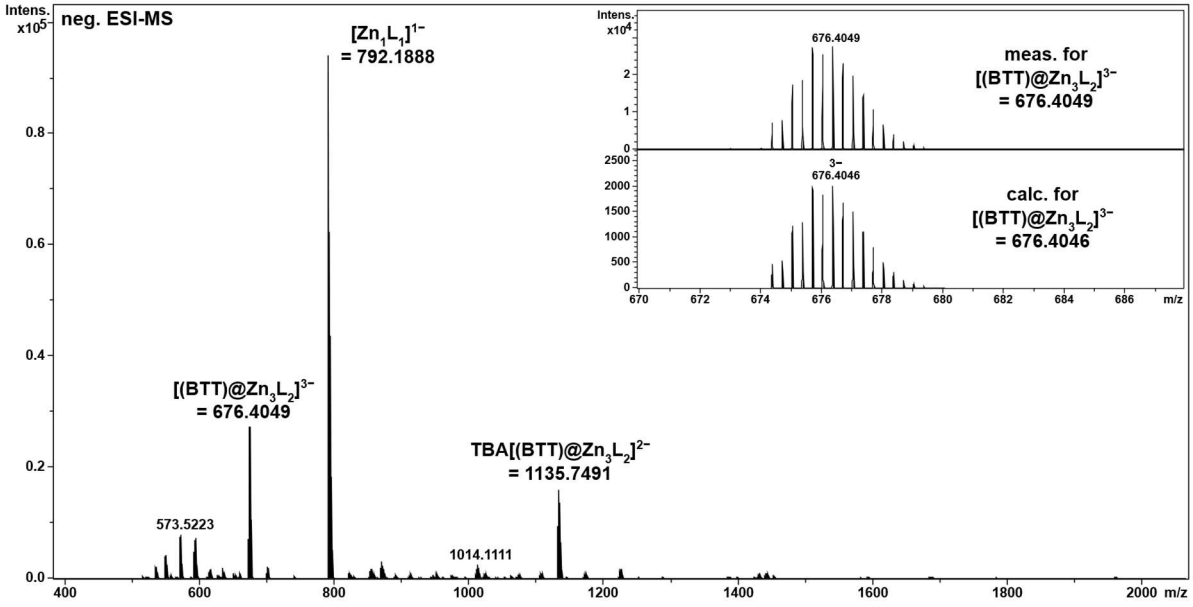

Figure 5.36 Negative ESI-MS spectrum of [(BTT)@ $Zn_3L^{TP3}{}_2]^{3-}$ (DMSO:ACN 1:4, 30°C), the spectrum shows the desired host-guest system, its TBA adduct and a $[Zn_1L^{TP3}{}_1]^-$ species.

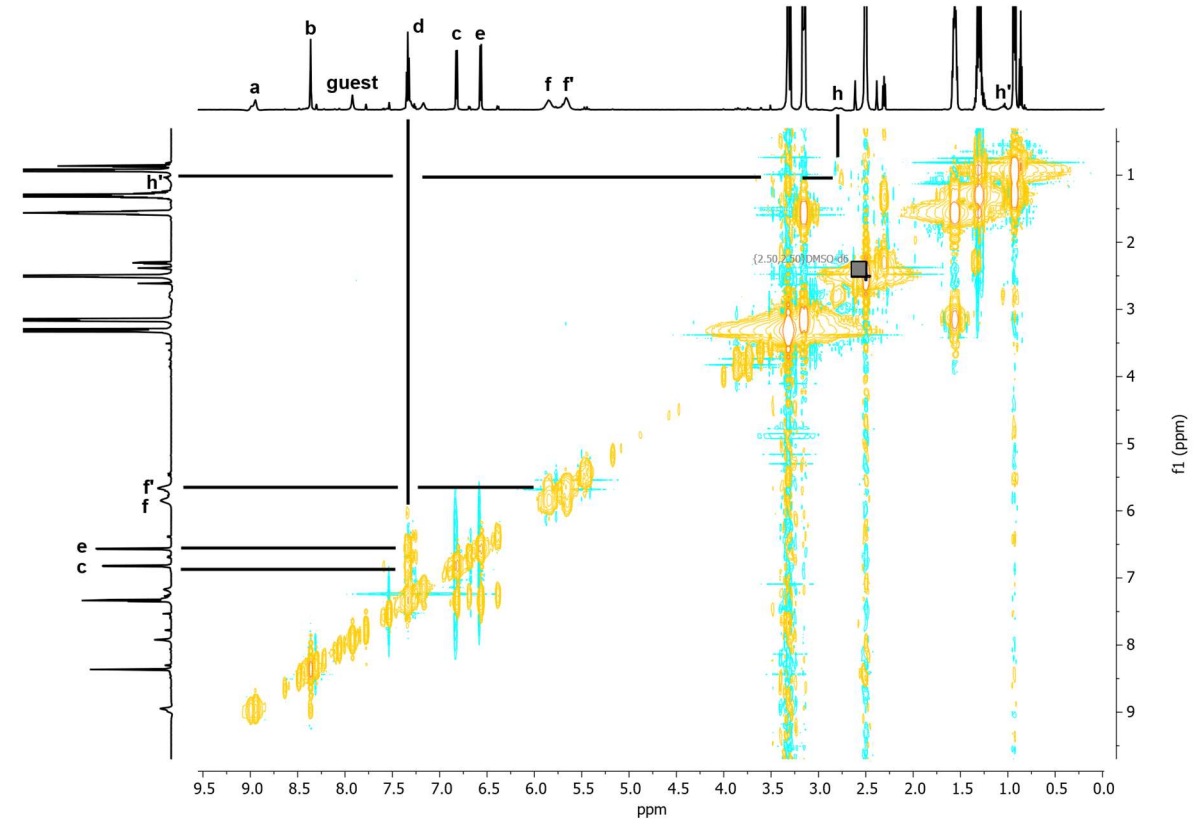

Figure 5.37: ^{1}H COSY spectrum of [(BTT)@ $Zn_3L^{TP3}{}_2]^{3-}$ (1 mM, 600 MHz, DMSO-d_6, 25°C).

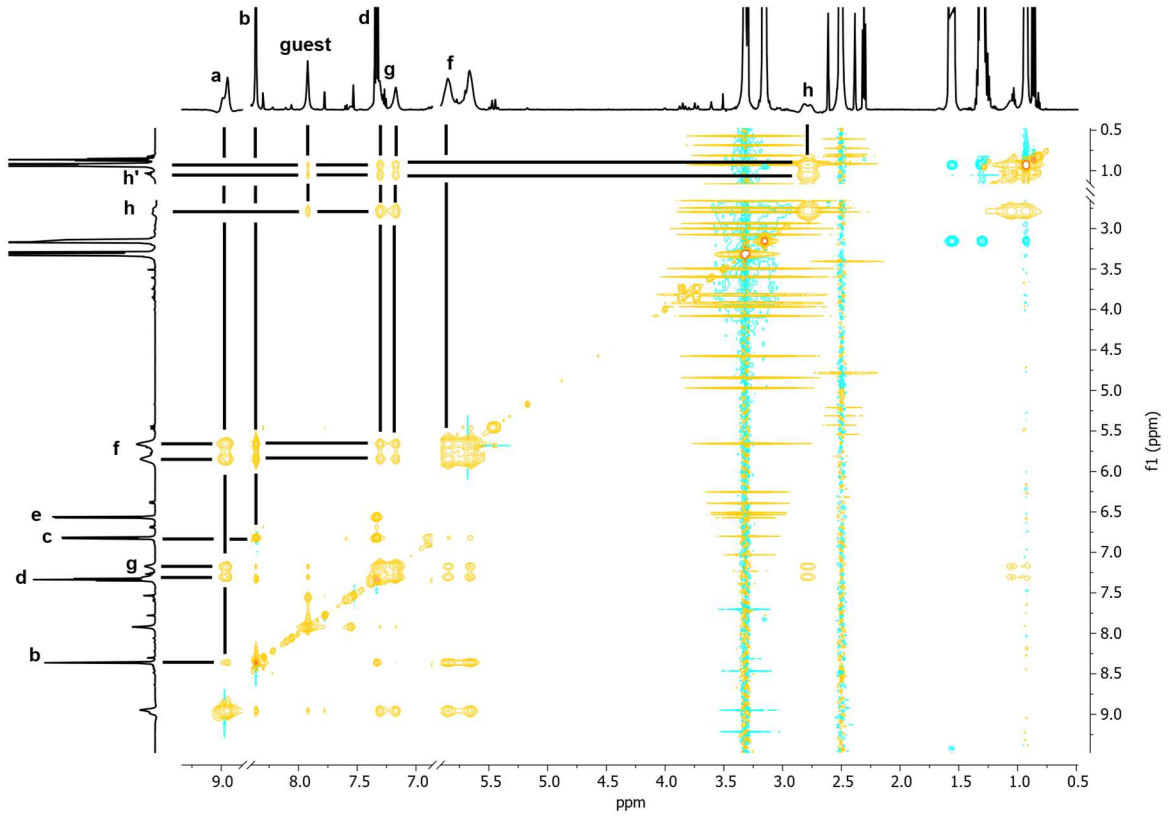

Figure 5.38: ^{1}H NOESY spectrum of [(BTT)@ $Zn_3L^{TP3}{}_2]^{3-}$ (1 mM, 600 MHz, DMSO-d_6, 25°C).

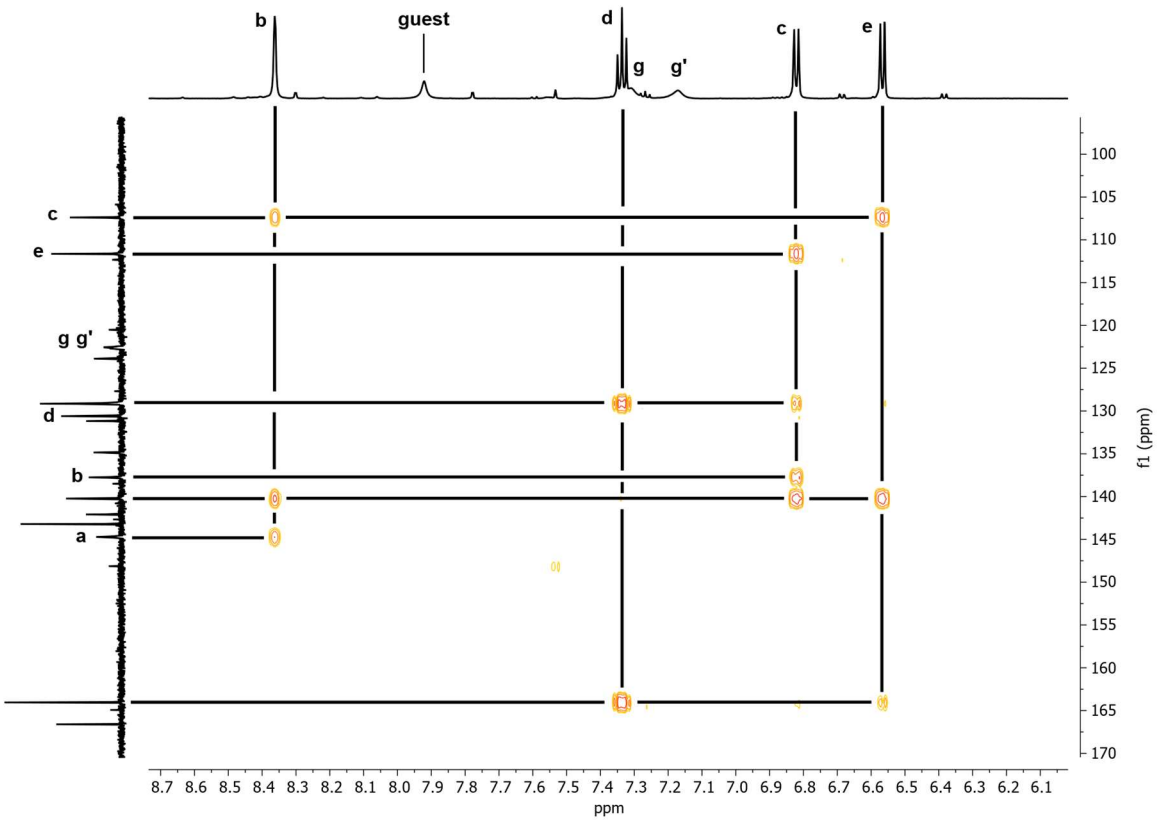

Figure 5.39: HMBC NMR spectrum of [(BTT)@ $Zn_3L^{TP3}{}_2]^{3-}$ (1 mM, 151 MHz, DMSO-d_6, 25°C).

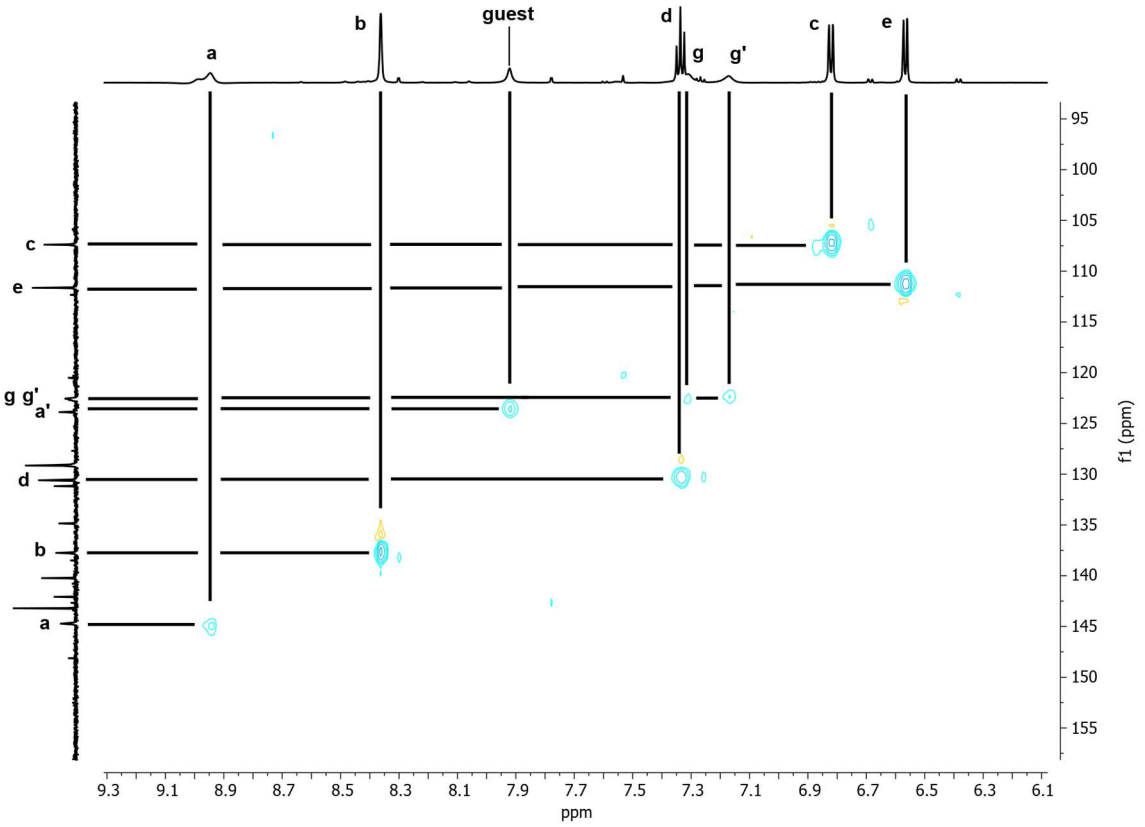

Figure 5.40: HSQC NMR spectrum of [(BTT)@ $Zn_3L^{TP3}{}_2]^{3-}$ (1 mM, 151 MHz, DMSO-d_6, 25°C).

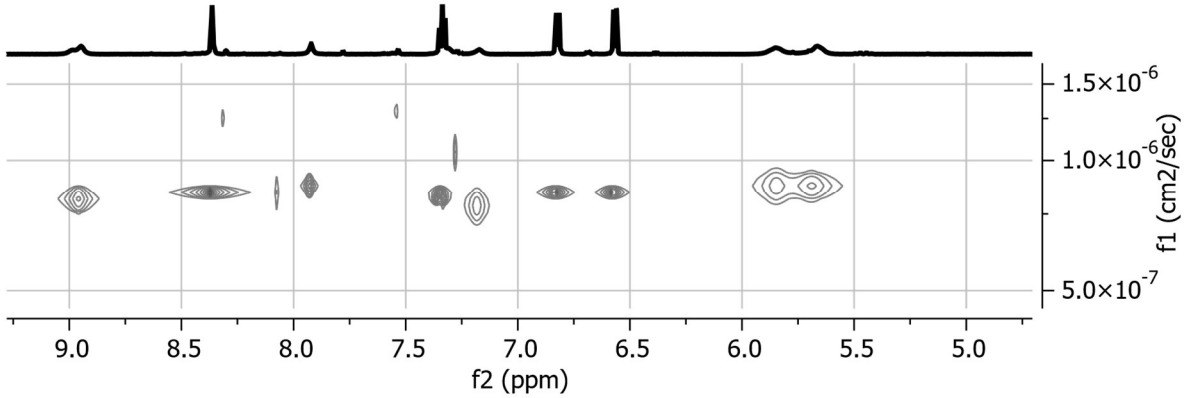

Figure 5.41: ^{1}H DOSY NMR spectrum of [(BTT)@ $Zn_3L^{TP3}{}_2]^{3-}$, D = 9.005 x 10^{-11} m^2 s^{-1}, r_H = 1.22 nm. (1 mM, 500 MHz, DMSO-d_6, 25°C).

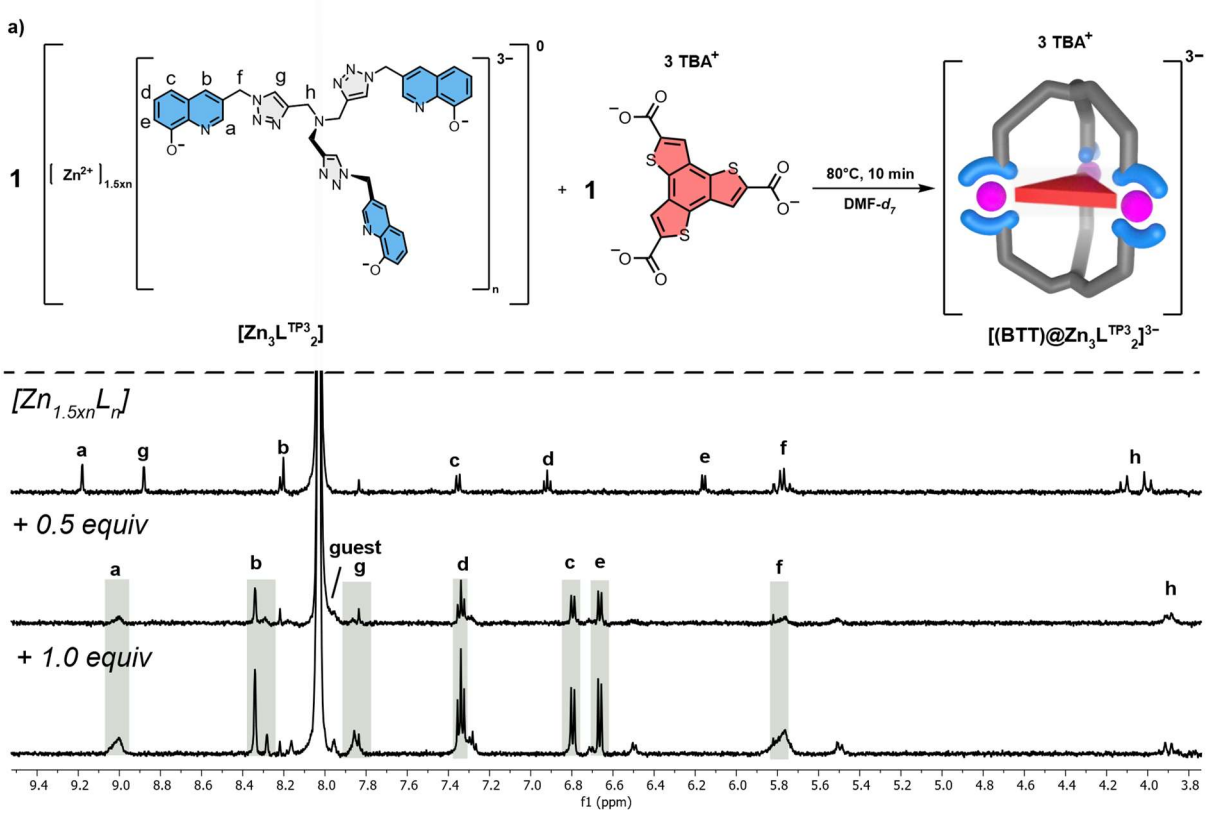

Figure 5.42: ^{1}H NMR spectra of [(BTT)@ $Zn_3L^{TP3}{}_2]^{3-}$ in DMF-d_7 at 25°C, recorded during gradual addition of TBA BTT. After each step of the addition, the sample was heated at 80°C for 10 minutes.

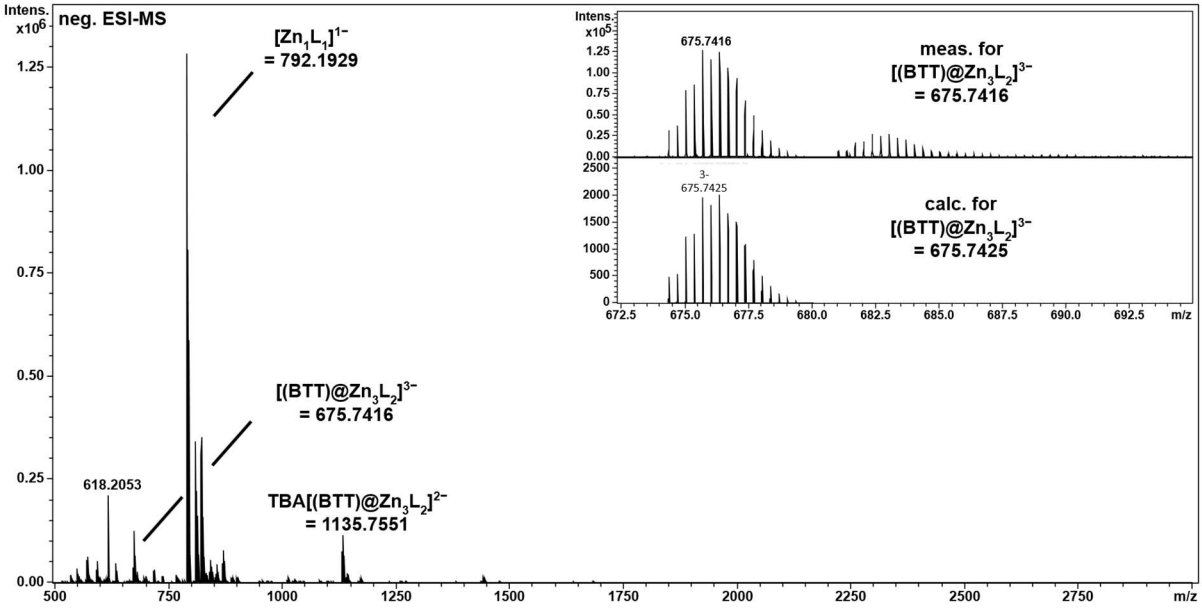

Figure 5.43: Negative ESI-MS spectrum of [(BTT)@ $Zn_3L^{TP3}{}_2]^{3-}$ (DMF:ACN 1:4, 30°C), the spectrum shows the desired host-guest system, its TBA adduct and a $[Zn_1L^{TP3}{}_1]^{1-}$ species.

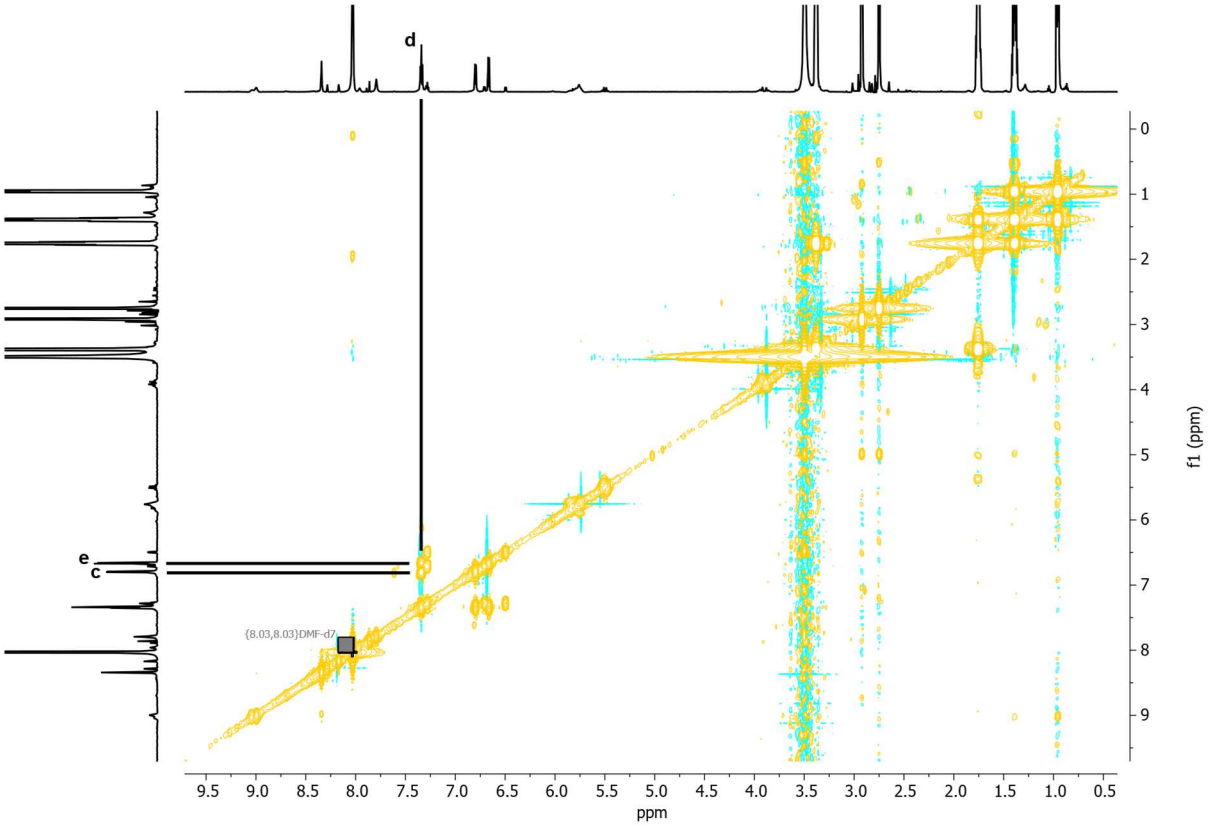

Figure 5.44: ^{1}H COSY spectrum of [(BTT)@ $Zn_3L^{TP3}{}_2]^{3-}$ (1 mM, 700 MHz, DMF-d_7, 25°C).

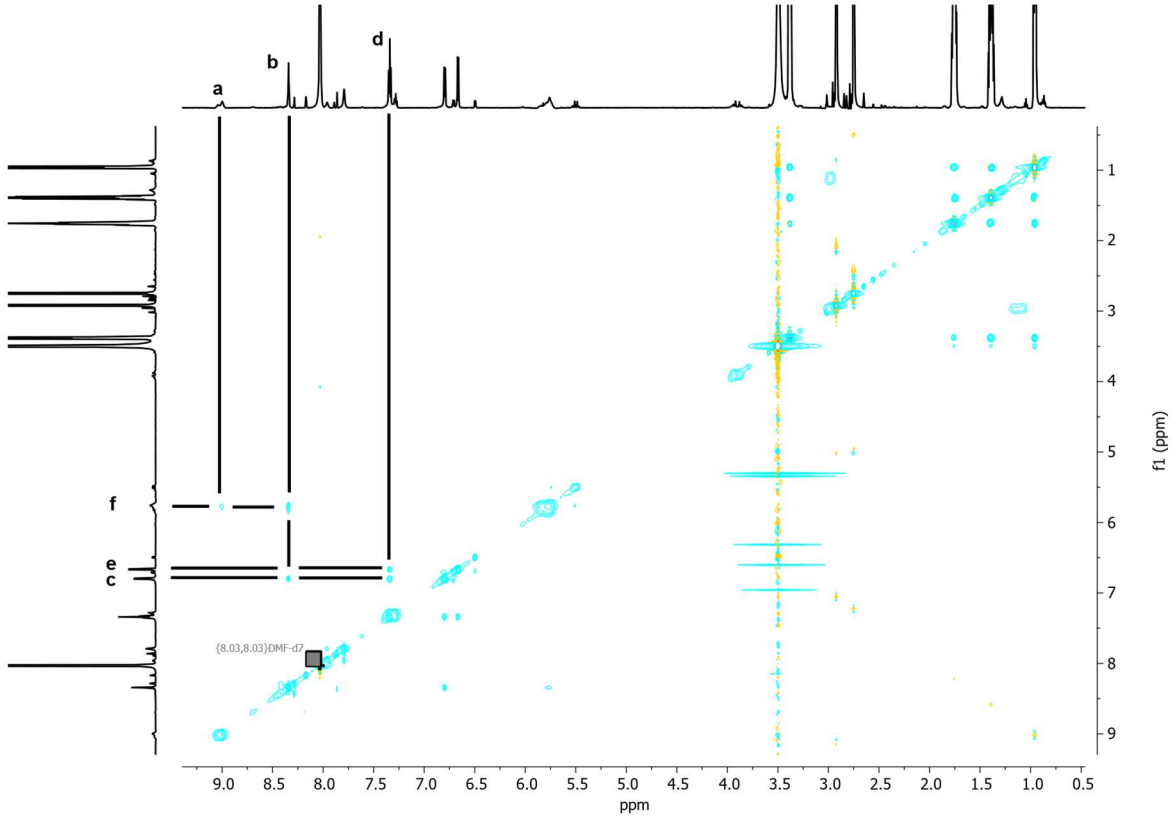

Figure 5.45: ^{1}H NOESY spectrum of [(BTT)@ $Zn_3L^{TP3}{}_2]^{3-}$ (1 mM, 700 MHz, DMF-d_7, 25°C).

5.6.7 Synthesis of [(TRI)@L_2Zn_3]$^{3-}$ and [(TRI)@L_4Zn_6]$^{3-}$ in DMSO and DMF

According to the general procedure of the host-guest complex formation, the suspended [$Zn_{1.5xn}L^{TP3}{}_n$] (1 equiv.) was treated with TBA TRI (2 x 0.5 equiv.) and was then heated for 10 min at 80°C. ^{1}H NMR showed the formation of [(TRI)@$Zn_3L^{TP3}{}_2$]$^{3-}$ and a minor [$Zn_1L^{TP3}{}_1$] species.

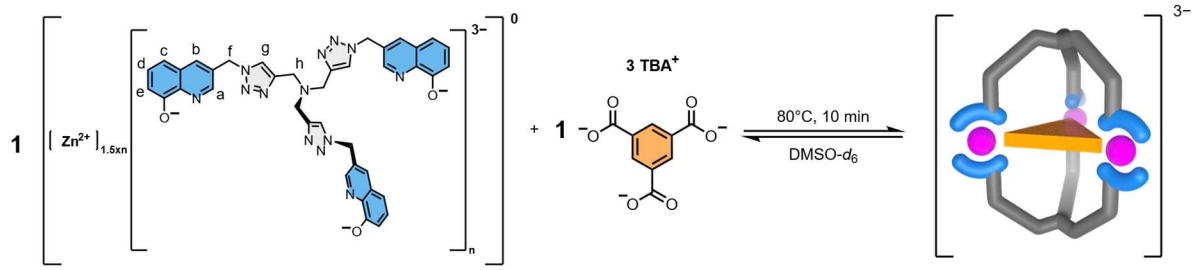

Figure 5.46: Templated self-assembly of the weakly soluble [$Zn_{1.5xn}L^{TP3}{}_n$] aggregate with TBA Trimesate 1:1 in DMSO at 80°C into a negatively charged host-guest complex [(TRI)@ $Zn_3L^{TP3}{}_2$]$^{3-}$.

^{1}H NMR (500 MHz, DMSO-d_6, 25°C): δ = 8.66 (s, 6H), 8.38 (s, 3H), 8.15 (s, 6H), 7.76 (s, 6H), 7.27 (t, *J* = 7.9 Hz, 6H), 6.73 (d, *J* = 8.0 Hz, 6H), 6.48 (d, 7.8, 1.2 Hz, 6H), 5.80 – 5.59 (m, 12H), 3.48 (m, 6H, the signals are overlapping with H_2O) ppm. **^{13}C NMR** (151 MHz, DMSO-d_6, 25°C): δ = 171.3183, 164.0292, 144.8012, 143.9611, 140.5223, 136.9492, 134.5949, 133.0201, 130.4579, 129.1821, 129.0217, 122.6011, 111.1874, 107.0566, 49.9358, 48.3725 ppm. **HRMS** (negative ESI-MS, ACN/DMSO 80:20, 30°C): m/z = 619.7664 [$(C_9H_3O_6)$@$(C_{39}H_{31}N_{13}O_3)_2Zn_3$]$^{3-}$, calc. 619.7662.

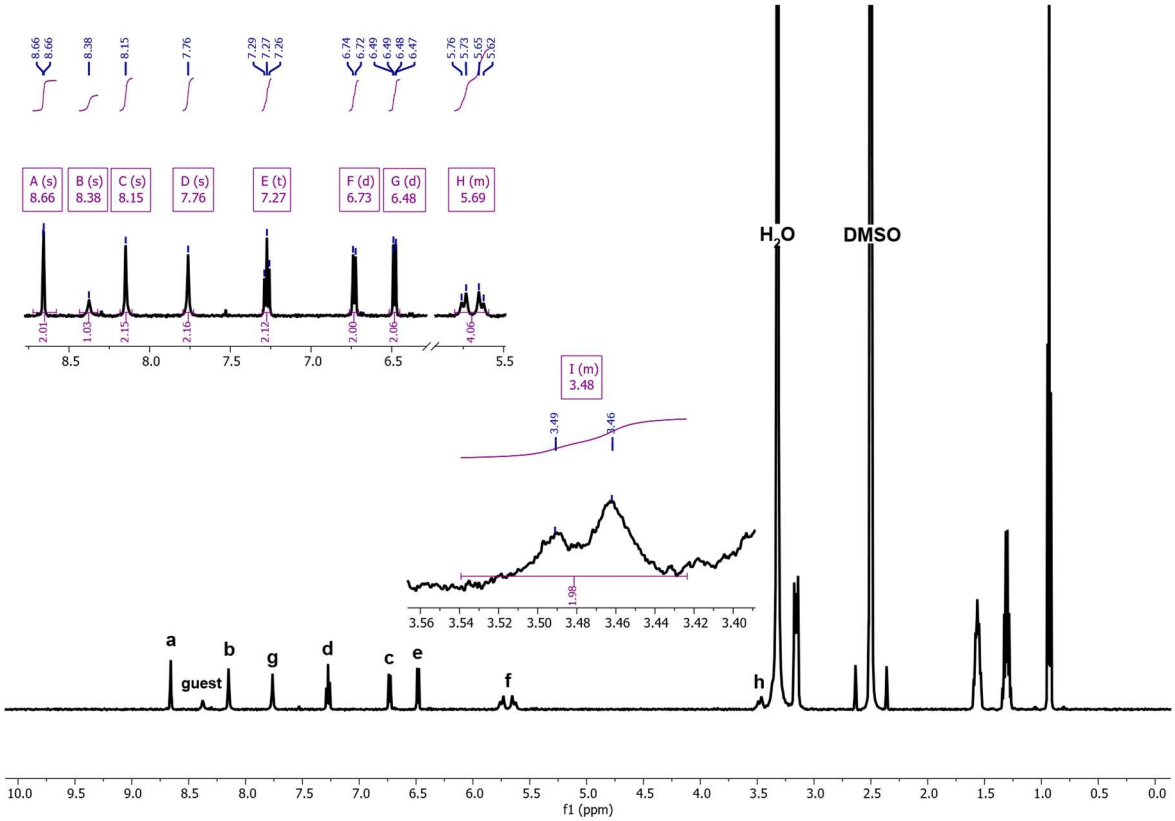

Figure 5.47: ^{1}H NMR spectrum of [(TRI)@ $Zn_3L^{TP3}{}_2$]$^{3-}$ (1 mM, 500 MHz, DMSO-d_6, 25°C).

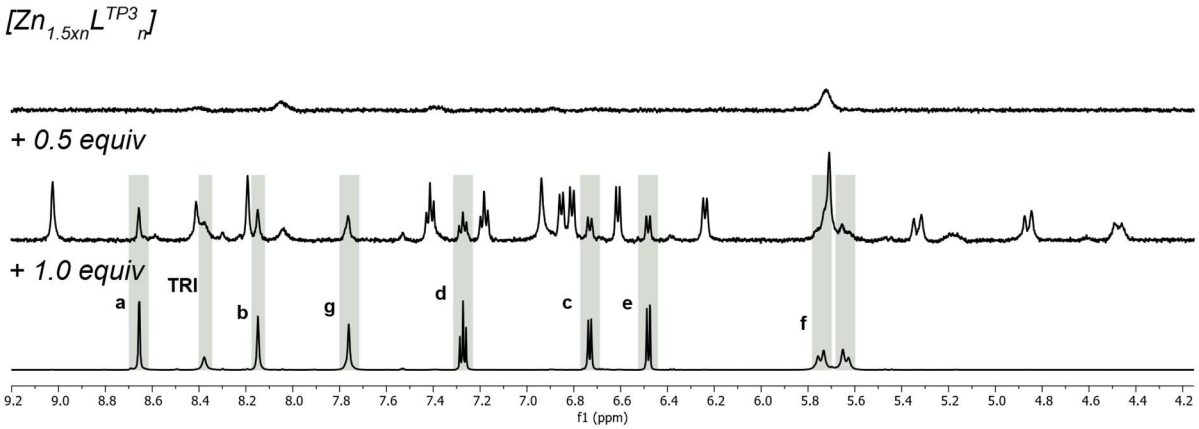

Figure 5.48: ^{1}H NMR spectra of [(TRI)@ $Zn_3L^{TP3}{}_2]^{3-}$ in DMSO-d_6 at 25°C, recorded during gradual addition of TBA TRI. After each step of the addition, the sample was heated at 80°C for 10 minutes.

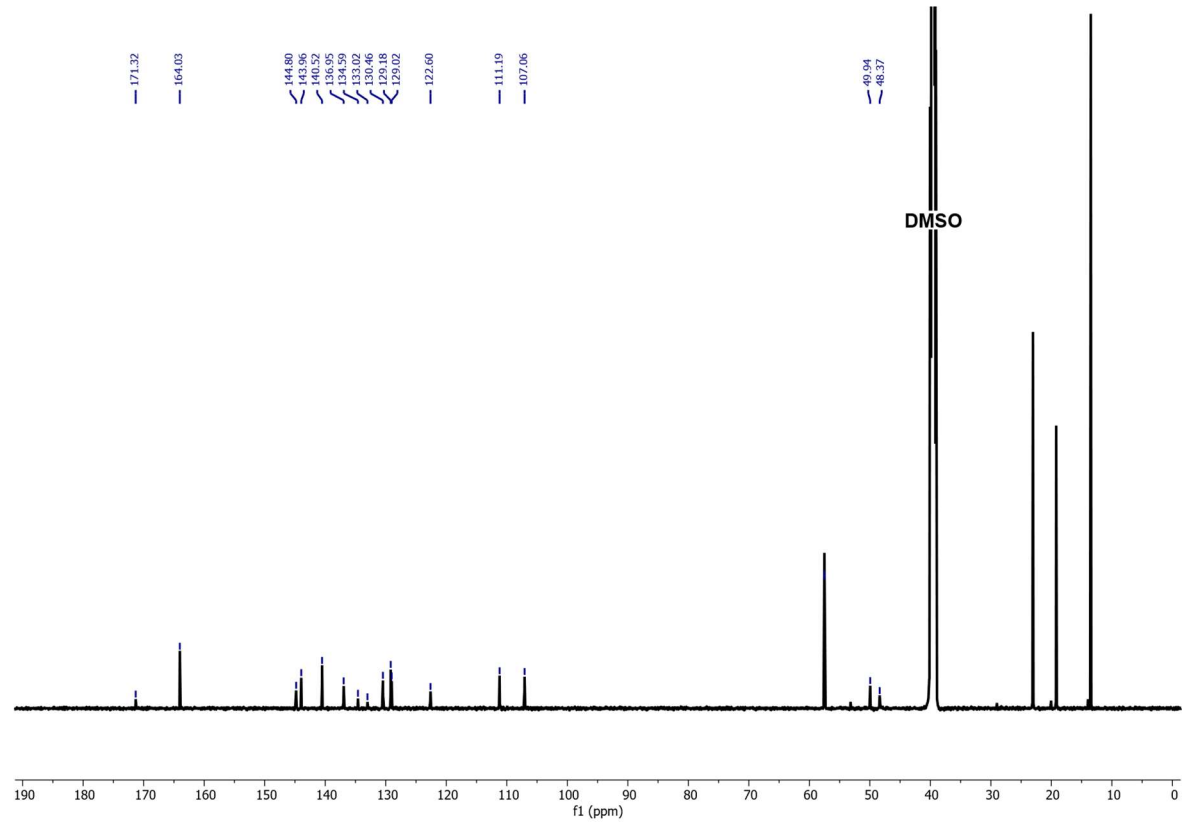

Figure 5.49: ^{13}C NMR spectrum of [(TRI)@ $Zn_3L^{TP3}{}_2]^{3-}$ (1 mM, 151 MHz, DMSO-d_6, 25°C).

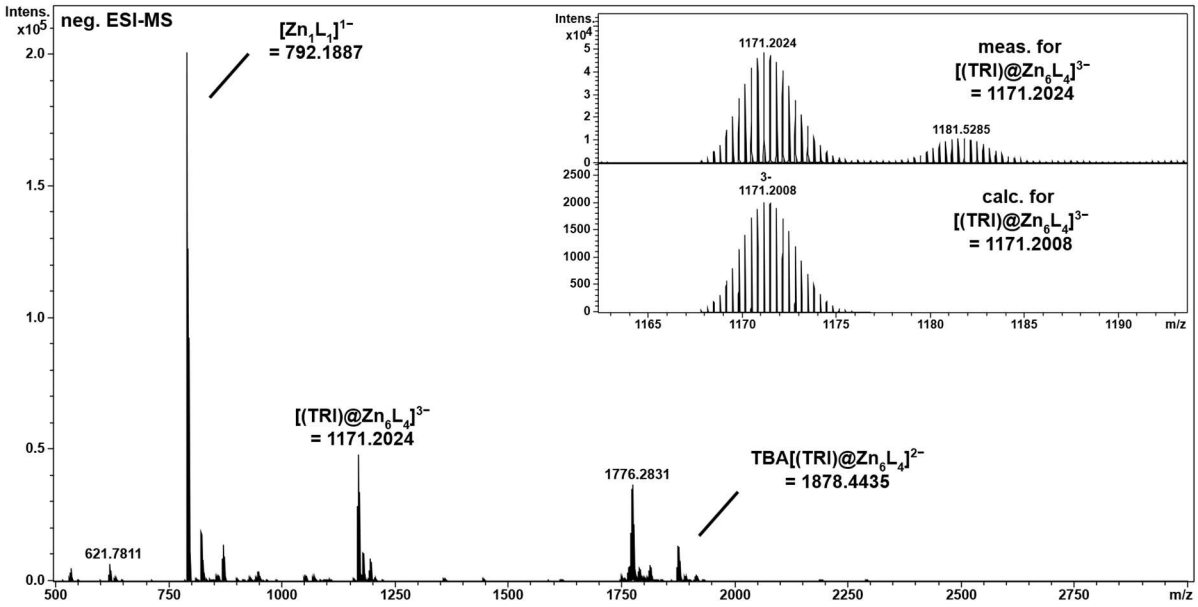

Figure 5.50: Negative ESI-MS spectrum of [(TRI)@ $Zn_6L^{TP3}{}_4]^{3-}$ (0.5 equiv. TBA TRI, DMSO:ACN 1:4, 30°C), the spectrum shows the desired host-guest system, its TBA adduct and a $[Zn_1L^{TP3}{}_1]^{1-}$ species.

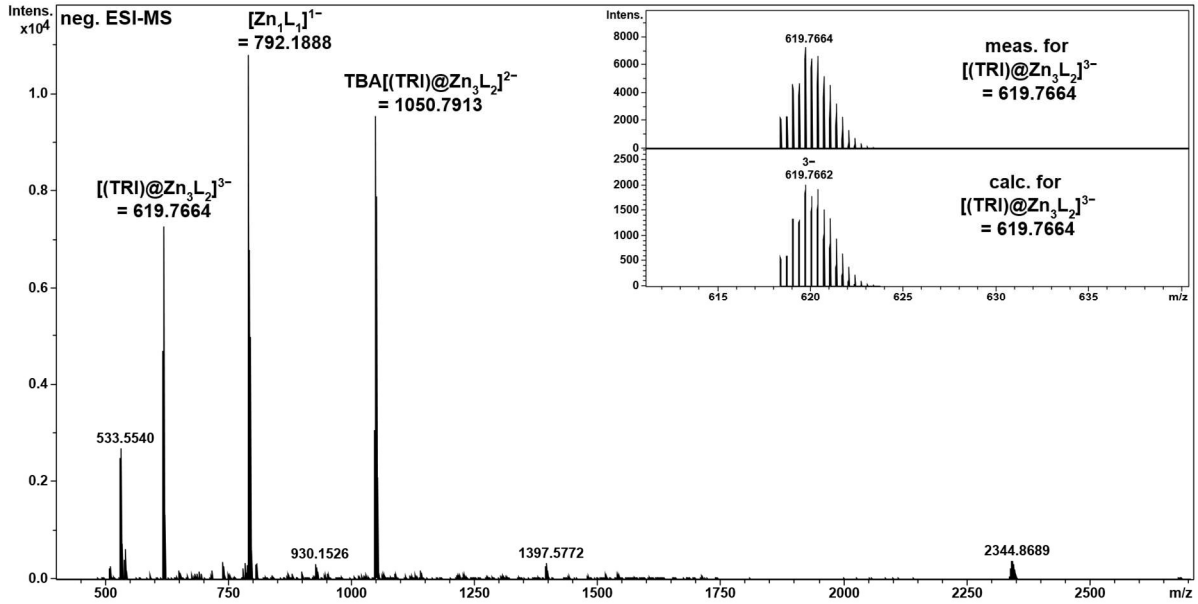

Figure 5.51: Negative ESI-MS spectrum of [(TRI)@ $Zn_3L^{TP3}{}_2]^{3-}$ (excess TBA TRI, DMSO:ACN 1:4, 30°C), the spectrum shows the desired host-guest system, its TBA-adduct and a $[Zn_1L^{TP3}{}_1]^{1-}$ species.

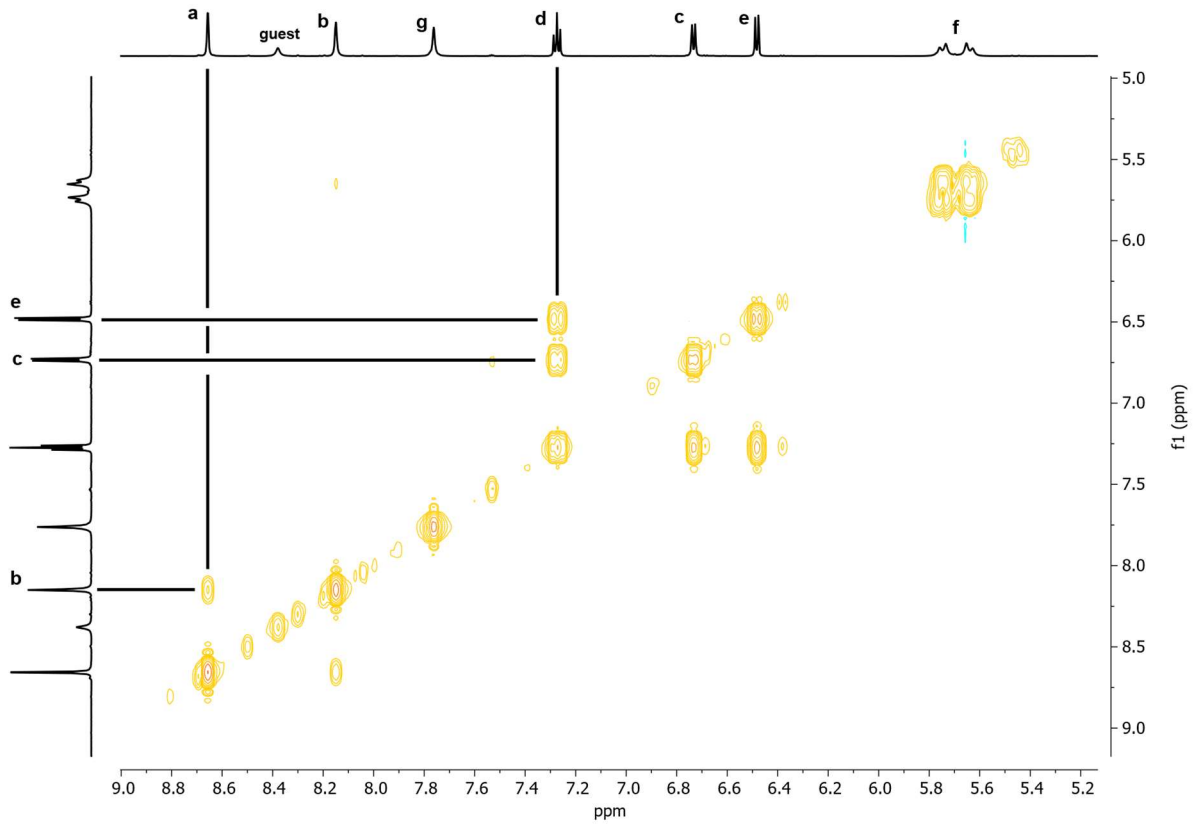

Figure 5.52: ^{1}H COSY spectrum of [(TRI)@ $Zn_3L^{TP3}{}_2]^{3-}$ (1 mM, 600 MHz, DMSO-d_6, 25°C).

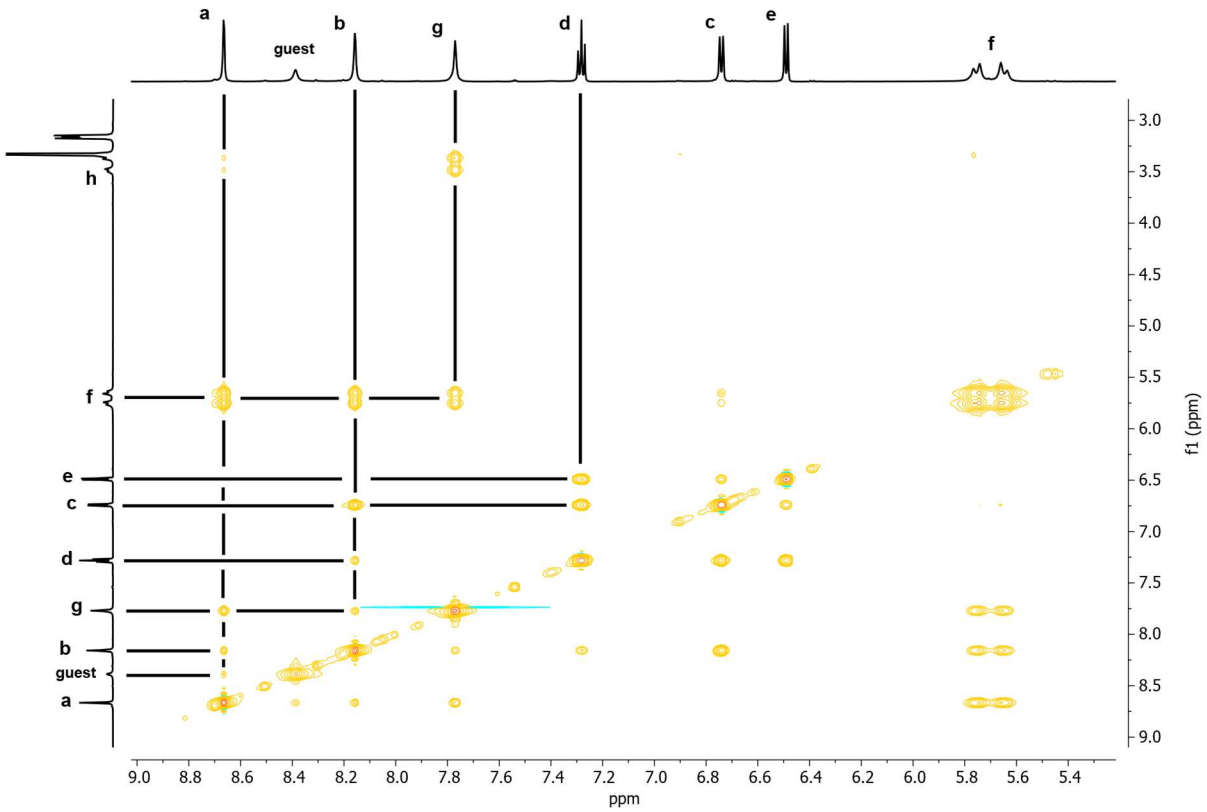

Figure 5.53: ^{1}H NOESY spectrum of [(TRI)@ $Zn_3L^{TP3}{}_2]^{3-}$ (1 mM, 600 MHz, DMSO-d_6, 25°C).

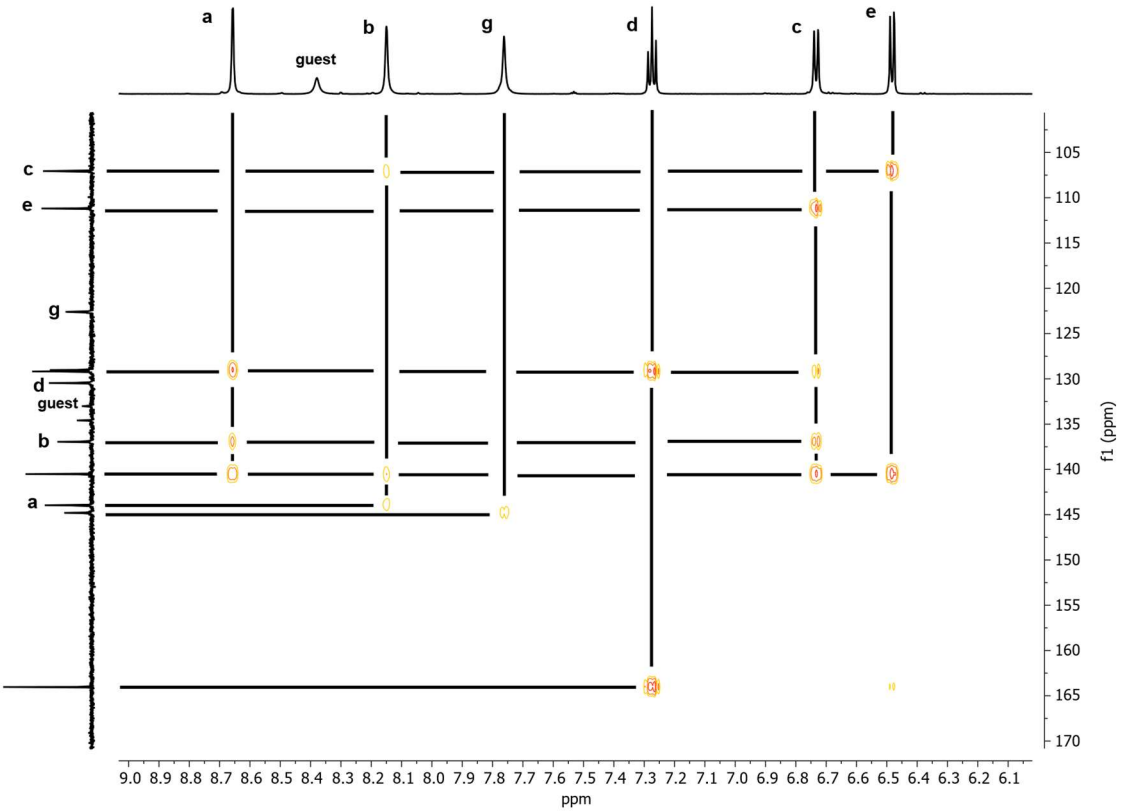

Figure 5.54 HMBC spectrum of [(TRI)@ $Zn_3L^{TP3}{}_2]^{3-}$ (1 mM, 151 MHz, DMSO-d_6, 25°C).

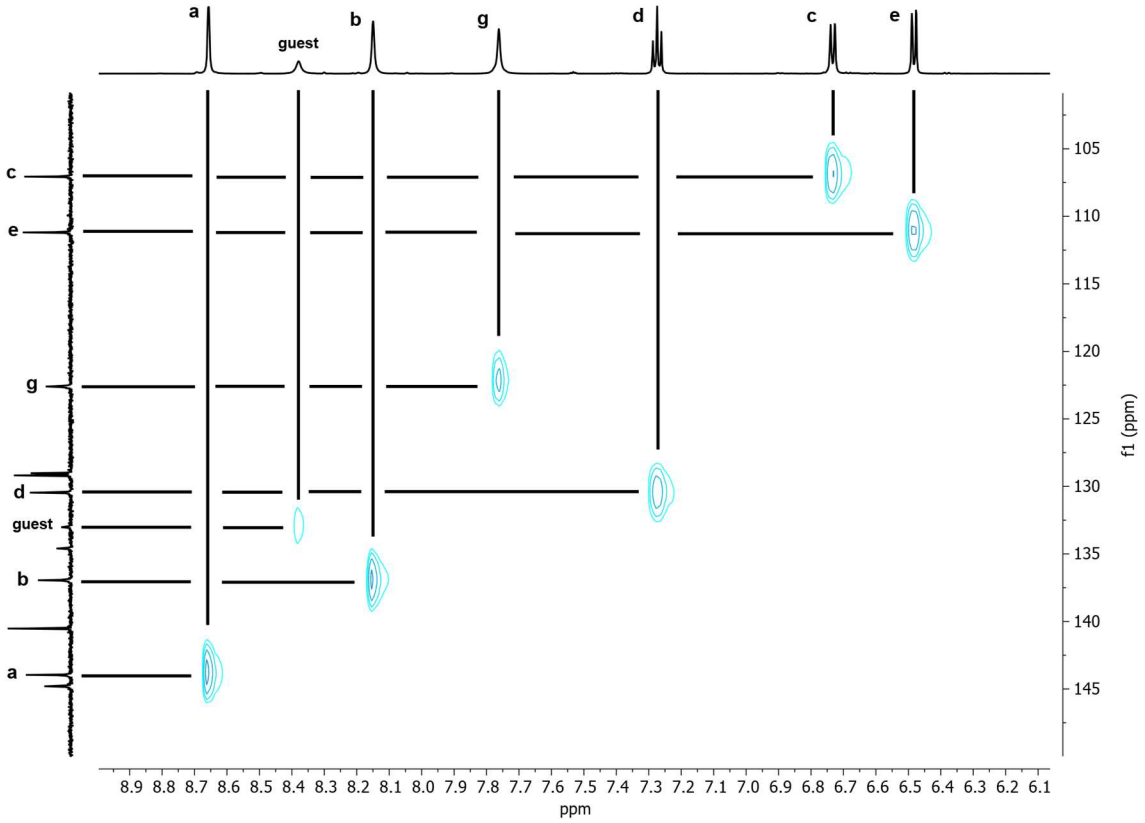

Figure 5.55: HSQC spectrum of [(TRI)@ $Zn_3L^{TP3}{}_2]^{3-}$ (1 mM, 151 MHz, DMSO-d_6, 25°C).

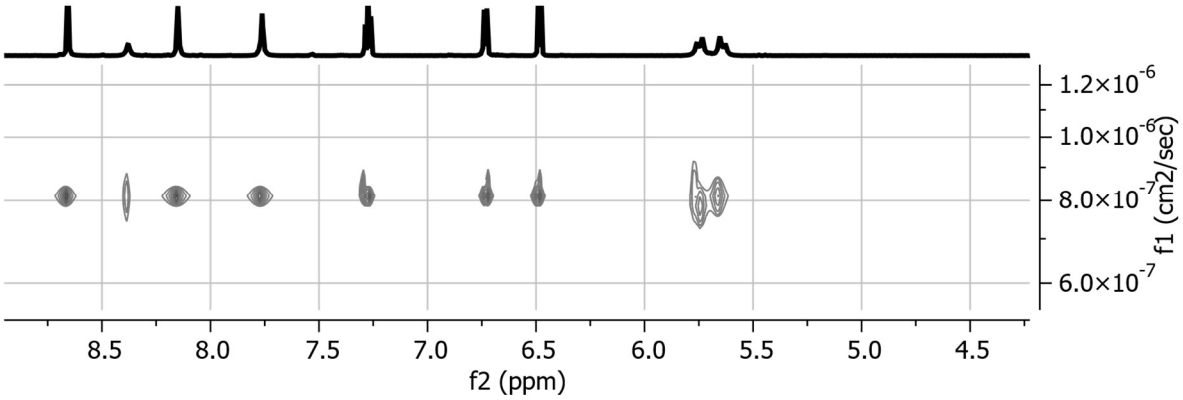

Figure 5.56: ^{1}H DOSY spectrum of [(TRI)@ $Zn_3L^{TP3}{}_2]^{3-}$, D = 9.142 x 10^{-11} m^2 s^{-1}, r_H = 1.20 nm (1 mM, 500 MHz, DMSO-d_6, 25°C).

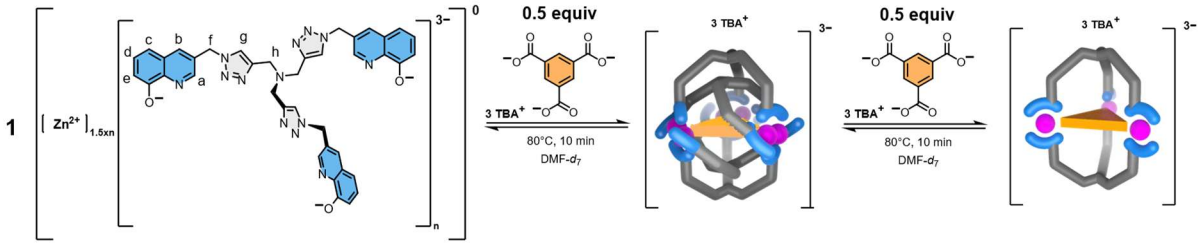

Figure 5.57: Templated self-assembly of the weakly soluble [$Zn_{1.5xn}L^{TP3}{}_n$] aggregate with TBA TRI in DMF-d_7 at 80°C into negatively charged host-guest complexes [(TRI)@ $Zn_3L^{TP3}{}_2]^{3-}$ and [(TRI)@ $Zn_6L^{TP3}{}_4]^{3-}$.

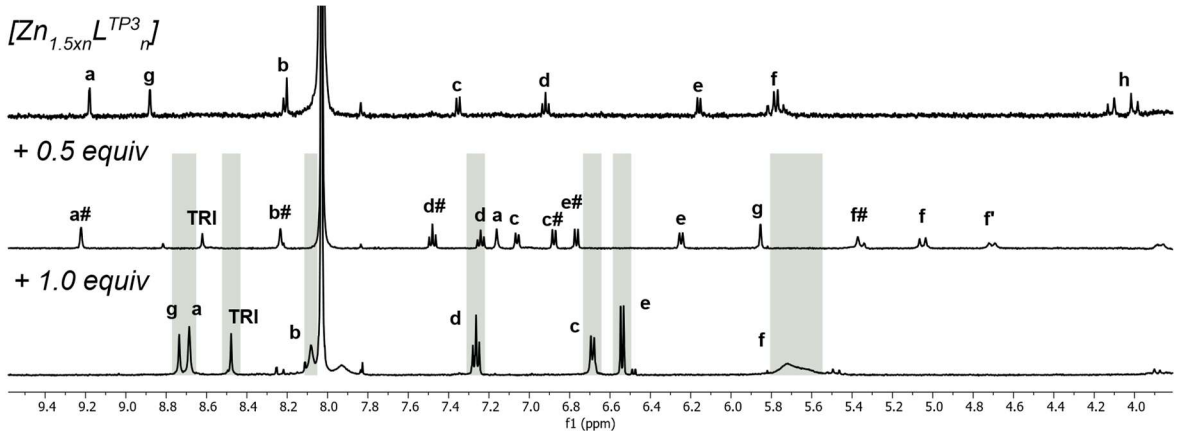

Figure 5.58: Two step ^{1}H NMR titration of the weakly soluble [$Zn_{1.5xn}L^{TP3}{}_n$] aggregate and TBA TRI in DMF-d_7 at 25°C. After each step of the addition, the sample was heated at 80°C for 10 minutes.

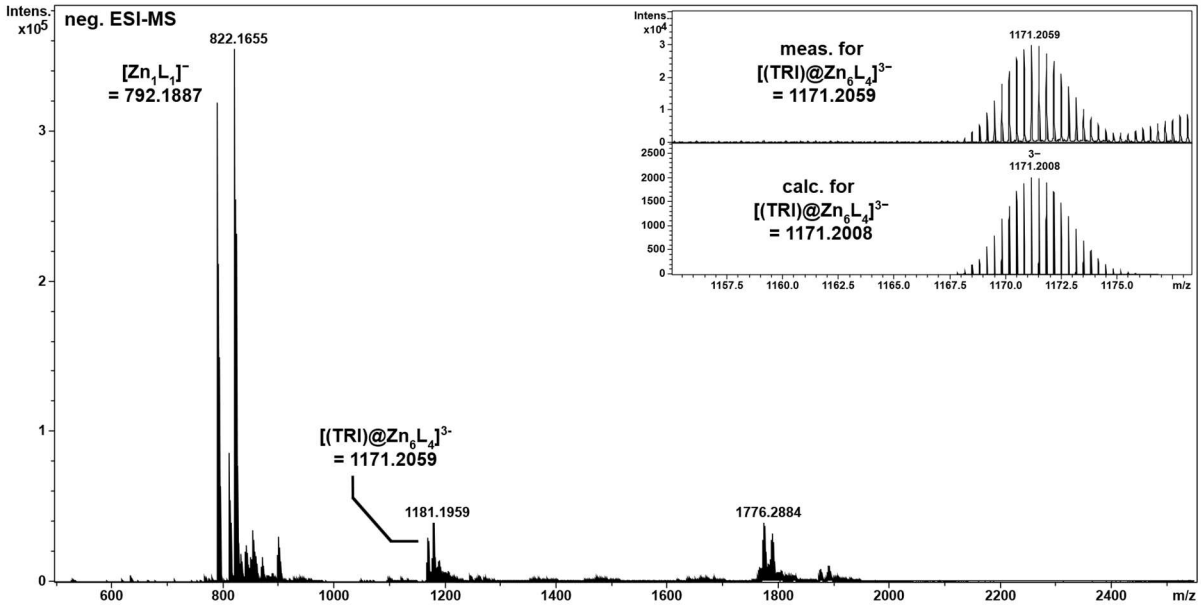

Figure 5.59: Negative ESI-MS spectrum of $[(TRI)@Zn_6L^{TP3}{}_4]^{3-}$ (0.5 equiv. TBA TRI, DMF:ACN 1:4, 30°C), the spectrum shows the desired host-guest system, its TBA adduct and a $[Zn_1L^{TP3}{}_1]^-$ species.

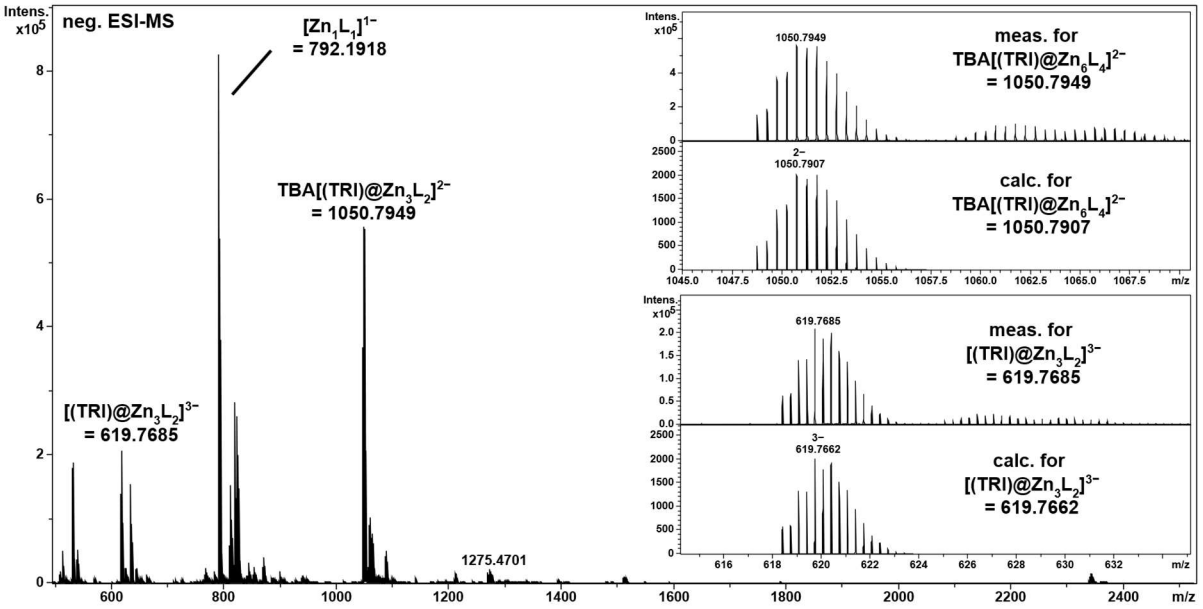

Figure 5.60: Negative ESI-MS spectrum of $[(TRI)@\ Zn_3L^{TP3}{}_2]^{3-}$ (excess TBA TRI, DMF:ACN 1:4, 30°C), the spectrum shows the desired host-guest system, its TBA adduct and a $[Zn_1L^{TP3}{}_1]^-$ species.

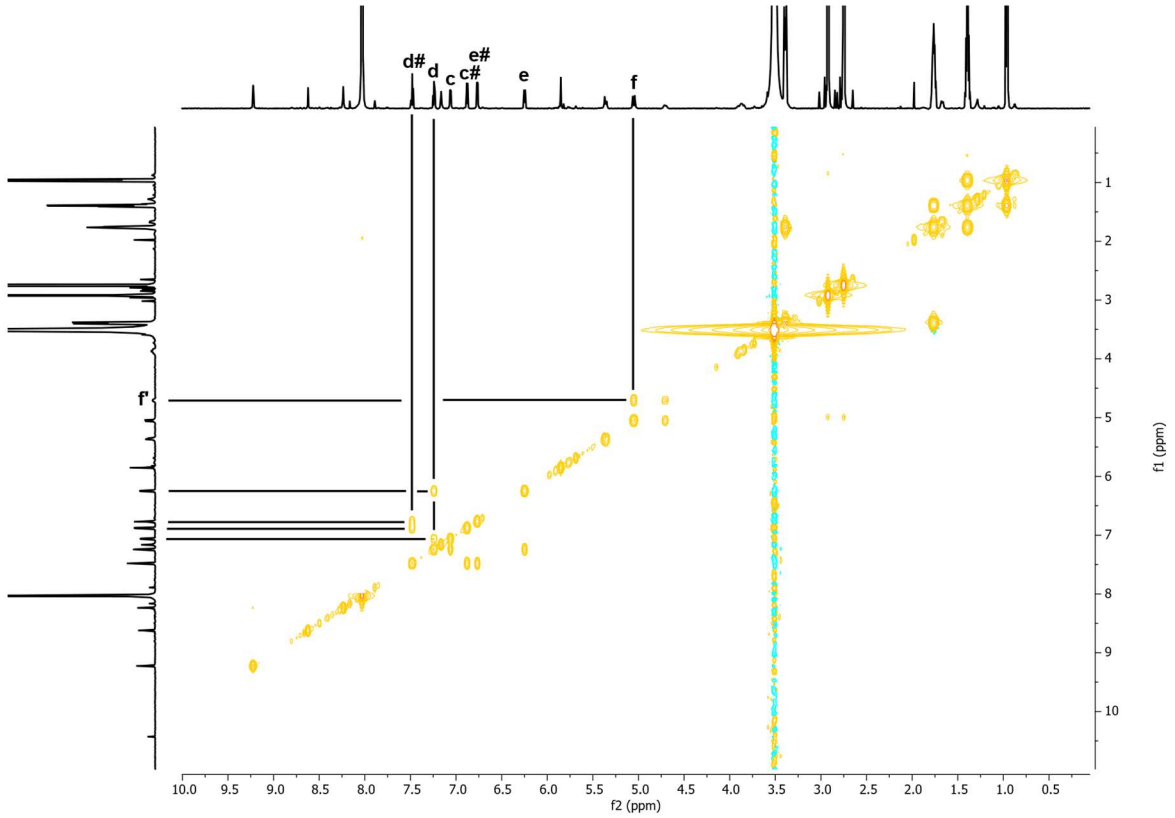

Figure 5.61: ^{1}H COSY NMR spectrum of the [(TRI)@ $Zn_6L^{TP3}{}_4]^{3-}$ complex (0.5 equiv. TBA TRI). The interpretation is hampered because of overlapping signals with H_2O (DMF-d_7, 500 µM, 25°C).

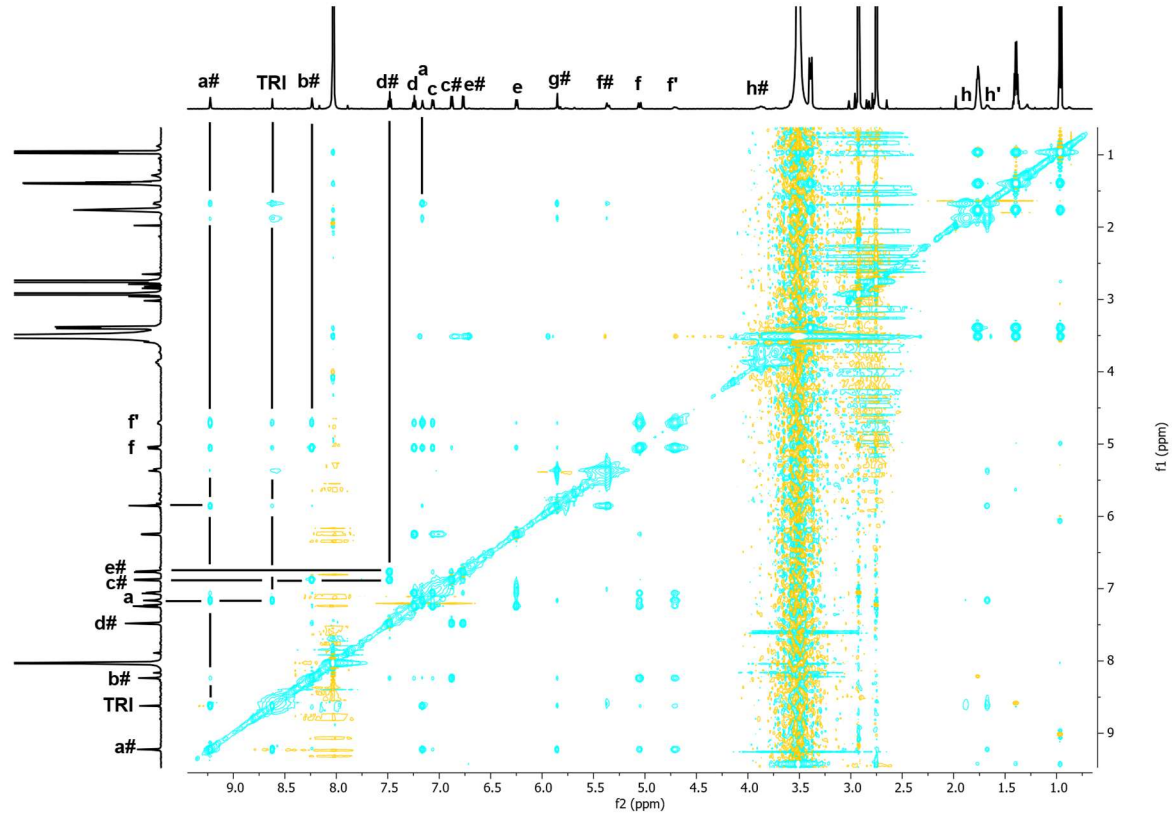

Figure 5.62: ^{1}H NOESY NMR spectrum of the [(TRI)@ $Zn_6L^{TP3}{}_4]^{3-}$ complex (0.5 equiv. TBA TRI). The interpretation is hampered because of overlapping signals with the solvent DMF-d_7 and H_2O. (DMF-d_7, 500 µM, 25°C)

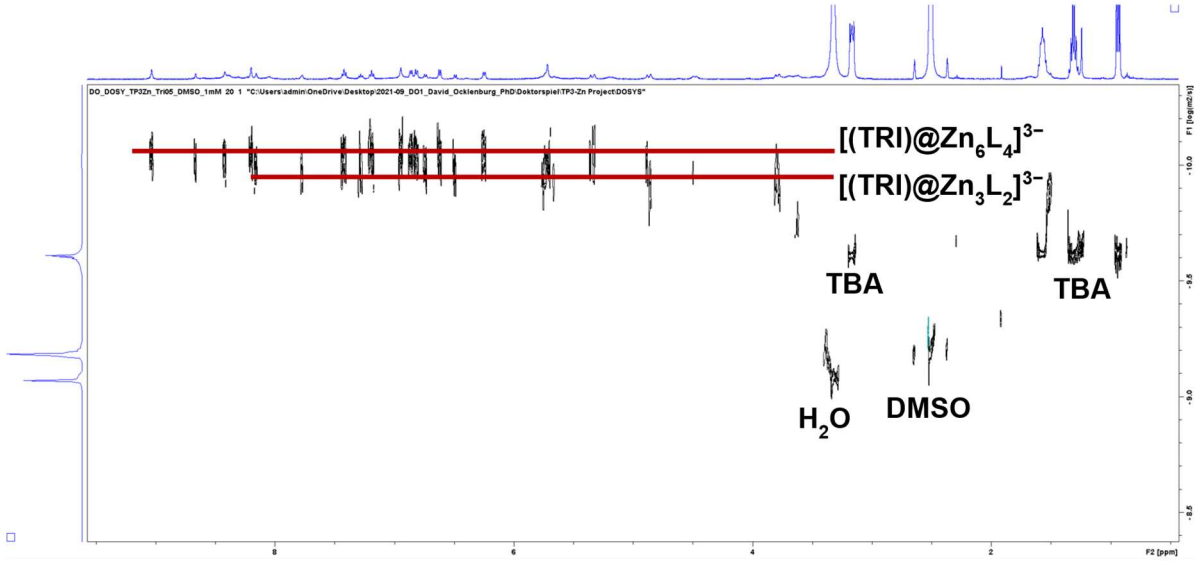

Figure 5.63: ^{1}H DOSY spectrum of a 1:2 mixture of [$Zn_{1.5xn}L_n$] and TBA TRI after heating to 80°C for 10 min. (DMSO-d_6, 500 MHz, 25°C)

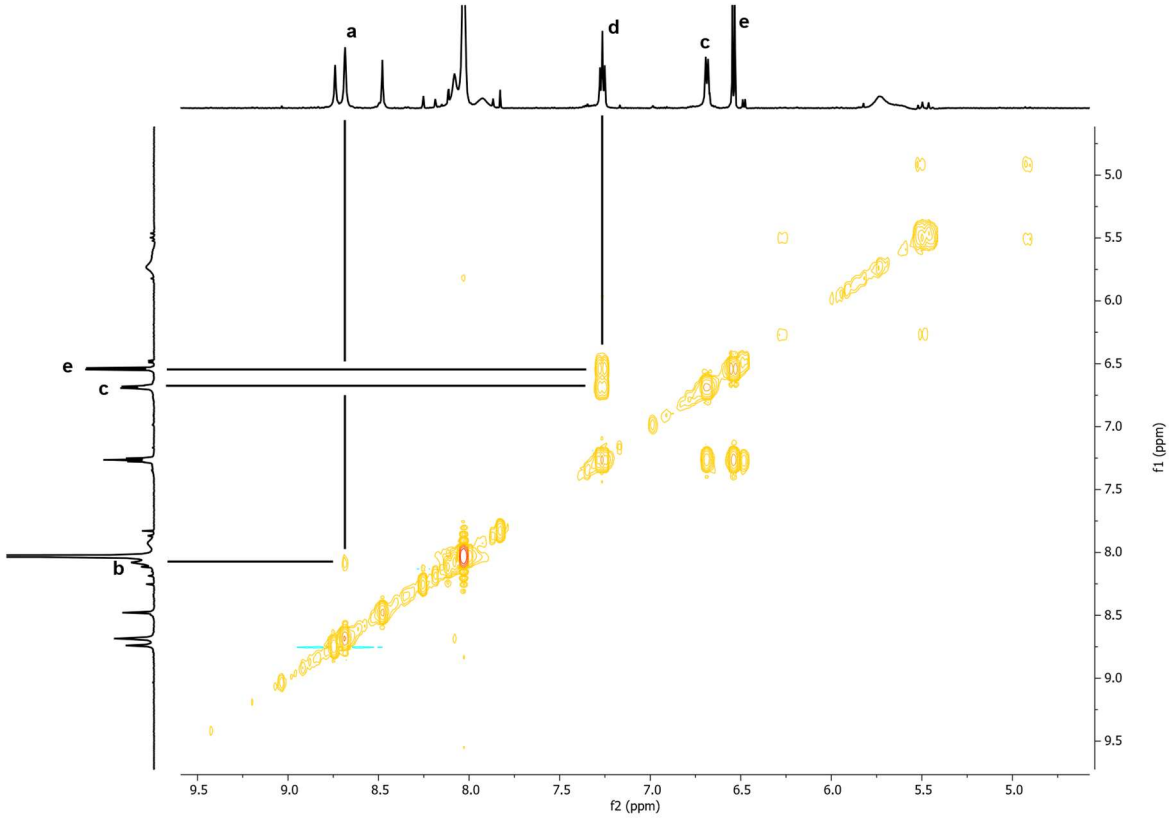

Figure 5.64: ^{1}H COSY NMR spectrum of the [(TRI)@ $Zn_3L^{TP3}{}_2]^{3-}$ complex (2 equiv. TBA TRI) (DMF-d_7, 500 µM 25°C).

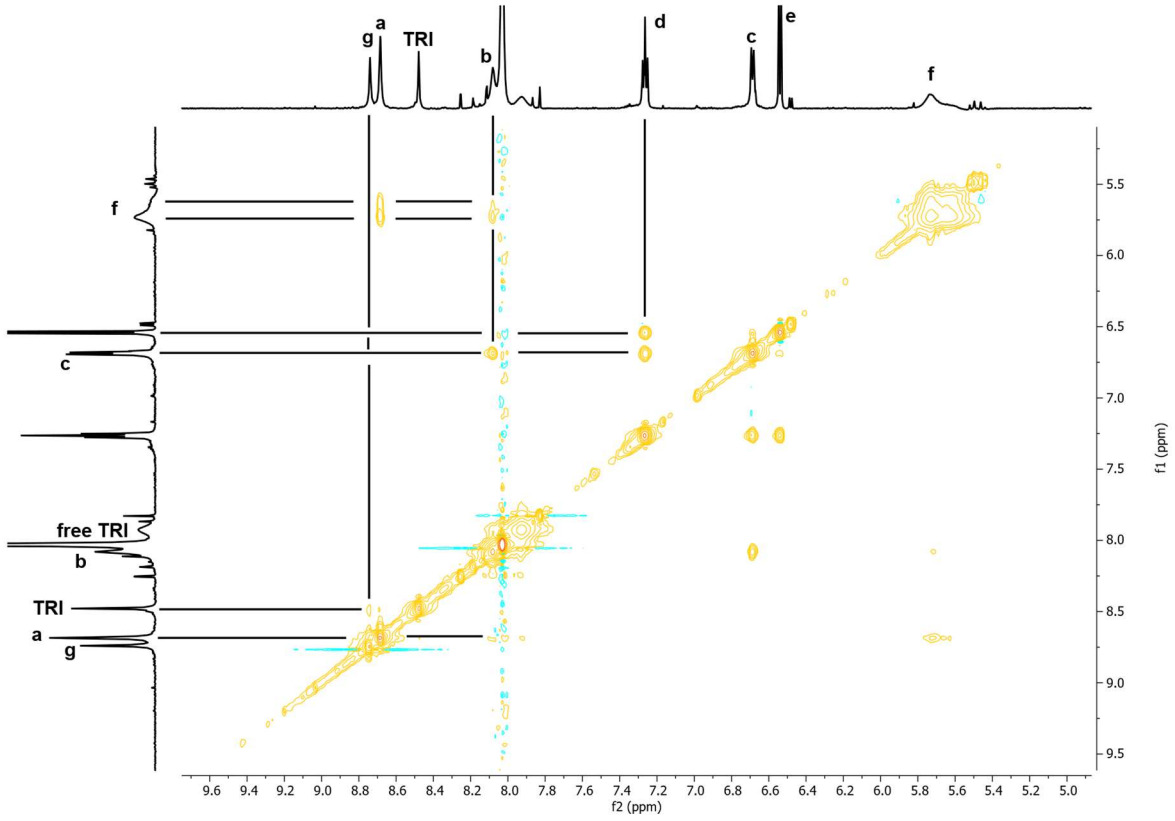

Figure 5.65: ^{1}H NOESY NMR spectrum of the [(TRI)@ $Zn_3L^{TP3}{}_2]^{3-}$ complex (2 equiv. TBA TRI) (DMF-d_7, 500 µM 25°C).

5.6.8 Synthesis of $[(CYC)@L_4Zn_6]^{3-}$ in DMSO-d_6 and DMF-d_7

According to the general procedure of the host-guest complex formation, the suspended $[Zn_{1.5xn}L^{TP3}{}_n]$ (1 equiv.) was treated with TBA CYC (2 x 0.5 equiv.) and was then heated for 10 min at 80°C. ^{1}H NMR showed the formation of $[(CYC)@Zn_6L^{TP3}{}_4]^{3-}$.

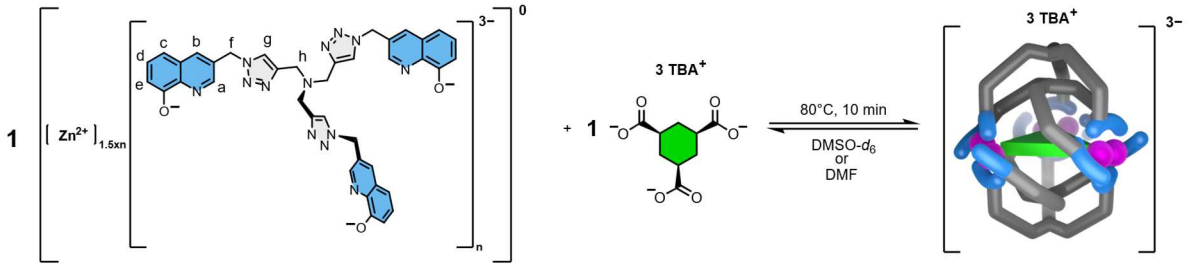

Figure 5.66: Templated self-assembly of the weakly soluble $[Zn_{1.5xn}L^{TP3}{}_n]$ aggregate with TBA CYC in DMSO-d_6 or DMF-d_7 at 80°C into a negatively charged host-guest complex $[(CYC)@Zn_6L^{TP3}{}_4]^{3-}$.

^{1}H NMR (500 MHz, DMSO-d_6, 25°C): δ = 9.08 (s, 3H), 8.77 (s, 3H), 8.34 (d, *J* = 2.0 Hz, 3H), 8.23 (d, *J* = 2.0 Hz, 3H), 7.56 (d, *J* = 2.0 Hz, 3H), 7.35 (t, *J* = 8.0 Hz, 3H), 7.27 (t, *J* = 8.0 Hz, 3H), 6.86 (dd, *J* = 7.8, 1.2 Hz, 3H), 6.78 (dd, *J* = 8.2, 1.2 Hz, 3H), 6.62 (d, *J* = 2.1 Hz, 3H), 6.58 (dd, *J* = 8.3, 1.2 Hz, 3H), 6.43 (dd, *J* = 7.9, 1.1 Hz, 3H), 5.56 (d, *J* = 16.2 Hz, 3H), 5.38 (d, *J* = 15.6 Hz, 3H), 5.06 (d, *J* = 16.3 Hz, 3H), 4.64 (d, *J* = 15.5 Hz, 3H), 4.40 (d, *J* = 13.2 Hz, 3H), 3.42 (d, *J* = 13.2 Hz, 3H), 2.38 (d, 3H), 1.94 (d, *J* = 12.7 Hz, 3H), 1.77 – 1.68 (m, 3H), 1.55 – 1.50 (m, 3H), 1.25 – 1.19 (m, 3H). **^{13}C NMR** (151 MHz, DMSO-d_6, 25°C): δ = 180.4563, 163.7238, 163.5505, 143.5441, 142.9302, 140.8265, 140.0660, 139.6116, 137.5604, 134.4294, 130.6593, 130.2475, 129.3736, 128.8880, 128.7469, 127.2368, 127.1581, 126.7246, 112.1624, 111.0285, 107.8594, 107.0633, 49.8829, 49.6192, 47.6186, 47.4742, 44.4913, 34.0178 ppm. **HRMS** (negative ESI-MS, ACN/DMSO 80:20, 30°C): m/z = 621.7823 $[(C_9H_9O_6)@(C_{39}H_{31}N_{13}O_3)_2Zn_3]^{3-}$, calc. 621.7819.

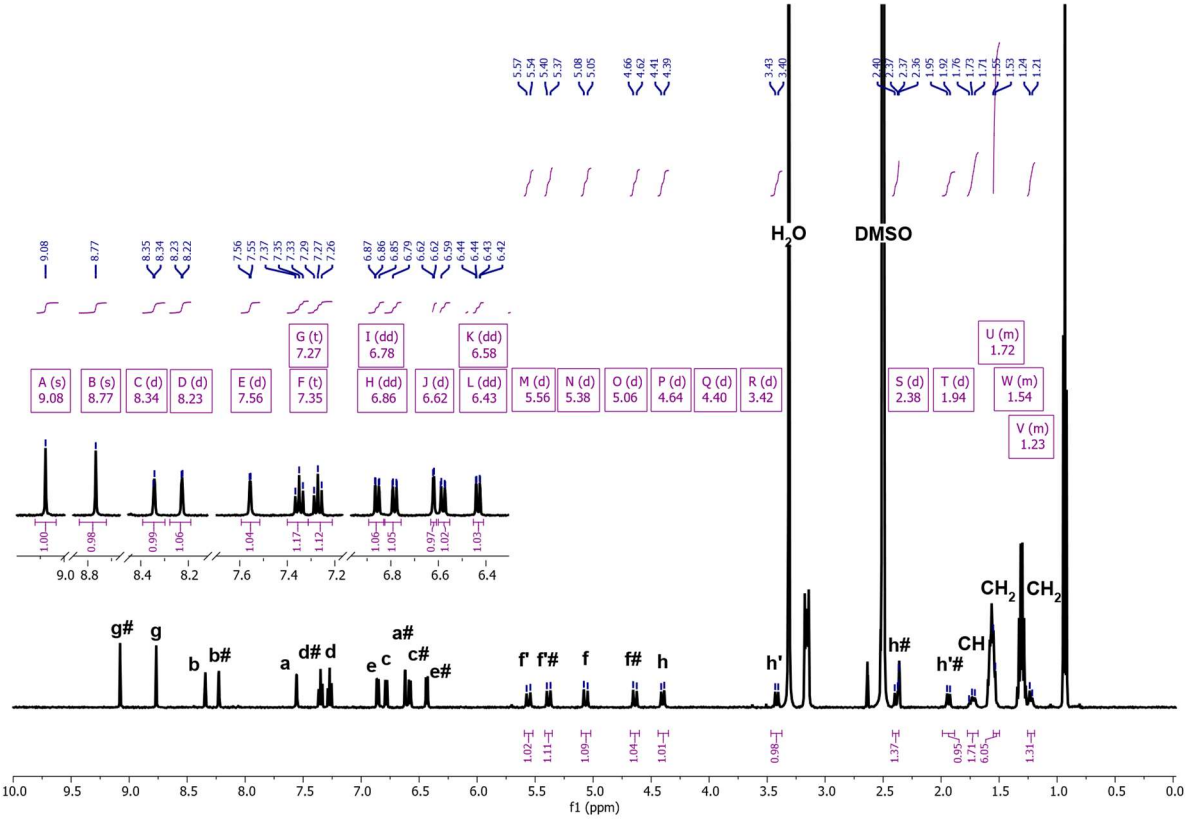

Figure 5.67: ^{1}H NMR spectrum of $[(CYC)@Zn_6L^{TP3}{}_4]^{3-}$, hashtag marks the outer-shell of the onion. (1 mM, 500 MHz, DMSO-d_6, 25°C).

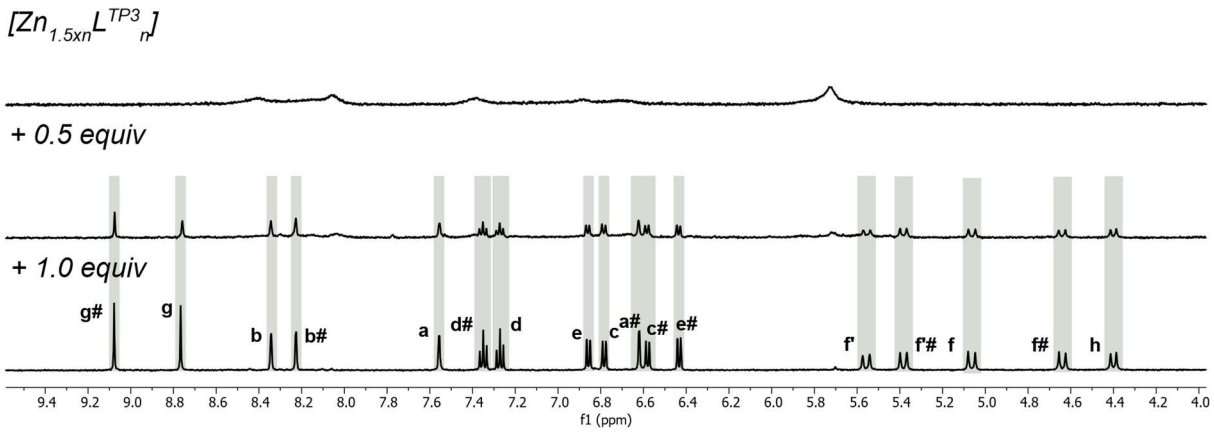

Figure 5.68: ^{1}H NMR spectra of [(CYC)@Zn$_6$L$^{TP3}_4$]$^{3-}$ in DMSO-d$_6$ at 25°C, recorded during gradual addition of TBA CYC. After each step of the addition, the sample was heated at 80°C for 10 minutes.

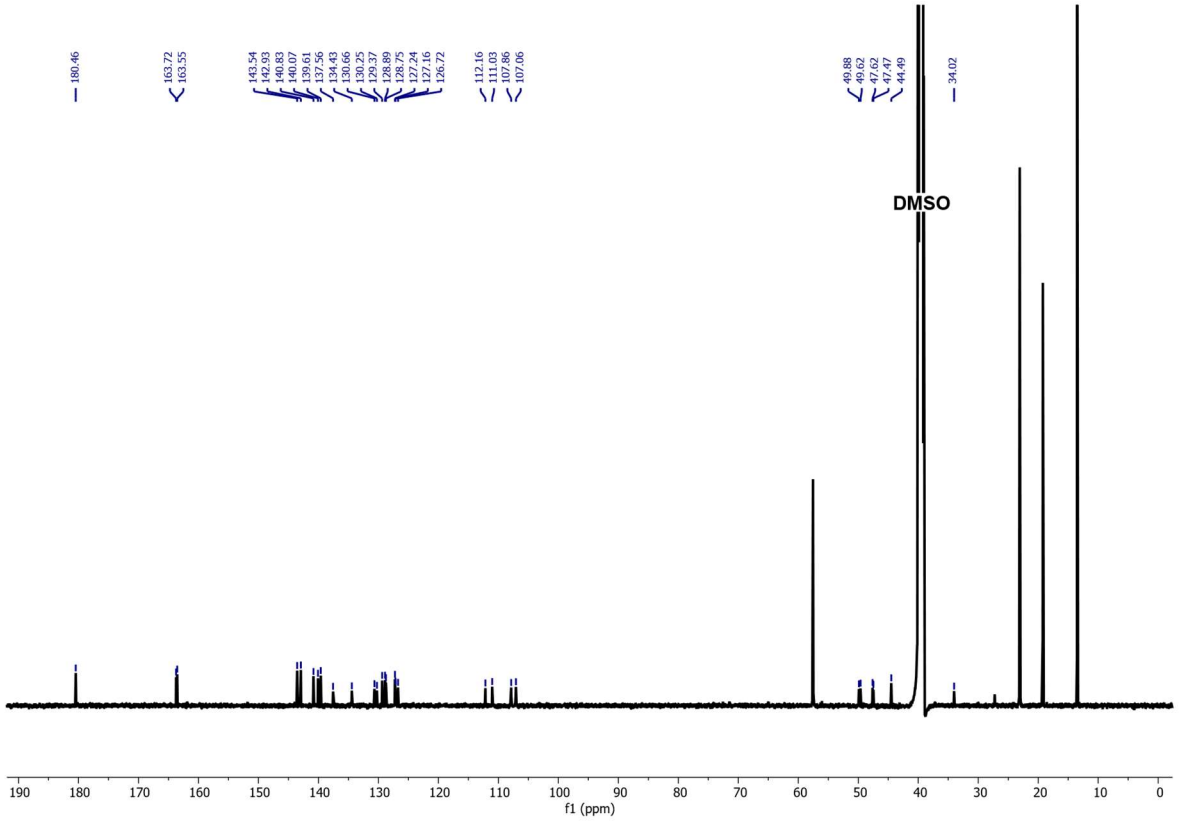

Figure 5.69: ^{13}C NMR spectrum of [(CYC)@Zn$_6$L$^{TP3}_4$]$^{3-}$ (1 mM, 151 MHz, DMSO-d$_6$, 25°C).

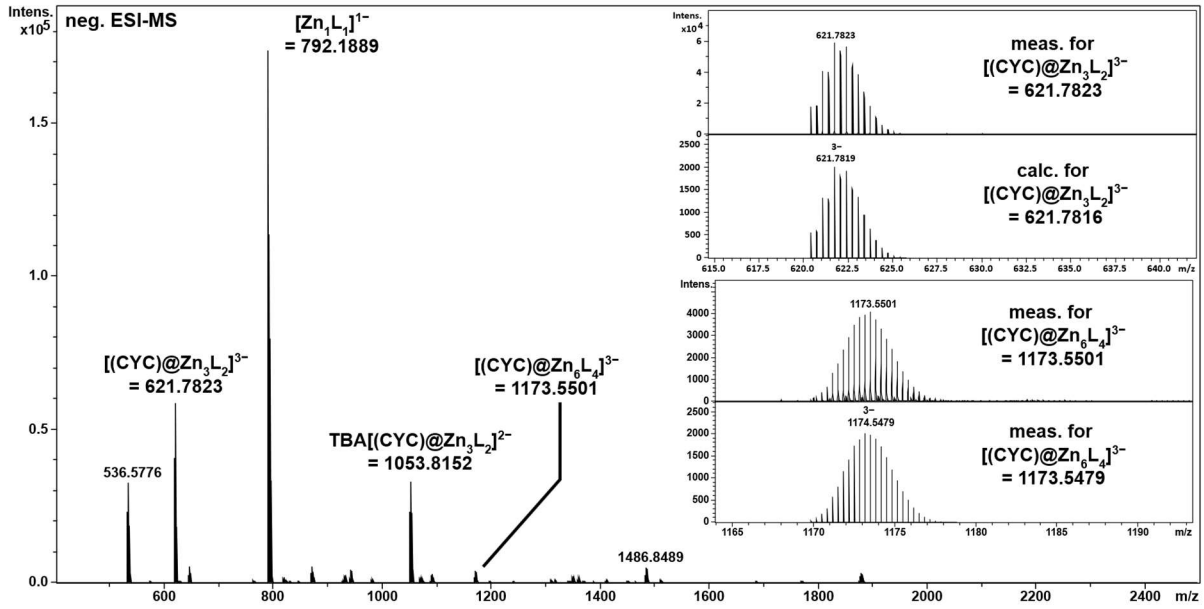

Figure 5.70: Negative ESI-MS spectrum of [(CYC)@Zn$_6$L$^{TP3}_4$]$^{3-}$ (DMSO:ACN 1:4, 30°C), the spectrum shows the desired host-guest system, its TBA adduct and a [Zn$_1$L$^{TP3}_1$]$^{1-}$ species.

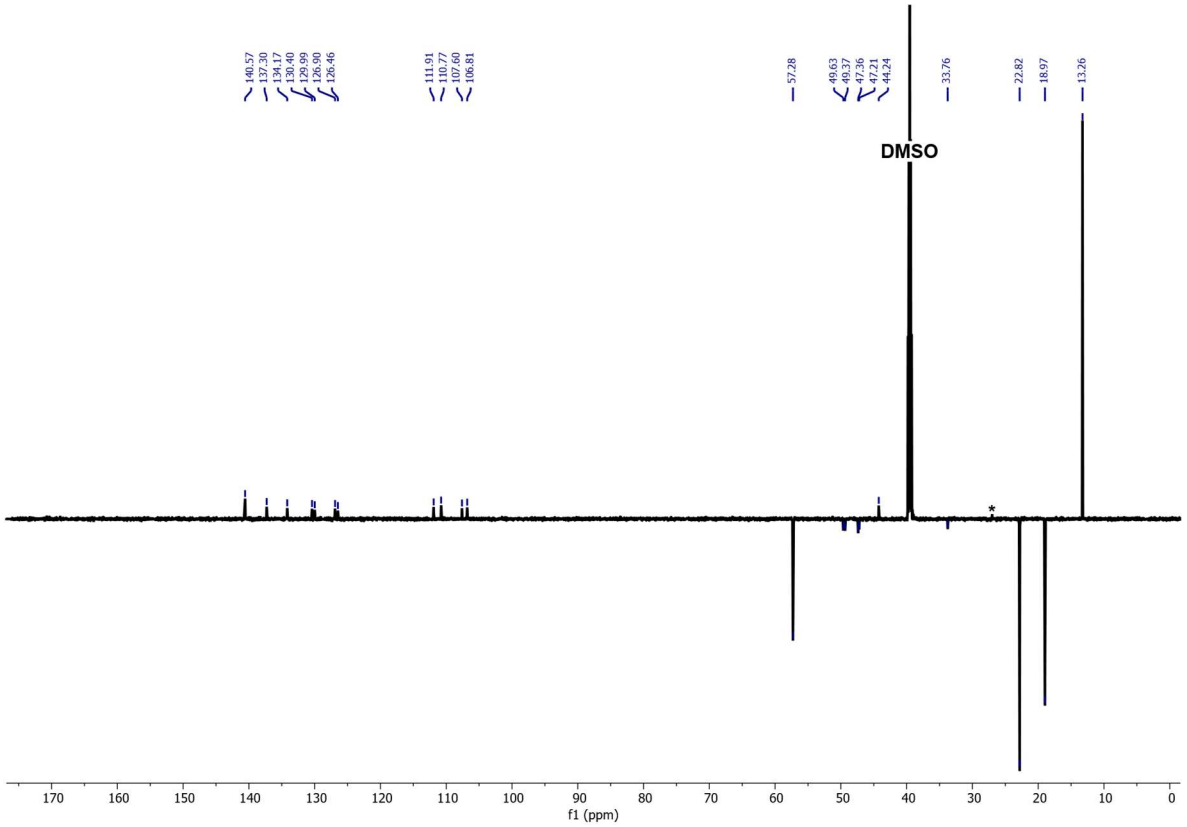

Figure 5.71: DEPT$_{135}$ NMR spectrum of [(CYC)@Zn$_6$L$^{TP3}_4$]$^{3-}$ (1 mM, 151 MHz, DMSO-d$_6$, 25°C).

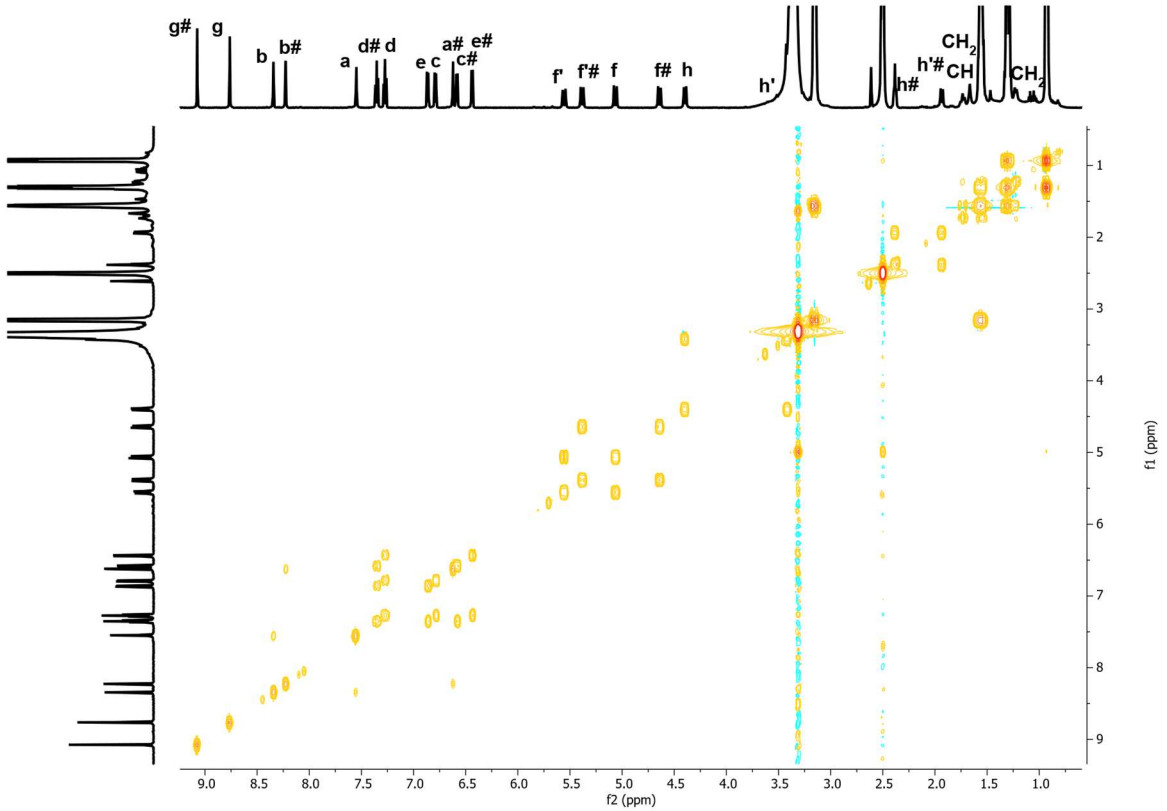

Figure 5.72: ^{1}H COSY NMR spectrum of [(CYC)@Zn$_6$L$^{TP3}{}_4$]$^{3-}$, hashtag marks the outer-shell of the onion. (1 mM, 500 MHz, DMSO-d$_6$, 25°C).

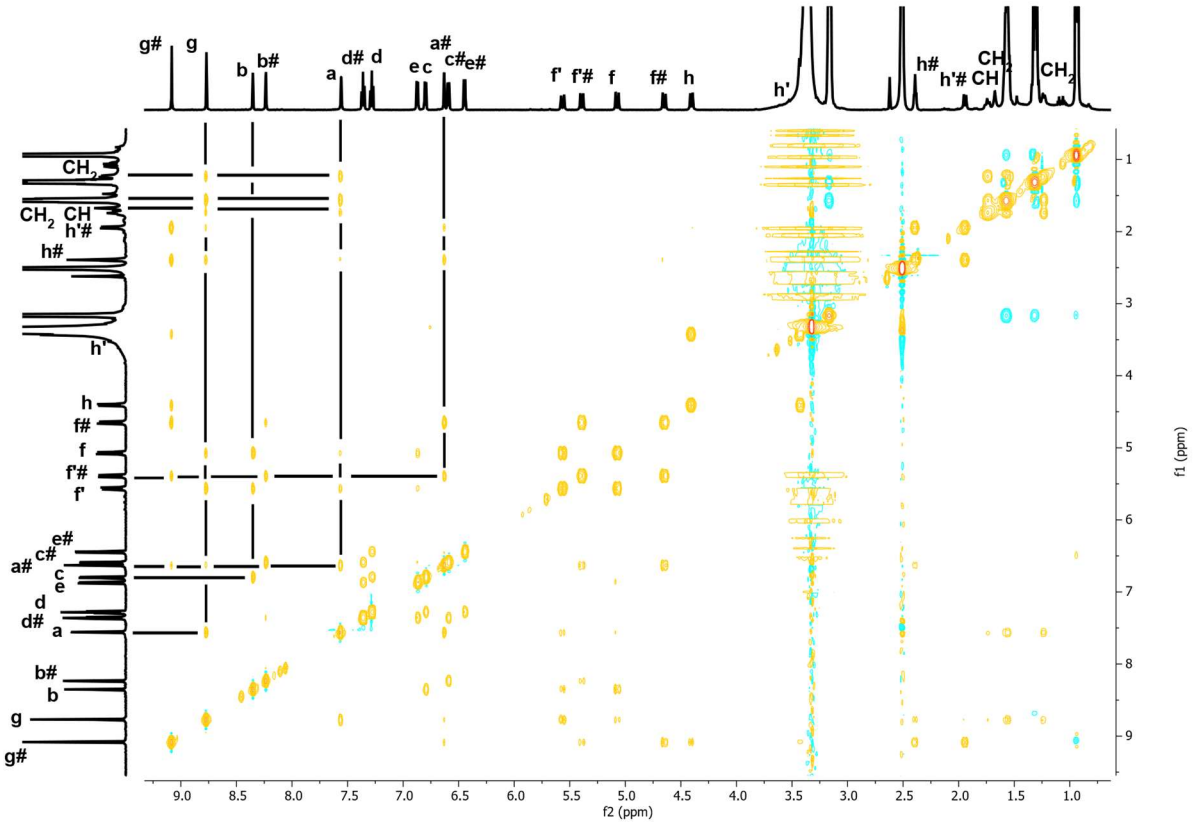

Figure 5.73: ^{1}H NOESY NMR spectrum of [(CYC)@Zn$_6$L$^{TP3}{}_4$]$^{3-}$, hashtag marks the outer-shell of the onion. (1 mM, 500 MHz, DMSO-d$_6$, 25°C).

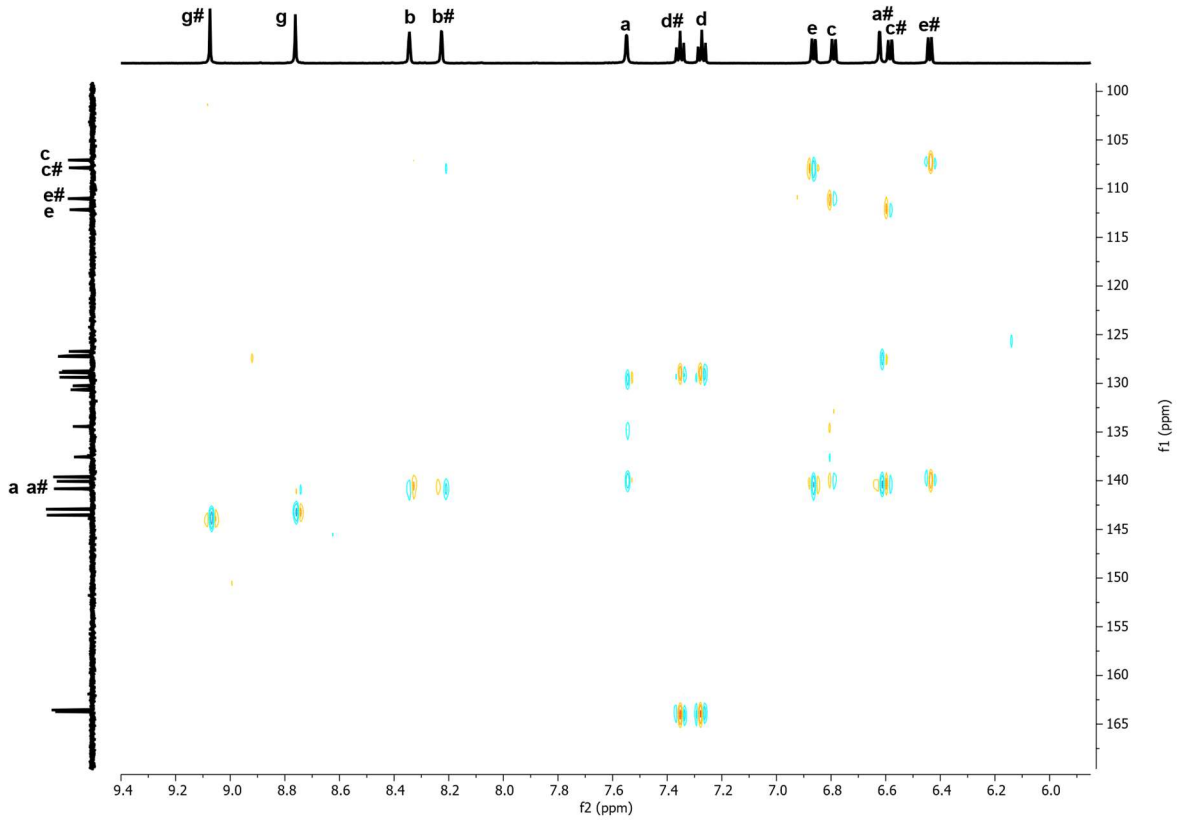

Figure 5.74: HMBC NMR spectrum of [(CYC)@Zn$_6$L$^{TP3}_4$]$^{3-}$, hashtag marks the outer-shell of the onion. (1 mM, 151 MHz, DMSO-d$_6$, 25°C).

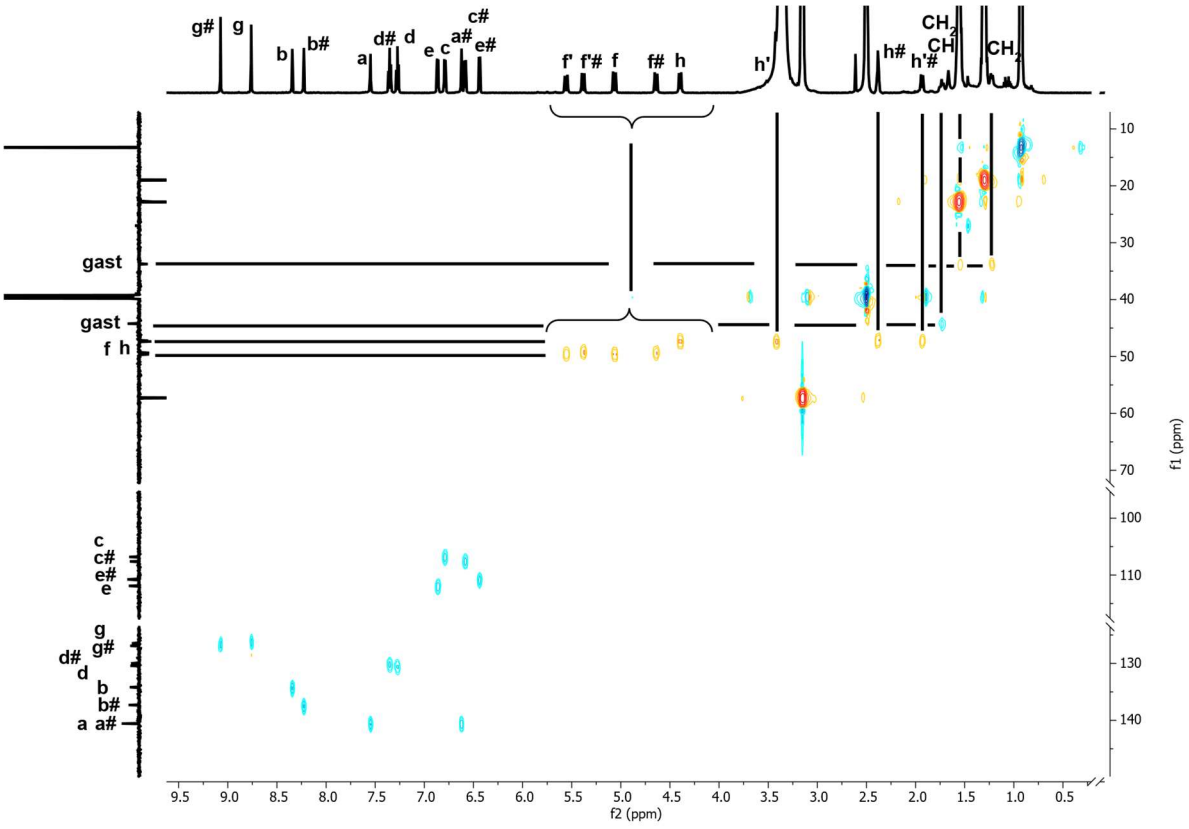

Figure 5.75: HSQC NMR spectrum of [(CYC)@Zn$_6$L$^{TP3}_4$]$^{3-}$, hashtag marks the outer-shell of the onion. (1 mM, 151 MHz, DMSO-d$_6$, 25°C).

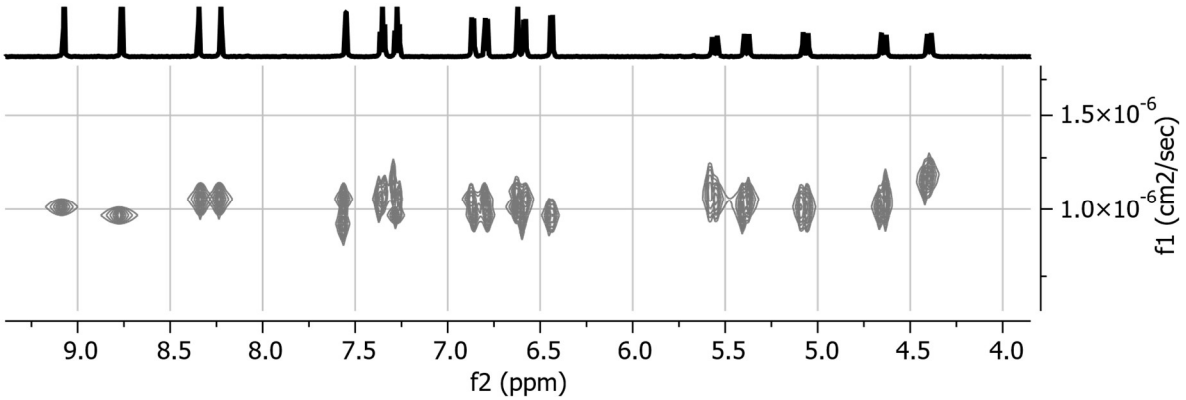

Figure 5.76: ^{1}H DOSY NMR spectrum of [(CYC)@Zn$_6$L$^{TP3}_4$]$^{3-}$, D = 1.156 x 10^{-10} m^2 s^{-1}, r$_H$ = 0.95 nm (1 mM, 500 MHz, DMSO-d$_6$, 25°C).

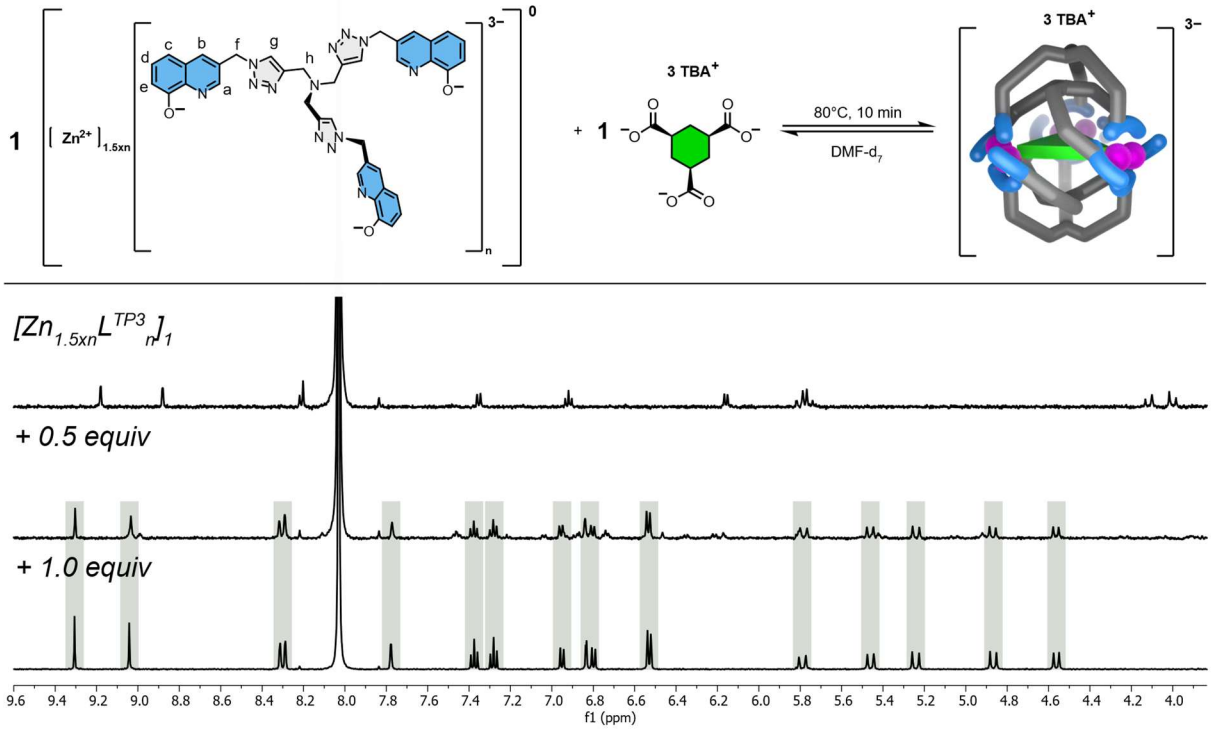

Figure 5.77: ^{1}H NMR spectra of [(CYC)@Zn$_6$L$^{TP3}_4$]$^{3-}$ in DMF-d$_7$ at 25°C, recorded during gradual addition of TBA CYC. After each step of the addition, the sample was heated at 80°C for 10 minutes.

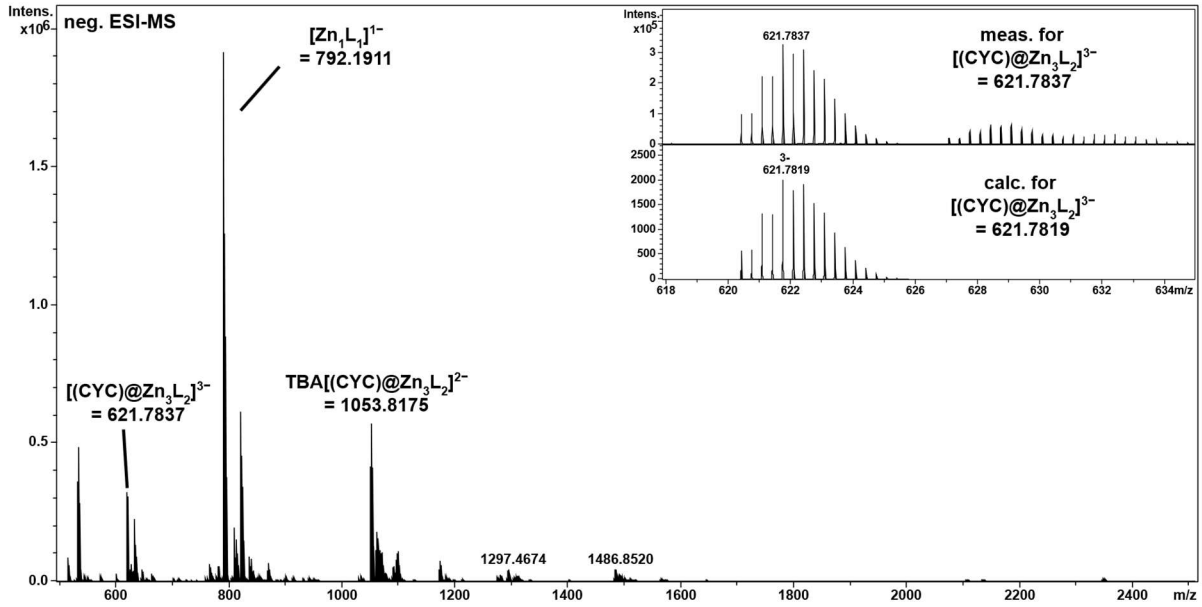

Figure 5.78: Negative ESI-MS spectrum of [(CYC)@ $Zn_6L^{TP3}{}_4]^{3-}$ (DMF:ACN 1:4, 30°C), the spectrum shows the host-guest system as [(CYC)@ $Zn_6L^{TP3}{}_4]^{3-}$, it's TBA adduct and a $[Zn_1L^{TP3}{}_1]^{1-}$ species.

5.6.9 Synthesis of $[(BtA)@Zn_6L^{TP3}{}_4]^{3-}$

According to the general procedure of the host-guest complex formation, the suspended $[Zn_{1.5nx}L_n]$ (1 equiv.) was treated with TBA BtA (1 equiv.) and was then heated for 10 min at 80°C. The ^{1}H NMR spectrum showed the quantitative formation of $[(BtA)@Zn_6L^{TP3}{}_4]^{3-}$.

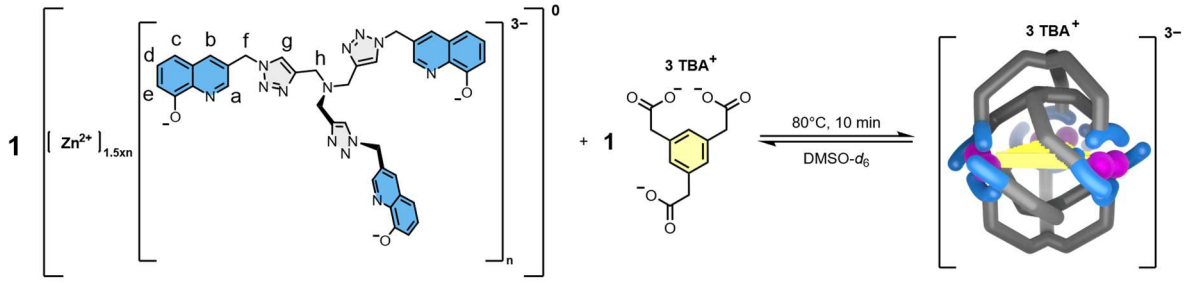

Figure 5.79: Templated self-assembly of the weakly soluble $[Zn_{1.5nx}L_n]$ aggregate with TBA BtA in DMSO-d_6 at 80°C into a negatively charged host-guest complex $[(BtA)@Zn_6L^{TP3}{}_4]^{3-}$.

^{1}H NMR (600 MHz, DMSO-d_6, 25°C) δ = 8.76 (s, 3H), 8.43 (d, *J* = 2.1 Hz, 3H), 6.02 (d, *J* = 2.1 Hz, 3H), 5.81 (d, *J* = 15.3 Hz, 3H), 5.32 (d, *J* = 15.9 Hz, 3H), 5.02 – 4.97 (m, 3H), 4.58 (d, *J* = 15.8 Hz, 3H), 4.17 (d, *J* = 13.1 Hz, 3H), 3.37 (d, 3H), 3.17 (d, 3H), 3.10 (d, *J* = 15.5 Hz, 3H), 1.85 (dd, *J* = 150.3, 12.7 Hz, 6H) ppm. **^{13}C NMR** (151 MHz, DMSO-d_6, 25°C) δ = 178.7584, 164.3910, 164.2904, 148.6085, 144.0313, 142.9321, 142.8540, 140.2690, 139.9711, 138.2949, 136.5004, 136.0739, 131.1628, 130.6412, 129.6845, 129.0994, 127.4563, 127.0758, 126.4307, 125.6292, 124.6721, 120.9813, 112.0580, 111.2552, 107.6624, 107.5335, 50.7698, 49.6327, 49.0702, 47.7931, 46.7280, 44.0545 ppm. **HRMS** (negative ESI-MS, ACN/DMSO 80:20, 30°C): m/z = 633.7797 $[(C_{12}H_9O_6)@(C_{39}H_{31}N_{13}O_3)_2Zn_3]^{3-}$, calc. 633.7807.

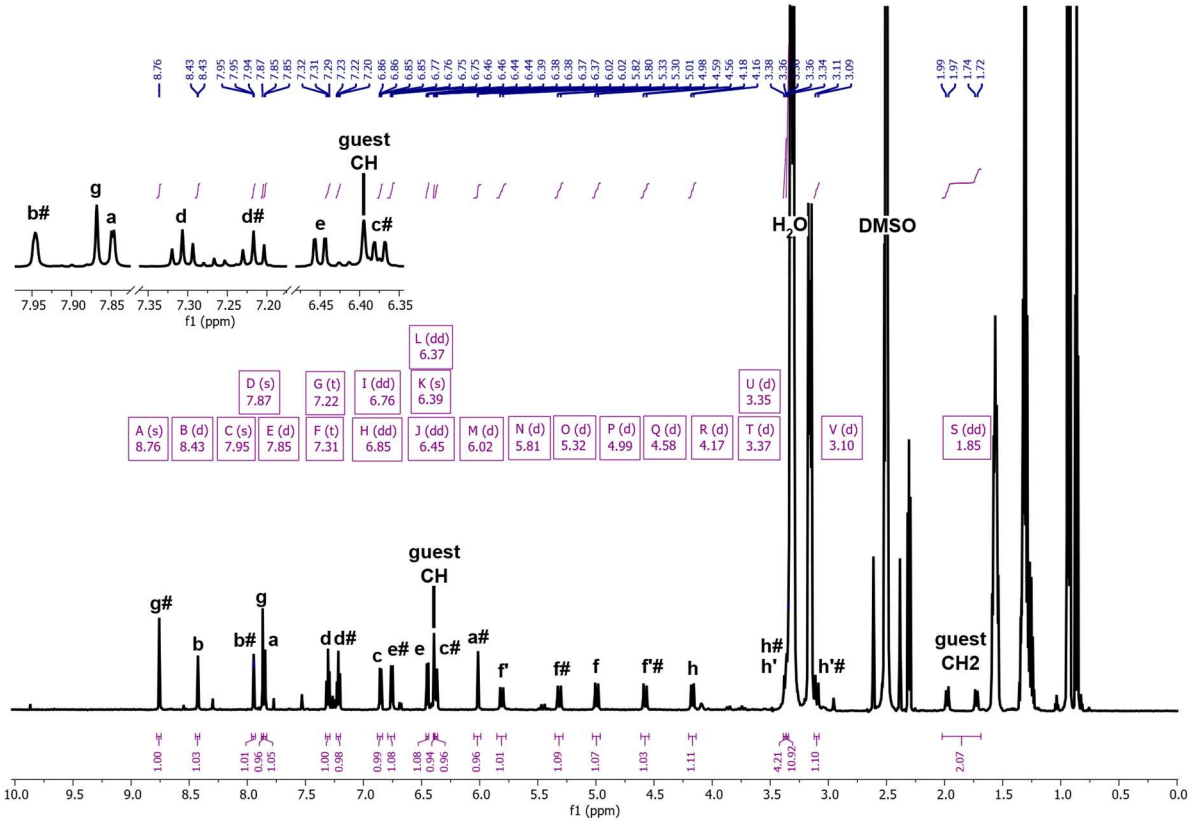

Figure 5.80: ^{1}H NMR spectrum of [(BtA)@ $Zn_6L^{TP3}{}_4]^{3-}$, hashtag marks the outer-shell of the onion. (1 mM, 600 MHz, DMSO-d_6, 25°C).

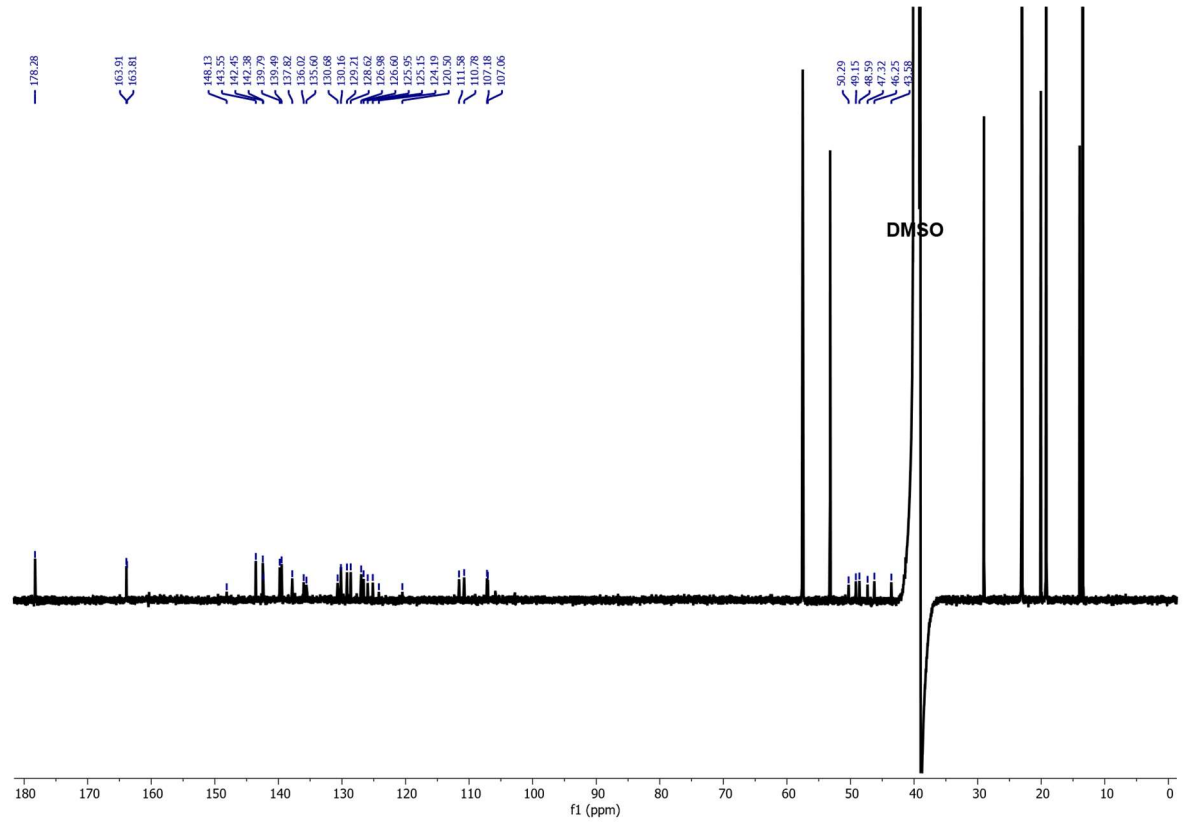

Figure 5.81: ^{13}C NMR spectrum of [(BtA)@$Zn_6L^{TP3}{}_4]^{3-}$ (500 µM, 151 MHz, DMSO-d_6, 25°C).

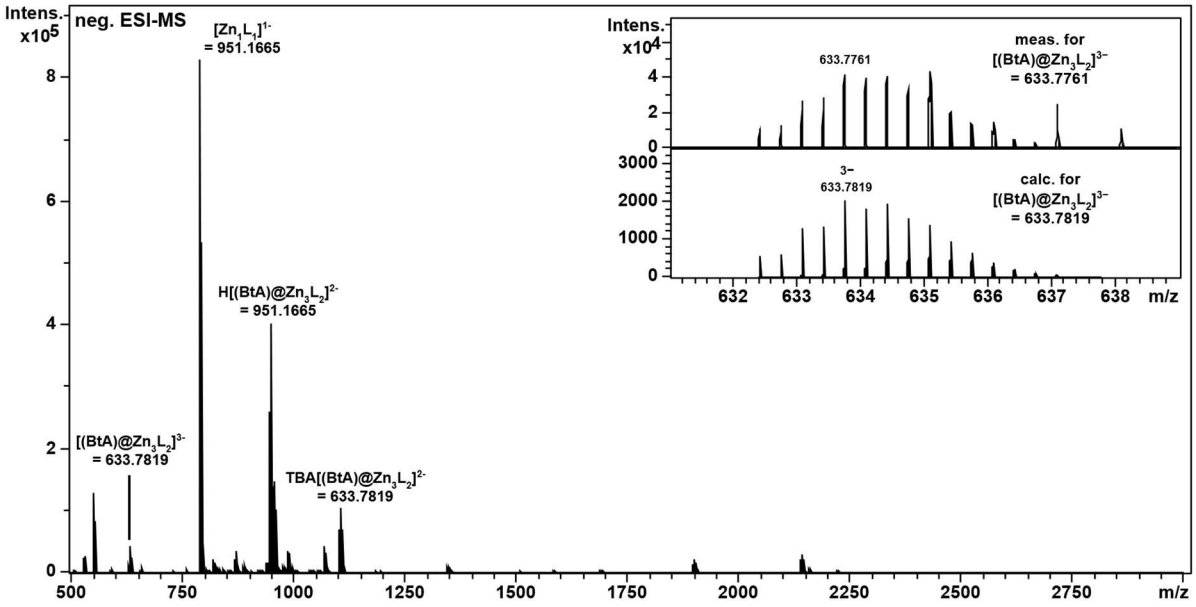

Figure 5.82: Negative ESI-MS spectrum of [(BtA)@ $Zn_6L^{TP3}{}_4]^{3-}$ (DMSO:ACN 1:4, 30°C), the spectrum shows the desired host-guest system, its TBA-adduct and a $[Zn_1L^{TP3}{}_1]^{1-}$ species.

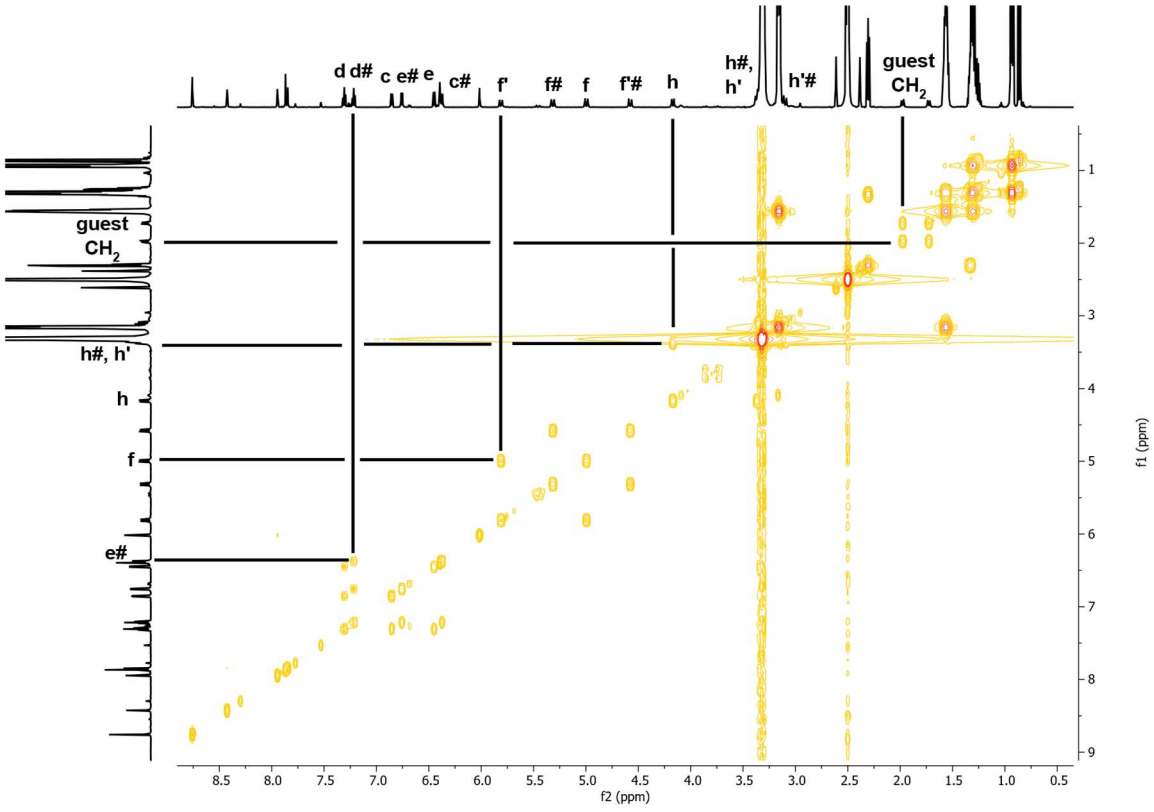

Figure 5.83: ^{1}H COSY NMR spectrum of $[(BtA)@Zn_6L_4]^{3-}$ (1 mM, 600 MHz, DMSO-d_6, 25°C).

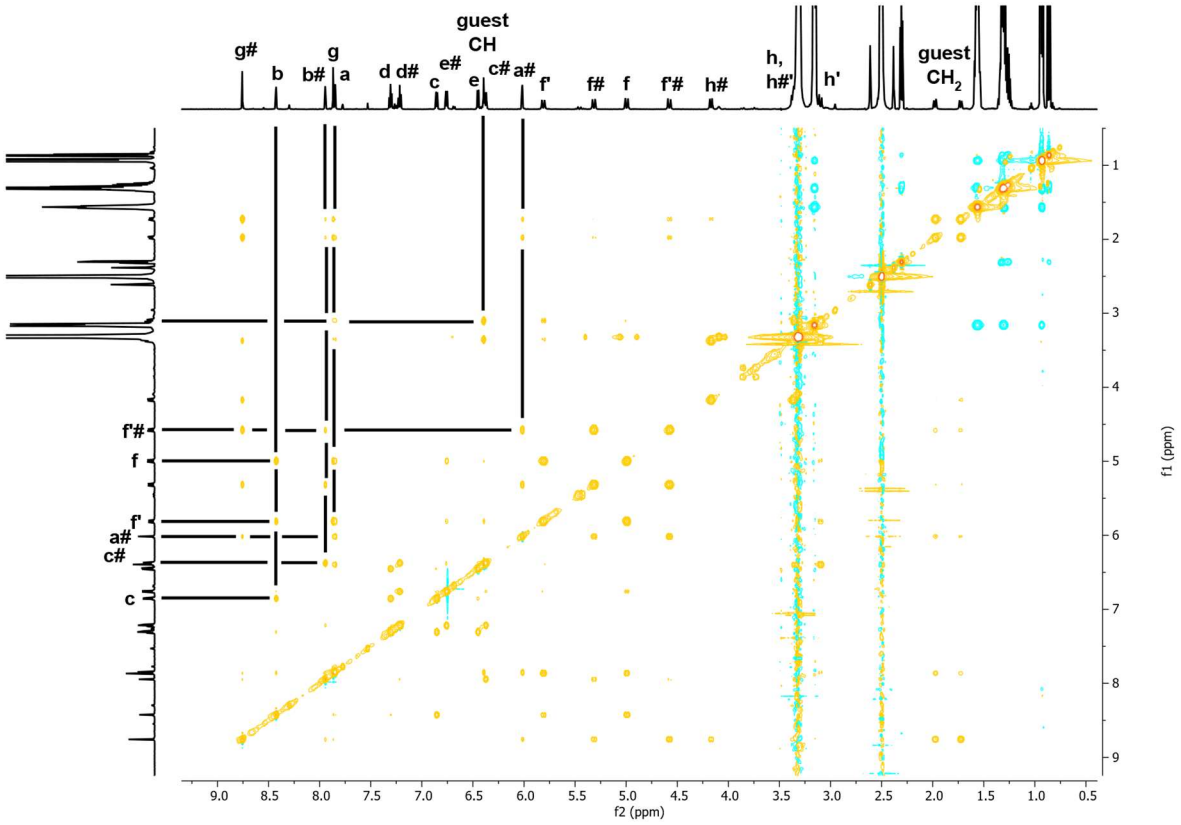

Figure 5.84: ^{1}H NOESY NMR spectrum of [(BtA)@Zn$_6$L$_4$]$^{3-}$ (1 mM, 600 MHz, DMSO-d$_6$, 25°C).

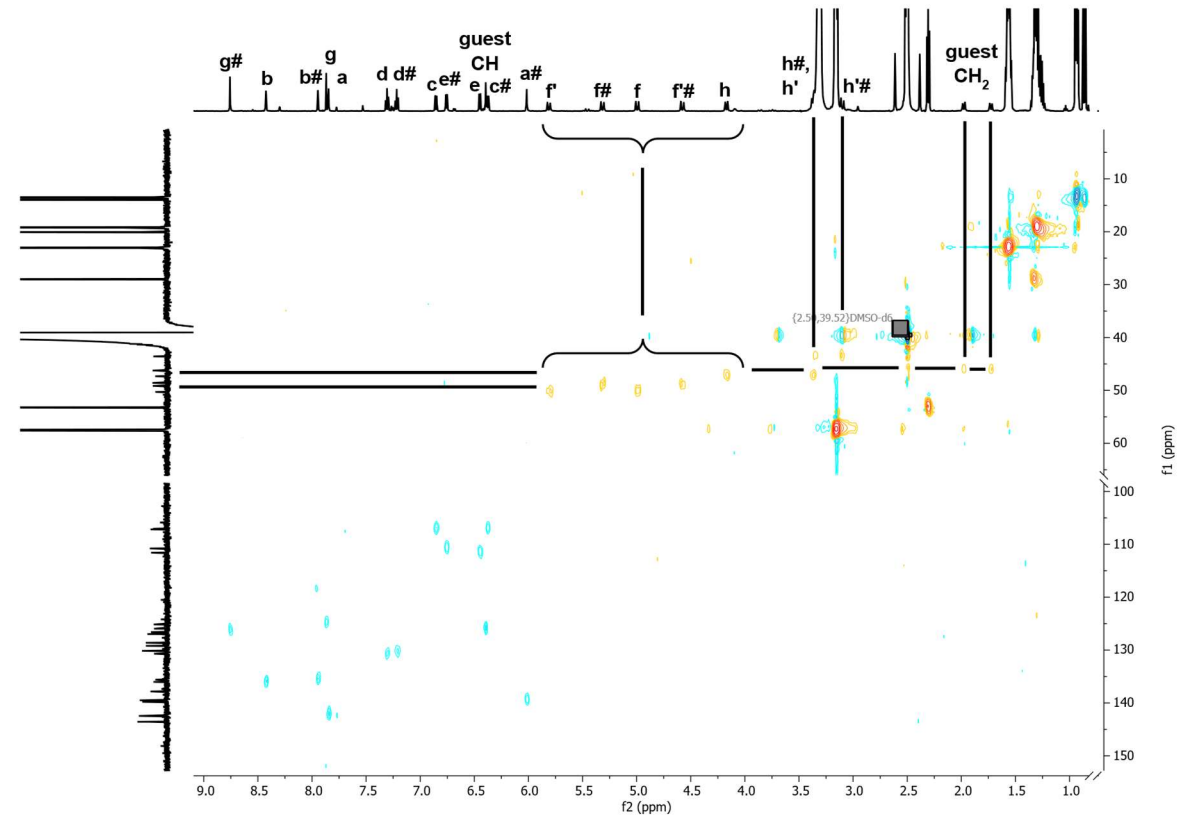

Figure 5.85: HSQC NMR spectrum of [(BtA)@Zn$_6$L$_4$]$^{3-}$ (1 mM, 600 MHz, DMSO-d$_6$, 25°C).

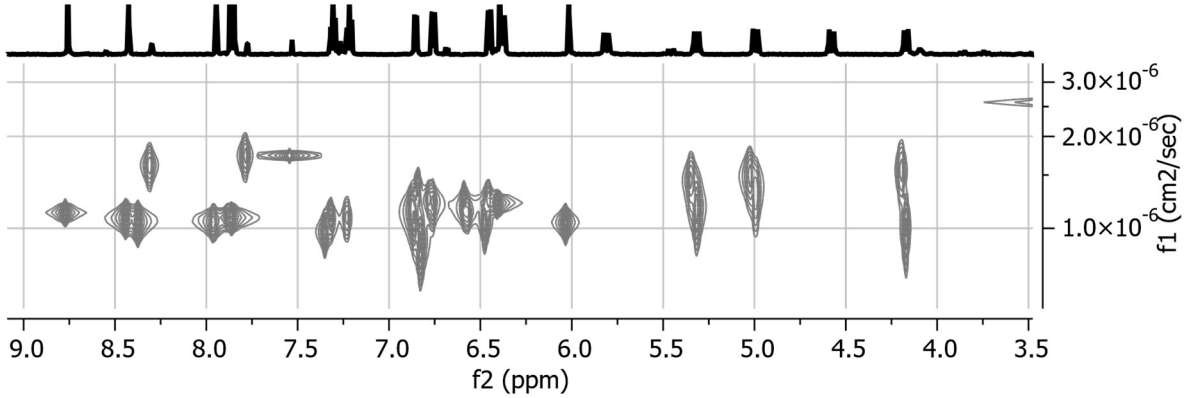

Figure 5.86: ^{1}H DOSY NMR spectrum of $[(BtA)@Zn_6L_4]^{3-}$, D = 1.319 x 10^{-10} m^2 s^{-1}, r_H = 0.83 nm (1 mM, 500 MHz, DMSO-d_6, 25°C).

5.6.10 Kinetic Investigation of guest-exchange induced transformation

Determination of k

The demonstrated ^{1}H NMR competition experiments in chapter 5.4 showed that the guest BTT^{3-} of $[(BTT)@Zn_3L_2]^{3-}$ was readily displaced by TRI^{3-} within five minutes at room temperature to form $[(TRI)@Zn_3L_2]^{3-}$, whereas the exchange of TRI^{3-} with CYC^{3-} and its corresponding transformation from a tri- to the hexanuclear host-guest assembly $[(CYC)@Zn_6L_4]^{3-}$ (equation 9) required more than 4 h under identical conditions.

Equation 9

$$2\,[(\mathrm{TRI})@\mathrm{Zn_3L_2}]^{3-} + CYC^{3-} \rightarrow [(\mathrm{CYC})@\mathrm{Zn_6L_4}]^{3-} + TRI^{3-}$$

To investigate this phenomenon, a kinetic evaluation of the guest exchange $TRI^{3-} \rightarrow CYC^{3-}$ was performed. Considering the host-guest system $[(TRI)@Zn_3L_2]^{3-}$ and CYC^{3-} as the reactants A and B, and assuming that only a single species is formed while neglecting that the stoichiometric requirement of two equivalents of $[(TRI)@Zn_3L_2]^{3-}$ are necessary for the transformation, we define the process as guest exchange. Under these assumptions, the equilibrium can be described as a pseudo second-order reaction (equation 10).[108]

Equation 10

$$\mathrm{A} + \mathrm{B} \xrightarrow{k} \mathrm{AB}$$

The course of this pseudo second-order guest exchange was observed via ^{1}H NMR spectroscopy and conducted at five different temperatures (25, 30, 35, 40 and 45°C). The rate constant k for each temperature was determined via the fully integrated rate law of a second-order reaction, where each temperature has the same initial concentration $[A]_0$.

For the general case of a reaction between particles A and B, the reaction rate is given by:

Equation 11

$$v = -\frac{d[A]}{dt} = -\frac{d[B]}{dt} = \frac{d[AB]}{dt} = k[A][B]$$

For the special case where the initial concentrations of A and B are equal, or two identical particles react with each other, equation simplifies to:

Equation 12

$$v = -\frac{d[A]}{dt} = -\frac{d[B]}{dt} = \frac{d[AB]}{dt} = k[A]^2$$

Integration and separation of variables give:

Equation 13

$$\frac{1}{[A]} = kt + C$$

For the initial conditions t_0, it follows that $[A] = [A]_0$ and $C = \frac{1}{[A]_0}$

The fully integrated rate law of a second-order reaction is the following:

Equation 14

$$\frac{1}{[A]} = kt + \frac{1}{[A]_0}$$

A plot of $\frac{1}{[A]}$ against the time gave a straight line with the slope of k. The differences in the initial times are due to technical factors.

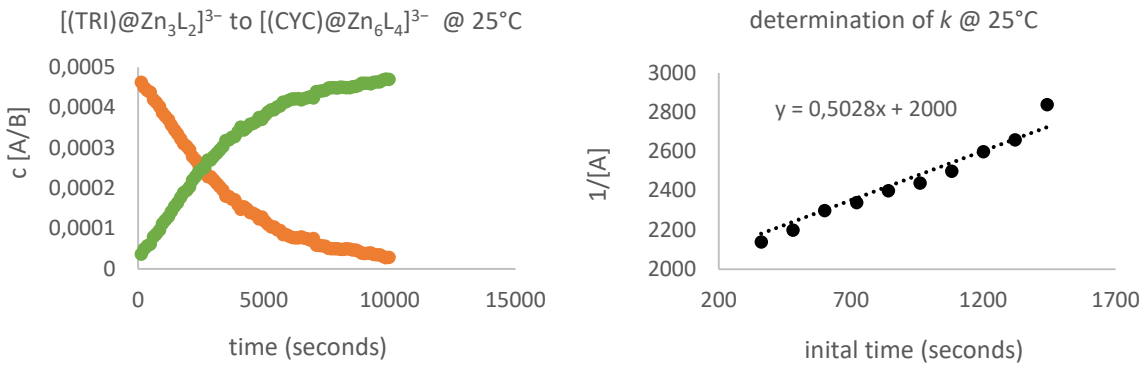

Figure 5.87: Left: Guest exchange and transformation $[(TRI)@Zn_3L_2]^{3-}$ to $[(CYC)@Zn_6L_4]^{3-}$. Right: initial rate and linear regression for the determination of k at 25°C via the fully integrated second-order rate law. (500 µM, DMSO-d_6, 25°C)

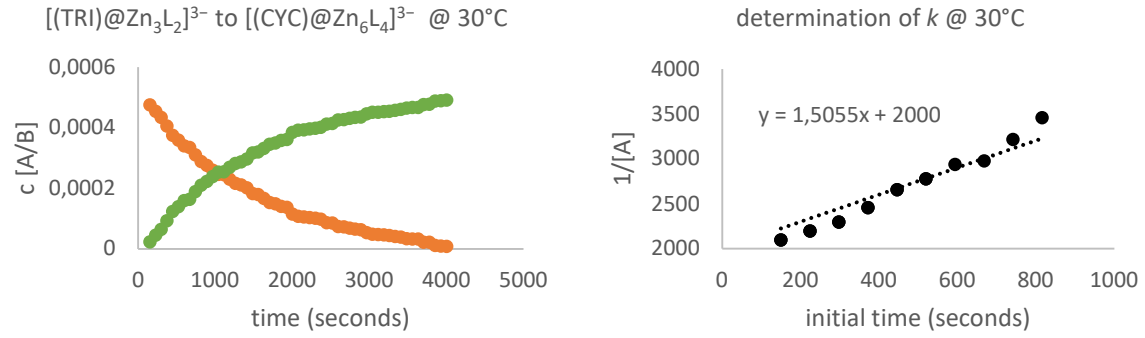

Figure 5.88: Left: Guest exchange and transformation $[(TRI)@Zn_3L_2]^{3-}$ to $[(CYC)@Zn_6L_4]^{3-}$. Right: initial rate and linear regression for the determination of k at 30°C via the fully integrated second-order rate law. (500 µM, DMSO-d_6, 30°C)

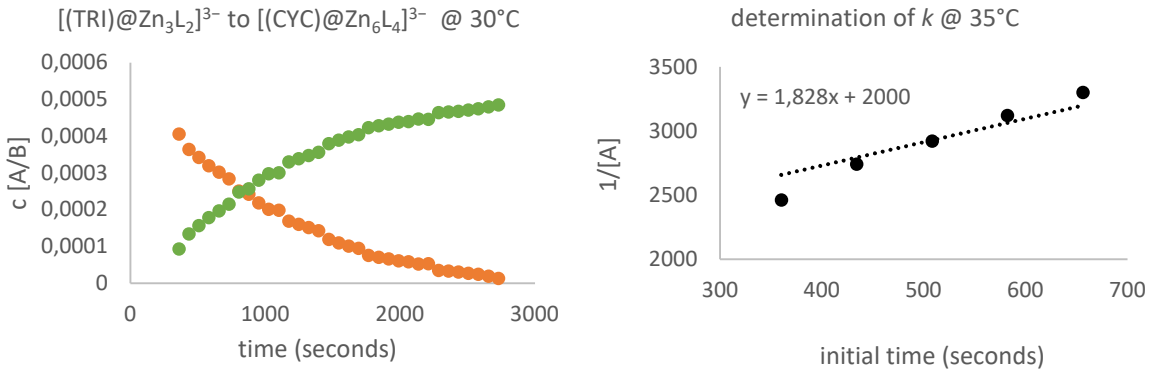

Figure 5.89: Left: Guest exchange and transformation $[(TRI)@Zn_3L_2]^{3-}$ to $[(CYC)@Zn_6L_4]^{3-}$. Right: initial rate and linear regression for the determination of k at 35°C via the fully integrated second-order rate law. (500 µM, DMSO-d_6, 35°C)

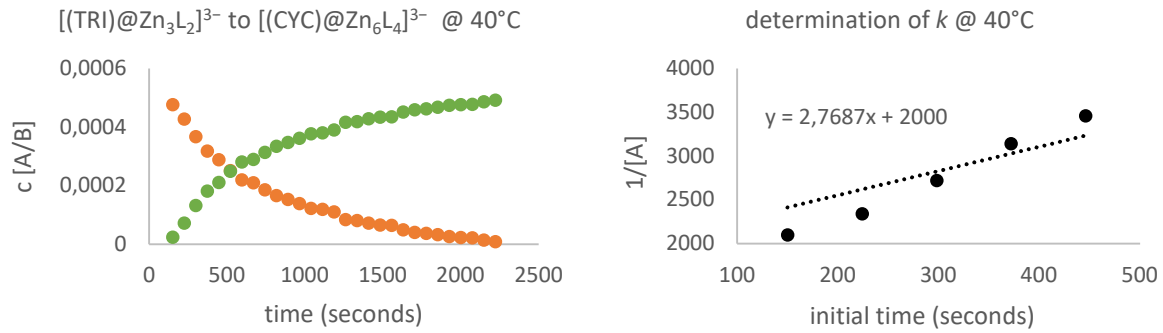

Figure 5.90: Left: Guest exchange and transformation $[(TRI)@Zn_3L_2]^{3-}$ to $[(CYC)@Zn_6L_4]^{3-}$. Right: initial rate and linear regression for the determination of k at 40°C via the fully integrated second-order rate law. (500 µM, DMSO-d6, 40°C)

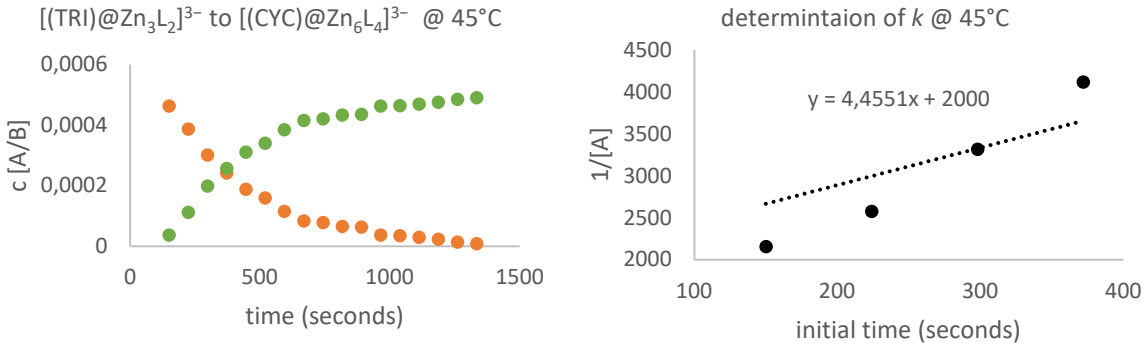

Figure 5.91: Left: Guest exchange and transformation of $[(TRI)@Zn_3L_2]^{3-}$ to $[(CYC)@Zn_6L_4]^{3-}$. Right: initial rate and linear regression for the determination of k at 45°C via the fully integrated second-order rate law. (500 µM, DMSO-d6, 45°C)

Table 1: Summary of the determination of k for each temperature.

$T\ [°C]$	$k\ [L\ mol^{-1}s^{-1}]$	$ln(k)$
25	0.5028	-0.6875
30	1.5055	1.5005
35	1.828	1.828
40	2.7687	2.7687
45	4.4551	8.9549

5.6.11 Activation energy calculation – ARRHENIUS – and calculation of the thermodynamic parameters of the transition state – EYRING

For the determination of the guest-exchanges activation energy (ΔE_a), the natural logarithm of k was plotted as a function of the inverse temperature in agreement with the Arrhenius equation. The value of ΔE_a can be calculated with the slope of the corresponding graph.[108] The Arrhenius equation is the following:

Equation 15

$$k = Ae^{\frac{-E_a}{RT}}$$

Taking the natural logarithm and rearranging gives:

Equation 16

$$\ln k = \frac{-E_a}{R}\left(\frac{1}{T}\right) + \ln A$$

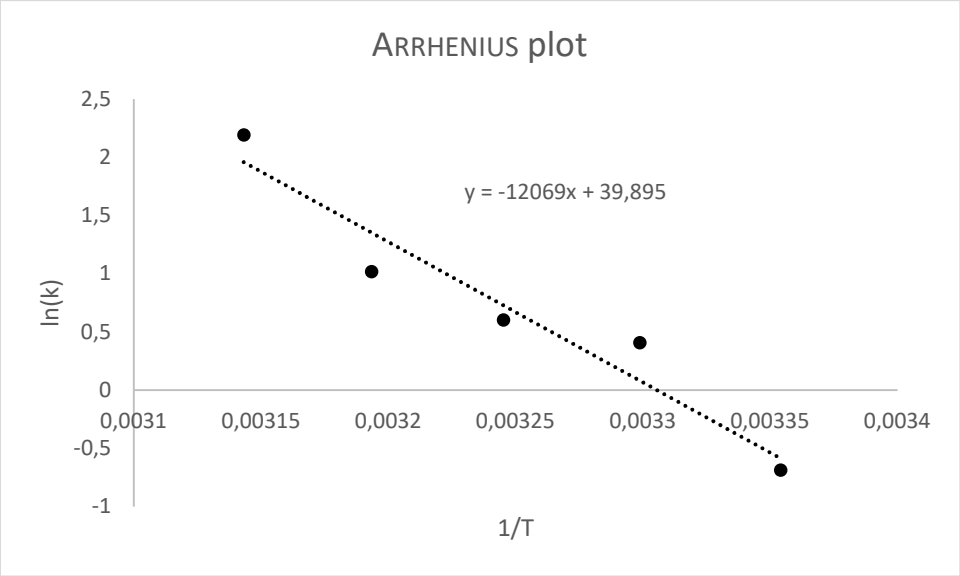

Figure 5.92: ARRHENIUS plot of the guest-exchange and transformation of [(TRI)@Zn_3L_2]$^{3-}$ to [(CYC)@Zn_6L_4]$^{3-}$.

The EYRING equation describes changes in the rate of a chemical reaction against the temperature. It's based on the transition state theory. The EYRING equation describes the free energy of a transition state.[109] For a unimolecular reaction, the parameters in the Arrhenius equation (ΔE_a and A) can be linked to the enthalpy and the entropy of the transition state.

Equation 17

$$\Delta G^{\ddagger} = \Delta H^{\ddagger} - T\Delta S^{\ddagger}$$

Equation 18

$$E_a = \Delta H^{\ddagger} + RT$$

Equation 19

$$A = \frac{k_B T}{h} e^{1+\frac{\Delta S^{\ddagger}}{R}}$$

The Eyring equation is the following:

Equation 20

$$k = \frac{k_B T}{h} e^{-\frac{\Delta G^{\ddagger}}{RT}}$$

Transforming it to its straight linear form, it's possible to extract the enthalpy and entropy of the transition state:

Equation 21

$$\ln\left(\frac{k}{T}\right) = -\frac{\Delta H^{\ddagger}}{R}\frac{1}{T} + \ln(\frac{k_B}{h}) + \left(\frac{\Delta S^{\ddagger}}{R}\right)$$

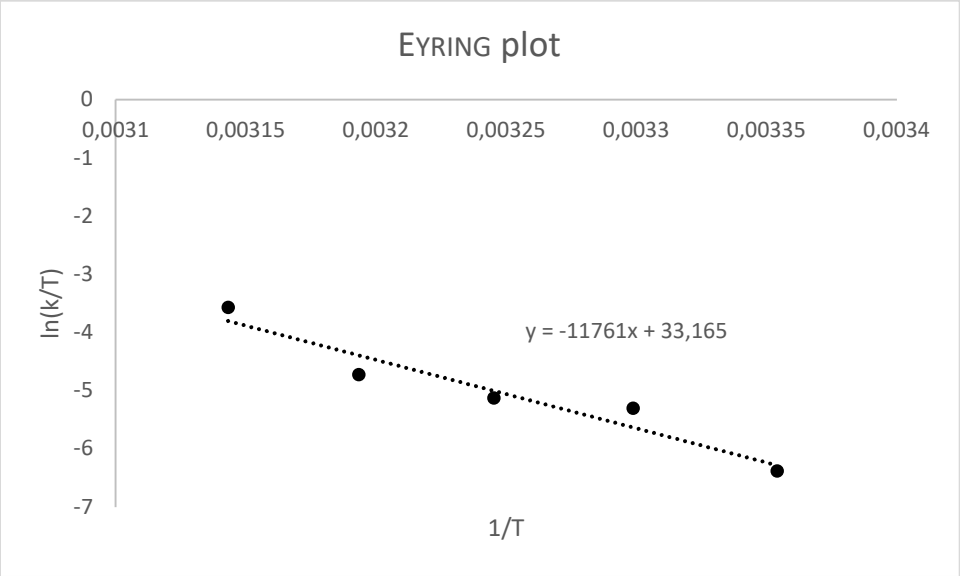

Figure 5.93: Eyring-plot of the guest-exchange and transformation of $[(TRI)@Zn_3L_2]^{3-}$ to $[(CYC)@Zn_6L_4]^{3-}$.

Table 2: Summary of the calculated values from the EYRING and ARRHENIUS plots.

Eyring			Arrhenius
$\Delta G^{\ddagger}$	$\Delta H^{\ddagger}$	$\Delta S^{\ddagger}$	E_a
$74.5\ kJ\ mol^{-1}$	$97.8\ kJ\ mol^{-1}$	$78.2\ J\ K^{-1}\ mol^{-1}$	$100.3\ kJ\ mol^{-1}$

5.6.12 Computational Studies – DFT calculations

The following relevant information was used in the input file's header for geometry optimization for the hexanuclear host-guest complex $[(BTT)@Zn_3L^{TP3}{}_2]^{3-}$ at the ωB97-3c[95]/def2-SVP[96,97] level of theory with ORCA 5.0.3[99,98]:

!ωB97-3c def2-SVP Opt

%maxcore 11250

%pal nprocs 4 end

%scf autoTRAH false end

%geom trust -0.1 end

*xyz -3 1

XYZ data for the optimized structure of **$[(BTT)@Zn_3L^{TP3}{}_2]^{3-}$**:

C	-4.72679528280118	-0.66601099317903	3.64999840303500
H	-2.77220617512829	1.57404502470050	7.76221295642855
C	-2.03038462871860	2.36985488851803	7.78525978722102
N	-0.09482457461068	4.36775331849752	7.78390636209694
C	-2.13091495205175	3.44470165352556	6.93281090264084
C	-0.93466042243930	2.27133941298865	8.67602823705641
C	0.06182000117601	3.28391107555929	8.57955652703356
C	-1.15756757070193	4.46308572139267	7.00942039789094
C	-0.74702911896222	1.20688898479511	9.58521192030106
C	0.41968586787164	1.16383895320132	10.32570615265730
C	1.44351824432646	2.11154801529519	10.18252669585641
C	1.33407310079373	3.16864934912245	9.26681594925581
H	2.37114430017105	2.01093195615097	10.73888851929011
H	-1.49893100876592	0.42744016735206	9.66717944956284
H	0.56964110662007	0.34281014728455	11.02460079265449
O	2.29250860789887	4.00194062270670	9.00750405256359
C	-3.21308139916770	3.60054980441440	5.88864864753348
C	-4.46112434344764	0.51180648386066	4.53100841128048
N	-5.30468404543232	0.79441208739517	5.56878962925874
N	-4.93294875526664	1.90754149434376	6.13886522696539
N	-3.84300652984287	2.35149008357108	5.48351380943992

C	-3.50886569559533	1.50935053363593	4.47302024154230
H	-2.66144611354603	1.68505963574970	3.82385317392801
C	-4.06052088839210	-2.80465891390854	2.77574030938368
H	-2.78512791481701	4.06640597528161	4.99312886699309
N	-3.61359629372407	-1.63143659051908	3.55405963012753
H	-5.64426742099284	-1.14877230782969	4.04066822414349
H	-4.95327557173706	-0.32070802126194	2.63395859298798
H	-4.84898359973535	-3.36571520217542	3.31520934167095
H	-3.20101115431532	-3.47755995060036	2.67084246441255
H	-1.21091414202417	5.33640092285909	6.36293332596803
H	-4.01913391572059	4.24830750747839	6.25484197539954
C	-3.24641886026643	-2.07233942140473	4.91506517924666
H	-4.13333730835507	-2.43937675895865	5.46836933444095
H	-2.86946972188083	-1.19614482482773	5.45618607326129
H	-1.03963739214924	-6.37750590666693	3.26657192126450
C	-0.01354582108858	-6.47238000740530	2.91670294673276
N	2.60188346431315	-6.64726867241587	1.98779176066338
C	1.01887989718970	-5.88615713325083	3.61155959746962
C	0.24733126454007	-7.17317482983522	1.71536846249816
C	1.59357577178491	-7.16949876376300	1.25128442195426
C	2.33579270323797	-6.04939546473800	3.13287536056782
C	-0.74762157843029	-7.80260825488733	0.93521108589874
C	-0.38604115090193	-8.36285361494115	-0.27586254388026
C	0.92107300887489	-8.29874825003923	-0.78009117341956
C	1.94486257265232	-7.65383364999152	-0.07024849842145
H	1.15475330091886	-8.69968962878478	-1.76234104861406
H	-1.77811812285618	-7.81055872622430	1.27803088166761
H	-1.15062880037322	-8.84512246718081	-0.88235152496743
O	3.13919593810871	-7.46554253692988	-0.53751699428243
C	0.83074181178393	-5.05337028291612	4.85944624562514
C	-2.23212238819907	-3.16874886620840	4.97183190312647
N	-2.52975638173533	-4.34357827383206	5.60437103161664
N	-1.47441521150543	-5.11015815717798	5.61432425665063

N	-0.48725913155453	-4.44530394370691	4.98277784118072
C	-0.91585370608229	-3.22890900735046	4.56045656411560
H	-0.27563027296043	-2.53635440884390	4.03062878854468
H	1.57471190794406	-4.24828366392955	4.87351365169140
H	3.18108272832837	-5.61246960166921	3.66036445403886
H	0.97449455167581	-5.66186411974495	5.76084911340086
H	-6.72553626184166	0.03163535361518	-0.57662640282547
C	-6.30414443234254	0.51681879150166	-1.45497665257818
N	-5.15895160441886	1.77378659940641	-3.65571901580477
C	-5.43960462404742	-0.16335803051045	-2.28135870733113
C	-6.62097403950071	1.87030690461273	-1.71955781984955
C	-5.94951076901554	2.48226663322731	-2.81634577953933
C	-4.92921494670112	0.49708232404703	-3.41823833083938
C	-7.49559726432446	2.64777964593010	-0.92858683655449
C	-7.64040627690513	3.99076155317895	-1.22311863738580
C	-6.92454353392252	4.62294000301407	-2.25013439223155
C	-6.01138048734068	3.91363581714267	-3.04458252877275
H	-7.02020874368778	5.69277951086036	-2.41277630679243
H	-8.01316956119736	2.19319270495384	-0.08891736372784
H	-8.31058086489524	4.59430605962882	-0.61356254049534
O	-5.23885849195547	4.46689925761526	-3.92616598986959
C	-4.98139323834267	-1.58345272239848	-2.03842219827324
C	-4.61790049443277	-2.48950201474661	1.42505290868317
N	-5.89121464715566	-2.86984574843721	1.10402428804865
N	-6.12935189873431	-2.57690197863702	-0.14462218816732
N	-5.01919913338317	-1.99744958025485	-0.64179158420365
C	-4.04943050827055	-1.91863947691840	0.30415927664638
H	-3.07712077527066	-1.48668216859994	0.10845142016281
H	-3.95035654656510	-1.69695412455287	-2.39326871042283
H	-4.25378528192313	-0.01037410604429	-4.10361413043286
H	-5.60867399228924	-2.29675686506161	-2.58717191717516
C	7.09091598687333	2.59950550115447	-1.53234072096460
H	6.34676201992063	6.91135992735978	3.76881879780453

C	5.61400292758913	6.51990089348900	4.47302453732464
N	3.73988434000666	5.50360694712506	6.24755116284057
C	5.46627271312802	5.15799089707666	4.63500779864319
C	4.79996280955939	7.41669852056961	5.20157882035144
C	3.83809618962063	6.83517583461561	6.07968051807357
C	4.50856907774955	4.68681792636998	5.55329611669195
C	4.86685479584883	8.82381764304945	5.10016553401385
C	3.98221446599646	9.58438138267882	5.84410324422077
C	3.00677433967986	9.02428715389487	6.68155636355907
C	2.87028317718001	7.63302493771435	6.81243885526555
H	2.31118486352290	9.66053063385928	7.22106355013350
H	5.59002405600609	9.28527793610122	4.43407212528416
H	4.02911545670742	10.66924375822086	5.76467813908115
O	1.95801359690830	7.05339476562659	7.51740283744941
C	6.31862397017111	4.14631031680580	3.90520820443758
C	6.46759497201683	4.71471504924077	0.35269473839517
N	7.68261263340329	5.13539816070402	0.81548882755582
N	7.72978286891443	4.97950797648349	2.10955247017900
N	6.54966555255776	4.45564067623604	2.49723981224956
C	5.72835519747015	4.27991271475565	1.43324531478281
H	4.73239978649543	3.87126430553971	1.52445350988881
C	5.61647507668841	3.61224426307254	-3.15196700791383
H	5.85464207661097	3.15545682236143	3.96734688687679
N	5.89296432492226	3.44771635977118	-1.70905268972616
H	7.99070576207713	3.07356701851151	-1.97061513704816
H	6.48421126482193	4.04860445147226	-3.68417682167482
H	4.34391955282878	3.62083862008536	5.70232946246313
H	7.31550373370956	4.07970629939511	4.35613168427554
C	6.13769702516643	4.77367499449536	-1.10262634238531
H	6.97377322941414	5.29948890470386	-1.60371227243989
H	1.60235961431231	5.20744231494666	-6.21147128009830
C	0.60155857159208	4.94346645160046	-5.87275672656000
N	-1.93816076096509	4.26269396104058	-4.98903542797513

C	0.22151366124446	5.19128444837677	-4.57037270014136
C	-0.29675651377038	4.32476197589306	-6.77186808505011
C	-1.57889690965750	3.97615522029612	-6.25409744822932
C	-1.08047075127248	4.83672982965512	-4.16751813021956
C	-0.00020192769003	4.02125716361430	-8.11894029230909
C	-0.96092645281033	3.37966656817896	-8.88050441209268
C	-2.21085115126553	2.99751632994311	-8.37268677189157
C	-2.56252730803217	3.24836654918582	-7.03661958955525
H	-2.92165504850343	2.46549331525549	-8.99834147231577
H	0.97221935458368	4.27572398748535	-8.53027505774337
H	-0.73361951404759	3.14119254880368	-9.91822425897918
O	-3.66967066322628	2.87133503583213	-6.49152352686121
C	1.12016880584511	5.87200131056797	-3.56442375007680
C	4.44092256948902	4.48756831314701	-3.43858988983405
N	4.58700955040892	5.65754958004814	-4.12931254577087
N	3.42576477501771	6.24107918685690	-4.24147228301936
N	2.51835461742504	5.45802918356685	-3.62477591884374
C	3.10721280479231	4.34867981176880	-3.11477042390280
H	2.55686160029308	3.58851482598810	-2.57960744717876
H	0.75129185857581	5.68421692614936	-2.54975580940620
H	-1.41999033447008	4.99568680755811	-3.14516690812011
H	1.12842745104309	6.95673711899966	-3.72294897093947
H	8.31823655172439	-2.56325769156308	-1.83876168804222
C	7.53919440412215	-3.24541411799324	-1.50124751007477
N	5.53687595716283	-4.96086876371407	-0.63904134139434
C	6.24908446702351	-3.11152849740437	-1.97069560801532
C	7.85461604736072	-4.25313420078250	-0.56180829629546
C	6.77922287969061	-5.08848768732749	-0.13750788563567
C	5.26652560426906	-4.00980573448348	-1.51232702661122
C	9.13954544887041	-4.46601215336186	-0.01570810570514
C	9.30174915797498	-5.46654970302199	0.92605653083497
C	8.24535991202610	-6.26902443475767	1.38035307358083
C	6.93857799672485	-6.09656372637543	0.89637426207558

H	8.41291615169908	-7.02019964651368	2.14676704181458
H	9.97011787907386	-3.83779195709917	-0.32403311529258
H	10.29051943410236	-5.63008918403342	1.35153887358298
O	5.91333212462420	-6.75851395210229	1.31519890502619
C	5.85021171527258	-2.07270734066488	-2.99243125662078
C	6.96237044898761	1.24686326718557	-2.15183542840731
N	7.79549241961662	0.85491208493835	-3.16168960578560
N	7.48103819467652	-0.35404940519327	-3.53686934687428
N	6.44233198657895	-0.75590746491547	-2.77730763112787
C	6.08997393144427	0.20984288760565	-1.89368064637943
H	5.27929780720383	0.09011976508685	-1.18964911935844
H	4.75993242415444	-1.96179731348210	-3.00349070862594
H	4.23119492777039	-3.93209384822645	-1.84057409730813
H	6.16699004549425	-2.37398700994429	-3.99770795290654
Zn	4.15591391925747	-6.13063137879423	0.55214345997598
Zn	1.92495883745769	5.04543067322577	7.33859130163779
Zn	-3.78012775720860	3.22778916458204	-4.50990708640467
H	7.27052690168315	2.50272687836521	-0.45535527650263
H	5.23693153173397	5.37833288005369	-1.25816748806742
H	5.45028818231735	2.61349671780115	-3.57194879265595
C	-0.12077637194855	0.00616759217808	0.13875250610300
C	0.75674740510110	-0.79510566257178	0.90278987102667
C	1.19435705207817	-0.29881326616561	2.14638803175851
C	0.78388069744404	0.96222934000101	2.63343011903559
C	-0.09005066224303	1.72853900702004	1.83746294569236
C	-0.55640128529266	1.26925560687346	0.58539334911011
C	1.21444460772186	1.66666662375334	3.79473492880132
C	0.71591179469526	2.93188483921628	3.86738429055194
S	-0.34243903104006	3.31485940131640	2.52023436285082
C	-1.33948275590063	1.94746710226525	-0.39301657928310
C	-1.47121856534720	1.24475883504418	-1.55224308815841
S	-0.66147226691531	-0.31145389175491	-1.48962451195433
C	1.38778209335651	-2.02601945584039	0.56027705762646

C	2.29381192047572	-2.43829904012666	1.48977131405109
S	2.39472061787348	-1.34547065353804	2.85994181141726
C	3.20240370402333	-3.61434669059807	1.44784188322169
C	-2.12868842489719	1.65534327422374	-2.82094706370961
C	1.00451918711310	3.98824021593090	4.87284583988889
O	0.54008033160743	5.12781661487274	4.67864316886731
O	1.71914663478153	3.59996830727739	5.86059902931471
O	-2.01822322363846	0.90328814109181	-3.80820392369582
O	4.04436916754288	-3.73755707316569	2.35789904592482
O	3.01449007908087	-4.39672389913552	0.45273440333452
O	-2.75439664141295	2.76977176950028	-2.75996069483019
H	1.88719859980756	1.27663869598947	4.54995928369396
H	-1.77906825281838	2.93078671295165	-0.27068984582068
H	1.20817094791175	-2.59055985615270	-0.34752509075255

*

The following relevant information was used in the input file's header for geometry optimization for the trinuclear host-guest complex $[(TRI)@Zn_3L^{TP3}{}_2]^{3-}$ at the ωB97-3c[95]/def2-SVP[96,97] level of theory with ORCA 5.0.3[99,98]:

!ωB97-3c def2-SVP Opt

%maxcore 11250

%pal nprocs 4 end

%scf autoTRAH false end

%geom trust -0.1 end

*xyz -3 1

XYZ data for the optimized structure of **$[(TRI)@Zn_3L^{TP3}{}_2]^{3-}$**:

C	3.78990481291193	16.53535481217953	-0.75329260013443
H	5.91285364879495	19.82783176413029	2.59867823763424
C	6.87463932160979	20.20488947330967	2.25297147107930
N	9.31280248048317	21.15712059105922	1.34667235243639
C	6.97009898063466	20.84170894102366	1.03294335805652
C	8.02240799932042	20.01761686376592	3.05420693172161
C	9.25079169536577	20.52137644157889	2.53144463843739
C	8.22962504463614	21.30805097588589	0.60915548405373
C	8.02482271361522	19.36586471614173	4.30675859361226
C	9.22719274165557	19.22884663950744	4.97890651674360
C	10.44478975079264	19.69971040075728	4.47083555482952
C	10.51834268246477	20.34732995360720	3.22429170805666
H	11.36848250719710	19.55002192297399	5.02236354269076
H	7.09902540720500	18.96874767467032	4.71276494966956
H	9.23408738373199	18.72013881237611	5.94167943701688
O	11.61024583703622	20.76538510125929	2.68856195775840
C	5.76504780071894	21.06805297698635	0.15019659573430
C	4.08975696064329	17.92518231131628	-0.30181713478750
N	3.28439657982669	18.60111537979234	0.56693310986270
N	3.78602686056646	19.79020348334898	0.77926866554446
N	4.91395314423228	19.88686387530628	0.04965041575755

C	5.14667866208919	18.74387245058614	-0.63572878445403
H	6.00762901453420	18.60804531767056	-1.27342913864140
C	4.72622482233540	14.37831753075479	-1.31023702241645
H	6.08192314479866	21.35570781247868	-0.85859684271137
N	4.96507571980511	15.66091120341613	-0.63279501167697
H	2.92424773451360	16.16050033446896	-0.17246725653674
H	3.48988826343636	16.54160347045206	-1.80946768640812
H	3.79620981361077	13.88712244501144	-0.96268385613343
H	5.55914655984356	13.71130602976367	-1.05264503008295
H	8.36032845783238	21.79382442533968	-0.35725273755655
H	5.12591465549726	21.86479697432964	0.54713738308104
C	5.30545161756982	15.44143290562887	0.78038941080212
H	4.55560095403206	14.81495396627134	1.30241488672034
H	5.30578671332028	16.42114620304391	1.27574534062182
H	8.66560417720507	11.98372034267806	-0.58336495111269
C	9.50198136688083	12.29740130185155	-1.20644358820546
N	11.62993809046490	13.10972090170008	-2.78218966097317
C	10.32013709795389	13.33061702505617	-0.80109930312737
C	9.72727734343335	11.64774016121961	-2.44080415339467
C	10.83086618864048	12.11546617401737	-3.21320204296576
C	11.39027628839600	13.71299081727157	-1.63395658432909
C	8.93149795361907	10.59680722783310	-2.94690694335854
C	9.24639592079060	10.06612667701808	-4.18609668368064
C	10.31279460327425	10.53007845388839	-4.96741675504727
C	11.13760416653608	11.58274094295420	-4.53137138255261
H	10.50892495253490	10.10102461800724	-5.94586536145994
H	8.08257497317634	10.23541243649238	-2.37379416215338
H	8.63053391095963	9.26050868282901	-4.58293238521448
O	12.10193046260136	12.08204406465663	-5.22162611117038
C	10.12756385643105	14.04956137152154	0.51474652879220
C	6.64222236914830	14.79720663029124	0.93338468234707
N	6.84574511948724	13.72481336260966	1.75105587440458
N	8.10755002527312	13.38379405007851	1.70358949773176

N	8.72241992467254	14.23275846925089	0.85816872654594
C	7.84517248506828	15.12730614600792	0.34757480541190
H	8.13307272113516	15.89135815158359	-0.35919074865572
H	10.60870951814515	15.03381629572830	0.48408284268584
H	12.04707385574941	14.54164867765839	-1.37147863842163
H	10.56928896828565	13.48230994957643	1.34216625488469
H	3.19126115090705	16.93685299349758	-5.46525014324275
C	3.95865576687883	17.54459338039650	-5.94305196152018
N	5.92687125618519	19.07577250377259	-7.14934604934557
C	5.15118256358807	16.97306827163057	-6.33463053829703
C	3.72773241262835	18.92421717027901	-6.14017403658042
C	4.78028378068467	19.66257788002428	-6.75820143074092
C	6.12621832598926	17.78863576503609	-6.94144339637208
C	2.54719075468412	19.59926652589863	-5.76006088164125
C	2.45948850534641	20.96107046464444	-5.99287197413283
C	3.49187167506188	21.70435552323107	-6.57971964613397
C	4.70044337824420	21.09969268582730	-6.96991154136411
H	3.38892619928552	22.77620696616373	-6.72249417589219
H	1.74027717581396	19.05241298160004	-5.28102025291506
H	1.55308500729435	21.48594843372177	-5.69497355808318
O	5.69885352286176	21.73430045086852	-7.47481203703386
C	5.43533880649648	15.49958866296517	-6.15909205274118
C	4.64597601742870	14.53825372116074	-2.79098816249380
N	3.61563208085281	14.02857016053346	-3.52531192100752
N	3.81543034717147	14.29899494164139	-4.78912962972725
N	4.97287852388790	14.98230616339983	-4.87604375464675
C	5.52238425379900	15.16151324332091	-3.65293360101657
H	6.44911328648669	15.69468128671802	-3.50039149199469
H	6.51106023658504	15.30802987163965	-6.24378335598853
H	7.09450066175946	17.38963648421629	-7.24176534319049
H	4.92340760527182	14.90454565139421	-6.92401577875390
C	17.43803360814044	20.67244659268344	-7.10151308328130
H	16.63910937551144	23.78001602878606	-0.98396747940113

C	15.72555755166723	23.32966623781570	-0.59648733073266
N	13.38665677573499	22.16818944063445	0.33261126765518
C	15.52409928100556	21.96968007132471	-0.70312366419844
C	14.73401761235840	24.15521505626992	-0.02430115864738
C	13.53731603181209	23.50647736871174	0.40205996810725
C	14.33259282346272	21.41414512844063	-0.19873259079172
C	14.84391901973065	25.55748914998302	0.11056628429402
C	13.77001861862948	26.25896315468522	0.62925465743885
C	12.57097922921494	25.64297023360999	1.01156637515946
C	12.38775445309300	24.25371517315785	0.88833839644342
H	11.73989636138947	26.23467747594188	1.38470335017111
H	15.74951784753934	26.06261092717493	-0.21302080113246
H	13.84846257666248	27.34049356830776	0.72993117612341
O	11.28971183363976	23.64117449125821	1.16049349594294
C	16.53336970426808	21.06803477617804	-1.37215962029757
C	17.06069158147747	22.34454937425996	-4.69239961943987
N	18.26148349371400	22.53697590034643	-4.07188297893528
N	18.19003397616889	22.08411256027695	-2.84792296714036
N	16.95049255656366	21.58605447038521	-2.67455458065388
C	16.20813496230980	21.73474278444842	-3.79665833675698
H	15.17966111778848	21.41070568219591	-3.86387604019090
C	16.00559965916903	22.20153781290038	-8.29426783247277
H	16.11075799610855	20.06597113655124	-1.50814915967855
N	16.37141869916830	21.67862558519084	-6.96745207729205
H	18.32438342570832	21.07731913876901	-7.62886995700682
H	16.84057748202404	22.75839501056601	-8.76365580101602
H	14.11748109081545	20.34673558480559	-0.25608889071164
H	17.45304453862317	20.97687409671104	-0.78389729367882
C	16.82429258974877	22.77943643629427	-6.10051718005246
H	17.75950036696044	23.24142662270956	-6.47398220417085
H	11.51663119905768	23.95154600180661	-10.45673223418541
C	10.71850010731595	23.40836269941720	-9.95116439518498
N	8.73168754422712	21.99609243883158	-8.63392264110461

C	10.56115639797311	23.52163462374144	-8.58555059358245
C	9.87681227316767	22.55707755673656	-10.69871784716125
C	8.89612921190433	21.82910185264664	-9.96144754576557
C	9.52646762212775	22.80426973742902	-7.95552448719802
C	9.97363155295724	22.36323895374050	-12.09507225162786
C	9.12664626823502	21.44952503309235	-12.69681683904214
C	8.18713996465162	20.69514979961269	-11.98141520591014
C	8.04867753322300	20.82586934673370	-10.58766132480707
H	7.56216805804308	19.96561185159181	-12.48859686224505
H	10.71854287317969	22.90932725118322	-12.66676662462810
H	9.20182947744742	21.29285709516489	-13.77190493483442
O	7.25082704926719	20.11757188699888	-9.86902762029581
C	11.48911894473833	24.36740309402527	-7.74859889163812
C	14.82098609953423	23.10840516163799	-8.25167339720883
N	14.86776298894527	24.37521260207103	-8.75855955417035
N	13.69833214003763	24.94001606895851	-8.61177100850756
N	12.89484864640449	24.04921798889175	-7.99944747640035
C	13.55069666596852	22.88892051481178	-7.76237933615339
H	13.08195875196499	22.03828850347118	-7.28914233649952
H	11.27572537302526	24.21898126270683	-6.68378126949283
H	9.35535969874383	22.85021693043076	-6.87948418579533
H	11.38669437495345	25.43408415194075	-7.97565551694681
H	17.59545534486577	15.40405841286841	-7.78855785452712
C	16.73097420823893	15.04683714257089	-7.22923311028767
N	14.52110073426676	14.20271827475487	-5.78698983063859
C	15.46213183249681	15.46120855487026	-7.57729752532940
C	16.92509580222266	14.19581907446196	-6.12039415354308
C	15.75417033103135	13.82479799248814	-5.39461863581127
C	14.36233059292143	14.99279894420509	-6.83386150414222
C	18.18533643679778	13.73474628094005	-5.67757944704671
C	18.24143747133129	12.95848588021204	-4.53363657672107
C	17.10640612652129	12.62204934144197	-3.78399553102759
C	15.82326498030479	13.06148941541806	-4.15773036380378

H	17.19889479321923	12.03665142111107	-2.87361382464296
H	19.08438462530808	14.01274082212444	-6.22015933691549
H	19.21124457292450	12.60569574125597	-4.18571841590348
O	14.75472376681679	12.84239062211969	-3.47634676218613
C	15.23191062079086	16.43704479285222	-8.70508894717789
C	16.99121700419143	19.45092478691475	-7.83353279024859
N	17.63300402994195	19.00809118390265	-8.95417714963203
N	17.05501461390330	17.91445536956709	-9.37627175123324
N	16.03116656085914	17.65203812711551	-8.54126807638004
C	15.95830584985644	18.57999227079062	-7.55856594163766
H	15.21386768427110	18.54557138779857	-6.77621366469335
H	14.17235165634387	16.71281596320214	-8.75501030358721
H	13.33642882630841	15.28696877557214	-7.05841794562751
H	15.52793792674905	16.02159635249343	-9.67425937525832
Zn	13.06407982935301	13.62599663153786	-4.31797473056695
Zn	11.37259010082876	21.62130098615926	0.86336926090568
Zn	7.31399852628426	20.56875981441145	-7.87630578824044
H	10.19877369814862	17.78161462681345	-6.11293561252912
C	10.45944989360019	18.19752454650958	-5.14603389973015
C	11.12922400801014	19.24693052509699	-2.64602911971693
C	11.30264232609008	17.47740067959436	-4.29667154464301
C	9.95562639069341	19.44044015901199	-4.75978236173015
C	10.29577497493355	19.96062735247803	-3.50858204018463
C	11.63260554241817	18.00778505179938	-3.04897265950512
H	9.90355182325989	20.92703535559746	-3.21215694142182
H	12.28494303762486	17.45762398362103	-2.38006615023234
C	11.82719202032545	16.13178910161281	-4.73426757119043
C	9.04225482795362	20.22817753036530	-5.66703968013549
C	11.49472050928335	19.78694938531874	-1.28519317214999
O	12.23309356453493	19.11437041116487	-0.54191818946721
O	8.65518541069613	21.35623526417210	-5.31094029242786
O	11.47372951675677	15.66848895603628	-5.83422366433442
O	12.62279319427040	15.55005622131766	-3.90293723371965

O	10.99835599142949	20.94079979573379	-0.99439768124233
O	8.72561421886452	19.64754408925186	-6.77418282567723
H	17.76196583500798	20.40094151333712	-6.08916143094504
H	16.04943499470042	23.55562188797111	-6.12557915727083
H	15.79201719342174	21.33977742542044	-8.93896312161550

*

The following relevant information was used in the input file's header for geometry optimization for the hexanuclear host-guest complex $[(TRI)@Zn_6L^{TP3}{}_4]^{3-}$ at the ωB97-3c[95]/def2-SVP[96,97] level of theory with ORCA 5.0.3[99,98]:

!ωB97-3c def2-SVP Opt

%scf

MaxIter 1000

end

%maxcore 8000

%pal nprocs 10 end

%geom trust -0.1 end

* xyz -3 1

XYZ data for the optimized structure of **$[(TRI)@Zn_6L^{TP3}{}_4]^{3-}$**:

Zn	13.58900	3.08000	5.12700
O	13.89500	5.16500	5.66100
O	15.57200	2.61300	4.89300
N	14.00200	3.44200	2.95000
O	12.52600	1.32600	5.07500
N	10.71100	7.33400	2.86900
N	11.62000	3.78600	4.81700
N	10.97400	6.81600	1.64200
N	12.00600	7.40700	1.19300
N	13.14400	5.09400	-1.54900
C	16.08300	2.64900	3.69300
C	12.46100	8.29700	2.12000
C	13.15900	3.86600	1.99800
C	13.59100	3.98800	0.56900
C	9.63300	6.80300	3.64600
C	11.61300	8.22200	3.18900
C	15.26100	3.07900	2.59600
C	11.20000	5.05800	4.53500
C	9.91400	5.36800	4.08800
C	14.86900	3.63300	0.30800

C	15.75600	3.17000	1.28400
C	17.06900	2.70400	1.04700
C	17.81800	2.28700	1.98400
C	17.40700	2.20600	3.40200
C	12.57700	4.45900	-0.38500
C	10.73100	2.77300	4.57500
C	11.31700	1.44200	4.74700
C	9.38500	2.97500	4.17100
C	8.92600	4.43900	3.92300
C	8.41500	1.89100	4.08800
C	10.48300	0.37000	4.60900
C	9.04600	0.62200	4.00200
N	13.98700	5.16100	-3.49700
N	13.44600	4.34300	-2.66800
C	13.41500	6.28800	-1.68800
C	13.69700	9.21100	1.87900
C	13.96500	6.57300	-3.12000
C	15.36700	7.41700	-3.75300
Zn	10.82400	12.58800	5.12700
O	12.47700	11.28100	5.66100
O	9.42800	11.10500	4.89300
N	10.93100	12.05000	2.95000
O	9.83700	14.38600	5.07500
N	15.94700	12.95400	2.86900
N	12.42000	13.94000	4.81700
N	15.36700	12.98500	1.64200
N	15.36300	11.79600	1.19300
N	12.79100	11.96700	-1.54900
C	9.20400	10.64400	3.69300
C	15.90700	10.95700	2.12000
C	11.72000	12.56800	1.99800
C	11.61000	12.13300	0.56900
C	16.02600	14.15300	3.64600

C	16.26600	11.72900	3.18900
C	9.98800	11.14100	2.59600
C	13.73200	13.66800	4.53500
C	14.64400	14.62700	4.08800
C	10.66300	11.20300	0.30800
C	9.81900	10.66700	1.28400
C	8.75900	9.76300	1.04700
C	8.02300	9.32300	1.98400
C	8.15900	9.71900	3.40200
C	12.52500	12.77500	-0.38500
C	11.98800	15.21700	4.57500
C	10.54200	15.37500	4.74700
C	12.83600	16.28100	4.17100
C	14.33300	15.94700	3.92300
C	12.38100	17.66400	4.08800
C	10.03100	16.63400	4.60900
C	10.96700	17.75200	4.00200
N	12.42800	11.20300	-3.49700
N	11.99000	12.08100	-2.66800
C	13.69000	11.13600	-1.68800
C	16.08000	9.42900	1.87900
C	13.66100	10.51700	-3.12000
C	13.69100	8.88000	-3.75300
Zn	16.31400	3.08000	6.82600
O	16.00800	5.16500	6.29200
O	14.33100	2.61300	7.05900
N	15.90100	3.44200	9.00300
O	17.37700	1.32600	6.87800
C	14.95200	7.26100	5.97600
N	19.19200	7.33400	9.08400
N	18.28300	3.78600	7.13600
N	18.92900	6.81600	10.31000
N	17.89700	7.40700	10.76000

C	14.95200	5.72600	5.97600
N	16.75900	5.09400	13.50200
C	13.82000	2.64900	8.25900
C	17.44200	8.29700	9.83200
C	16.74400	3.86600	9.95400
C	16.31200	3.98800	11.38400
C	20.27000	6.80300	8.30700
C	18.29000	8.22200	8.76400
C	14.64200	3.07900	9.35600
C	18.70300	5.05800	7.41800
C	19.98900	5.36800	7.86500
C	15.03400	3.63300	11.64400
C	14.14700	3.17000	10.66900
C	12.83400	2.70400	10.90600
C	12.08500	2.28700	9.96800
C	12.49600	2.20600	8.55100
C	17.32600	4.45900	12.33700
C	19.17200	2.77300	7.37700
C	18.58600	1.44200	7.20500
C	20.51800	2.97500	7.78100
C	20.97700	4.43900	8.03000
C	21.48800	1.89100	7.86500
C	19.42100	0.37000	7.34400
C	20.85700	0.62200	7.95100
N	15.91600	5.16100	15.45000
N	16.45700	4.34300	14.62000
C	16.48800	6.28800	13.64000
C	16.20600	9.21100	10.07400
C	15.93800	6.57300	15.07200
C	14.53600	7.41700	15.70600
Zn	20.44100	10.22900	5.12700
O	18.48300	9.45100	5.66100
O	19.85400	12.17900	4.89300

N	19.92100	10.40500	2.95000
C	16.16700	7.93100	5.97600
O	22.49100	10.18500	5.07500
N	18.19600	5.60900	2.86900
N	20.81400	8.17000	4.81700
N	18.51300	6.09600	1.64200
N	17.48600	6.69400	1.19300
N	18.92000	8.83600	-1.54900
C	19.56700	12.60400	3.69300
C	16.48700	6.64300	2.12000
C	19.97500	9.46300	1.99800
C	19.65400	9.77600	0.56900
C	19.19500	4.94100	3.64600
C	16.97600	5.94600	3.18900
C	19.60600	11.67700	2.59600
C	19.92300	7.17100	4.53500
C	20.29700	5.90200	4.08800
C	19.32200	11.06000	0.30800
C	19.28000	12.06000	1.28400
C	19.02700	13.43000	1.04700
C	19.01400	14.28700	1.98400
C	19.28900	13.97100	3.40200
C	19.75200	8.66200	-0.38500
C	22.13600	7.90600	4.57500
C	22.99500	9.07900	4.74700
C	22.63400	6.64000	4.17100
C	21.59600	5.51100	3.92300
C	24.05800	6.34200	4.08800
C	24.34100	8.89300	4.60900
C	24.84200	7.52300	4.00200
N	18.44000	9.53300	-3.49700
N	19.41900	9.47300	-2.66800
C	17.75000	8.47300	-1.68800

N	14.95100	8.63200	2.28500
C	15.07700	7.25600	1.87900
C	17.22900	8.80700	-3.12000
N	14.95100	8.63200	-3.21500
C	15.79600	9.60000	-3.75300
Zn	9.46200	10.22900	6.82600
O	11.42000	9.45100	6.29200
O	10.04900	12.17900	7.05900
N	9.98200	10.40500	9.00300
C	13.73600	7.93100	5.97600
O	7.41200	10.18500	6.87800
C	13.76400	9.31700	5.97600
N	11.70700	5.60900	9.08400
N	9.08900	8.17000	7.13600
N	11.39000	6.09600	10.31000
N	12.41700	6.69400	10.76000
C	12.43400	10.08500	5.97600
N	10.98300	8.83600	13.50200
C	10.33600	12.60400	8.25900
C	13.41600	6.64300	9.83200
C	9.92800	9.46300	9.95400
C	10.24900	9.77600	11.38400
C	10.70800	4.94100	8.30700
C	12.92700	5.94600	8.76400
C	10.29700	11.67700	9.35600
C	9.98000	7.17100	7.41800
C	9.60600	5.90200	7.86500
C	10.58100	11.06000	11.64400
C	10.62300	12.06000	10.66900
C	10.87600	13.43000	10.90600
C	10.88900	14.28700	9.96800
C	10.61400	13.97100	8.55100
C	10.15100	8.66200	12.33700

C	7.76700	7.90600	7.37700
C	6.90800	9.07900	7.20500
C	7.26900	6.64000	7.78100
C	8.30700	5.51100	8.03000
C	5.84500	6.34200	7.86500
C	5.56200	8.89300	7.34400
C	5.06100	7.52300	7.95100
N	11.46300	9.53300	15.45000
N	10.48400	9.47300	14.62000
C	12.15300	8.47300	13.64000
C	14.82600	7.25600	10.07400
C	12.67400	8.80700	15.07200
C	14.10700	9.60000	15.70600
Zn	19.07900	12.58800	6.82600
O	17.42600	11.28100	6.29200
O	20.47500	11.10500	7.05900
N	18.97200	12.05000	9.00300
C	14.95200	10.03500	5.97600
O	20.06600	14.38600	6.87800
C	16.13900	9.31800	5.97600
N	13.95600	12.95400	9.08400
N	17.48300	13.94000	7.13600
N	14.53600	12.98500	10.31000
N	14.54000	11.79600	10.76000
C	17.46800	10.08600	5.97600
N	17.11200	11.96700	13.50200
C	20.69900	10.64400	8.25900
C	13.99600	10.95700	9.83200
C	18.18300	12.56800	9.95400
C	18.29300	12.13300	11.38400
C	13.87700	14.15300	8.30700
C	13.63700	11.72900	8.76400
C	19.91500	11.14100	9.35600

C	16.17200	13.66800	7.41800
C	15.25900	14.62700	7.86500
C	19.24000	11.20300	11.64400
C	20.08400	10.66700	10.66900
C	21.14400	9.76300	10.90600
C	21.88000	9.32300	9.96800
C	21.74400	9.71900	8.55100
C	17.37800	12.77500	12.33700
C	17.91500	15.21700	7.37700
C	19.36100	15.37500	7.20500
C	17.06700	16.28100	7.78100
C	15.57000	15.94700	8.03000
C	17.52200	17.66400	7.86500
C	19.87200	16.63400	7.34400
C	18.93600	17.75200	7.95100
N	17.47500	11.20300	15.45000
N	17.91300	12.08100	14.62000
C	16.21300	11.13600	13.64000
N	14.95100	8.63200	9.66700
C	13.82300	9.42900	10.07400
C	16.24200	10.51700	15.07200
N	14.95100	8.63200	15.16800
C	16.21200	8.88000	15.70600
H	12.14580	4.12540	2.26730
H	9.49430	7.42490	4.53030
H	8.72050	6.82090	3.05000
H	11.67610	8.78250	4.11000
H	11.90300	5.86740	4.66560
H	15.22370	3.71130	-0.70910
H	17.44790	2.70250	0.03570
H	18.81890	1.97150	1.72880
H	18.06880	1.83420	4.17020
H	11.98450	3.60410	-0.71090

H	11.92210	5.16930	0.11960
H	7.91530	4.69890	3.64480
H	7.34470	2.03540	4.09150
H	10.79590	-0.62020	4.90570
H	8.53160	-0.19030	3.51010
H	12.51320	6.87910	-1.52840
H	14.16620	6.57360	-0.95160
H	13.75350	9.43440	0.81360
H	13.55170	10.14410	2.42340
H	13.11890	6.99270	-3.66420
H	15.41980	7.41810	-4.84170
H	16.29400	7.06580	-3.29970
H	12.45130	13.31570	2.26750
H	16.63410	13.96210	4.53020
H	16.49780	14.93430	3.05000
H	16.72050	11.39440	4.10980
H	14.08150	12.65450	4.66560
H	10.55350	10.85630	-0.70900
H	8.56840	9.43540	0.03570
H	7.24870	8.61470	1.72870
H	7.50660	9.33120	4.17030
H	13.46940	12.97410	0.12150
H	12.09120	13.72210	-0.70570
H	15.06320	16.69250	3.64480
H	13.04090	18.51890	4.09150
H	9.01720	16.85840	4.90610
H	10.52060	18.60350	3.50990
H	13.55790	10.34160	-0.95340
H	14.65350	11.61890	-1.52510
H	16.24530	9.26840	0.81360
H	16.96070	9.08810	2.42330
H	14.44730	11.03980	-3.66450
H	12.90920	8.24050	-3.34340

H	13.70220	8.86390	-4.84280
H	17.75710	4.12560	9.68430
H	20.40870	7.42490	7.42270
H	21.18250	6.82090	8.90300
H	18.22720	8.78260	7.84310
H	18.00000	5.86740	7.28740
H	14.67920	3.71160	12.66100
H	12.45490	2.70220	11.91730
H	11.08400	1.97160	10.22280
H	11.83410	1.83390	7.78300
H	17.91900	3.60430	12.66250
H	17.98040	5.16970	11.83220
H	21.98750	4.69880	8.30880
H	22.55830	2.03540	7.86220
H	19.10850	-0.62040	7.04760
H	21.37130	-0.19020	8.44320
H	15.73340	6.56960	12.90560
H	17.38740	6.88150	13.47620
H	16.35160	10.13630	9.51650
H	16.15150	9.44920	11.13630
H	16.78420	6.99280	15.61590
H	13.59090	7.05980	15.29690
H	14.52840	7.43450	16.79580
H	17.10250	7.39120	5.97600
H	20.25630	8.45570	2.26740
H	19.63810	4.14670	3.04530
H	18.72780	4.50330	4.52820
H	16.45900	5.72020	4.11000
H	18.87060	7.37540	4.66550
H	19.07600	11.32770	-0.70900
H	18.83850	13.75900	0.03570
H	18.78770	15.31180	1.72890
H	19.27970	14.72990	4.17030

H	20.78870	8.57490	-0.71030
H	19.46290	7.74010	0.11960
H	21.87630	4.50580	3.64470
H	24.46800	5.34290	4.09150
H	25.04180	9.65930	4.90580
H	25.80280	7.48380	3.51040
H	17.68930	7.39640	-1.52860
H	17.12680	8.98060	-0.95180
H	14.95090	8.63200	3.29500
H	14.85520	7.19300	0.81370
H	14.34180	6.66340	2.42350
H	17.28880	7.86470	-3.66450
H	14.95090	8.63190	-2.20500
H	15.76860	9.64540	-4.84170
H	15.63690	10.57830	-3.29950
H	12.80060	7.39110	5.97600
H	9.64690	8.45570	9.68420
H	11.17720	4.50980	7.42270
H	10.26720	4.14190	8.90300
H	13.44390	5.71990	7.84310
H	11.03240	7.37540	7.28750
H	10.82730	11.32780	12.66090
H	11.06440	13.75920	11.91720
H	11.11550	15.31180	10.22270
H	10.62310	14.73020	7.78290
H	10.45220	7.74520	11.83020
H	9.11370	8.56280	12.65690
H	8.02670	4.50600	8.30890
H	5.43500	5.34280	7.86220
H	4.86110	9.65950	7.04780
H	4.10020	7.48380	8.44260
H	12.77450	8.98540	12.90570
H	12.21690	7.39720	13.47650

H	15.04710	7.19370	11.13950
H	15.56170	6.66350	9.53020
H	12.61420	7.86450	15.61630
H	14.27050	10.59680	15.29630
H	14.12620	9.59830	16.79580
H	14.95190	11.11500	5.97600
H	17.45160	13.31550	9.68410
H	13.41060	14.93380	8.90770
H	13.26420	13.96710	7.42490
H	13.18230	11.39460	7.84320
H	15.82290	12.65430	7.28770
H	19.34940	10.85610	12.66090
H	21.33490	9.43530	11.91720
H	22.65420	8.61450	10.22290
H	22.39670	9.33120	7.78290
H	16.43360	12.97350	11.83030
H	17.81140	13.72240	12.65730
H	14.84000	16.69250	8.30880
H	16.86200	18.51890	7.86210
H	20.88600	16.85840	7.04760
H	19.38240	18.60350	8.44310
H	15.25040	11.62200	13.48090
H	16.34090	10.34290	12.90330
H	14.95090	8.63200	8.65700
H	13.65910	9.26890	11.13970
H	12.94160	9.08800	9.53100
H	15.45550	11.03980	15.61630
H	14.95080	8.63190	14.15800
H	16.23750	8.83420	16.79470
H	16.97970	8.25270	15.25290

*

6 Conclusion and Outlook

The first chapter of this thesis demonstrated the functionalization of the ligand backbone of the parent [Zn_2L_2] MOC. The ligand backbone was functionalized in two complementary ways. On the one hand, the π-surface of the backbone was increased and on the other hand, a crown-ether moiety was introduced. The second chapter delt with the limitations of the parent [Zn_2L_2] MOC, regarding discrete binding of the challenging oxalate anion. Nevertheless, the system was tested with a range of anions, including monocarboxylates and halides. The third chapter built on the design principles established in the other two previous chapters to create a more confined supramolecular architecture in contrast to the rather open "window-like" parent [Zn_2L_2] cages. Which resulted in a tripodal bis(bidentate) ligand, which formed ill-defined complexes in a self-assembly with $Zn(OAc)_2$. However, in the presence of tricarboxylate templates, such as trimesate, guest-induced formation of tri- and hexanuclear assemblies was observed.

Concluding my personal delve into the world of supramolecular chemistry with some suggestions and ideas for future experiments and scientific pathways for the demonstrated systems. First, the limitation of solubility is a major issue, which does come along with the hydroxyquinolate coordination units for metal complexation. Hydroxyquinolate-metal complexes are prone to be weakly soluble, which is linked to the overall charge-neutrality of the systems. Nevertheless, it comes along with possibilities in using the demonstrated systems in the separation of metal-ions. Also, as already demonstrated by our group, chiral guests could have a big impact on the applications of the systems presented. A bachelor's thesis supervised by me delt with the binding of prolinate by the parent [Zn_2L_2] cage and the use of the host-guest system as catalyst in a MICHEAL-addition. Unfortunately, weak binding of prolinate makes it challenging to use the host-guest system as catalyst. Especially when the guest itself shows catalytic activity for the investigated reaction.

Another approach for the development of the presented systems, especially for the guest induced self-assembly of the tripodal ligand L^{TP3}-H_3, is creating chiral, confined onion-type hexanuclear assemblies, which could lead to CPL and CD effects, or even catalytic reactivity. The modification of the tripropargyl amine is a possibility. Preliminary studies showed that an iodinated, L^{TP3}-derived ligand can be synthesized in which the triazole C-H atoms are substituted with iodine. This provides access to SONOGASHIRA cross-coupling reactions and, consequently, enables diverse post-modification to introduce tailored functionalities. Another opportunity is the synthesis of chiral tricarboxylate guests, such as monofunctionalized trimesate anions, that induce a discrete formation of a confined onion-type structure, thereby providing a functional cavity effectively shielded from the bulk phase.

Looking at the ligands demonstrated in the first two chapters it is obvious where the modulation of the system's functionalities can take place and how easy it is to implement chirality to the ligand's backbone. Preliminary studies with an alanine modified backbone, which are not included in this work, demonstrated another facile backbone modification. In this case, more functional amino acids like tryptophane could be more interesting, as this amino acid is a key intrinsic fluorophore in proteins, emitting fluorescence due to its indole heterocycle. Alternatively, as demonstrated in a bachelor's thesis supervised by me, a ligand bearing a polymerization unit on the backbone can be synthesized. Although the project was shelved due to low yields, incorporation of this ligand into a polymer network, where it could act as a cross-linking motif via Zn(II) complexation, thereby enabling modulation of the material properties, may still be an interesting scientific path to take.

To keep the charge-neutrality of the host-complexes, but to increase solubility, modifications of the hydroxyquinolate units could lead to challenging synthetic steps but also rewarding scientific results. Nevertheless, there are other complexation units, such as picolinate, which could not only expand the family of charge-neutral Zn(II) based MOCs, but also to new opportunities for applications. Another approach, which is well known in literature, is to use the copper(II)-paddlewheel to obtain charge neutrality of metal organic cages.

8-Hydroxyquinoline are derivates found many applications in the scientific world, besides fundamental supramolecular chemistry. Thinking outside of the box and use the present ligands in a medicinal chemistry way might be a little bit crazy, but no one knows. The best lines of script for the technological and scientific milestones were found by coincidence, as well as doing stuff nobody believed in at first.

7 Acknowledgment

First, I want to thank myself for always believing in me. And of course, I want to acknowledge my family. Without the unconditional support of my parents, Karola and Andreas, my academic path would not have been what it was; I do not know whether it would even have been possible.

Along this path, I met many remarkable people and experienced very different academic cultures. I also encountered situations that highlighted how important responsible mentorship and supportive supervision are for students' development and well-being. Those experiences reinforced for me how much leadership, empathy and integrity matter in academia, especially in senior positions.

Against that background, it was even more meaningful to meet David Van Craen. He offered me a position, I received the scholarship and the rest is history, already written above. Our association with the Clever Lab enriched my PhD experience enormously. Frequent scientific discussion with international and emotionally intelligent colleagues, an environment where you feel seen, where your abilities are trusted and where you can grow freely with the support of the group. In particular, Elie, Armin, and Jacopo made my arrival in the group much easier. I could ask them anything, and they would support me, while also challenging me to improve.

I also want to thank everybody I met at the TU Dortmund. Starting with Rudolf Walther, Laura Schneider, Laura Neukirch, Maike Wolters, Malavika Kallarikal, Anbinhu, Sami Ansawi, Silvia Lessing, Ljuba Iovkova, Wibke Langenkamp, Joseph Openy, Guido Clever, Christina Krabbe, Julian Holstein, Astrid Riedel, Weichao Xue, Jennifer Bremer, Gabi TK, Birgit Thormann, and many more. Thank you! Not to forget all my students I was allowed to support. Yannic, Viktoria, Alma, Sopiyas and Lennart.

Joe Giuseppe Joseph von und zu Prangenberg. Danke. Thank you supporting me from the day I enrolled. Thank you for keeping me company on the drive to Dortmund and for helping me submit my enrollment papers. Thank you for still being my friend. Even though our paths took completely different directions, we will always be family. Oschauer Jungs, vonner Benne, in die Welt.

Special thanks to David Mroß. Dziekuje za wszystko. Von der Mathe-Vorübung und dem ersten gemeinsamen Fass am Martin-Schmeißer Platz über die Schillerstraße zur Ardeystraße und bis ans Ende der Promotion, danke für deine Freundschaft.

I also want to thank Elie personally for being a friend I can always rely on. Our open and honest relationship is a pleasure. Especially the moments together in the coffee room or on the dancefloors of Tresor. More to come!

In the same breath I want to thank Armin for being one of the best lab mates I have met in Clever lab. Besides the great time in lab we, you Elie and I, we had a great time together. Cannot wait to visit Südtirol together with you. I also want to mention Alexandre and his jokes in the coffee room, our almost daily encounters were always a little spark for my day. Thank you!

Gostaria também de agradecer à minha namorada Iasmin pelo apoio incondicional durante o meu doutorado. Muito obrigado por todas as horas que me escutou falar sobre coisas da universidade.

Zu guter Letzt möchte ich, nochmals auf Deutsch, meiner Familie danken. Meiner Mutter Karola, meinem Vater Andreas und meiner Schwester Liza und Tim. Vielen Dank für euren bedingungslosen Support. Egal wann, egal wo. Ich weiß, es war nicht immer leicht. Jedoch weiß ich, was ich will. Und nun sind wir hier, gemeinsam, am Ende meiner akademischen Laufbahn. Vielen Dank.

Everybody I did not mention, but you know that you were part of it, thank you!

From Orsoy, with love to the world – thank you, everybody.

8 References

[1] a) C. J. Pedersen, *Angew. Chem. Int. Ed. Engl.* **1988**, *27*, 1021; b) C. J. Pedersen, *J. Am. Chem. Soc.* **1967**, *89*, 2495.

[2] a) B. Dietrich, J. M. Lehn, J. P. Sauvage, *Tetrahedron Letters* **1969**, *10*, 2889; b) R.-C. Brachvogel, F. Hampel, M. von Delius, *Nature communications* **2015**, *6*, 7129.

[3] C. D. Gutsche, B. Dhawan, K. H. No, R. Muthukrishnan, *J. Am. Chem. Soc.* **1981**, *103*, 3782.

[4] R. W. Saalfrank, A. Stark, K. Peters, H. G. von Schnering, *Angew. Chem. Int. Ed. Engl.* **1988**, *27*, 851.

[5] a) P. W. K. Rothemund, *Nature* **2006**, *440*, 297; b) J. M. Lehn, A. Rigault, J. Siegel, J. Harrowfield, B. Chevrier, D. Moras, *Proceedings of the National Academy of Sciences of the United States of America* **1987**, *84*, 2565; c) H. Wang, X. Zheng, *Physical chemistry chemical physics: PCCP* **2022**, *24*, 19011.

[6] D. L. Caulder, R. E. Powers, T. N. Parac, K. N. Raymond, *Angew. Chem. Int. Ed.* **1998**, *37*, 1840.

[7] M. Fujita, D. Oguro, M. Miyazawa, H. Oka, K. Yamaguchi, K. Ogura, *Nature* **1995**, *378*, 469.

[8] T. Kusukawa, M. Fujita, *Angewandte Chemie International Edition* **1998**, *37*, 3142.

[9] a) K. Omoto, S. Tashiro, M. Kuritani, M. Shionoya, *J. Am. Chem. Soc.* **2014**, *136*, 17946; b) D. Zhu, B. Sun, L. Tong, Y. Wu, M. M. Cetin, H. Li, *Organic letters* **2022**, *24*, 8980; c) K. P. de Carvasal, G. Vergoten, J.-J. Vasseur, M. Smietana, F. Morvan, *Biomacromolecules* **2023**, *24*, 756; d) S. J. Dettmer, H. D. Williams, R. Napier, J. M. Beames, S. Walker-Griffiths, T. D. Craggs, M. J. Hannon, *Angew. Chem. Int. Ed.* **2025**, *64*, e202504866.

[10] J. Gemen, J. R. Church, T.-P. Ruoko, N. Durandin, M. J. Białek, M. Weißenfels, M. Feller, M. Kazes, M. Odaybat, V. A. Borin et al., *Science* **2023**, *381*, 1357.

[11] a) H. Cheng, R. Liu, R. Zhang, L. Huang, Q. Yuan, *Nanoscale advances* **2023**, *5*, 2394; b) T. Keijer, T. Bouwens, J. Hessels, J. N. H. Reek, *Chemical science* **2020**, *12*, 50.

[12] A. B. Søgaard, A. B. Pedersen, K. B. Løvschall, P. Monge, J. H. Jakobsen, L. Džabbarova, L. F. Nielsen, S. Stevanovic, R. Walther, A. N. Zelikin, *Nature communications* **2023**, *14*, 1646.

[13] S. Löffler, J. Lübben, L. Krause, D. Stalke, B. Dittrich, G. H. Clever, *J. Am. Chem. Soc.* **2015**, *137*, 1060.

[14] a) R. Kluifhooft, T. Wachsmuth, B. Barthel, M. Müller, A.-K. Rückert, M. Kathan, *Angew. Chem. Int. Ed.* **2025**, e20085; b) T. Wachsmuth, R. Kluifhooft, M. Müller, L. Zeiß, M. Kathan, *Science (New York, N.Y.)* **2025**, *389*, 526.

[15] Y. Yang, Y. Du, A. W. Heard, J. R. Nitschke, *Nat. Synth* **2025**, *4*, 776.

[16] a) L.-J. Chen, H.-B. Yang, M. Shionoya, *Chemical Society reviews* **2017**, *46*, 2555; b) A. J. McConnell, *Chemical Society reviews* **2022**, *51*, 2957; c) T. Tateishi, M. Yoshimura, S. Tokuda, F. Matsuda, D. Fujita, S. Furukawa, *Coordination Chemistry Reviews* **2022**, *467*, 214612; d) E. Benchimol, J. Tessarolo, G. H. Clever, *Nature chemistry* **2024**, *16*, 13; e) E. Benchimol, B.-N. T. Nguyen, T. K. Ronson, J. R. Nitschke, *Chemical Society reviews* **2022**, *51*, 5101; f) S. Pullen, J. Tessarolo, G. H. Clever, *Chemical science* **2021**, *12*, 7269; g) F. J. Rizzuto, L. K. S. von Krbek, J. R. Nitschke, *Nature reviews. Chemistry* **2019**, *3*, 204; h) M. Yoshizawa, J. K. Klosterman, M. Fujita, *Angew. Chem. Int. Ed.* **2009**, *48*, 3418; i) C. M. Hong, R. G. Bergman, K. N. Raymond, F. D. Toste, *Accounts of chemical research* **2018**, *51*, 2447; j) M. D. Ward, P. R. Raithby, *Chemical Society reviews* **2013**, *42*, 1619; k) T. R. Cook, P. J. Stang, *Chem. Rev.* **2015**, *115*, 7001; l) R. Chakrabarty, P. S. Mukherjee, P. J. Stang, *Chem. Rev.* **2011**, *111*, 6810; m) N. B. Debata, D. Tripathy, H. S. Sahoo, *Coordination Chemistry Reviews* **2019**, *387*, 273; n) C. J. T. Cox, J. Hale, P. Molinska, J. E. M. Lewis, *Chemical Society reviews* **2024**, *53*, 10380; o) T. Abe, N. Sanada, K. Takeuchi, A. Okazawa, S. Hiraoka, *J. Am. Chem. Soc.* **2023**, *145*, 28061; p) J.-J. Xuan, Z.-J. Xia, D.-N. Yan, S.-J. Hu, L.-P. Zhou, L.-X. Cai, Q.-F. Sun, *Inorganic chemistry* **2022**, *61*, 8854; q) B. Zhang, H. Lee, J. J. Holstein, G. H. Clever, *Angew. Chem. Int. Ed.* **2024**, *63*, e202404682; r) H. Wu, Y. Wang, L.

Đorđević, P. Kundu, S. Bhunia, A. X.-Y. Chen, L. Feng, D. Shen, W. Liu, L. Zhang et al., *Nature* **2025**, *637*, 347; s) A. Tarzia, G. M. Pavan, *Predicting stable cage structures by enumerating stoichiometry and topology*, **2025**; t) T. Li, P. Wang, T. Wu, *Chemistry, an Asian journal* **2025**, *20*, e00867; u) H. D. Williams, S. J. Dettmer, S. Bajpai, M. J. Hannon, *J. Am. Chem. Soc.* **2025**, *147*, 40992.

[17] J. Liu, Z. Wang, P. Cheng, M. J. Zaworotko, Y. Chen, Z. Zhang, *Nature reviews. Chemistry* **2022**, *6*, 339.

[18] K. Wu, E. Benchimol, A. Baksi, G. H. Clever, *Nature chemistry* **2024**, *16*, 584.

[19] S. R. Seidel, P. J. Stang, *Accounts of chemical research* **2002**, *35*, 972.

[20] J. R. Bradbury, J. L. Hampton, D. P. Martone, A. W. Maverick, *Inorg. Chem.* **1989**, *28*, 2392.

[21] A. W. Maverick, F. E. Klavetter, *Inorg. Chem.* **1984**, *23*, 4129.

[22] A. W. Maverick, S. C. Buckingham, Q. Yao, J. R. Bradbury, G. G. Stanley, *J. Am. Chem. Soc.* **1986**, *108*, 7430.

[23] D. L. Caulder, K. N. Raymond, *Angew. Chem. Int. Ed. Engl.* **1997**, *36*, 1440.

[24] B. Kersting, M. Meyer, R. E. Powers, K. N. Raymond, *J. Am. Chem. Soc.* **1996**, *118*, 7221.

[25] M. Scherer, D. L. Caulder, D. W. Johnson, K. N. Raymond, *Angew. Chem. Int. Ed.* **1999**, *38*, 1587.

[26] F. E. Yates, *Self-Organizing Systems*. *The Emergence of Order*, Springer, New York, NY, **1987**.

[27] R. M. Yeh, J. Xu, G. Seeber, K. N. Raymond, *Inorganic chemistry* **2005**, *44*, 6228.

[28] a) H.-B. Zhu, Y.-F. Wu, Y.-B. Lou, J. Hu, *Synthetic Metals* **2014**, *190*, 34; b) P. W. V. Butler, P. E. Kruger, J. S. Ward, *Chemical communications (Cambridge, England)* **2019**, *55*, 10304; c) M. Hong, Y. Zhao, W. Su, R. Cao, M. Fujita, Z. Zhou, A. S. C. Chan, *J. Am. Chem. Soc.* **2000**, *122*, 4819.

[29] Y. Yang, S. Y. Hu, T. K. Ronson, P. C. Teeuwen, S. Gaikwad, A. W. Heard, D. J. Wales, J. R. Nitschke, *Angew. Chem. Int. Ed.* **2025**.

[30] C. V. Craescu, S. Stahl, T. L. F. Correia, S. M. Bierschenk, N. S. Settineri, R. G. Bergman, K. N. Raymond, F. D. Toste, *J. Am. Chem. Soc.* **2025**, *147*, 32600.

[31] H. Kurz, P. C. P. Teeuwen, T. K. Ronson, J. B. Hoffman, P. Pracht, D. J. Wales, J. R. Nitschke, *J. Am. Chem. Soc.* **2024**, *146*, 30958.

[32] D. Luo, Z.-J. Yuan, L.-J. Ping, X.-W. Zhu, J. Zheng, C.-W. Zhou, X.-C. Zhou, X.-P. Zhou, D. Li, *Angew. Chem. Int. Ed.* **2023**, *62*, e202216977.

[33] S. Dey, R. Banerjee, N. Hickey, P. S. Mukherjee, *J. Am. Chem. Soc.* **2025**, *147*, 32904.

[34] L. A. Faulkner, J. D. Crowley, *Chem. Eur. J.* **2024**, *10*, 440.

[35] a) D. Zhang, T. K. Ronson, Y.-Q. Zou, J. R. Nitschke, *Nature reviews. Chemistry* **2021**, *5*, 168; b) E. G. Percástegui, T. K. Ronson, J. R. Nitschke, *Chem. Rev.* **2020**, *120*, 13480.

[36] a) S. Bhattacharyya, M. R. Black, B. S. Pilgrim, *Chemical science* **2025**, *16*, 21238; b) S. Chen, L.-J. Chen, *Chem. Eur. J.* **2022**, *4*, 494; c) R. G. DiNardi, S. Rasheed, S. S. Capomolla, M. H. Chak, I. A. Middleton, L. K. Macreadie, J. P. Violi, W. A. Donald, P. J. Lusby, J. E. Beves, *J. Am. Chem. Soc.* **2024**, *146*, 21196.

[37] D. Fiedler, R. G. Bergman, K. N. Raymond, *Angew. Chem. Int. Ed.* **2006**, *45*, 745.

[38] a) H. Wang, Z. Qiu, H. Liu, A. M. D. S. Jayawardhana, Z. Yue, H. Daghlas, D. J. Bowers, B. Datta, Y.-R. Zheng, *Frontiers in chemistry* **2019**, *7*, 39; b) G. Montà-González, E. Ortiz-Gómez, R. López-Lima, G. Fiorini, R. Martínez-Máñez, V. Martí-Centelles, *Molecules (Basel, Switzerland)* **2024**, *29*.

[39] a) N. Dey, C. J. E. Haynes, *ChemPlusChem* **2021**, *86*, 418; b) A. Bajer, V. Mangili, A. R. Stefankiewicz, *Chem* **2025**, 102784; c) N. Suzuki, K. Miyata, Y. Ono, Y. Yamasaki, T. Haino, *J. Am. Chem. Soc.* **2025**.

[40] V. M. Dong, D. Fiedler, B. Carl, R. G. Bergman, K. N. Raymond, *J. Am. Chem. Soc.* **2006**, *128*, 14464.

[41] J. L. Brumaghim, M. Michels, D. Pagliero, K. N. Raymond, *Eur. J. Org. Chem.* **2004**, *2004*, 5115.
[42] P. Mal, B. Breiner, K. Rissanen, J. R. Nitschke, *Science* **2009**, *324*, 1697.
[43] M. Yamashina, Y. Sei, M. Akita, M. Yoshizawa, *Nature communications* **2014**, *5*, 4662.
[44] S. Hasegawa, S. L. Meichsner, J. J. Holstein, A. Baksi, M. Kasanmascheff, G. H. Clever, *J. Am. Chem. Soc.* **2021**, *143*, 9718.
[45] R. Baliyan, G. Bailey, *Molecular Cages as Encapsulants for the Stabilization of Reactive Iron-Sulfur Cofactor Models*, **2024**.
[46] D. Samanta, J. Gemen, Z. Chu, Y. Diskin-Posner, L. J. W. Shimon, R. Klajn, *Proceedings of the National Academy of Sciences of the United States of America* **2018**, *115*, 9379.
[47] D. Samanta, S. Mukherjee, Y. P. Patil, P. S. Mukherjee, *Chem. Eur. J.* **2012**, *18*, 12322.
[48] D. Samanta, D. Galaktionova, J. Gemen, L. J. W. Shimon, Y. Diskin-Posner, L. Avram, P. Král, R. Klajn, *Nature communications* **2018**, *9*, 641.
[49] A. I. Hanopolskyi, S. De, M. J. Białek, Y. Diskin-Posner, L. Avram, M. Feller, R. Klajn, *Beilstein journal of organic chemistry* **2019**, *15*, 2398.
[50] L. Pesce, C. Perego, A. B. Grommet, R. Klajn, G. M. Pavan, *J. Am. Chem. Soc.* **2020**, *142*, 9792.
[51] J. Gemen, M. J. Białek, M. Kazes, L. J. W. Shimon, M. Feller, S. N. Semenov, Y. Diskin-Posner, D. Oron, R. Klajn, *Chem. Eur. J.* **2022**, *8*, 2362.
[52] Olof Ramström, *The Nobel Prize in Chemistry 2016*, Stockholm, **2016**.
[53] Z.-J. Xia, Y.-M. Zhong, S.-J. Hu, L.-X. Cai, Q.-F. Sun, *Inorganic chemistry* **2023**, *62*, 8293.
[54] A. Walther, I. Regeni, J. J. Holstein, G. H. Clever, *J. Am. Chem. Soc.* **2023**, *145*, 25365.
[55] D. E. Koshland, *Proceedings of the National Academy of Sciences of the United States of America* **1958**, *44*, 98.
[56] B. Hasenknopf, J.-M. Lehn, N. Boumediene, E. Leize, A. van Dorsselaer, *Angew. Chem. Int. Ed.* **1998**, *37*, 3265.
[57] E. G. Percástegui, *Eur. J. Inorg. Chem.* **2021**, *2021*, 4425.
[58] A. V. Davis, K. N. Raymond, *J. Am. Chem. Soc.* **2005**, *127*, 7912.
[59] M. L. C. Quan, D. J. Cram, *J. Am. Chem. Soc.* **1991**, *113*, 2754.
[60] M. D. Pluth, K. N. Raymond, *Chemical Society reviews* **2007**, *36*, 161.
[61] A. V. Davis, D. Fiedler, G. Seeber, A. Zahl, R. van Eldik, K. N. Raymond, *J. Am. Chem. Soc.* **2006**, *128*, 1324.
[62] a) D. J. Cram, M. T. Blanda, K. Paek, C. B. Knobler, *J. Am. Chem. Soc.* **1992**, *114*, 7765; b) T. A. Bobbins, D. J. Cram, *J. Chem. Soc., Chem. Commun.* **1995**, 1515.
[63] a) D. J. Cram, R. Jaeger, K. Deshayes, *J. Am. Chem. Soc.* **1993**, *115*, 10111; b) M. L. C. Quan, D. J. Cram, *J. Am. Chem. Soc.* **1991**, *113*, 2754.
[64] J. Yoon, D. J. Cram, *Chem. Commun.* **1997**, 1505.
[65] S. C. N. Hsu, M. Ramesh, J. H. Espenson, T. B. Rauchfuss, *Angew. Chem. Int. Ed.* **2003**, *42*, 2663.
[66] D. M. Kaphan, F. D. Toste, R. G. Bergman, K. N. Raymond, *J. Am. Chem. Soc.* **2015**, *137*, 9202.
[67] a) S. M. Bierschenk, R. G. Bergman, K. N. Raymond, F. D. Toste, *J. Am. Chem. Soc.* **2020**, *142*, 733; b) T. A. Bender, R. G. Bergman, K. N. Raymond, F. D. Toste, *J. Am. Chem. Soc.* **2019**, *141*, 11806; c) D. Fiedler, D. H. Leung, R. G. Bergman, K. N. Raymond, *Accounts of chemical research* **2005**, *38*, 349; d) D. Fiedler, R. G. Bergman, K. N. Raymond, *Angew. Chem. Int. Ed.* **2004**, *43*, 6748; e) S. M. Bierschenk, J. Y. Pan, N. S. Settineri, U. Warzok, R. G. Bergman, K. N. Raymond, F. D. Toste, *J. Am. Chem. Soc.* **2022**, *144*, 11425.
[68] H. Xu, T. K. Ronson, A. W. Heard, P. C. P. Teeuwen, L. Schneider, P. Pracht, J. D. Thoburn, D. J. Wales, J. R. Nitschke, *Nature chemistry* **2025**, *17*, 289.
[69] a) R. Zhu, J. Lübben, B. Dittrich, G. H. Clever, *Angew. Chem. Int. Ed.* **2015**, *54*, 2796; b) M. Fukuda, R. Sekiya, R. Kuroda, *Angew. Chem. Int. Ed.* **2008**, *47*, 706; c) S. Ganta, A. S. Mikherdov, A. Baksi, C. Drechsler, G. H. Clever, *Angew. Chem. Int. Ed.* **2025**, e202516952; d) S. Freye, J.

Hey, A. Torras-Galán, D. Stalke, R. Herbst-Irmer, M. John, G. H. Clever, *Angew. Chem. Int. Ed.* **2012**, *51*, 2191; e) G. H. Clever, P. Punt, *Accounts of chemical research* **2017**, *50*, 2233.
[70] a) M. Frank, M. D. Johnstone, G. H. Clever, *Chem. Eur. J.* **2016**, *22*, 14104; b) J. Martí-Rujas, A. Famulari, *Angew. Chem. Int. Ed.* **2024**, *63*, e202407626.
[71] S. Freye, R. Michel, D. Stalke, M. Pawliczek, H. Frauendorf, G. H. Clever, *J. Am. Chem. Soc.* **2013**, *135*, 8476.
[72] B. Odell, M. V. Reddington, A. M. Z. Slawin, N. Spencer, J. F. Stoddart, D. J. Williams, *Angew. Chem. Int. Ed. Engl.* **1988**, *27*, 1547.
[73] I. Regeni, B. Chen, M. Frank, A. Baksi, J. J. Holstein, G. H. Clever, *Angew. Chem. Int. Ed.* **2021**, *60*, 5673.
[74] T. Tateishi, S. Takahashi, A. Okazawa, V. Martí-Centelles, J. Wang, T. Kojima, P. J. Lusby, H. Sato, S. Hiraoka, *J. Am. Chem. Soc.* **2019**, *141*, 19669.
[75] Z.-Y. Zeng, X. Zhao, J. Huang, J. Zhu, T. Jin, L. Hu, W.-T. Dou, L. Xu, *Synlett* **2024**, *35*, 130.
[76] D. van Craen, M. G. Kalarikkal, J. J. Holstein, *J. Am. Chem. Soc.* **2022**, *144*, 18135.
[77] K. V. Krishnamurty, G. M. Harris, *Chem. Rev.* **1961**, *61*, 213.
[78] E. J. Baran, *Geochemistry* **2016**, *76*, 449.
[79] D. P. August, G. S. Nichol, P. J. Lusby, *Angew. Chem. Int. Ed.* **2016**, *55*, 15022.
[80] a) L. A. Pérez-Márquez, M. D. Perretti, R. García-Rodríguez, F. Lahoz, R. Carrillo, *Angew. Chem. Int. Ed.* **2022**, *61*, e202205403; b) T. Fiehn, R. Goddard, R. W. Seidel, S. Kubik, *Chem. Eur. J.* **2010**, *16*, 7241; c) Q.-Q. Wang, V. W. Day, K. Bowman-James, *Angew. Chem. Int. Ed.* **2012**, *51*, 2119.
[81] Y. Liu, W. Zhao, C.-H. Chen, A. H. Flood, *Science* **2019**, *365*, 159.
[82] M. G. Kalarikkal, C. Drechsler, G. Tusha, L. V. Schäfer, D. Van Craen, *Chem. Eur. J.* **2023**, *29*, e202301613.
[83] a) C. Bravin, A. Guidetti, G. Licini, C. Zonta, *Chemical science* **2019**, *10*, 3523; b) C. Bravin, G. Mason, G. Licini, C. Zonta, *J. Am. Chem. Soc.* **2019**, *141*, 11963; c) F. Begato, R. Penasa, G. Licini, C. Zonta, *ACS sensors* **2022**, *7*, 1390.
[84] F. Begato, G. Licini, C. Zonta, *Chemical science* **2023**, *14*, 8147.
[85] C. Bravin, E. Badetti, R. Puttreddy, F. Pan, K. Rissanen, G. Licini, C. Zonta, *Chem. Eur. J.* **2018**, *24*, 2936.
[86] F. Begato, R. Penasa, G. Licini, C. Zonta, *Chem. Com.* **2021**, *57*, 10019.
[87] P. Belser, S. Bernhard, U. Guerig, *Tetrahedron* **1996**, *52*, 2937.
[88] E. Ziegler, G. Haberhauer, *Eur. J. Org. Chem.* **2009**, *2009*, 3432.
[89] V. Haridas, S. Sahu, P. P. Praveen Kumar, A. R. Sapala, *RSC Adv.* **2012**, *2*, 12594.
[90] P. Thordarson, *Chemical Society reviews* **2011**, *40*, 1305.
[91] D. Brynn Hibbert, P. Thordarson, *Chem. Com.* **2016**, *52*, 12792.
[92] V. Luca, J. J. Tejada, D. Vega, G. Arrachart, C. Rey, *Inorg. Chem.* **2016**, *55*, 7928.
[93] X. Liu, Z. Han, Z. Wang, K. Ding, *Sci. China Chem.* **2014**, *57*, 1073.
[94] S. Suzuki, K. Matsuura, K. Nakazono, T. Takata, *Polym J* **2014**, *46*, 355.
[95] M. Müller, A. Hansen, S. Grimme, *The Journal of chemical physics* **2023**, *158*, 14103.
[96] F. Weigend, R. Ahlrichs, *Physical chemistry chemical physics: PCCP* **2005**, *7*, 3297.
[97] F. Weigend, *Physical chemistry chemical physics: PCCP* **2006**, *8*, 1057.
[98] *Software update: The ORCA program system–Version 5.0, WIREs Comput. Mol. Sci., 12, e1606*, **2022**.
[99] *Software update: The ORCA program system–Version 5.0, WIREs Comput. Mol. Sci., 12, e1606*, **2022**.
[100] D. Ocklenburg, D. van Craen, *Beilstein journal of organic chemistry* **2024**, *20*, 3007.
[101] A. S. K. Hashmi, L. Molinari, F. Rominger, T. Oeser, *Eur. J. Org. Chem.* **2011**, *2011*, 2256.

[102] a) E. J. Baran, *Journal of Coordination Chemistry* **2014**, *67*, 3734; b) V. Jordanovska, R. Trojko, N. Galešić, *Thermochimica Acta* **1992**, *198*, 369.
[103] P. Gans, A. Sabatini, A. Vacca, *Talanta* **1996**, *43*, 1739.
[104] A. Najibi, L. Goerigk, *Journal of computational chemistry* **2020**, *41*, 2562.
[105] V. Barone, M. Cossi, *J. Phys. Chem. A* **1998**, *102*, 1995.
[106] C. Bannwarth, E. Caldeweyher, S. Ehlert, A. Hansen, P. Pracht, J. Seibert, S. Spicher, S. Grimme, *WIREs Comput Mol Sci* **2021**, *11*.
[107] C. Bannwarth, S. Ehlert, S. Grimme, *Journal of chemical theory and computation* **2019**, *15*, 1652.
[108] P. W. Atkins, J. de Paula, J. J. Keeler, *Physikalische Chemie,* 6. Aufl., WILEY-VCH, Weinheim, **2022**.
[109] H. Eyring, *The Journal of chemical physics* **1935**, *3*, 107.

9 *Eidesstattliche Versicherung (Affidavit)*

Name, Vorname
(Surname, first name)

Matrikel-Nr.
(Enrolment number)

Belehrung:
Wer vorsätzlich gegen eine die Täuschung über Prüfungsleistungen betreffende Regelung einer Hochschulprüfungsordnung verstößt, handelt ordnungswidrig. Die Ordnungswidrigkeit kann mit einer Geldbuße von bis zu 50.000,00 € geahndet werden. Zuständige Verwaltungsbehörde für die Verfolgung und Ahndung von Ordnungswidrigkeiten ist der Kanzler/die Kanzlerin der Technischen Universität Dortmund. Im Falle eines mehrfachen oder sonstigen schwerwiegenden Täuschungsversuches kann der Prüfling zudem exmatrikuliert werden, § 63 Abs. 5 Hochschulgesetz NRW.

Die Abgabe einer falschen Versicherung an Eides statt ist strafbar.

Wer vorsätzlich eine falsche Versicherung an Eides statt abgibt, kann mit einer Freiheitsstrafe bis zu drei Jahren oder mit Geldstrafe bestraft werden, § 156 StGB. Die fahrlässige Abgabe einer falschen Versicherung an Eides statt kann mit einer Freiheitsstrafe bis zu einem Jahr oder Geldstrafe bestraft werden, § 161 StGB.

Die obenstehende Belehrung habe ich zur Kenntnis genommen:

Official notification:

Any person who intentionally breaches any regulation of university examination regulations relating to deception in examination performance is acting improperly. This offence can be punished with a fine of up to EUR 50,000.00. The competent administrative authority for the pursuit and prosecution of offences of this type is the chancellor of the TU Dortmund University. In the case of multiple or other serious attempts at deception, the candidate can also be unenrolled, Section 63, paragraph 5 of the Universities Act of North Rhine-Westphalia.

The submission of a false affidavit is punishable.

Any person who intentionally submits a false affidavit can be punished with a prison sentence of up to three years or a fine, Section 156 of the Criminal Code. The negligent submission of a false affidavit can be punished with a prison sentence of up to one year or a fine, Section 161 of the Criminal Code.

I have taken note of the above official notification.

Ort, Datum
(Place, date)

Unterschrift
(Signature)

Titel der Dissertation:
(Title of the thesis):

Ich versichere hiermit an Eides statt, dass ich die vorliegende Dissertation mit dem Titel selbstständig und ohne unzulässige fremde Hilfe angefertigt habe. Ich habe keine anderen als die angegebenen Quellen und Hilfs mittel benutzt sowie wörtliche und sinngemäße Zitate kenntlich gemacht.
Die Arbeit hat in gegenwärtiger oder in einer anderen Fassung weder der TU Dortmund noch einer anderen Hochschule im Zusammenhang mit einer staatlichen oder akademischen Prüfung vorgelegen.

I hereby swear that I have completed the present dissertation independently and without inadmissible external support. I have not used any sources or tools other than those indicated and have identified literal and analogous quotations.

The thesis in its current version or another version has not been presented to the TU Dortmund University or another university in connection with a state or academic examination.*

*Please be aware that solely the German version of the affidavit ("Eidesstattliche Versicherung") for the PhD thesis is the official and legally binding version.

Ort, Datum
(Place, date)

Unterschrift
(Signature)